Design, synthesis and characterization of polylysine dendrones for biomedical applications

Mirsharghi, Sahar

Publication date:
2016

Document Version
Publisher's PDF, also known as Version of record

Design, Synthesis and Characterization of Polylysine Dendrons for Biomedical Applications

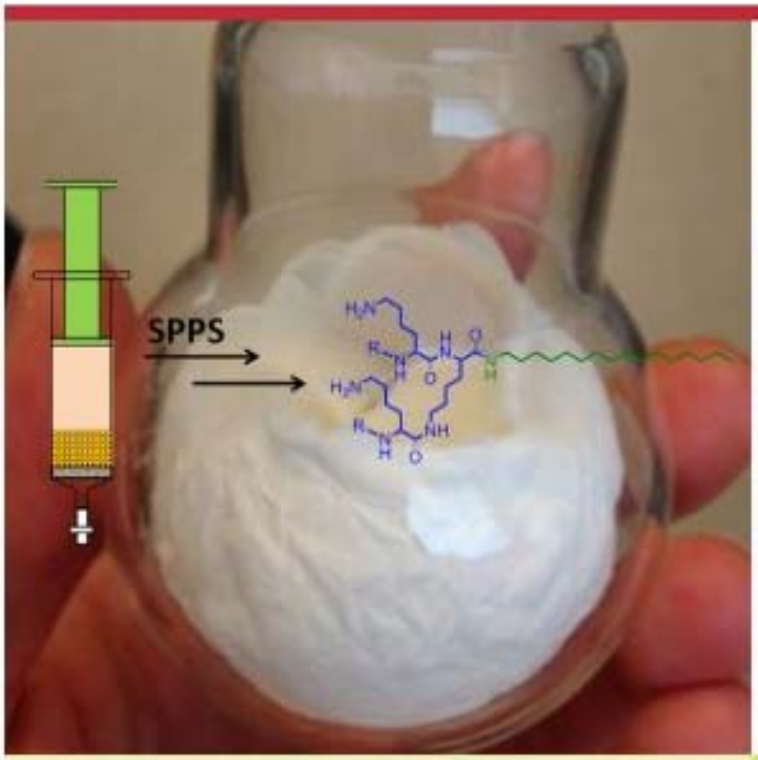

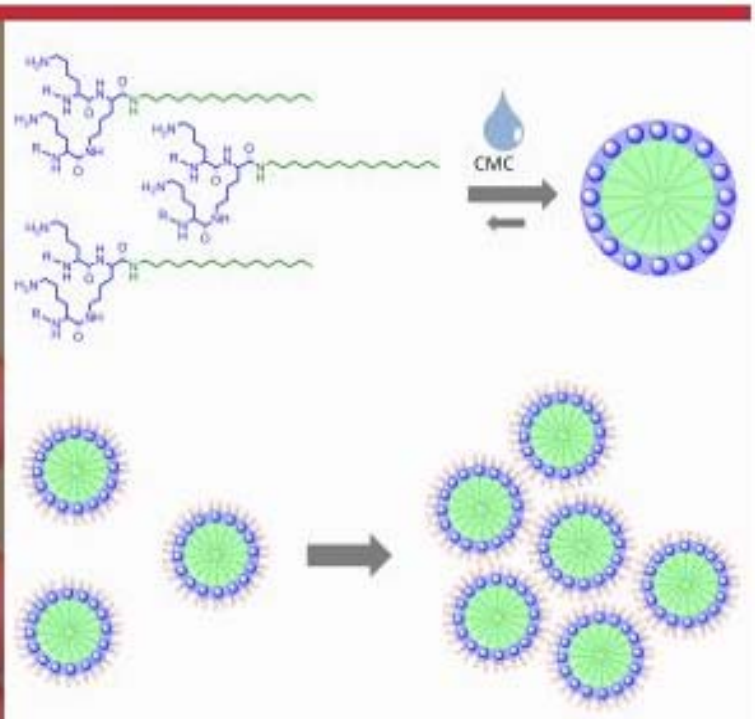

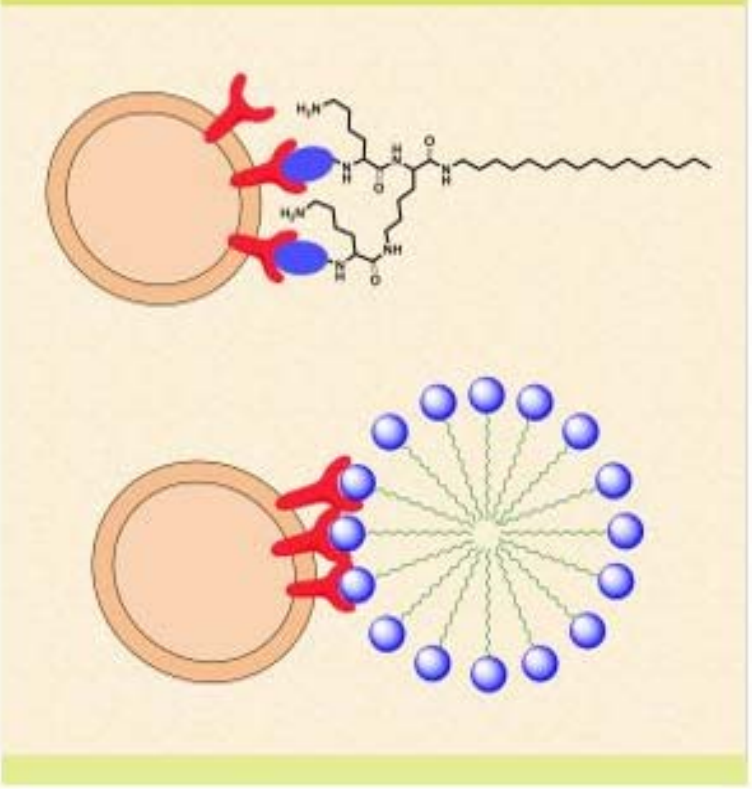

Sahar Mirsharghi

August 2016

DTU Vet
National Veterinary Institute

Design, Synthesis and Characterization of Polylysine Dendrons for Biomedical Applications

Ph.D. Thesis

by

Sahar Mirsharghi

Section for Immunology and Vaccinology

National Veterinary Institute

Technical University of Denmark

August 2016

List of publications

Publication I

D. K. Svenssen, S. Mirsharghi and U. Boas, Solid-Phase Synthesis of Polyfunctional Polylysine Dendrons using Aldehyde Linkers, *Tet. Lett.*, **2014**, 55, 3942-3945.

Publication II

U. Boas and S. Mirsharghi, Color Test for Selective Detection of Secondary Amines on Resin and in Solution, *Org. Lett.*, **2014**, 16, 5918-5921.

Publication III

S. Mirsharghi, K. D. Knudsen, S. Bagherifam, B. Nyström and U. Boas, Preparation and Self-Assembly of Amphiphilic Polylysine Dendrons, *New J. Chem.*, **2016**, 40, 3597-3611.

Preface

The work presented in this thesis summarizes the research performed from August 2013 to August 2016 under the supervision of Associate Professor Ulrik Boas and Professor Peter M. H. Heegaard at the Section for Immunology and Vaccinology, National Veterinary Institute, Technical University of Denmark, as well as research performed from December 2014 to April 2015 under the supervision of Professor Bo Nyström at the Department of Chemistry, University of Oslo. Thus far the work has resulted in three publications, which can be found in the Appendix.

Apart from the research presented in this thesis, I have had the pleasure of teaching bachelor and master students in Bioconjugate Chemistry (24007, 3 weeks course in June 2014 and June 2015) and Applied Peptide Synthesis (24008, 3 weeks course in January 2016). Furthermore, I have passed the following courses, Advanced Medicinal and Organic Chemistry (8 ECTS, KU), Dynamic Light Scattering (5 ECTS, DTU), Neutron Scattering Methods for Materials Research (3 ECTS, IFE), N11 Drug Delivery (3 ECTS, iNANO, AU), PolyNano Summer School (5 ECTS, DTU) and Biostructures and Molecular Modelling in Drug Research (6.5 ECTS, KU). In addition, I have also attended the following conferences and meetings: DTU Vet meetings (Denmark, April 2014, October 2014 and September 2015, oral presentations), group meeting at the University of Oslo (Norway, December 2014, oral presentation), Polymer Meeting organized by the Polymer Group at the University of Oslo (Norway, March 2015, oral presentation), PhD Day at DTU Vet (Denmark, September 2015, poster presentation), 13th Meeting in Future Trends in Protein Science (Denmark, December 2015, poster presentation), 5th International Symposium on Biological Applications of Dendrimers (Copenhagen, Denmark, August 2016, poster presentation).

First of all, I would like to give my profound thanks to my supervisors Ulrik Boas and Peter M. H. Heegaard for giving me the opportunity to work with such an exciting and multidisciplinary PhD project, which has allowed me to evolve both personally and professionally. The support and encouraging guidance throughout the last three years has been enormously valuable and led to many fruitful discussions.

Furthermore, I am extremely grateful to Professor Bo Nyström for welcoming me as a student in his group and making me feel like home. Although the external stay only lasted five months, it resulted in very productive months thanks to his admirable mentoring and continuous support. In addition, I would like to express my gratitude to Dr. Kenneth D. Knudsen for performing the small angle neutron scattering experiments and always being available for discussions of the results when needed. Moreover, I would like to thank the students in Bo Nyströms group and others for making my stay in Oslo very enjoyable, especially Sara Bekhradnia, Shahla Bagherifam, Elahe Jafari, Bárbara Claro, Vahid Fooroqi and Leva Momtazi who have all become dear friends.

I would also like to thank my previous supervisor Professor Trond Ulven for sparking my interest in medicinal chemistry and my dear friends Professor Pawan K. Sharma and Professor Mehdi Bakavoli whom have been invaluable throughout the years.

Moreover, I am deeply thankful to Professor Charlotte H. Gotfredsen and Professor Jens Ø. Duus at the Department of Chemistry, Technical University of Denmark for the permission to use the departments NMR apparatus and appreciate the indispensable NMR recordings performed by Dr. Kasper Enemark-Rasmussen and Laboratory Technician Anne E. Hector.

Furthermore, I would like to express my gratitude to a good friend Dr. Michael D. Jensen and technical staff at the University of Southern Denmark for performing the HRMS analysis.

In addition, I would like to thank Postdoc Julia Hütter and Senior Researcher Katharina Lahl at the Section for Virology, National Veterinary Institute, Technical University of Denmark for performing the preliminary immunological *in vitro* experiments.

I would like to thank dear colleagues at DTU Vet and DTU Nanotech for creating a pleasant atmosphere and being tremendously helpful, especially Niels Schytte, Danny Darby, Bjørn R. Hørsving, Associate Professor Vasileios Bekiaris, Nicki Frederiksen, Martin K. Kræmer, Postdoc Rasmus Eliasen, Simon Welner, Miguel A. Pena-Espinoza, Abdellatif Elghazi, Bettina Nonnemann, Mogens H. Kristensen, Pernille Schwarzer, Finn S. Nielsen, Hue T. T. Tran and Martin A. Povlsen. In addition, I would like to thank Senior Researcher Kerstin Skovgaard and Head of Section Jørgen Schøller for support when needed and Postdoc Chris J. Hedegaard for his fun and unique humor.

Special thanks go to Dr. Maria E. Due-Hansen and Dr. Mads C. Nielsen for proofreading of this thesis and constructive feedback.

Finally, I would like to thank my amazing parents for their unconditional love and support, my wonderful friends, especially Maria E. Due-Hansen, Sophie Hytteballe, Tuyen Nguyen, Elina Ferdosi, Shang Yu, Helle Søndergaard, Pablo M. Antúnez, Marie L. L. Busk, Ane H. Landt, Jimmy C. Kromann and Julie Groizeleau for support and motivation when I needed it most. Last but not least, I would like to thank Luca for his continuous love and support, which has meant the world to me. Without all of you, I would not have come so far.

Abbreviations and symbols

For standard abbreviations, the reader is referred to *The Journal of Organic Chemistry* Guidelines for Authors 2016. The non-standard abbreviations included in this thesis are listed in the following:

AAA	amino acid analysis
Ac-Mur	*N*-acetylmuramic acid
AcOH	acetic acid
Ac_2O	acetic anhydride
Ala	alanine
ATR	attenuated technique reflectance
BAL	backbone amide linker
B cells	bone marrow-derived lymphocytes
Bromophenol blue	3′,3″,5′,5″-tetrabromophenol sulfophtalein
BSA	bovine serum albumin
Caco-2	human epithelial cells
CC_{50}	cytotoxic concentration causing death to 50% of viable cells
Chloranil	tetrachloro-1,4-benzoquinone
CMC	critical micelle concentration
CpG ODN	cytosine-guanine oligodeoxynucleotide
C-terminal	carboxyl-terminal
DABITC	4-*N*,*N*′-dimethylaminoazobenzene-4′-isothiocyanate
DBF	dibenzofulvene
DC	dendritic cell
DESC	1-methyl-2-(4′-nitrophenyl)-imidazol(1,2-*a*)pyrimidinium perchlorate
DIC	*N*,*N*′-diisopropyl carbodiimide
DIPEA	*N*,*N*-diisopropylethyl amine
DLS	dynamic light scattering
DNPH	2,4-dinitrophenylhydrazine
DVB	divinylbenzene
ELISA	enzyme-linked immunosorbent assay
FCS	fetal calf serum
fMLP	*N*-formylmethionyl-leucyl-phenylalanine, fMet-Leu-Phe
FMPB	4-(4-formyl-3-methoxyphenoxy)butanoic acid
FPR	formyl-peptide receptor
Gly	glycine
G*n*	generation number
GPCR	G protein-coupled receptor
HBTU	*N*,*N*,*N*′,*N*′-tetramethyl-*O*-(1*H*-benzotriazol-1-yl)uronium hexafluorophosphate
HEK 293T	human embryonic kidney cells
HepG2	human liver hepatocellular carcinoma cells

HIV	human immunodeficiency virus
IFN	interferon
IL	interleukin
Isatin	2,3-indolinedione
^{D}isoGln	D-isoglutamine
KWW	Kohlrausch-Williams-Watts
Leu	leucine
Lys	lysine
M	molecular ion
MALS	multi angle light scattering
MAP	multiple antigenic peptide
MCF-7	human breast cancer cells
MDP	muramyl dipeptide, *N*-acetylmuramic acid-L-alanyl-D-isoglutamine
MDMA	3,4-methylenedioxymethamphetamine
MeOH	methanol
MTS	[3-(4,5-dimethylthiazol-2-yl)-5-(3-carboxymethyoxyphenyl)-2-(4-sulfophenyl)-2*H*-tetrazolium]
NADPH	reduced nicotinamide adenine dinucleotide phosphate
NIH/3T3	mouse fibroblast cells
NLRs	NOD-like receptors
NOD	nucleotide-binding oligomerization domain
N-terminal	amino-terminal
PAMAM	poly(amidoamine)
PAMPs	pathogen-associated molecular patterns
PBS	phosphate buffered saline
PEGA	poly(ethylene glycol)-poly-*N*,*N*-dimethylacrylamide
PEG	poly(ethylene glycol)
PES	phenazine ethosulfate
PGNs	peptidoglycans
Phe	phenylalanine
poly(I:C)	polyinosinic-polycytidylic acid
PPI	poly(propylene imine)
PRRs	pattern recognition receptors
Pro	proline
PS	polystyrene
PTFE	polytetrafluoroethylene
PyBOP	(benzotriazol-1-yloxy)tripyrrolidinophosphonium hexafluorophosphate
Rink amide	4-(2′,4′-dimethoxyphenyl-Fmoc-aminomethyl)-phenoxy
RNA	ribonucleic acid
SANS	small angle neutron scattering
SAXS	small angle X-ray scattering
SDS	sodium dodecyl sulfate

SPPS	solid-phase peptide synthesis
SVEC4-10	murine endothelial cells
TBTU	*N*,*N*,*N'*,*N'*-tetramethyl-*O*-(benzotriazol-1-yl)uronium hexafluoroborate
T cells	thymus-derived lymphocytes
TG	Tentagel
TIS	triisopropylsilane
TLRs	Toll-like receptors
TNF	tumor necrosis factor
TNBSA	trinitrobenzenesulfonic acid
TYKDT	threonine-tyrosine-lysine-aspartic acid-threonine, Thr-Tyr-Lys-Asp-Thr
UPLC-MS	ultra-performance liquid chromatography mass spectrometry
7TM	seven-transmembrane
A	amplitude of the relaxation mode
$a(K)$	sum of polynomial terms
B	instrumental parameter
bkg	incoherent scattering from the background
d	length scale
D	diffusion coefficient
d_h	hydrodynamic diameter
$g^2(q,t)$	experimentally recorded intensity autocorrelation function
$g^1(q,t)$	theoretical first-order electric field autocorrelation function
$I(q)$	scattering intensity
k_B	Boltzmann constant
N(agg)	aggregation number
N_A	Avogadro's constant
n	refractive index
$P(q)$	form factor
q	scattering vector
R	radius
r_s	outer radius of the shell
r_c	radius of the core
R_t	retention time
$scale$	a factor proportional to the concentration
$S(q)$	structure factor
V_c	volume of the core
V_s	volume of the shell
β	a measure of distribution of relaxation times (polydispersity)
λ	wavelength
ρ_c	scattering length density of the core
ρ_s	scattering length density of the shell
ρ_{solv}	scattering length density of the solvent
σ	diameter of the spherical particle

ω	volume fraction
ψ	particle number density
η	viscosity of the medium
θ	scattering angle
τ_e	effective relaxation time
Γ	gamma function
ϕ	density of water

Table of contents

Abstract

Since dendrimers and dendrons are molecularly well-defined (monodisperse) hyperbranched molecules with multiple surface functional groups, they are an excellent choice for the attachment of biologically relevant molecules. Dendritic structures based on peptides (e.g., polylysine) have an additional advantage of being biocompatible and biodegradable, which are important for biomedical applications. Modification of the multiple surface functional groups in polylysine dendrons with peptide antigens or other immunomodulatory groups makes these dendrons exceptional for vaccine purposes and additional modification with lipid groups can further enhance this antigenicity by improving interactions with the cell membrane.

In Chapter 2 and publication I, a straightforward solid-phase peptide synthetic approach is described whereby a variety of C-terminal functionalities can be introduced in polylysine dendrons through acid labile backbone amide linkers. This developed method was employed for the synthesis of polylysine dendron libraries presented throughout the thesis. The backbone amide linkers were attached onto an aminomethyl functionalized polystyrene resin by employing peptide coupling reagents followed by reductive amination for the introduction of desired C-terminal functionalities. Hereafter, the dendron was grown divergently. The method proved to yield polyfunctional polylysine dendrons of high crude purity and was well-suited for automatization.

Chapter 3 and publication II describe the development of a selective colorimetric method for the detection of secondary amines, which showed to be indispensable for on-bead reaction monitoring of the reductive amination and subsequent acylation steps during the synthesis of C-terminally modified polylysine dendrons. The colorimetric method proved to be valid for a broad range of secondary amines on polystyrene resins and further modified in order to be applicable on "polystyrene deficient" resins.

The synthesis of a library of G1 and G2 polylysine dendrons modified with different alkyl chain lengths at the C-terminal is described in Chapter 4 and publication III. The self-assembling properties of selected dendrons were characterized by small angle neutron scattering (SANS) and dynamic light scattering (DLS). It was demonstrated that self-assembling and micelle formation was governed by factors such as length of the alkyl chain, concentration, electrostatic interactions and steric hindrance. The chapter also includes a brief introduction to the SANS and DLS techniques to give the reader an overview of the principles. Micellar self-assemblies (ca. 5 nm) were observed by SANS for dendrons having an alkyl chain length above C12, which additionally showed to form clusters of micelles (65-370 nm) by DLS. Polylysine dendrons with shorter alkyl chains either did not self-assemble or formed more random assemblies probably due to hydrophobic interactions of the dynamic alkyl chains. Finally, the dendrons showed to be biocompatible up to a concentration of 20 μM, which is surprising as cationic surface functionalities are known to be cytotoxic. Therefore, the polylysine dendrons are excellent systems for further modification with biologically relevant molecules for biomedical applications.

In Chapter 5, chosen polylysine dendrons were further modified at the N-terminal with immunostimulatory motifs in order to investigate the immunoactivity of the dendrons as a function of multivalency and alkyl chain length. Synthetic difficulties encountered are described and probable causes discussed. Finally, preliminary results from immunological studies on cultured whole mouse spleen cells and dendritic cell subsets isolated from mouse spleen are presented and discussed. The preliminary studies demonstrate interesting findings, such as moderate levels of immunoactivity of G1 and G2 dendrons modified with two or four immunostimulatory motifs, respectively. The activity seems to be influenced by the length of the alkyl chain, depending on the localization of the putative receptor (i.e., cell membrane or cytosol) and steric effects. In addition, some dendrons exhibited cross-antagonistic activities against known Toll-like receptor agonists (i.e., synthetic analogues of viral double-stranded RNA [poly(I:C)] and bacterial unmethylated cytosine-guanine DNA motifs [CpG oligodeoxynucleotide]), which may be explained by electrostatic interactions of the anionic agonists with the cationic polylysine dendrons resulting in complexation rendering them less available for receptor interaction.

Resumé

Eftersom dendrimerer og dendroner er molekylært veldefinerede (monodisperse) hyperforgrenede molekyler med adskillige overfladefunktionelle grupper, er de et glimrende valg til påsætning af biologisk relevante molekyler. Dendritiske strukturer der er baseret på peptider (f.eks. polylysin) har den ekstra fordel, at de er biokompatible og biologisk nedbrydelige, hvilket er vigtige faktorer for biomedicinske anvendelser. Modifikation af de adskillige overfladefunktionelle grupper i polylysin dendroner med peptidantigener eller andre immunmodulerende grupper gør disse dendroner exceptionelle til brug i vaccine sammenhænge og yderligere modifikation med lipid grupper kan forbedre deres antigenicitet ved, at øge interaktioner med cellemembranen.

I kapitel 2 og publikation I beskrives en enkel fast-fase peptid syntetisk fremgangsmåde, hvorved en række C-terminale funktionaliteter kan introduceres i polylysin dendroner gennem syrelabile backbone amid linkere. Den udviklede metode blev anvendt til syntese af polylysin dendron biblioteker præsenteret gennem hele afhandlingen. Backbone amid linkere blev fastgjort på en aminomethyl funktionaliseret polystyrenresin vha. peptidkoblingsreagenser efterfulgt af reduktiv aminering til introduktion af ønskede C-terminale funktionaliteter. Herefter blev dendronen opbygget divergent. Metoden viste sig at give polyfunktionelle polylysin dendroner med høj råprodukt renhed og var velegnet til automatisering.

Kapitel 3 og publikation II beskriver udviklingen af en selektiv kolorimetrisk metode til påvisning af sekundære aminer, som viste sig at være uundværlig for ”on-bead” reaktion monitorering af den reduktive aminering og efterfølgende acyleringstrin under syntesen af C-terminal modificerede polylysin dendroner. Den kolorimetriske metode viste sig at virke for et bredt udvalg af sekundære aminer på polystyrenresiner og yderligere modificeret for, at kunne anvendes på resiner med underskud eller mangel på polystyren.

Syntesen af et bibliotek af G1 og G2 polylysin dendroner modificeret med forskellige alkylkædelængder i C-terminalen er beskrevet i kapitel 4 og publikation III. Udvalgte dendroners egenskab til sammenpakning blev karakteriseret ved small angle neutronspredning (SANS) og dynamisk lysspredning (DLS). Det blev påvist at sammenpakning og micelledannelse blev styret af faktorer såsom længden af alkylkæden, koncentration, elektrostatiske interaktioner og sterisk hindring. Kapitlet indeholder også en kort introduktion til SANS og DLS teknikkerne for at give læseren et overblik over principperne. Micelledannelse (ca. 5 nm) blev observeret med SANS for dendroner med en alkylkædelængde over C12, som desuden viste sig at danne klumper af miceller (65-370 nm) med DLS. Polylysin dendroner med kortere alkylkæder kunne enten ikke danne miceller eller kun danne tilfældige strukturer sandsynligvis pga. hydrofobe interaktioner af de dynamiske alkylkæder. Til sidst viste dendronerne at være biokompatible op til en koncentration af 20 µM, hvilket er overraskende da kationiske overflade funktionaliteter er kendt for at være cytotoksiske. Derfor er polylysin dendronerne fremragende systemer til yderligere modifikation med biologisk relevante molekyler for biomedicinske anvendelser.

I kapitel 5 blev udvalgte polylysin dendroner yderligere modificeret ved N-terminalen med immunstimulerende motiver for, at undersøge immunaktiviteten af dendronerne som funktion af multivalens og alkylkædelængde. Syntetiske vanskeligheder er beskrevet og sandsynlige årsager diskuteret. Til sidst præsenteres og diskuteres foreløbige resultater fra immunologiske undersøgelser på dyrkede milt celler fra mus og dendrit celler isoleret fra milten af mus. De foreløbige undersøgelser viser interessante resultater, såsom moderat immunaktivitet af G1 og G2 dendroner modificeret med hhv. to eller fire immunstimulerende motiver. Aktiviteten synes at være påvirket af længden af alkylkæden, afhængig af lokaliseringen af den formodede receptor (dvs. cellemembran eller cytosol) og steriske effekter. Derudover udviste nogle dendroner kryds-antagonistiske aktiviteter mod kendte Toll-like receptor agonister (dvs. syntetiske analoger af viral dobbeltstrenget RNA [poly(I:C)] og bakteriel ikke-methyleret cytosin-guanin DNA motiver [CpG oligodeoxynukleotid]), hvilket muligvis kan forklares vha. elektrostatiske interaktioner af de anioniske agonister med de kationiske polylysin dendroner, som resulterer i kompleksdannelse og gør dem mindre tilgængelige for receptor interaktion.

1 Introduction

The principal aim of this project was to design and synthesize a library of polylysine dendrons with variable alkyl chains and to modify relevant dendrons with immunomodulatory motifs for possible use as vaccine adjuvants. From this, the following main objectives were established:

- Development and optimization of a quick and feasible solid-phase peptide synthetic strategy whereby libraries of polyfunctional polylysine dendrons could be synthesized.

- Synthesis of a library of polylysine dendrons with different alkyl chains at the C-terminal and characterization of their physicochemical properties, in order to obtain a better understanding of the relationship between lipidation degree and self-assembly.

- The synthesis of a library of dendrons modified with a multivalent display of immunostimulatory motifs (i.e., muramyl dipeptide, ^{D}isoGln-Ala or *N*-formylmethionine) for the investigation of the effect of multivalency on the ability to induce an activation of immune cells.

In the following sections, the background and motivation for the project is given together with relevant examples of dendritic constructs containing immunomodulatory motifs.

1.1 Immunological background

The immune system consists of a variety of white blood cells (leucocytes) and molecules that protect the host from pathogens. Immunity occurs through the interplay of two important systems, namely the innate and adaptive immune response. The non-specific and rapid (minutes) first line of defense is conducted by the innate immune response. The specific, potent and slower (hours or days) second line of defense is coordinated by the adaptive immune response, which develops during an individual's lifetime and is initiated by the cells of the innate immune system.[1]

The initial defense against infection is maintained by physical and chemical barriers, e.g., skin, respiratory and gastrointestinal epithelia, oral mucosa and secreted antimicrobial agents. The cells of the innate immune system (e.g., the phagocytic macrophages, dendritic cells and neutrophils) come into play when these barriers are breached. Macrophages, dendritic cells and neutrophils engulf and kill invading pathogens and also function as sensor cells initiating inflammatory responses by producing inflammatory mediators such as cytokines and chemokines. These sensor cells recognize pathogen-associated molecular patterns (PAMPs) by pattern recognition receptors (PRRs). The simple pathogenic molecular patterns recognized include oligosaccharides, peptidoglycans, lipopolysaccharides and nucleic acid motifs that have been conserved during evolution. Important PRRs include the Toll-like receptors (TLRs), NOD-like receptors (NLRs) and the fMet-Leu-Phe (fMLP) receptor. Ligand recognition by PRRs triggers phagocytosis and

degradation of pathogens and release of important inflammatory mediators (e.g., interferons, interleukins and tumor necrosis factors) aiding the fight against pathogens. Subsequently, the adaptive immune response is initiated by antigen presentation mainly on dendritic cells, which are recognized by specific antigen receptors on B and T lymphocytes (B and T cells). This ultimately leads to long-term protective immunological memory. Hence, a future encounter of a specific pathogen will lead to a faster and stronger immune response preventing re-infection by utilizing T cells or antibodies (produced by B cells).[1,2]

Although the immune system is successfully able to combat a range of pathogens, many are still able to evade its guard and cause deadly diseases. In the late 18th century, Edward Jenner developed a procedure termed vaccination, whereby a deliberate stimulation of an immune response with an inactive form of a pathogen results in immunization. Roughly a century later, the method was further refined by Louis Pasteur and other scientists were attracted to the field in order to elucidate the mechanisms behind vaccination. Since then, vaccines have markedly decreased deaths from infectious diseases. Nevertheless, infectious diseases continue to be the main cause of death worldwide and vaccines against, e.g., malaria, tuberculosis and HIV still need to be developed.[1]

For the development of vaccines an important factor to be considered is the ability to induce an immune response leading to long-term protective immunological memory without causing deadly disease. Therefore, vaccines are usually based on live attenuated pathogens or purified components from killed organisms. Killed inactivated pathogens usually induce a weaker immune response and several doses are needed for full protection. Vaccines based on live attenuated pathogens are more potent, but might on rare occasions regain virulence and pose a risk to the individual. Additionally, vaccines based on live attenuated pathogens pose a risk to immunodeficient individuals. Consequently, a safer approach is to employ subunit vaccines based on smaller components of the pathogen, e.g., peptide or polysaccharide fragments. However, in order to be effective, these vaccines have to be employed together with adjuvants (molecules that potentiate and/or modulate the immune response) or large carrier molecules.[1,3,4]

In this project polylysine dendrons were employed for the attachment of surface immunostimulatory motifs. The aim was to see if the dendritic structure would lead to an increased activation of immune cells due to a multivalent presentation of relevant PAMP motifs and accordingly be employed as possible adjuvant. The chosen PAMPs were muramyl dipeptide, desmuramyl dipeptide (i.e., L-alanyl-D-isoglutamine without the *N*-acetylmuramic acid moiety) and *N*-formylmethionine.

Muramyl dipeptide

Peptidoglycans (PGNs) are found in bacterial cell walls and consist of repeating units of *N*-acetyl glucosamine linked to *N*-acetylmuramic acid. Furthermore, the *N*-acetylmuramic acid units are linked to D/L-amino acid oligopeptides. Muramyl dipeptide (MDP, *N*-acetylmuramic acid-L-alanyl-D-isoglutamine) is the minimal pro-inflammatory motif of PGNs and a powerful adjuvant (Fig. 1.1).[5,6] Thus, it can be employed together with vaccines and thereby increase their potency through synergistic effects. MDP is an agonist to the nucleotide-binding oligomerization domain 2 (NOD2)

receptor situated in the cytosol and Toll-like receptor 2 (TLR2) situated on the cell membrane. Activation of the NOD2 receptor and TLR2 results in production and release of pro-inflammatory and antiviral cytokines such as interleukin 6 and 12 (IL-6 and IL-12), tumor necrosis factor-α (TNF-α), interferon-α and -β (IFN-α and IFN-β).[1,7]

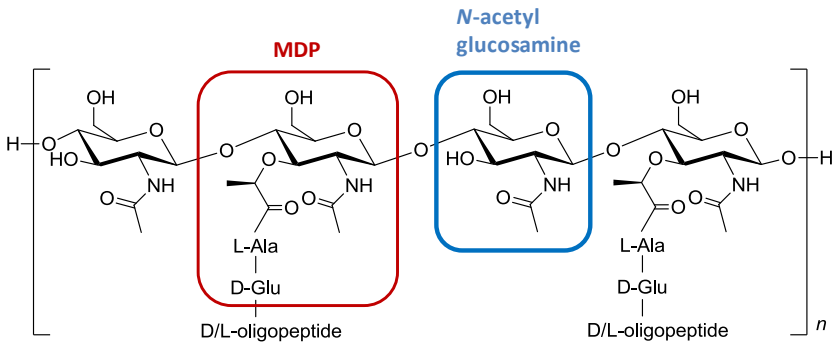

Figure 1.1 The molecular structure of peptidoglycans consisting of alternating MDP (red) and *N*-acetyl glucosamine (blue) units cross-linked through oligopeptides on MDP.

N-formylmethionine peptides

N-formylmethionine peptides are either secreted by bacterial invaders or released from the mitochondria of dead host cells during cell lysis. The synthetic tripeptide, *N*-formylmethionyl-leucyl-phenylalanine (fMet-Leu-Phe or fMLP) (Fig. 1.2), is a high affinity agonist for the formyl-peptide receptor 1 (FPR1), which is a seven-transmembrane (7TM) G protein-coupled receptor (GPCR).

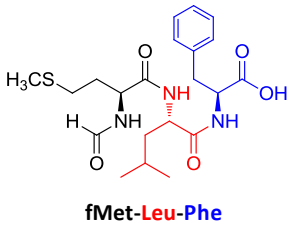

Figure 1.2 Molecular structure of *N*-formylmethionyl-leucyl-phenylalanine (fMet-Leu-Phe).

FPR1 is not specific for fMLP and also binds to other ligands including different *N*-formylated peptides and non-formylated peptides containing ≥ five amino acids. Even though the *N*-formylmethionine group is not prerequisite for binding, it still has a potential effect on ligand activity compared to non-formylated derivatives, because of hydrogen bonding interaction of the formyl group with the binding site. Additionally, the sulfur atom in the methionine side chain is relatively electron-rich and may interact with positively charged areas of the receptor. FPR1 is present on phagocytic cells and its activation leads to increased antimicrobial activity and guides leucocytes to the site of inflammation.[1,8,9]

1.2 Dendrimers and dendrons

Dendrimers and dendrons are molecularly well-defined (monodisperse) hyperbranched molecules with nano-scalar dimensions. The first successful synthesis of dendritic structures was reported in 1978 by Buhleier *et al.*[10], which initially termed these poly(propylene imine) [PPI] structures as *cascade* molecules. Several years later the field was revisited by Tomalia *et al.*[11] who described the synthesis of bigger poly(amidoamine) [PAMAM] structures and named branched macromolecular structures as "dendrimers" (derived from the Greek words "dendri" [branched] and "mer" [part of]).[12,13] Around the same time, Newkome *et al.*[14] independently described the synthesis of similar poly(etheramide) [Arborol] structures (Fig. 1.3).

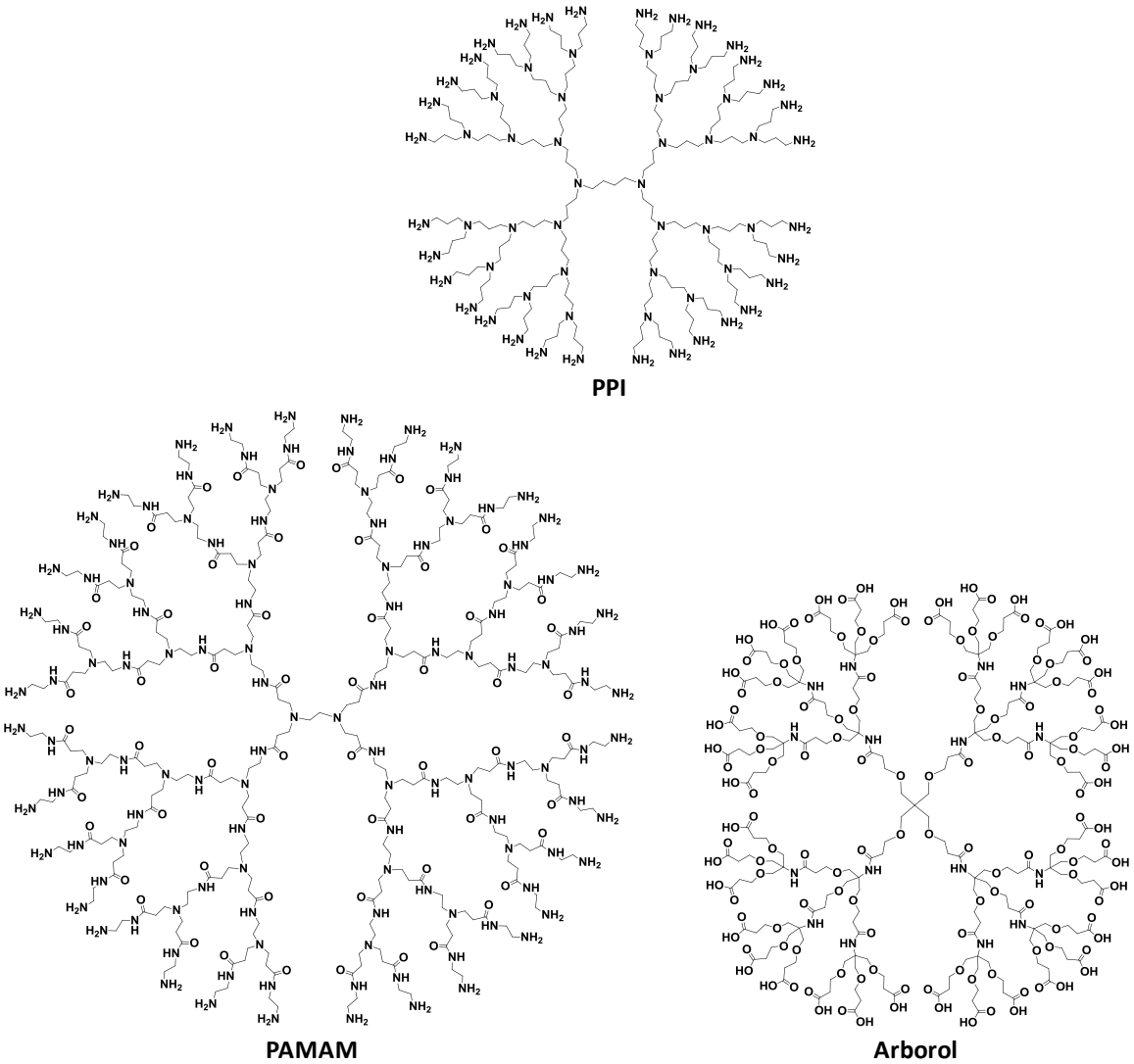

Figure 1.3 A molecular representation of the first dendritic families reported showing a G4-PPI, a G4-PAMAM and a G2-Arborol dendrimer.

Dendrimers can be synthesized in a controllable manner by a stepwise approach from the core to the periphery (divergent approach, Section 1.2.1) or by coupling two or more dendrons together

(convergent approach, Section 1.2.2). Therefore, dendrimers have a globular structure of concentric shells with a core that is lacking in dendrons. Dendrimers and dendrons are labeled by their generation numbers (G*n*) according to the number (*n*) of branching points of repeating monomer units from the core, or for dendrons from the origin, to the periphery. The number of functional end groups grows with each generation number and depends on the number of end groups available on the repeating branching monomer (usually two or three). The end groups on the dendritic target can then be further modified or covalently linked to relevant motifs (Fig. 1.4).[12,15] However, dendrimers and dendrons have a critical branching state where further growth cannot be successfully obtained due to steric crowding and can therefore not be grown continuously without structural defects.[15]

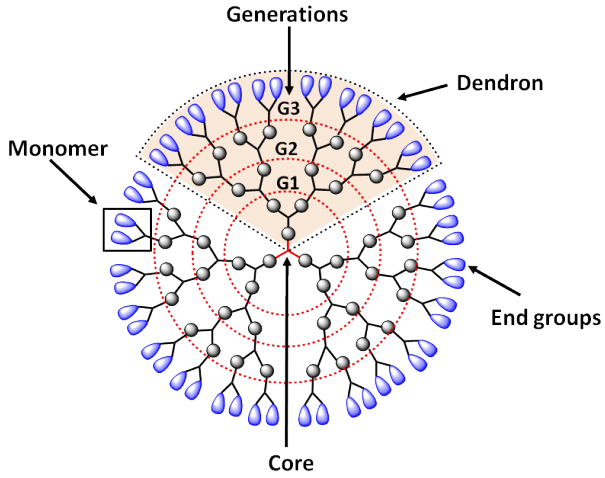

Figure 1.4 Schematic illustration of the structural components of dendrimers and dendrons.

1.2.1 Divergent Synthesis

The first dendritic structures reported by Buhleier *et al.*[10], Tomalia *et al.*[11] and Newkome *et al.*[14] were prepared by divergent synthesis. In this approach, the dendrimer or dendron is prepared by building from a multifunctional core or origin towards the periphery in a stepwise manner (Fig. 1.5). To prepare the first generation (G1, one branching point with $n = 1$), the active functionalities on the core molecule (blue ellipse) are reacted with an excess amount of the monomer with protected end groups (grey sphere). Subsequently, by-products and excess reagents are removed by purification steps and the end groups of the G1 product are deprotected and activated towards reaction with another cycle of monomers. These steps are repeated until the desired generation is obtained and the end groups can be further linked to preferred molecular motifs (Fig. 1.5).[12,13]

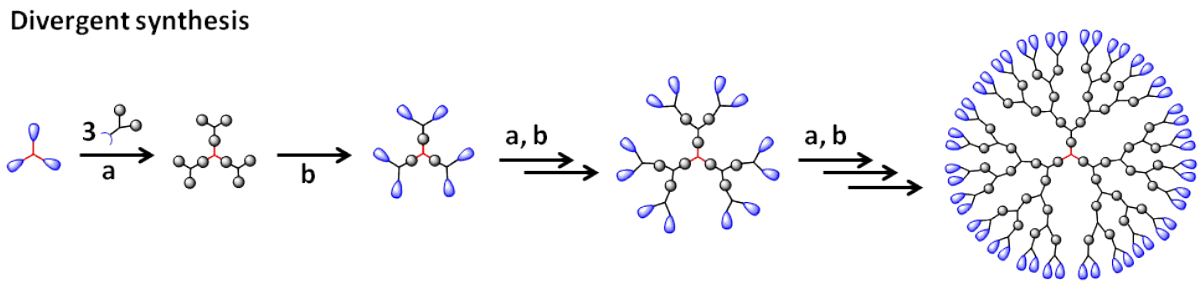

Figure 1.5 Divergent synthesis of dendrimers. (a) Dendritic growth by reaction of the core molecule with an excess amount of monomers. (b) Deprotection and activation of the dendritic end groups for further dendritic growth.

As the generation and the number of end groups grow a considerable amount of monomer and reagents are needed for reaction completion. The increased number of end groups gives rise to steric crowding in higher generations. As a consequence, the likelihood of so-called deletions with incomplete derivatization rises. These deletion by-products are difficult to separate efficiently from the desired product by standard purification methods due to molecular similarities. Regardless, the divergent approach is widely employed for a large variety of dendrimers and is the method of choice for most commercially available dendrimers.[12,13,16]

1.2.2 Convergent Synthesis

The convergent approach was first introduced in 1990 by Hawker and Fréchet[17] for the synthesis of poly-benzylether dendrimers. In this approach, in contrast to the divergent method, the dendritic structure is built from the periphery towards the core by coupling dendrons to a desired core molecule. Typically, the dendrons are synthesized first using the same activation/deactivation steps as for the divergent method (Fig. 1.6). During these synthetic steps the dendron origin is protected (green sphere). When the desired dendron generation is reached, the dendron origin is deprotected and activated, after which it is coupled to a preferred core molecule. Subsequently, the end groups of the resulting dendrimer can be activated and linked to desired molecular motifs (Fig. 1.6).[12,13,16]

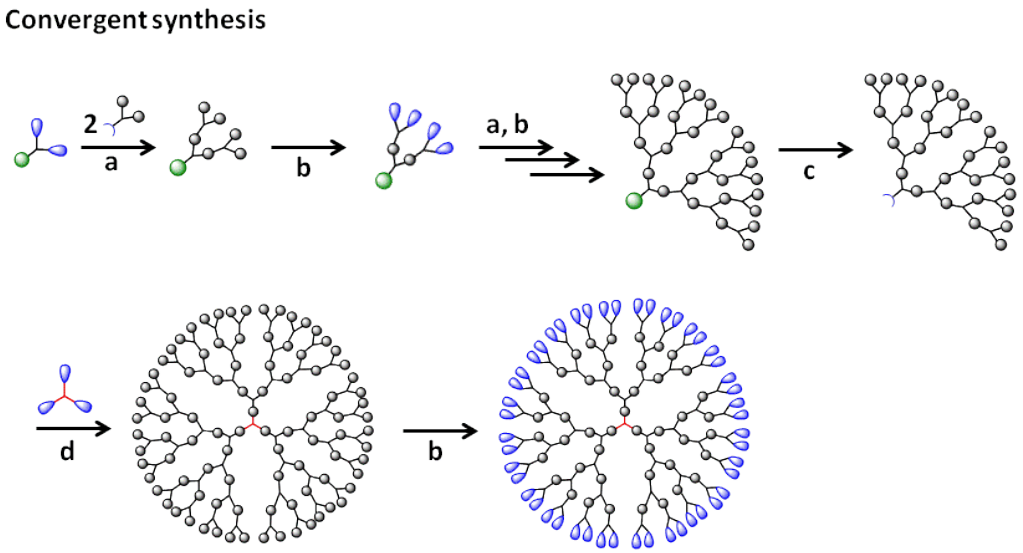

Figure 1.6 Convergent synthesis of dendrimers. (a) Dendritic growth by reaction of two or more monomers. (b) Deprotection and activation of the dendritic end groups for further dendritic growth. (c) Deprotection and activation of the dendron origin. (d) Coupling of the dendron to a desired core molecule.

The last coupling step of higher generation dendrons to the desired core molecule is difficult due to steric hindrance making preparation of higher generation dendrons (above G6) less straightforward.[17] Consequently, not all core molecules can be fully derivatized and a purification step is needed. Nevertheless, a great advantage of the convergent approach is the relatively facile purification step due to dendrons being less molecularly similar to the more complex target dendrimer. Additionally, the convergent approach is an excellent choice for the synthesis of bifunctional dendrimers. This is achieved by coupling dendrons with different end groups together.[12,13,16]

1.2.3 Dendrimers based on lysine

One important group of dendritic structures are based on peptides (e.g., polylysine). The first polylysine dendrons (based on L-lysine) were developed and patented by Denkewalter and co-workers in the early 1980s.[18,19] Lysine has two amine functionalities (at the α and ε position) and is therefore an excellent choice as branching unit in dendritic structures (Fig. 1.7).

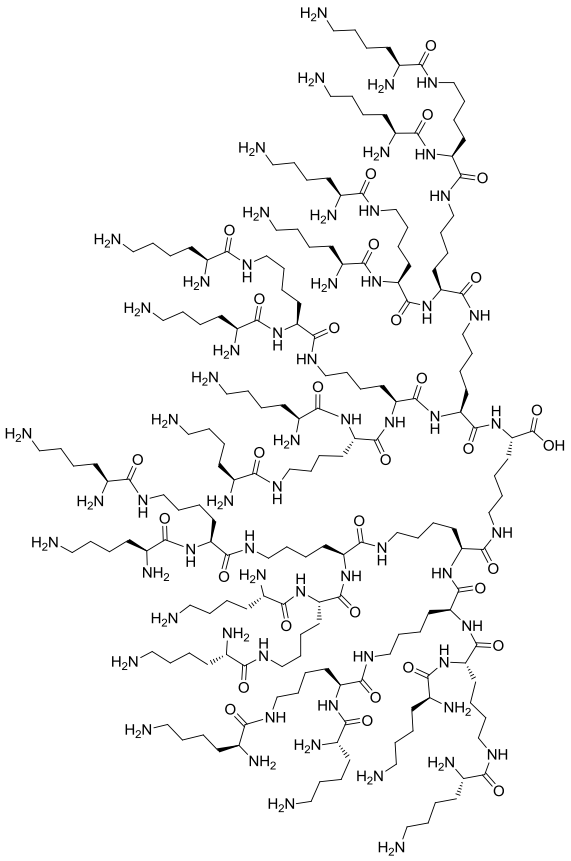

G4 Poly-L-lysine dendron

Figure 1.7 Molecular structure of a Denkewalter-type G4 poly-L-lysine dendron containing 32 surface amine groups that can be modified.

The fundamental advantages of dendritic structures based on amino acids including Denkewalter-type dendrons are their biocompatibility and biodegradability, since they can be cleaved in the presence of enzymes or acids. In conjunction with their dendritic multivalency, they are highly relevant for biomedical applications.[20,21] Multivalent molecules are abundant in nature, e.g., protein aggregates on virions and bacteria, and interact with relevant receptors in a polyvalent manner. In polyvalent interactions, two or more ligands associate with multiple binding sites on the receptor, which can result in a more effective and specific response compared to monovalent interactions. The enhanced binding ability is due to the multiple ligands being in close proximity favoring subsequent binding events.[22-24] Therefore, multivalency in dendritic structures (termed the *dendritic effect*[12]) is a highly attractive property. The biocompatibility and multivalency are probably the main reasons for the large number of polylysine dendritic structures being reported in the literature.[20,23,25-27]

1.3 Synthetic immunomodulators based on dendrimers and dendrons

Synthetic ligands for the PRRs have been explored as adjuvants and have been shown to be relatively safe and selective.[4] To increase the immunostimulatory activity of such small molecular weight ligands they should be polymerized or conjugated to bigger carriers for a multimeric presentation. In this respect, dendrimers and dendrons are ideal candidates as carriers. This is attributed to their well-defined (monodisperse) hyperbranched nature with multiple surface functional groups that can be conjugated with a molecule of choice (e.g., adjuvant) for a multivalent display.[28] Therefore, dendrimers and dendrons have the ability to enhance the immunostimulatory activity of PAMPs through the *dendritic effect* as demonstrated for MDP by Sorensen *et al.*[29] (Fig. 1.8).[12]

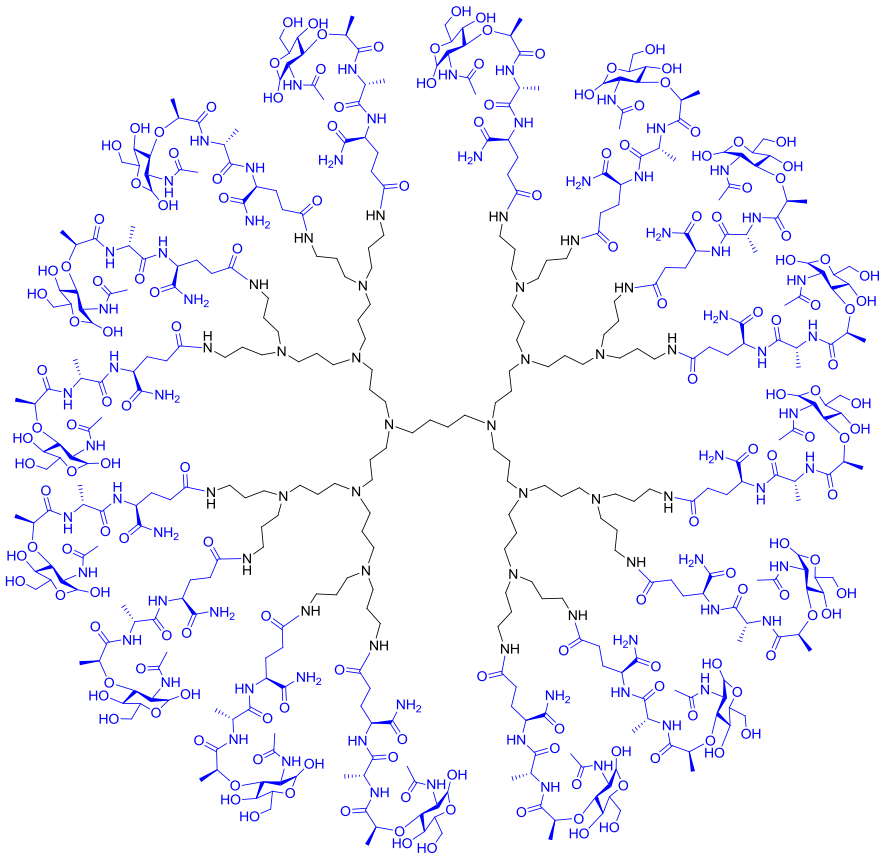

Figure 1.8 Multimeric presentation of MDP (blue) on a G3-PPI dendrimer demonstrating enhanced immunostimulatory effects.

One of the most important peptide-based dendritic systems is the multiple antigenic peptide (MAP) developed by Tam in the late 1980s.[30] The MAP construct is based on Denkewalter-type dendrons where the amine groups on the surface are modified with peptide antigens for use in vaccines. In this construct the need for large carrier molecules is avoided. Thus, the MAP system can be directly employed as immunizing antigen due to the multivalent presentation of peptide antigens with the lysine core only representing a minor portion of the total dendritic structure.[30]

The initial MAPs were intended for vaccine applications, but have found additional use in other applications, e.g., diagnostics, mimetics, drug and gene delivery.[23] Furthermore, MAPs have been designed with a dendrimer structure having a core, which is lacking in the original dendron structure.[12] When employing lysine as the branching unit in MAPs, asymmetrical dendrons are produced. If a symmetrical construct is desired, the repeating branching unit can be exchanged with Lys(β-Ala) (Fig. 1.9).[31]

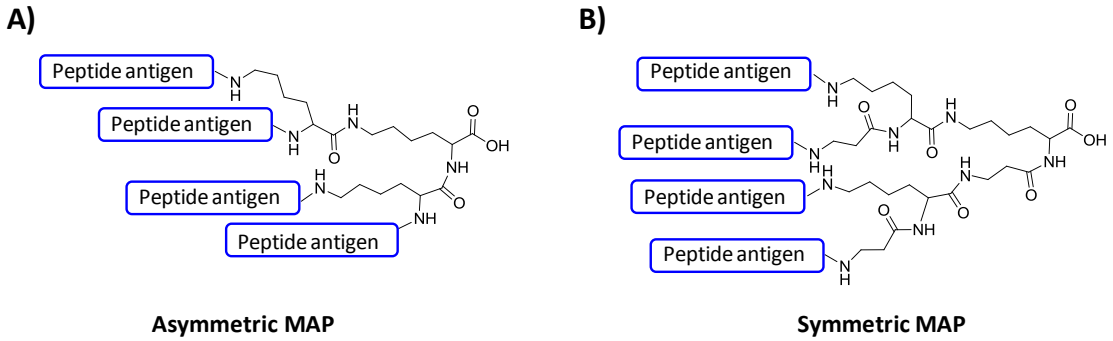

Figure 1.9 (A) Asymmetrical MAP with lysine as the branching unit. (B) Symmetrical MAP with Lys(β-Ala) as the branching unit. Peptide antigens on the N-terminal surface are indicated in blue.

Moreover, lipidated versions of the MAP constructs have been developed by anchoring lipid groups (e.g., palmitic acid, tripalmitoyl-*S*-glyceryl cysteine[31-33] and lipidic α-amino acids[34]) at the C-terminal/origin of the dendron resulting in enhanced antigenicity due to improved cell membrane interactions (Fig. 1.10). Additionally, this modification allows delivery through endosomal pathways, uptake by epithelial tissues for oral and nasal delivery and incorporation into liposomes or micelles thereby amplifying the peptide antigen presentation.[25]

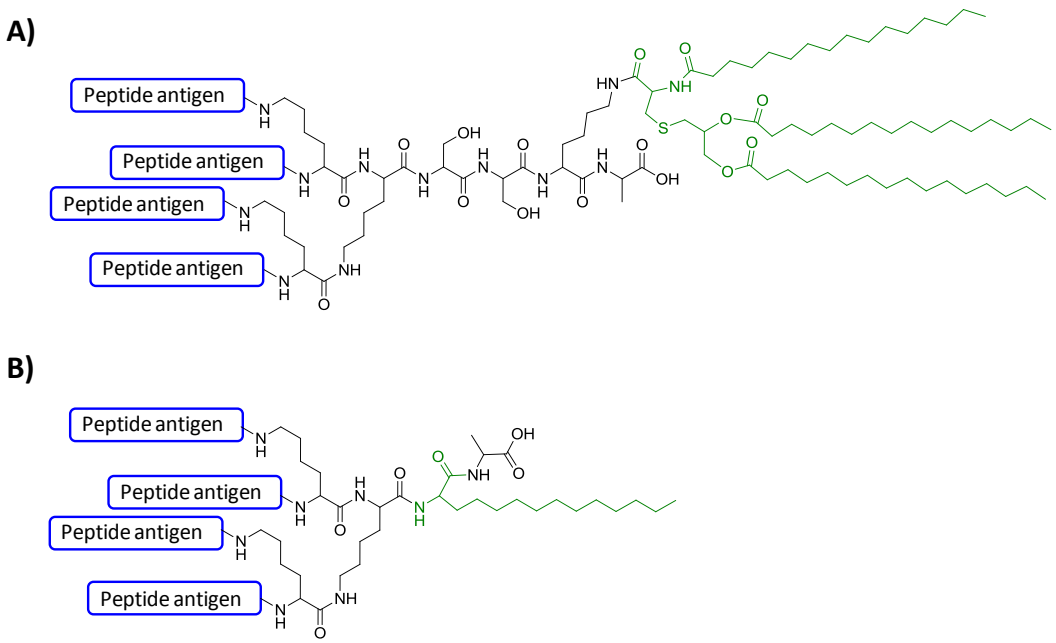

Figure 1.10 MAP modified at the C-terminal with tripalmitoyl-*S*-glyceryl cysteine (A) and a lipidic α-amino acid (B) indicated in green. Peptide antigens on the N-terminal surface are indicated in blue.

Florence and co-workers synthesized a series of MAP constructs with a lipidated surface for possible drug delivery purposes. The physicochemical properties were analyzed by varying the generation number (G1-G6) and alkyl chain length (C8, C12 and C16). Only the G4 dendron having 16 lipid groups was reported to self-assemble into cylindrical tubules in aqueous environments.[35] Furthermore, a cationic G2 MAP dendron with a lipidated surface and C-terminal was synthesized by the same group. The cationic dendron was shown to self-assemble into vesicular/bilayered structures in aqueous solutions with a diameter of approximately 311 nm. Moreover, the possibility to use this type of system as drug carrier was supported by the dendrons ability to encapsulate benzylpenicillin (a water soluble and orally labile antibiotic).[36]

From these examples it is apparent that MAP constructs, with or without lipid functionalities, can be an excellent construct for vaccine purposes[37-39] and other relevant biomedical applications such as gene delivery[40], drug delivery[36,41], anticancer agents[42], antiviral agents[43] and antimicrobials[44]. Consequently, this pushed us towards further exploration of polylysine dendrons.

2 Solid-phase synthesis of modified polylysine dendrons

This chapter describes the work performed for the development of a straightforward approach for the solid-phase synthesis of C-terminally modified polylysine dendrons by employing backbone amide linkers. The method showed to be suitable for a variety of C-terminal functionalities yielding dendrons of high crude purity and was conveniently implemented for solid-phase automated synthesis. Additionally, the scope of the method for the preparation of diverse libraries for biomedical application (e.g., vaccine purposes) was proven by N^{α}-terminal pentapeptide (half T cell epitope) modification of the dendritic structure. The work is described in publication I.

2.1 Solid-phase peptide synthesis

Dendritic structures based on peptides (e.g., polylysine dendrons) can both be prepared by traditional solution-phase methods or solid-phase peptide synthesis (SPPS) and the concepts are similar to common peptide synthesis employing coupling reagents and protected amino acids.

The SPPS approach was chosen over conventional solution-phase for the preparation of polylysine dendrons due to the ability to drive reactions to completion by employing excess reagents. In this approach, excess reagents and soluble by-products can easily be removed after reaction completion by consecutive washing and filtering of the resin avoiding time-consuming purifications and characterizations of intermediates between steps. Therefore, SPPS allows for a fast and reliable way to prepare diverse libraries of complex compounds, e.g., polylysine dendrons. However, it is important to stress the limitations of the SPPS approach. Since isolation and characterization of intermediates cannot be performed, it becomes more difficult to remove deletion impurities (due to incomplete couplings or deprotections) and by-products (due to side reactions on the resin) closely resembling the desired product. Moreover, simple solution-phase reaction monitoring is not possible. Thus, the reactions are typically monitored on-bead by, e.g., colorimetric or infrared methods.[20,26,45]

The solid-phase method[46] was successfully developed by Merrifield in 1963 for the synthesis of linear peptides.[47] The polylysine dendrons were grown in a stepwise divergent manner (Section 1.2.1) from the C-terminal to the N-terminal (N←C) on an insoluble polymeric support, i.e., a functionalized polystyrene (PS) resin cross-linked with divinylbenzene (DVB). The basic repetitive operations of stepwise SPPS and final cleavage from the resin are summarized in Scheme 2.1. In the initial step, the first amino acid is anchored onto the solid support containing a suitable linker (handle) through its carboxyl group while the side chain and α-amino group are protected. The protecting groups can either be identical (removed simultaneously) or orthogonal (removed under different conditions). Two different N^{α}-protecting group strategies are commonly employed in SPPS, i.e., *tert*-butyloxycarbonyl (Boc)[48] and 9-Fluorenylmethyloxycarbonyl (Fmoc)[49,50] strategies. For the preparation of polylysine dendrons the Fmoc strategy was employed.

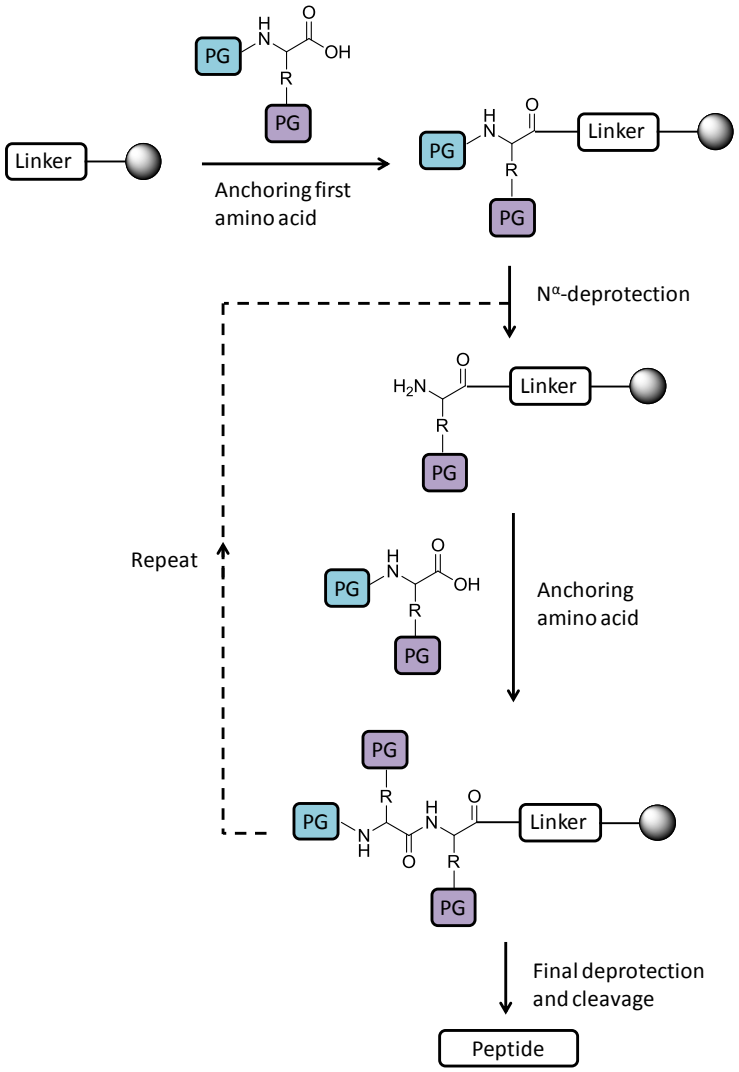

Scheme 2.1 Basic repetitive operations during solid-phase peptide synthesis. Protecting groups are abbreviated PG with blue and purple boxes referring to orthogonal protecting groups, e.g., Fmoc and Boc/*tert*-butyl.

After the first amino acid is attached to the polymeric support, the α-amino protecting group is removed and excess amounts of the second amino acid together with a suitable coupling reagent are added.[45] The polymeric support is washed thoroughly between each deprotection and coupling cycle to remove excess reagents and the reaction completion monitored colorimetrically by, e.g., the ninhydrin test.[51,52] For the synthesis of polylysine dendrons the branching lysine units have identical N^{α}- and N^{ε}-protecting groups (i.e., Fmoc), which are removed simultaneously by piperidine and coupled with the next N^{α} and N^{ε} Fmoc-protected lysine until the desired dendron generation is obtained. Hereafter, the next lysine is orthogonally protected (i.e., N^{α}-Fmoc and N^{ε}-Boc) and further modified in a linear manner until cleavage and deprotection of the final dendron from the resin (Scheme 2.1).

2.2 C-terminal modification by backbone amide linkers

In order to pursue our goal for the preparation of a large library of multifunctional dendritic structures for biomedical applications, we wanted to investigate backbone amide linkers as a way to introduce an extra functionality in Denkewalter-type polylysine dendrons. This led to the development of a simple solid-phase peptide synthetic (SPPS) method with a broad scope.

Linkers or handles are bifunctional molecules with one side functioning as anchor point for the growing molecule to the resin and another side functioning as protecting group. The linker determines the C-terminal functionality of the final product and generally a carboxylic acid or amide is released after cleavage.[53]

If C-terminal modifications are desired, they can be introduced by employing linkers based on tris- and bisalkoxybenzaldehydes, e.g., backbone amide linker (BAL, with a substituted pentanoic or butanoic acid spacer *ortho*[54] [**2.1**] or *para* [**2.2**] to the aldehyde functionality) and 4-(4-formyl-3-methoxyphenoxy)butanoic acid (FMPB [**2.3**], with a *para* substituted butanoic acid spacer) linker, respectively (Fig. 2.1).[55-59]

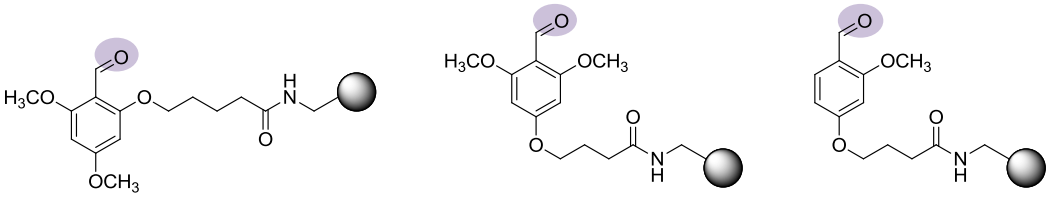

Figure 2.1 Tris- and bisalkoxybenzaldehyde linkers attached to a suitable resin (e.g., aminomethyl PS) by amide linkage. Attachment point to the linker is indicated by a purple circle on the *ortho* BAL (**2.1**), *para* BAL (**2.2**) and FMPB linker (**2.3**).

Aminomethyl PS resin (1% or 10% [rigid macroporous] DVB cross-linked, loading: 2.0 mmol/g) was chosen as a suitable resin with an amino functionality for linker attachment. Only the *para*-BAL and FMPB linker were commercially available and attached onto the resin amino group through the carboxylic acid functionality by employing a coupling reagent (i.e., PyBOP [(benzotriazol-1-yloxy)tripyrrolidinophosphonium hexafluorophosphate] together with DIPEA [*N*,*N*-diisopropylethyl amine]). To avoid steric crowding on the resin during the subsequent dendritic growth[13] (Section 1.2.1), loading of the linker was decreased and residual aminomethyl groups quenched by capping with acetic anhydride in the presence of DIPEA. Therefore, halved resin loadings (i.e., 1.0 mmol/g) were employed to calculate the amount of reagents needed for the following synthetic steps.

The backbone amide linker method allows for subsequent attachment of amines with a large variety of functional groups by reductive amination resulting in a secondary amine (Scheme 2.2).

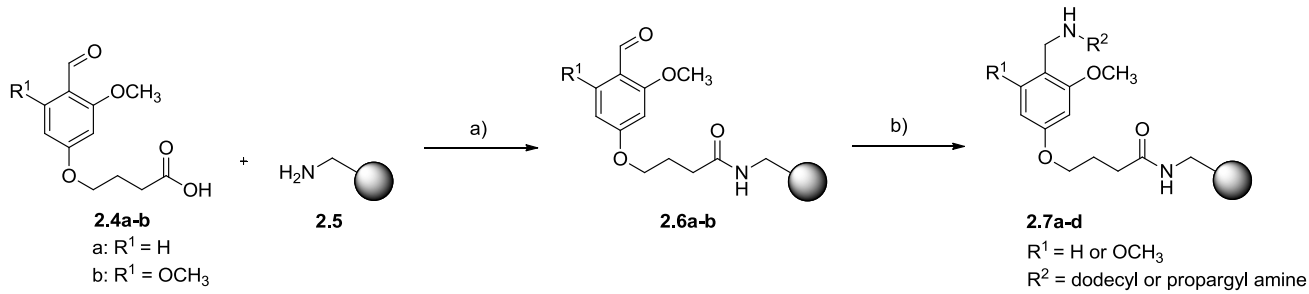

Scheme 2.2 The attachment of bis- and trisalkoxybenzaldehyde linkers to aminomethyl PS resin and subsequent reductive amination step. (a) FMPB or *para*-BAL linker, PyBOP, DIPEA, NMP, rt, 1-2 h; acetic anhydride, DIPEA, dichloromethane, rt, 2 h. (b) Propargyl or dodecyl amine, $NaBH_3CN$, 5 vol. % acetic acid, NMP, rt, 2 h followed by 1 h reaction repeat in the case of dodecyl amine.

The C-terminal functionality of the polylysine dendrons was introduced by reductive amination employing sodium cyanoborohydride ($NaBH_3CN$) in a polar aprotic solvent (*N*-methyl-2-pyrrolidone, NMP) under mild acidic catalysis, 5 vol. % acetic acid (Scheme 2.2), since strong acids tend to protonate the amino group whereby the nucleophilicity is lost.[60]

The presence of aldehyde groups on the BAL or FMPB derivatized resin was monitored colorimetrically and by infrared (IR) spectroscopy directly on the resin beads. A carbonyl aldehyde band at approximately 1715 cm^{-1} together with a carbonyl amide band at approximately 1650 cm^{-1} were seen by IR spectroscopy (Fig. 2.2). 2,4-dinitrophenylhydrazine (DNPH) was employed for colorimetric monitoring as described by Shannon and Barany[61]. The reaction between DNPH and resin-bound aldehydes under dilute acidic conditions yields a red phenylhydrazone (**2.9**) (Scheme 2.3). Hence, a red to dark orange coloration of the resin beads is indicative for the presence of aldehyde groups (positive test).[61]

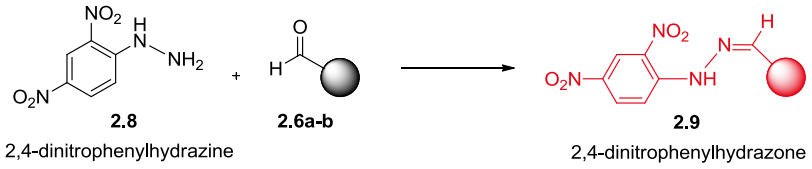

Scheme 2.3 On-bead aldehyde monitoring by DNPH yielding red to dark orange beads as positive test.

The completion of the subsequent reductive amination was also monitored by IR and DNPH test with reaction times typically being 2 h or repeated 1 h in the case of dodecyl amine. On-bead IR analysis showed a marked reduction of the aldehyde band (Fig. 2.2) and the absence of aldehyde groups was indicated by a negative DNPH test (yellow beads). Furthermore, reductive amination with dodecyl groups also showed an increase in C-H stretching at 2900 cm^{-1} (Fig. 2.2).

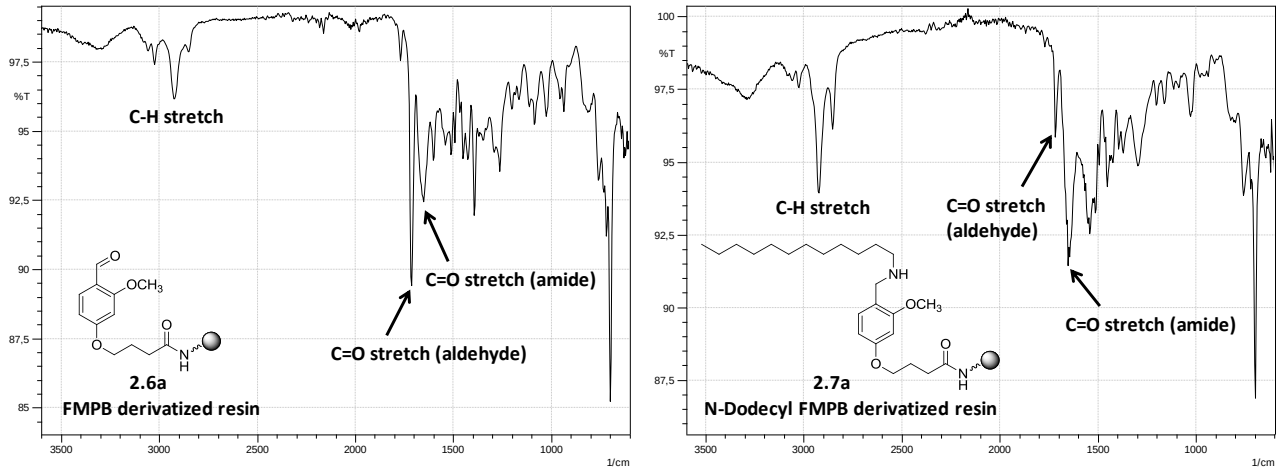

Figure 2.2 An example of reaction monitoring by IR spectroscopy when employing the FMPB linker (similar pattern observed for BAL derivatized resins). Left: FMPB derivatized resin (**2.6a**) showing a strong C=O aldehyde band at approximately 1715 cm^{-1} together with a C=O amide band at approximately 1650 cm^{-1}. Right: *N*-dodecyl FMPB derivatized resin (**2.7a**) showing a decreased C=O aldehyde band and increased C-H stretching at approximately 2900 cm^{-1}.

2.3 Synthesis of polylysine dendrons modified with peptides

After attachment of the backbone amide linker onto the resin and subsequent reductive amination, the resulting secondary amine was acylated with lysine by the symmetric anhydride method[62] employing *N*,*N*′-diisopropyl carbodiimide (DIC) as the coupling reagent. Two equivalents of the carboxylic acid were employed and the acylation was typically repeated once or twice for 2 h. DIC showed to be superior to other coupling reagents (i.e., PyBOP and *N*,*N*,*N*′,*N*′-tetramethyl-*O*-[1*H*-benzotriazol-1-yl]uronium hexafluorophosphate [HBTU] giving active esters) for the acylation of the secondary amine under the employed reaction conditions. Similar observations were reported by Jensen and co-workers.[55] The two amino groups in lysine served as dendritic branching points whereby G1 and G2 polylysine dendrons could be grown by a divergent Fmoc-based SPPS approach having a pentapeptide (indicated in blue) at the N-terminal and a propargyl or dodecyl group at the C-terminal (Scheme 2.4).

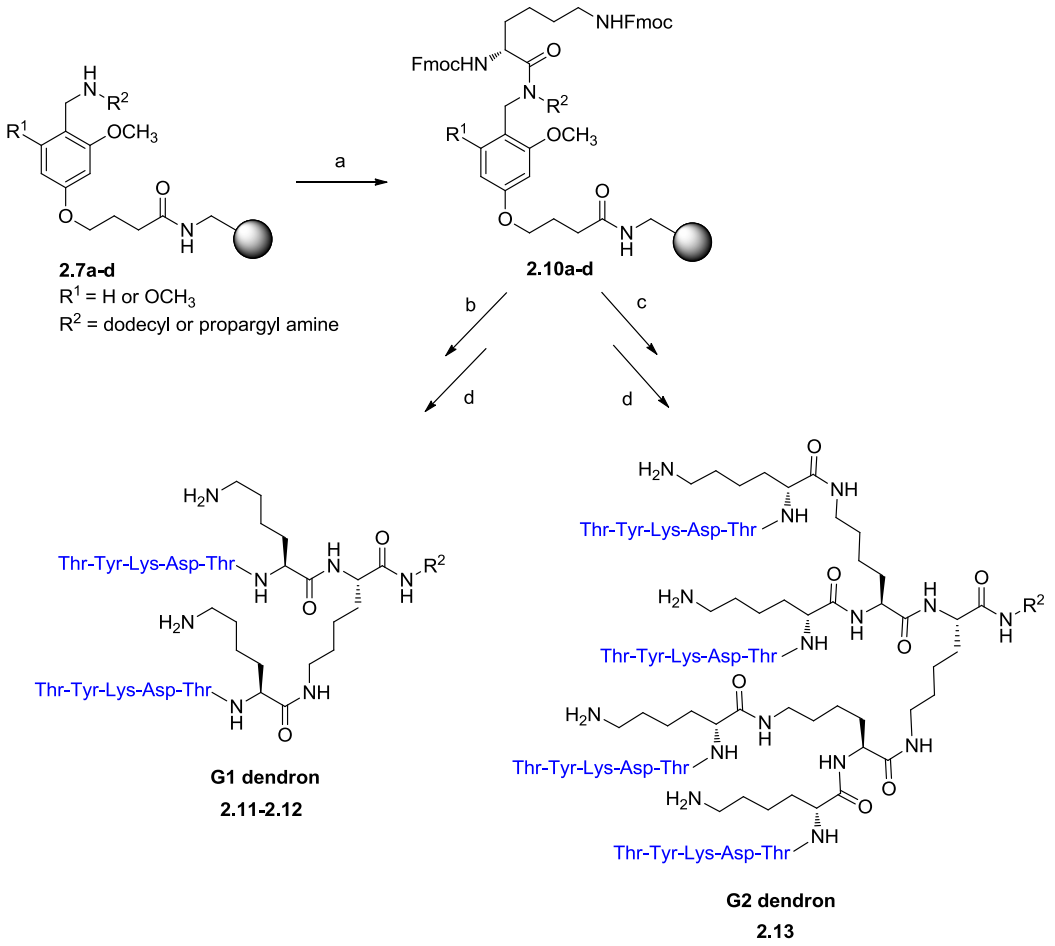

Scheme 2.4 Stepwise manual and automated SPPS of G1 and G2 polylysine dendrons with two or four N-terminal pentapeptides (indicated in blue), respectively, and a propargyl or dodecyl group at the C-terminal. Automatic synthesis is indicated by * in the following text. (a) Fmoc-Lys(Fmoc)-OH, DIC, dichloromethane/NMP (9:1), rt, 2 h. Repeated 1-2 times. (b) Fmoc deprotection between acylation steps: piperidine/NMP (1:4), rt, 3 + 20 + 30 min or 5 + 15 min*; linkage of Fmoc-Lys(Boc)-OH followed by pentapeptide (starting from Thr-Asp-Lys-Tyr-Thr) in six acylation steps: amino acid, PyBOP or TBTU*, DIPEA or *N*-methylmorpholine*, NMP, rt, 2.5 h or 1 h*. (c) Fmoc deprotection between acylation steps*: piperidine/NMP (1:4), rt, 5 + 15 min; linkage of Fmoc-Lys(Fmoc)-OH followed by pentapeptide in seven acylation steps*: amino acid, TBTU, *N*-methylmorpholine, NMP, rt, 1 h. (d) trifluoroacetic acid/dichloromethane (1:1), rt, 2 h.

The resin loadings were determined after attachment of the first lysine by measuring the UV absorbance of the released dibenzofulvene-piperidine adduct at 290 nm. This was performed on several milligrams of dry Fmoc-amino acid derivatized resin (**2.10a-d**) by treatment with 20 vol. % piperidine in NMP for 30 min.[53] Since both the α- and ε-amines in the first lysine were Fmoc-protected, the actual resin loadings were halved. The rigid macroporous (10% DVB cross-linked) aminomethyl resin generally yielded two to eight times lower loadings (i.e., 0.04 mmol/g and 0.11 mmol/g for dodecyl and propargyl derivatized resins, respectively) compared to the 1% DVB cross-linked aminomethyl resin (0.31 mmol/g and 0.18-0.24 mmol/g for dodecyl and propargyl derivatized resins, respectively). The higher degree of cross-linkage renders the polymeric support less flexible, which in turn affects the swelling properties. Polymeric supports with good swelling properties are vital for the success of SPPS. Solvent uptake by the resin results in an increase in

volume (swelling) whereby the permeability for reagents is improved. A successful solid-phase reaction is dependent on interactions between reagents in the solution and resin-bound functional groups. Hence, less flexible polymeric supports slow down reaction kinetics due to their impaired swelling (Fig. 2.3A).[63] Nevertheless, macroporous resins do not necessarily require swelling to allow access of reagents to the interior polymeric network due to the presence of a permanent network of pores (Fig. 2.3B).[64] Yet, with the conditions employed for the synthesis of the G1 and G2 polylysine dendrons, it was apparent the macroporous nature of the resin had an unfavorable effect leading to low loadings and yields.

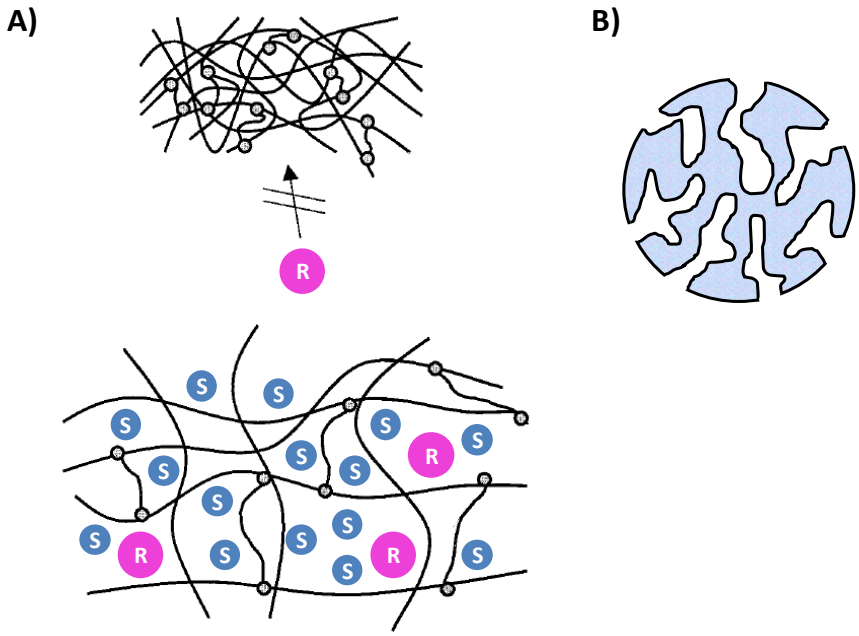

Figure 2.3 (A) Top: Non-swollen polymeric network impermeable to reagent molecules (purple circles). (A) Bottom: Polymeric network swollen in an appropriate solvent (blue circles) allowing permeability for reagent molecules to the interior. Adapted from Vaino and Janda.[63] (B): An illustrative example of a permanent network of pores in macroporous resins.

For the preparation of G1 polylysine dendrons, the amino functionalities of the second lysine were protected with orthogonal groups (e.g., N^{α}-Fmoc and N^{ε}-Boc) allowing selective α-amino modification with a pentapeptide. Subsequent one-pot Boc deprotection and resin cleavage resulted in G1 dendrons containing two pentapeptides (Scheme 2.4). Conversely, the additional branching point the G2 polylysine dendron required the second lysine to be protected with identical groups (i.e., N^{α}-Fmoc and N^{ε}-Fmoc) for simultaneous deprotection and subsequent acylation. Hereafter, the third lysine was again orthogonally protected, since the desired branching number was reached. Further stepwise SPPS and final cleavage yielded a G2 dendron consisting of four pentapeptides at the N-terminal (Scheme 2.4). The method was shown to be well-suited for automated peptide synthesis after manual introduction of the first lysine group on the secondary amine by a symmetric anhydride approach. In manual divergent growth of the dendrons, two equivalents of amino acid per amine were sufficient to afford complete acylations after 2.5 h, compared to 4-5 equivalents typically needed in SPPS.[53] However, for automated dendron growth, standard or higher

equivalents up to eight were employed, to ensure complete acylations after 1 h, since reaction completion could not be monitored between acylation steps. Additionally, TBTU (*N*,*N*,*N'*,*N'*-tetramethyl-*O*-[benzotriazol-1-yl]uronium hexafluoroborate) was applied as coupling reagent instead of PyBOP due to its superior stability when prepared as stock solution for automated synthesis.[45] During successive amino acid couplings, reaction monitoring by the ninhydrin test occasionally showed to be inconclusive (i.e., false negative read-outs) and was overcome by prolonged heating (5 min. at 80 °C) during analysis.

G1 and G2 dendrons modified with two or four N-terminal pentapeptides, respectively, having either a C-terminal dodecyl (**2.11**) or propargyl (**2.12** or **2.13**) group were successfully synthesized by the method (Table 2.1, Fig. 2.4).

Table 2.1 Synthesized dendrons and their isolated yields

#	Compound[d]	Yield (%)
2.11	G1(TYKDT)$_2$-*N*-dodecyl	42[a] 29[b]
2.12	G1(TYKDT)$_2$-*N*-propargyl	44[b]
2.13	G2(TYKDT)$_4$-*N*-propargyl	32[b,c]

[a] Manual SPPS. [b] Mixed manual-automated SPPS. [c] A somewhat higher loading (0.11 mmol/g) and lower isolated yield was obtained due to the lack of capping of the free amine groups on the resin. [d] Nomenclature for synthesized dendrons. G*n*: generation number, (TYKDT)$_n$: the number of pentapeptides attached to the N-terminal, T: Thr, Y: Tyr, K: Lys, D: Asp, *N*-: the group attached to the nitrogen at the C-terminal end of the dendron.

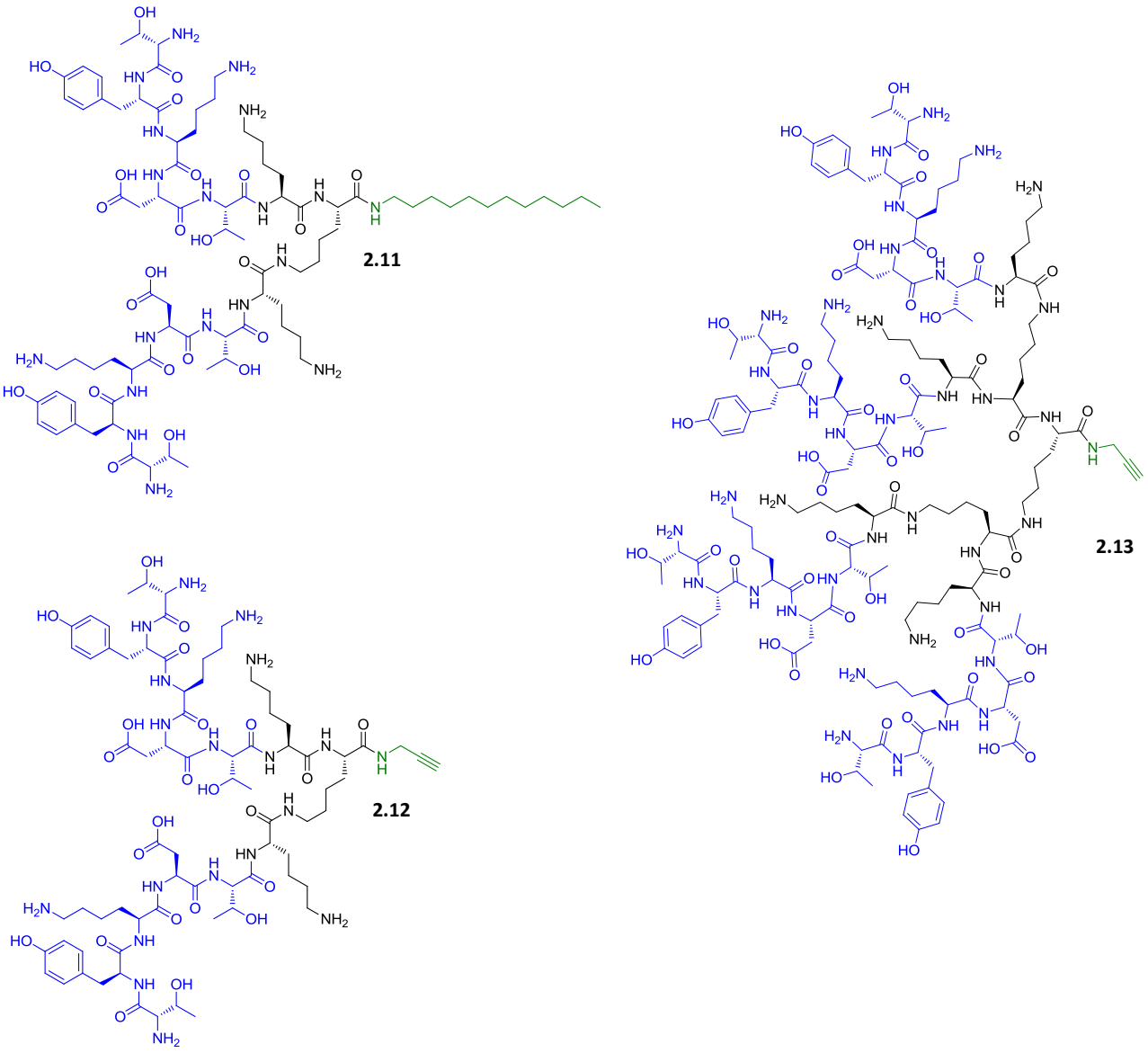

Figure 2.4 Molecular structures of synthesized polyfunctional polylysine dendrons. G1(TYKDT)$_2$-*N*-dodecyl (**2.11**), G1(TYKDT)$_2$-*N*-propargyl (**2.12**) and G2(TYKDT)$_4$-*N*-propargyl (**2.13**). C-terminal group indicated in green. Pentapeptide indicated in blue.

Both manual and mixed manual-automated SPPS were employed yielding dendrons in high crude purities by UPLC-MS (ultra-performance liquid chromatography mass spectrometry). A minor deletion impurity with an M – 128 mass was observed during automated synthesis of dendron **2.11** resulting from a dendron missing one lysine group. This could be due to steric effects induced by the hydrophobic dodecyl chain and/or amount of resin employed (Fig. 2.5). Therefore, to ensure complete acylations the amount of resin employed during automated synthesis was reduced from 100 mg to 50 mg for the synthesis of dendron **2.12** and **2.13**. A further optimization strategy for the automated synthesis could be to increase the acylation times.

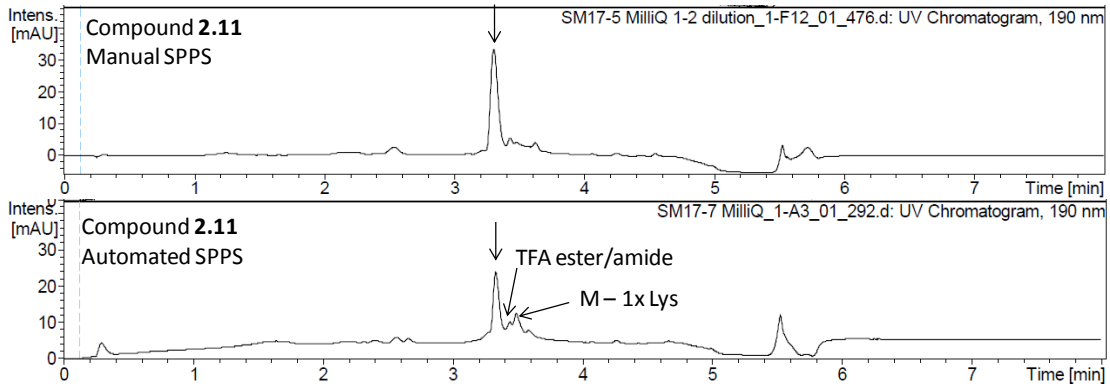

Figure 2.5 UV chromatograms of compound **2.11** synthesized by manual or mixed manual-automated SPPS. Automated SPPS led to a deletion impurity due to incomplete acylation resulting in a dendron missing one lysine (M – 1x Lys). Minor TFA ester or TFA amide impurity observed due to cleavage conditions.

Compound **2.13** showed a high crude purity, but a minor impurity with an M + 96 mass was observed for both for compound **2.11** and **2.12**. This could result from a trifluoroacetic acid (TFA) ester or amide formed during the resin cleavage conditions (Fig. 2.5 and 2.6).

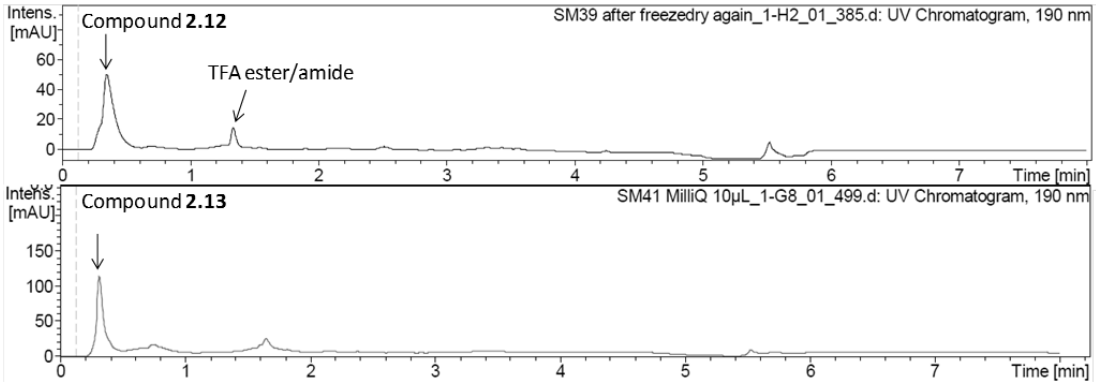

Figure 2.6 UV chromatograms of dendron **2.12** and **2.13** showing high crude purities with only a minor TFA ester or amide impurity for compound **2.12** due to cleavage conditions.

The propargyl group in compound **2.12** and **3.13** was chosen strategically to prove the broad application of the method, since it allows introduction of numerous functionalities via triazole linkage by a click chemistry approach.[65-67]

The structure and purity of dendron **2.12** and **2.13** was additionally determined by amino acid analysis (AAA) and found to be in agreement with the expected amino acid composition. The AAA of dendron **2.12** and **2.13** showed the following composition $Lys_5Thr_4Asp_2Tyr_2$ and $Lys_{11}Thr_8Asp_4Tyr_4$, respectively.

2.4 Conclusion

A simple and easy SPPS method was developed for the synthesis of polyfunctional polylysine dendrons in good yields and high crude purities as proved by UPLC-MS and AAA. This method employs backbone amide linkers as a way to insert desired C-terminal functionalities on dendrons

by SPPS including functionalities for further transformation by, e.g., click chemistry in solution-phase. The scope of the method was further demonstrated by N-terminal pentapeptide modifications yielding G1 and G2 dendrons that may be used for biomedical applications such as vaccines. Finally, the method showed to be fully compatible for automated peptide synthesis. Consequently, any functionality containing a primary amine group at one end can be successfully introduced at the C-terminal and the divergent SPPS approach enables further N-terminal modifications.

3 Selective detection of secondary amines on solid-phase

"In the field of observation,
chance favors only the prepared mind"
Louis Pasteur, 1854

Following our developed solid-phase backbone amide linker approach towards the synthesis of a variety of polylysine dendron libraries, we were of need for a quick and reliable colorimetric method to selectively detect various resin-bound secondary amine intermediates obtained after reductive amination. Up to then, we were relying on IR spectroscopy to detect a reduced carbonyl aldehyde band together with an increased C-H stretch when applicable (long alkyl chains) and the colorimetric DNPH test for detecting aldehyde groups. However, sometimes the DNPH test gave partly positive read-outs (i.e., orange beads) and IR spectroscopy tyoically showed a carbonyl aldehyde band although noticeably decreased. Hence, we needed to complement with an additional and reliable on-resin method for detecting secondary amines. As a result, this chapter describes the work done for the modification of an already known amine test (chloranil) to a selective test for secondary amines, which came to our notice during an unexpected observation (Publication II).

3.1 Colorimetric reaction monitoring

Reaction monitoring in solid-phase is not as straightforward as in solution-phase where traditional methods (e.g., thin layer chromatography [TLC]) are employed, since the intermediates are bound to the resin and cleavage between reaction steps is impractical. Therefore, colorimetric methods for on-bead monitoring of functional groups are essential for quick and reliable determination of reaction completion. In principle, a small amount of the derivatized resin is treated with a colorimetric test solution inducing a visible coloration upon the presence of relevant functional groups.[68]

Because amino groups are central to SPPS, several on-bead colorimetric methods have been developed for their detection. In 1970, a colorimetric method based on ninhydrin and phenol was developed by Kaiser and well-established in SPPS for the selective detection of primary amines indicated by a purple-blue coloration (Ruhemann's purple).[51] Other colorimetric visualization methods for the detection of both primary and secondary amines include TNBSA (trinitrobenzenesulfonic acid)[69], Bromophenol blue (3′,3″,5′,5″-tetrabromophenol sulfophtalein)[70,71], DABITC (4-*N*,*N*′-dimethylaminoazobenzene-4′-isothiocyanate)[72], DESC (1-methyl-2-[4′-nitrophenyl]-imidazol[1,2-*a*]pyrimidinium perchlorate)[73], 2-amino-3-chloro-1,4-naphthoquinone[74]. Moreover, a nondestructive colorimetric monitoring of amines and thiols has been reported where the colorimetric dye can be removed from the resin after the color test.[75] The only reported on-bead method for selective detection of secondary amines (proline) is the isatin (2,3-indolinedione)[72,76] test giving a blue proline-isatin complex in the presence of an acid (e.g., Boc-phenylalanine). In addition, a colorimetric method for the detection of secondary amines in solution employing acetaldehyde together with sodium nitroprusside in alkaline solution has been reported[77,78] and

employed for the quantitative determination of secondary amines as well.[79] However, there are some disadvantages with the reported method including the instability of the colored solution, which fades after several minutes and it is not suited for very sterically hindered secondary amines (e.g., where the nitrogen group is attached to two R′-CH-R″ groups).[79] Nowadays, the method is primarily employed for the detection of narcotics containing secondary amines, e.g., ecstacy (3,4-methylenedioxymethamphetamine [MDMA]) and methamphetamine (*N*-methylamphetamine).[80] Another widely employed method for the detection of both primary and secondary amines on solid-phase is the chloranil (tetrachloro-1,4-benzoquinone) method. The original method was reported to be selective for primary or secondary amines, when employing chloranil in toluene with acetaldehyde or acetone, respectively, giving blue/green colored resins.[81] However, a re-examination of the colorimetric method showed it to be selective for resin-bound secondary amines, when employing 2 vol. % chloranil with 2 vol. % acetaldehyde *instead* of acetone. Herein, toluene was exchanged with DMF (*N*,*N*-dimethylformamide) as solvent to increase the sensitivity of the test and a side-by-side examination with the original chloranil test employing acetone showed it only to give positive read-outs in four out of eleven cases.[82] A closer look in the literature gives a somewhat controversial picture of the selectivity of the chloranil method, and generally it should be employed together with the ninhydrin test for conclusive analysis.[83,84]

3.2 Development of a selective secondary amine test

Due to the developed backbone amide linker approach for the synthesis of polylysine dendrons, a selective visualization method for various resin-bound secondary amine intermediates was needed. As such, the chloranil test was attempted to be implemented as a standard reaction monitoring procedure. However, selectivity between primary and secondary amines was not observed by the chloranil test. Unexpectedly, it was found that upon adding two drops of 2 vol. % acetaldehyde in DMF (without chloranil) to samples of PS resin-bound secondary amines, the resin changed color within 3-5 min at room temperature giving dark orange-red to brown beads (Fig. 3.1A).

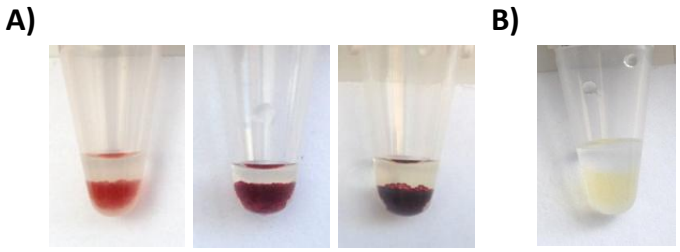

Figure 3.1 (A) Dark orange-red to brown color change variations when adding two drops of 2 vol. % acetaldehyde solution to PS resin-bound secondary amines. (B) No color change observed for PS resin-bound primary amines treated with 2 vol. % acetaldehyde solution.

No color change was observed when treating a sample of PS resin-bound primary amines with the acetaldehyde solution (Fig. 3.1B). Following the exciting discovery, examination of the observations were further pursued to see if this was a general trend or only valid for *N*-methylamine substrates (**3.1**) (Fig. 3.2A). When exposing other secondary amine substrates to the acetaldehyde

solution a similar color change was noticed. The amount of time needed for a full coloration was somewhat longer (ca. 5 min) for secondary amine substrates containing a long alkyl chain, e.g., C16 (**3.2**) (Fig. 3.2B), compared to *N*-methylamine (**3.1**) (Fig. 3.2A) presumably due to steric effects.

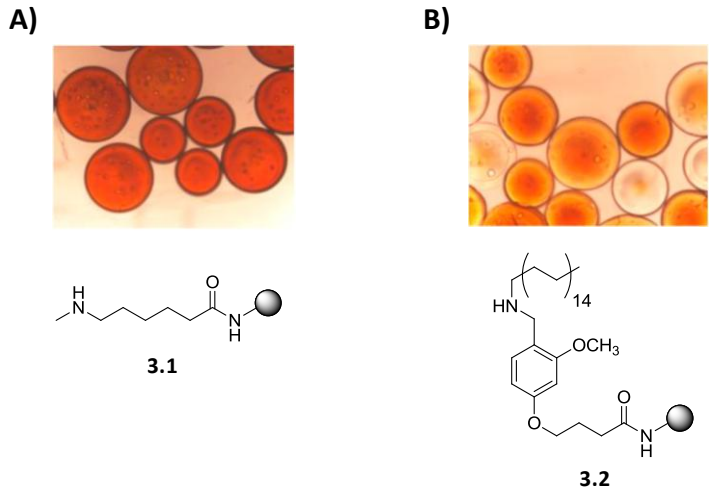

Figure 3.2 Micrograph of (A) an *N*-methylamine substrate (**3.1**) and (B) a long alkyl chain (C16) secondary amine substrate (**3.2**) on PS resins exposed to the acetaldehyde solution showing a positive readout.

The methods ability to distinguish between primary and secondary resin-bound amines was further demonstrated by conjugating an Fmoc-protected lysine, proline and alanine directly onto an aminomethyl PS. No color change was observed when exposing the Fmoc-derivatized resin to the acetaldehyde solution. Upon Fmoc-deprotection, only the proline derivatized resin (**3.3**) containing a secondary amine gave a positive readout (Fig. 3.3A). In addition, no coloration was observed with an underivatized aminomethyl PS resin (**2.5**) containing free primary amino groups (Fig. 3.3B). Furthermore, a range of secondary amine substrates produced by the backbone amide linker approach were acylated by an Fmoc-protected lysine. Exposure to the acetaldehyde solution before and after Fmoc-deprotection of the derivatized resins gave negative readouts similar to Fig. 3.1B (see Fig. 3.3C for an example of a micrographic picture).

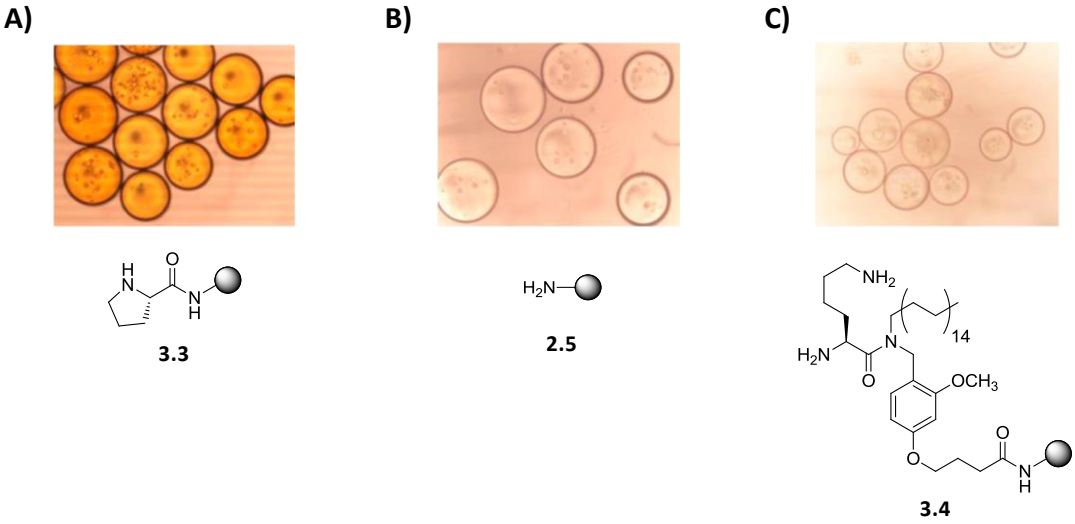

Figure 3.3 Micrograph after acetaldehyde solution treatment of a (A) PS-bound proline (**3.3**) containing a secondary amine, (B) underivatized aminomethyl PS (**2.5**) containing primary amino groups and (C) acylated secondary amine (**3.4**) attached to PS through the backbone amide linker approach having a C16 alkyl chain and a deprotected lysine.

The specificity of the acetaldehyde test was verified by looking at other functional groups on PS, i.e., carbonyl, chloro and dithiocarbamate functionalities. Two carbonyl containing PS resins were chosen, such as one derivatized with the FMPB linker (**2.6a**) and a commercially available indole aldehyde resin (**3.5**). As for the analysis of chloro functionalities, the commercially available chloromethyl PS (**3.6**) was chosen. The resin beads were colorless upon treatment with the acetaldehyde solution (Fig. 3.4). Thus, the presence of carbonyl and chloro functionalities does not affect the acetaldehyde test.

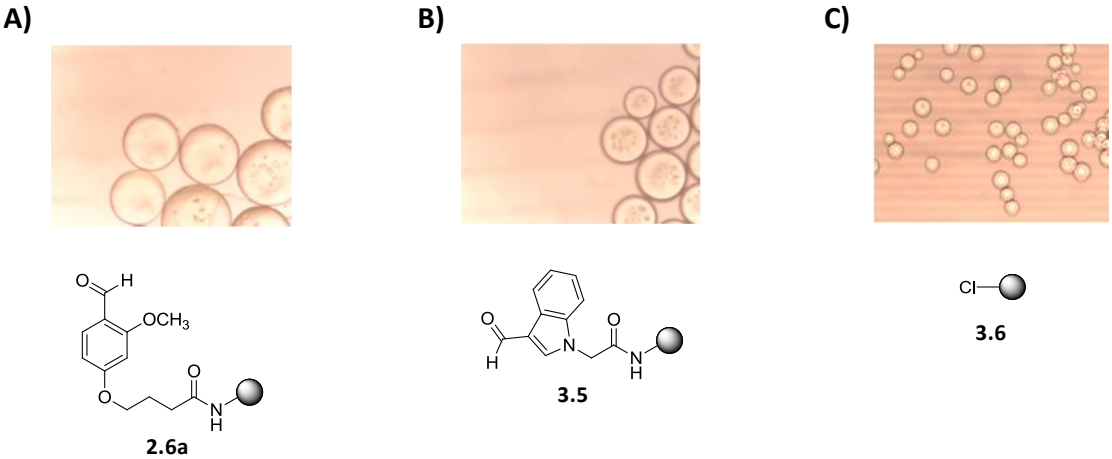

Figure 3.4 Micrograph of an (A) FMPB linker derivatized PS (**2.6a**), (B) indole aldehyde PS (**3.5**) and (C) a chloromethyl PS (**3.6**) showing negative readouts.

The dithiocarbamate functionalities were prepared by treating aminomethyl (**2.5**) and *N*-methylamine PS (**3.1**) with carbon disulfide. The dithiocarbamate derivatized aminomethyl resin (**3.7**) showed colorless beads upon treatment with the acetaldehyde solution (Fig. 3.5A). However,

the dithiocarbamate derivatized *N*-methylamine resin (**3.8**) displayed a slight coloration (Fig. 3.5B). The weak positive readout was presumably due to dithiocarbamate decomposing back to the secondary *N*-methylamine and carbon disulfide.

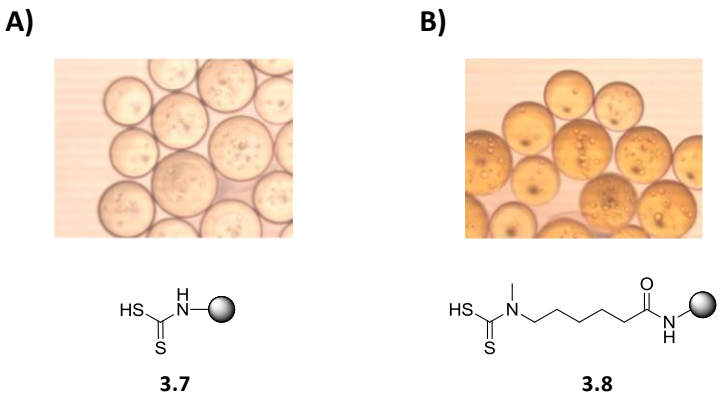

Figure 3.5 Micrograph of dithiocarbamate derivatized (A) aminomethyl (**3.7**) and (B) *N*-methylamine (**3.8**) PS.

Solvents with good PS swelling properties (e.g., NMP and tetrahydrofuran [THF]) other than DMF were examined displaying comparable results. NMP was preferred over DMF, since the latter can decompose to dimethylamine upon standing leading to consumption of the acetaldehyde thereby decreasing the sensitivity of the test. In addition, quenching the test after 5 min by washing the resin beads with NMP was found to be necessary to avoid false positive readouts overnight.

The acetaldehyde test was employed on PS resins with different degrees of cross-linkage, i.e., 1% and 10% DVB, and displayed similar colorations when positive. Furthermore, the compatibility of the acetaldehyde test was tested on different types of resins, i.e., proline derivatized Tentagel[85] (TG, a polyethylene glycol [PEG] functionalized PS resin) and PEGA[86] (poly[ethylene glycol]-poly-*N*,*N*-dimethylacrylamide copolymer). Upon acetaldehyde treatment the PEGA resin remained colorless and only a weak positive readout (yellow beads) was observed for the TG resin upon standing for 10 min. In addition, no coloration was observed in the presence of secondary amines, when employing the acetaldehyde test in traditional solution phase. It was apparent the coloration was somehow dependent on aromatic PS groups, which were markedly reduced in the TG resin composed mainly of PEG units and completely missing in the PEGA resin consisting of cross-linked PEG units to acrylamide (Fig. 3.6).[45,53,87]

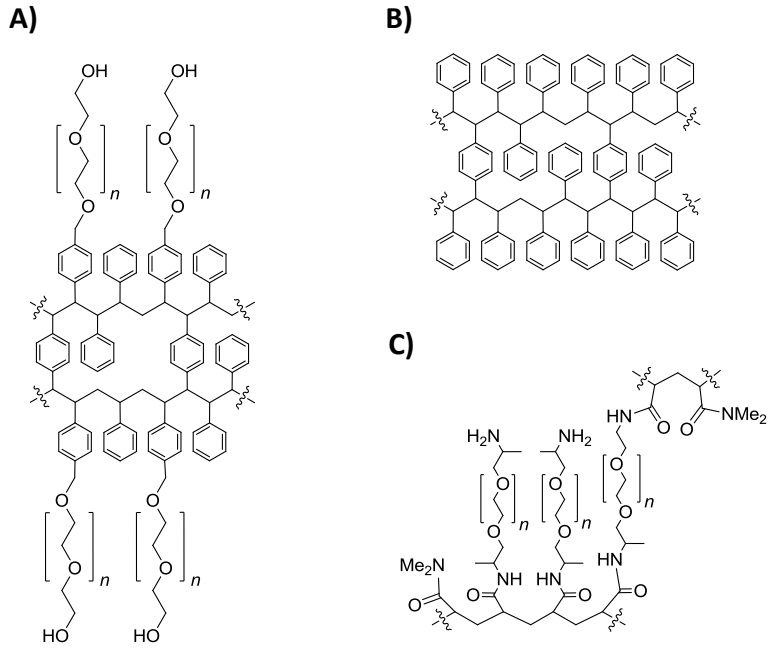

Figure 3.6 Structural presentation of (A) Tentagel resin consisting of PEG units attached to DVB cross-linked PS, (B) DVB cross-linked PS resin and (C) PEGA resin consisting of PEG units attached to acrylamide. *n:* number of polymeric PEG units.

An orange-red colored supernatant was observed, when performing the acetaldehyde test on Fmoc-deprotected primary amines present on PS resins. This color formation could be due to the presence of trace amounts of dibenzofulvene (DBF) from the prior Fmoc-deprotection with piperidine. Since Fmoc-protected amino acids rapidly release DBF upon reaction with amines in polar solvents[88], a small amount of an Fmoc-protected amino acid (Fmoc-Gly-OH) was added to the acetaldehyde solution. Upon adding a few drops of this modified solution the Fmoc group may be removed by the secondary amine present on the PEGA or TG resin thereby releasing DBF. Subsequently, the enamine formed between the secondary amine and acetaldehyde could attack the reactive DBF forming a colored adduct. As anticipated, this modification resulted in an orange-red coloration on proline derivatized TG and PEGA resins and was also valid for solution phase analysis. The selectivity of the modified solution towards secondary amines was maintained, since no coloration was observed upon treatment of a TG resin having primary amine groups with the modified acetaldehyde solution (Fig. 3.7).

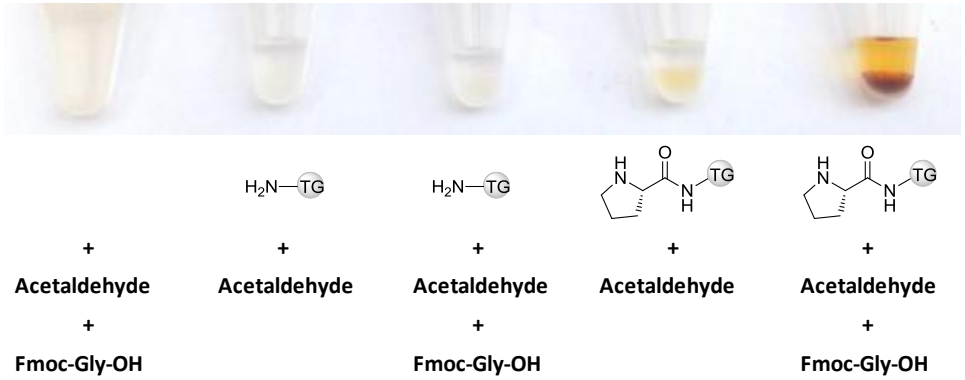

Figure 3.7 The effect of adding Fmoc-Gly-OH to the acetaldehyde solution analyzed on a TG resin having primary or secondary amines.

The sensitivity of the newly developed acetaldehyde test was examined on a Rink amide PS (4-[2′,4′-dimethoxyphenyl-Fmoc-aminomethyl]-phenoxy resin) and TG resins by a similar method as reported by Yang and co-workers.[75] Herein, the sensitivity of a colorimetric method was evaluated by quenching 90% of the resin-bound secondary amine groups with an Fmoc-Leu-OH. The derivatized PS and TG resins were prepared by anchoring different ratios of Fmoc-Pro-OH and Boc-Gly-OH similar to the method described by Claerhout and co-workers.[73] After initial loading determination and Fmoc-deprotection the secondary amines on the resins were quenched with 0.9 equivalents of Fmoc-Leu-OH. The sensitivity tests were performed with an acetaldehyde solution containing Fmoc-Phe-OH as additive and color visualization was obtained for loadings down to ~3-6 µmol/g (Fig. 3.8). The TG resin showed visible coloration after 5 min at the detection limit, whereas the Rink amide PS resin required 10 min for a conclusive readout.

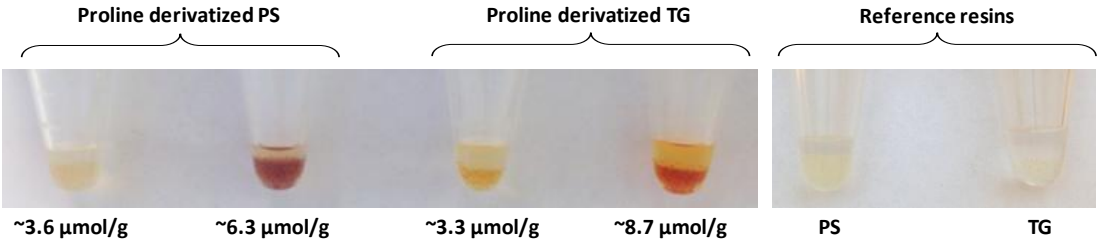

Figure 3.8 Sensitivity tests on Rink amide PS and TG resins derivatized with a secondary amino acid (proline) employing an acetaldehyde solution with Fmoc-Phe-OH as additive.

Even though uncertainty exists about the exact mechanism responsible for the coloration, it is evident the coloration is dependent on the presence of aromatic molecules (i.e., PS/DVB and DBF) and iminium/enamines from the reaction between the secondary amine and acetaldehyde. As mentioned above, DBF may be released from the Fmoc-protected amino acid employed as additive in the acetaldehyde solution under the presence of secondary amines. Even though alkenes are nucleophilic, when conjugated to an electron-withdrawing group one end of the C=C bond becomes electrophilic (like in the case of DBF) and can undergo Michael addition (conjugate addition) with nucleophiles.[60] Since enamines are known to undergo Michael addition to electrophilic alkenes (Michael acceptors)[60], it is proposed that after its formation the enamine (**3.10**) makes a

nucleophilic attack on DBF (**3.9**) to form an iminium adduct (**3.11**) with a delocalized negative charge on the fluorene moiety. This then undergoes proton transfer whereby the aromaticity is regained resulting in a stable DBF-enamine adduct (**3.12**), which is presumed to cause the red-brown coloration (Scheme 3.1).

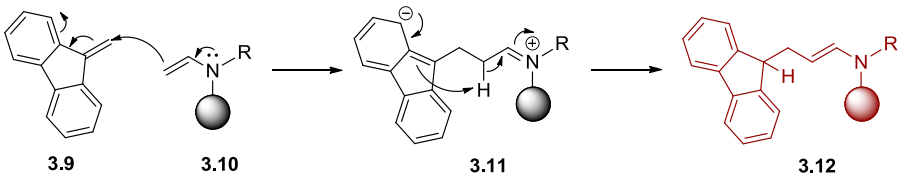

Scheme 3.1 Proposed mechanism for the formation of a red-brown DBF-enamine adduct (**3.12**).

No Fmoc-protected amino acids were needed as additive to induce coloration in PS resins cross-linked with DVB. During co-polymerization of styrene with DVB a significant amount of vinyl groups remain unreacted.[64] Hence, a reasonable explanation could be that residual reactive vinyl groups on the resin would undergo a similar Michael addition with the resin-bound nucleophilic enamine as proposed in Scheme 3.1 resulting in a colored DVB-enamine adduct (**3.13**) (Fig. 3.9).

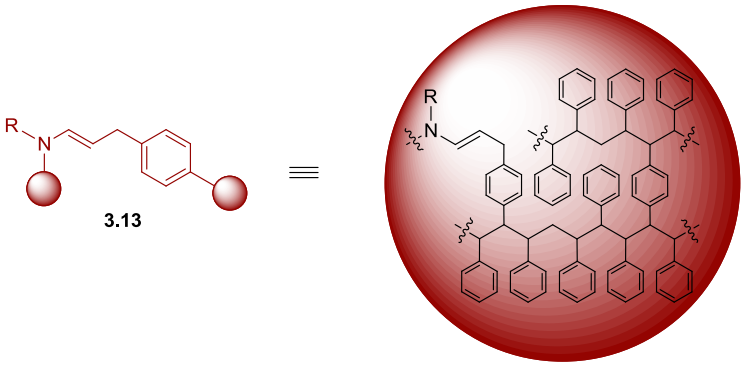

Figure 3.9 Proposed formation of a DVB-enamine adduct (**3.13**) from reaction between unreacted vinyl groups on the resin and resin-bound enamines. For simplicity the red-brown resin beads are drawn as two separate beads (left), however the reaction occurs inside one bead (right).

Furthermore, an increased presence of aromatic residues in the system (i.e., PS or Fmoc-protected aromatic amino acids) seems to increase the intensity of the coloration and make visualization more rapid.

3.3 Conclusion

Modification of the chloranil test led to a colorimetric method for selective detection of secondary amines, the acetaldehyde test. The method was shown to be valid for a broad range of secondary amines on PS resins and applicable for different degrees DVB cross-linkage showing excellent specificity. Further modification of the acetaldehyde test with Fmoc-protected amino acids as additives broadened the scope of the method to include detection of secondary amines in solution and on "PS deficient" resins, i.e., Tentagel and PEGA. Additionally, the sensitivity of the

acetaldehyde test was examined on PS and Tentagel resins showing a satisfactory detection limit of ~3-6 μmol/g. Moreover, it was apparent that the coloration was dependent on the presence of aromatic molecules, and so the coloration was proposed to be due to the DBF-enamine and/or DVB-enamine adducts. The acetaldehyde test greatly aided the synthesis of polylysine dendrons by the solid-phase backbone amide linker approach. By this method, colorimetric reaction monitoring of the reductive amination step is easy and quick. In addition, the method can be complemented by the ninhydrin and DNPH tests and IR spectroscopy.

4 Do dendrons with variable alkyl chains self-assemble?

A library of G1 and G2 polylysine dendrons with variable alkyl chains lengths (C1 – C18) and a benzyl group at the C-terminal were synthesized by the backbone amide linker approach for the investigation of self-assembling behavior as a function of lipidation degree and generation number. Small angle neutron scattering (SANS) and dynamic light scattering (DLS) characterization techniques were employed to test the hypothesis of self-assembly of dendrons in aqueous solutions and the charge density of the moieties was checked with zeta potential measurements. Additionally, the biocompatibility of the polylysine dendrons was investigated by cytotoxicity experiments. The physicochemical characterizations were performed at the University of Oslo during a five months external stay. Not all possible combinations (G1 vs. G2 with/without partially acetylated α-amino groups) of dendrons in each family of alkyl chain lengths were successfully synthesized before the external stay. Therefore, the study was focused on a selection of dendrons carefully chosen from the available dendron library to give the most coherent data collection and reported in publication III. In addition, several G1 and G2 poly-D-lysine dendrons were also prepared, since D amino acids are known to be abundant in bacteria[89] and the future plan was to perform immunological tests on synthesized dendrons. In the following, all synthesized compounds from the dendron library are included and physicochemical results obtained from selected dendrons are described.

4.1 Characterization techniques for self-assembly

When analyzing the structure of dendritic macromolecules including supramolecular structures formed by self-assemblies a broader array of analytical methods (e.g., SANS and DLS) are typically applied, because methods for analyzing small molecules (e.g., nuclear magnetic resonance [NMR], elemental analysis and IR spectroscopy) have limitations when applied on macromolecules, e.g., giving highly complex spectra. By using DLS, the molecules and complexes will be studied on a global dimensional scale, whereas SANS probes the species on a more local dimensional scale.

4.1.1 Small angle neutron scattering

SANS is a powerful non-destructive tool to determine the size and shape of various nanomaterials, e.g., biological macromolecules, polymers and dendritic structures in solution. It is an ideal characterization method for probing mesoscopic structures, since neutrons have the ability to penetrate through matter. An advantage of neutron scattering over other scattering techniques (e.g., X-ray scattering) is the ability of the neutrons to detect light atoms (hydrogen) in the presence of heavier atoms. Additionally, good contrasts can be obtained with SANS by isotope labeling or employing deuterated solvents due to the large difference between the neutron scattering profile of hydrogen (1 proton, 0 neutrons) and deuterium (1 proton, 1 neutron). Hence, after measurements one can subtract the scattering data obtained from the deuterated solvent and by exchanging specific hydrogen atoms in the sample with deuterium they can be made “invisible”.[90-92]

During a typical SANS experiment, the sample is irradiated with neutrons of a certain wavelength. The neutrons penetrate the sample and are scattered by the atomic nuclei. The 2D scattering intensity with respect to the incoming beam is recorded at a detector (Fig. 4.1).

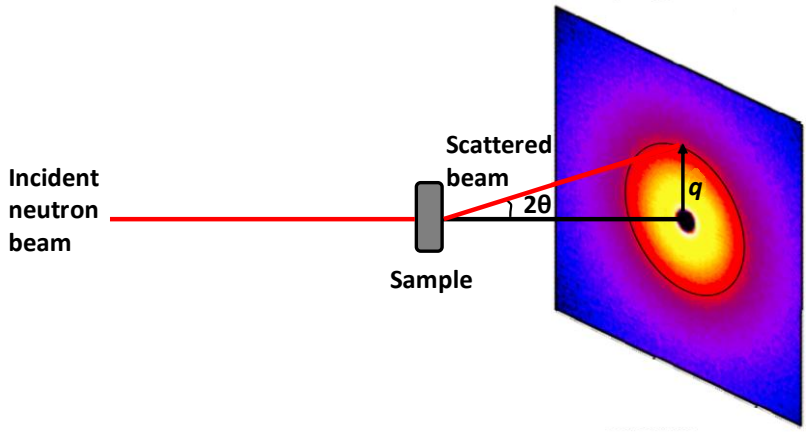

Figure 4.1 A simplified schematic presentation of the SANS setup resulting in a 2D scattering pattern. The incident neutron beam is scattered by the sample in an angle of 2θ and the scattering vector *q* is the difference between the vector of the incident beam and scattered beam. Adapted from Hammouda.[93]

The scattering vector *q* is expressed in $Å^{-1}$ or nm^{-1} and is given by:

$$q = \left(\frac{4\pi n}{\lambda}\right) \cdot \sin\left(\frac{\theta}{2}\right) \approx \frac{2\pi\theta}{\lambda} \tag{4.1}$$

where λ is the wavelength of the incident beam, *n* is the refractive index of the medium (by convention *n* = 1 in SANS), and θ is the scattering angle, which in SANS by definition is 2θ. From Eq. 4.1 it is clear that small angles (θ) or high wavelengths (λ) give low *q*-values. Therefore, the scattering vector *q* can be approximated to $2\pi\theta/\lambda$, which is valid for small angles employed in SANS. Introducing Eq. 4.1 in Braggs law gives the relationship between *q* and the observable length scale *d*:[94,95]

Braggs Law: $$H\lambda = 2d \cdot \sin\theta \tag{4.2}$$

$$q = \frac{4\pi}{\lambda} \cdot \sin\theta \Rightarrow q = \frac{1}{2d \cdot \sin\theta} 4\pi \cdot \sin\theta \Rightarrow q = \frac{2\pi}{d} \tag{4.3}$$

where *H* is an integer and set to 1.

Typically SANS measurements take minutes to hours to complete. Before conducting an experiment, the required *q*-range has to be considered and an optimal wavelength and detector distance has to be acquired. A *q*-range of 0.008-0.25 $Å^{-1}$ was employed for the SANS experiments on selected dendrons corresponding to an observable length scale of 2.5-78.5 nm. The scattering

intensity is plotted against the scattering vector q and analyzed by model fitting whereby the size and shape of structures in the sample are obtained.[95]

For N number of monodisperse particles the scattered intensity in its simplest form is given by:

$$I(q) = N \cdot P(q) \cdot S(q) \tag{4.4}$$

where $P(q)$ is the form factor and $S(q)$ the structure factor.

The form factor describes the *intra*-particle contribution and gives information about the form and size of the particles. The structure factor describes the *inter*-particle contribution and can give information about the distances between particles in the sample.[96]

The SANS data obtained for the polylysine dendrons were fitted by a core-shell particle model containing an interparticle repulsive term. A spherical core-shell structure was employed for the form factor term:[97]

$$P(q) = \frac{scale}{V_s}\left[\begin{array}{l} 3V_c(\rho_c - \rho_s)\dfrac{[\sin(qr_c) - qr_c \cdot \cos(qr_c)]}{(qr_c)^3} \\ +\,3V_s(\rho_s - \rho_{solv})\dfrac{[\sin(qr_s) - qr_s \cdot \cos(qr_s)]}{(qr_s)^3} \end{array}\right]^2 + bkg \tag{4.5}$$

where V_c is the volume of the core, V_s the volume of the shell, r_s the outer radius of the shell and r_c the radius of the core, *scale* is a factor proportional to the concentration and *bkg* is the incoherent scattering from the background. ρ_c, ρ_s and ρ_{solv} are the scattering length densities of the core, shell and solvent, respectively.

Here, the average scattering length density of the shell (ρ_s) corresponds to the hydrophilic polylysine head groups forming the shell of the micelle together with water molecules. Theoretical values were employed for the scattering length density of deuterium oxide (ρ_{solv} = 6.3 x 10^{-6} Å^{-2}) and the alkyl chain (ρ_c = -0.34 x 10^{-6} Å^{-2}).

The structure factor employed was developed by Hayter and Penfold:[98]

$$S(K) = \frac{1}{1 - 24\omega a(K)} \tag{4.6}$$

where $K = q\sigma$ (σ is the diameter of the spherical particle), $\omega = \pi\psi\sigma^3/6$ is the volume fraction (ψ is the particle number density) and $a(K)$ is a sum of polynomial terms including the effects of particle charge, counterions and additional ions present in the solution (not shown here).

4.1.2 Dynamic light scattering

In DLS the beam source is a laser rather than neutrons and the same scattering principles as SANS and other scattering techniques are valid. However, here the sample is observed on a more global length scale. In DLS the sample is solvated in an appropriate solvent and the size of the molecules can be determined. A laser beam is directed through the sample and time dependent fluctuations in the intensity of the scattered light as a result of the Brownian motion of the molecules (random movements due to colliding solvent molecules) are probed in form of a correlation function that is analyzed.[99]

In a typical DLS experiment the sample is irradiated by a laser source, which is scattered at a scattering angle θ as it hits the particles or molecules in the scattering volume of the sample (Fig. 4.2). The scattering vector q is given by Eq. 4.1, as described above.

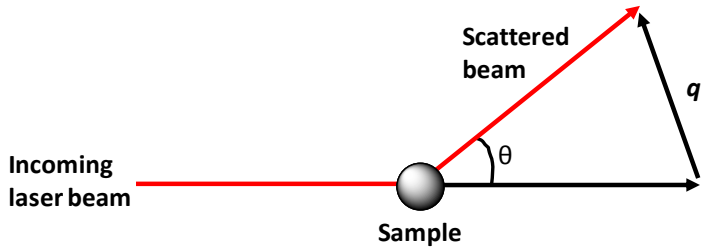

Figure 4.2 Simple schematic presentation of the scattering process in DLS. The incoming laser beam is scattered by the sample at a scattering angle θ. The scattering vector q is the difference between the vector of the incoming beam and scattered beam.

The DLS experiments on selected dendrons were performed using a multi angle light scattering (MALS) spectrometer to obtain simultaneous data at eight angles thereby increasing experimental quality and covering a larger q-range. The data were analyzed by expressing the time-dependent scattering intensity fluctuations in terms of correlation functions. The duration of the fluctuations depends on the size of the particle in the sample, where larger particles show slower Brownian motion resulting in longer fluctuation times compared to smaller particles.[100] The experimentally recorded intensity autocorrelation function $g^2(q,t)$ is related to the theoretically manageable first-order electric field autocorrelation function $g^1(q,t)$ through the Siegert relation:[101]

$$g^2(q,t) = 1 + B\left|g^1(q,t)\right|^2 \tag{4.7}$$

where B (≤ 1) is an instrumental parameter.

In simple systems, where we allow some size distribution of the moieties, the decay of the correlation function can be fitted by a stretched exponential with only one relaxation mode:[102]

$$g^1(t) = A \cdot \exp\left[-\left(\frac{t}{\tau_e}\right)^{\beta}\right] \tag{4.8}$$

where A is the amplitude of the relaxation mode, τ_e is the effective relaxation time and β ($0 \leq \beta \leq 1$) is a measure of the distribution of relaxation times (a measure of the polydispersity of the sample with $\beta = 1$ for monodisperse samples). The mean relaxation time is given by:[102]

$$\tau = \left(\frac{\tau_e}{\beta}\right) \cdot \Gamma\left(\frac{1}{\beta}\right) \tag{4.9}$$

where $\Gamma(1/\beta)$ is the gamma function of β^{-1}.

For bimodal systems the decay of the correlation function can be fitted by the sum of two stretched exponentials. The two relaxation modes observed for bimodal systems can be described by the Kohlrausch-Williams-Watts (KWW) function:[103]

$$g^1(t) = A_f \cdot \exp\left[-\left(\frac{t}{\tau_{fe}}\right)^{\beta_f}\right] + A_s \cdot \exp\left[-\left(\frac{t}{\tau_{se}}\right)^{\beta_s}\right] \tag{4.10}$$

where $A_f + A_s = 1$. The subscripts f and s denote parameters for the fast and slow relaxation modes, respectively.

The mean relaxation time for the fast and slow relaxation modes is as described above (Eq. 4.9) and q^2 dependent if the relaxation mode is diffusive. Therefore, the mean relaxation time is related to the diffusion coefficient D portraying the systems diffusive nature. The diffusion coefficient can be determined by:[102]

$$\tau^{-1} = D \cdot q^2 \tag{4.11}$$

The hydrodynamic diameter d_h can then be calculated from the Stokes-Einstein relationship by assuming the system consists of spherical structures:[102,104]

$$d_h = \frac{k_B T}{3\pi\eta D} \tag{4.12}$$

where k_B is the Boltzmann constant, T the absolute temperature and η the viscosity of the medium.

Both unimodal and bimodal autocorrelation functions were probed and the dendron samples always showed diffusive behavior. Therefore, the hydrodynamic diameters could be determined by the Stokes-Einstein relationship.

4.2 Dendron library synthesized by solid-phase

The G1 and G2 polylysine dendrons were synthesized by stepwise divergent SPPS employing the backbone amide linker approach (Chapter 2). To give the reader a better overview, two synthetic schemes are given together with the corresponding compound tables. Scheme 4.1 represents all synthesized polylysine dendrons, Table 4.1 indicates polylysine dendrons selected for physicochemical analysis and in Table 4.2 the remaining polylysine dendrons can be found.

Initially, an FMPB linker (**2.4a**) was attached onto an aminomethyl PS resin (**2.5**) (1% DVB cross-linked, loading: 2.0 mmol/g) employing PyBOP or HBTU as the coupling reagents together with DIPEA. The loading on the resin was reduced to avoid steric crowding and residual aminomethyl groups quenched with acetic anhydride employing DIPEA as base (Section 1.2.1). Subsequently, an alkyl chain or benzyl group was attached by reductive amination. Reaction completion for these two steps was monitored by IR spectroscopy and the DNPH test, as described in Section 2.2. In addition, the presence of the secondary amine after the reductive amination step was monitored by the acetaldehyde test, as described in Chapter 3, giving a positive readout (orange-brown beads). Consequently, the secondary amine was acylated with two equivalents of Fmoc-Lys(Fmoc)-OH (either the D or L enantiomer) employing DIC as the coupling reagent in a dichloromethane (DCM)/NMP (95:5) mixture (Scheme 4.1).

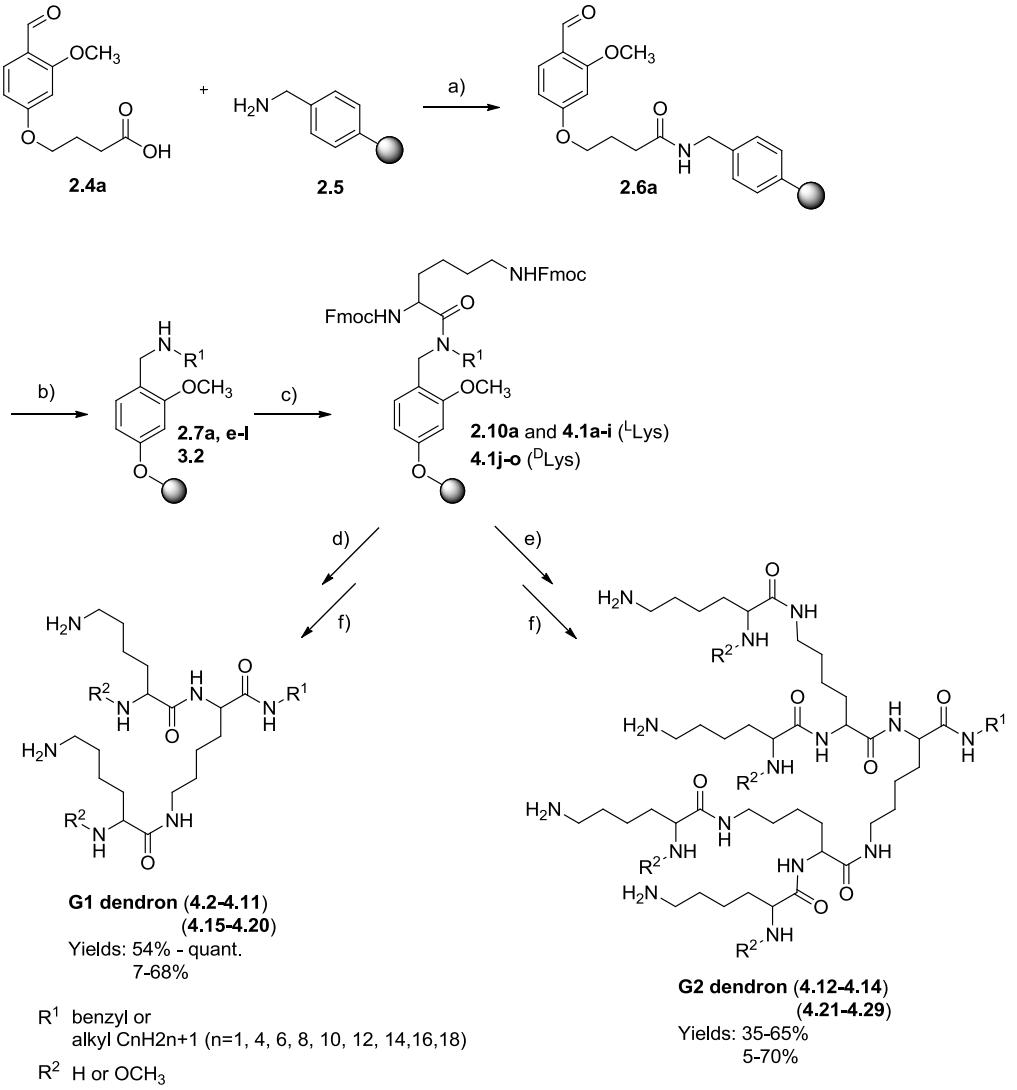

Scheme 4.1 Stepwise divergent SPPS of G1 and G2 polylysine dendrons with variable alkyl chain lengths. The protected lysines employed were either solely the D or L enantiomers. (a) PyBOP or HBTU, DIPEA, NMP, rt, 22 h; acetic anhydride, DIPEA, DCM, rt, 2-4 h. (b) Alkyl amine, $NaBH_3CN$, 5 vol. % acetic acid, NMP, rt, 20 h or 3 + 2h. (c) Fmoc-Lys(Fmoc)-OH, DIC, DCM/NMP (95:5), rt, 20 h or 2 + 2h. (d) Fmoc deprotection: piperidine/NMP (1:4), rt, 3 + 30 + 20 min; linkage of the second lysine group: Fmoc-Lys(Boc)-OH, PyBOP, DIPEA, NMP, rt, 3 h or 20 h or until negative readout by the ninhydrin test. (e) Fmoc deprotection: piperidine/NMP (1:4), rt, 3 + 30 + 20 min; linkage of the second lysine group: Fmoc-Lys(Fmoc)-OH, PyBOP, DIPEA, rt, 3 h or until negative readout by the ninhydrin test; Fmoc deprotection: piperidine/NMP (1:4), rt, 3 + 30 + 20 min; linkage of the third lysine group: Fmoc-Lys(Boc)-OH, PyBOP, DIPEA, NMP, rt, 3 h or 20 h or until negative readout by the ninhydrin test; Fmoc deprotection: piperidine/NMP (1:4), rt, 3 + 30 + 20 min. (f) R^2 = H: TFA/DCM (1:1), rt, 2 h; R^2 = OCH_3: acetic anhydride/DIPEA/DCM (10/5/85), rt, 3 h; TFA/DCM (1:1), rt, 2 h.

Later it was found that both the reductive amination and subsequent acylation of the secondary amine could be optimized by employing halved resin loadings (i.e., 1.0 mmol/g) for reagent calculations and increasing the reaction time from 2-3 h to typically 20 h. Thereby, the reductive amination and acylation reactions became much more cost-effective eliminating the need for reaction repeat and use of high amounts of reagents. Moreover, the optimization made the resin

washing steps less demanding. Hereafter, the reaction completion was again monitored by the acetaldehyde test giving a negative readout (colorless beads) and the resin loadings were determined as described in Chapter 2 and typically ranged from 0.14 to 0.47 mmol/g. Deprotection of the Fmoc-amines between the following acylation steps were performed by 20 vol. % piperidine in NMP and the resulting free primary amine groups were monitored by the ninhydrin test.[51,52] However, the reliability of the ninhydrin test was low for derivatized resins containing alkyl chain lengths above C12 leading to false negative readouts. The second and third lysines were attached employing PyBOP as the coupling reagent in NMP together with DIPEA and the reaction repeated if necessary. The second lysine in G1 dendrons and third lysine in G2 dendrons was an orthogonally protected Fmoc-Lys(Boc)-OH (either the D or L enantiomer). Since an extra branching point was needed in G2 dendrons, an Fmoc-Lys(Fmoc)-OH (either the D or L enantiomer) was employed as the second lysine. For the synthesis of dendrons with partial acetylated N-terminal amines, the derivatized resin was treated with acetic anhydride in DCM together with DIPEA after Fmoc deprotection of the α-amines (Scheme 4.1). The target dendrons were cleaved of the resin by employing TFA/DCM (1:1) giving the dendrons in moderate to good yields and high crude purity (Table 4.1). However, for a small number of dendrons purification by preparative reversed-phase HPLC was required giving poor yields (Table 4.2). Furthermore, in few cases TFA was exchanged with HCl, since at first small angle X-ray scattering (SAXS) was planned instead of SANS and the electronegative fluoride ion had on previous occasions disturbed X-ray measurements on similar dendrons. The anion exchange was achieved by treating the lyophilized dendron twice with 0.1M HCl for 1 h at rt.

Table 4.1 Synthesized G1 and G2 polylysine dendrons included in Publication III.

#	Compound[c]	Yield[a] (%)
4.2	G1-C1	70
4.3	G1-C8	64
4.4	G1-C12	54
4.5	G1-C14	Quantitative
4.6	G1-C16	79[b]
4.7	G1-C18	Quantitative
4.8	G1(acetyl)-C4	81
4.9	G1(acetyl)-C6	73
4.10	G1(acetyl)-C10	Quantitative
4.11	G1(acetyl)-C16	72
4.12	G2-C1	35
4.13	G2-C12	43
4.14	G2-C16	65

[a] TFA salt. [b] Dendron based on poly-D-lysine. [c] (acetyl) corresponds to $R^2 = OCH_3$ in Scheme 4.1.

Table 4.2 Remaining G1 and G2 polylysine dendrons.

#	Compound	Yield (%)
4.15	G1-PDL(acetyl)-C4	60[a]
4.16	G1-PDL(acetyl)-C6	62[a]
4.17	G1-PDL(acetyl)-C8	23[b]
4.18	G1-PDL-C10	32[a]
4.19	G1-PDL-C12	7[a]
4.20	G1-benzyl	68[a]
4.21	G2-C4	63[b]
4.22	G2(acetyl)-C4	24[b]
4.23	G2-PDL(acetyl)-C4	15[b]
4.24	G2(acetyl)-C8	62[a]
4.25	G2-PDL-C8	9[b]
4.26	G2-C10	70[a]
4.27	G2-PDL-C12	17[a]
4.28	G2-PDL-C16	67[a]
4.29	G2-benzyl	5[a]

[a] TFA salt. [b] HCl salt. PDL: poly-D-lysine. [c] (acetyl) corresponds to $R^2 = OCH_3$ in Scheme 4.1.

The molecular weight of the synthesized dendrons was confirmed by UPLC-MS. The chemical structure of dendrons from Table 4.1 was confirmed by ^{1}H-NMR, ^{13}C-NMR, DEPT-135 ^{13}C-NMR, COSY and HSQC (see Publication III for spectra and chromatograms). The chemical structure of dendrons from Table 4.2 was confirmed by ^{1}H-NMR and ^{13}C-NMR by comparing with thoroughly assigned NMR spectra of dendrons from Table 4.1. In addition, the size and shape of selected dendrons (Table 4.1) were further characterized by SANS and DLS, which is described in the following.

4.3 Dendron self-assembly studied by small angle neutron scattering

Self-assembly of small readily accessible dendrons enables a quick and simple way to generate bigger and more complex dendritic systems through non-covalent interactions, since time-consuming synthetic steps are eliminated.[105] In addition, the multivalency in the corresponding dendritic systems will be amplified compared to single dendrons and can be used as a way to increase ligand binding affinity.[24,106] Dendrons containing hydrophobic and hydrophilic groups (i.e., amphiphilic dendrons) behave like surfactants in aqueous environments by self-assembling into dendritic micelles or vesicles at concentrations greater than the critical micelle concentration (CMC). The self-assembly into micellar structures is typically in the nanoscale range (5-20 nm) and can be controlled through the choice of the hydrophobic group at the dendron branching point.[21,105,107] Therefore, it was hypothesized that the amphiphilic polylysine dendrons may aggregate in aqueous solutions to form supramolecular entities through non-covalent intermolecular interactions. To test this hypothesis and reveal the structure and shape of possible supramolecular entities as a function of the length of the alkyl chain and generation number, selected dendrons were analyzed by SANS (Table 4.1). The hypothesis was indeed proven and micellar self-assemblies

with polylysine head groups and alkyl chains were clearly observed for several dendrons by examining the scattering behavior (Fig. 4.3).

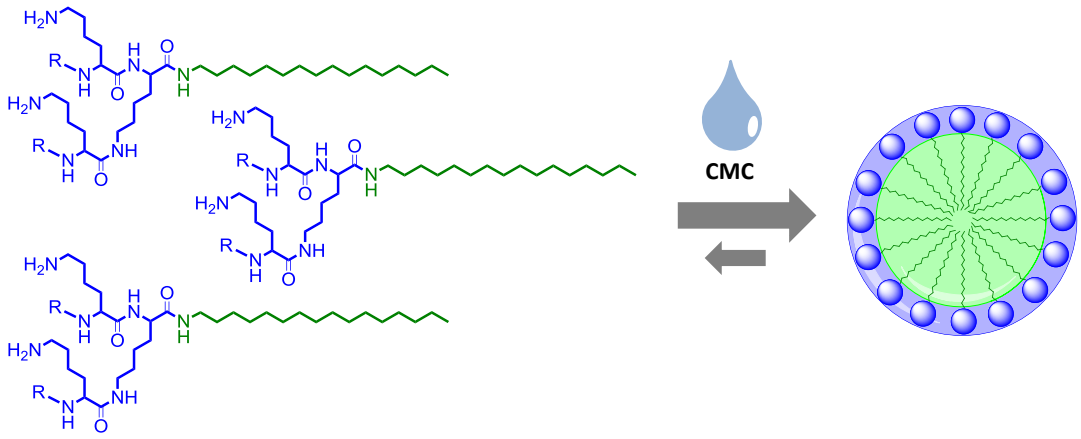

Figure 4.3 An illustrative example of micellar self-assemblies formed by amphiphilic polylysine dendrons in aqueous solutions above the CMC (here a G1 dendron with a C16 tail is shown as an example). Blue spheres and shell: hydrophilic polylysine head groups. Green sphere: hydrophobic alkyl tails forming the micellar core. R: H or OCH_3.

The CMC values of similar dendritic systems have been reported in the literature. Cationic PAMAM dendrons containing a hydrophobic alkyl chain (C10, C14 or C18) were reported to have CMC values in the range of 0.03 to 2.72 mM.[108] In another example, the CMC of a linear-dendritic co-polymer surfactant consisting of poly(ethylene oxide) and a G3 polylysine was measured to be 0.08 mM.[109] Therefore, the concentrations chosen to examine the self-assembling properties of the polylysine dendrons were 9, 18 and 27 mM and they are all well above the CMC.

The scattering data for G1-C16 (**4.6**) and G1-C18 (**4.7**) showed a correlation peak at around q = 0.045 $Å^{-1}$ demonstrating strong interparticle interactions (Fig. 4.4). The corresponding interparticle distance calculated from equation 4.3 was around 14 nm. Since the overall diameter of the micelles were found to be around 5 nm (see below), it is apparent from the interparticle distance that the micelles are somewhat separated (Table 4.3).

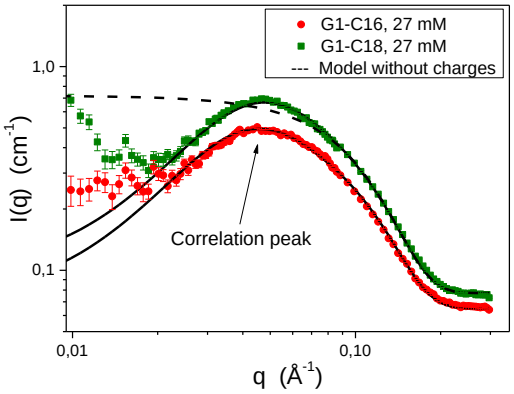

Figure 4.4 SANS scattering data of the G1-C16 and G1-C18 dendrons in aqueous solutions at a concentration of 27 mM. Continuous lines are fits with a spherical core-shell model having an interparticle repulsive term. The dashed line for G1-C18 represents the same core-shell model without the repulsive term.

At q values below 0.015 $Å^{-1}$ an upturn is observed in the scattering data indicating the presence of larger aggregates in the sample (Fig. 4.4). However, this was not included in the fitting of the data and instead further analyzed by DLS (Section 4.4).

The scattering data for G1-C16 and G1-C18 were fitted by a core-shell particle model having an interparticle repulsive term (Eq. 4.4-4.6) and the results are shown in Table 4.3. Removing the repulsive term from the core-shell model (dashed line) did not show a good fit of the scattering data (Fig. 4.4). And so, it was apparent that charges due to the presence of protonated amine groups (dendrons were synthesized as TFA salts) in the head group needed to be included in the model (Eq. 4.6) thereby leading to a depression of the curve to the left side of the correlation peak giving a better fit of the data (Fig. 4.4). In agreement with protonated amines being present in the head groups, the micelles were found to have an estimated total effective charge of ca. + 8 when taking the distribution of charges from counterions close to the surface into account. As expected, the total charge units for micelles formed by G1-C16 and G1-C18 are similar, since the head groups in G1-C16 and G1-C18 are identical (Table 4.3).

Table 4.3 Fitted parameters for G1-C16 and G1-C18 from the core-shell particle model with a repulsive term.

#	Compound	Conc. [mM]	Radius[a] (core) [nm]	Thickness[a] (shell) [nm]	Radius[a] (total) [nm]	Charge[b] [+]	N(agg)[c]
4.6	G1-C16	27	1.20	1.23	2.43	7.9	33
4.7	G1-C18	27	1.28	1.19	2.47	8.0	35

[a] Error ± 0.04nm. [b] Error ± 0.5 *e*. [c] Error ±5.

The core radius of the micelles formed by self-assembly of G1-C16 dendrons is slightly smaller than for G1-C18, i.e., 1.20 nm vs. 1.28 nm. Even though this difference is minor (within errors), a difference of two carbon atoms in the alkyl tail seems to have an effect on the core size resulting in a slightly bigger core in G1-C18 as expected. The total radius of the micelle is ca. 2.5 nm corresponding to a diameter of ca. 5 nm. Assuming that the alkyl chain is fully stretched in a zig-zag pattern, the total length spanned by the alkyl tail can be calculated by trigonometry knowing the C-C bond length (0.154 nm) and angle (108°). Hence, the total length spanned by a C16-C18 tail is roughly 2 nm. Taking into account the thickness of the shell being around 1 nm, the micellar diameter is likely spanned by two dendrons with a total diameter of roughly 6 nm (Fig. 4.3).

In Table 4.3, the number of dendrons interacting to form one micelle are also indicated by the aggregation number, N(agg) = V(total) / V(dendron). The aggregation number was roughly estimated by employing the volume of a sphere for the micelles (i.e., V (total) = $(4/3)\pi R^3$) with the total radius (core + shell) listed in Table 4.3 employed as R. The volume of one dendron is given by $M_w/(N_A \cdot \phi)$ where M_w is the molecular weight (dendron + TFA), N_A is Avogadro's constant (6.02 x 10^{23} mol^{-1}) and ϕ is the density of water (1 g/cm^3). Since the dendrons were prepared as TFA salts, a minimum number of TFA molecules associated with the amine groups in the polylysine dendron head were included in the calculation. Hence, for G1-C16 (**4.6**) and G1-C18 (**4.7**) having four free amine groups the total M_w was calculated by including four TFA molecules. The estimated aggregation numbers for G1-C16 and G1-C18 were 33 ± 5 and 35 ± 5, respectively (Table 4.3). The

large error bars indicated in Table 4.3 are due to the uncertainty of the exact number of counterions associated with each dendron. In addition, the employed density may be slightly overestimated. A larger number of counterions and a lower density would reduce the aggregation number. And so, the error bars were calculated by including five TFA molecules per dendron and taking a lower value for the density (0.9 g/cm^3). The estimated aggregation numbers for G1-C16 and G1-C18 (i.e., 33 and 35) are markedly smaller than what is generally seen with smaller amphiphiles, e.g., micelles (ca. 2 nm) formed by sodium dodecyl sulfate (SDS) having an aggregation number of around 60.[110] Nevertheless, this was expected since the sulfate head group in SDS is much smaller than the bulky polylysine head group (Fig. 4.5).

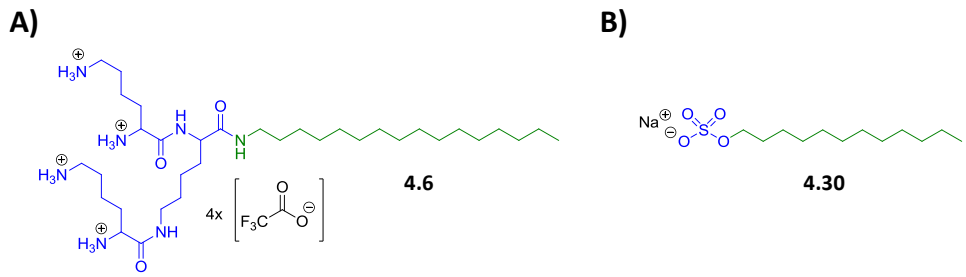

Figure 4.5 Molecular structures of the (A) G1-C16 dendron (**4.6**) and (B) SDS detergent (**4.30**) comparing the size of the head groups. Green: hydrophobic alkyl tail. Blue: head group. Black: counterions.

A G1(acetyl)-C16 dendron (**4.11**) was examined in order to explore the effect of charges in the head groups towards the dendrons ability to self-assemble into micelles. Compared to the four protonated amino groups in G1-C16 (**4.6**), the G1(acetyl)-C16 dendron has only two protonated amines thereby reducing the Coulombic repulsion between dendron head groups in the micellar shell. Comparing the SANS data of G1-C16 and G1(acetyl)-C16 it is evident that a reduced charge in the dendron head group has a stabilizing effect of the micelle formation (Fig. 4.6).

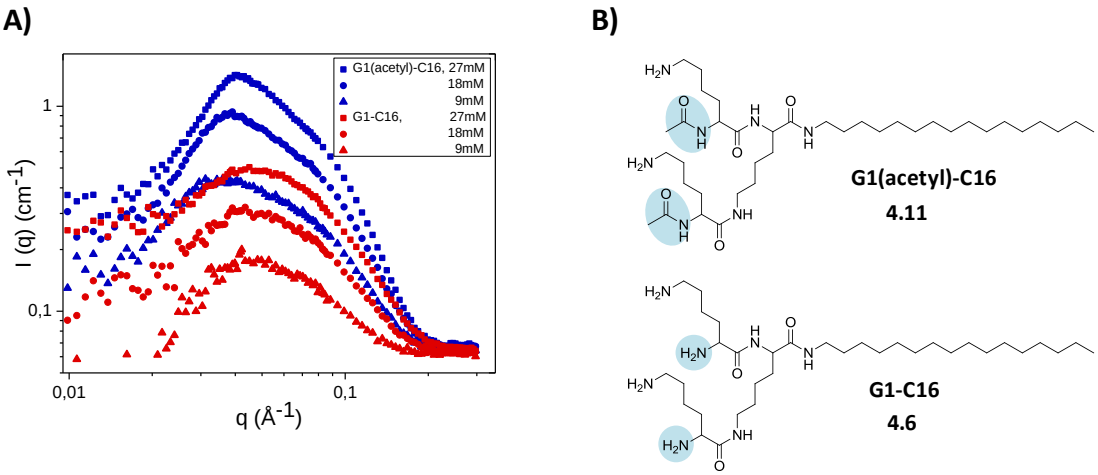

Figure 4.6 (A) Comparison of SANS scattering data from G1(acetyl)-C16 (blue) and G1-C16 (red). (B) Molecular structures of G1(acetyl)-C16 (**4.11**) having two free amine groups and G1-C16 (**4.6**) having four free amine groups with head group differences marked by blue circles.

The correlation peaks for the less charged G1(acetyl)-C16 are more established and narrower with an increased scattering intensity compared to G1-C16 revealing a well-defined average distance between the micelles (Fig. 4.6). Therefore, it is likely that the increased positive charge in the head group of G1-C16 has a stronger repulsive effect in the micellar shell thereby working against the formation of stable micelles (Fig. 4.7).

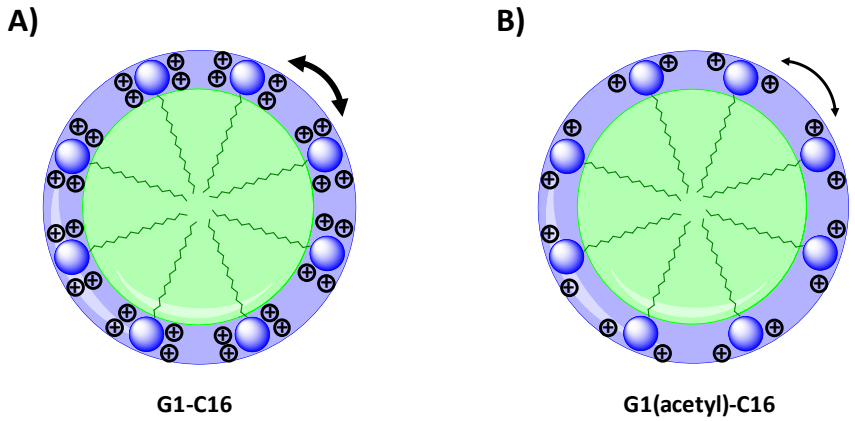

Figure 4.7 Schematic illustration of the effect of repulsive head groups in the micellar shell of (A) G1-C16 vs. (B) G1(acetyl)-C16. A stronger repulsion (bold arrow) is seen for G1-C16 compared to G1(acetyl)-C16.

The thickness of the shell obtained by fitting the scattering data by the core-shell model for G1(acetyl)-C16 showed to be similar (ca. 1 nm) as for G1-C16 and G1-C18 when comparing at the same concentrations (27 mM). This was expected, since the size of the polylysine head group does not change (i.e., G1) and apparently partial acetylation of the α-amino groups in G1(acetyl)-C16 does not have a noteworthy impact on the shell thickness. Furthermore, the thickness of the micellar shell remains nearly constant for G1(acetyl)-C16 at increasing concentrations (Table 4.4).

Table 4.4 Fitted parameters for G1(acetyl)-C16 from the core-shell particle model with a repulsive term.

#	Compound	Conc. [mM]	Radius[a] (core) [nm]	Thickness[a] (shell) [nm]	Radius[a] (total) [nm]	Charge[b] [+]	*N*(agg)
4.11	G1(acetyl)-C16	9	1.34	1.25	2.59	10	47
		18	1.57	1.17	2.74	15	55
		27	1.67	1.13	2.80	16	59

[a] Error ± 0.02nm. [b] Error ± 0.5 *e*.

The core radius and the total radius of the micelles increase slightly at higher concentrations and are also somewhat higher compared to G1-C16 at the same concentration (27 mM), i.e., a core radius of 1.7 nm vs. 1.2 nm and total radius of 2.8 nm vs. 2.4 nm. The increased core radius and total radius with higher concentrations is indicative of more dendrons being incorporated into each micelle and is also demonstrated by the increased aggregation number and effective charge (Table 4.4).

To examine the effect of the alkyl chain length and generation number towards the dendrons micelle forming ability, SANS data were collected for several dendrons having short alkyl chains including G2 dendrons (Fig. 4.8).

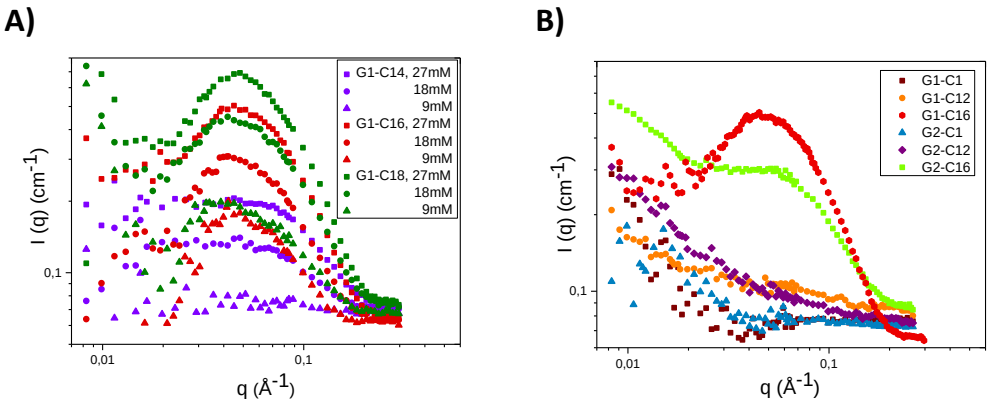

Figure 4.8 SANS scattering data for (A) G1-C14, G1-C16 and G1-C18 at different concentrations and (B) G1 and G2 dendrons with different alkyl chain lengths at a concentration of about 20 mg/mL.

A noticeable difference is observed between the SANS scattering profiles of G1-C14, G1-C16 and G1-C18 at different concentrations. It is apparent that concentration effects are the strongest for G1-C14, where the correlation peak is practically absent for the lowest concentration (9 mM) and gradually more present with increasing concentrations (Fig. 4.8A). In contrast, correlation peaks are seen at all concentrations for G1-C16 and G1-C18 showing to be strongest for the latter. It is assumed that at higher concentrations the dendrons are pushed towards forming micelles, since more dendrons are available for self-assembly. As a result, the intensity of the correlation peak tends to increase with higher concentrations and micelles can form at even low concentrations, when the alkyl chain is sufficiently long (i.e., C16 and C18) (Fig. 4.8A).

Comparing the scattering from different generations (i.e., G1-C16 and G2-C16) at a concentration of about 20 mg/mL, it seems the larger head group in G2-C16 interferes with the formation of micelles, since the correlation peak is quite different with respect to G1-C16 (Fig. 4.8B). Furthermore, only very weak scattering is seen for G1-C1/C12 and G2-C1/C12 indicating no micelle formation, presumably due to the short alkyl chains (Fig. 4.8B). Therefore, the overall results indicate that the ability to form stable micelles may be a function of both the size of the head group and alkyl chain length with the best results obtained for G1 dendrons having an alkyl chain length of C14 and above.

4.4 Dendron self-assembly studied by dynamic light scattering

The self-assembling behavior of the dendrons as a function of generation number and alkyl chain length was further analyzed by DLS to obtain information on a more global scale compared to the mesoscopic size information obtained by SANS. Additionally, the effects of concentration, temperature and pH on the self-assembling behavior were examined on selected dendrons.

The concentration effects were examined on the G2-C12 and G2-C16 dendrons at 4, 9 and 18 mM to see if this would have an effect on the size of the assemblies. The autocorrelation functions were fitted by a stretched exponential with only one relaxation mode (Eq. 4.8). The hydrodynamic

diameters (d_h) remained constant with increasing concentrations and were found to be 95 and 65 nm for G2-C12 and G2-C16, respectively (Fig. 4.9).

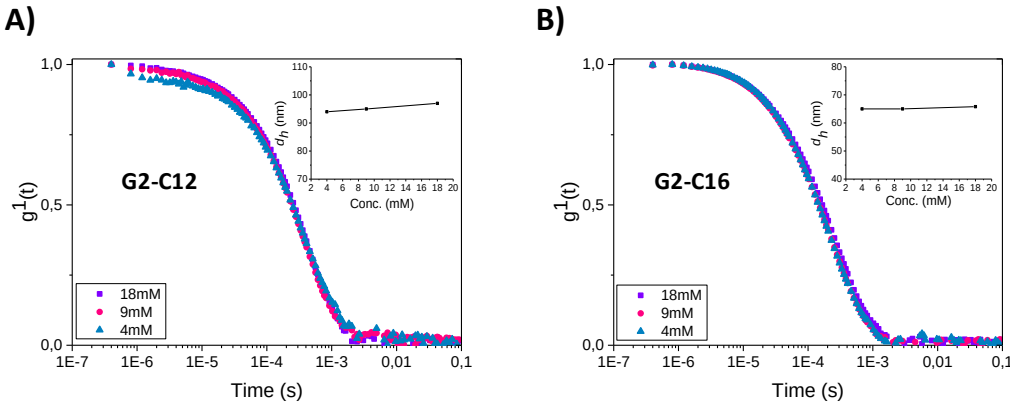

Figure 4.9 Autocorrelation functions plotted against time for different concentrations of (A) G2-C12 and (B) G2-C16 dendrons at 25°C and pH 3-5 with the hydrodynamic diameter indicated in the insets.

The much larger sizes found by DLS indicate the presence of large assemblies presumably formed by many micelles colliding and clustering together due to electrostatic interactions between positively charged amines in the head groups and TFA counterions (Fig. 4.10A). For dendrons not showing micelle formation by SANS (i.e., below C14) these large entities observed by DLS presumably are formed by random assemblies due to the hydrophobic interactions of the alkyl chains (Fig. 4.10B). In solution, these alkyl chains are not expected to be fully extended and therefore can adopt many dynamic conformations resulting in random assemblies.

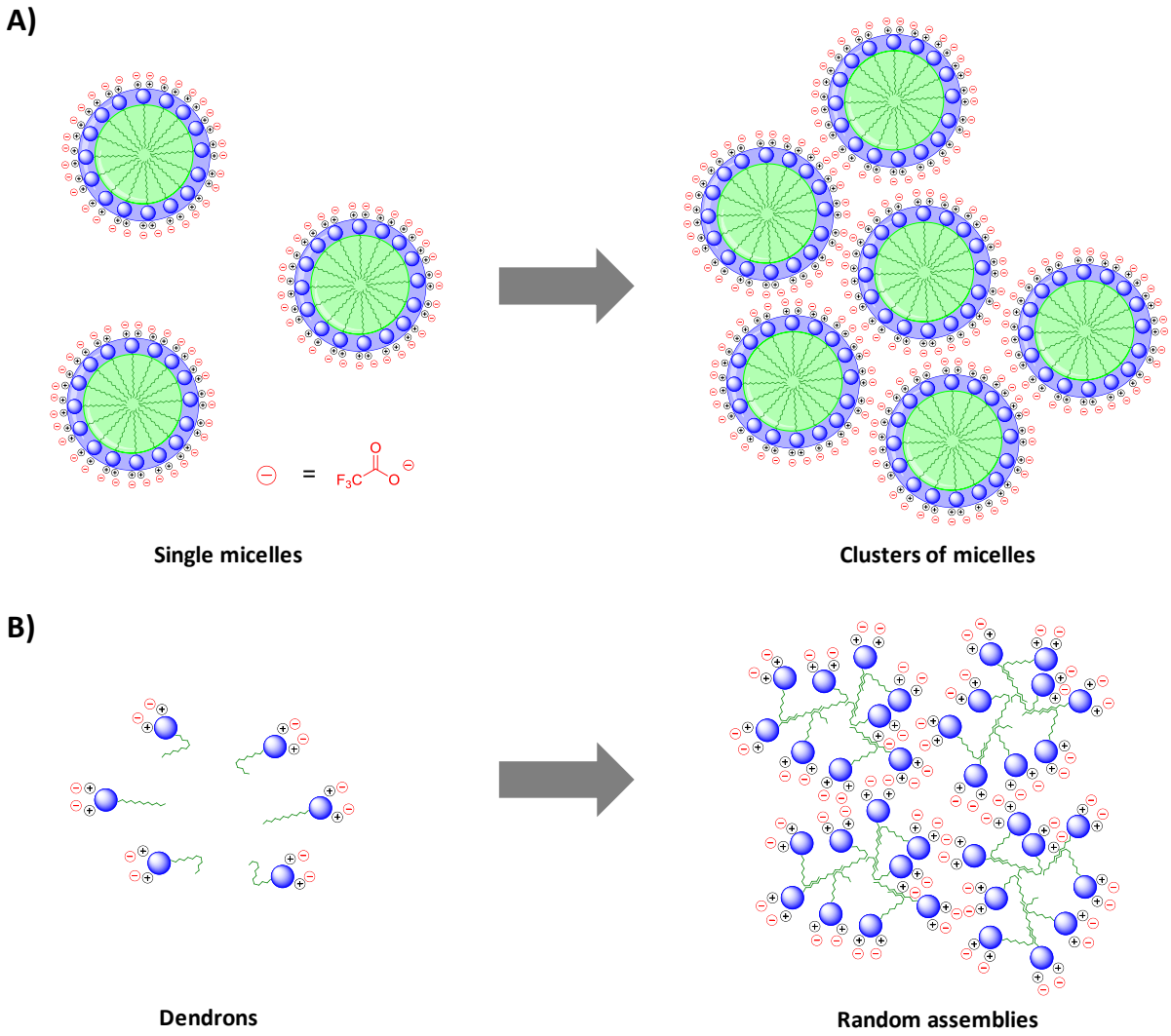

Figure 4.10 (A) Illustrative example of single micelles (observed by SANS) forming clusters of micelles (observed by DLS) due to electrostatic interactions between positively charged head groups and negatively charged TFA counterions. (B) Illustrative example of dendrons forming random assemblies, which is only observed by DLS.

The temperature effect was examined for several dendrons (i.e., G1-C8, G1-C16, G1(acetyl)-C10, G1(acetyl)-C16, G2-C12 and G2-C16) at a concentration of 18 mM, and no influence of temperature on the sizes of the clusters was observed (see Fig. 4.11 for selected examples).

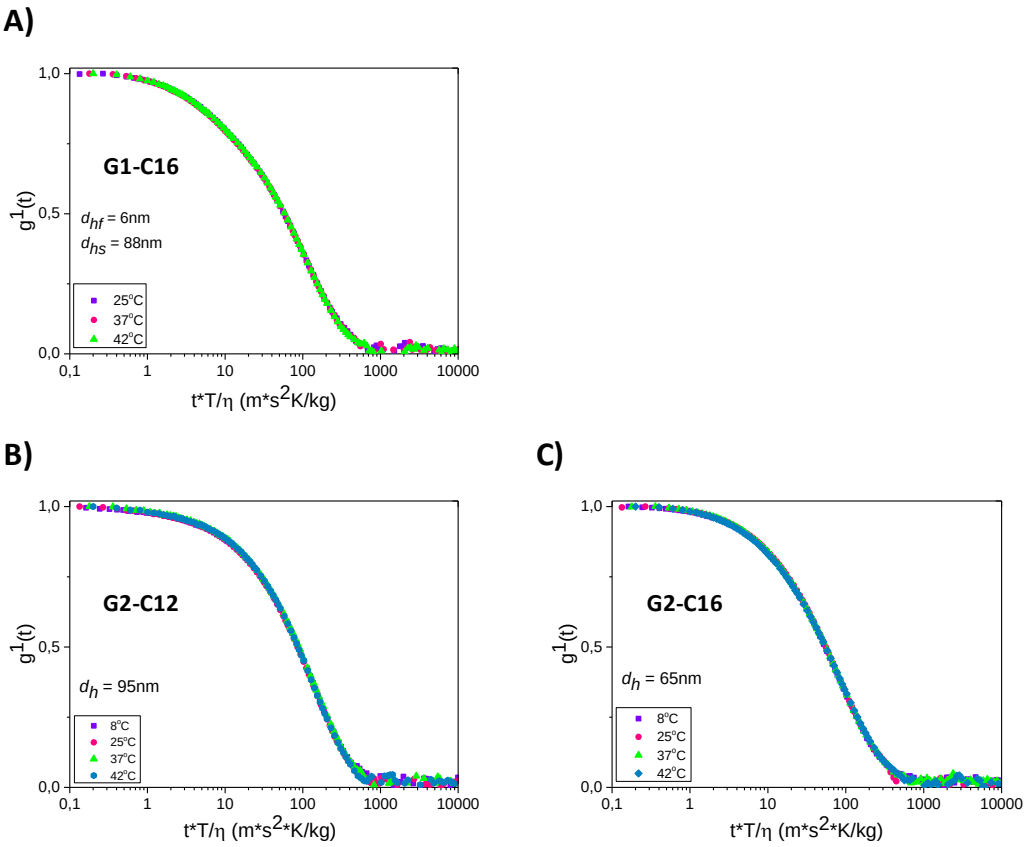

Figure 4.11 Autocorrelation functions at different temperatures plotted against $t \cdot T/\eta$ for (A) G1-C16, (B) G2-C12, (C) G2-C16 at a concentration of 18 mM.

The autocorrelation functions are plotted against $t \cdot T/\eta$ in order to remove temperature dependent viscosity changes of the solvent (Fig. 4.11). The autocorrelation function for G1-C16 showed a bimodal behavior and was fitted with Eq. 4.10 giving hydrodynamic diameters for single micelles (d_{hf} = 6 nm, corresponding well with SANS results) together with clusters of micelles (d_{hs} = 88 nm). The autocorrelation functions for G2-C12 and G2-C16 showed unimodal behaviors as before and were fitted by Eq. 4.8 with no change in the observed sizes (Fig. 4.11). The explanation for the difference in self-assembling behavior observed between G1-C16 and G2-C12/C16 (i.e., bimodal vs. unimodal) is uncertain. Presumably the bulky head groups in the G2-C12 and G2-C16 are more prone to form clusters of random self-assemblies or micelles, respectively. The lack of temperature effects indicate that hydrogen bonds are not essential for the formation of clusters, since these would be broken at the high temperatures employed resulting in a decrease in the size of the assemblies. Since also no concentration effects were observed, the formation of large clusters seem to be determined by other forces and are not dependent on hydrophobic interactions or hydrogen bonds.

To examine the pH effect towards self-assembling behavior, G2-C16 was chosen and studied at pH 5, 7.4 and 9 in a phosphate buffered saline (PBS) solution. At pH 5 the dendron was solvated and

showed aggregation with increased size of the micellar clusters (212 nm) compared to the size measured at pH 4 (117 nm) (Fig. 4.12).

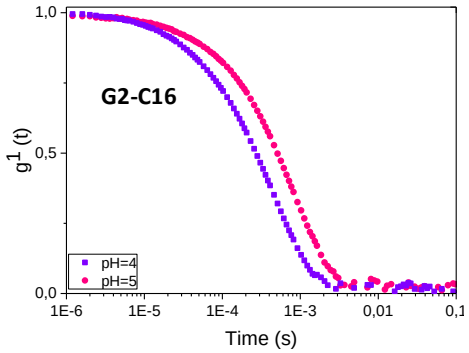

Figure 4.12 Autocorrelation functions of G2-C16 against time at pH 4 and 5 in a phosphate buffered saline solution measured at 25°C demonstrating an increased size at pH 5.

pH 7.4 and 9 led to macroscopic phase separation (precipitation) with the hydrophobic alkyl chains being shielded from the aqueous solution to minimize water exposure. This is a result of the removal of positive charges on the amine head groups at higher pH values making electrostatic forces ineffective. Therefore, it seems that an acidic pH is important for self-assembly confirming the assumption that micellar clusters are formed by electrostatic interactions between positively charged amine groups and negatively charged TFA counterions (Fig. 4.10A).

DLS measurements of the rest of the dendrons showed no self-assembling behavior for dendrons with alkyl chain lengths below C8 and the samples showed to be reasonably monodisperse (β = 0.8-1.0). Since only micelles were observed by SANS for dendrons having alkyl chain lengths above C12, the large entities observed for these dendrons by DLS presumably are due to random assemblies as mentioned above. G1-C12 did not show any self-assembly by DLS, which came as a surprise, since dendrons with shorter alkyl chains were showing self-assembling behavior (i.e., G1-C8 and G1(acetyl)-C10). In an attempt to explain this observation the zeta potentials (charge densities) were measured on all dendrons ranging from 11 mV to 55 mV. However, no clear correlation could be determined between zeta potentials and the dendrons self-assembling abilities. The hydrodynamic diameters of the assemblies for G1-C8/C14/C16/C18, G1(acetyl)-C10/C16 and G2-C12/C16 ranged from 65 nm to 370 nm (Fig. 4.13).

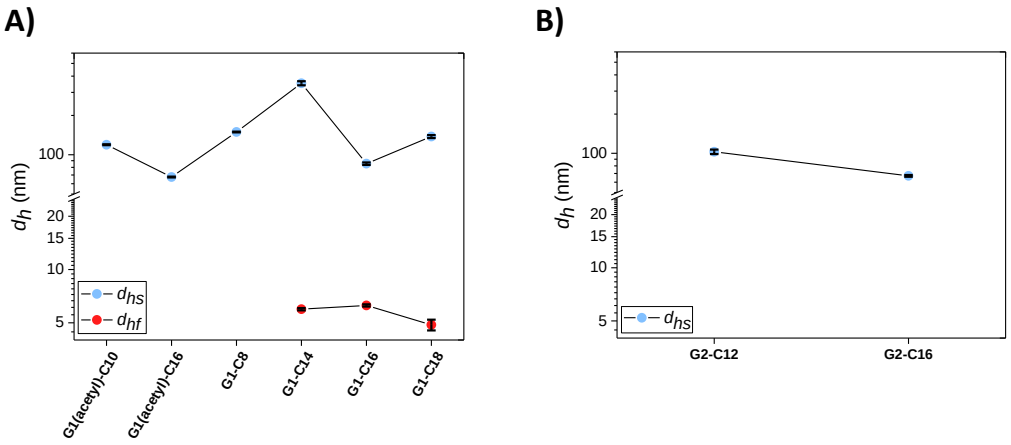

Figure 4.13 The hydrodynamic diameters (d_h) obtained by DLS for (A) G1 and (B) G2 dendrons with error bars.

Only G1-C14, G1-C16 and G1-C18 showed bimodal behaviors having single micelles coexisting with clusters of micelles. The sizes of single micelles measured by DLS for these dendrons ranged from 4-6 nm corresponding well with SANS results. The highest hydrodynamic diameter was observed for G1-C14 showing micellar clusters of 370 nm, whereas G1-C16 and G1-C18 yielded hydrodynamic diameters of 88 nm and 133 nm, respectively (Fig. 4.13A). G1(acetyl)-C16 showed a unimodal behavior, even though micelles were detected by SANS indicating the coexistence of single micelles with clusters of micelles as for G1-C14/C16/C18 (Fig. 4.13A). This may be due to the fast relaxation mode (due to single micelles) in the autocorrelation function having small amplitude compared to the slow mode (due to clusters of micelles) thereby making it undetectable during the fitting procedure. The reason for the decrease in the hydrodynamic diameter, when going from G2-C12 to G2-C16 is not clear (Fig. 4.13B), but could be attributed to a decreased efficiency in packing longer alkyl chains in the interior of the assemblies resulting in fewer dendrons in each micelle, which in turn reduces the overall size of the micellar clusters. However, one could also argue for an increased efficiency in packing the more hydrophobic C16 alkyl chains in the interior of each micelle leading to more compressed micelles and micellar clusters in contrast to the less hydrophobic C12. Moreover, the observation could also be ascribed to G2-C12 forming random assemblies, whereas G2-C16 forms clusters of micelles and therefore is more vulnerable to steric effects. The random assemblies formed by G2-C12 dendrons may have a higher packing efficiency, since they are not already organized in micelles. This makes G2-C12 dendrons more flexible with higher degrees of freedom to form closely packed assemblies.

4.5 Test of dendron toxicity

The cytotoxicity profile of dendritic structures is mainly determined by their surface functionalities and size. As dendritic structures can be synthesized in a controllable manner, the surface groups can easily be modified to obtain the desired biological properties. Dendritic structures with cationic surface functionalities (e.g., amine groups) are generally cytotoxic due to interaction and disruption of the negatively charged surface groups on the cell membrane. Consequently, higher generation (above G5) dendritic structures with an increased number of cationic surface groups will tend to

show increased cytotoxicity compared to lower generations. The degree of substitution on the nitrogen has an effect on the cytotoxicity profile, i.e., primary amines are more toxic than secondary and tertiary amines. Hence, removal of the positive charge by acylation and acetylation will generally result in a decreased cytotoxicity. In addition, cytotoxicity is also observed with dendritic structures containing lipid groups possibly due to hydrophobic interactions with the cellular lipid membrane resulting in membrane disruption and cell lysis.[12,91]

The *in vitro* cytotoxicity of selected dendrons was evaluated on mouse fibroblast (NIH/3T3) and human embryonic kidney (HEK 293T) cells in order to explore the biocompatibility by comparing alkyl chain lengths and generation numbers. NIH/3T3 cells were chosen as a common model for connective tissues in the body. HEK 293T cells were chosen as a chemical sensitive model, since the kidney is the main site for excretion of drugs and their metabolites and therefore a major target for organ damage caused by drug toxicity.[111-113] The cytotoxicity was measured by determining the number of viable cells in the culture. A commercially available colorimetric solution containing a tetrazolium compound (MTS, [3-(4,5-dimethylthiazol-2-yl)-5-(3-carboxymethyoxyphenyl)-2-(4-sulfophenyl)-2*H*-tetrazolium][114]) and an electron coupling reagent (phenazine ethosulfate [PES]) was employed. The enzymatic reduction of MTS to a colored formazan occurs in the cytoplasm or mitochondria of metabolically active cells due to the presence of reducing cofactors, i.e., NADH/NADPH (Scheme 4.2). Hence, the amount of formazan measured by UV absorbance at 490 nm is directly proportional to the number of viable cells in the culture.[115,116]

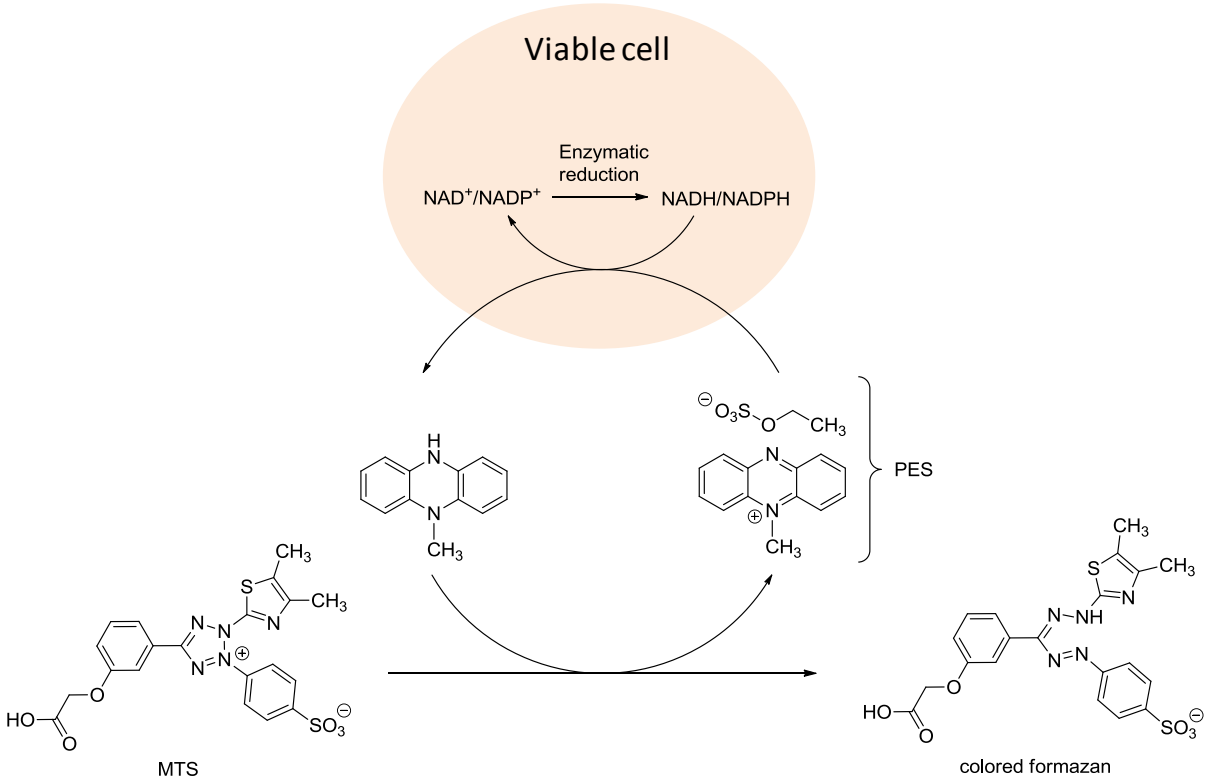

Scheme 4.2 Enzymatic reduction of MTS to a colored formazan by metabolically active cells.

The concentrations chosen for the cytotoxicity experiments were inspired from results published by Ma *et al.*[67] Herein, seven G2 polylysine dendrons modified with propargyl at the C-terminal were conjugated to a β-cyclodextrin through triazole linkages and evaluated in human breast cancer (MCF-7) cells. Ma and co-workers did not observe any cytotoxicity at concentrations up to 6.3 µM (50 µg/mL), hence concentrations of 5, 10 and 20 µM (corresponding to 2-23 µg/mL) were chosen for the much smaller alkyl chain modified G1 and G2 polylysine dendrons.

G1 dendrons with four cationic primary amine groups were expected to show higher cytotoxicity relative to partially acetylated G1 dendrons having only two cationic primary amine groups. In addition, the cytotoxicity was expected to increase with higher dendron concentrations (see above). However, the G1 dendrons displayed similar biocompatibilities and where not cytotoxic for NIH/3T3 and HEK 293T cell lines at the employed concentrations (Fig. 4.14).

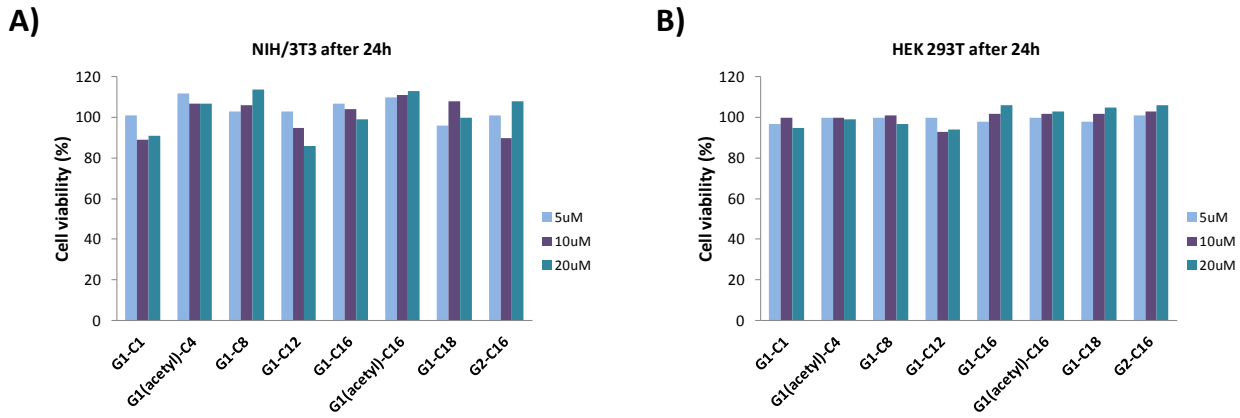

Figure 4.14 Cell viability of (A) NIH/3T3 and (B) HEK 293T cells relative to untreated control cells. The cell viability was assessed by an MTS assay after treating the cells with G1 and G2 dendrons at 5, 10 and 20 µM concentrations. The standard deviation was calculated to be less than 0.05 and 0.01 for NIH/3T3 and HEK 293T cells, respectively.

G2-C16 was selected as representative for evaluation of the cytotoxicity of G2 dendrons at the three chosen concentrations. An increased cytotoxicity was expected when going from a G1 to a G2 dendron, since the number of cationic primary amines would double (i.e., G1-C16 vs. G2-C16). As for G1 dendrons, also here a higher cytotoxicity was expected at elevated concentrations. However, no cytotoxicity was observed for the G2-C16 dendron displaying similar biocompatibility profile as seen for the other dendrons (Fig. 4.14). Hence, the dendrons showed to be quite biocompatible at concentrations up to 20 µM showing cell viabilities above 80%.

Literature search of *in vitro* cell viability studies on dendritic structures based on polylysine yielded some interesting findings. A cationic amino terminated G6 polylysine dendron consisting of 63 lysine residues, 64 primary amine groups and a glycine residue at the C-terminal was reported by Al-Jamal *et al.* for the study of intrinsic fluorescence.[117] Contrary to what is typically expected with higher generations and increased number of amino surface functionalities, no cytotoxicity was observed at dendron concentrations below 614 µM (5 mg/mL) in human epithelial cells (Caco-2). Conversely, in a different study regarding antiangiogenic properties Al-Jamal *et al.* observed a 51-

fold higher cytotoxicity of an identical dendron in murine endothelial cells (SVEC4-10), where concentrations above 12 µM (0.1 mg/mL) were cytotoxic.[42] These results are quite fascinating considering the presence of a high amount of cationic amino groups and clearly show the importance of choosing two or more cell lines for cytotoxicity evaluations. The cytotoxicity of a G3 polylysine dendron with a methyl ester at the C-terminal (having 15 lysine residues and 16 surface amino groups) was investigated in Caco-2 cells by Avaritt *et al.* and showed to be non-toxic at concentrations below 100 µM (2 g/mL).[118] Comparing the results obtained by Al-Jamal and Avaritt for Caco-2 cells it is somewhat puzzling that the cytotoxicity seems to decrease with higher generations, even though the two results cannot be completely compared due to different C-terminal functionalities (glycine vs. methyl ester). As an example of polylysine dendrons with lipid functionalities it is worth to mention the findings of Azmi and co-workers.[44] A series of short cationic lipopetides were investigated for antibacterial purposes including two G1 polylysine dendrons (three lysines) with one (**4.31**) or two (**4.32**) 12-carbon atom lipidic α-amino acids at the C-terminal and two or four primary amino groups, respectively (Fig. 4.15). The cell viability tests were carried out on HEK293T (human embryonic kidney cells) and HepG2 (human liver hepatocellular carcinoma cells). The cytotoxicity was reported as the CC_{50} value (cytotoxic concentration causing death to 50% of viable cells) and was above 15 µM (corresponding to 10.2 or 11.9 mg/mL for a G1 dendron with one or two lipidic α-amino acids, respectively).[44] Hence, a low generation dendron modified with one or more lipid functionalities can exhibit increased cytotoxicity compared to higher generations without lipid groups. This can be attributed to hydrophobic interactions with the cell membrane as mentioned above.

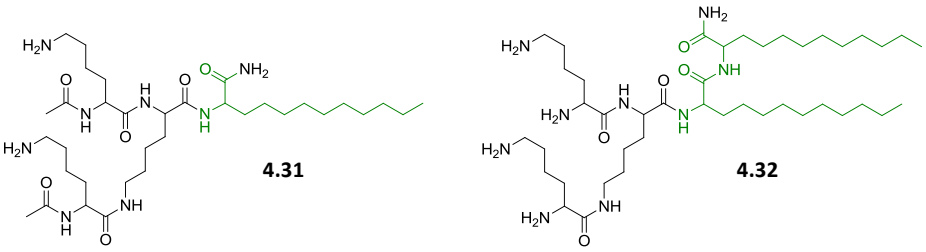

Figure 4.15 G1 polylysine dendron with one (**4.31**) or two (**4.32**) 12-carbon lipidic α-amino acids at the C-terminal (green).

The examined G1 and G2 polylysine dendrons in this project did not seem to show cytotoxicity up to 20 µM (cell viability above 80%), whereas the G1 polylysine dendrons (Fig. 4.15) reported by Azmi *et al.*[44] exhibited higher cytotoxicity at lower concentrations (i.e., concentrations above 15 µM showing cell viability below 50%).

4.6 Conclusion

A library of G1 and G2 polylysine dendrons modified with different alkyl chain lengths at the C-terminal were successfully synthesized by SPPS employing the backbone amide linker approach. The synthesized dendrons had amphiphilic properties due to the hydrophilic polylysine head groups and hydrophobic alkyl chain. Therefore, they were hypothesized to behave like surfactants and self-

assemble into micelles. The self-assembling hypothesis was proven by SANS revealing micellar structures with the hydrophobic interior consisting of alkyl chains and hydrophilic shell consisting of polylysine head groups. The observed micelles were around 5 nm in diameter, which corresponds to two dendrons spanning the diameter and a rough calculation of the number of G1 dendrons per micelle showed to be around 33-59. A correlation was observed between the length of the alkyl chain and the ability of dendrons to self-assemble into micelles. Dendrons with alkyl chain lengths below C14 were not able to form micellar structures. Furthermore, the amount of positively charged amine groups in the polylysine head groups seemed to have an effect on the stability of the micelles. Reducing the number of positively charged amines in the head groups seemed to have a stabilizing effect on micelle formation (G1-C16 vs. G1(acetyl)-C16) presumably due to the reduction of electrostatic repulsion in the micellar shell. In addition, the size of the polylysine head group appeared to be an important factor for successful micelle formation. The bulky head group in a G2 dendron seemed to have an impaired effect on the micelle formation resulting in less stable micelles compared to the corresponding G1 dendron. Further investigation of the self-assembly by DLS demonstrated much larger entities with sizes ranging from 65-370 nm. For dendrons observed to self-assemble into micelles by SANS (i.e., alkyl chain lengths above C12) these larger entities were presumed to be attributed to micellar clusters held together by electrostatic forces. However, large entities seen by DLS for dendrons with alkyl chain lengths below C14 were presumed to be due to random assemblies that may be formed by hydrophobic interactions between the alkyl chains. Finally, the cytotoxicity of the dendrons was investigated in NIH/3T3 and HEK 293T cells and they exhibited biocompatibility up to a concentration of 20 μM (cell viability above 80-90%). Hence, these polylysine dendrons are excellent systems for biomedical applications through further modification with relevant surface motifs at the N-terminal.

5 Synthesis of dendrons modified with PAMP motifs and preliminary tests

This chapter describes the synthesis of two small libraries of G1 and G2 polylysine dendrons containing a multivalent presentation of PAMP motifs on the N-terminal surface and a C-terminal C1 or C16 alkyl chain. Furthermore, preliminary results from immunological cell culture studies for the exploration of immunostimulatory properties of the dendrons as a function of multivalency and alkyl chain are also discussed. The preliminary immunological cell culture studies were performed by Postdoc Julia Hütter and Senior Researcher Katharina Lahl at the Section for Virology, National Veterinary Institute, Technical University of Denmark.

5.1 Synthesis of dendron libraries containing PAMP motifs

The G1 and G2 polylysine dendron libraries containing multivalent presentations of PAMP motifs were prepared by stepwise divergent SPPS through the backbone amide linker approach (Chapter 2). The FMPB derivatized PS resin (**2.6a**) was prepared according to section 4.2 followed by C-terminal modification (i.e., C1 or C16) by reductive amination and employed for the synthesis of PAMP modified polylysine dendrons.

5.1.1 Muramyl dipeptide library

The muramyl dipeptide library was composed of a total of six G1 dendrons with a C-terminal C16 alkyl chain (Table 5.1). Three dendrons were synthesized with PAMP motifs (**5.2**, **5.3** and **5.4**) for evaluation of the multivalency effect towards activation of immune cells. Additionally, three dendrons were prepared without PAMP motifs (**4.6**, **4.11** and **5.1**) to examine possible intrinsic immunostimulatory properties.

Table 5.1 Synthesized polylysine dendrons with or without PAMP motifs.

#	Compound[a]	Yield[b] (%)
4.6	G1-PDL-C16	79
4.11	G1(acetyl)-C16	72
5.1	G1-C16	36
5.2	G1(^{D}isoGln-Ala)$_2$-C16	91
5.3	G1(MDP)$_2$-C16	20
5.4	G1(^{D}isoGln-Ala)$_4$-C16	15

[a] Nomenclature for synthesized dendrons. G*n*: generation number, PDL: poly-D-lysine. [b] TFA salt.

The secondary amine (**3.2**) was acylated with two equivalents of Fmoc-Lys(Fmoc)-OH (either the D or L enantiomers) employing DIC as the coupling reagent in a DCM/NMP (95:5) mixture (Scheme 5.1). The reaction completion was monitored colorimetrically by the acetaldehyde test giving a negative readout (colorless beads) (Chapter 3).

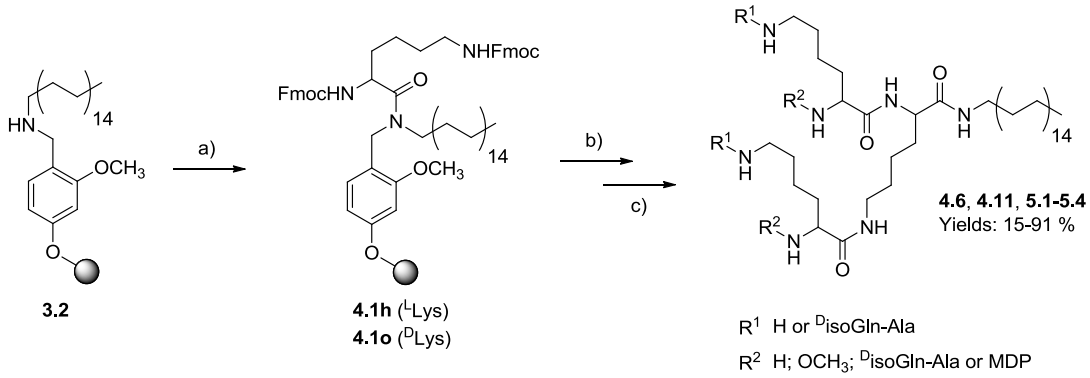

Scheme 5.1 Stepwise divergent SPPS of G1-C16 polylysine dendrons with/without PAMP motifs. The protected lysines employed were either solely the D or L enantiomers. (a) Fmoc-Lys(Fmoc)-OH, DIC, DCM/NMP (95:5), rt, 20 h or 2 + 2 h. (b) Fmoc deprotection between acylations: piperidine/NMP (1:4), rt, 3 + 30 + 20 (+ 30) min; linkage of second lysine group: Fmoc-Lys(Boc)-OH or Fmoc-Lys(Fmoc)-OH, PyBOP, DIPEA, NMP, rt, 3 h or 20 h or until negative ninhydrin test. (c) Fmoc deprotection between acylations: piperidine/NMP (1:4), rt, 3 + 30 + 30 + 20 min; R^1 = H and R^2 = H: TFA/DCM (1:1), rt, 2 h; R^1 = H and R^2 = OCH_3: acetic anhydride/DIPEA/DCM (10/5/85), rt, 3 h; TFA/DCM (1:1), rt, 2 h; R^1 = H or ^{D}isoGln-Ala and R^2 = ^{D}isoGln-Ala: amino acid, PyBOP, DIPEA, NMP, rt, 20 h; TFA/DCM (1:1), rt, 2 h; R^1 = H and R^2 = MDP: *N*-acetylmuramic acid, PyBOP, DIPEA, NMP, rt, 20 + 23 h (on resin derivatized with two α-amino ^{D}isoGln-Ala groups); TFA/DCM (1:1), rt, 2 h.

The resin loadings were determined as described in Chapter 2 and ranged from 0.19 to 0.25 mmol/g. The Fmoc protected amines on the employed amino acids were deprotected by 20 vol. % piperidine in NMP between each acylation step. The completion of Fmoc deprotections and acylation steps were monitored by the ninhydrin test.[51,52] As mentioned in section 4.2, the reliability of the ninhydrin test was low due to the long alkyl chain (C16). To ensure complete removal of Fmoc protecting groups, the original procedure was optimized to include an additional 30 min deprotection time after the linkage of the second lysine group. After attachment of the first lysine with DIC, all sequential acylations were performed with PyBOP as the coupling reagent together with DIPEA (Scheme 5.1). Generally, the acylation reactions were complete after 20 h employing two equivalents of amino acid, which were calculated using halved resin loadings (i.e., 1 mmol/g). However, acylation with *N*-acetylmuramic acid was not as straightforward and repeating the reaction 23 h still did not result in full conversion (see discussion below). Later it was found for dendron **5.4**, that even as low as one equivalent of amino acid after linkage of the second lysine was sufficient for a full conversion, since the amounts were based on 1 mmol/g loadings and well above the determined loadings (e.g. 0.19-0.25 mmol/g). For the synthesis of dendron **4.11**, the α-amino groups were acetylated with acetic anhydride and DIPEA before the final cleavage step. The target dendrons were cleaved from the resin by TFA/DCM (1:1) giving the dendrons in poor to good yields (Scheme 5.1) and the purities and structures confirmed by UPLC-MS and NMR.

Two equivalents of *N*-acetylmuramic acid (**5.5**, Ac-Mur) were employed for the preparation of dendron **5.3** (Scheme 5.2). After 20 h, the ninhydrin test showed a partially positive readout (pale purple supernatant). Therefore, the reaction was repeated an additional 23 h giving a negative ninhydin test.

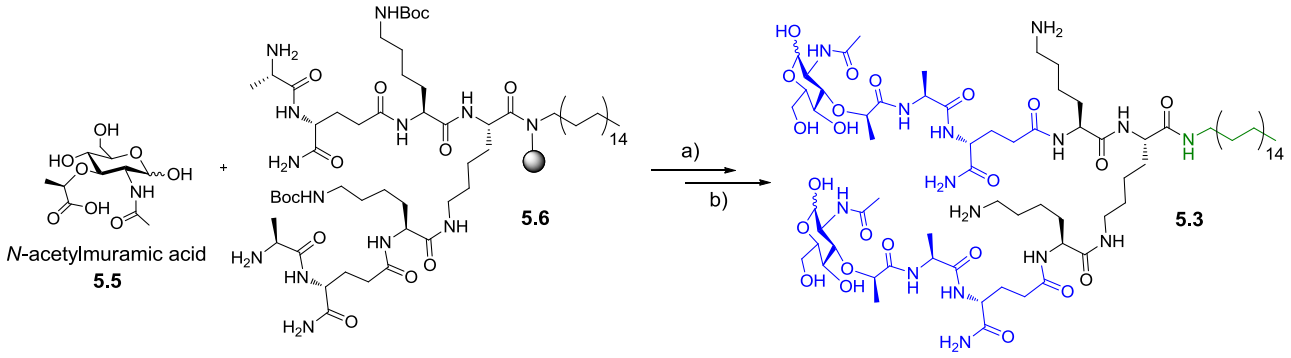

Scheme 5.2 Acylation of a ^{D}isoGln-Ala derivatized PS resin (**5.6**) with *N*-acetylmuramic acid (**5.5**) for the preparation of dendron **5.3** with two MDP motifs (blue) and a C16 alkyl chain (green). (a) PyBOP, DIPEA, NMP, rt, 20 h + 23 h. (b) TFA/DCM (1:1), rt, 2 h.

Even though the acylation reaction was repeated, a full conversion was not obtained. Three main peaks of similar intensities were observed for the crude product of **5.3** by UPLC-MS resulting from unsuccessful acylations with Ac-Mur. Peak 1 and 2 were due to deletions missing two or one Ac-Mur moieties, respectively, with peak 3 resulting from the target dendron (Fig. 5.1).

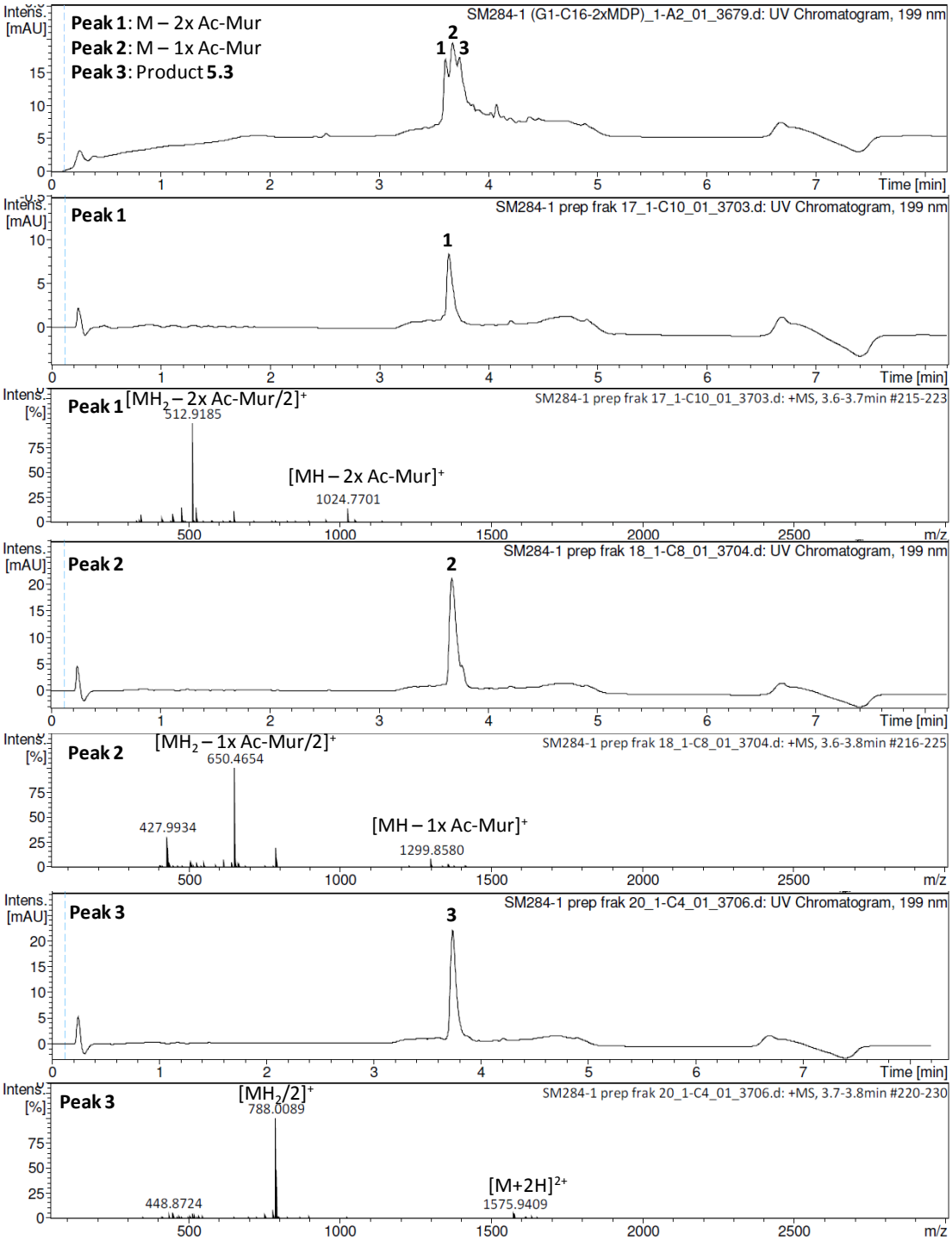

Figure 5.1 UV chromatogram of the crude product of **5.3** showing two deletion impurities (peak 1 and 2) together with the target product (peak 3) having similar intensities and UPLC-MS data of the three peaks after purification with preparative reversed-phase HPLC. Peak 1: dendron missing two Ac-Mur moieties. Peak 2: dendron missing one Ac-Mur moiety. Peak 3: target product (**5.3**).

An attempt to prepare a G1(MDP)$_4$-C16 (**5.8**) by the same procedure proved to be unsuccessful (Scheme 5.3) and UPLC-MS analysis revealed multiple peaks with very close retention times, which were difficult to identify (data not shown). Nevertheless, one peak was identified belonging to a deletion missing four Ac-Mur moieties (i.e., dendron **5.4**).

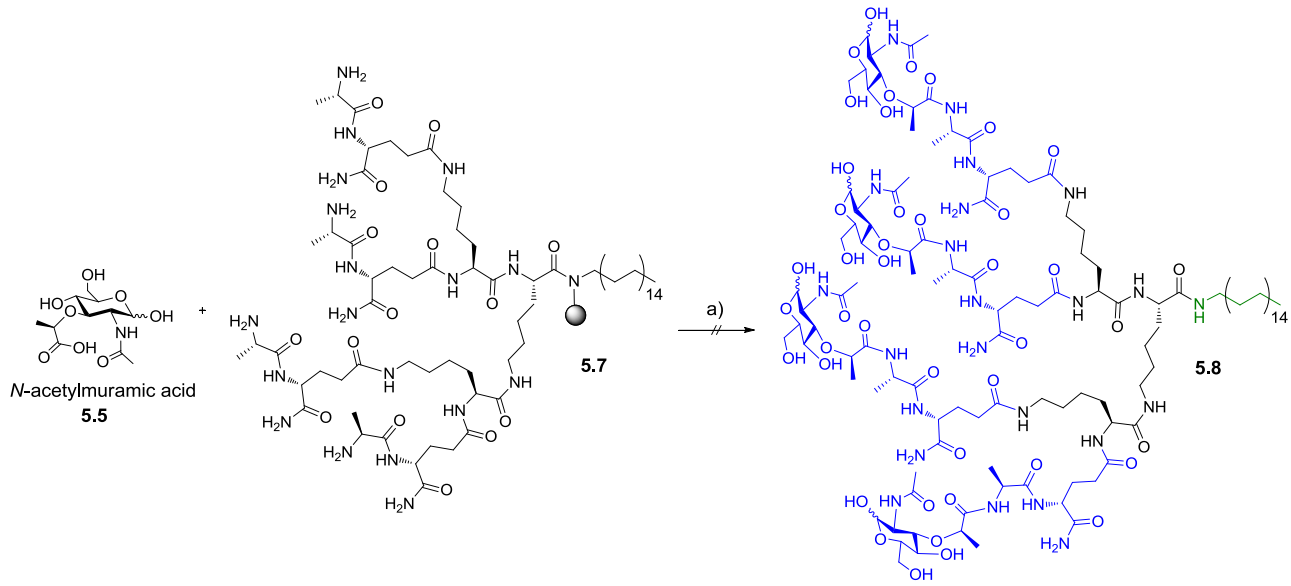

Scheme 5.3 Unsuccessful acylation of a ^{D}isoGln-Ala derivatized PS resin (**5.7**) with *N*-acetylmuramic acid (**5.5**) for the preparation of dendron **5.8** with four MDP motifs (blue) and a C16 alkyl chain (green). (a) PyBOP, DIPEA, NMP, rt, 20 h + 23 h; TFA/DCM (1:1), rt, 2 h.

One cause for the synthetic failure in preparing dendron **5.8** was reasoned to be due to steric effects. Dendron **5.8** was much more crowded compared to dendron **5.3**, which would make the primary amines less accessible for acylation with Ac-Mur (**5.5**). Four parallel reactions were performed in an attempt to address this issue (Table 5.2). The less sterically hindered HBTU was compared to PyBOP at room temperature and elevated temperatures in an attempt to drive the reaction to completion.

Table 5.2 Different acylation conditions examined for the preparation of G1(MDP)$_4$-C16 (**5.8**).

Entry	Coupling reagent	Temp.	Rx time	Ninhydrin test
1	HBTU	rt	21 h	(+) dark purple
2	HBTU	60 °C	21 h	(-) pale grey
3	PyBOP	rt	21 h	(+) dark purple
4	PyBOP	60 °C	21 h	(+) pale purple

From the ninhydrin tests it was apparent that HBTU was as ineffective as PyBOP at rt. Increasing the temperature to 60 °C appeared to have a positive effect (Table 5.2). However, a closer examination of the cleaved crude product showed similar UPLC-MS as before, albeit with the multiple peaks superimposing into a very broad peak (data not shown).

Since Ac-Mur (**5.5**) was employed with unprotected hydroxyl groups, the multiple peaks seen on UPLC-MS are likely due to side reactions arising from deprotonation and subsequent activation of the hydroxyl groups making them prone to nucleophilic attack. The pK_a values of the hydroxyl groups in D-glucose have been theoretically calculated and range from 14-20 for C1 (anomeric, highest acidity), C4 and C6.[119] Similar pK_a values can be expected for the hydroxyl groups of Ac-

Mur. Although DIPEA (pK_a of conjugate acid ~ 11[120]) preferably deprotonates the ether bound lactic acid group (pKa ~ 3.6[121]), deprotonation can still occur on the hydroxyl groups rendering them able to react with phosphonium or uronium reagents. In addition, it could be speculated that the nucleophilic ethanolates of Ac-Mur could react with another molecule of Ac-Mur yielding many possible side products. Therefore, it was decided to employ a hydroxyl protected derivative of Ac-Mur for the synthesis of G1(MDP)$_4$-C16 (**5.8**).

Acetyl groups are commonly employed protecting groups in carbohydrate chemistry, therefore they were the first choice of protecting groups for the hydroxyl functionalities in Ac-Mur. A general straightforward procedure involves treating the carbohydrate with acetic anhydride in pyridine.[122] Ac-Mur (**5.5**) was treated with 10 equiv. of acetic anhydride and pyridine per hydroxyl group at rt. for 23 h (Scheme 5.4).

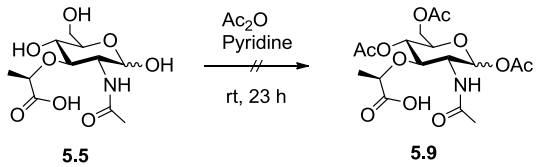

5.5 **5.9**

Scheme 5.4 Attempted acetylation of Ac-Mur (**5.5**) with acetic anhydride and pyridine for the preparation of 1,4,6-*O*-triacetyl-*N*-acetylmuramic acid (**5.9**).

UPLC-MS analysis showed the formation of a diacetylated derivative of Ac-Mur (**5.14**) and a dioxanone by-product (**5.13**) with a ratio of 2:3, respectively, obtained by integration of the UV chromatogram (Fig. 5.2).

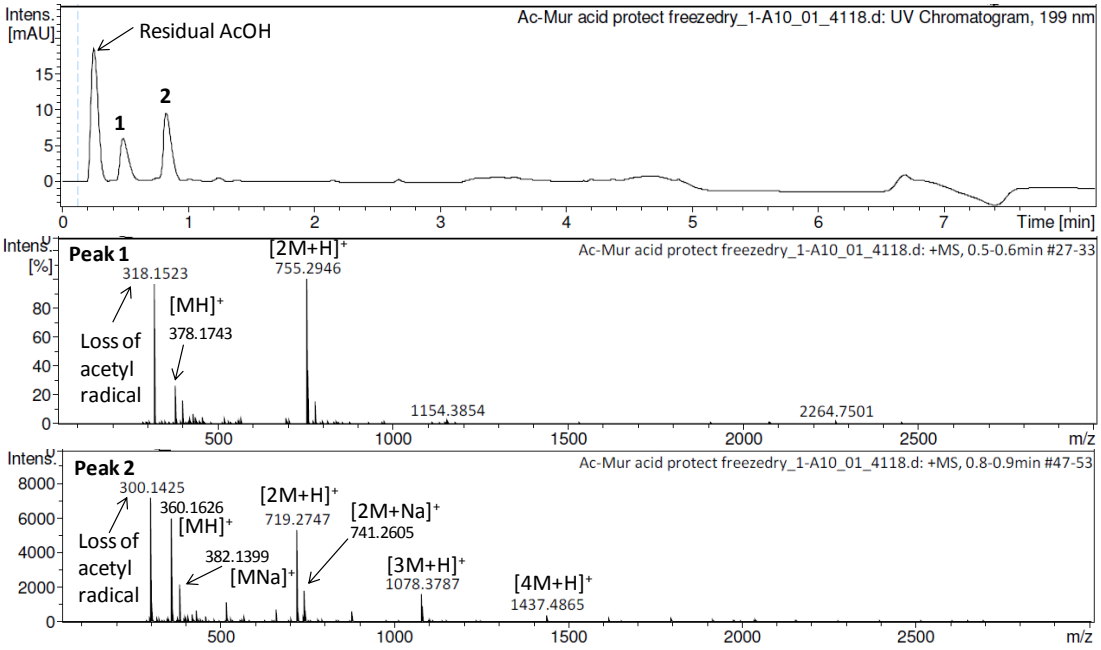

Figure 5.2 UPLC-MS analysis of the product mixture from the reaction between *N*-acetylmuramic acid (**5.5**) and acetic anhydride in the presence of pyridine. The hydrophilic peak is due to residual acetic acid (AcOH) after work-up and lyophilization. Peak 1 (diacetylated derivative of Ac-Mur, **5.14**) and peak 2 (dioxanone by-product, **5.13**) with a ratio of 2:3, respectively.

The dioxanone by-product (**5.13**) is presumably formed by an intramolecular ring closure of the ether bound lactic acid group, which may occur as proposed in Scheme 5.5. Since the ether bound lactic acid group contains the most acidic proton, it is most likely deprotonated first by pyridine (pKa = 5.2[60]) yielding an ether bound lactate intermediate (**5.10**), which can attack acetic anhydride forming an anhydride intermediate (**5.11**) prone to nucleophilic attack. The order of the next deprotonation steps is uncertain and most likely the anomeric hydroxyl will be deprotonated next, since it is the most acidic. However, for simplicity that is ignored in the proposed mechanism and the next deprotonation proposed to occur at the hydroxyl group adjacent to the ether bound lactic acid anhydride. The probability for the oxygen to make an intramolecular nucleophilic attack on the adjacent ether bound lactic acid anhydride to form a six-membered ring is higher than an intermolecular attack on acetic anhydride present in the reaction solution. Therefore, a dioxanone intermediate (**5.12**) is produced and further acetylation yields the dioxanone by-product (**5.13**) as observed by UPLC-MS. The diacetylated derivative of Ac-Mur (**5.14**), also observed by UPLC-MS, is formed by hydrolysis of the dioxanone by-product (**5.13**) in the presence of water in the reaction mixture, since the reaction was not performed under dry conditions (Scheme 5.5).

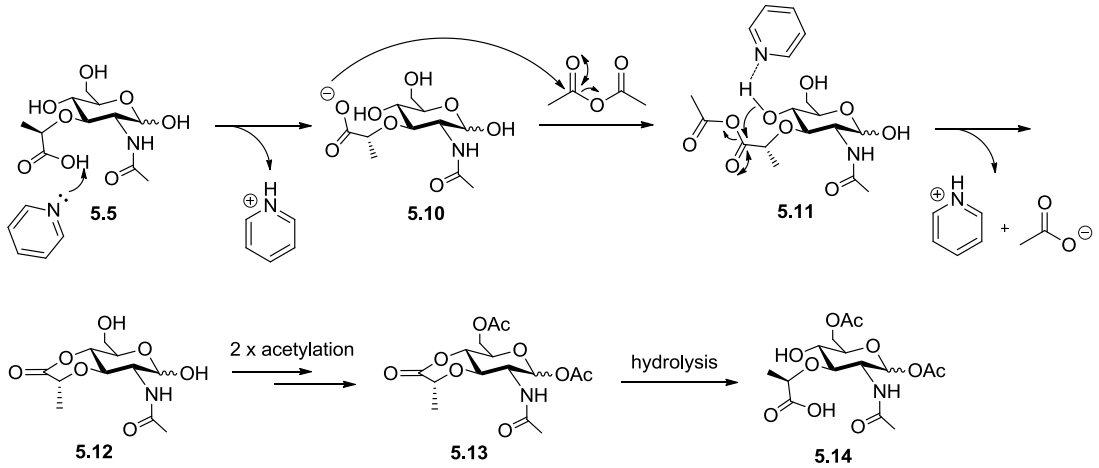

Scheme 5.5 Proposed mechanism for the formation of the dioxanone by-product (**5.13**) through an intramolecular ring closure of the ether bound lactate group and further hydrolysis to the diacetylated derivative of Ac-Mur (**5.14**).

Deng and co-workers reported sonication as a technique to enhance the efficiency (e.g., reduced reaction times, increased reactivity and stereoselectivity) of several carbohydrate reactions such as hydroxyl group protection by acetylation.[123] Therefore, sonochemistry was attempted in order to test whether that would drive the reaction towards the formation of the desired triacetylated Ac-Mur (**5.9**) product. The reaction mixture was sonicated for 20 min and reaction completion followed by TLC showing a single spot (developed with 4M H_2SO_4). However, further analysis by UPLC-MS showed a similar profile as before, albeit with the main peak being due to the dioxanone by-product (**5.13**) (Fig. 5.3).

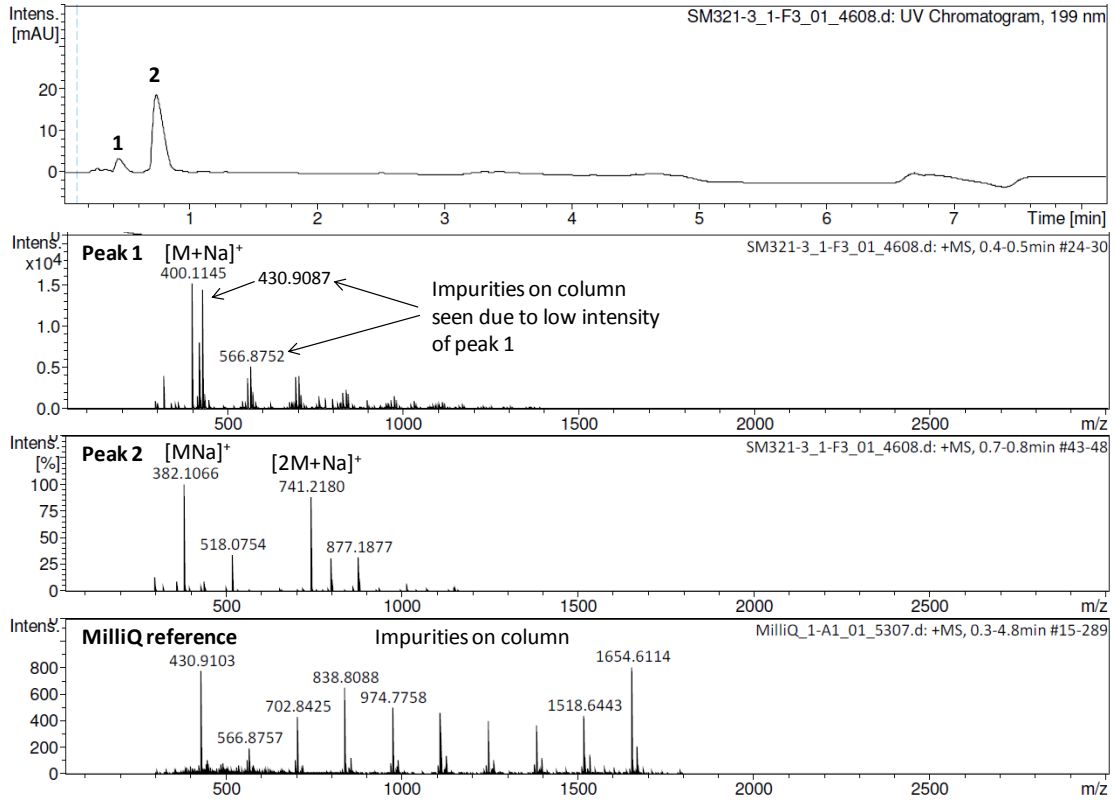

Figure 5.3 UPLC-MS analysis of the product mixture from the sonication reaction. Peak 1 (diacetylated derivative of Ac-Mur, **5.14**) and peak 2 (dioxanone by-product, **5.13**) with a ratio of 1:7.3, respectively. The MS spectrum arising from a MilliQ reference is also shown demonstrating impurities on the column, which can also be seen in the MS spectrum of peak 1 due its low concentration.

Formation of the dioxanone by-product (**5.13**) was further confirmed by ^{1}H-NMR showing both anomers (i.e., α anomer [51%] and β anomer [49%]) (Fig. 5.4A) and ^{13}C-NMR also confirmed the structure of the dioxanone by-product (Fig. 5.4B). The two anomeric peaks were assigned by consulting previously reported ^{1}H-NMR data from Ac-Mur and a derivative protected with a methoxy group at the anomeric carbon.[124-126]

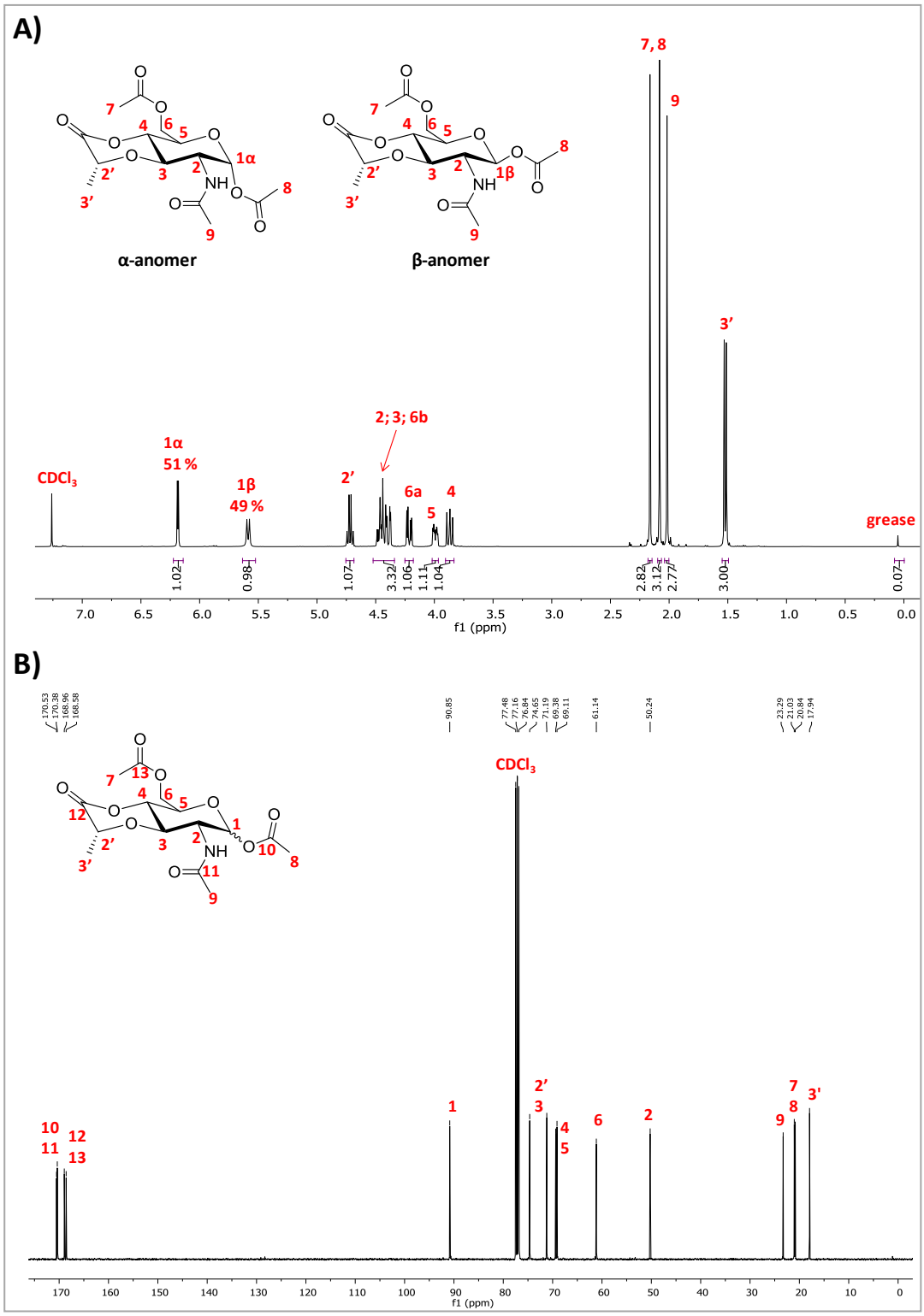

Figure 5.4 (A) ^{1}H-NMR (400 MHz, $CDCl_3$) obtained for the dioxanone by-product (**5.13**) showing 51% of the α-anomer and 49% of the β-anomer. (B) ^{13}C-NMR (101 MHz, $CDCl_3$) confirming the structure of the dioxanone by-product.

Therefore, it was realized that other protecting group strategies for the protection of the hydroxyl groups on Ac-Mur (**5.5**) were necessary and preferably introduced in the absence of the reactive

ether bound lactic acid group. After a thorough literature search, it was decided to employ benzylidene and benzyl groups as the hydroxyl protecting groups. Therefore, a glucopyranose derivative with a 4,6-*O*-benzylidene and benzyl group on the anomeric oxygen (**5.15**) was purchased and the ether bound lactic acid group introduced by the Williamson ether reaction employing (*S*)-2-chloropropionic acid (**5.16**) and NaH in dioxane (Scheme 5.6).[127-130] By inversion of configuration (*S* → *R*) via an S_N2 mechanism[60] this yielded the desired Benzyl-2-acetamido-4,6-*O*-benzylidene-3-*O*-(*R*-1′-carboxyethyl)-2-deoxy-α-D-glucopyranoside (benzylidene-benzyl Ac-Mur, **5.17**) in 57% yield after purification by preparative reversed-phase HPLC.

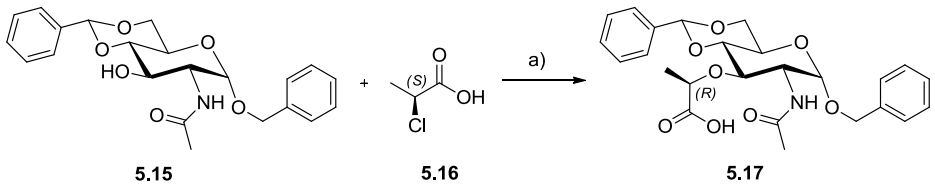

Scheme 5.6 Synthesis of benzylidene-benzyl Ac-Mur (**5.17**) by a Williamson ether reaction between benzylidene-benzyl glucopyranose (**5.15**) and (*S*)-chloropropionic acid (**5.16**). (a) NaH, dry dioxane, 70 °C, 23 h (57%).

Before employing benzylidene-benzyl Ac-Mur (**5.17**) for the synthesis of G1$(MDP)_4$-C16 (**5.8**), it was examined whether the benzylidene group could be removed in a one-pot fashion under the resin cleavage conditions. The benzylidene acetal is generally removed under acidic conditions (e.g., 60-70 vol. % aqueous acetic acid at 70 °C or 90 vol. % aqueous TFA at 0 °C) or hydrogenation.[122,131] Chen and co-workers[132] successfully employed 23 vol. % TFA in DCM at 0 °C for 30 min and Willems *et al.*[133] employed 20 vol. % TFA together with 2.5 vol. % triisopropylsilane (TIS) in DCM at rt for 3 h. Therefore, it was expected that treatment with TFA/DCM (1:1) at rt for 2h would successfully yield benzyl Ac-Mur (**5.18**) (Scheme 5.7).

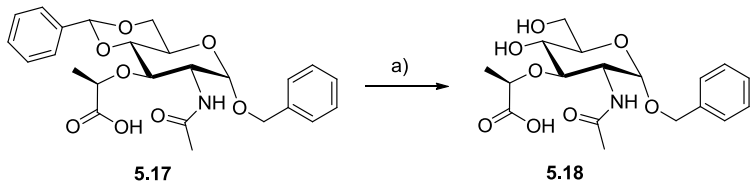

Scheme 5.7 Removal of the benzylidene acetal by acid hydrolysis yielding benzyl Ac-Mur (**5.18**). (a) TFA/DCM (1:1), rt, 2 h (100%).

Examination by UPLC-MS showed a proof of concept with an excellent 91% conversion to benzyl Ac-Mur (**5.18**) obtained by integration of the UV chromatogram (Fig. 5.5).

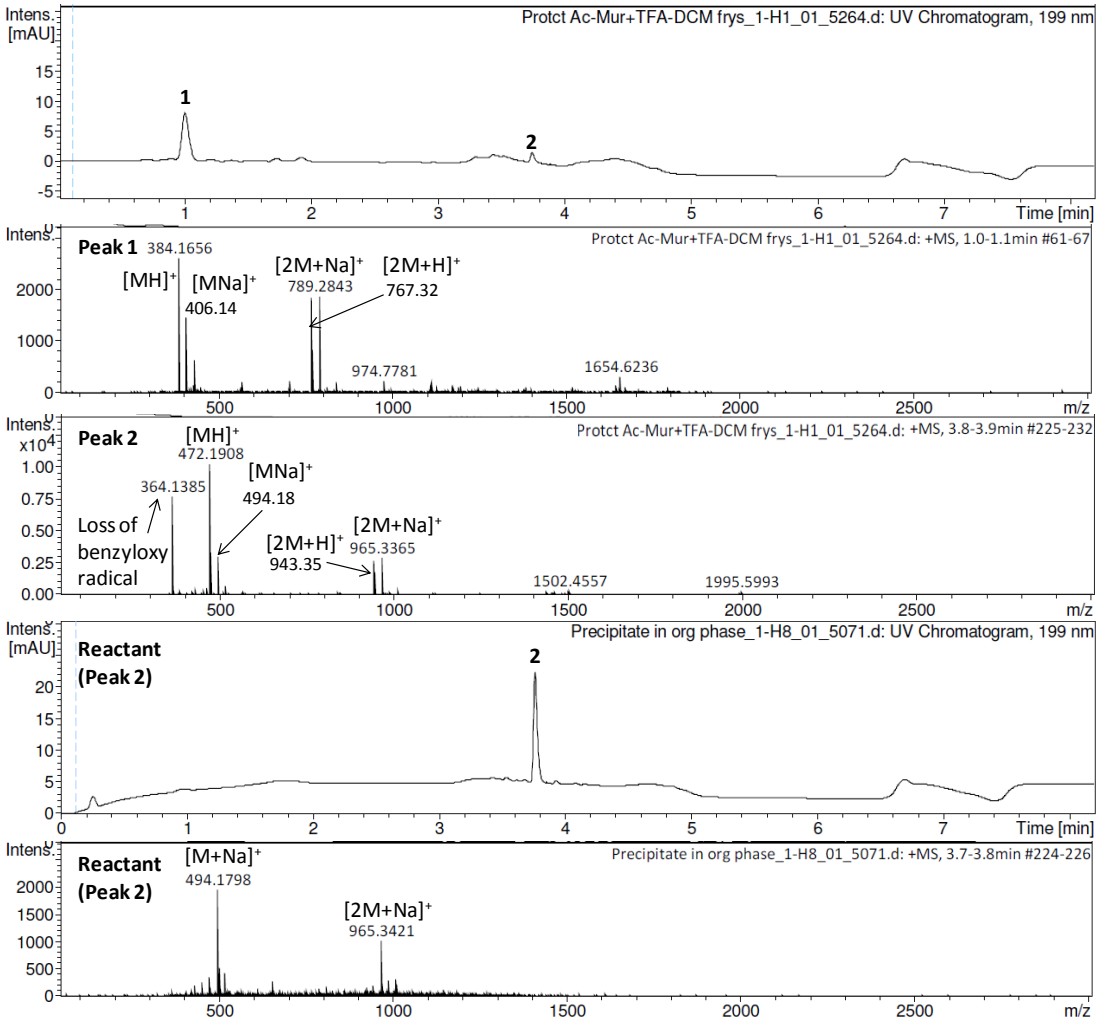

Figure 5.5 UPLC-MS analysis of the product mixture from the acid hydrolysis with TFA/DCM (1:1) and the reactant prior to acid hydrolysis. Peak 1 (benzyl Ac-Mur, **5.18**) and peak 2 (benzylidene-benzyl Ac-Mur reactant, **5.17**) with a ratio of 10.1:1 (91% vs. 9%) for the acid hydrolysis reaction, respectively.

The synthesis of G1(benzyl-MDP)$_4$-C16 (**5.19**) was performed by acylation of a ^{D}isoGln-Ala derivatized PS resin (**5.7**) with 4 equiv. of benzylidene-benzyl Ac-Mur (**5.17**) employing HBTU as the coupling reagent in the presence of DIPEA (Scheme 5.8). After 23 h, the completion of the reaction was monitored by the ninhydrin test giving a negative readout (yellow supernatant).

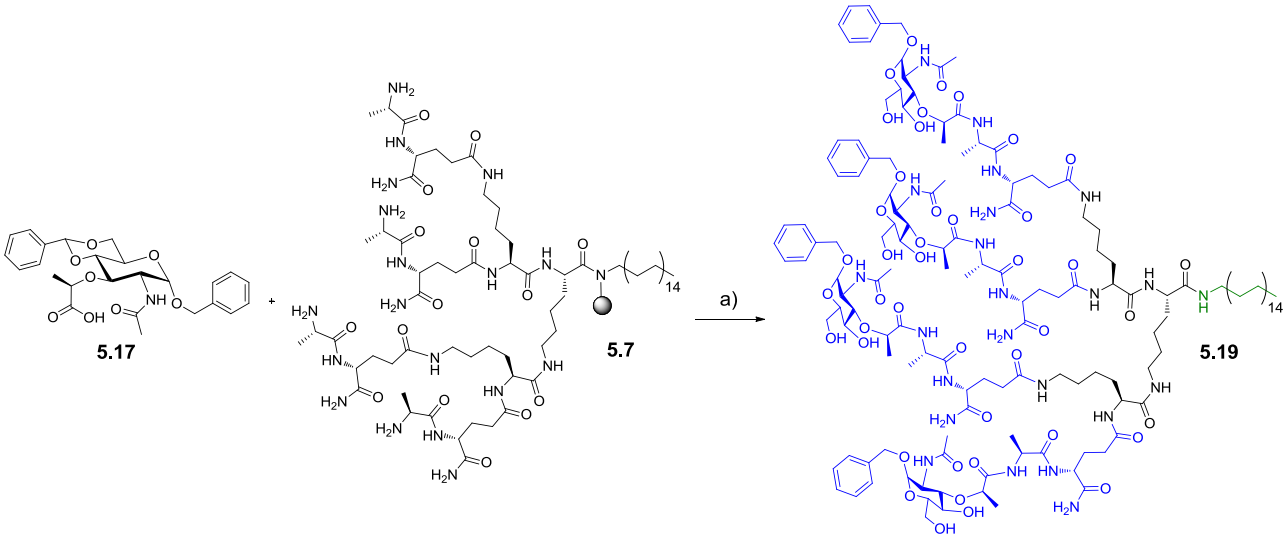

Scheme 5.8 Synthesis of G1(benzyl-MDP)$_4$-C16 (**5.19**) with benzyl-MDP groups marked in blue and the C16 alkyl chain in green. (a) HBTU, DIPEA, NMP, rt, 23 h; 5 vol. % TIS in TFA/DCM (1:1), rt, 2h.

The benzylidene-benzyl Ac-Mur (**5.17**) was not pre-activated before being added to the derivatized resin. The pre-activation proved to be a vital for a successful reaction, since UPLC-MS analysis of the cleaved product displayed four main peaks resulting from dendrons containing one, two and three guanidinium groups and peak 4 resulting from the target product (**5.19**) (Fig. 5.6).

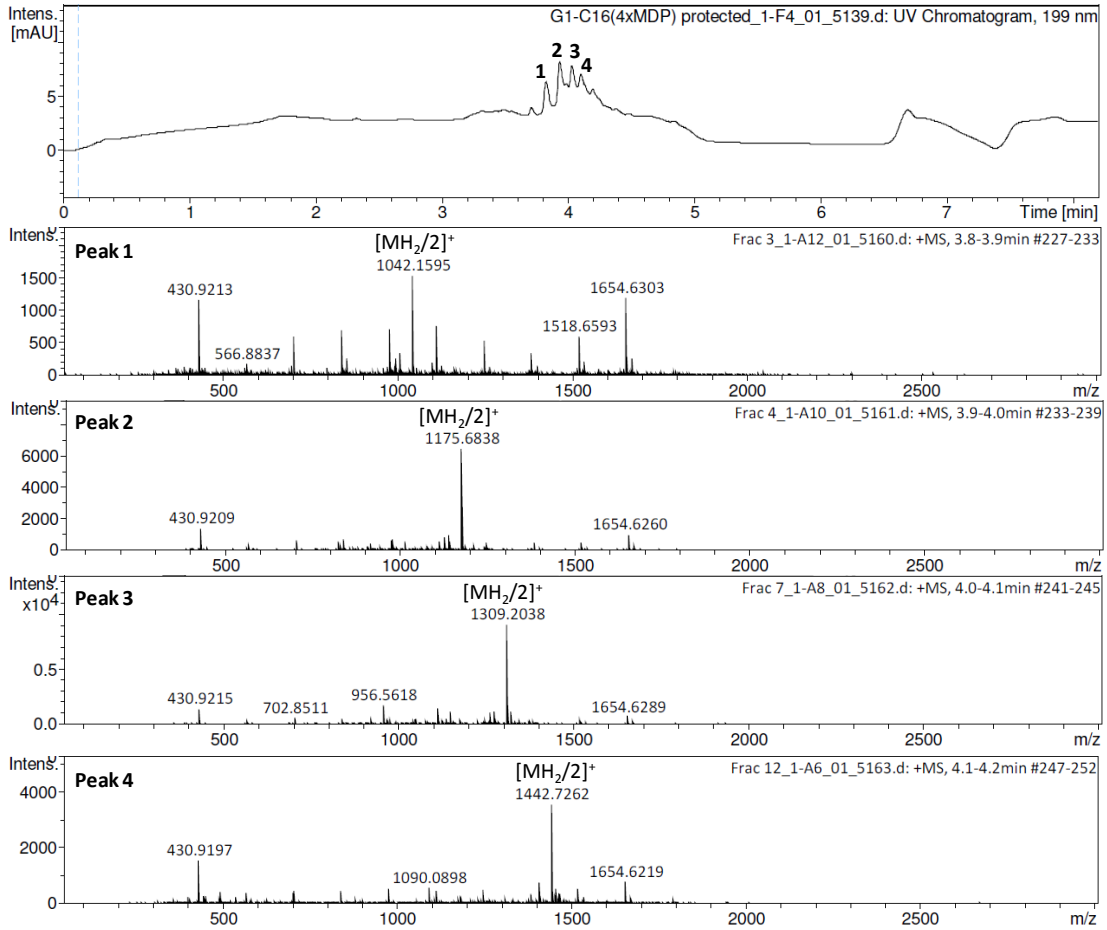

Figure 5.6 UV chromatogram of the product mixture obtained from the acylation reaction with benzylidene-benzyl Ac-Mur (**5.17**) after resin cleavage and MS spectra corresponding to the indicated peaks after isolation by preparative reversed-phase HPLC. Peak 1, 2 and 3 correspond to G1(benzyl-MDP)$_1$(guanidinium)$_3$-C16 (**5.20**), G1(benzyl-MDP)$_2$(guanidinium)$_2$-C16 (**5.21**) and G1(benzyl-MDP)$_3$(guanidinium)$_1$-C16 (**5.22**), respectively. Peak 4 corresponds to the target product, G1(benzyl-MDP)$_4$-C16 (**5.19**).

The irreversible formation of the guanidinium by-product is a known side reaction that can take place with uronium reagents and occurs through a nucleophilic attack of the amine (Scheme 5.9). Hence, when employing uronium reagents pre-activation of the carboxylic acid is essential before the amine is introduced to the reaction mixture.[134]

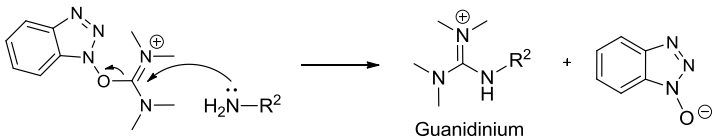

Scheme 5.9 Irreversible formation of a guanidinium by-product as a result of nucleophilic attack of the amine on uronium reagents.

An example of possible structures of the dendron by-products with guanidinium groups is given in Fig. 5.7. However, without a detailed structural analysis the exact positional combinations of the guanidinium groups are difficult to predict.

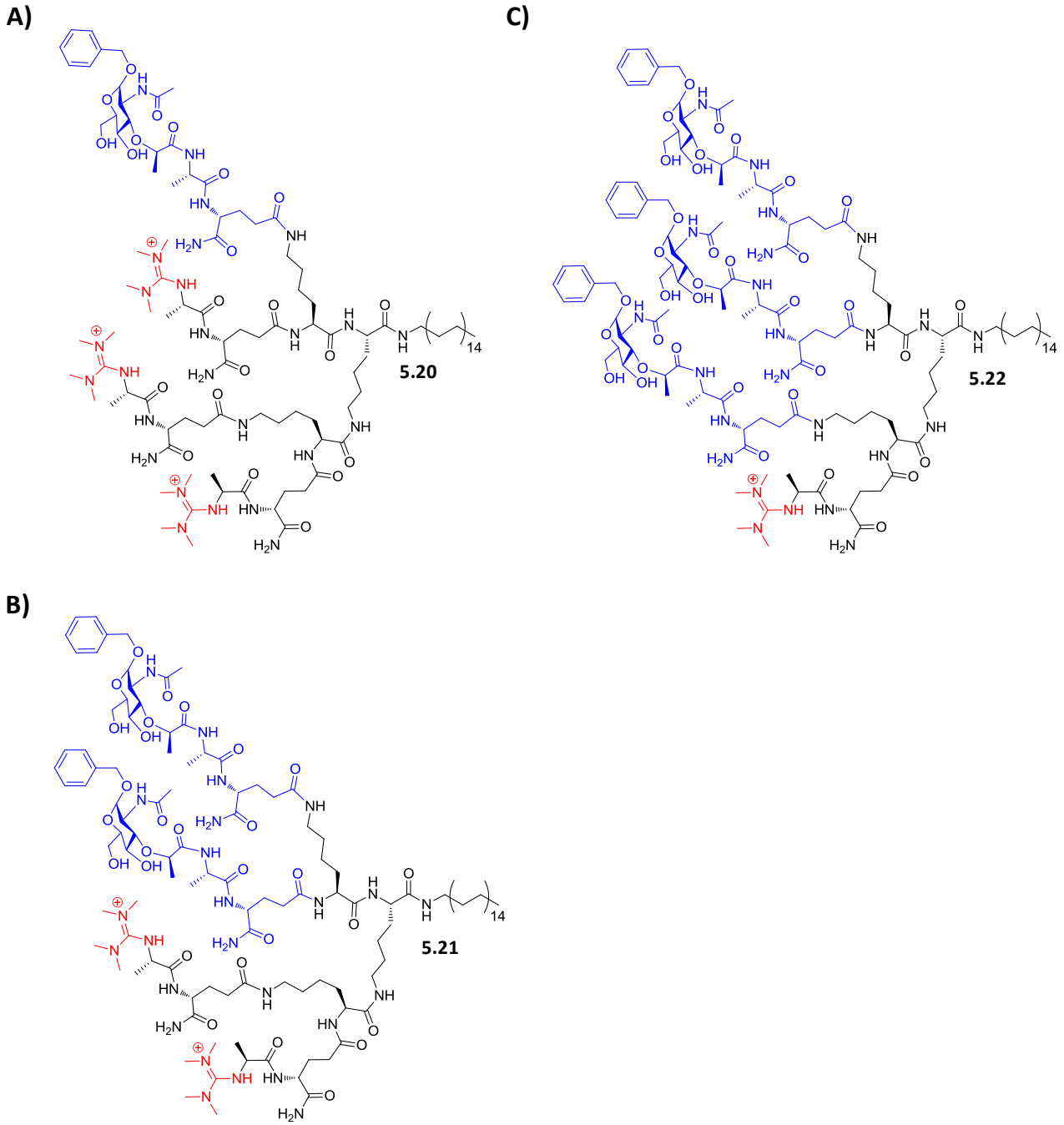

Figure 5.7 Possible structural combinations of dendron by-products containing guanidinium groups (red) and benzyl-MDP (blue). (A) G1(benzyl-MDP)$_1$(guanidinium)$_3$-C16 (**5.20**). (B) G1(benzyl-MDP)$_2$(guanidinium)$_2$-C16 (**5.21**). (C) G1(benzyl-MDP)$_3$(guanidinium)$_1$-C16 (**5.22**).

Scheme 5.8 was followed once again, however the ether bound lactic acid group of benzylidene-benzyl Ac-Mur (**5.17**) was pre-activated for 15 min at rt before being added to a new batch of ^{D}isoGln-Ala derivatized PS resin (**5.7**). After 23 h, the completion of the reaction was monitored by the ninhydrin test giving a partially positive readout (pale purple supernatant). UPLC-MS analysis of the cleaved product displayed two main peaks resulting from the cleaved reactant, G1(^{D}isoGln-Ala)$_4$-C16 (**5.4**), and the target product, G1(benzyl-MDP)$_4$-C16 (**5.19**) (Fig. 5.8).

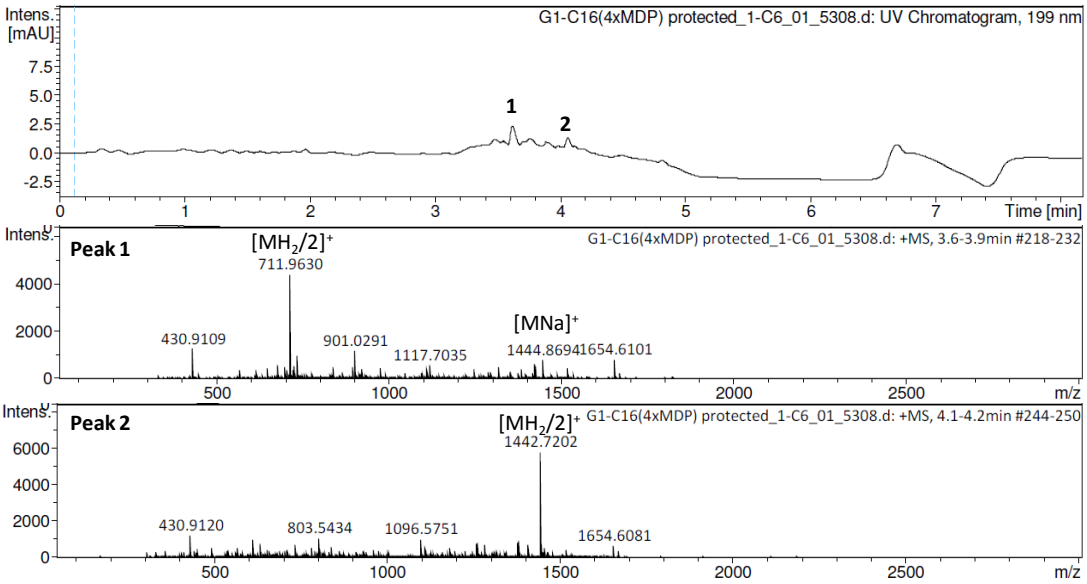

Figure 5.8 UPLC-MS analysis of the cleaved product from the acylation reaction with benzylidene-benzyl Ac-Mur (**5.17**) and 15 min pre-activation. Peak 1 and 2 correspond to the cleaved reactant G1(^{D}isoGln-Ala)$_4$-C16 (**5.4**) and target product G1(benzyl-MDP)$_4$-C16 (**5.19**).

In addition, purification by preparative reversed-phase HPLC revealed a small amount of G1(benzyl-MDP)$_3$(^{D}isoGln-Ala)$_1$-C16 and presumably the additional peaks observed between peak 1 and 2 in Fig. 5.8 are due to partially benzyl-MDP derivatized dendrons. Therefore, it was reasoned that benzylidene-benzyl Ac-Mur (**5.17**) is too steric to be coupled to the already crowded dendron. In addition, these effects would be augmented when performing the synthesis on a polymeric support compared to traditional solution-phase. An obvious future approach could be to employ stronger coupling reagents (e.g., carbodiimides or fluorinating reagents) to drive the acylation reaction to completion. Another option could be to perform the acylation in solution-phase after cleavage of the G1(^{D}isoGln-Ala)$_4$-C16 dendron (**5.4**) from the resin thereby increasing reaction kinetics. In a different approach, the protected MDP could be prepared separately and subsequently attached to the ^{D}isoGln-Ala derivatized PS resin (**5.7**). Cleavage of the target dendron would yield the benzyl protected MDP dendron (**5.19**) and the benzyl ether group can be deprotected through catalytic hydrogenolysis over a Pd catalyst (e.g., 10 wt. % Pd over carbon and H_2)[60,122,128]

5.1.2 *N*-formylmethionine library

A total of four G1 and G2 dendrons were modified with *N*-formylmethionine (fMet) as the PAMP motif to examine the effect of multivalency on immune cell activation (Table 5.3). In addition, the C-terminal of the dendrons was modified with either C1 or C16 to examine the effect of the alkyl chain length on the immunostimulatory properties.

Table 5.3 Synthesized polylysine dendrons modified with fMet

#	Compound[a]	Yield[b] (%)
5.23	G1(fMet)$_2$-C1	31
5.24	G1(fMet)$_2$-C16	83
5.25	G2(fMet)$_4$-C1	12
5.26	G2(fMet)$_4$-C16	10

[a] Nomenclature for synthesized dendrons. G*n*: generation number, [b] TFA salt.

After reductive amination, the resulting secondary amine was acylated with two equivalents of Fmoc-Lys(Fmoc)-OH employing DIC as the coupling reagent (Scheme 5.10). The reaction completion was monitored by the acetaldehyde test giving a negative readout (colorless beads). Following the attachment of the first lysine group, the resin loadings were determined ranging from 0.21 to 0.24 mmol/g.

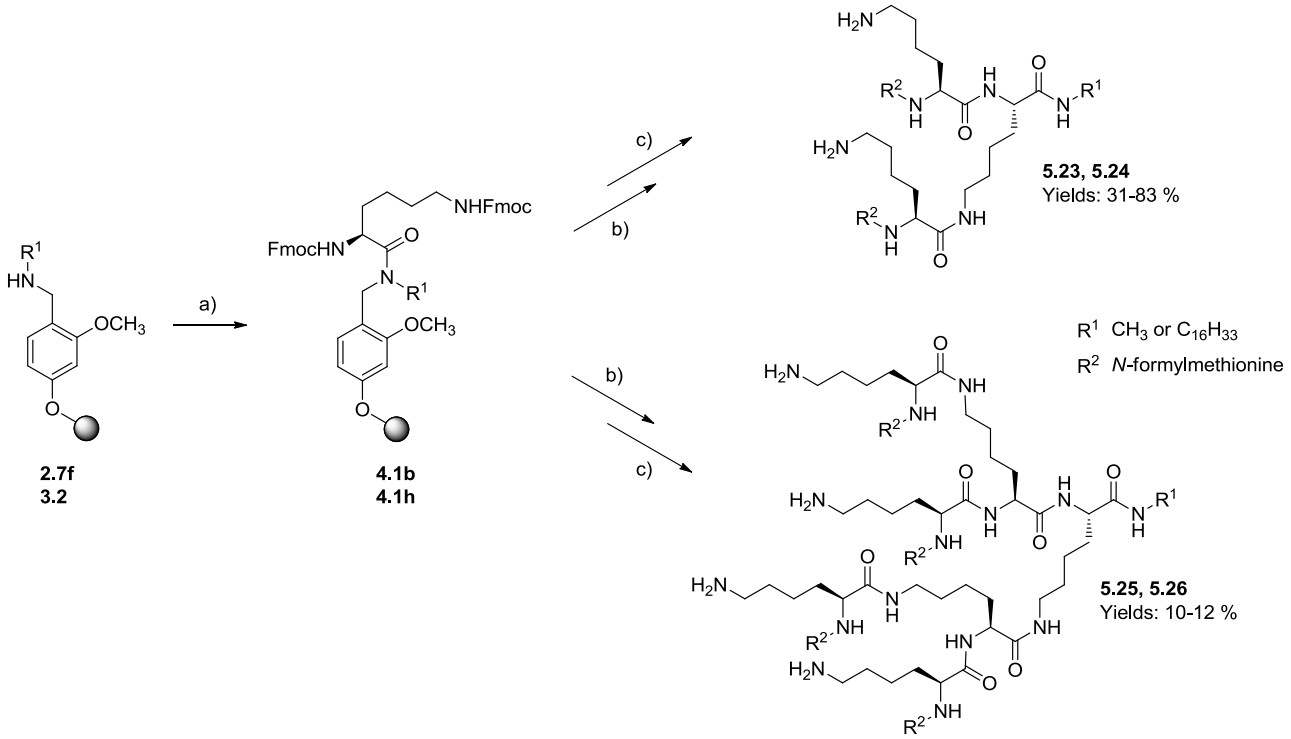

Scheme 5.10 Stepwise divergent SPPS of G1 and G2 polylysine dendrons having a C1 or C16 alkyl chain and modified with *N*-formylmethionine. (a) Fmoc-Lys(Fmoc)-OH, DIC, DCM/NMP (95:5), rt, 20 h. (b) Fmoc deprotection between acylation steps: piperidine/NMP (1:4), rt, 3 + 30 + 30 + 20 min; linkage of second lysine: Fmoc-Lys(Boc)-OH or Fmoc-Lys(Fmoc)-OH, PyBOP, DIPEA, NMP, rt, 20 h; linkage of third lysine in G2 dendrons: Fmoc-Lys(Boc)-OH, PyBOP, DIPEA, NMP, rt, 20 h. (c) Linkage of PAMP motif: *N*-formylmethionine, PyBOP, DIPEA, NMP, rt, 20 h; cleavage: TFA/DCM (1:1), rt, 2 h.

In between acylation steps, the Fmoc group was removed by employing 20 vol. % piperidine in NMP and the completion of the deprotections and subsequent acylations were monitored by the ninhydrin test. The acylations were performed with PyBOP and generally a coupling time of 20 h was sufficient for reaction completion, when employing two equivalents of the amino acids. In the

final step, the dendrons were cleaved of the resin by TFA/DCM (1:1) for 2 h giving poor to excellent yields (Scheme 5.10). The purity of the synthesized dendrons was examined by UPLC-MS and the structure confirmed by fingerprint regions in NMR.

Since fMLP is known to have a high affinity for the formyl peptide receptor 1 (Section 1.1), the synthesis of G1 and G2 dendrons modified with fMLP was pursued with the aim to expand the fMet library. A G1(fMLP)$_2$-C16 dendron (**5.28**) was prepared following the same procedure as Scheme 5.10 up to the attachment of the second lysine. After Fmoc deprotection of the second lysine (**5.27**), the amino acids in the PAMP motif were attached individually in the following order: 1) Fmoc-Phe-OH, 2) Fmoc-Leu-OH and 3) fMet and subsequently the dendron was cleaved of the resin (Scheme 5.11).

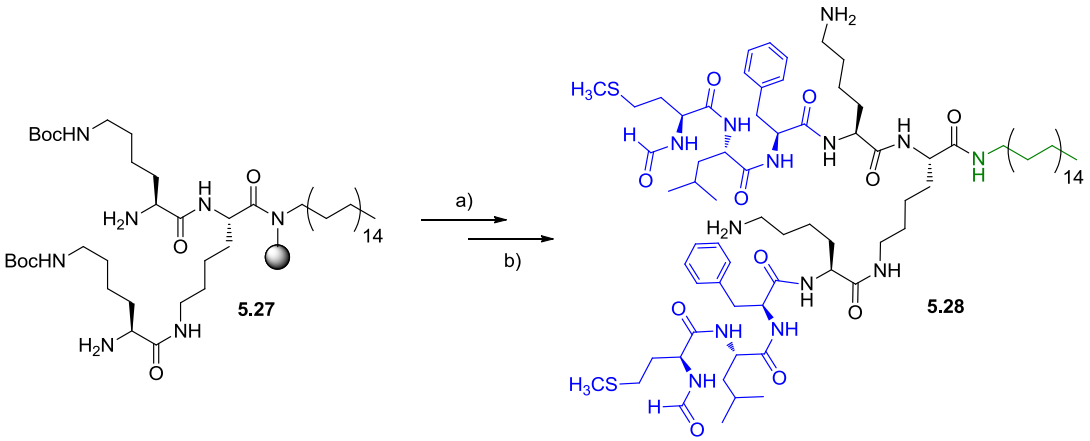

Scheme 5.11 Synthesis of G1(fMLP)$_2$-C16 (**5.28**) with the PAMP motifs marked in blue and the C16 alkyl chain in green. (a) Fmoc deprotection between acylation steps: piperidine/NMP (1:4), rt, 3 + 30 + 30 + 20 min; amino acid (1. Fmoc-Phe-OH, 2. Fmoc-Leu-OH and 3. fMet), PyBOP, DIPEA, NMP, rt, 20 h. (b) TFA/DCM (1:1), rt, 2 h.

Four equivalents of amino acid appeared to be sufficient for reaction completion as monitored by the ninhydrin test. PyBOP was employed as the standard coupling reagent together with DIPEA and reaction times were typically 20 h at rt. Following the last acylation, the target dendron was cleaved of the resin employing TFA/DCM (1:1) for 2 h. UPLC-MS analysis of the crude product displayed three peaks, which were further isolated by preparative reversed-phase HPLC showing identical masses (Fig. 5.9). In addition, the same pattern was observed when repeating the reaction on different batches.

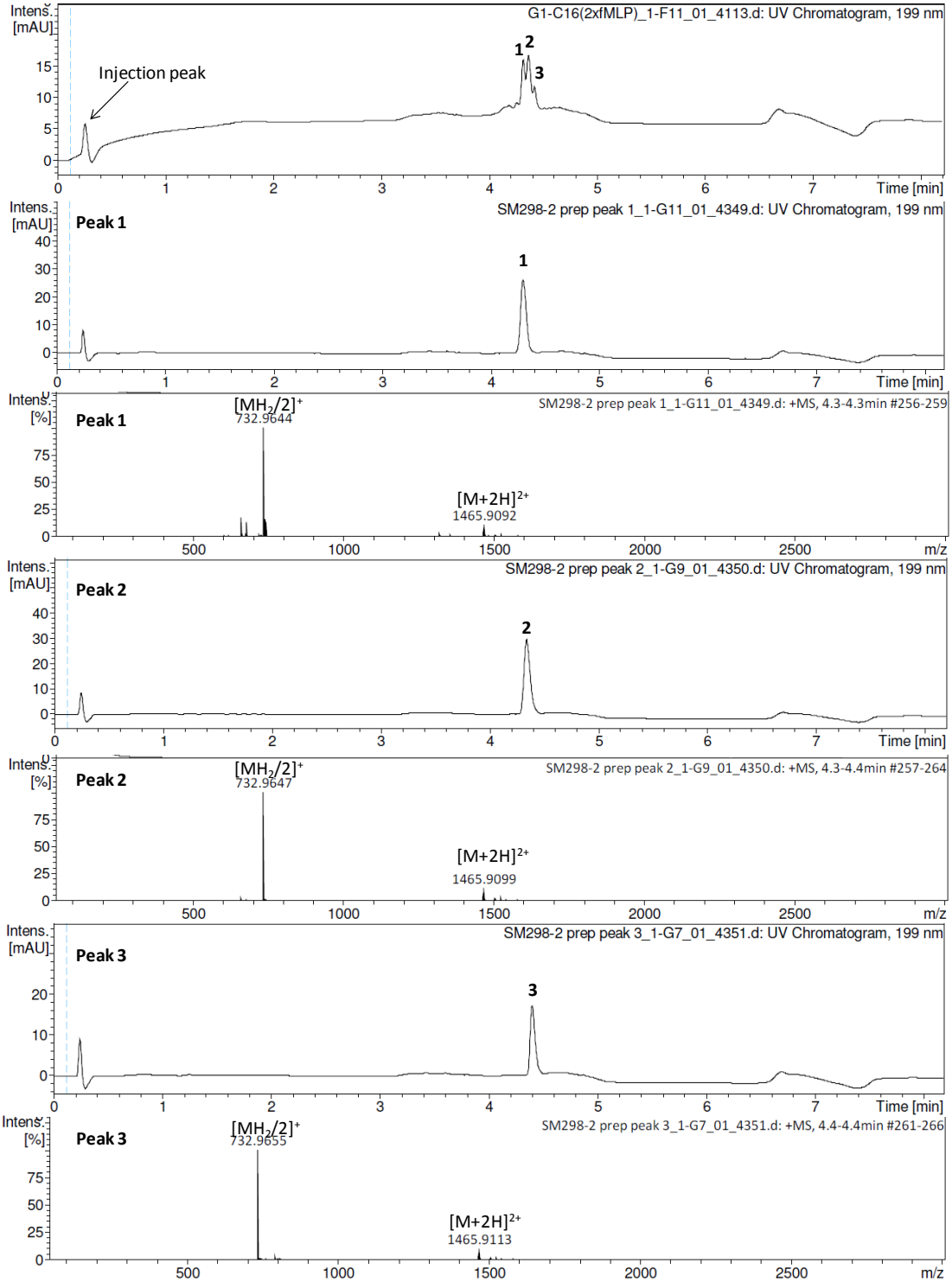

Figure 5.9 UV chromatogram of the crude product (**5.28**) after resin cleavage showing three peaks and UPLC-MS analysis of the three peaks after preparative reversed-phase HPLC purification showing identical masses corresponding to the target product (**5.28**)

At first it was reasoned that the three peaks may be due to some type of rearrangement giving rise to constitutional isomers. Possible rearrangements during the acidic cleavage conditions could occur on the fMet group. One of the UV-chromatogram peaks could be caused by an intramolecular attack

of the sulfur on the positively charged electrophilic formyl carbon (**5.29**) giving a compound with a six-membered ring (**5.30**). Further protonation of the amine in the six-membered ring (**5.31**) may result in a formyl group migration to the sulfur atom (**5.32**) causing another UV-chromatogram peak (Scheme 5.12).

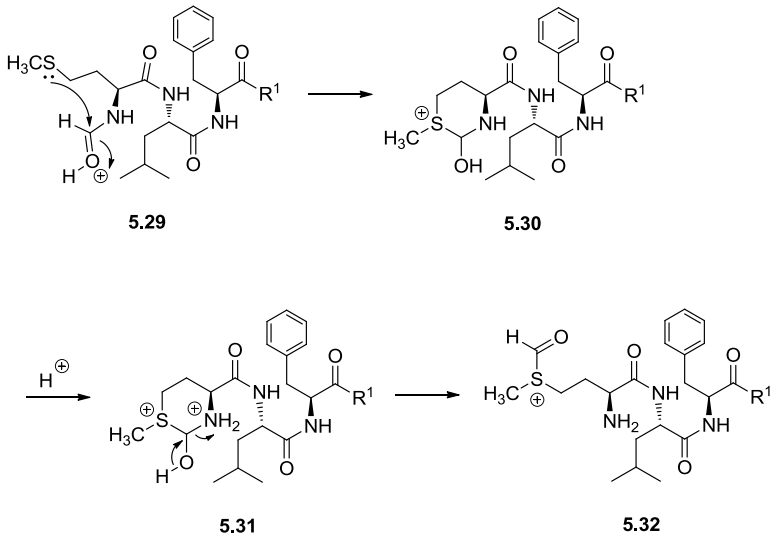

Scheme 5.12 Possible rearrangements on fMet giving rise to constitutional isomers.

However, the hypothesis would not explain why the same was not observed for dendrons containing only the fMet group (Table 5.3). Since constitutional isomers would exhibit different IR and NMR spectra, the three peaks were isolated by preparative reversed-phase HPLC for further analysis. The hypothesis was contradicted by IR analysis giving completely identical spectra for the three peaks (Fig. 5.10). Since the yield of peak 3 after purification was too low, only peak 1 and 2 were further examined by ^{1}H-NMR. Also here, the superimposed spectra contradicted the constitutional isomer hypothesis (Fig. 5.11).

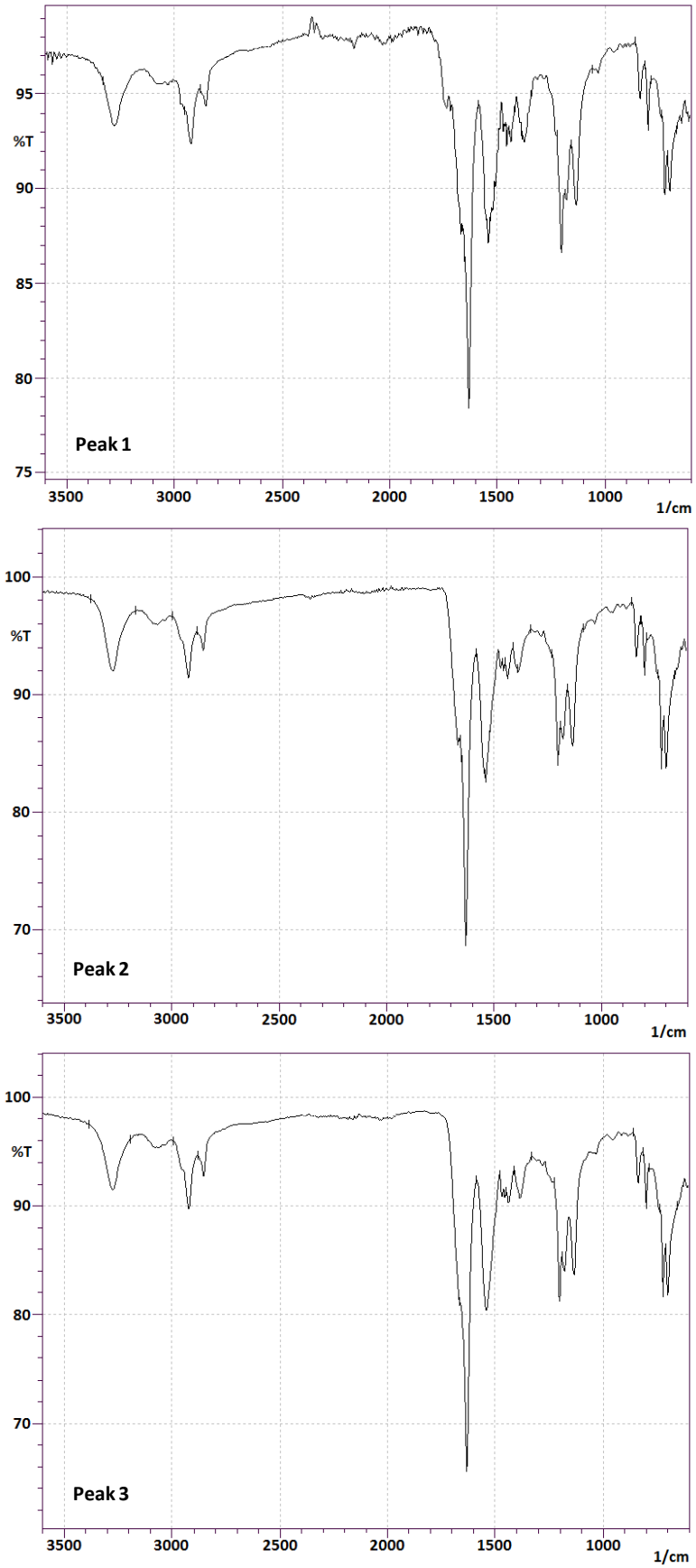

Figure 5.10 IR analysis of peak 1, 2 and 3 showing identical spectra.

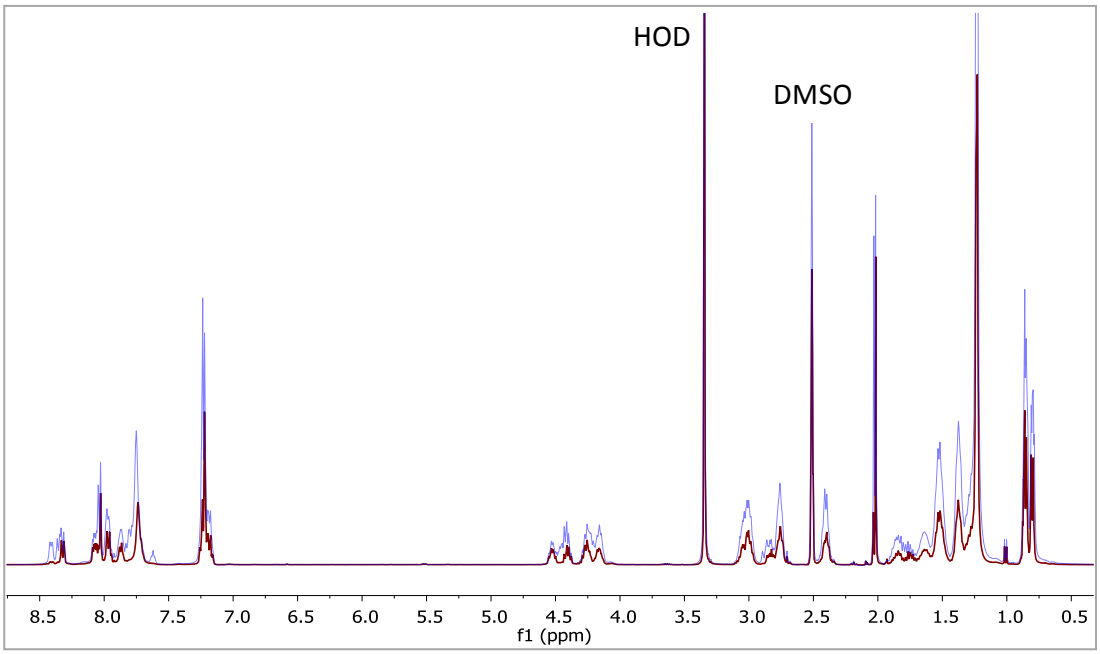

Figure 5.11 Superimposed ^{1}H-NMR (400 MHz in DMSO) spectra for peak 1 (dark red) and peak 2 (violet blue).

Therefore, it could be concluded that the peaks observed on UPLC-MS could not be due to rearrangements resulting in constitutional isomers.

Next, several dendrons [i.e., G1(fMet-Leu)$_2$-C16 (**5.33**), G1(fMet-Phe)$_2$-C16 (**5.34**) and G2(fMLP)$_4$-C16 (**5.35**)] were synthesized following the procedure in Scheme 5.10 and 5.11 showing similar UPLC-MS patterns with identical masses as observed before (Fig. 5.12).

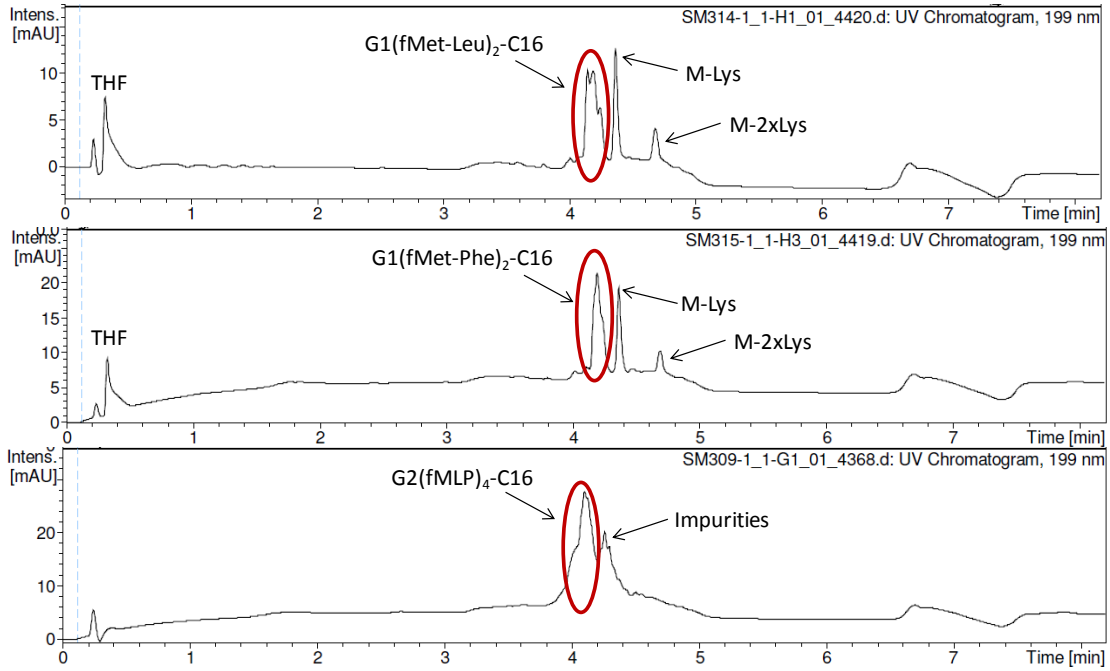

Figure 5.12 UV chromatograms of G1(fMet-Leu)$_2$-C16 (**5.33**), G1(fMet-Phe)$_2$-C16 (**5.34**) and G2(fMLP)$_4$-C16 (**5.35**) having multiple peaks with identical masses (red circle).

Since the pattern was not observed for dendrons only modified with fMet, it was reasoned the effect may be due to higher levels of sterical hindrance, when linking additional amino acids (e.g., Leu and Phe) on the dendron and some level of hydrophobic interactions of Leu and Phe in polar solvents (e.g., NMP) resulting in aggregated structures on the resin. These effects may slow down the activated fMet or reaction kinetics in the final acylation step. Thereby, the contact with the basic medium (i.e., DIPEA) is prolonged resulting in racemization through formation of an oxazolone intermediate (**5.39**). Following activation of the formylated amino acid (**5.37**), the N^{α} proton is removed by a base in the medium and subsequently the negatively charged oxygen makes an intramolecular nucleophilic attack on the activated carbonyl (**5.38**) whereby the oxazolone is formed (**5.39**). Consequently, the α-proton is removed yielding a carbanion intermediate (**5.40**) stabilized by resonance. Re-protonation of the carbanion reforms oxazolone, which can further react with the amine giving a racemic product (**5.41**) (Scheme 5.13).[135,136]

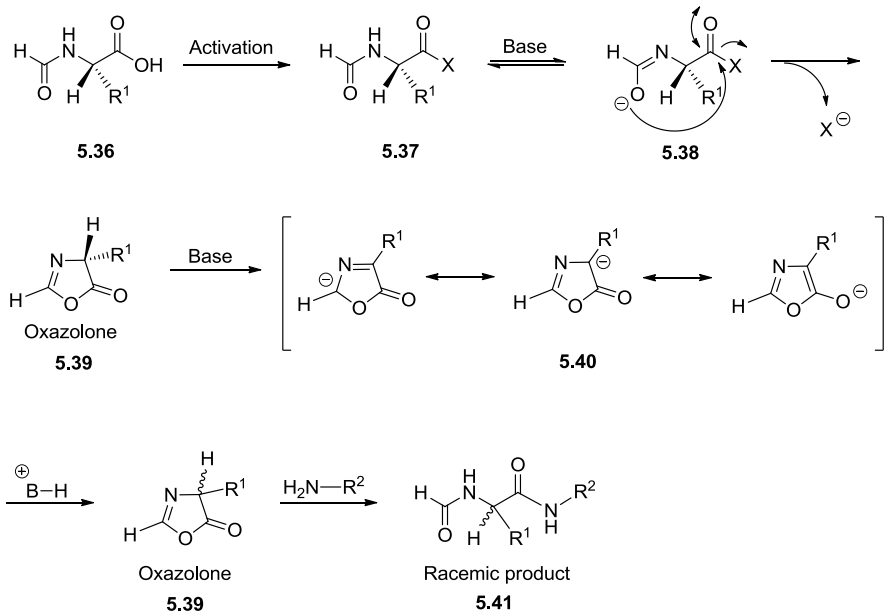

Scheme 5.13 Proposed mechanism for racemization of N^{α}-formylated amino acids through oxazolone (**5.39**) formation. X: activating group. R^1: amino acid side chain. R^2: amino acid with a free amino group.

The N^{α}-protecting group is the key factor determining the rate of formation of the oxazolone intermediate. The electron-withdrawing effects of *N*-acyl groups (e.g., formyl or acetyl) tend to increase the likelihood of oxazolone formation due to an increase in the N^{α}-proton acidity making proton abstraction favorable (Scheme 5.14A). In addition, the stability of the carbanion is also enhanced by such groups (Scheme 5.14B), which drives the racemization process. Conversely, in carbamate protected (e.g., Fmoc and Boc) α-amino acids the N^{α}-proton is less acidic due to electron donation from the alkoxy group (OR) making proton abstraction less favorable and the alkoxy group also has a destabilizing effect on the carbanion (Scheme 5.14C and 5.14D).[136] In addition to electronic effects, the formyl group is small facilitating the attack on the activated carbonyl yielding the oxazolone (**5.39**) (Scheme 5.13).

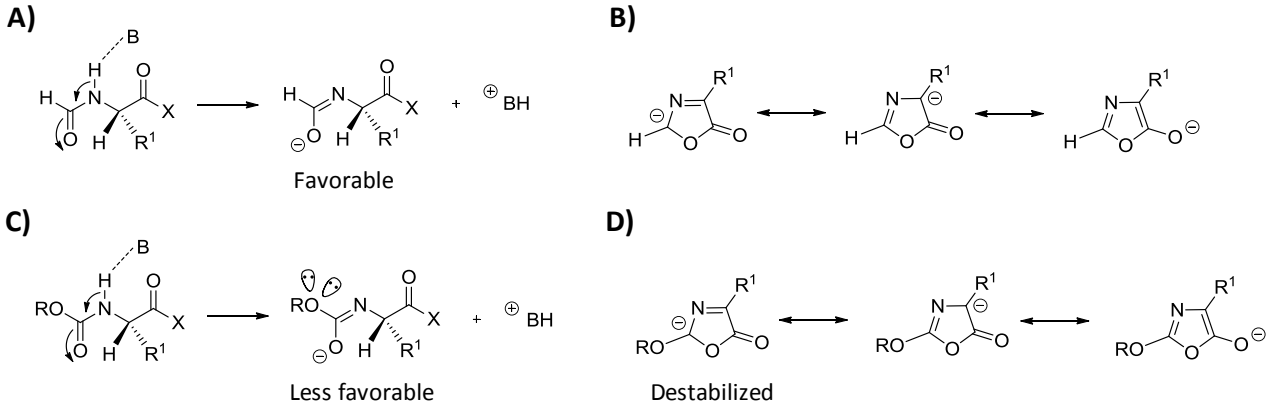

Scheme 5.14 The effect of *N*-substituents on oxazolone formation through stabilization/destabilization of intermediates. (A) The *N*-formyl group withdraws electrons increasing the acidity of the N^{α}-proton making proton abstraction favorable. (B) The carbanion intermediate is stabilized through resonance. (C) The alkoxy group has a destabilizing effect through electron donation making the N^{α}-proton less acidic and proton abstraction less favorable due to oxygen-oxygen electron repulsion in the conjugate base. (D) Electron donating groups like, e.g., the alkoxy group (OR) have a destabilizing effect on the carbanion.

Consequently, the formyl group on the α-amine of fMet renders it prone to racemization through oxazolone formation. G1 and G2 dendrons contain two and four fMet groups, respectively. The number of stereoisomers can be calculated by 2^n, where *n* is the number of chiral groups that can racemize. Therefore, the racemization of fMet in the G1 and G2 dendrons can give four (2^2) or sixteen (2^4) stereoisomers (i.e., two or eight diastereomeric pairs of enantiomers), respectively. The diastereomers may exhibit different retention times on the achiral column employed for UPLC-MS analysis, which may make it possible to distinguish them from each other.[137] Hence, the additional peaks observed on UPLC-MS having an identical mass may well be caused by diastereomers. Since stereochemical homogeneity of the dendrons was important and it was not possible to know the exact stereochemistry without employing all possible stereoisomers as reference, dendrons modified with fMLP were not pursued further. In addition, the best solubility profiles were also obtained for dendrons only modified with fMet making them a better choice for purification by HPLC and for *in vitro* studies.

5.2 Preliminary results from immunological cell culture studies

The immunostimulatory properties of PAMP modified polylysine dendrons (Table 5.4, corresponding to dendrons from Table 5.1 and 5.3) were examined by investigating the effect of multivalency towards the initiation of immune cell activation. Immune activation was measured as the interleukin-6 (IL-6) concentration in supernatants of cultured whole mouse spleen cells or dendritic cell subset ($CD11c^+$) isolated from mouse spleen. PGN (peptidoglycan from *Staphylococcus aureus*), MDP, fMet and fMLP were employed as positive controls. In addition, the effect of the length of the C-terminal alkyl chain (C1 vs. C16) was examined on dendrons modified with fMet. Furthermore, co-stimulatory effects of chosen dendrons from the MDP library were studied by examining the activation of immune cells in the presence of known TLR ligands (i.e., polyinosinic-polycytidylic acid [poly(I:C)] and CpG oligodeoxynucleotide [CpG ODN]).

Table 5.4 MDP and fMet dendron libraries

#	Dendron[a]
	MDP library
4.6	G1-PDL-C16
4.11	G1(acetyl)-C16
5.1	G1-C16
5.2	G1(^{D}isoGln-Ala)$_2$-C16
5.3	G1(MDP)$_2$-C16
5.4	G1(^{D}isoGln-Ala)$_4$-C16
	fMet library
5.23	G1(fMet)$_2$-C1
5.24	G1(fMet)$_2$-C16
5.25	G2(fMet)$_4$-C1
5.26	G2(fMet)$_4$-C16

[a] Nomenclature for synthesized dendrons. G*n*: generation number, PDL: poly-D-lysine.

Murine CD11c^{+} dendritic cells were treated with dendrons from the MDP library in order to evaluate the immunostimulatory effects relative to positive controls (PGN and MDP) by measuring the concentration of IL-6 in the supernatant of cultured cells. The MDP dendron library consisted of an N-terminally unmodified dendron with an L-lysine (**5.1**) and D-lysine (**4.6**) core, a partially acetylated dendron with reduced positive charge (**4.11**), a dendron modified with two (**5.2**) or four (**5.4**) ^{D}isoGln-Ala moieties and a dendron with two MDP (**5.3**) moieties (Fig. 5.13).

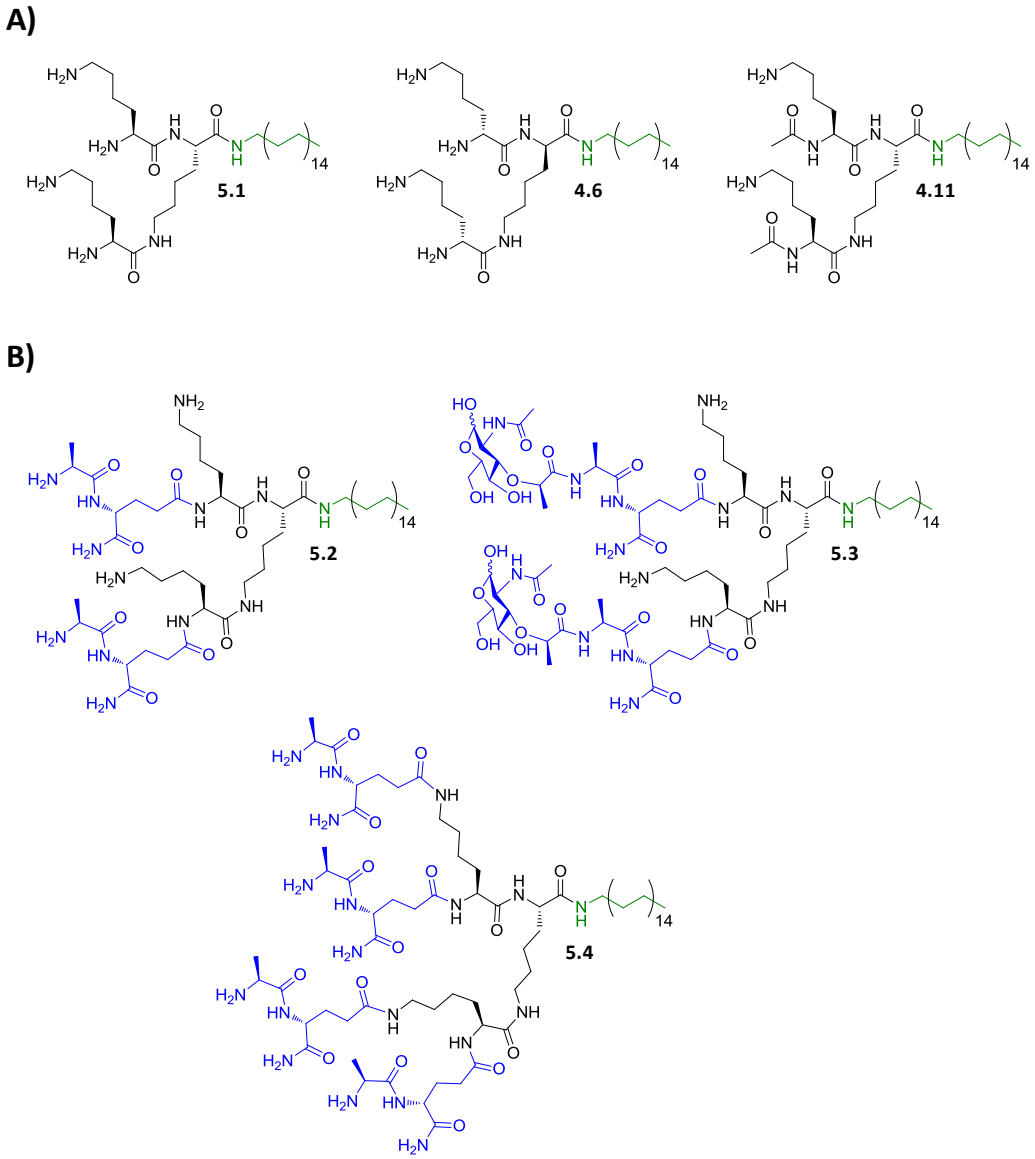

Figure 5.13 MDP dendron library. (A) unmodified dendrons with a C16 alkyl chain (green): G1-C16 (**5.1**), G1-PDL-C16 (**4.6**) and G1(acetyl)-C16 (**4.11**). (B) PAMP (blue) modified dendrons with a C16 alkyl chain (green): G1(^{D}isoGln-Ala)$_2$-C16 (**5.2**), G1(MDP)$_2$-C16 (**5.3**) and G1(^{D}isoGln-Ala)$_4$-C16 (**5.4**).

The response obtained after treatment of murine CD11c$^+$ dendritic cells with the MDP dendron library at a concentration of 25 µM demonstrated that unmodified G1 dendrons (**5.1**, **4.6** and **4.11**) did not exhibit any intrinsic immunostimulatory effects, although it seems strange that the IL-6 levels are below the blank (125 pg/mL) (Fig. 5.14). This may indicate that the unmodified dendrons show some level of cytotoxicity resulting in cell death or weakening of the cells, thereby reducing the basic level of IL-6 production. Therefore, cell viability studies should be performed in order to exclude cytotoxic effects. Sorensen *et al.*[29] observed maximum cytokine response employing 10 µg/mL PGN. Therefore, a concentration of 12.5 µg/mL PGN was chosen for the positive control giving an IL-6 response of 1950 pg/mL. Since D amino acids are known to be abundant in bacteria,[89] an unmodified dendron having a D-lysine core (**4.6**) was hypothesized to induce some

level of immune cell activation. However, the D-lysine core apparently does not induce an immunostimulatory activity in the G1 polylysine dendron (Fig. 5.14). Furthermore, no detectable difference was observed between an unmodified G1 dendron with four positively charged amino groups (**5.1**) and a partially acetylated G1 dendron with only two positively charged amino groups (**4.11**) (Fig. 5.14).

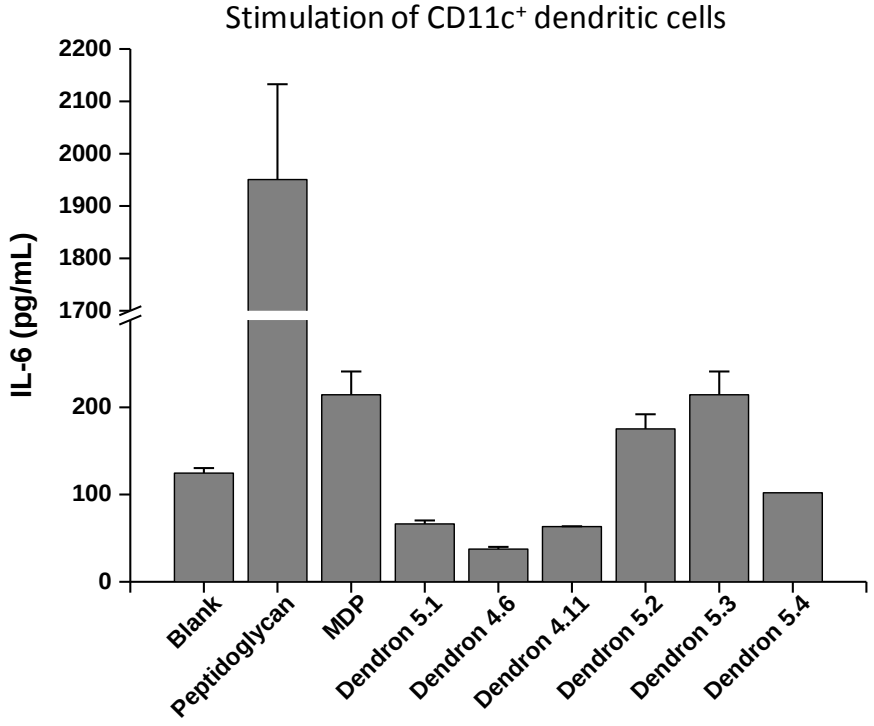

Figure 5.14 IL-6 levels (ELISA) after stimulation of $CD11c^+$ dendritic cells with the MDP dendron library at 25 µM concentrations. Positive controls: Peptidoglycan (12.5 µg/mL) and MDP (10 µg/mL) resulting in IL-6 concentrations of 1950 pg/mL and 215 pg/mL, respectively. Mean of blank (culture medium only, n = 4) was 125 pg/mL +/- 5.7 pg/mL (standard deviation, SD). Mean and standard error of mean (SEM) of duplicate cultures are shown.

Interestingly, only dendrons modified with two ^{D}isoGln-Ala (**5.2**) or MDP (**5.3**) motifs showed a moderate degree of immunostimulatory effect (Fig. 5.14). Although the induced IL-6 levels for these dendrons are comparable with levels induced by free MDP (215 pg/mL), they cannot be directly compared since equimolar concentrations with respect to the MDP motif were not employed for dendron **5.3** and the Ac-Mur moiety is lacking in dendron **5.2**. An MDP concentration of 20 µM (10 µg/mL) would correspond to 10 µM of dendron (**5.3**), thus the applied concentration was 2.5-fold higher. Since only dendron **5.3** consists of the complete MDP motif, a single concentration (25 µM) was chosen in order to be able to compare results between dendrons. The slightly higher IL-6 levels (although a statistical significance cannot be drawn) observed for G1$(MDP)_2$-C16 (**5.3**) relative to a dipeptide modified dendron (**5.2**) lacking the Ac-Mur moiety corresponds well with the general observation of MDP being the minimal PGN motif required for immune activation.[6] Nevertheless, it is interesting to see that the dipeptide (^{D}isoGln-Ala) also is able to exhibit moderate immunoactivity when multivalently presented on a G1 polylysine dendron. The lack of immunostimulatory activity for a dendron having four ^{D}isoGln-Ala motifs (**5.4**) came as

a surprise (Fig. 5.14), since it was hypothesized that an increased multivalency (i.e., increased number of PAMP motifs) in dendron **5.4** would lead to an enhanced immunostimulatory activity (i.e., higher IL-6 levels) or at least display similar activity compared to dendron **5.2** as reported by Sorensen *et al.*[29] Herein, they report comparable immunostimulatory activities for MDP-dendrimers (PAMAM or PPI) carrying 16 (G3) or 32 (G4) MDP motifs. The lack of immunostimulatory activity of the closely packed dendron **5.4** may be attributed to crowding effects hindering receptor interaction, whereas dendron **5.2** displays the dipeptide motifs with larger spacing reducing steric effects. In addition, one could also imagine the need for hydrogen bonding interactions at the distance of the free ε-amino groups on lysines and the active site of the putative receptor (i.e., TLR2 and NOD2). However, other explanations are certainly possible and molecular modelling may help explaining these observations.

The co-stimulatory property of dendron **5.2**, **5.3** and **5.4** was further evaluated in murine whole spleen cells by examining the IL-6 production upon simultaneous treatment with known TLR agonists (poly[I:C] and CpG ODN) (Fig. 5.15). Whole spleen cells were examined instead of isolated DC subsets in order to achieve a less selective view of the immune activating effect of the dendrons. Internalized poly(I:C) [a synthetic analogue of viral double-stranded RNA[138,139]] and CpG ODN [a synthetic analogue of bacterial unmethylated cytosine-guanine DNA motifs[140,141]] are recognized by TLR3 and TLR9, respectively, which are located in the cytosol.[140,142] Stimulation with only poly(I:C) or CpG ODN yielded IL-6 levels of ca. 145 pg/mL. Surprisingly, co-stimulation with the dendrons display antagonistic effects with dendrons **5.3** and **5.4** completely blocking the action of poly(I:C), while dendron **5.2** and **5.3** completely block CpG ODN activity. The effect seems to be cross-antagonistic, since the MDP and ^{D}isoGln-Ala modified dendrons are not expected ligands for TLR3 and TLR9. Therefore, additional tests are certainly needed in order to get more information on the mechanism behind this apparent cross-antagonism. Additional test may also elucidate why dendron **5.2** (two ^{D}isoGln-Ala motifs) and **5.4** (four ^{D}isoGln-Ala motifs) exhibit different degrees of antagonistic activities towards poly(I:C) and CpG ODN. Dendron **5.2** seems to be a full antagonist of CpG ODN, but partial antagonist of poly(I:C), whereas the opposite is true for dendron **5.4**. Cationic dendrimers and dendrons can be employed as transfection agents, since they form complexes with RNA and DNA through electrostatic interactions with the negatively charged phosphodiester backbone.[66,91] Therefore, a possible explanation of the antagonistic activity may be due to poly(I:C) and CpG ODN forming complexes with the cationic polylysine dendrons. Instead of promoting cytosolic delivery the complexation may actually render the agonists less available for interaction with the receptors (i.e., TLR3 and TLR9).

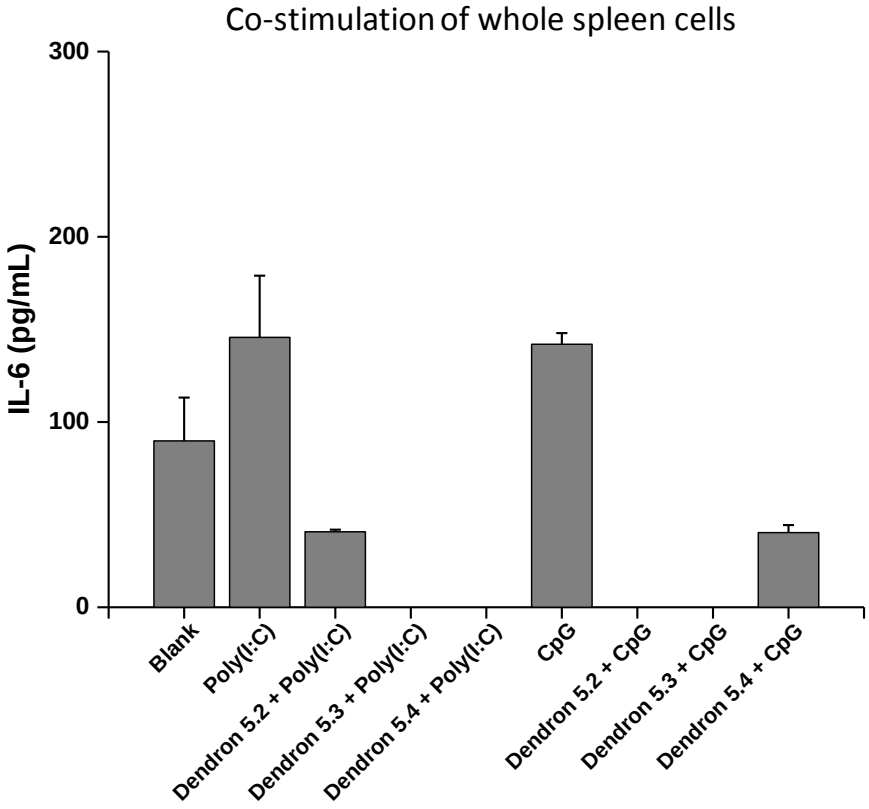

Figure 5.15 IL-6 levels (ELISA) after co-stimulation of whole spleen cells with MDP dendron library (100 µM) and poly(I:C) or CpG. Controls: poly(I:C) [20 µg/mL] and CpG [5 µg/mL] resulting in IL-6 concentrations of 146 pg/mL and 142 pg/mL, respectively. Mean of blank (culture medium only, n = 4) was 90 pg/mL +/- 23.4 pg/mL (SD). Mean and SEM of duplicate cultures are shown.

Next, the fMet dendron library was evaluated in murine whole spleen cells (Table 5.4). Also here, the immunostimulatory effects were studied by measuring the concentration of IL-6 in the supernatant of cultured cells and fMet and fMLP were employed as positive controls. In order to examine the effects of the alkyl chain, the dendrons were synthesized having a C1 or C16 alkyl chain at the C-terminal. The fMet dendron library consisted of G1 and G2 dendrons with two or four fMet motifs at the N-terminal, respectively, having a C1 or C16 alkyl chain (Fig. 5.16).

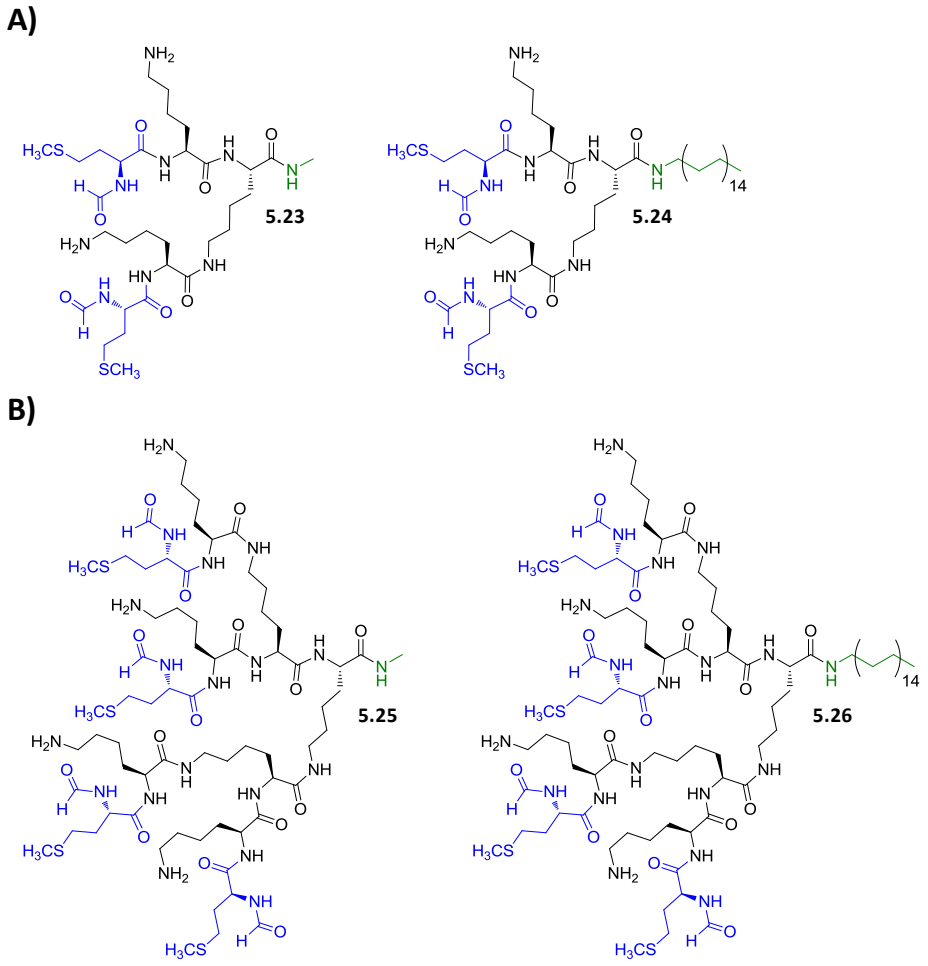

Figure 5.16 fMet dendron library. (A) G1 dendrons with two fMet motifs (blue) and a C1 (**5.23**) or C16 (**5.24**) alkyl chain (green). (B) G2 dendrons with four fMet motifs (blue) and a C1 (**5.25**) or C16 (**5.26**) alkyl chains (green).

Stimulation of whole spleen cells with positive controls (fMet and fMLP) did not show any response indicating that the employed concentrations were too low. What seems puzzling however, is the fact that the measured IL-6 levels are actually somewhat lower than the blank (90 pg/mL) (Fig. 5.17). This may again indicate some level of cytotoxicity resulting in cell death or weakening of the cells and cell viability studies should be performed in order to exclude cytotoxic effects from positive controls. Unfortunately, it was later realized that free fMet and fMet-dendrons were not tested in correct equimolar concentrations with respect to the fMet motif. A concentration of 100 µM fMet corresponds to 50 µM (G1 dendrons with two fMet) or 25 µM (G2 dendrons with four fMet). Therefore, the concentration employed for the dendrons (100 µM) is 2 to 4-fold higher than the equimolar concentration, which makes the results incomparable with the positive control. Nevertheless, the results obtained for the dendrons can be compared with each other and it is apparent that the effect of having a short alkyl chain (i.e., C1) has an enhancing impact on the immunostimulatory activity. Conversely, G1 and G2 dendrons having a longer alkyl chain (i.e., C16) do not display immunoactivity (Fig. 5.17). This may be attributed to the long flexible C16 chain blocking the receptor interaction due to steric hindrance. In addition, it can also be assumed that the hydrophobic alkyl chain may result in cell membrane interaction and penetration, thereby

internalizing the dendrons. The internalization would render the dendrons unavailable for interaction with the putative receptor (i.e., FPR1), which is a seven-transmembrane GPCR.[1] Interestingly, this hypothesis also fits with the observed immunostimulatory activity (presuming the interacting receptor is NOD2, which is present in the cytosol[1]) (Fig. 5.14) and cross-antagonistic activity (Fig. 5.15) of the MDP dendron library. However, the hypothesis does not hold true if the immunostimulatory activity is caused by TLR2 recognition, since this receptor is situated on the cell membrane.[1]

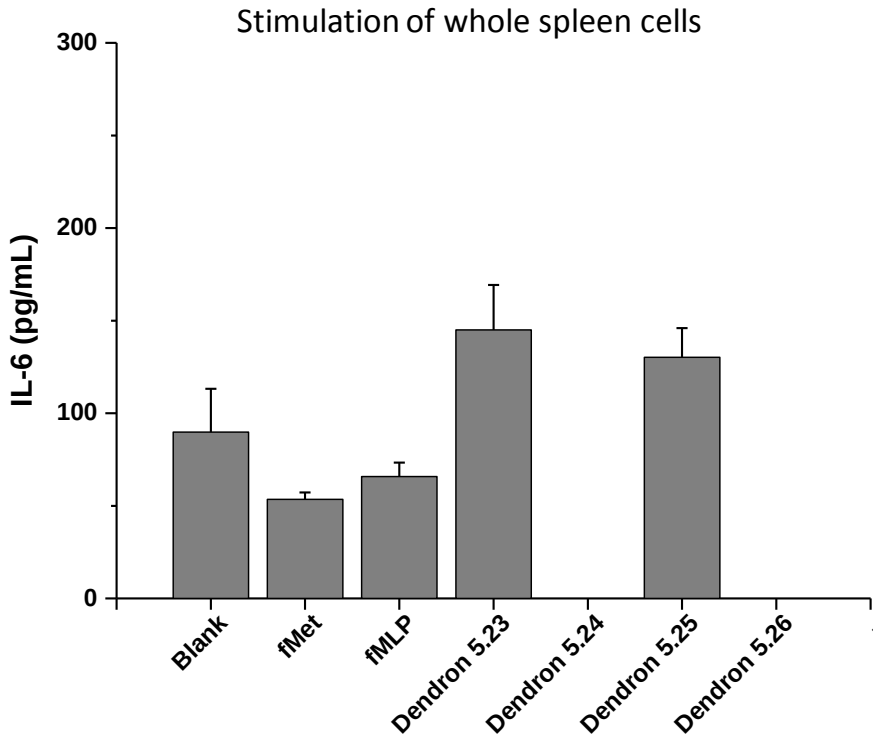

Figure 5.17 IL-6 levels (ELISA) after stimulation of whole spleen cells with fMet dendron library at 100 µM concentrations. Positive controls: fMet and fMLP at 100 µM concentrations. Mean of blank (culture medium only, n = 4) was 90 pg/mL +/- 23.4 pg/mL (SD). Mean and SEM of duplicate cultures are shown.

An increased fMet-multimerization in the G2 dendron (**5.25**) did not enhance the immunostimulatory property and somewhat lower IL-6 values were observed compared to the G1 dendron (**5.23**) (Fig. 5.17). Although the IL-6 values are very close, the somewhat lower values obtained for the G2 dendron could be attributed to steric effects due a bigger lysine head group making receptor interactions more difficult. Nevertheless, it is ambitious to give a statistical significance to the difference observed, as the high standard deviations (24.2 pg/mL for **5.23** and 15.8 pg/mL for **5.25**) will hide the small difference observed.

5.3 Preliminary conclusion

Two small libraries of G1 and/or G2 polylysine dendrons with a C1 and/or C16 alkyl chain modified with PAMP motifs were successfully synthesized by SPPS. The employed PAMP motifs

were MDP, ^{D}isoGln-Ala (dipeptide component of MDP) and fMet. The synthesis of G1(MDP)$_4$-C16 proved to be difficult and attempts to optimize the procedure by employing HBTU and benzylidene-benzyl protected Ac-Mur did not yield satisfactory results. The benzylidene-benzyl protected Ac-Mur apparently was too sterically hindered for a successful coupling with the already crowded dendron. Furthermore, solid-phase reactions generally have slower reaction kinetics, since the reagents have to work in a two-phase system and have to reach the functional groups in the interior of the polymeric network. Therefore, possible approaches to optimize the coupling reaction could be by employing stronger coupling reagents in order to push the reaction to completion or performing the last coupling in solution phase. In addition, the the protected MDP could be prepared separately and subsequently coupled to the dendron. An attempt to expand the fMet library with fMLP modified dendrons was unsuccessful. UPLC-MS analysis of different dendrons modified with fMLP, fMet-Phe or fMet-Leu displayed several peaks by UPLC-MS with identical masses. Since IR and ^{1}H-NMR of the isolated peaks were identical, the peaks could not be due to rearrangements at the fMet group yielding constitutional isomers. Instead it was reasoned the different peaks may be caused by stereoisomers due to racemization at fMet through oxazolone formation. Since this pattern was not observed with dendrons modified with only fMet, a rational explanation could be due to the linkage of additional amino acids (i.e., Phe and Leu) increasing the steric crowding thereby slowing down reaction kinetics. Therefore, the prolonged contact of activated fMet with the basic medium may result in deprotonation of the acidic N^{α}-proton and racemization.

Although the preliminary immunological tests have to be optimized and repeated, some interesting preliminary conclusions can be drawn from the observations. The unmodified polylysine dendrons from the MDP library did not display any intrinsic immunostimulatory activity and exchanging the L-lysine core with D-lysine did not change this. Only G1(^{D}isoGln-Ala)$_2$-C16 (**5.2**) and G1(MDP)$_2$-C16 (**5.3**) from the MDP library displayed immunostimulatory activity. The lack of activity observed for G1(^{D}isoGln-Ala)$_4$-C16 (**5.4**) was speculated to be due to an increased sterical hindrance obstructing interaction with the putative receptor. Furthermore, these dendrons displayed exciting cross-antagonistic activities against poly(I:C) and CpG ODN by complete or partial inhibition and additional tests are needed in order to elucidate the mechanism behind this effect, which may be due to electrostatic effects from complexation with the cationic polylysine dendrons. Moreover, only G1 and G2 dendrons from the fMet library having a C1 alkyl chain exhibited immunostimulatory activity. A possible explanation could be due to the long flexible C16 alkyl chain hindering receptor interaction. In addition, it could also be proposed that the hydrophobic C16 alkyl chain displays improved cell membrane interactions resulting in internalization of the dendrons making them unavailable for interaction with the putative GPCR receptor (FPR1). Increasing the multivalent presentation of fMet (G1 vs. G2) did not amplify the immunostimulatory activity. This may be attributed to the larger lysine head group in the G2 dendron having a negative impact on receptor interaction. Since free fMet and MDP were not employed in equimolar concentrations, the immunological tests have to be repeated in order to obtain results of higher quality. Additional tests hopefully will also elucidate the mechanism behind the immunostimulatory activity observed for certain dendrons and cross-antagonistic activities. Furthermore, it could be

interesting to expand the MDP library with G2 dendrons and dendrons having a C1 alkyl chain. Finally, cell viability studies are certainly needed in order to elucidate if the reduced basic level of IL-6 seen with some dendrons are due to cytotoxic effects.

6 Conclusions

Due to their molecularly well-defined (monodisperse) nature, multiple functionalizable amino surface groups, biocompatibility and biodegradability, polylysine dendrons were chosen as molecular scaffolds for multivalent presentation of immunostimulatory motifs in the quest to develop new possible adjuvants.

A straightforward solid-phase peptide synthetic approach employing backbone amide linkers was developed and described in Chapter 2. With this method, which was well-suited for automatization, it was possible to introduce desired C-terminal functionalities in polylysine dendrons whereby polyfunctional dendrons with preferred properties could be prepared. G1 and G2 polylysine dendrons were prepared in high crude purities by a divergent approach containing N-terminal antigenic pentapeptide motifs (half T cell epitope) and a dodecyl chain or alkyne at the C-terminal demonstrating the scope of the method. The alkyne functionality was chosen to illustrate the possibility for further functionalization by a click chemistry approach. With the developed approach, a reliable and fast colorimetric method for on-bead reaction monitoring of the reductive amination (whereby the C-terminal functionality was introduced) and subsequent acylation step was needed. This led to the development of the acetaldehyde test for selective detection of secondary amines with a broad scope (Chapter 3).

In order to investigate the self-assembling properties of the polylysine dendron scaffold, a library of G1 and G2 dendrons with variable alkyl chain lengths at the C-terminal were synthesized and characterized by SANS and DLS (Chapter 4). The amphiphilic polylysine dendrons exhibited self-assembling properties above the CMC. By SANS it was shown, that dendrons containing an alkyl chain above C12 would self-assemble into micellar structures of around 5 nm in diameter with hydrophobic alkyl chains in the interior and hydrophilic polylysine head groups forming the shell. The micelle forming ability was controlled by the length of the alkyl chain, electrostatic interactions and steric factors. Electrostatic interactions seemed to play an important role in the micelle forming ability, since reduction of positively charged amines in the polylysine head groups displayed stabilizing effects. In addition, the size of the polylysine head group also played a role as the bulky head group in a G2 dendron appeared to destabilize the micellar structure relative to a G1 dendron. Further characterization by DLS revealed larger entities (65-370 nm), which for dendrons having alkyl chain lengths above C12 presumably were formed by clusters of micelles. However, for dendrons with alkyl chain lengths below C14 these larger structures were apparently due to more random assemblies. Importantly, the polylysine scaffolds proved to be biocompatible up to 20 µM exhibiting cell viability well above 80%, which was impressive considering the multiple cationic amino surface groups and hydrophobic alkyl chain.

Finally in Chapter 5, chosen dendrons were modified with immunostimulatory motifs. The ability of the polylysine scaffold to enhance the immunostimulatory activity of chosen PAMPs through the *dendritic effect* was investigated. The preliminary results demonstrated no intrinsic immunoactivity of polylysine scaffolds. Moderate levels of immunoactivity were observed for G1 dendrons with

two MDP (**5.3**) or ^{D}isoGln-Ala (**5.2**) motifs, whereas a G1 dendron modified with four ^{D}isoGln-Ala (**5.4**) motifs exhibited no immunoactivity. Since equimolar concentrations with respect to free MDP were not employed, it is difficult to state whether the moderate level of immunoactivity was due to the *dendritic effect* without further studies. The lacking activity of **5.4** appears to be due to steric hindrance blocking interaction with the putative receptor. In addition, cross-antagonistic activities were observed for these dendrons (**5.2**, **5.3** and **5.4**), which displayed full or partial antagonistic activity against known TLR agonists. Additional studies are needed in order to elucidate the mechanism behind this observation, which could very well be due to complexation of the anionic TLR agonists and cationic polylysine dendrons hindering successful interaction with the receptors. Furthermore, G1 and G2 dendrons modified with two (**5.23**) or four (**5.25**) fMet motifs having a C-terminal methyl group exhibited moderate and comparable immunoactivities. Therefore, the increased multivalency in G2 dendrons does not seem to further enhance the immunostimulatory activity of the PAMP motifs compared to G1 dendrons, which was the original hypothesis. The lack of immunoactivity of similar dendrons with a C16 alkyl chain (**5.24** and **5.26**) may be explained by steric effects or internalization hindering receptor interaction. Nevertheless, the preliminary results need to be optimized and repeated in order to validate the observations and hypotheses. In addition, cell viability studies should be performed to exclude cytotoxic effects. Furthermore, it could be interesting to include other relevant immunomodulatory motifs on polylysine dendrons in future studies and optimize the synthetic procedure for the synthesis of G1$(MDP)_4$-C16 (**5.8**), which due to synthetic difficulties could not be prepared in time for preliminary tests. Moreover, the modified dendrons should be characterized by SANS and DLS in order to compare with results obtained from polylysine scaffolds and acquire a better understanding of the physicochemical properties. Finally, as well as being explored as possible adjuvants, the project may very well be broadened to include research in applying these biocompatible polyfunctional dendrons as, e.g., gene delivery and drug delivery systems.

7 Experimental section

This chapter contains experimental procedures for compound **5.17**, **5.19**, **5.28** and compounds from Table 4.2, 5.1 and 5.3, which are not already described in publication I-III. The experimental procedures are ordered according to corresponding chapters in the thesis, where the compounds are presented. The FMPB derivatized resin was prepared according to publication III, where physicochemical (SANS, DLS, zeta potential and pH) and cell viability methods also can be found. Experimental procedures for the sensitivity tests employed in Chapter 3 can be found in publication II together with synthetic procedures for the preparation of resin substrates.

General Remarks

All starting materials were purchased from Sigma-Aldrich, IRIS Biotech GmBH, Merck Chemicals, Bachem and Carbosynth Limited and used without further purification. Solvents of HPLC grade were purchased from Fischer Scientific and VWR International and dry (anhydrous) dioxane was purchased from Sigma-Aldrich. Aminomethylated PS (50-100 mesh; 2 mmol/g loading; 1% DVB cross-linked) was employed for the synthesis of dendrons. The solid-phase reactions were performed in polypropylene syringes equipped with a polytetrafluroethylene (PTFE) filter placed on a shaker. Manual washing of the resins was carried out on Torviq plates using around 30 mL/g resin for each wash. After the reductive amination step, the resin was typically washed with MeOH (3x), NMP and DCM (15x), MeOH (3x), NMP (5x), DCM (5x) and MeOH (2x). Washing for the subsequent steps was typically performed with NMP and DCM (10x) and MeOH (3x). Fmoc deprotection was typically carried out with 20 vol. % piperidine in NMP (20 mL/g resin) for 3 + 30 + (30) + 20 min. TLC analysis was performed on silica gel 60 F_{254} plates. Compounds were characterized by ^{1}H-NMR (600 MHz or 400 MHz) and ^{13}C-NMR (151 MHz or 101 MHz) using a Bruker Ultrashield AVANCE and AVANCE II 600 (University of Olso) or Bruker Ascend 400 with cryo platforms. Spectra were calibrated relative to residual solvent peaks (^{1}H-NMR [D_2O: 4.79 ppm; DMSO-d_6: 2.50 ppm; $CDCl_3$: 7.26 ppm], ^{13}C-NMR [DMSO-d_6: 39.52 ppm; $CDCl_3$: 77.16 ppm]). ^{1}H-NMR and ^{13}C-NMR spectra of dendrons from Chapter 4 were assigned by comparing with spectra of similar dendrons (Table 4.1), which were thoroughly characterized in publication III. PAMP modified dendrons from Chapter 5 were characterized by looking at fingerprint regions in ^{1}H-NMR and ^{13}C-NMR by comparing with spectra from unmodified dendrons. ^{13}C-NMR spectra are not included for all compounds due to the poor quality in few cases. The ^{1}H integrals of some protons occasionally deviates from the proposed dendron structure and are marked with a dagger (†). Presumably this is due to slow relaxation. However, UPLC-MS chromatograms and ^{13}C spectra correlate nicely with the proposed structure. The numbers of carbon atoms in the ^{13}C spectra are not always equal to the number present in the molecular formula presumably due to the high number of peaks overlapping and equivalent carbons giving rise to only one peak. Reversed-phase UPLC-MS analysis was conducted on an equipment comprising of a Shimadzu Nexera X2 and a Bruker MicrOTOF-Q III, using a Phenomenex Kinetex C8 column (2.6 µm, 100 Å, 50x2.1 mm) or Ascentis Express Peptide ES-C18 column (2.7µm, 160 Å, 50x2.1 mm) and a 1 mL/min linear gradient 0-2.7 min (0-20% buffer B), 2.7-6.0 min (20-100% buffer B), 6.0-7.0 min (100-0% buffer

B), stop time 8.2 min. Buffer A: 0.025% TFA in 10% aqueous MeCN. Buffer B: 0.025% TFA in 90% aqueous MeCN. Preparative reversed-phase HPLC purification was conducted on a Prominence UFLC CBM-20A system from Shimadzu, using an Ascentis C18 column (5 µm, 100 Å, 250x10 mm) or a Phenomenex Jupiter C18 column (10 µm, 300 Å, 250x30 mm). The linear gradient of buffer A and B was adjusted according to the compound to be purified. The flow rates employed were 8 mL/min or 55 mL/min for Ascentis C18 and Phenomenex Jupiter C18 columns, respectively. Infrared spectroscopy (IR) was performed directly on the resin beads by a Shimadzu IR-affinity spectrometer using attenuated technique of reflectance (ATR). High-resolution mass spectra (HRMS) of PAMP modified dendrons were obtained (except dendrons **5.19**, **5.26** and **5.28**) on a Bruker micrOTOF-Q II (ESI) (University of Southern Denmark).

General Procedures

In general procedure III and IV the employed reagents were calculated based on halved resin loadings (i.e., 1 mmol/g). However, in few cases the calculations were based on full loading (i.e., 2 mmol/g) and indicated with an asterisk (*). A plus (+) sign between reaction times indicates removal of the reaction mixture by washing and addition of fresh reagents for subsequent reaction repeat. In cases were protected L-lysine or D-lysine is mentioned, the dendrons were synthesized only containing one enantiomer and never a mixture in order to maintain stereochemical homogeneity. Thus, when employing D-lysine the subsequent lysines were of the D-configuration and vice versa.

General procedure (GP) I: Cleavage from resin

The derivatized resin was treated with TFA/DCM (1:1) or 5 vol. % TIS in TFA/DCM (1:1) (20 mL/g resin) and shaken for 2 h, followed by filtration and collection of the cleavage mixture in a round bottomed flask. Evaporation *in vacuo* and precipitation in cold Et_2O yielded the product.

GP II: TFA exchange with HCl[143]

Anion-exchange was performed treating the dendron twice with 0.1 M HCl (30 mL) for 2 h under stirring at rt following lypophilization, which yielded the final product.

GP III: G1 dendrons

The FMPB-derivatized resin (500 mg, [0.5 mmol] or [1.0 mmol]*, 1 equiv.), $NaBH_3CN$ ([5 mmol, 10 equiv.] or [12.5 mmol , 12.5 equiv.]*) and amine ([5 mmol, 10 equiv] or [12.5 mmol, 12.5 equiv.]*) were suspended in a 5 vol. % AcOH in NMP solution (6mL) in a 20 mL filter syringe and shaken at rt. After 20 h or 2 + 3 h*, the resin was washed followed by air-drying and drying *in vacuo*. DNPH test (negative, pale orange to yellow beads) and acetaldehyde test (positive, orange-brown beads) were performed. Fmoc-^{L}Lys(Fmoc)-OH or Fmoc-^{D}Lys(Fmoc)-OH ([2.5 mmol] or [5 mmol]*, 5 equiv.) and DIC ([1.25 mmol] or [2.5 mmol]*, 2.5 equiv.) were added to the filter syringe containing the derivatized resin and DCM/NMP (95:5, 10 mL). The suspension was mixed using a spatula until a waxy mass was obtained with evenly distributed beads. After 20 h or 2 + 2 h*, the resin was washed followed by air-drying and drying *in vacuo*. Acetaldehyde test (negative,

colorless beads) was carried out. Fmoc deprotection was conducted followed by washing. Fmoc-^{L}Lys(Boc)-OH or Fmoc-^{D}Lys(Boc)-OH (2 mmol, 4 equiv.), PyBOP (1.9 mmol, 3.8 equiv.) and DIPEA (3.9 mmol, 7.8 equiv.) were transferred to the filter syringe containing the derivatized resin and NMP (6mL) and shaken for 3-20 h at rt, or repeated until ninhydrin test was negative. The resin was washed followed by Fmoc deprotection. Cleavage of the final dendron from the resin was conducted as described in GP I.

GP IV: G2 dendrons

The G2 dendrons were synthesized according to GP III up to and including Fmoc deprotection of the first lysine residue followed by washing. Fmoc-^{L}Lys(Fmoc)-OH or Fmoc-^{D}Lys(Fmoc)-OH (2 mmol, 4 equiv.), PyBOP (1.9 mmol, 3.8 equiv.) and DIPEA (3.9 mmol, 7.8 equiv.) were added to the filter syringe containing the derivatized resin and NMP (6 mL) and shaken for 3-20 h at rt, or repeated until ninhydrin test was negative. The resin was washed followed by Fmoc deprotection. Fmoc-^{L}Lys(Boc)-OH or Fmoc-^{D}Lys(Boc)-OH (2 mmol, 4 equiv.), PyBOP (1.9 mmol, 3.8 equiv.) and DIPEA (3.9 mmol, 7.8 equiv.) were transferred to the filter syringe containing the derivatized resin and NMP (6mL) and shaken for 3-20 h at rt, or repeated until ninhydrin test was negative. The resin was washed followed by Fmoc deprotection. Cleavage of the final dendron from the resin was conducted as described in GP I.

GP V: Partially acetylated G1 and G2 dendrons

The partially acetylated G1 and G2 dendrons were synthesized according to GP III. However, prior to the cleavage step, the derivatized resin was treated with Ac_2O/DIPEA/DCM (20 mL/g resin, 10/5/85) and shaken for 3 h or until ninhydrin test was negative. The resin was washed followed by air-drying. Cleavage of the final dendron from the resin was performed by following GP I.

Compounds from Chapter 4

G1-PDL(acetyl)-C4 (4.15)

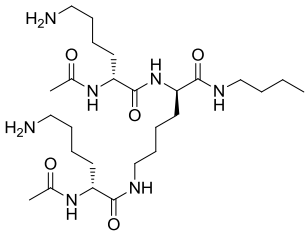

Dendron **4.15** was prepared according to GP III and V to give 104 mg (60% as TFA salt) of the title compound as a white powder. UPLC-MS data R_t: 0.5-0.7 min. MS(ESI$^+$), calcd $C_{26}H_{51}N_7O_5$: 541.40 g/mol, found: m/z 542.40 $[MH]^+$. ^{1}H-NMR (400 MHz, D_2O): δ 4.30 – 4.11 (m, 3H), 3.18 (m, 4H), 3.06 – 2.93 (m, 4H), 2.03 (s, 5H)†, 1.87 – 1.60 (m, 10H), 1.58 – 1.22 (m, 10H) †, 0.88 (t, *J* = 7.3 Hz, 3H). ^{13}C-NMR (101 MHz, D_2O) δ 174.23, 174.16, 173.93, 173.85, 173.44, 53.97, 53.61, 39.13, 38.97, 38.91, 30.51, 30.45, 30.37, 27.78, 26.27, 26.25, 22.34, 22.11, 21.99, 21.64, 21.58, 19.28, 12.92.

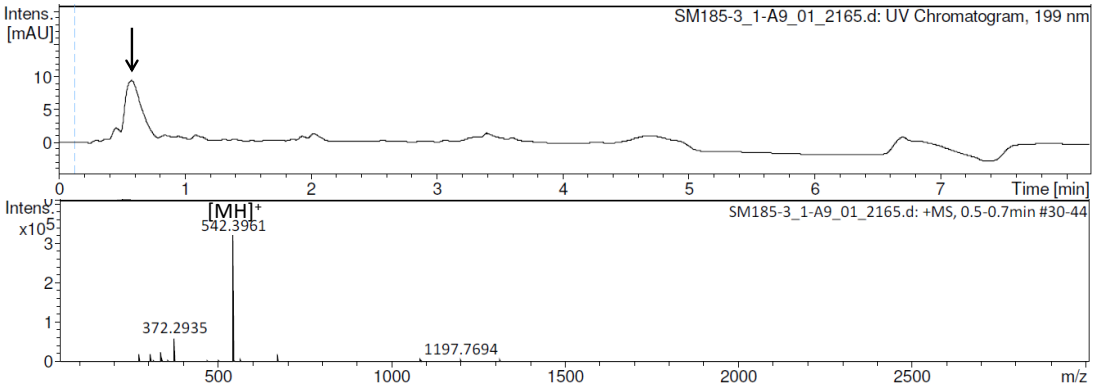

G1-PDL(acetyl)-C6 (4.16)

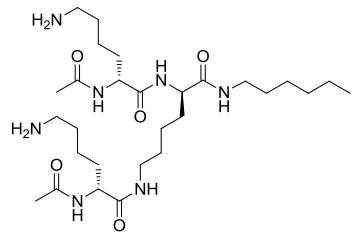

Dendron **4.16** was prepared according to GP III and V to give 101 mg (62% as TFA salt) of the title compound as a white powder. UPLC-MS data R_t: 1.8-2.0 min. MS(ESI$^+$), calcd $C_{28}H_{55}N_7O_5$: 569.43 g/mol, found: m/z 285.72 $[MH_2/2]^+$; 570.42 $[MH]^+$; 1139.83 $[2M+H]^+$. ^{1}H-NMR (400 MHz, D_2O) δ 4.32 – 4.12 (m, 3H), 3.28 – 3.09 (m, 4H), 3.05 – 2.94 (m, 4H), 2.04 (s, 5H)†, 1.87 – 1.60 (m, 10H), 1.57 – 1.33 (m, 6H)†, 1.28 (m, 7H)†, 0.93 – 0.80 (m, 3H). ^{13}C-NMR (101 MHz, D_2O) δ 174.22, 174.14, 173.87, 173.82, 173.40, 53.96, 53.61, 39.25, 39.13, 38.93, 30.62, 30.53, 30.50, 30.46, 28.17, 27.78, 26.28, 26.26, 25.61, 22.34, 22.12, 22.01, 21.92, 21.65, 21.60, 13.32.

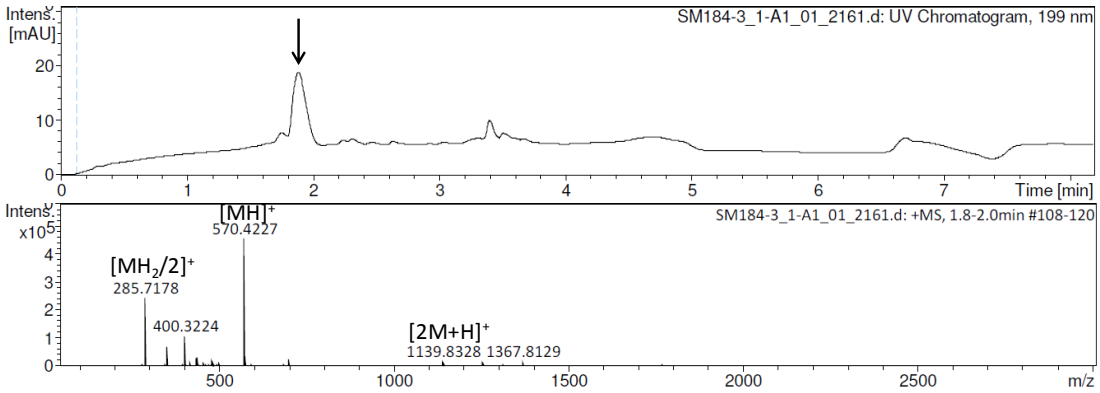

G1-PDL(acetyl)-C8 (4.17)

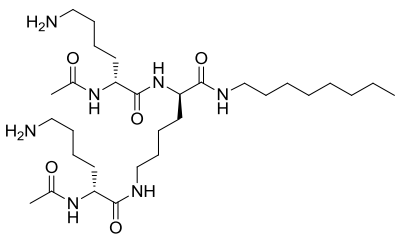

Dendron **4.17** was prepared according to GP III and V. Anion-exchange was performed according to GP II. Preparative reversed-phase HPLC purification yielded 26 mg (23% as HCl salt) of the title compound as a white powder. UPLC-MS data R_t: 2.0-2.2 min. MS(ESI$^+$), calcd $C_{30}H_{59}N_7O_5$: 597.46 g/mol, found: m/z 598.45 $[MH]^+$; 1195.86 $[2M+H]^+$. ^{1}H-NMR (400 MHz, D_2O) δ 4.31 – 4.14

(m, 3H), 3.20 (m, 4H), 3.00 (m, 5H)†, 2.04 (s, 6H), 1.86 – 1.63 (m, 7H)†, 1.48 (m, 6H)†, 1.28 (m, 12H)†, 0.91 – 0.81 (m, 3H). ^{13}C-NMR (101 MHz, D_2O) δ 174.24, 174.15, 173.88, 173.81, 173.41, 53.97, 53.95, 53.60, 39.24, 39.14, 38.95, 31.05, 30.54, 30.52, 30.46, 28.38, 28.27, 28.17, 27.80, 26.28, 26.26, 25.91, 22.35, 22.13, 22.01, 21.66, 21.60, 13.42.

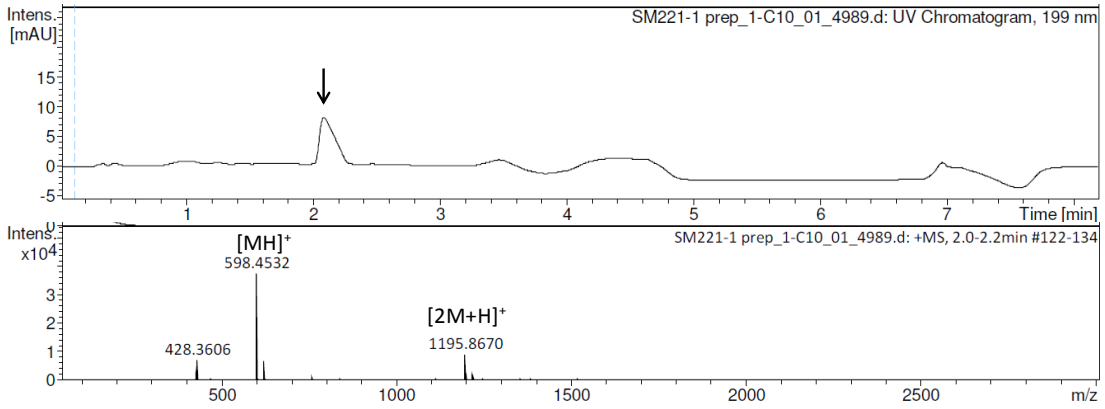

G1-PDL-C10 (4.18)

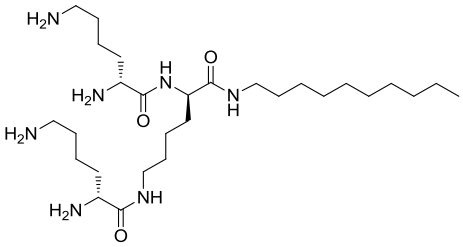

Dendron **4.18** was prepared according to GP III. Preparative reversed-phase HPLC purification yielded 66 mg (32% as TFA salt) of the title compound as a white powder. UPLC-MS data R_t: 1.9-2.2 min. MS(ESI$^+$), calcd $C_{28}H_{59}N_7O_3$: 541.47 g/mol, found: m/z 542.48 $[MH]^+$; 1083.91 $[2M+H]^+$. ^{1}H-NMR (400 MHz, D_2O) δ 4.25 (t, *J* = 7.4 Hz, 1H), 4.05 (t, *J* = 6.5 Hz, 1H), 3.95 (t, *J* = 6.7 Hz, 1H), 3.33 – 3.07 (m, 4H), 3.02 (m, 4H), 1.91 (q, *J* = 8.2 Hz, 4H), 1.73 (m, 6H), 1.63 – 1.36 (m, 6H)†, 1.29 (m, 15H)†, 0.87 (t, *J* = 6.5 Hz, 3H). ^{13}C-NMR (101 MHz, D_2O) δ 172.98, 169.33, 169.23, 54.29, 53.08, 52.66, 39.28, 38.97, 38.95, 31.18, 30.59, 30.39, 30.37, 28.68, 28.66, 28.48, 28.30, 28.19, 27.88, 26.34, 26.33, 25.97, 22.47, 22.04, 21.33, 21.06, 13.43.

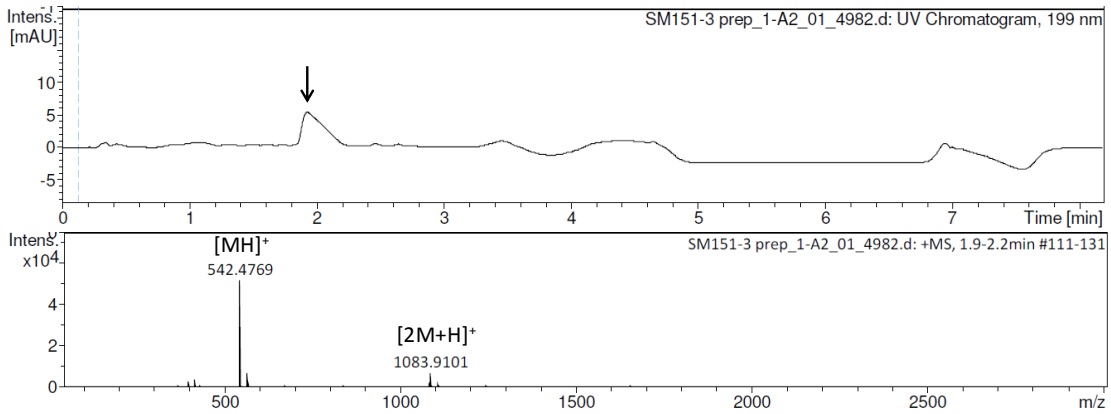

G1-PDL-C12 (4.19)

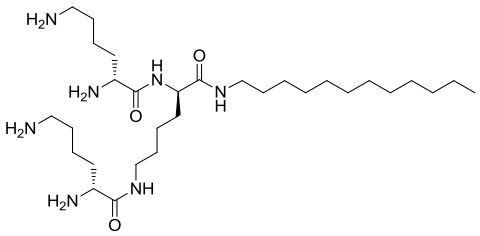

Dendron **4.19** was prepared according to GP III. Preparative reversed-phase HPLC purification yielded 10 mg (7% as TFA salt) of the title compound as a white powder. UPLC-MS data R_t: 2.8-3.0 min. MS(ESI$^+$), calcd $C_{30}H_{63}N_7O_3$: 569.50 g/mol, found: m/z 570.51 $[MH]^+$; 1139.98 $[2M+H]^+$. ^{1}H NMR (400 MHz, D_2O) δ 4.25 (t, *J* = 7.4 Hz, 1H), 4.03 (t, *J* = 6.5 Hz, 1H), 3.93 (t, *J* = 6.7 Hz, 1H), 3.33 – 3.08 (m, 4H), 3.01 (m, 4H), 1.91 (m, 4H), 1.73 (m, 6H), 1.62 – 1.34 (m, 6H)†, 1.29 (m, 18H), 0.87 (t, *J* = 6.5 Hz, 3H).

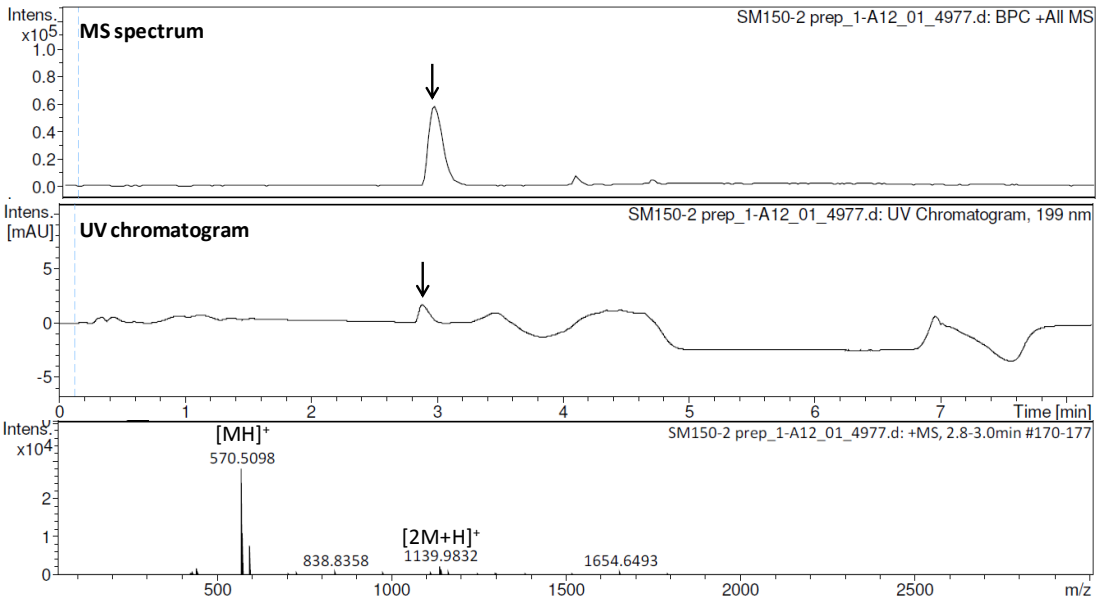

G1-benzyl (4.20)

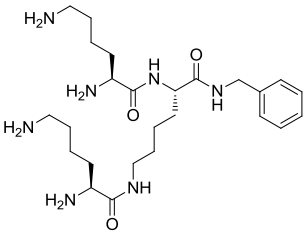

Dendron **4.20** was prepared according to GP III to give 131 mg (68% as TFA salt) of the title compound as an off-white powder. UPLC-MS data R_t: 0.2-0.4 min. MS(ESI$^+$), calcd $C_{25}H_{45}N_7O_3$: 491.36 g/mol, found: m/z 492.35 $[MH]^+$. ^{1}H-NMR (600 MHz, D_2O) δ 7.48 – 7.43 (m, 2H), 7.41 – 7.33 (m, 3H), 4.55 – 4.28 (m, 3H), 4.06 (t, *J* = 6.5 Hz, 1H), 3.95 (t, *J* = 6.7 Hz, 1H), 3.26 – 3.21 (m, 2H), 3.06 – 2.99 (m, 2H), 2.88 (t, *J* = 7.7 Hz, 2H), 1.97 – 1.87 (m, 4H), 1.86 – 1.77 (m, 2H), 1.77 – 1.69 (m, 2H), 1.69 – 1.62 (m, 2H), 1.61 – 1.53 (m, 2H), 1.51 – 1.30 (m, 3H)†. ^{13}C-NMR (151 MHz, D_2O) δ 173.35, 169.44, 169.27, 137.85, 128.77, 127.51, 127.24, 54.32, 53.11, 52.67, 42.95, 39.27, 38.97, 38.90, 30.45, 30.39, 30.36, 27.82, 26.35, 26.31, 22.44, 21.32, 20.98.

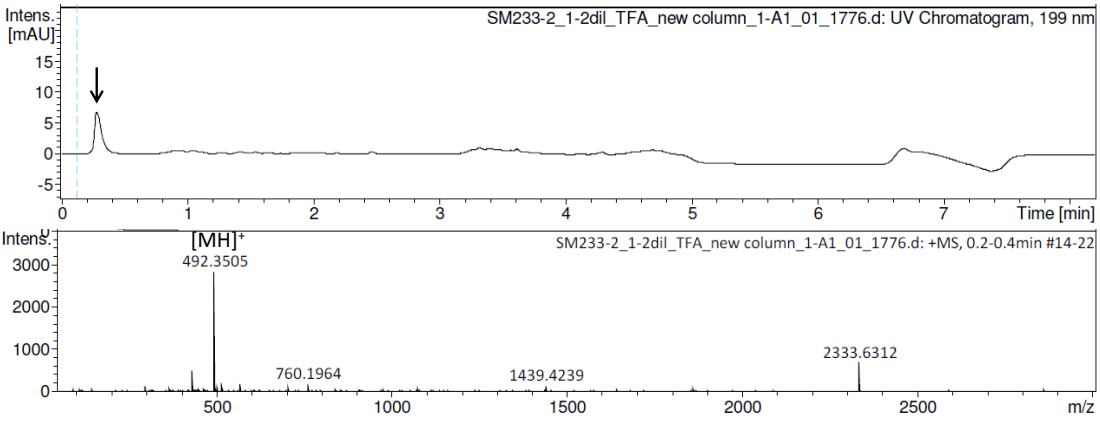

G2-C4 (4.21)

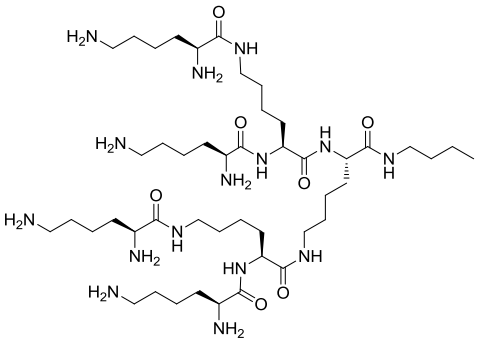

Dendron **4.21** was prepared according to GP IV. Anion-exchange was performed according to GP II to give 70 mg (63% as HCl salt) of the title compound as a white powder. UPLC-MS data R_t: 0.2-0.3 min. MS(ESI$^+$), calcd $C_{46}H_{95}N_{15}O_7$: 969.75 g/mol, found: m/z 485.87 $[MH_2/2]^+$; 970.71 $[MH]^+$. ^{1}H-NMR (600 MHz, D_2O) δ 4.38 (t, *J* = 7.0 Hz, 1H), 4.29 (t, *J* = 7.3 Hz, 1H), 4.22 (t, *J* = 7.3 Hz, 1H), 4.14 – 4.06 (m, 2H), 4.01 (t, *J* = 6.7 Hz, 2H), 3.34 – 3.10 (m, 12H)†, 3.10 – 3.01 (m, 8H), 2.00 – 1.89 (m, 8H), 1.88 – 1.68 (m, 14H), 1.67 – 1.27 (m, 29H)†, 0.97 – 0.86 (m, 5H)†. ^{13}C-NMR (151 MHz, D_2O) δ 173.36, 173.30, 173.23, 169.61, 169.55, 169.34, 169.31, 54.36, 54.34, 53.85, 53.14, 52.73, 39.34, 39.32, 39.17, 39.03, 30.67, 30.64, 30.59, 30.45, 30.43, 30.39, 30.38, 28.01, 27.97, 27.92, 26.38, 26.35, 22.56, 22.46, 22.22, 21.37, 21.36, 21.19, 21.16, 19.36, 13.01.

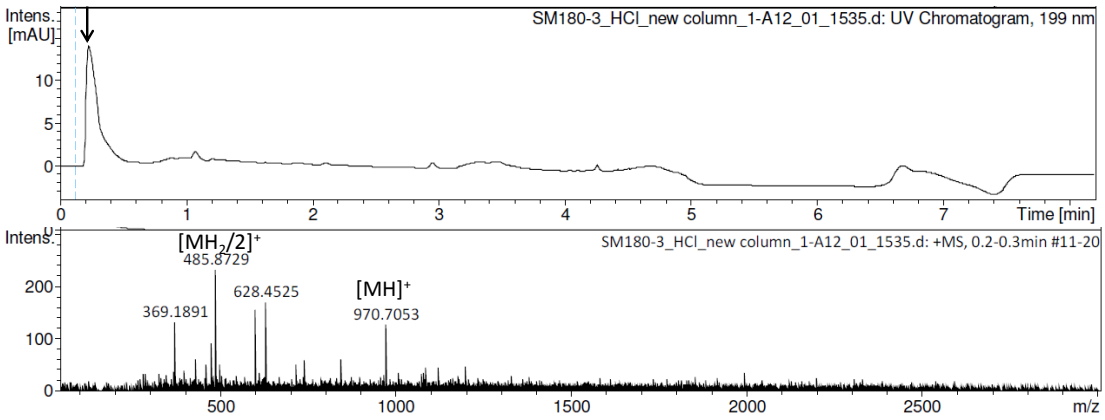

G2(acetyl)-C4 (4.22)

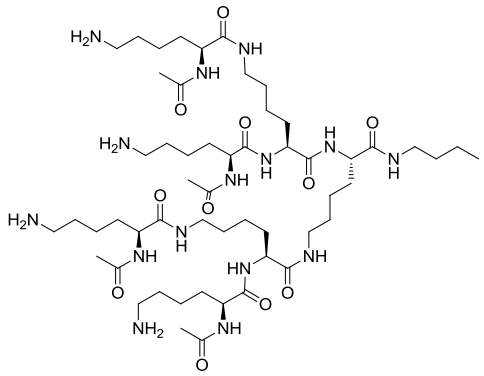

Dendron **4.22** was prepared according to GP IV and V. Anion-exchange was performed according to GP II. Preparative reversed-phase HPLC purification yielded 25 mg (24% as HCl salt) of the title compound as an off-white powder. UPLC-MS data R_t: 0.3-0.4 min. MS(ESI$^+$), calcd $C_{54}H_{103}N_{15}O_{11}$: 1137.80 g/mol, found: m/z 569.91 $[MH_2/2]^+$; 1138.77 $[MH]^+$. ^{1}H-NMR (400 MHz, D_2O) δ 4.33 – 4.12 (m, 7H), 3.29 – 3.10 (m, 6H)†, 3.01 (m, 8H), 2.04 (s, 11H)†, 1.90 – 1.63 (m, 11H)†, 1.61 – 1.22 (m, 15H)†, 0.88 (t, *J* = 7.3 Hz, 3H). ^{13}C-NMR (101 MHz, D_2O) δ 174.30, 174.27, 174.20, 174.16, 174.04, 173.89, 173.72, 173.57, 173.42, 54.15, 54.01, 53.97, 53.66, 53.60, 39.16, 38.99, 38.93, 30.51, 30.48, 30.45, 30.41, 27.81, 26.26, 22.40, 22.32, 22.14, 22.08, 22.05, 22.01, 21.69, 21.66, 19.31, 12.97.

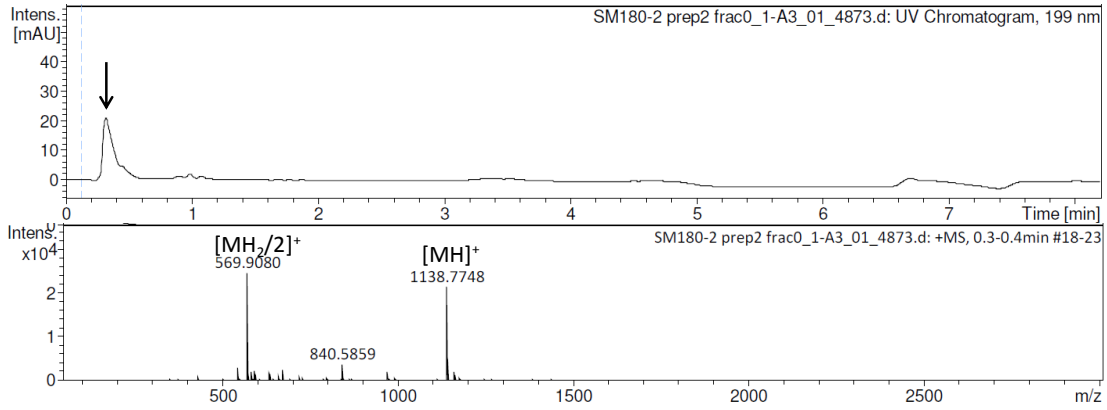

G2-PDL(acetyl)-C4 (4.23)

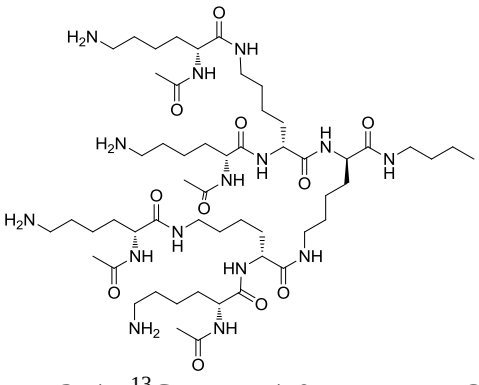

Dendron **4.23** was prepared according to GP IV and V. Anion-exchange was performed according to GP II. Preparative reversed-phase HPLC purification yielded 26 mg (15% as HCl salt) of the title compound as an off-white powder. UPLC-MS data R_t: 0.3-0.4 min. MS(ESI$^+$), calcd $C_{54}H_{103}N_{15}O_{11}$: 1137.80 g/mol, found: m/z 569.91 $[MH_2/2]^+$; 1138.77 $[MH]^+$. ^{1}H-NMR (400 MHz, D_2O) δ 4.32 – 4.12 (m, 7H), 3.25 – 3.13 (m, 7H)†, 3.00 (m, 9H)†, 2.04 (s, 11H)†, 1.87 – 1.61 (m, 12H)†, 1.58 – 1.22 (m, 13H)†, 0.88 (t, *J* = 7.3 Hz, 3H). ^{13}C-NMR (101 MHz, D_2O) δ 174.30, 174.27, 174.19, 174.16, 174.04, 173.88, 173.72, 173.57, 173.41, 54.14, 54.01, 53.66, 53.60, 39.16, 38.98, 38.93, 30.50, 30.42, 30.38, 27.81, 26.26, 22.39, 22.32, 22.14, 22.08, 22.04, 21.69, 21.66, 19.31, 12.96.

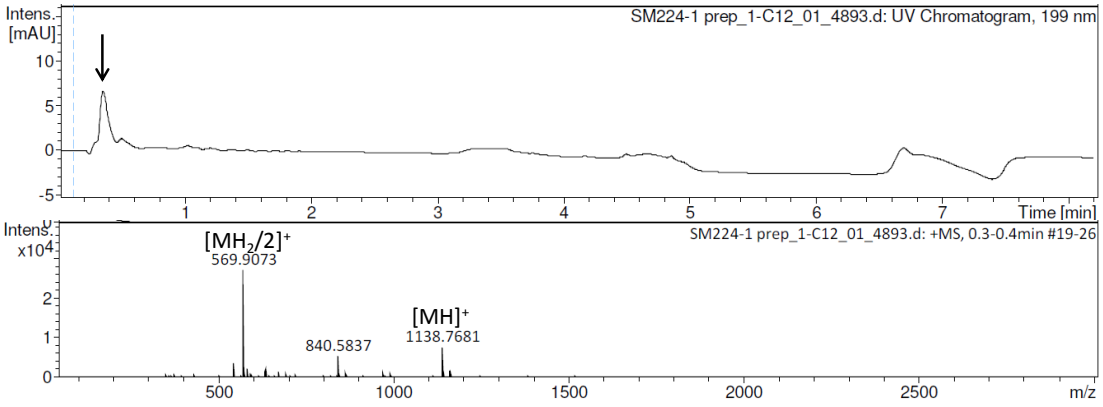

G2(acetyl)-C8 (4.24)

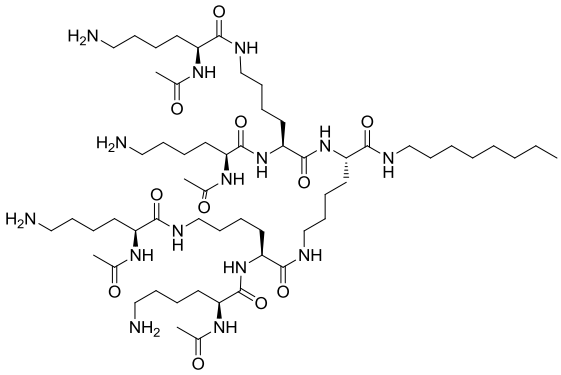

Dendron **4.24** was prepared according to GP IV and V to give 180 mg (62% as TFA salt) of the title compound as a white powder. UPLC-MS data R_t: 1.8-1.9 min. MS(ESI$^+$), calcd $C_{58}H_{111}N_{15}O_{11}$: 1193.86 g/mol, found: m/z 597.91 $[MH_2/2]^+$; 1194.78 $[MH]^+$. ^{1}H-NMR (600 MHz, D_2O) δ 4.36 – 4.15 (m, 7H), 3.30 – 3.13 (m, 5H)†, 3.07 – 2.97 (m, 8H), 2.07 (s, 12H), 1.89 – 1.65 (m, 11H)†, 1.63 – 1.35 (m, 9H)†, 1.35 – 1.23 (m, 17H)†, 0.89 (t, J = 6.8 Hz, 4H)†. ^{13}C-NMR (151 MHz, D_2O) δ 174.29, 174.28, 174.16, 174.13, 173.98, 173.85, 173.82, 173.59, 173.51, 173.36, 54.14, 53.98, 53.94, 53.69, 53.67, 53.62, 39.27, 39.17, 39.00, 38.97, 31.08, 31.07, 30.56, 30.49, 30.47, 30.45, 28.42, 28.39, 28.33, 28.29, 28.24, 27.86, 27.85, 26.29, 25.96, 25.93, 22.42, 22.36, 22.16, 22.09, 22.06, 22.04, 22.02, 21.69, 21.66, 13.46.

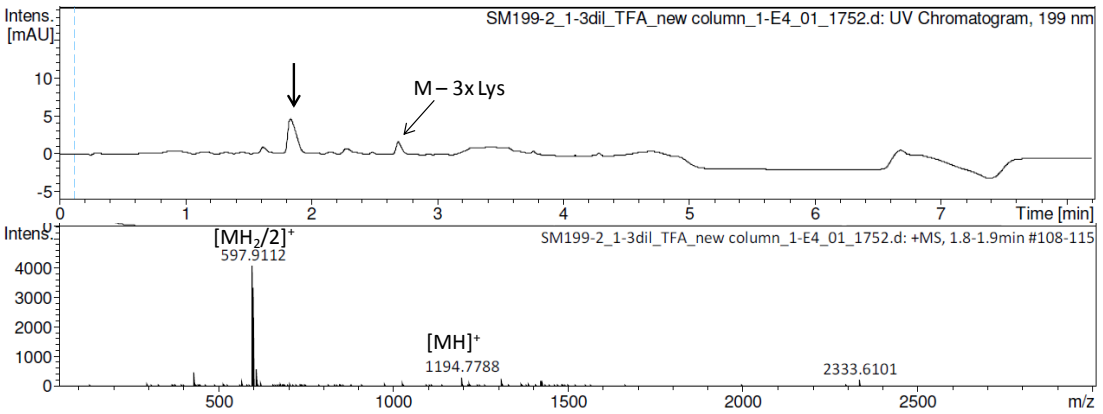

G2-PDL-C8 (4.25)

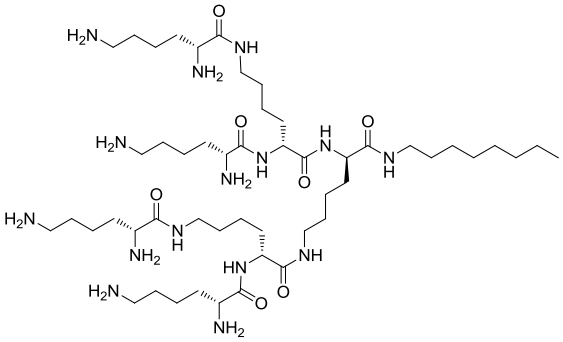

Dendron **4.25** was prepared according to GP IV. Anion-exchange was performed according to GP II. Preparative reversed-phase HPLC purification yielded 23 mg (9% as HCl salt) of the title compound as a white powder. UPLC-MS data R_t: 1.0-1.1 min. MS(ESI$^+$), calcd $C_{50}H_{103}N_{15}O_7$: 1025.82 g/mol, found: m/z 513.91 $[MH_2/2]^+$; 1026.79 $[MH]^+$. ^{1}H-NMR (400 MHz, D_2O) δ 4.35 (t, *J* = 7.2 Hz, 1H), 4.26 (t, *J* = 7.2 Hz, 1H), 4.20 (t, *J* = 7.3 Hz, 1H), 4.09 (t, *J* = 6.7 Hz, 2H), 3.98 (t, *J* = 6.8 Hz, 2H), 3.34 – 3.10 (m, 7H)†, 3.10 – 2.97 (m, 8H), 2.02 – 1.86 (m, 8H), 1.85 – 1.68 (m, 14H), 1.64 – 1.34 (m, 17H)†, 1.33 – 1.22 (m, 10H), 0.92 – 0.81 (m, 3H). ^{13}C-NMR (101 MHz, D_2O) δ 173.32, 173.21, 173.17, 169.58, 169.52, 169.31, 169.28, 54.30, 53.83, 53.10, 52.69, 39.32, 39.30, 39.25, 39.16, 39.00, 31.06, 30.64, 30.44, 30.41, 30.37, 28.40, 28.30, 28.23, 27.97, 27.89, 26.35, 26.32, 25.96, 22.55, 22.46, 22.03, 21.35, 21.16, 21.14, 13.47.

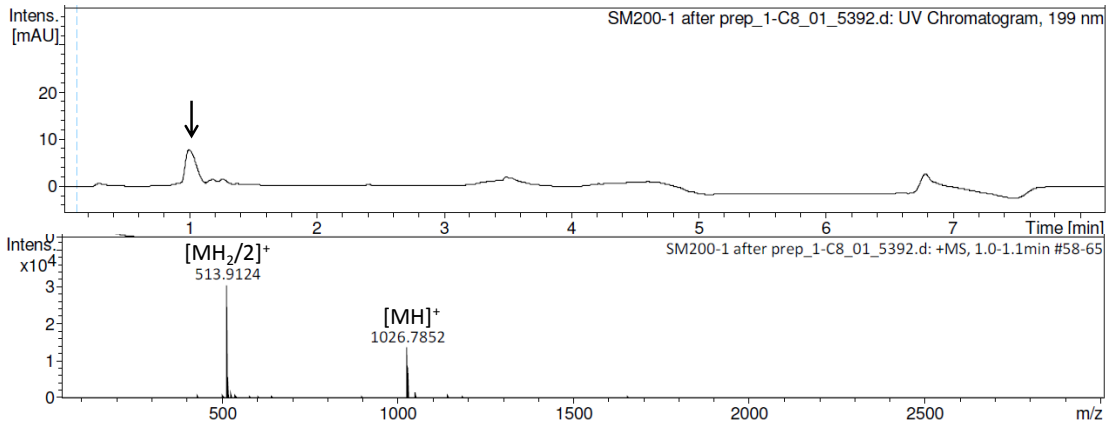

G2-C10 (4.26)

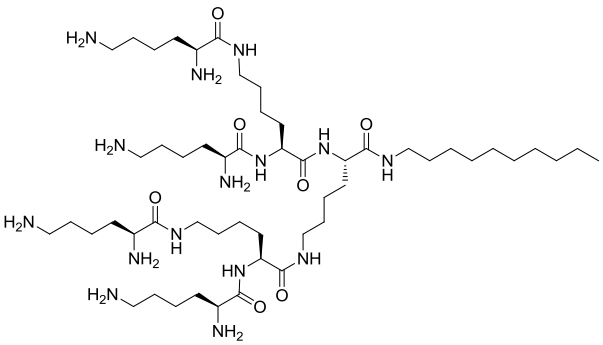

Dendron **4.26** was prepared according to GP IV to give 270 mg (70% as TFA salt) of the title compound as a white powder. UPLC-MS data R_t: 1.1-1.5 min. MS(ESI$^+$), calcd $C_{52}H_{107}N_{15}O_7$: 1053.85 g/mol, found: m/z 527.92 $[MH_2/2]^+$; 1054.79 $[MH]^+$. ^{1}H-NMR (600 MHz, D_2O) δ 4.38 – 4.32 (m, 1H), 4.30 – 4.24 (m, 1H), 4.21 (t, *J* = 7.4 Hz, 1H), 4.07 (t, *J* = 6.6 Hz, 2H), 3.97 (t, *J* = 6.7 Hz, 2H), 3.36 – 3.11 (m, 8H), 3.10 – 3.00 (m, 8H), 1.99 – 1.87 (m, 8H), 1.86 – 1.67 (m, 13H)†, 1.63 – 1.35 (m, 7H)†, 1.35 – 1.24 (m, 18H)†, 0.89 (t, *J* = 6.9 Hz, 3H). ^{13}C-NMR (151 MHz, D_2O) δ 173.25, 173.11, 173.06, 169.54, 169.46, 169.27, 169.25, 54.29, 54.25, 53.83, 53.12, 52.73, 39.36, 39.32, 39.25, 39.19, 39.00, 38.97, 31.18, 30.73, 30.66,

30.45, 30.42, 30.39, 28.71, 28.68, 28.67, 28.65, 28.49, 28.32, 28.22, 28.04, 27.99, 27.92, 26.37, 26.33, 25.95, 22.56, 22.54, 22.45, 22.05, 21.35, 21.17, 21.15, 13.46.

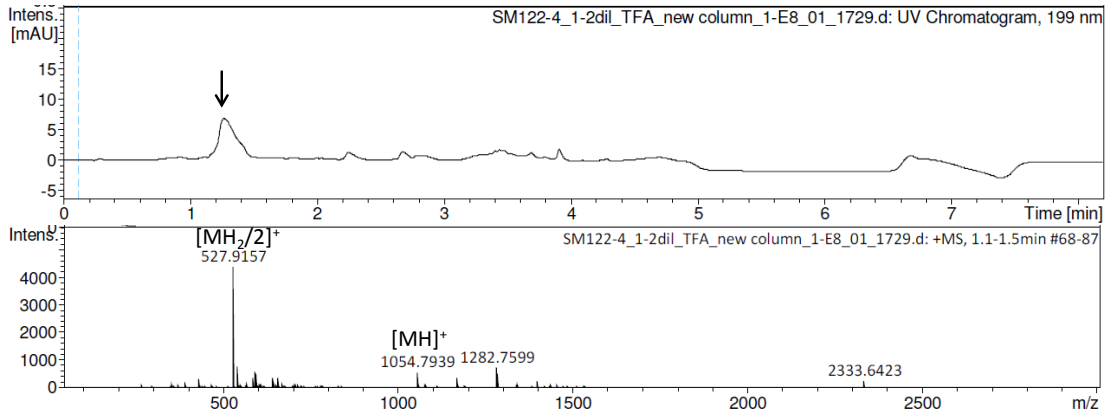

G2-PDL-C12 (4.27)

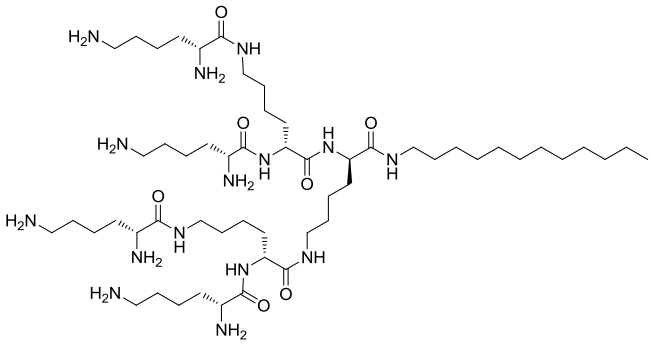

Dendron **4.27** was prepared according to GP IV. Preparative reversed-phase HPLC purification yielded 57 mg (17% as TFA salt) of the title compound as a white powder. UPLC-MS data R_t: 1.7-2.0 min. MS(ESI$^+$), calcd $C_{54}H_{111}N_{15}O_7$: 1081.88 g/mol, found: m/z 541.95 $[MH_2/2]^+$; 1082.86 $[MH]^+$. ^{1}H-NMR (400 MHz, D_2O) δ 4.33 (t, *J* = 7.1 Hz, 1H), 4.25 (t, *J* = 7.3 Hz, 1H), 4.19 (t, *J* = 7.3 Hz, 1H), 4.05 (t, *J* = 6.6 Hz, 2H), 3.95 (t, *J* = 6.7 Hz, 2H), 3.32 – 3.08 (m, 8H), 3.07 – 2.95 (m, 8H), 2.01 – 1.83 (m, 9H)†, 1.83 – 1.63 (m, 15H)†, 1.63 – 1.32 (m, 12H)†, 1.33 – 1.23 (m, 19H)†, 0.87 (t, *J* = 6.6 Hz, 3H). ^{13}C-NMR (101 MHz, D_2O) δ 173.22, 173.10, 173.04, 169.51, 169.43, 169.23, 169.21, 54.27, 54.24, 53.80, 53.08, 52.69, 39.33, 39.30, 39.23, 39.16, 38.97, 38.95, 31.19, 30.70, 30.64, 30.43, 30.41, 30.37, 28.76, 28.75, 28.66, 28.63, 28.50, 28.29, 28.19, 28.02, 27.96, 27.90, 26.34, 26.30, 25.92, 22.53, 22.42, 22.04, 21.33, 21.14, 13.44.

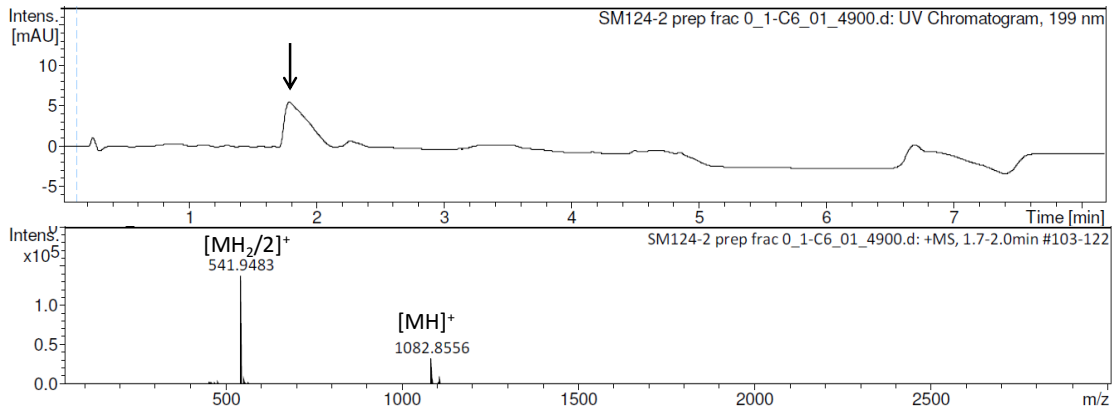

G2-PDL-C16 (4.28)

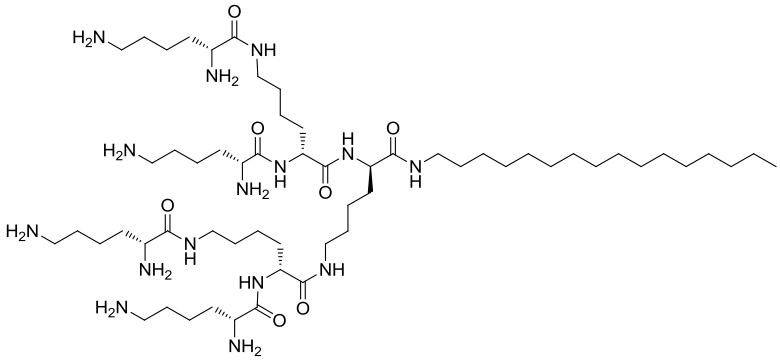

Dendron **4.28** was prepared according to GP IV to give 172 mg (67% as TFA salt) of the title compound as a white powder. UPLC-MS data R_t: 3.3-3.4 min. MS(ESI$^+$), calcd $C_{58}H_{119}N_{15}O_7$: 1137.94 g/mol, found: m/z 569.97 $[MH_2/2]^+$; 1138.90 $[MH]^+$. ^{1}H-NMR (400 MHz, D_2O) δ 4.35 (t, *J* = 7.2 Hz, 1H), 4.31 – 4.17 (m, 2H), 4.14 – 4.02 (m, 2H), 3.99 – 3.91 (m, 2H), 3.37 – 3.08 (m, 5H)†, 3.03 (m, 8H), 2.02 – 1.84 (m, 8H), 1.85 – 1.64 (m, 14H)†, 1.62 – 1.32 (m, 15H)†, 1.28 (s, 26H), 0.95 – 0.82 (m, 3H). ^{13}C-NMR (101 MHz, D_2O) δ 173.10, 173.07, 173.01, 169.53, 169.47, 169.23, 169.21, 54.22, 54.07, 53.80, 53.07, 52.70, 39.34, 39.28, 39.20, 38.99, 38.96, 31.50, 30.89, 30.77, 30.68, 30.42, 29.21, 29.18, 29.15, 29.08, 29.06, 28.89, 28.72, 28.45, 28.06, 27.90, 26.33, 26.28, 22.62, 22.58, 22.51, 22.28, 21.36, 21.17, 13.62.

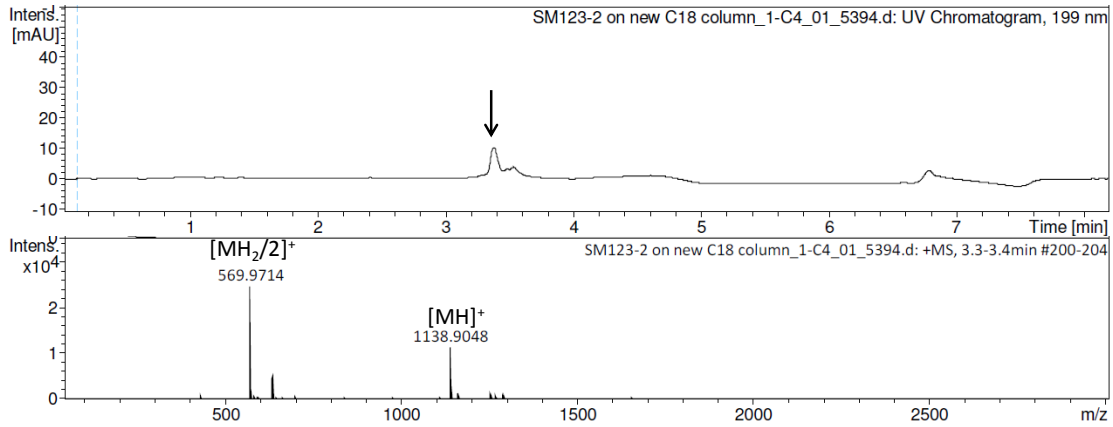

G2-benzyl (4.29)

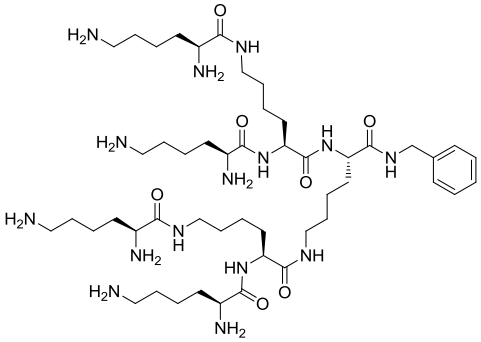

Dendron **4.29** was prepared according to GP IV. Preparative reversed-phase HPLC purification yielded 24 mg (5% as TFA salt) of the title compound as a white powder. UPLC-MS data R_t: 0.3-0.4 min. MS(ESI$^+$), calcd $C_{49}H_{93}N_{15}O_7$: 1003.74 g/mol, found: m/z 502.88 $[MH_2/2]^+$; 1004.71 $[MH]^+$. ^{1}H-NMR (400 MHz, D_2O) δ 7.48 – 7.23 (m, 5H), 4.51 – 4.17 (m, 5H), 4.04 (t, *J* = 6.7 Hz, 2H), 3.97 – 3.83 (m, 2H), 3.28 – 3.08 (m, 6H), 3.08 – 2.92 (m, 8H), 1.99 – 1.83 (m, 9H)†, 1.81 – 1.63 (m, 11H)†, 1.60 – 1.24 (m, 9H)†. ^{13}C-NMR (101 MHz, D_2O) δ 173.56, 173.28, 173.12, 169.51, 169.45, 169.25, 169.18, 137.76, 128.75, 127.47, 127.21, 127.18, 127.14, 54.30, 54.25, 53.81, 53.08, 53.05, 52.68, 42.85, 39.27, 39.24,

39.12, 38.95, 38.92, 30.61, 30.49, 30.41, 30.39, 30.33, 27.88, 27.80, 26.33, 26.30, 22.49, 22.41, 22.36, 21.31, 21.28, 21.14, 21.11.

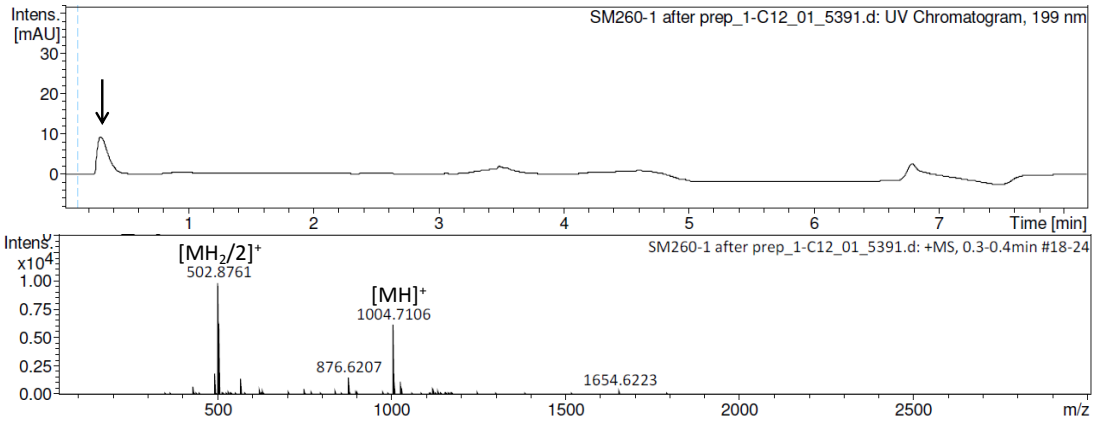

Compounds from Chapter 5

G1-C16 (5.1)

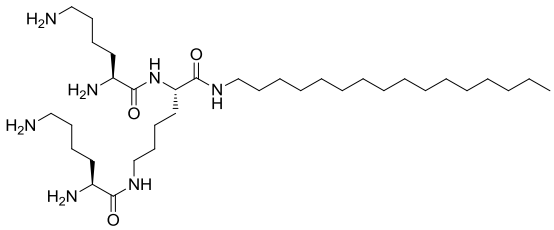

Dendron **5.1** was prepared according to GP III employing Fmoc-Lys(Fmoc)-OH instead of Fmoc-Lys(Boc)-OH as the second lysine. Preparative reversed-phase HPLC purification yielded 16 mg (36% as HCl salt) of the title compound as a white powder. UPLC-MS data R_t: 3.5-3.7 min. MS(ESI$^+$), calcd $C_{34}H_{71}N_7O_3$: 625.56 g/mol, found: m/z 313.83 $[MH_2/2]^+$; 626.59 $[MH]^+$. ^{1}H-NMR (400 MHz, D_2O) δ 4.25 (t, *J* = 7.4 Hz, 1H), 4.06 – 3.98 (m, 1H), 3.96 – 3.88 (m, 1H), 3.33 – 3.08 (m, 4H), 3.05 – 2.97 (m, 4H), 1.98 – 1.83 (m, 4H), 1.82 – 1.65 (m, 6H), 1.64 – 1.34 (m, 6H)†, 1.28 (s, 26H), 0.91 – 0.81 (m, 3H).

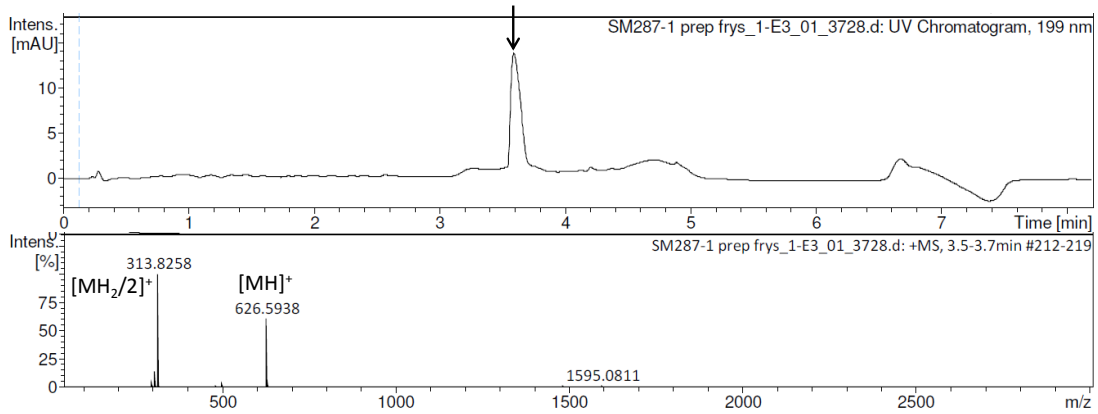

G1(^{D}isoGln-Ala)$_2$-C16 (5.2)

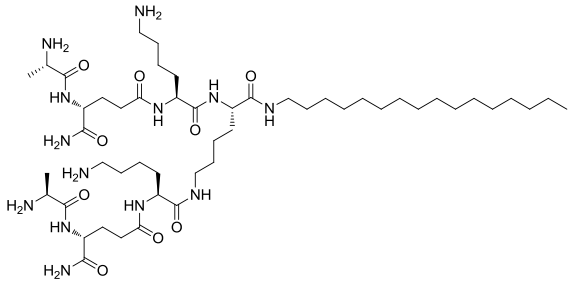

Dendron **5.2** was prepared according to GP III up to and including Fmoc deprotection of the second lysine residue followed by washing. Fmoc-^{D}isoGln-OH (0.8 mmol, 4 equiv.), PyBOP (0.76 mmol, 3.8 equiv.) and DIPEA (1.56 mmol, 7.8 equiv.) were added to the filter syringe containing the derivatized resin (200 mg, 0.2 mmol, 1 equiv.) and NMP (2 mL) and shaken for 20 h at rt. The resin was washed followed by Fmoc deprotection. Fmoc-Ala-OH (0.8 mmol, 4 equiv.), PyBOP (0.76 mmol, 3.8 equiv.) and DIPEA (1.56 mmol, 7.8 equiv.) were added to the filter syringe containing the derivatized resin and NMP (2 mL) and shaken for 20 h at rt. The resin was washed followed by Fmoc deprotection. Cleavage of the final dendron from the resin was conducted as described in GP I to give 51 mg (91% as TFA salt) of the title compound as a white powder. UPLC-MS data R_t: 3.5-3.6 min. MS(ESI$^+$), calcd $C_{50}H_{97}N_{13}O_9$: 1023.75 g/mol, found: m/z 342.29 $[MH_3/3]^+$; 512.92 $[MH_2/2]^+$; 1024.78 $[MH]^+$. ESI-HRMS calcd for $C_{50}H_{98}N_{13}O_9$ (M+H) 1024.7605, found 1024.7584. ^{1}H-NMR (400 MHz, D_2O) δ 4.36 – 4.26 (m, 3H), 4.26 – 4.18 (m, 2H), 4.18 – 4.10 (m, 2H), 3.34 – 3.05 (m, 4H), 3.05 – 2.92 (m, 4H), 2.53 – 2.34 (m, 3H)†, 2.23 – 2.07 (m, 2H), 2.07 – 1.95 (m, 2H), 1.87 – 1.62 (m, 11H)†, 1.56 (d, *J* = 7.1 Hz, 6H), 1.53 – 1.35 (m, 4H)†, 1.27 (s, 26H), 0.92 – 0.79 (m, 3H). ^{13}C-NMR (101 MHz, D_2O) δ 175.54, 174.68, 174.53, 173.64, 173.52, 173.20, 170.95, 53.95, 53.85, 53.56, 53.08, 49.05, 39.30, 39.13, 39.03, 31.40, 30.72, 30.51, 29.08, 28.56, 28.34, 27.96, 26.92, 26.30, 22.51, 22.20, 22.09, 16.57, 13.58.

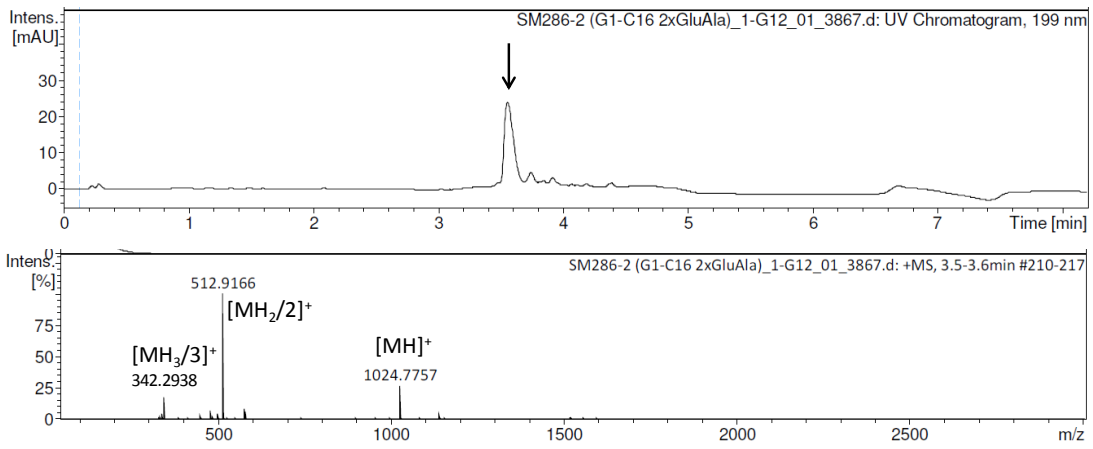

G1(MDP)$_2$-C16 (5.3)

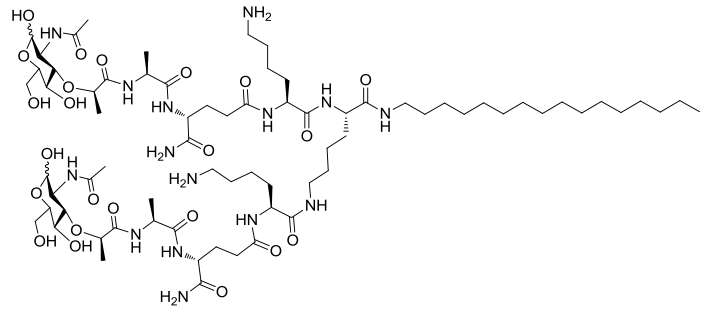

Dendron **5.3** was prepared as dendron **5.2** up to and including Fmoc deprotection after addition of Fmoc-Ala-OH. *N*-acetylmuramic acid (0.4 mmol, 4 equiv.), PyBOP (0.38 mmol, 3.8 equiv.) and DIPEA (0.78 mmol, 7.8 equiv.) were added

to the filter syringe containing the derivatized resin (100 mg, 0.1 mmol, 1 equiv.) and NMP (2 mL) and shaken for 20 + 23 h at rt followed by washing. Cleavage of the final dendron from the resin was conducted as described in GP I. Preparative reversed-phase HPLC purification yielded 7 mg (20% as TFA salt) of the title compound as a white powder. UPLC-MS data R_t: 3.7-3.8 min. MS(ESI$^+$), calcd $C_{72}H_{131}N_{15}O_{23}$: 1573.95 g/mol, found: m/z 788.02 $[MH_2/2]^+$; 1575.96 $[M+2H]^{2+}$. ESI-HRMS calcd for $C_{72}H_{132}N_{15}O_{23}$ (M+H) 1574.9615, found 1574.9556. ^{1}H-NMR (400 MHz, D_2O) δ 5.18 (s, 1H), 4.38 – 4.10 (m, 5H), 4.01 – 3.42 (m, 7H)†, 3.35 – 3.05 (m, 5H)†, 3.04 – 2.92 (m, 4H), 2.41 (s, 5H)†, 2.29 – 2.07 (m, 2H), 1.99 (s, 4H)†, 1.89 – 1.60 (m, 2H)†, 1.56 (d, *J* = 7.1 Hz, 1H)†, 1.47 – 1.34 (m, 7H)†, 1.26 (s, 26H), 0.90 – 0.80 (m, 3H).

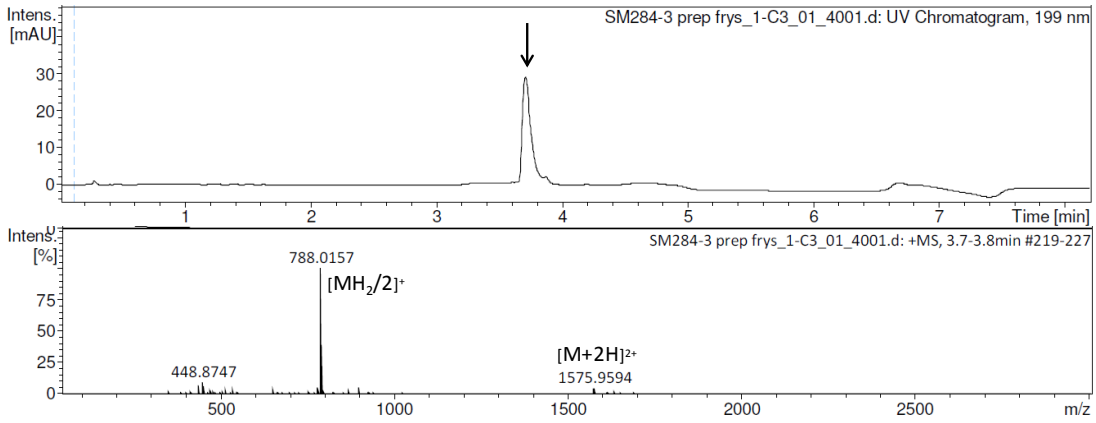

G1(^{D}isoGln-Ala)$_4$-C16 (5.4)

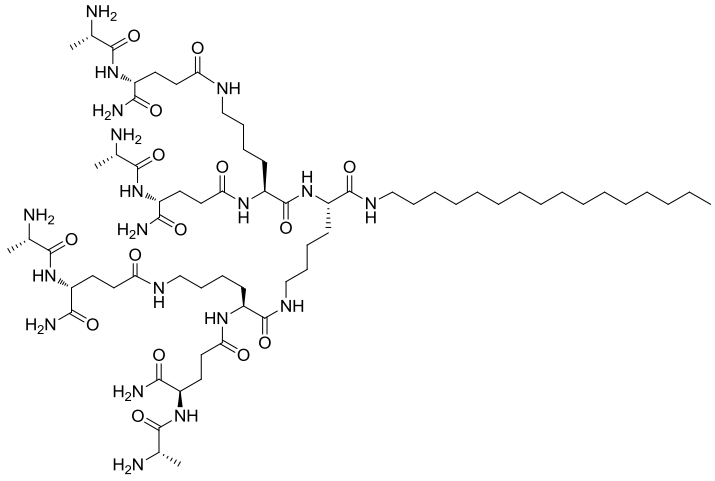

Dendron **5.4** was prepared as dendron **5.2** employing Fmoc-Lys(Fmoc)-OH as the second lysine residue during GP III and 400 mg derivatized resin (0.4 mmol, 1 equiv.). Preparative reversed-phase HPLC purification yielded 15 mg (15% as TFA salt) of the title compound as a white powder. UPLC-MS data R_t: 3.6-3.7 min. MS(ESI$^+$), calcd $C_{66}H_{123}N_{19}O_{15}$: 1421.94 g/mol, found: m/z 475.03 $[MH_3/3]^+$; 712.01 $[MH_2/2]^+$; 1422.96 $[MH]^+$. ESI-HRMS calcd for $C_{66}H_{124}N_{19}O_{15}$ (M+H) 1422.9519, found 1422.9450. ^{1}H-NMR (400 MHz, D_2O) δ 4.39 – 4.22 (m, 5H), 4.22 – 4.07 (m, 4H)†, 3.30 – 3.00 (m, 8H), 2.52 – 2.24 (m, 9H)†, 2.23 – 2.06 (m, 4H), 2.05 – 1.89 (m, 4H), 1.85 – 1.60 (m, 8H)†, 1.55 (d, *J* = 7.1 Hz, 12H), 1.52 – 1.42 (m, 8H)†, 1.24 (s, 26H), 0.92 – 0.80 (m, 3H). ^{13}C-NMR (101 MHz, D_2O) δ 175.54, 175.51, 175.47, 174.52, 174.47, 174.10, 174.04, 173.63, 173.02, 170.97, 170.94, 54.04, 53.77, 53.15, 49.07, 39.33, 39.03, 31.88, 31.71, 31.47, 30.99, 30.83, 29.49, 29.16, 29.02, 28.68, 28.07, 27.19, 26.97, 26.53, 22.61, 22.45, 16.63, 16.60, 13.80.

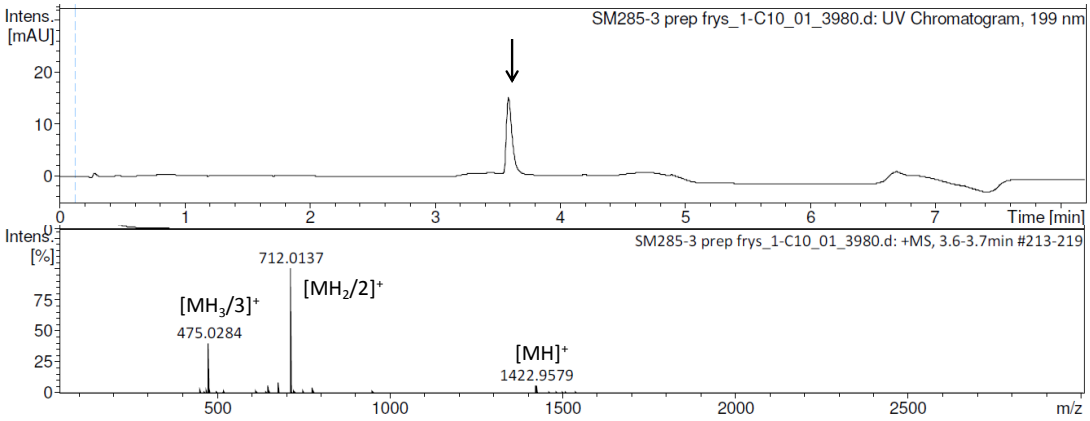

Benzyl-2-acetamido-4,6-*O*-benzylidene-3-*O*-(*R*-1'-carboxyethyl)-2-deoxy-α-D-glucopyranoside (5.17)

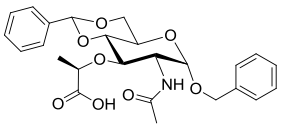

Benzyl-2-acetamido-4,6-*O*-benzylidene-2-deoxy-α-D-glucopyranoside (**5.15**) (1.2 g, 3 mmol, 1 equiv.) was added to hot (~85 °C) dry dioxane (100 mL) in a 250 mL round bottomed flask equipped with a condenser and stirred until completely dissolved. The temperature was lowered to 70 °C and NaH (0.4 g, 10 mmol, 3.33 equiv., 60% dispersion in mineral oil) was added. The reaction mixture was stirred for 1 h at 95 °C, then cooled to 65 °C and a solution of (*S*)-2-chloropropionic acid (1.6 mL, 18.4 mmol, 6.1 equiv.) in dry dioxane (5 mL) was added dropwise. After 1 h stirring at 65 °C additional NaH (1.6 g, 40 mmol, 13.3 equiv.) was added and the reaction mixture was stirred at 70 °C for 22 h. The reaction mixture was cooled on ice-water bath and ice cold MilliQ water (20 mL) was added cautiously. The mixture was concentrated *in vacuo* to a thick yellow-brown paste. MilliQ water (30 mL) was added and the mixture washed chloroform (3x25 mL). The organic layers were collected and concentrated *in vacuo* to a thick pale brown paste and lyophilized. MilliQ water (120 mL) was added to the lyophilized product and the cloudy solution was made acidic (pH 2-3) by dropwise addition of 4M HCl under ice-water cooling. The white slurry was placed in a refrigerator overnight to improve crystallization. The crystals were centrifuged and washed with cold MilliQ water (4x60 mL) and lyophilized yielding white crystals (1.85 g). Preparative reversed-phase HPLC purification yielded 810 mg (57%) of the title compound as white crystals. UPLC-MS data R_t: 3.7-3.8 min. MS(ESI^+), calcd $C_{25}H_{29}NNaO_8$: 494.18 g/mol, found: m/z 494.18 $[M+Na]^+$; 965.34 $[2M+Na]^+$. ^{1}H-NMR (400 MHz, DMSO-d_6) δ 12.87 (s, 1H), 7.97 (d, *J* = 6.2 Hz, 1H), 7.47 – 7.25 (m, 10H), 5.70 (s, 1H), 5.04 (d, *J* = 3.4 Hz, 1H), 4.70 (d, *J* = 12.4 Hz, 1H), 4.49 (d, *J* = 12.4 Hz, 1H), 4.30 (q, *J* = 6.9 Hz, 1H), 4.20 – 4.11 (m, 1H), 3.86 – 3.66 (m, 5H), 1.85 (s, 3H), 1.28 (d, *J* = 6.9 Hz, 3H). ^{13}C-NMR (101 MHz, DMSO) δ 175.24, 169.36, 137.61, 137.58, 128.79, 128.26, 128.15, 127.65, 127.61, 125.83, 100.24, 96.80, 81.51, 75.09, 75.05, 68.95, 67.86, 62.87, 53.49, 22.61, 18.68. NMR data is in accordance with literature.[130]

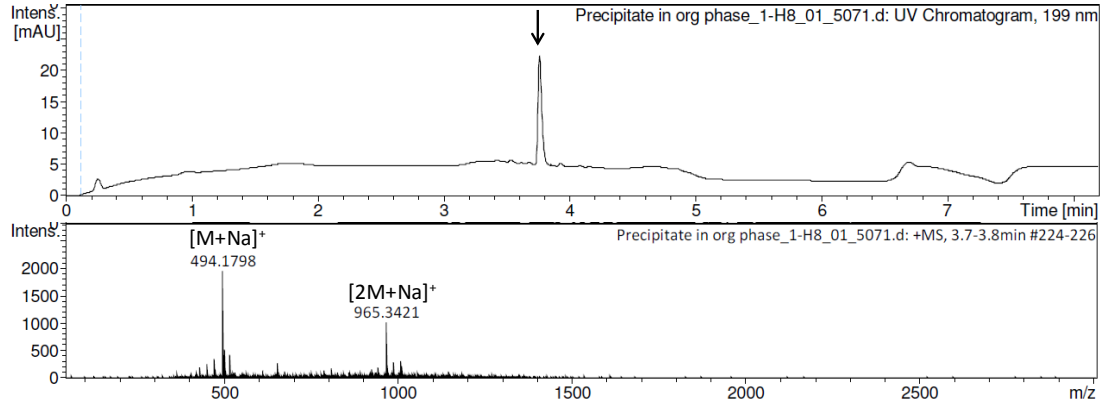

G1(benzyl-MDP)$_4$-C16 (5.19)

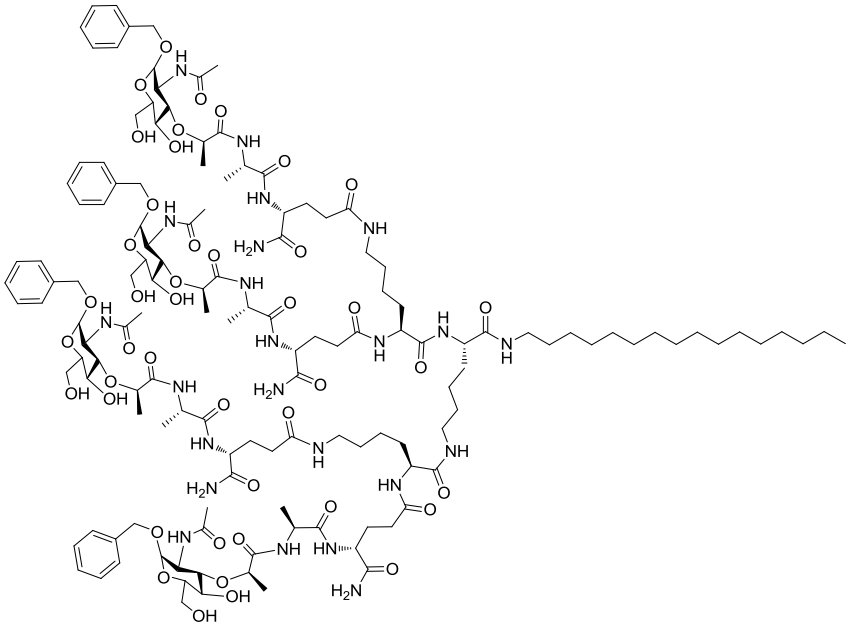

Dendron **5.19** was prepared as dendron **5.2** up to and including Fmoc deprotection after addition of Fmoc-Ala-OH employing 200 mg derivatized resin (0.2 mmol, 1 equiv.). Compound (**5.17**) (0.8 mmol, 4 equiv.), HBTU (0.76 mmol, 3.8 equiv.) and DIPEA (1.56 mmol, 7.8 equiv.) were dissolved in NMP (2 mL) and shaken for 15 min at rt. The reaction mixture was then added to the filter syringe containing the derivatized resin (200 mg, 0.2 mmol, 1 equiv.) and shaken for 20 h at rt. Ninhydrin test gave semi-positive readout (pale purple). Cleavage of the final dendron from the resin was conducted as described in GP I. Preparative reversed-phase HPLC purification was performed, but the yield too low to be determined. UPLC-MS data R_t: 4.1-4.2 min. MS(ESI$^+$), calcd $C_{138}H_{215}N_{23}O_{43}$: 2882.53 g/mol, found: m/z 962.17 $[MH_3/3]^+$; 1442.73 $[MH_2/2]^+$.

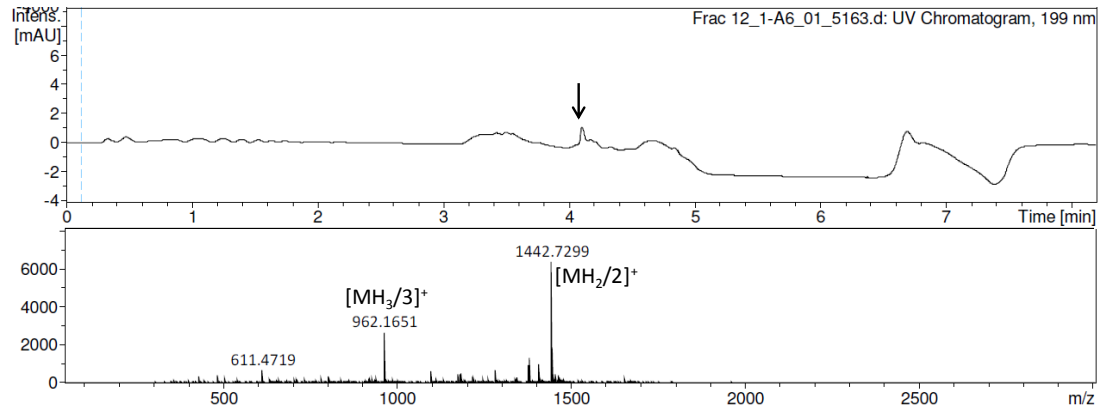

G1(fMet)$_2$-C1 (5.23)

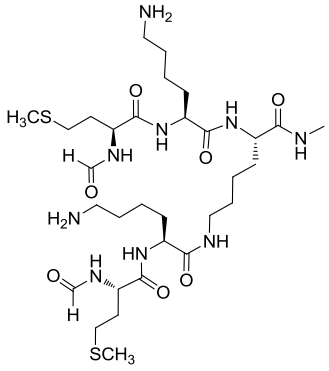

Dendron **5.23** was prepared according to GP III up to and including Fmoc deprotection of the second lysine residue followed by washing. *N*-formylmethionine (1.6 mmol, 4 equiv.), PyBOP (1.5 mmol, 3.8 equiv.) and DIPEA (3.1 mmol, 7.8 equiv.) were added to the filter syringe containing the derivatized resin (400 mg, 0.4 mmol, 1 equiv.) and NMP (5 mL) and shaken for 20 h at rt followed by washing. Cleavage of the final dendron from the resin was conducted as described in GP I. Preparative reversed-phase HPLC purification yielded 27 mg (31% as TFA salt) of the title compound as a white powder. UPLC-MS data R_t: 0.5-0.7 min. MS(ESI$^+$), calcd $C_{31}H_{59}N_9O_7S_2$: 733.40 g/mol, found: m/z 367.70 $[MH_2/2]^+$; 734.37 $[MH]^+$. ESI-HRMS calcd for $C_{31}H_{60}N_9O_7S_2$ (M+H) 734.4052, found 734.4058. ^{1}H-NMR (400 MHz, D_2O) δ 8.14 (s, 2H), 4.58 – 4.45 (m, 2H), 4.41 – 4.30 (m, 1H), 4.28 – 4.23 (m, 1H), 4.22 – 4.15 (m, 1H), 3.20 (t, *J* = 6.8 Hz, 2H), 3.07 – 2.94 (m, 4H), 2.75 (s, 3H), 2.67 – 2.48 (m, 4H), 2.11 (s, 6H), 2.08 – 1.95 (m, 4H), 1.90 – 1.62 (m, 4H)†, 1.60 – 1.18 (m, 7H)†.

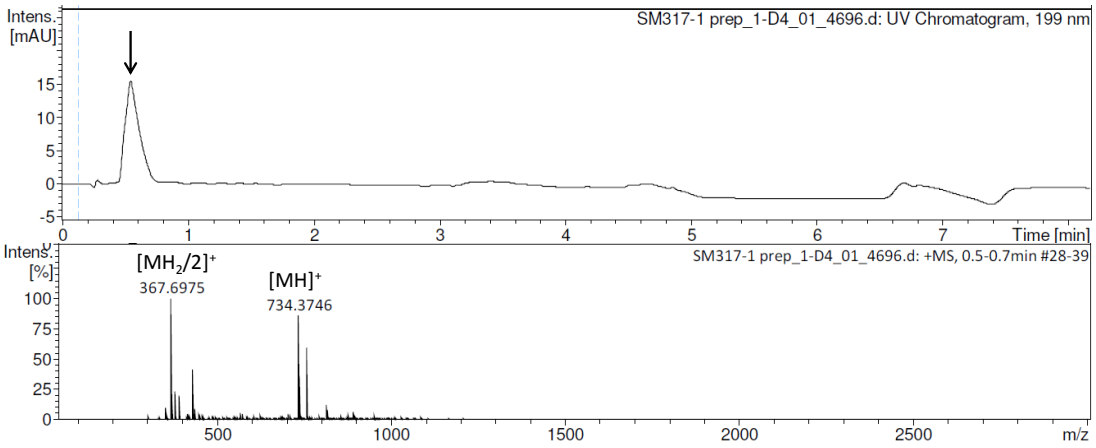

G1(fMet)$_2$-C16 (5.24)

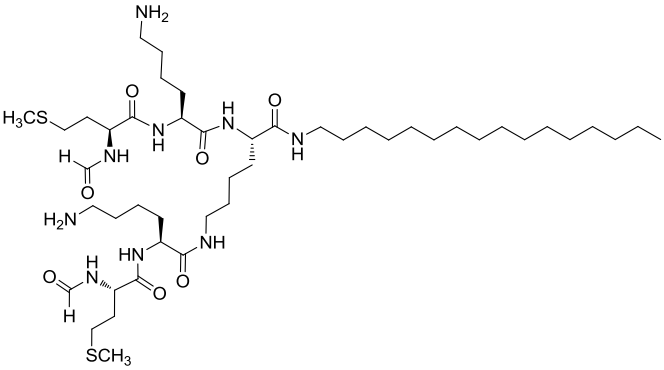

Dendron **5.24** was prepared according to GP III up to and including Fmoc deprotection of the second lysine residue followed by washing. *N*-formylmethionine (1.2 mmol, 4 equiv.), PyBOP (1.1 mmol, 3.8 equiv.) and DIPEA (2.3 mmol, 7.8 equiv.) were added to the filter syringe containing the derivatized resin (300 mg, 0.3 mmol, 1 equiv.) and NMP (4 mL) and shaken for 20 h at rt followed by washing. Cleavage of the final dendron from the resin was conducted as described in GP I to give 61 mg (83% as TFA salt) of the title compound as a white powder. UPLC-MS data R_t: 3.9-4.0 min. MS(ESI$^+$), calcd $C_{46}H_{89}N_9O_7S_2$: 943.63 g/mol, found: m/z 472.81 $[MH_2/2]^+$; 944.60 $[MH]^+$. ESI-

HRMS calcd for $C_{46}H_{90}N_9O_7S_2$ (M+H) 944.6399, found 944.6423. ^{1}H-NMR (400 MHz, DMSO-d_6) δ 8.46 – 8.05 (m, 3H), 8.02 (s, 2H), 7.93 – 7.66 (m, 8H), 4.48 – 4.32 (m, 2H), 4.28 – 4.05 (m, 3H), 3.11 – 2.89 (m, 4H), 2.81 – 2.66 (m, 4H), 2.47 – 2.37 (m, 4H), 2.09 – 1.98 (m, 6H), 1.96 – 1.71 (m, 3H)†, 1.70 – 1.42 (m, 8H)†, 1.42 – 1.28 (m, 4H)†, 1.23 (s, 30H)†, 0.92 – 0.77 (m, 3H).

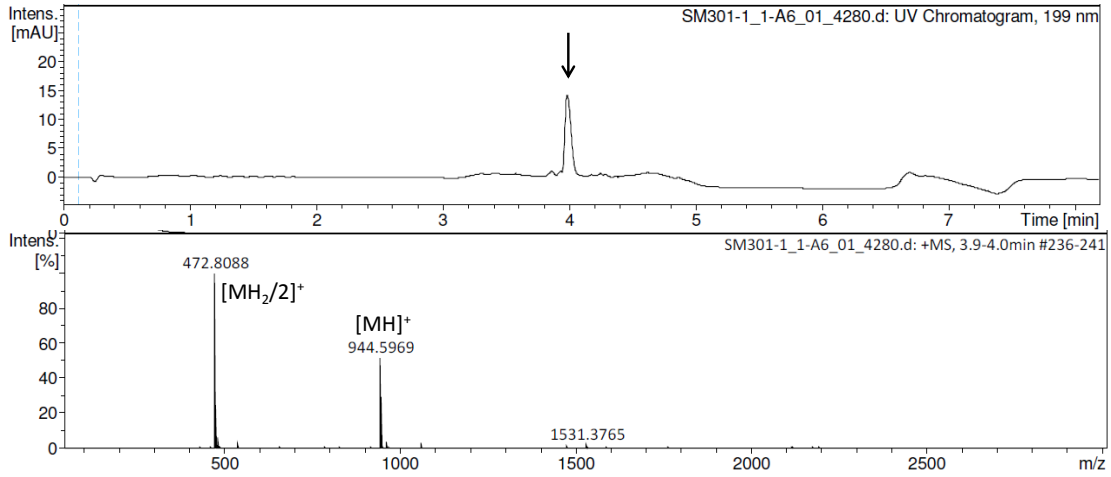

G2(fMet)$_4$-C1 (5.25)

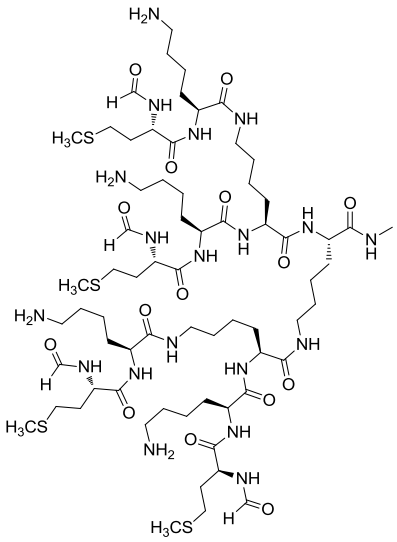

Dendron **5.25** was prepared according to GP IV up to and including Fmoc deprotection of the third lysine residue followed by washing. *N*-formylmethionine (1.6 mmol, 4 equiv.), PyBOP (1.5 mmol, 3.8 equiv.) and DIPEA (3.1 mmol, 7.8 equiv.) were added to the filter syringe containing the derivatized resin (400 mg, 0.3 mmol, 1 equiv.) and NMP (5 mL) and shaken for 20 h at rt followed by washing. Cleavage of the final dendron from the resin was conducted as described in GP I. Preparative reversed-phase HPLC purification yielded 24 mg (12% as TFA salt) of the title compound as a white powder. UPLC-MS data R_t: 1.1-1.3 min. MS(ESI$^+$), calcd $C_{67}H_{125}N_{19}O_{15}S_4$: 1563.85 g/mol, found: m/z 522.28 $[MH_3/3]^+$; 782.90 $[MH_2/2]^+$. ESI-HRMS calcd for $C_{67}H_{126}N_{19}O_{15}S_4$ (M+H) 1564.8558, found 1564.8497. ^{1}H-NMR (400 MHz, D_2O) δ 8.14 (s, 4H), 4.58 – 4.47 (m, 4H), 4.36 (m, 2H), 4.30 – 4.24 (m, 3H), 4.19 (t, *J* = 7.4 Hz, 2H), 3.27 – 3.14 (m, 6H), 3.05 – 2.94 (m, 9H)†, 2.75 (s, 3H), 2.67 – 2.50 (m, 8H), 2.11 (s, 13H)†, 2.10 – 1.96 (m, 6H)†, 1.90 – 1.63 (m, 12H)†, 1.59 – 1.22 (m, 13H)†.

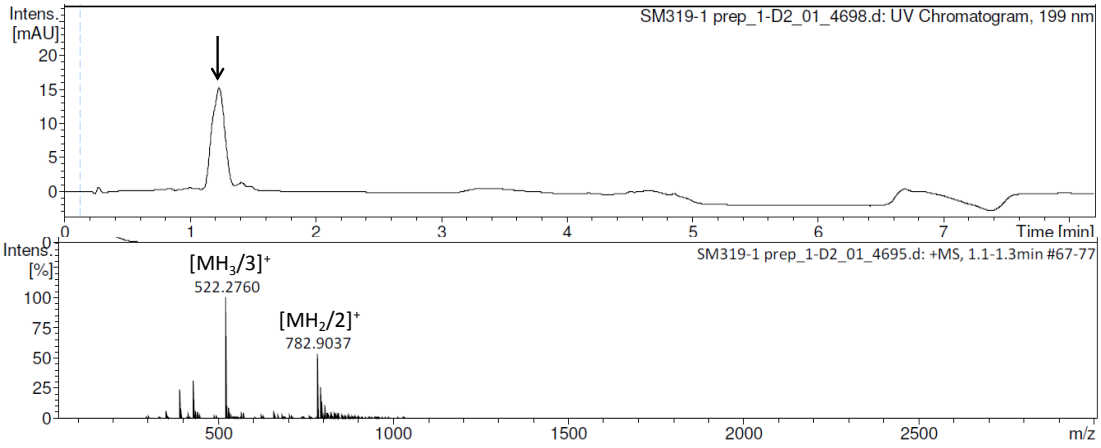

G2(fMet)$_4$-C16 (5.26)

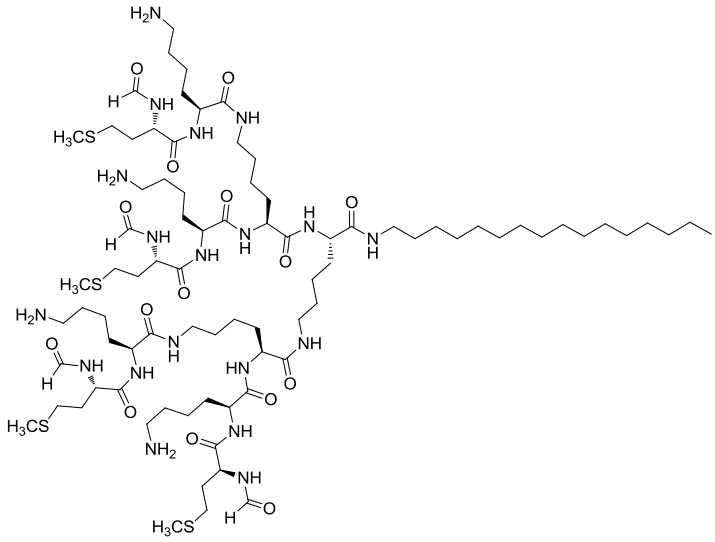

Dendron **5.26** was prepared as dendron **5.25**. Preparative reversed-phase HPLC purification yielded 19 mg (10% as TFA salt) of the title compound as a white powder. UPLC-MS data R_t: 3.7 min. MS(ESI$^+$), calcd $C_{82}H_{155}N_{19}O_{15}S_4$: 1774.08 g/mol, found: m/z 592.68 $[MH_3/3]^+$; 888.51 $[MH_2/2]^+$. ^{1}H-NMR (400 MHz, DMSO-d_6) δ 8.49 – 8.05 (m, 7H), 8.03 (s, 4H), 7.85 (s, 17H), 4.49 – 4.32 (m, 4H), 4.29 – 4.04 (m, 7H), 3.11 – 2.86 (m, 8H), 2.82 – 2.66 (m, 8H), 2.43 (m, 8H), 2.03 (s, 11H)†, 1.96 – 1.73 (m, 5H), 1.73 – 1.43 (m, 21H), 1.41 – 1.28 (m, 4H), 1.23 (s, 32H)†, 0.85 (t, J = 6.6 Hz, 3H).

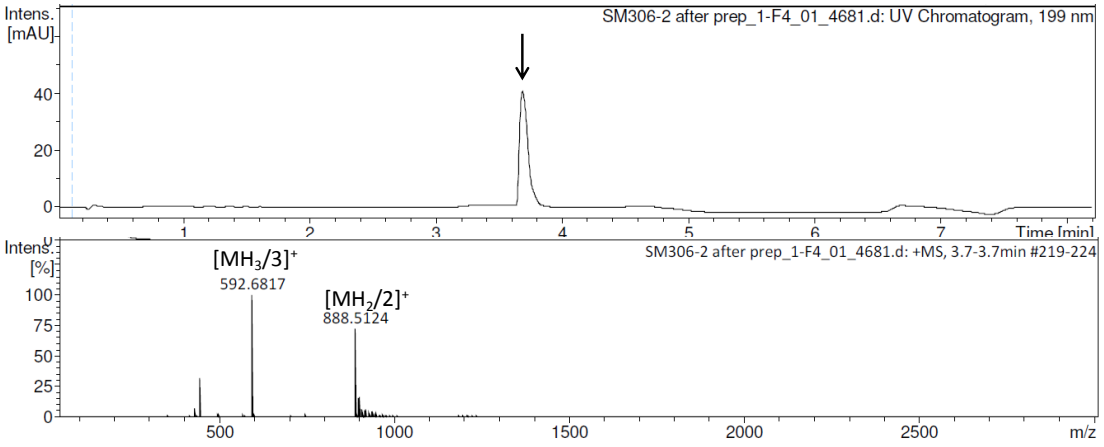

G1(fMLP)$_2$-C16 (5.28)

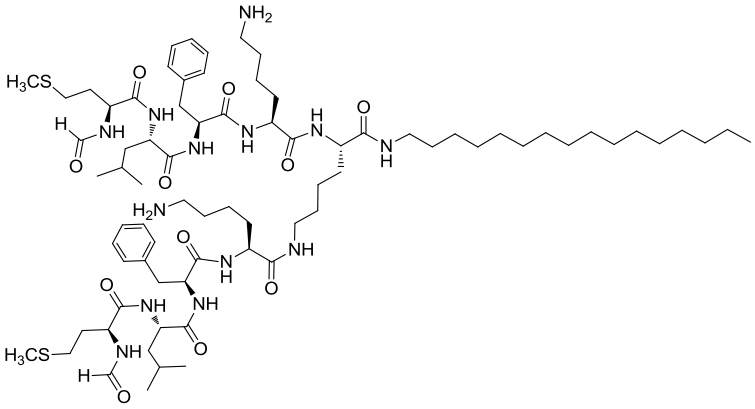

Dendron **5.28** was prepared according to GP III up to and including Fmoc deprotection of the second lysine residue followed by washing. The PAMP motif (fMLP) was added in the following order: 1. Fmoc-Phe-OH, 2. Fmoc-Leu-OH and 3. *N*-formylmethionine. Between acylation steps with Fmoc protected amino acids, the Fmoc group was removed followed by washing. Amino acid (2.4 mmol, 4 equiv.), PyBOP (2.3 mmol, 3.8 equiv.) and DIPEA (4.7 mmol, 7.8 equiv.) were added to the filter syringe containing the derivatized resin (600 mg, 0.6 mmol, 1 equiv.) and NMP (6 mL) and shaken for 20 h at rt followed by washing. Cleavage of the final dendron from the resin was conducted as described in GP I. Isolation of the three peaks by preparative reversed-phase HPLC yielded 15 mg (9% as TFA salt), 18 mg (11% as TFA salt) and 7 mg (4% as TFA salt) of peak 1, 2 and 3, respectively, as white powders. UPLC-MS data R_t: 4.3 min (peak 1), 4.3-4.4 min (peak 2) and 4.4 min (peak 3). MS(ESI$^+$), calcd $C_{76}H_{129}N_{13}O_{11}S_2$: 1463.94 g/mol, found: m/z 732.96 (peak 1 and 2) and 732.97 (peak 3) $[MH_2/2]^+$; 1465.91 (peak 1, 2 and 3) $[M+2H]^{2+}$ (see Fig. 5.8 for UPLC-MS data).

Immunological tests from Chapter 5

Reagents

Staphylococcus aureus peptidoglycan (PGN), *N*-formyl-L-methionine (fMet), *N*-formyl-Met-Leu-Phe (fMLP), poly(I:C) and bovine serum albumin (BSA) were purchased from Sigma Aldrich and muramyl dipeptide (MDP) from Bachem. CpG ODN was purchased from InvivoGen and collagenase digestion mix from Nordic BioSite. Phosphate-buffered saline (PBS, Ca^{2+} and Mg^{2+} free) and ethylenediaminetetraacetic acid (EDTA) were purchased from Life Technologies. Dynabeads mouse dendritic cell (DC) enrichment kit by Invitrogen were purchased from ThermoFisher Scientific. The cells were cultured in Roswell Park Memorial Institute (RPMI) 1640 medium containing 1% penicillin-streptomycin-glutamine (Life Technologies) and 10% fetal calf serum (FCS, Viralex). Red blood cell lysis buffer (Sigma Aldrich) consisting of 90% ammonium chloride (160 mM) and 10% tris(hydroxylmethyl)aminomethane (100 mM) at pH 7.4. Buffer employed for washing: PBS containing 0.1% BSA and 2 mM EDTA or 0.6% sodium citrate (Sigma Aldrich).

Mice

C57BL/6 mice were bred in house at the Section for Virology, National Veterinary Institute, Technical University of Denmark following Danish rules and regulations.

Isolation of whole mouse spleen cells

The spleens of four male wild type mice (3.5 month old) were harvested and collagenase digestion performed (0.5 mg/mL). Subsequently, the cells were flushed out, spun down at 1300 rpm for 7 min, and red blood cell lysis performed (3 mL red blood cell lysis buffer for 1 min at rt.)

Isolation of DC subsets ($CD11c^+$) from mouse spleen

The spleens of five male wild type mice (3.5 month old) were harvested and the cells flushed out followed by red blood cell lysis through a 70 µm cell strainer into a 50 mL tube and flushing with buffer. The cells were counted and re-suspended in buffer to a concentration of $1x10^8$ cells/mL. $CD11c^+$ DCs were isolated by negative selection using Dynabeads, which were washed with buffer prior to use. 100 µL of antibody mix (included in Dynabead mouse DC enrichment kit) was added to 500 µL ($5x10^7$ cell/mL) splenic mononuclear cells suspended in buffer. The mixture was incubated for 20 min at 2-8 °C and washed with buffer. The supernatant was removed by centrifugation and the cells re-suspended in 4.5 mL buffer. Subsequently, 500 µL of pre-washed dynabeads were added to bind the antibody-labeled non-dendritic cells and incubated 15 min at 2-8 °C. Hereafter, 5 mL of buffer was added and the mixture placed in a magnet for 3 min after which the supernatant containing the dendritic cells was collected.

Stimulation of DC subsets ($CD11c^+$) and whole spleen cells with dendrons

Stock solutions of MDP, fMet, fMLP, PGN and dendrons were prepared at 10 mM in PBS. The stock solutions were stored as aliquots at -20°C until use. Final dilutions of all compounds were made in complete medium. $CD11c^+$ DCs were cultured for 24 h (37 °C, 5% CO_2) with or without stimulators/dendrons in a total of 200 µL medium per well in a 96 u-bottom well plate (Sigma Aldrich) at a final concentration of $2x10^5$ cells/well (DCs) or $1x10^6$ cells/well (whole spleen cells) followed by collection of supernatants. PGN of *Staphylococcus aureus* (12.5 µg/mL), MDP (10 µg/mL or 100 µg/mL), fMet (100 µM) and fMLP (100 µM) were employed as positive controls. The $CD11c^+$ DCs were treated with 25 µM of each dendron from the MDP library and whole spleen cells were treated with 100 µM of MDP and fMet dendrons followed by collected of supernatants. All incubations were performed in duplicates. Supernatants were stored at -20 °C until analysis. The concentration of IL-6 was determined by sandwich enzyme-linked immunosorbent assay (ELISA) (BD Biosciences, BD OptEIA, cat. no. 55240) as described by the manufacturer using undiluted cell culture supernatants. During co-stimulation studies on whole spleen cells poly(I:C) (Sigma-Aldrich P0913) and CpG ODN (InVivogen, A type, 1585) were added simultaneously with chosen dendrons. The standard was an in-kit recombinant mouse IL-6 preparation and this was used in triplicates to calibrate plates with a lower limit of detection at 16.5 pg/mL IL-6. Sample concentrations of IL-6 were calculated from a curve fitted to the dilution series of the standard.

References

(1) K. Murphy and C. Weaver, *Janeway's Immunobiology 9th Ed.*, Garland Science, Taylor and Francis Group, **2016**

(2) T. J. Kindt, R. A. Goldsby and B. A. Osborne, *Kuby Immunology 6th Ed.*, W. H. Freeman and Company, **2007**

(3) C. Foged, T. Rades, Y. Perrie and S. Hook, *Subunit Vaccine Delivery*, Springer, **2015**

(4) B. Guy, The Perfect Mix: Recent Progress in Adjuvant Research, *Nat. Rev. Microbiol.*, **2007**, 5, 505-517

(5) S. E. Girardin, I. G. Boneca, J. Viala, M. Chamaillard, A. Labigne, G. Thomas, D. J. Philpott and P. J. Sansonetti, Nod2 Is a General Sensor of Peptidoglycan through Muramyl Dipeptide (MDP) Detection, *J. Biol. Chem.*, **2003**, 278, 8869-8872

(6) N. Inohara, Y. Ogura, A. Fontalba, O. Gutierrez, F. Pons, J. Crespo, K. Fukase, S. Inamura, S. Kusumoto, M. Hashimoto, S. J. Foster, A. P. Moran, J. L. Fernandez-Luna and G. Nuñez, Host Recognition of Bacterial Muramyl Dipeptide Mediated through NOD2, *J. Biol. Chem.*, **2003**, 278, 5509-5512

(7) C. Ogawa, Y.-J. Liu and K. S. Kobayashi, Muramyl Dipeptide and Its Derivatives: Peptide Adjuvant in Immunological Disorders and Cancer Therapy, *Curr. Bioact. Compd.*, **2011**, 7, 180-197

(8) N. Dufton and M. Perretti, Therapeutic Anti-Inflammatory Potential of Formyl-Peptide Receptor Agonists, *Pharmacol. Ther.*, **2010**, 127, 175-188

(9) D. A. Dorward, C. D. Lucas, G. B. Chapman, C. Haslett, K. Dhaliwal and A. G. Rossi, The Role of Formylated Peptides and Formyl Peptide Receptor 1 in Governing Neutrophil Function during Acute Inflammation, *Am. J. Pathol.*, **2015**, 185, 1172-1184

(10) E. Buhleier, W. Wehner and F. Vögtle, "Cascade" - and "Nonskid-Chain-Like" Synthesis of Molecular Cavity Topologies, *Synthesis*, **1978**, 155-158

(11) D. A. Tomalia, H. Baker, J. R. Dewald, M. Hall, G. Kallos, S. Martin, J. Roeck, J. Ryder and P. Smith, A New Class of Polymers: Starburst-Dendritic Macromolecules, *Polym. J.*, **1985**, 17, 117-132

(12) U. Boas, J. B. Christensen and P. M. H. Heegaard, *Dendrimers in Medicine and Biotechnology – New Molecular Tools*, RCS Publishing, **2006**

(13) M. Malkoch, E. Malmström and A. M. Nyström, Dendrimers: Properties and Applications, *Polym. Sci. Compre. Ref.*, **2012**, 6, 113-175

(14) G. R. Newkome, Z. Q. Yao, G. R. Baker and V. K. Gupta, Cascade Molecules: A New Approach to Micelles. A [27]-Arborol, *J. Org. Chem.*, **1985**, 50, 2003-2004

(15) M. Fischer and F. Vögtle, Dendrimers: From Design to Application – A Progress Report, *Angew. Chem. Int. Ed.*, **1999**, 38, 884-905

(16) A. Carlmark, C. Hawker, A. Hult and M. Malkoch, New Methodologies in the Construction of Dendritic Materials, *Chem. Soc. Rev.*, **2009**, 38, 352-362

(17) J. C. Hawker and J. M. J. Fréchet, Preparation of Polymers with Controlled Molecular Architecture. A New Convergent Approach to Dendritic Macromolecules, *J. Am. Chem. Soc.*, **1990**, 112, 7638-7647

(18) R. G. Denkewalter, J. Kolc and W. J. Lukasavage, Macromolecular Highly Branched Homogeneous Compound Based on Lysine Units, *US patent*, 4 289 872, **1981**

(19) R. G. Denkewalter, J. Kolc and W. J. Lukasavage, Macromolecular Highly Branched α,ω-Diamino Carboxylic Acids, *US patent*, 4 410 688, **1983**

(20) L. Crespo, G. Sanclimens, M. Pons, E. Giralt, M. Royo and F. Albericio, Peptide and Amide Bond-Containing Dendrimers, *Chem. Rev.*, **2005**, 105, 1663-1681

(21) F. S. Mehrabadi, W. Fischer and R. Haag, Dendritic and Lipid-Based Carriers for Gene/siRNA Delivery (a Review), *Curr. Opin. Solid State Mater. Sci.*, **2012**, 16, 310-322

(22) M. Mammen, S.-K. Choi and G. M. Whitesides, Polyvalent Interactions in Biological Systems: Implications for Design and Use of Multivalent Ligands and Inhibitors, *Angew. Chem. Int. Ed.*, **1998**, 37, 2754-2794

(23) K. Sadler and J. P. Tam, Peptide Dendrimers: Applications and Synthesis, *Rev. Mol. Biotechnol.*, **2002**, 90, 195-229

(24) D. J. Welsh and D. K. Smith, Comparing Dendritic and Self-Assembly Strategies to Multivalency – RGD Peptide-Integrin Interactions, *Org. Biomol. Chem.*, **2011**, 9, 4795-4801

(25) J. P. Tam, Recent Advances in Multiple Antigen Peptides, *J. Immunol. Methods*, **1996**, 196, 17-32

(26) Z. W. Gu, K. Luo, W. C. She, Y. Wu and B. He, New-Generation Biomedical Materials: Peptide Dendrimers and Their Application in Biomedicine, *Sci. China Chem.*, **2010**, 53, 458-478

(27) V. G. Joshi, V. D. Dighe, D. Thakuria, Y. S. Malik and S. Kumar, Multiple Antigenic Peptide (MAP): A Synthetic Peptide Dendrimer for Diagnostic, Antiviral and Vaccine Strategies for Emerging and Re-Emerging Viral Diseases, *Indian J. Virol.*, **2013**, 24, 312-320

(28) P. M. H. Heegaard, U. Boas and N. S. Sorensen, Dendrimers for Vaccine and Immunostimulatory Uses – A review, *Bioconjug. Chem.*, **2010**, 21, 405-418

(29) N. S. Sorensen, U. Boas and P. M. H. Heegaard, Enhancement of Muramyl Dipeptide (MDP) Immunostimulatory Activity by Controlled Multimerization on Dendrimers, *Macromol. Biosci.*, **2011**, 11, 1484-1490

(30) J. P. Tam, Synthetic Peptide Vaccine Design: Synthesis and Properties of a High-Density Multiple Antigenic Peptide System, *Proc. Natl. Acad. Sci. U.S.A*, **1988**, 85, 5409-5413

(31) W. Huang, B. Nardelli and J. P. Tam, Lipophilic Multiple Antigen Peptide System for Peptide Immunogen and Synthetic Vaccine, *Mol. Immunol.*, **1994**, 31, 1191-1199

(32) J.-P. Defoort, B. Nardelli, W. Huang, D. D. Ho and J. P. Tam, Macromolecular Assemblage in the Design of a Synthetic AIDS Vaccine, *Proc. Natl. Acad. Sci. USA*, **1992**, 89, 3879-3883

(33) J.-P. Defoort, B. Nardelli, W. Huang and J. P. Tam, A Rational Design of Synthetic Peptide Vaccine with a Built-In Adjuvant, *Int. J. Pept. Protein Res.*, **1992**, 40, 214-221

(34) I. Toth, M. Danton, N. Flinn and W. A. Gibbons, A Combined Adjuvant and Carrier System for Enhancing Synthetic Peptides Immunogenicity Utilising Lipidic Amino Acids, *Tet. Lett.*, **1993**, 34, 3925-3928

(35) T. Sakthivel, I. Toth and A. T. Florence, Synthesis and Physicochemical Properties of Lipophilic Polyamide Dendrimers, *Pharm. Res.*, **1998**, 15, 776-782

(36) K. T. Al-Jamal, T. Sakthivel and A. T. Florence, Dendrisomes: Cationic Lipidic Dendron Vesicular Assemblies, *Int. J. Pharm.*, **2003**, 254, 33-36

(37) I. Haro, S. Pérez, M. García, W. C. Chan and G. Ercilla, Liposome Entrapment and Immunogenic Studies of a Synthetic Lipophilic Multiple Antigenic Peptide bearing VP1 and VP3 Domains of the Hepatitis A Virus: A Robust Method for Vaccine Design, *FEBS Letters*, **2003**, 540, 133-140

(38) C. Cubillos, B. G. de la Torre, A. Jakab, G. Clementi, E. Borrás, J. Bárcena, D. Andreu, F. Sobrino and E. Blanco, Enhanced Mucosal Immunoglobulin A Response and Solid Protection against Foot-and-Mouth Disease Virus Challenge Induced by a Novel Dendrimeric Peptide, *J. Virol.*, **2008**, 82, 7223-7230

(39) S. Ota, T. Ono, A. Morita, A. Uenaka, M. Harada and E. Nakayama, Cellular Processing of a Multibranched Lysine Core with Tumor Antigen Peptides and Presentation of Peptide Epitopes Recognized by Cytotoxic T Lymphocytes on Antigen-Presenting Cells, *Cancer Res.*, **2002**, 62, 1471-1476

(40) D. S. Shah, T. Sakthivel, I. Toth, A. T. Florence and A. F. Wilderspin, DNA Transfection and Transfected Cell Viability Using Amphipathic Asymmetric Dendrimers, *Int. J. Pharm.*, **2000**, 208, 41-48

(41) K. T. Al-Jamal, W. T. Al-Jamal, J. T.-W. Wang, N. Rubio, J. Buddle, D. Gathercole, M. Zloh and K. Kostarelos, Cationic Poly-L-lysine Dendrimer Complexes Doxorubicin and Delays Tumor Growth *in Vitro* and *in Vivo*, *ACS Nano*, **2013**, 7, 1905-1917

(42) K. T. Al-Jamal, W. T. Al-Jamal, S. Akerman, J. E. Podestra, A. Yilmazer, J. A. Turton, A. Bianco, N. Vargesson, C. Kanthou, A. T. Florence, G. M. Tozer and K. Kostarelos, Systemic Antiangiogenic Activity of Cationic Poly-L-lysine Dendrimer Delays Tumor Growth, *PNAS*, **2010**, 107, 3966-3971

(43) A. Luganini, S. F. Nicoletto, L. Pizzuto, G. Pirri, A. Giuliani, S. Landolfo and G. Gribaudo, Inhibition of Herpes Simplex Virus Type 1 and Type 2 Infections by Peptide-Derivatized Dendrimers, *Antimicrob. Agents Chemother.*, **2011**, 55, 3231-3239

(44) F. Azmi, A. G. Elliott, N. Marasini, S. Ramu, Z. Ziora, A. M. Kavanagh, M. A. T. Blaskovich, M. A. Cooper, M. Skwarczynski and I. Toth, Short Cationic Lipopeptides as Effective Antibacterial Agents: Design, Physicochemical Properties and Biological Evaluation, *Bioorg. Med. Chem.*, **2016**, 24, 2235-2241

(45) W. C. Chan and P. D. White, *Fmoc Solid Phase Peptide Synthesis – A Practical Approach*, Oxford University Press, **2000**

(46) S. A. Kates and F. Albericio, *Solid-Phase Synthesis. A Practical Guide.* New York, Marcel Dekker Inc., **2000**

(47) R. B. Merrifield, Solid Phase Peptide Synthesis. I. The Synthesis of a Tetrapeptide, *J. Am. Chem. Soc.*, **1963**, 85, 2149-2154

(48) R. B. Merrifield, Solid-Phase Peptide Synthesis. III. An Improved Synthesis of Bradykinin, *Biochemistry*, **1964**, 3, 1385-1390

(49) L. A. Carpino and G. Y. Han, The 9-Fluorenylmethoxycarbonyl Function, a New Base-Sensitive Amino-Protecting Group, *J. Am. Chem. Soc.*, **1970**, 92, 5748-5749

(50) L. A. Carpino and G. Y. Han, The 9-Fluorenylmethoxycarbonyl Amino-Protecting Group, *J. Org. Chem.*, **1972**, 37, 3404-3409

(51) E. Kaiser, R. L. Colescott, C. D. Bossinger and P.I. Cook, Color Test for Detection of Free Terminal Amino Groups in the Solid-Phase Synthesis of Peptides, *Anal. Biochem.*, **1970**, 34, 595-598

(52) S. Yokoyama and J.-I. Hiramatsu, A Modified Ninhydrin Reagent Using Ascorbic Acid Instead of Potassium Cyanide, *J. Biosci. Bioeng.*, **2003**, 95, 204-205

(53) K. J. Jensen, P. T. Shelton and S. L. Pedersen, Eds., *Peptide Synthesis and Applications*, Humana Press, Springer, **2013**

(54) U. Boas, J. Brask, J. B. Christensen and K. J. Jensen, The Ortho Backbone Amide Linker (*o*-BAL) Is an Easily Prepared and Highly Acid-Labile Handle for Solid-Phase Synthesis, *J. Comb. Chem.*, **2002**, 4, 223-228

(55) K. J. Jensen, J. Alsina, M. F. Songster, J. Vágner, F. Albericio and G. Barany, Backbone Amide Linker (BAL) Strategy for Solid-Phase Synthesis of C-Terminal-Modified and Cyclic Peptides, *J. Am. Chem. Soc.*, **1998**, 120, 5441-5452

(56) K. J. Jensen, M. F. Songster, J. Vágner, J. Alsina, F. Albericio and G. Barany, *Peptides – Chemistry, Structure and Biology: Proceedings of the Fourteenth American Peptide Symposium (1995)*, Edited by P. T. P. Kaumaya and R. S. Hodges, Mayflower Scientific, Kingswinford, UK, **1996**

(57) J. Alsina, K. J. Jensen, F. Albericio and G. Barany, Solid-Phase Synthesis with Tris(alkoxy)benzyl Backbone Amide Linkage (BAL), *Chem. Eur. J.*, **1999**, 5, 2787-2795

(58) U. Boas, J. Brask and K. J. Jensen, Backbone Amide Linker in Solid-Phase Synthesis, *Chem. Rev.*, **2009**, 109, 2092-2118

(59) E. E. Swayze, Secondary Amide-Based Linkers for Solid Phase Organic Synthesis, *Tet. Lett.*, **1997**, 38, 8465-8468

(60) J. Clayden, N. Greeves, S. Warren and P. Wothers, *Organic Chemistry*, Oxford University Press, **2001**

(61) S. K. Shannon and G. Barany, Colorimetric Monitoring of Solid-Phase Aldehydes Using 2,4-Dinitrophenylhydrazine, *J. Comb. Chem.*, **2004**, 6, 165-170

(62) J. C. Sheehan and G. P. Hess, A New Method for Forming Peptide Bonds, *J. Am. Chem. Soc.*, **1955**, 77, 1067-1068

(63) A. R. Vaino and K. D. Janda, Solid-Phase Organic Synthesis: A Critical Understanding of the Resin, *J. Comb. Chem.*, **2000**, 2, 579-596

(64) D. C. Sherrington, Preparation, Structure and Morphology of Polymer Supports, *Chem. Commun.*, **1998**, 2275-2286

(65) X. Liu, J. Zhou, T. Yu, C. Chen, Q. Cheng, K. Sengupta, Y, Huang, H. Li, C. Liu, Y. Wang, P. Posocco, M. Wang, Q. Cui, S. Giorgio, M. Fermeglia, F. Qu, S. Pricl, Y. Shi, Z. Liang, P. Rocchi, J. J. Rossi and L. Peng, Adaptive Amphiphilic Dendrimer-Based Nanoassemblies as Robust and Versatile siRNA Delivery Systems, *Angew. Chem.*, **2014**, 126, 12016-12021

(66) T. Yu, X. Liu, A.-L. Bolcato-Bellemin, Y. Wang, C. Liu, P. Erbacher, F. Qu, P. Rocchi, J.-P. Behr and L. Peng, An Amphiphilic Dendrimer for Effective Delivery of Small Interfering RNA and Gene Silencing In Vitro and In Vivo, *Angew. Chem. Int. Ed.*, **2012**, 51, 8478-8484

(67) D. Ma, H.-B. Zhang, Y.-Y. Chen, J.-T. Lin and L.-M. Zhang, New Cyclodextrin Derivative Containing Poly(L-lysine) Dendrons for Gene and Drug Co-Delivery, *J. Colloid Interface Sci.*, **2013**, 405, 305-311

(68) Y. Teng and P. H. Toy, *Colorimetric Tests for Solid-Phase Organic Synthesis*, Edited by P. H. Toy and Y. Lam, *Solid-Phase Organic Synthesis: Concepts, Strategies, and Applications*, John Wiley & Sons Inc., **2012**, 83-93

(69) W. S. Hancock and J. E. Battersby, A New Micro-Test for Detection of Incomplete Coupling Reactions in Solid-Phase Peptide-Synthesis using 2,4,6-Trinitrobenzenesulphonic Acid, *Anal. Biochem.*, **1976**, 71, 260-264

(70) V. Krchňák, J. Vágner, P. Safár and M. Lebl, Noninvasive Continuous Monitoring of Solid-Phase Peptide Synthesis by Acid-Base Indicator, *Collect. Czech. Chem. Commun.*, **1988**, 53, 2542-2548

(71) M. Flegel and R. C. Sheppard, A Sensitive, General Method for Quantitative Monitoring of Continuous Flow Solid Phase Peptide Synthesis, *J. Chem. Soc. Chem. Commun.*, **1990**, 536-538

(72) A. Shah, S. S. Rahman, V. de Biasi and P. Camilleri, Development of Colorimetric Method for the Detection of Amines Bound to Solid Support, *Anal. Commun.*, **1997**, 34, 325-328

(73) S. Claerhout, D. S. Ermolat'ev and E. V. Van der Eycken, A New Colorimetric Test for Solid-Phase Amines and Thiols, *J. Comb. Chem.*, **2008**, 10, 580-585

(74) C. Blackburn, Solid-Phase Synthesis of 2-Amino-3-chloro-5 and 8-Nitro-1,4-naphtoquinones: A New and General Colorimetric Test for Resin-Bound Amines, *Tet. Lett.*, **2005**, 46, 1405-1409

(75) S.-J. Yang, X. Z. Tian and I. Shin, Colorimetric Monitoring of Amines and Thiols on a Solid Support, *Org. Lett.*, **2009**, 11, 3438-3441

(76) E. Kaiser, C. D. Bossinger, R. L. Colescott and D. B. Olsen, Color Test for Terminal Prolyl Residues in the Solid-Phase Synthesis of Peptides, *Anal. Chim. Acta*, **1980**, 118, 149-151

(77) L. Simon, *C. R. Acad. Sci.*, **1897**, 125, 1105

(78) F. Feigl and V. Anger, Nachweis von Aliphatischen Sekundären Aminen, Mikrochemische Nachweise Organischer Verbindungen mit Hilfe von Tüpfelreaktionen, *Mikrochim. Acta*, **1937**, 1, 121-141

(79) C. F. Cullis and D. J. Waddington, The Colorimetric Determination of Secondary Amines, *Anal. Chim. Acta*, **1956**, 15, 158-163

(80) K.-A. Kovar and M. Laudszun, Chemistry and Reaction Mechanisms of Rapid Tests for Drug of Abuse and Precursors Chemicals, *Scientific and Technical Notes, United Nations*, **1989**, SCITEC/6, V.89-51669

(81) T. Christensen, A Qualitative Test for Monitoring Coupling Completeness in Solid Phase Peptide Synthesis Using Chloranil, *Acta Chem. Scand.*, **1979**, B 33, 763-766

(82) T. Vojkovsky, Detection of Secondary Amines on Solid Phase, *Pept. Res.*, **1995**, 8, 236-237

(83) C. Kay, O. E. Lorthioir, N. J. Parr, M. Congreve, S. C. McKeown, J. J. Scicinski and S. V. Ley, Solid-Phase Reaction Monitoring – Chemical Derivatization and Off-Bead Analysis, *Biotechnol. Bioeng.*, **2000**/**2001**, 71, 110-118

(84) J. Vázquez, G. Qushair and F. Albericio, Qualitative Colorimetric Tests for Solid Phase Synthesis, *Methods Enzymol.*, **2003**, 369, 21-35

(85) E. Bayer, M. Dengler and B. Hemmasi, Peptide Synthesis on the New Polyoxyethylene-Polystyrene Graft Copolymer, Synthesis of Insulin B_{21-30}, *Int. J. Pept. Protein Res.*, **1985**, 25, 178-186

(86) M. Meldal, PEGA: A Flow Stable Polyethylene Glycol Dimethyl Acrylamide Copolymer for Solid Phase Synthesis, *Tet. Lett.*, **1992**, 33, 3077-3080

(87) F. Albericio and F. G. Martin, Solid Supports for the Synthesis of Peptides – From the First Resin Used to the Most Sophisticated in the Market, Focus on Peptides Supplement to *Chim. Oggi*, **2008**, 26, 29-34

(88) G. B. Fields, *Methods for Removing the Fmoc Group*, Edited by M. W. Pennington and B. M. Dunn, *Methods in Molecular Biology, Vol. 35 Peptide Synthesis Protocols*, Humana Press Inc., **1994**, 17-27

(89) A. D. Radkov and L. A. Moe, Bacterial Synthesis of D-amino Acids, *Appl. Microbiol. Biotechnol.*, **2014**, 98, 5363-5374

(90) K. Lefmann, *Neutron Scattering: Theory, Instrumentation, and Simulation,* Department of Materials Research, Risø National Laboratory, Technical University of Denmark, **2007**

(91) D. A. Tomalia, J. B. Christensen and U. Boas, *Dendrimers, Dendrons, and Dendritic Polymers – Discovery, Applications and the Future*, Cambridge University Press, **2012**

(92) F. Mezei, *Neutron Scattering,* Edited by T. Imae, T. Kanaya, M. Furusaka and N. Torikai, *Neutrons in Soft Matter*, John Wiley & Sons, Inc, **2011**, 1-28

(93) B. Hammouda, *Small-Angle Neutron Scattering* (Summer School Course Materials), National Institute of Standards and Technology, Center for Neutron Research, **2011**

(94) R. Pynn, *Neutron Scattering – A primer*, Los Alamos Neutron Science Center (LANSCE), **1990**

(95) I. Grillo, *Small-Angle Neutron Scattering and Applications in Soft Condensed Matter*, Edited by R. Borsali and R. Pecora, *Soft-Matter Characterization*, Springer-Verlag Berlin Heidelberg, **2008**, 725-782

(96) K. Mortensen, *Instrumentation,* Edited by T. Imae, T. Kanaya, M. Furusaka and N. Torikai, *Neutrons in Soft Matter*, John Wiley & Sons, Inc, **2011**, 29-56

(97) A. Guinier and G. Fournet, *Small-Angle Scattering of X-Rays,* John Wiley & Sons, Inc, **1955**

(98) J. B. Hayter and J. Penfold, An Analytic Structure Factor for Macroion Solutions, *Mol. Phys.*, **1981**, 42, 109-118

(99) R. Pecora, Dynamic Light Scattering Measurement of Nanometer Particles in Liquids, *J. Nanopart. Res.*, **2000**, 2, 123-131

(100) C. A. Williams, *Application of Photon Correlation Spectroscopy to a Macromolecular System*, Physics Department, the College of Wooster, **1998**

(101) A. J. F. Siegert, On the Fluctuations in Signals Returned by Many Independently Moving Scatterers, *Rad. Lab. Rep.*, No 465, Massachusetts Institute of Technology, **1943**

(102) R. A. Lauten, A.-L. Kjøniksen and B. Nyström, Adsorption and Desorption of Unmodified and Hydrophobically Modified Ethyl(hydroxyethyl)cellulose on Polystyrene Latex Particles in the Presence of Ionic Surfactants using Dynamic Light Scattering, *Langmuir*, **2000**, 16, 4478-4484

(103) A.-L. Kjøniksen and B. Nyström, Dynamic Light-Scattering of Poly(vinyl alcohol) Solutions and Their Dynamical Behavior During the Chemical Gelation Process, *Macromolecules*, **1996**, 29, 7116-7123

(104) R. Pecora, *Dynamic Light Scattering – Applications of Photon Correlation Spectroscopy*, Plenum Press, New York, **1985**

(105) D. K. Smith, A. R. Hirst, C. S. Love, J. G. Hardy, S. V. Brignell and B. Huang, Self-Assembly using Dendritic Building Blocks – Towards Controllable Nanomaterials, *Prog. Polym. Sci.*, **2005**, 30, 220-293

(106) A. Barnard and D. K. Smith, Self-Assembled Multivalency: Dynamic Ligand Arrays for High-Affinity Binding, *Angew. Chem. Int. Ed.*, **2012**, 51, 6572-6581

(107) A. Barnard, P. Posocco, S. Pricl, M. Calderon, R. Haag, M. E. Hwang, V. W. T. Shum, D. W. Pack and D. K. Smith, Degradeable Self-Assembling Dendrons for Gene Delivery: Experimental and Theoretical Insights into the Barriers to Cellular Uptake, *J. Am. Chem. Soc.*, **2011**, 133, 20288-20300

(108) T. Yoshimura, M. Saito and K. Esumi, Solution Properties of Tadpole-Type Cationic Amphiphilic Dendrimers Consisting of an Alkyl Chain, a Quaternary Ammonium, and a Poly(amidoamine) Dendron, *J. Oleo Sci.*, **2013**, 62, 213-221

(109) T. M. Chapman, G. L. Hillyer, E. J. Mahan and K. A. Shaffer, Hydraamphiphiles: Novel Linear Dendritic Block Copolymer Surfactants, *J. Am. Chem. Soc.*, **1994**, 116, 11195-11196

(110) N. J. Turro and A. Yekta, Luminescent Probes for Detergent Solutions. A Simple Procedure for Determination of the Mean Aggregation Number of Micelles, *J. Am. Chem. Soc.*, **1978**, 100, 5951-5952

(111) J. V. Bonventre, V. S. Vaidya, R. Schmouder, P. Feig and F. Dieterle, New-Generation Biomarkers for Detecting Kidney Toxicity, *Nat Biotechnol.*, **2010**, 28, 436-440

(112) G. F. Rush and J. B. Hook, *The Kidney as a Target Organ for Toxicity*, Edited by G. M. Cohen, *Target Organ Toxicity*, vol. II, CRC Press, Inc., **1999**, 1-18

(113) M. A. Perazella, Renal Vulnerability to Drug Toxicity, *Clin. J. Am. Soc. Nephrol.*, **2009**, 4, 1275-1283

(114) J. A. Barltrop and T. C. Owen, 5-(3-Carboxymethoxyphenyl)-2-(4,5-dimethylthiazolyl)-3-(4-sulfophenyl)tetrazolium, Inner Salt (MTS) and Related Analogs of 3-(4,5-Dimethylthiazolyl)-2,5-diphenyltetrazolium bromide (MTT) Reducing to Purple Water-Soluble Formazans as Cell-Viability Indicators, *Bioorg.Med. Chem. Lett.*, **1991**, 1, 611-614

(115) L. Kupcsik, *Estimation of Cell Number Based on Metabolic Activity: The MTT Reduction Assay*, Edited by M. J. Stoddart, *Mammalian Cell Viability – Methods and Protocols*, Methods in Molecular Biology, vol. 740, Humana Press, **2011**, 13-19

(116) J. M. Capasso, B. R. Cossío, T. Berl, C. J. Rivard and C. Jiménez, A Colorimetric Assay for Determination of Cell Viability in Algal Cultures, *Biomol. Eng.*, **2003**, 20, 133-138

(117) K. T. Al-Jamal, P. Ruenraroengsak, N. Hartell and A. T. Florence, An Intrinsically Fluorescent Dendrimer as a Nanoprobe of Cell Transport, *J. Drug Target.*, **2006**, 14, 405-412

(118) B. R. Avaritt and P. W. Swaan, Internalization and Subcellular Trafficking of Poly-L-lysine Dendrimers are Impacted by the Site of Fluorophore Conjugation, *Mol. Pharm.*, **2015**, 12, 1961-1969

(119) S. Feng, C. Bagia and G. Mpourmpakis, Determination of Proton Affinities and Acidity Constants of Sugars, *J. Phys. Chem. A*, **2013**, 117, 5211-5219

(120) D. D. Perrin, *Dissociation Constants of Organic Bases in Aqueous Solution*, Butterworths, London, **1965**, Supplement 1972

(121) L. R. Martin, S. P. Mezyk and B. J. Mincher, Determination of Arrhenius and Thermodynamic Parameters for the Aqueous Reaction of the Hydroxyl Radical with Lactic Acid, *J. Phys. Chem. A*, **2009**, 113, 141-145

(122) T. K. Lindhorst, *Essentials of Carbohydrate Chemistry and Biochemistry*, WILEY-VCH Verlag GmbH & Co. KGaA, Weinheim, **2007**

(123) S. Deng, U. Gangadharmath and C.-W. T. Chang, Sonochemistry: A Powerful Way of Enhancing the Efficiency of Carbohydrate Synthesis, *J. Org. Chem.*, **2006**, 71, 5179-5185

(124) Y. A. Knirel, N. A. Paramonov, E. V. Vinogradov, A. S. Shashkov, N. K. Kochetkov, Z. Sidorczyk and A. Swierzko, Structure of the O-Specific Polysaccharide of *Proteus penneri* 62 Containing 2-Acetamido-3-*O*-[(*S*)-1-carboxyethyl]-2-deoxy-D-glucose (*N*-acetylisomuramic acid), *Carbohydr. Res.*, **1992**, 235, C19-C23

(125) H. Merten and R. Brossmer, A Facile Two-Step Synthesis of *N*-acetylmuramic Acid by Selective Functionalization of HO-3 of 2-Acetamido-2-deoxy-D-glucose, *Carbohydr. Res.*, **1989**, 191, 144-149

(126) Y. Cai, C.-C. Ling and D. R. Bundle, Concise and Efficient Synthesis of 2-Acetamido-2-deoxy-β-D-hexopyranosides of Diverse Aminosugars from 2-Acetamido-2-deoxy-β-D-glucose, *J. Org. Chem.*, **2009**, 74, 580-589

(127) Y. Matsushima and J. T. Park, Stereospecific Synthesis of 2-Amino-3-*O*-(D-1'-carboxyethyl)-2-deoxy-D-glucose (Muramic Acid) and Related Compounds, *J. Org. Chem.*, **1962**, 27, 3581-3583

(128) H. M Flowers and R. W. Jeanloz, The Synthesis of 2-Acetamido-3-*O*-(D-1-carboxyethyl)-2-deoxy-α-D-glucose (*N*-Acetylmuramic Acid) and of Benzyl Glycoside Derivatives of 2-Amino-3-*O*-(D-1-carboxyethyl)-2-deoxy-D-glucose (Muramic Acid), *J. Org. Chem.*, **1963**, 28, 2983-2986

(129) H. M. Flowers and R. W. Jeanloz, The Synthesis of a Glucosaminyl-Muramic Acid Disaccharide: Methyl 6-*O*-(2-Acetamido-3,4,6-tri-*O*-acetyl-2-deoxy-β-D-glucopyranosyl)-2-acetamido-4-*O*-acetyl-2-deoxy-3-*O*-[D-1-(methyl carboxylate)ethyl]-α-D-glucopyranoside, *J. Org. Chem.*, **1963**, 28, 1564-1567

(130) K. Vlahoviček-Kahlina and A. Jakas, Synthesis of Orthogonally Protected Muramic Acid Building Blocks for Solid Phase Peptide Synthesis, *Croat. Chem. Acta*, **2015**, 88, 151-157

(131) S. Oscarson, *Protective Group Strategies*, Edited by D. E. Levy and P. Fügedi, *The Organic Chemistry of Sugars*, CRC Press, Taylor & Francis Group, **2005**, 53-87

(132) K.-T. Chen, D.-Y. Huang, C.-H. Chiu, W.-W. Lin, P.-H. Liang and W.-C. Cheng, Synthesis of Diverse *N*-Substituted Muramyl Dipeptide Derivatives and Their use in a Study of Human NOD2 Stimulation Activity, *Chem. Eur. J.*, **2015**, 21, 11984-11988

(133) M. M. J. H. P. Willems, G. G. Zom, N. Meeuwenoord, S. Khan, F. Ossendorp, H. S. Overkleeft, G. A. van der Marel, D. V. Filippov and J. D. C. Codée, Lipophilic Muramyl Dipeptide-Antigen Conjugates as Immunostimulating Agents, *ChemMedChem*, **2016**, 11, 190-198

(134) E. Valeur and M. Bradley, Amide Bond Formation: Beyond the Myth of Coupling Reagents, *Chem. Soc. Rev.*, **2009**, 38, 606-631

(135) P. Lloyd-Williams, F. Albericio and E. Giralt, *Chemical Approaches to the Synthesis of Peptides and Proteins*, CRC Press LCC, **1997**

(136) M. M. Joullié and K. M. Lassen, Evolution of Amide Bond Formation, *ARKIVOC*, 2010, viii, 189-250

(137) M. Driffield, D. M. Goodall and D. K. Smith, Synthesis of Dendritic Branches Based on L-lysine: is the Stereochemistry Preserved Throughout the Synthesis?, *Org. Biomol. Chem.*, **2003**, 1, 2612-2620

(138) V. Kunzmann, E. Kretzschmar, T. Herrmann and M. Wilhelm, Polyinosinic-Polycytidylic Acid-Mediated Stimulation of Human γδ T Cells via $CD11c^+$ Dendritic Cell-Derived Type I Interferons, *Immunology*, **2004**, 112, 369-377

(139) Y.-S. Cheng and F. Xu, Anticancer Function of Polyinosinic-Polycytidylic Acid, *Cancer Biol. Ther.*, **2010**, 10, 1219-1223

(140) C. Bode, G. Zhao, F. Steinhagen, T. Kinjo and D. M. Klinman, CpG DNA as Vaccine Adjuvant, *Expert Rev. Vaccines*, **2011**, 10, 499-511

(141) D. M. Klinman, Immunotherapeutic uses of CpG Oligodeoxynucleotides, *Nat. Rev. Immunol.*, **2004**, 4, 249-259

(142) K. Takeda and S. Akira, Toll-Like Receptors in Innate Immunity, *Int. Immunol.*, **2005**, 17, 1-14

(143) V. V. Andrushchenko, H. J. Vogel and E. J. Prenner, Optimization of the Hydrochloric Acid Concentration used for Trifluoroacetate Removal from Synthetic Peptides, *J. Pept. Sci.*, **2007**, 13, 37-43

Appendix

Publication I

D. K. Svenssen, S. Mirsharghi and U. Boas, Solid-Phase Synthesis of Polyfunctional Polylysine Dendrons using Aldehyde Linkers, *Tet. Lett.*, **2014**, 55, 3942-3945.

Publication II

U. Boas and S. Mirsharghi, Color Test for Selective Detection of Secondary Amines on Resin and in Solution, *Org. Lett.*, **2014**, 16, 5918-5921.

Publication III

S. Mirsharghi, K. D. Knudsen, S. Bagherifam, B. Nyström and U. Boas, Preparation and Self-Assembly of Amphiphilic Polylysine Dendrons, *New J. Chem.*, **2016**, 40, 3597-3611.

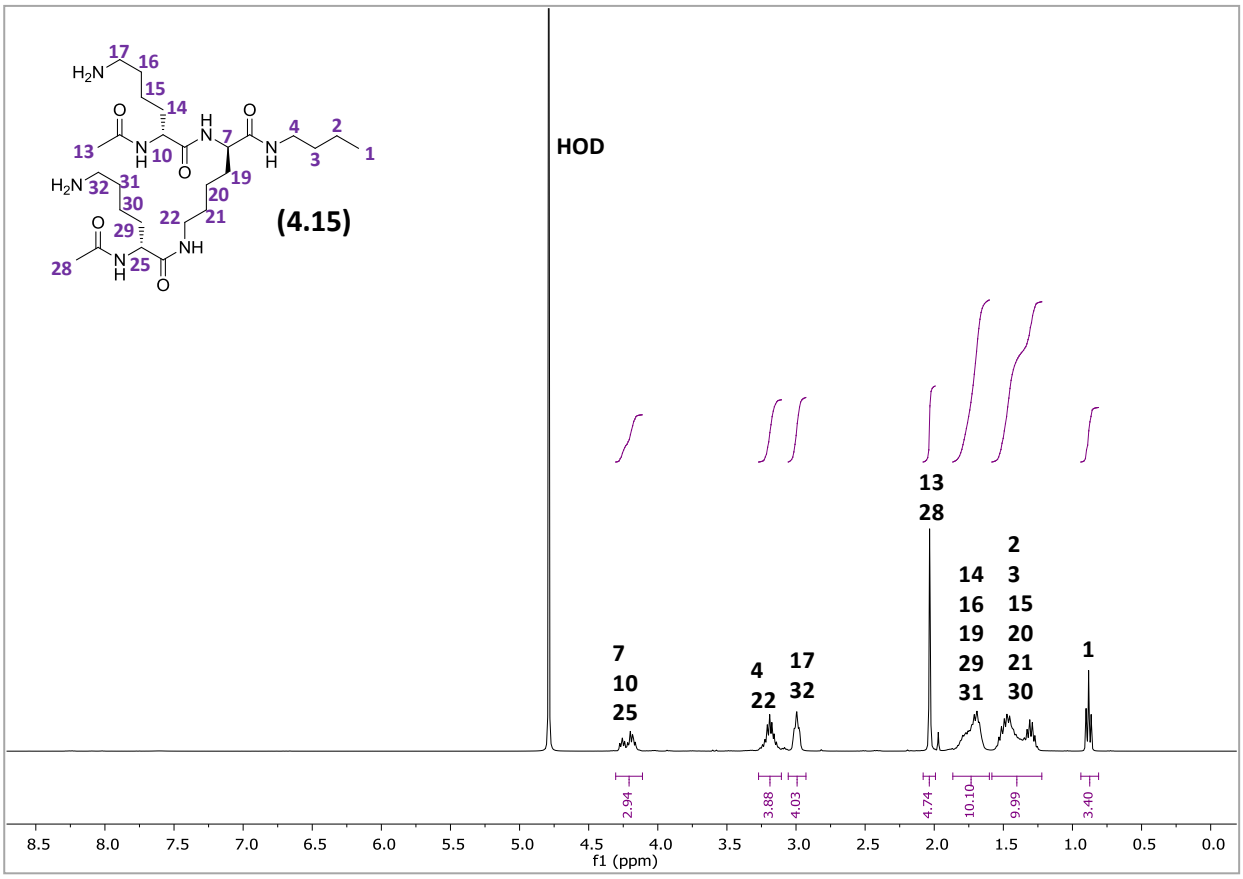
(4.15)
HOD
7
10
25
4
22
17
32
13
28
14
16
19
29
31
2
3
15
20
21
30
1
2.94
3.88
4.03
4.74
10.10
9.99
3.40
f1 (ppm)

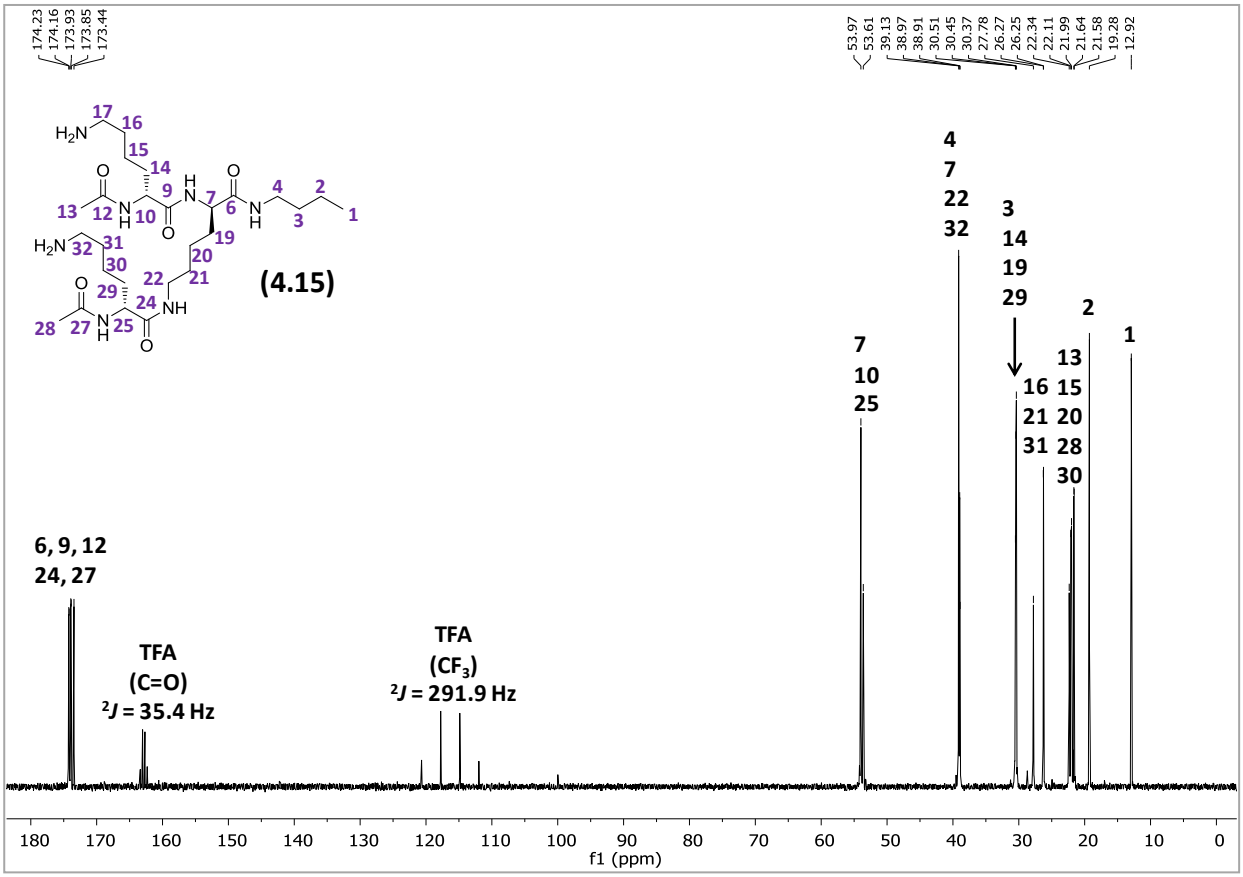
174.23
174.16
173.93
173.85
173.44
53.97
53.61
39.13
38.97
38.91
30.51
30.45
30.37
27.78
26.27
26.25
22.34
22.11
21.99
21.64
21.58
19.28
12.92
(4.15)
6, 9, 12
24, 27
TFA
(C=O)
²J = 35.4 Hz
TFA
(CF3)
²J = 291.9 Hz
4
7
22
32
3
14
19
29
2
1
7
10
25
16
21
31
13
15
20
28
30
f1 (ppm)

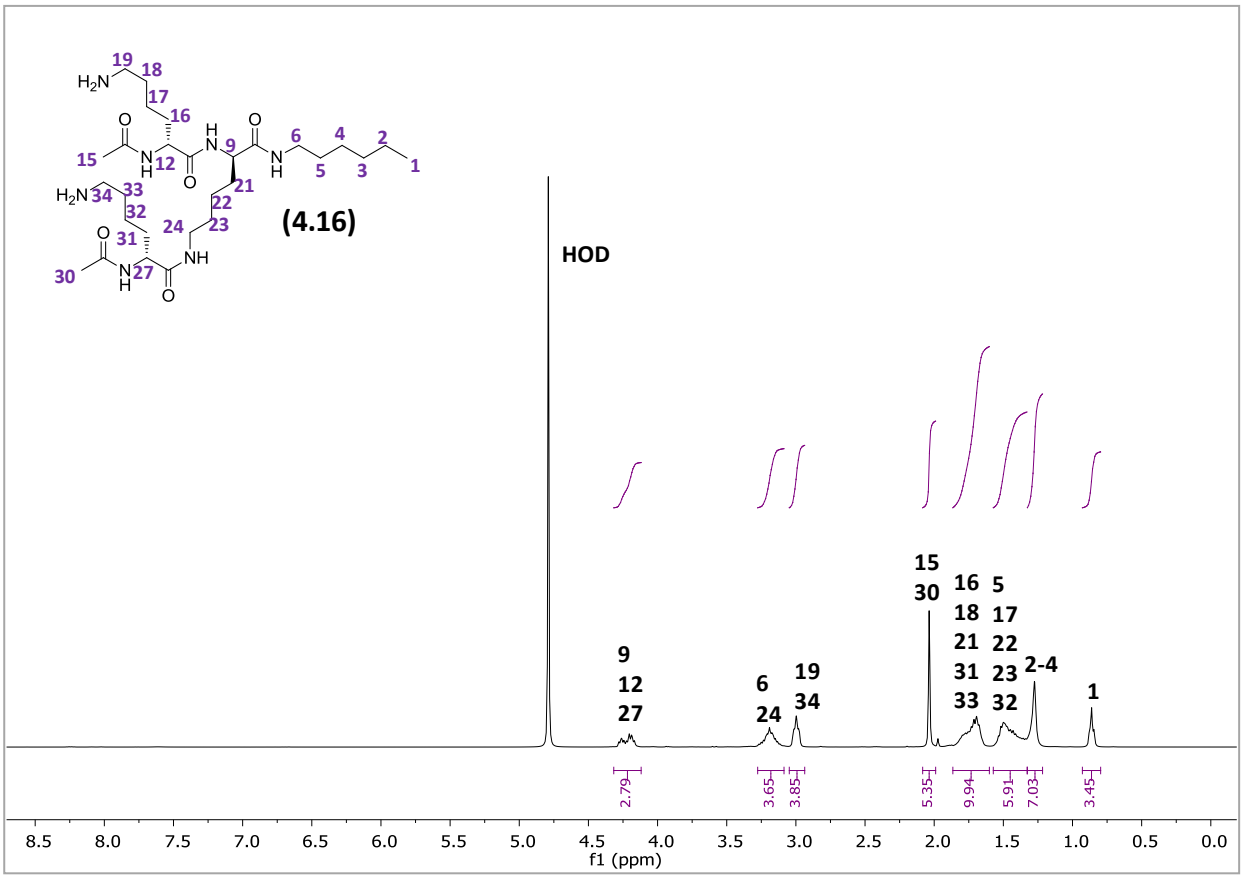
(4.16)
HOD
9
12
27
6
24
19
34
15
30
16
18
21
31
33
5
17
22
23
32
2-4
1
2.79
3.65
3.85
5.35
9.94
5.91
7.03
3.45
f1 (ppm)

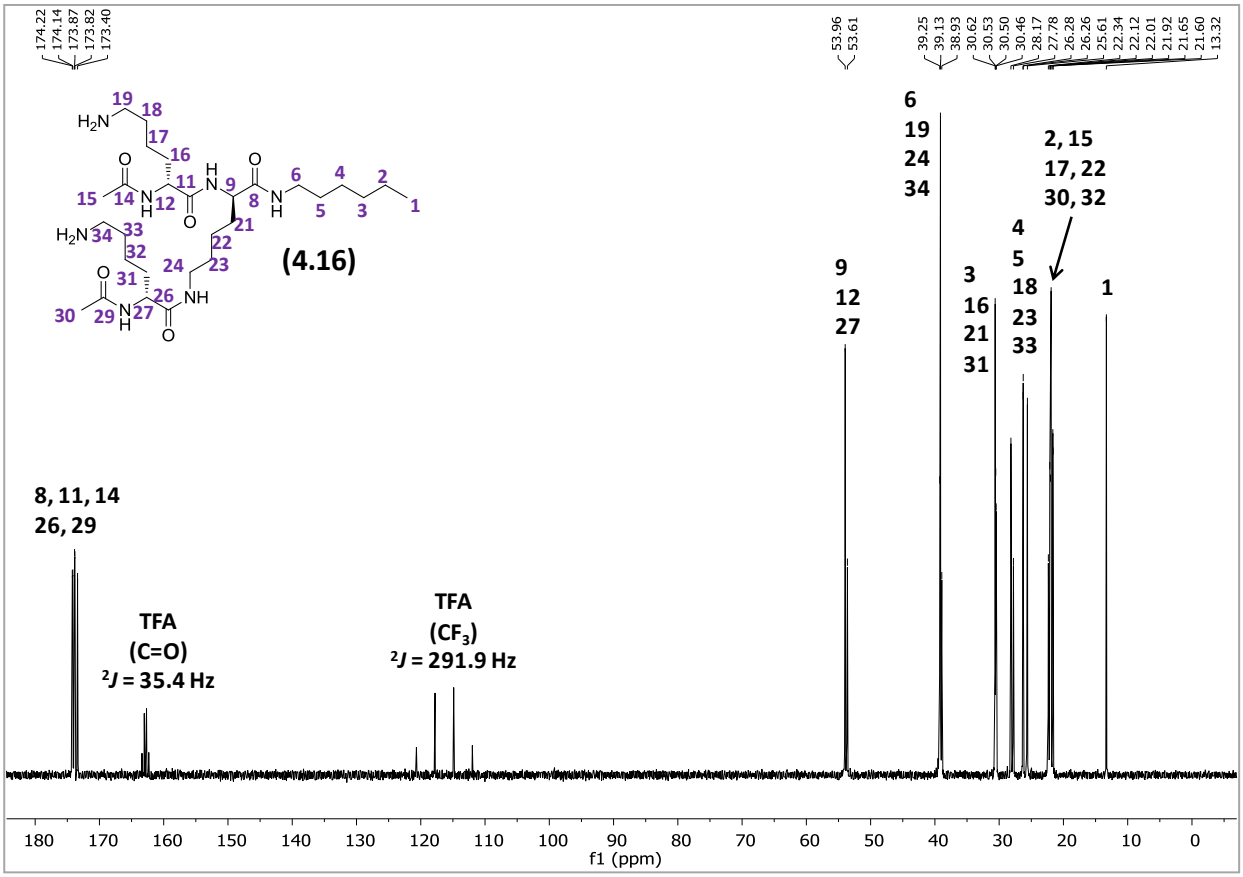
(4.16)
8, 11, 14
26, 29
TFA
(C=O)
²J = 35.4 Hz
TFA
(CF3)
²J = 291.9 Hz
9
12
27
6
19
24
34
3
16
21
31
4
5
18
23
33
2, 15
17, 22
30, 32
1
f1 (ppm)

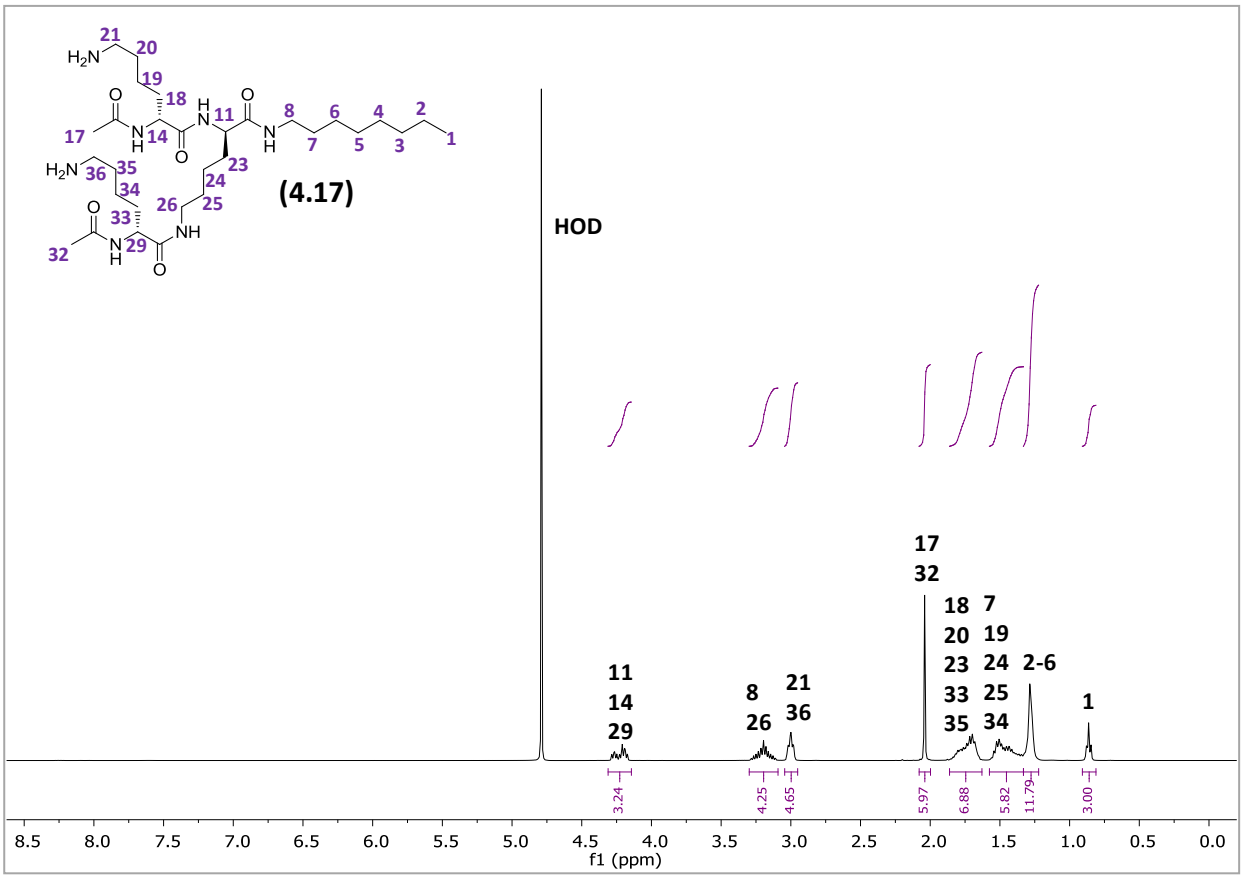
(4.17)
HOD
11
14
29
8
26
21
36
17
32
18
20
23
33
35
7
19
24
34
2-6
1
3.24
4.25
4.65
5.97
6.88
5.82
11.79
3.00
f1 (ppm)

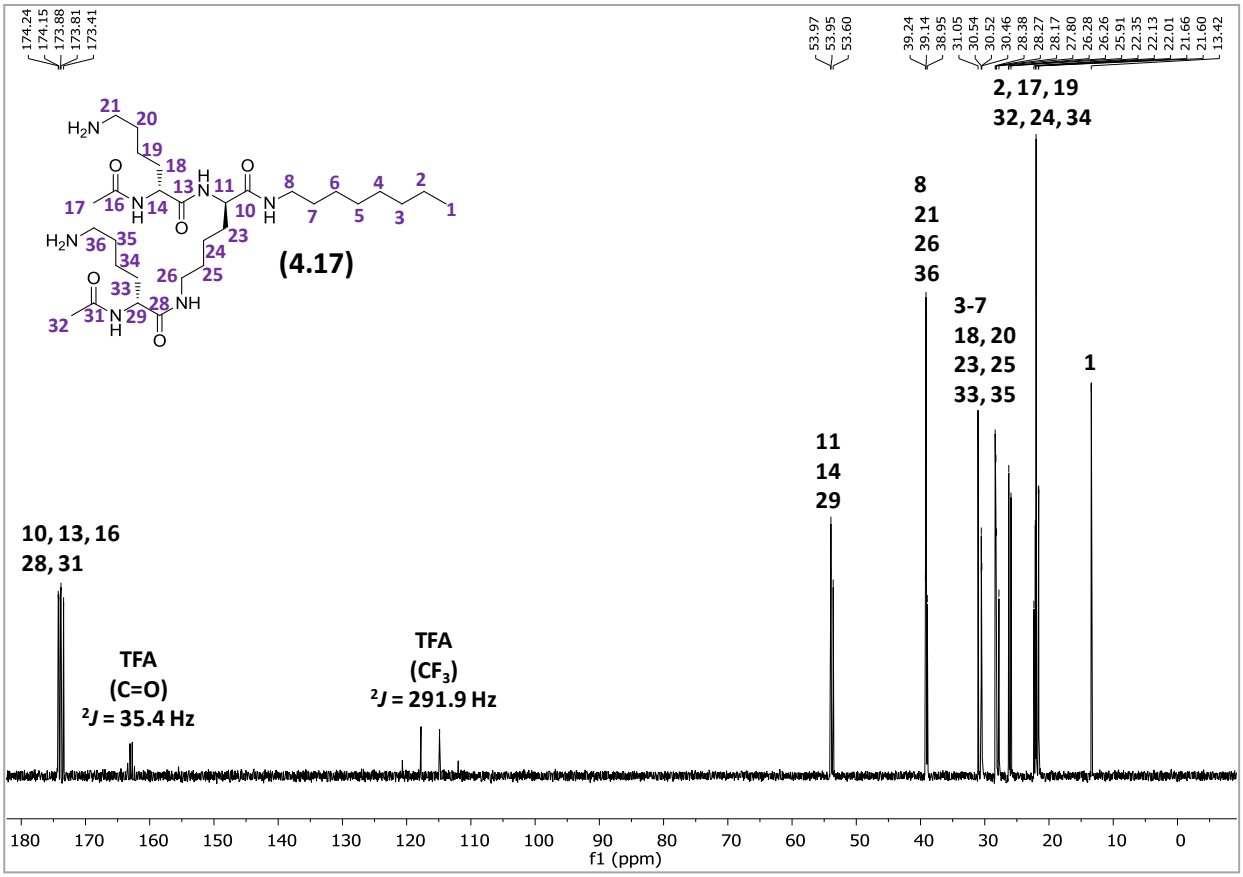
(4.17)
2, 17, 19
32, 24, 34
8
21
26
36
3-7
18, 20
23, 25
33, 35
1
11
14
29
10, 13, 16
28, 31
TFA
(C=O)
²J = 35.4 Hz
TFA
(CF3)
²J = 291.9 Hz
f1 (ppm)

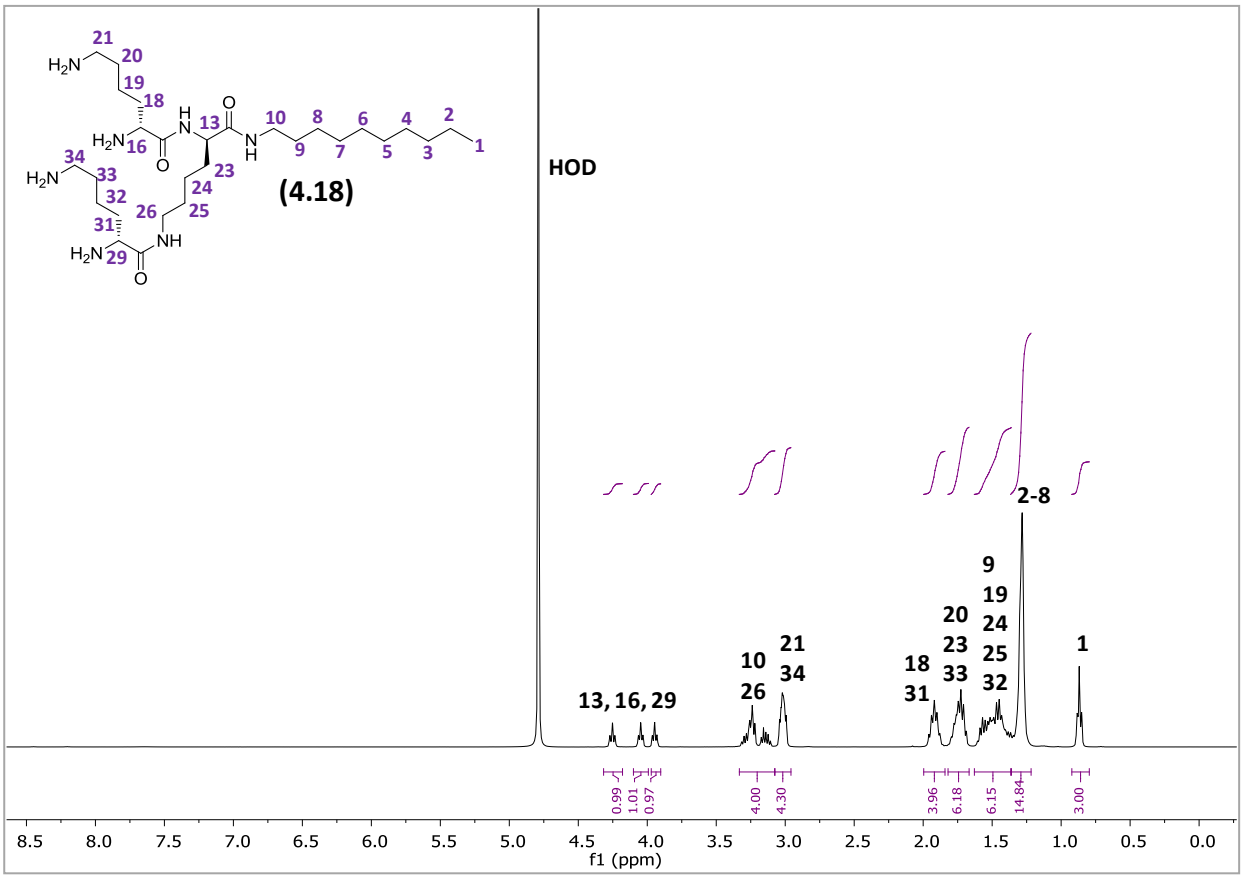
(4.18)
HOD
13, 16, 29
10
26
21
34
18
31
20
23
33
9
19
24
25
32
2-8
1
0.99
1.01
0.97
4.00
4.30
3.96
6.18
6.15
14.84
3.00
f1 (ppm)

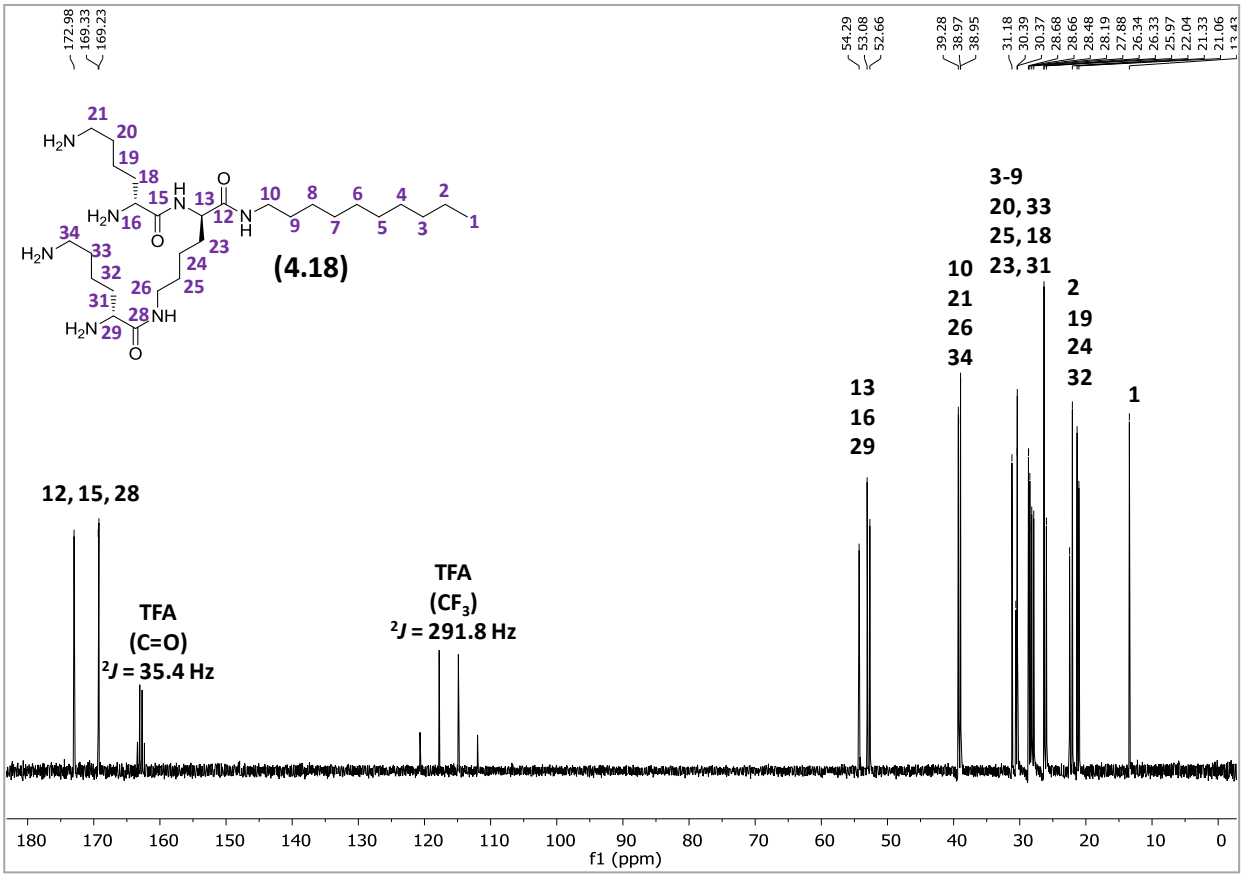
(4.18)
12, 15, 28
TFA
(C=O)
^2J = 35.4 Hz
TFA
(CF_3)
^2J = 291.8 Hz
13
16
29
10
21
26
34
3-9
20, 33
25, 18
23, 31
2
19
24
32
1
f1 (ppm)

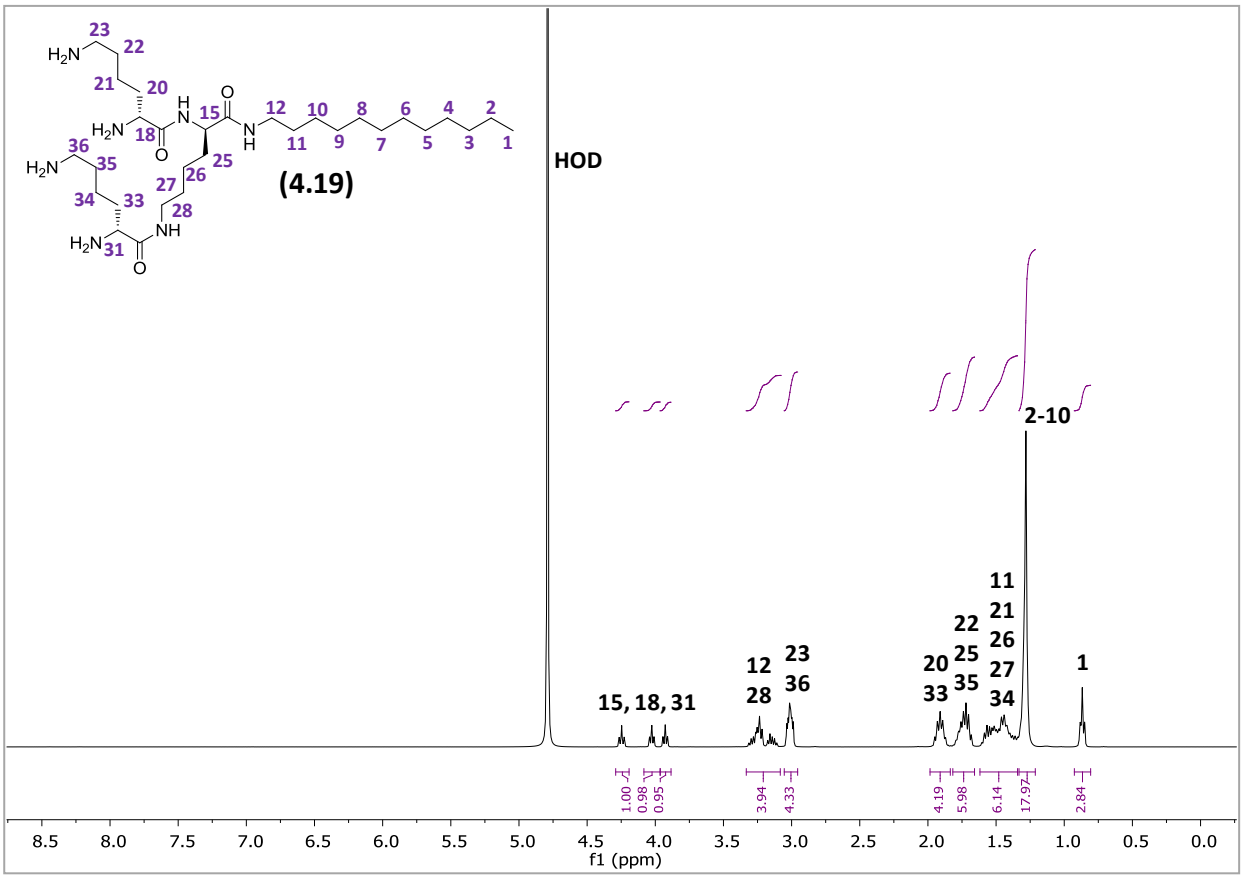
(4.19)
HOD
2-10
15, 18, 31
12
28
23
36
20
33
22
25
35
11
21
26
27
34
1
1.00
0.98
0.95
3.94
4.33
4.19
5.98
6.14
17.97
2.84
8.5
8.0
7.5
7.0
6.5
6.0
5.5
5.0
4.5
4.0
3.5
3.0
2.5
2.0
1.5
1.0
0.5
0.0
f1 (ppm)

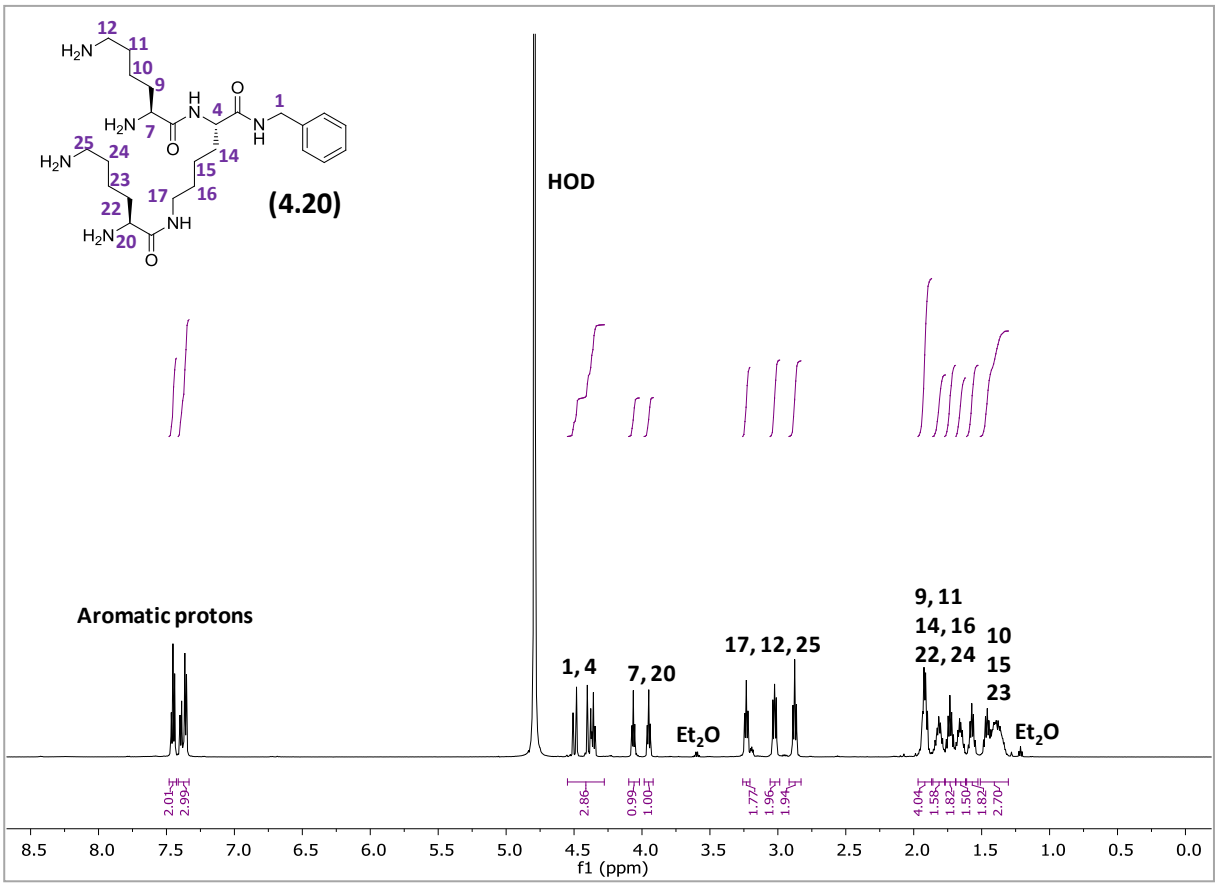
(4.20)
HOD
Aromatic protons
1, 4
7, 20
Et2O
17, 12, 25
9, 11
14, 16
22, 24
10
15
23
Et2O
f1 (ppm)

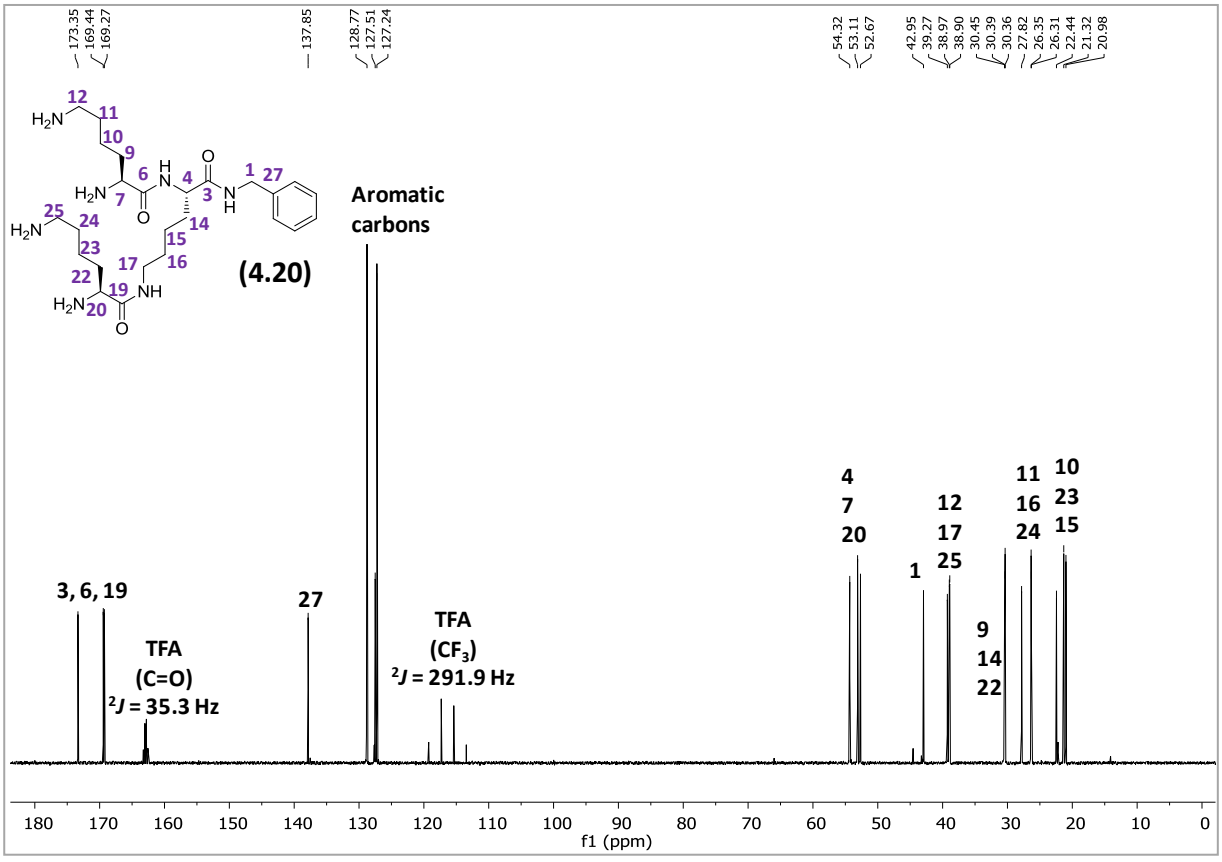
(4.20)
Aromatic carbons
3, 6, 19
TFA
(C=O)
2J = 35.3 Hz
27
TFA
(CF3)
2J = 291.9 Hz
4
7
20
1
12
17
25
9
14
22
11
16
24
10
23
15
f1 (ppm)

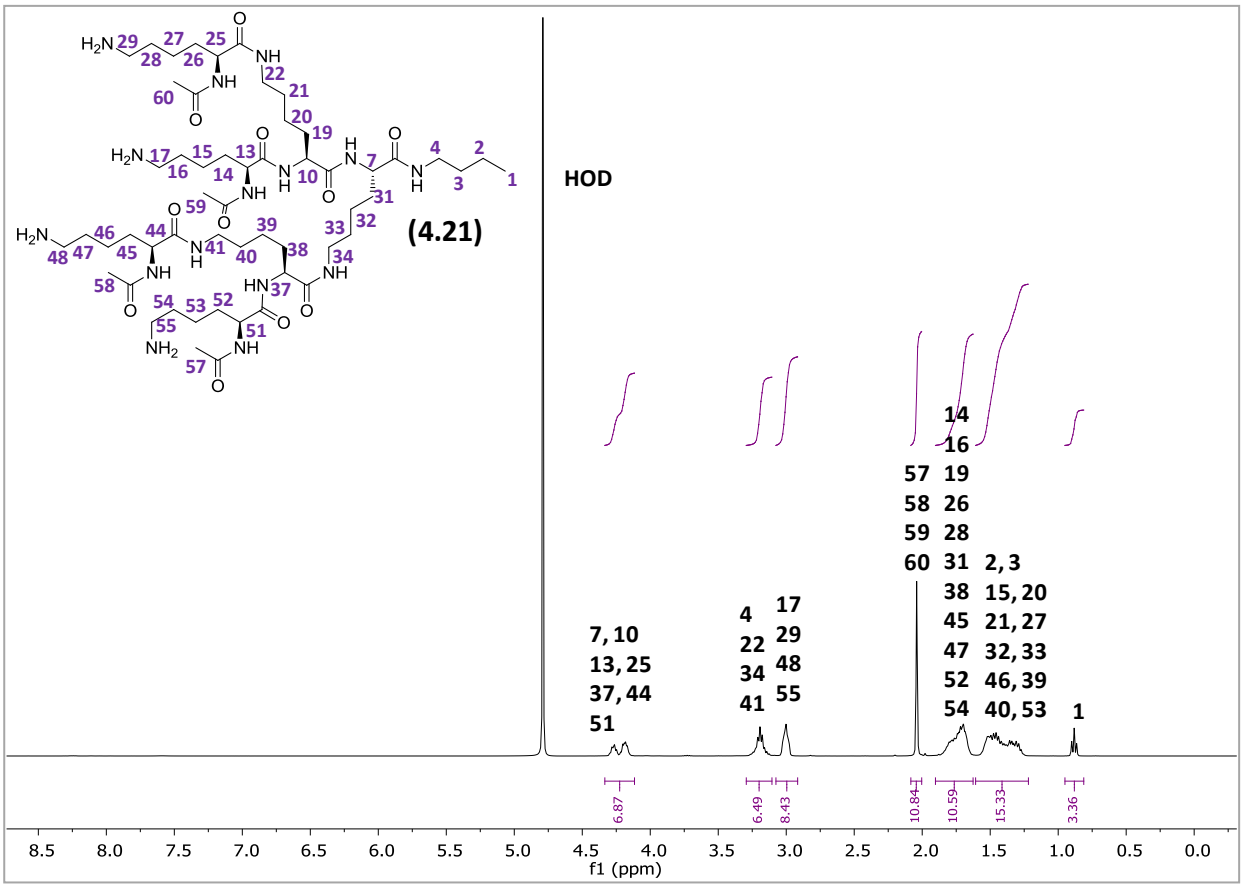
(4.21)
HOD
7, 10
13, 25
37, 44
51
4
22
34
41
17
29
48
55
57
58
59
60
14
16
19
26
28
31
38
45
47
52
54
2, 3
15, 20
21, 27
32, 33
46, 39
40, 53
1
6.87
6.49
8.43
10.84
10.59
15.33
3.36
f1 (ppm)

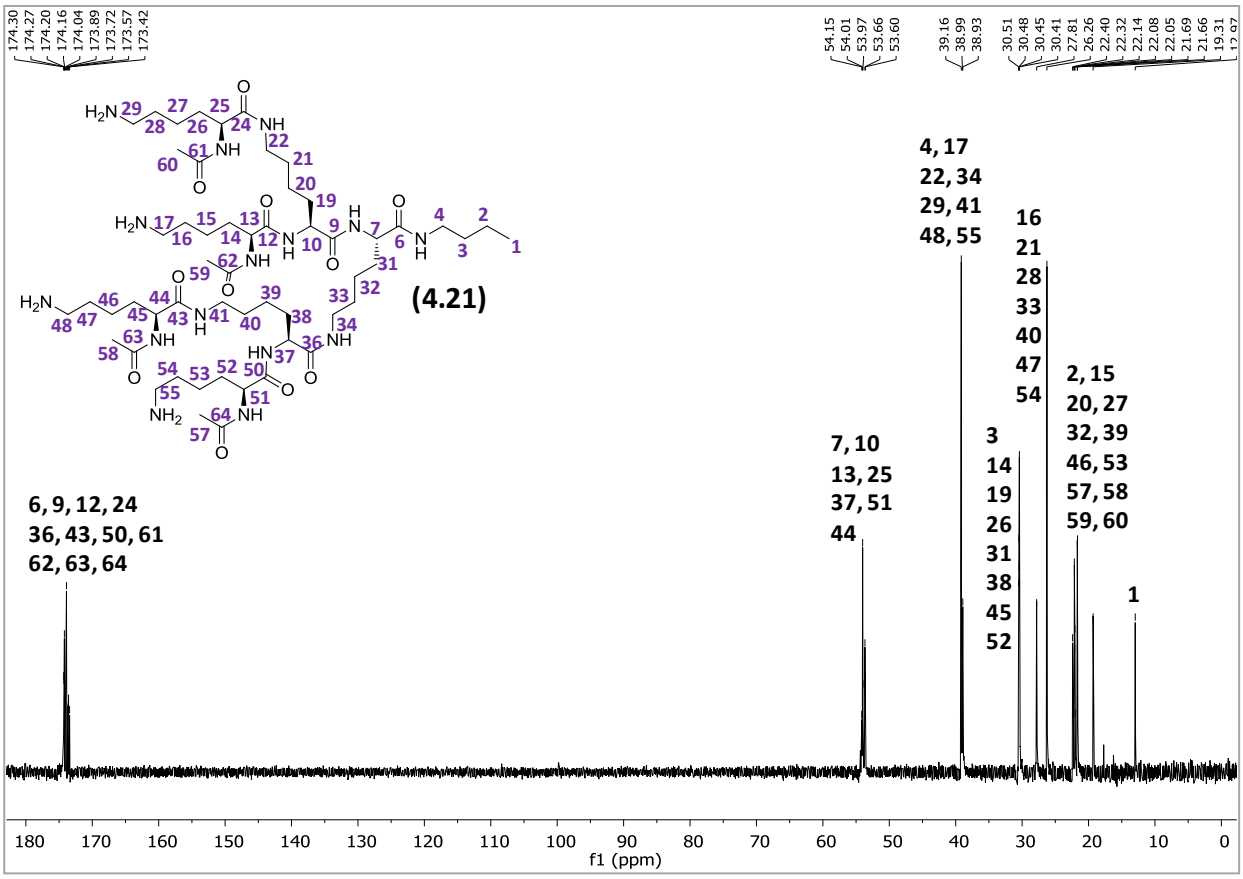
(4.21)
6, 9, 12, 24
36, 43, 50, 61
62, 63, 64
7, 10
13, 25
37, 51
44
4, 17
22, 34
29, 41
48, 55
3
14
19
26
31
38
45
52
16
21
28
33
40
47
54
2, 15
20, 27
32, 39
46, 53
57, 58
59, 60
1
f1 (ppm)

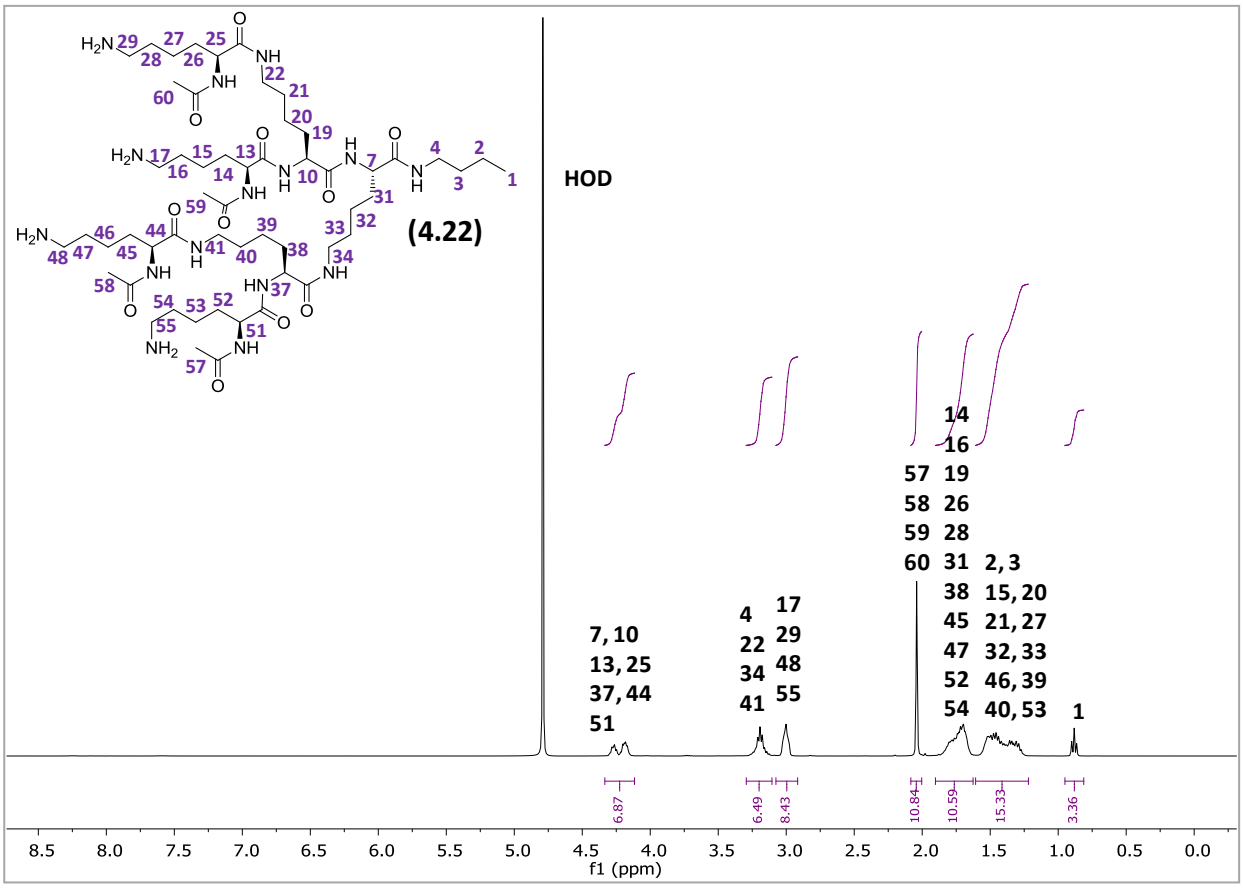
(4.22)
HOD
7, 10
13, 25
37, 44
51
4
22
34
41
17
29
48
55
57
58
59
60
14
16
19
26
28
31
38
45
47
52
54
2, 3
15, 20
21, 27
32, 33
46, 39
40, 53
1
6.87
6.49
8.43
10.84
10.59
15.33
3.36
f1 (ppm)

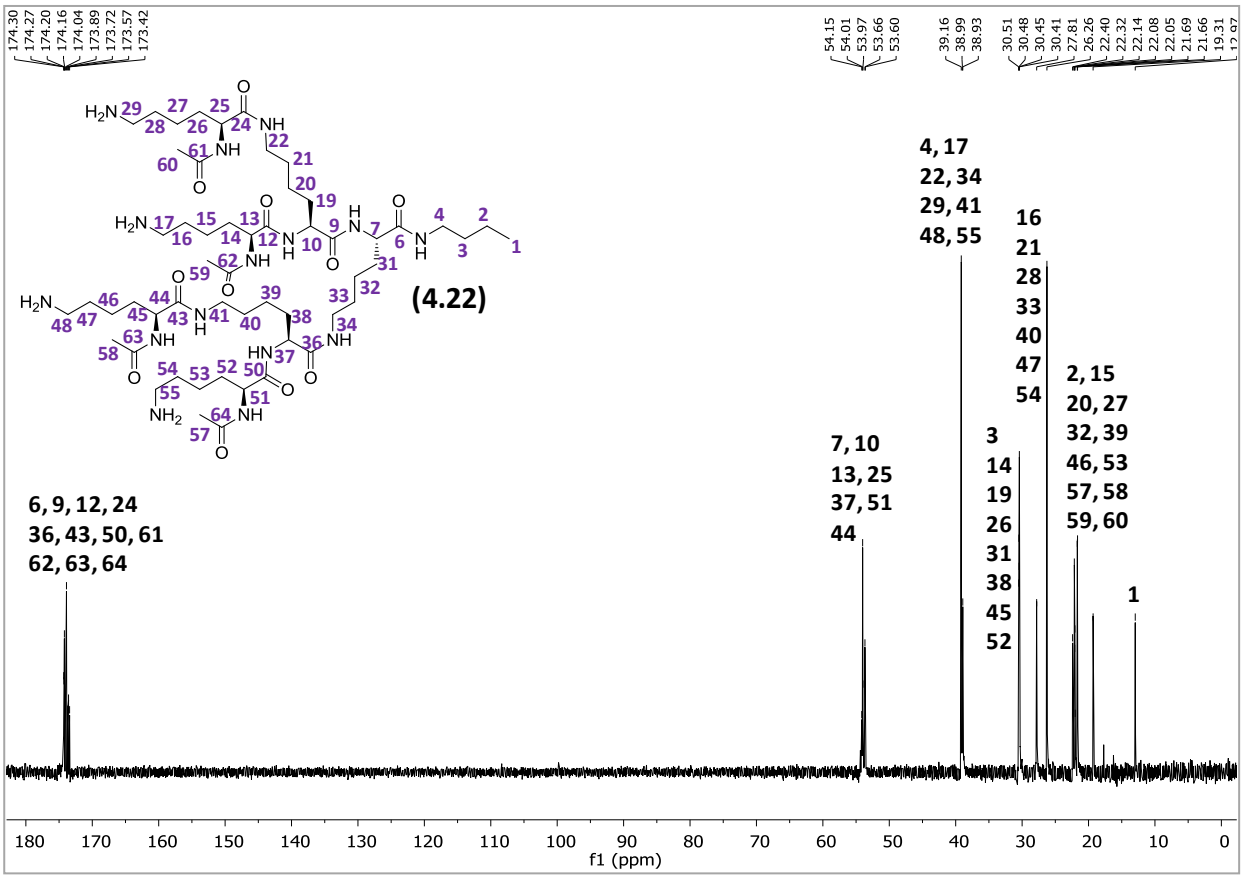
(4.22)
6, 9, 12, 24
36, 43, 50, 61
62, 63, 64
7, 10
13, 25
37, 51
44
4, 17
22, 34
29, 41
48, 55
3
14
19
26
31
38
45
52
16
21
28
33
40
47
54
2, 15
20, 27
32, 39
46, 53
57, 58
59, 60
1
f1 (ppm)

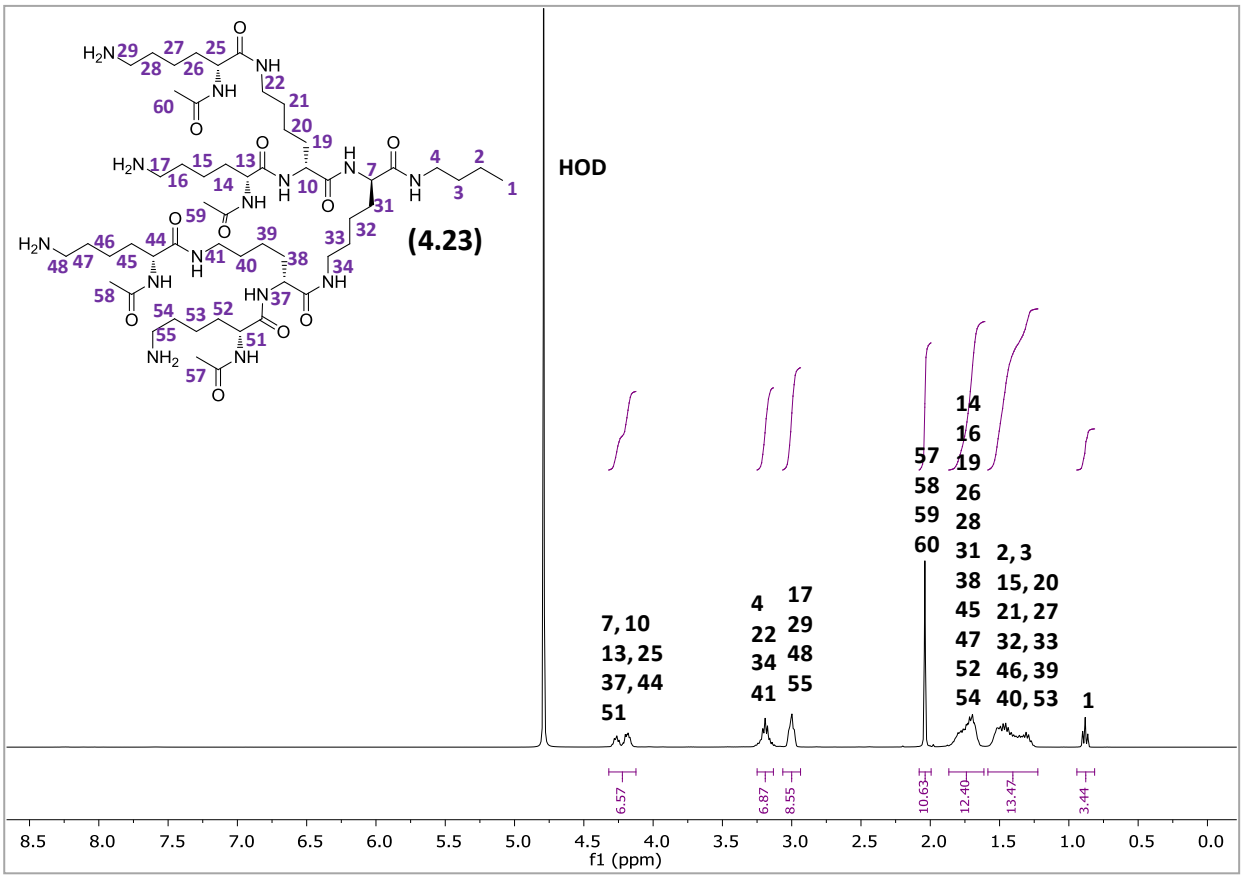
(4.23)
HOD
7, 10
13, 25
37, 44
51
4
22
34
41
17
29
48
55
57
58
59
60
14
16
19
26
28
31
38
45
47
52
54
2, 3
15, 20
21, 27
32, 33
46, 39
40, 53
1
6.57
6.87
8.55
10.63
12.40
13.47
3.44
f1 (ppm)

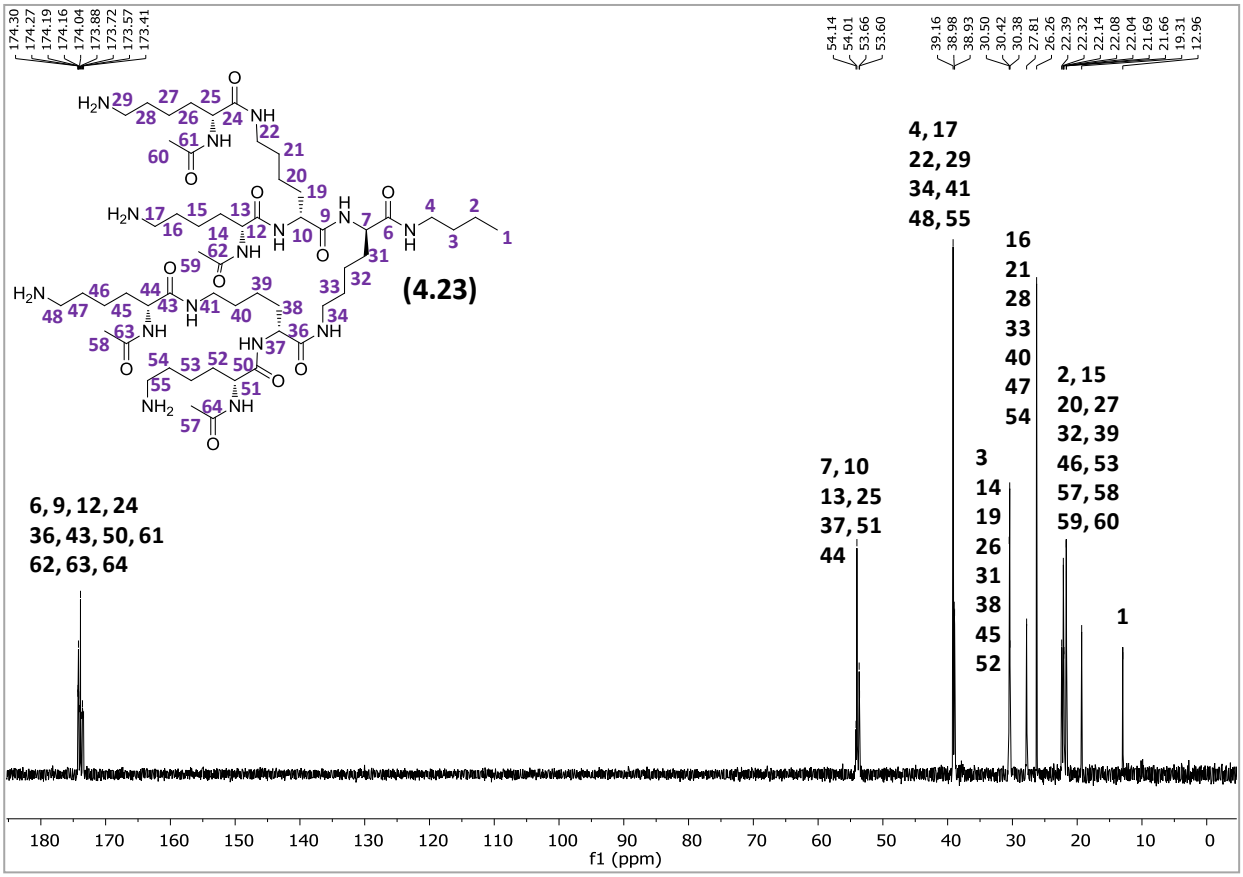
(4.23)
6, 9, 12, 24
36, 43, 50, 61
62, 63, 64
7, 10
13, 25
37, 51
44
4, 17
22, 29
34, 41
48, 55
3
14
19
26
31
38
45
52
16
21
28
33
40
47
54
2, 15
20, 27
32, 39
46, 53
57, 58
59, 60
1
f1 (ppm)

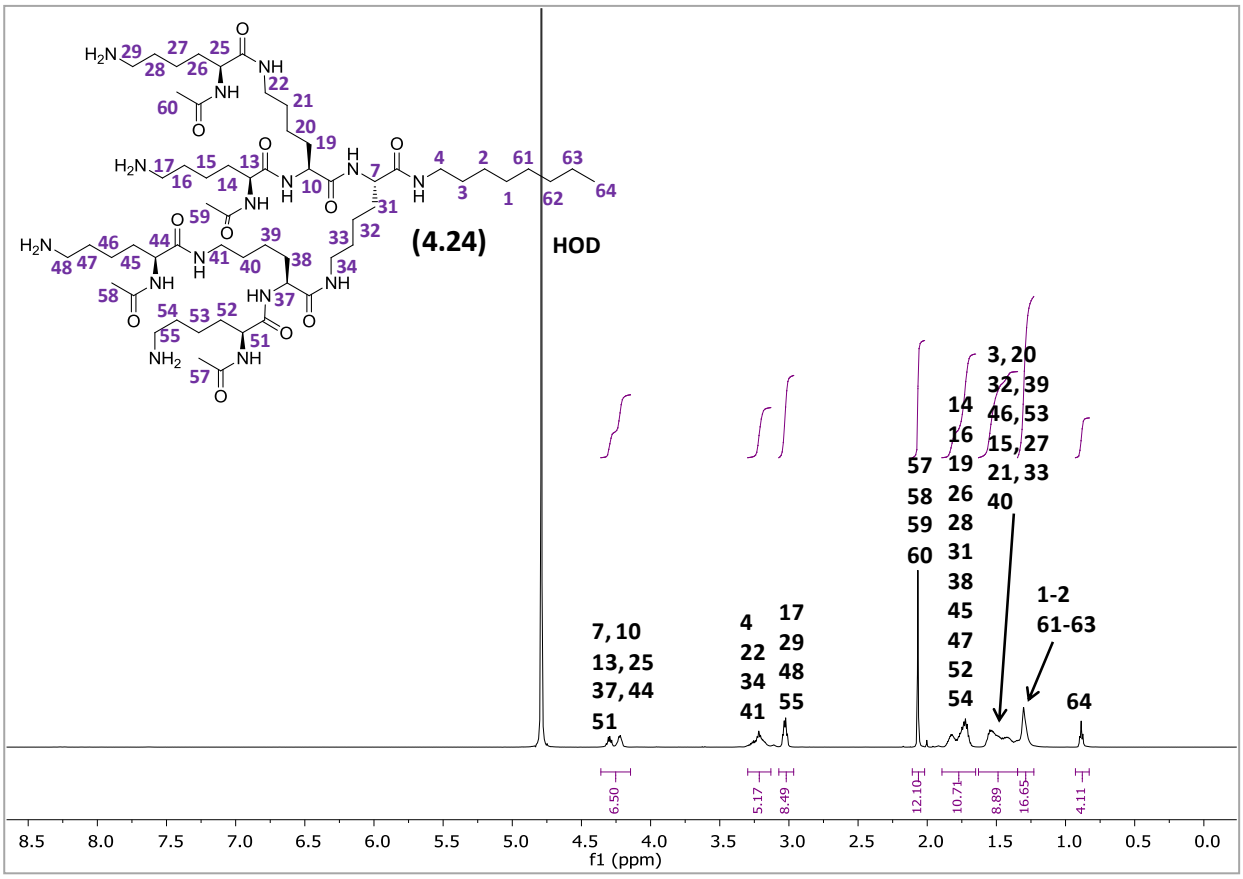
(4.24)
HOD
7, 10
13, 25
37, 44
51
4
22
34
41
17
29
48
55
57
58
59
60
14
16
19
26
28
31
38
45
47
52
54
3, 20
32, 39
46, 53
15, 27
21, 33
40
1-2
61-63
64
6.50
5.17
8.49
12.10
10.71
8.89
16.65
4.11
f1 (ppm)

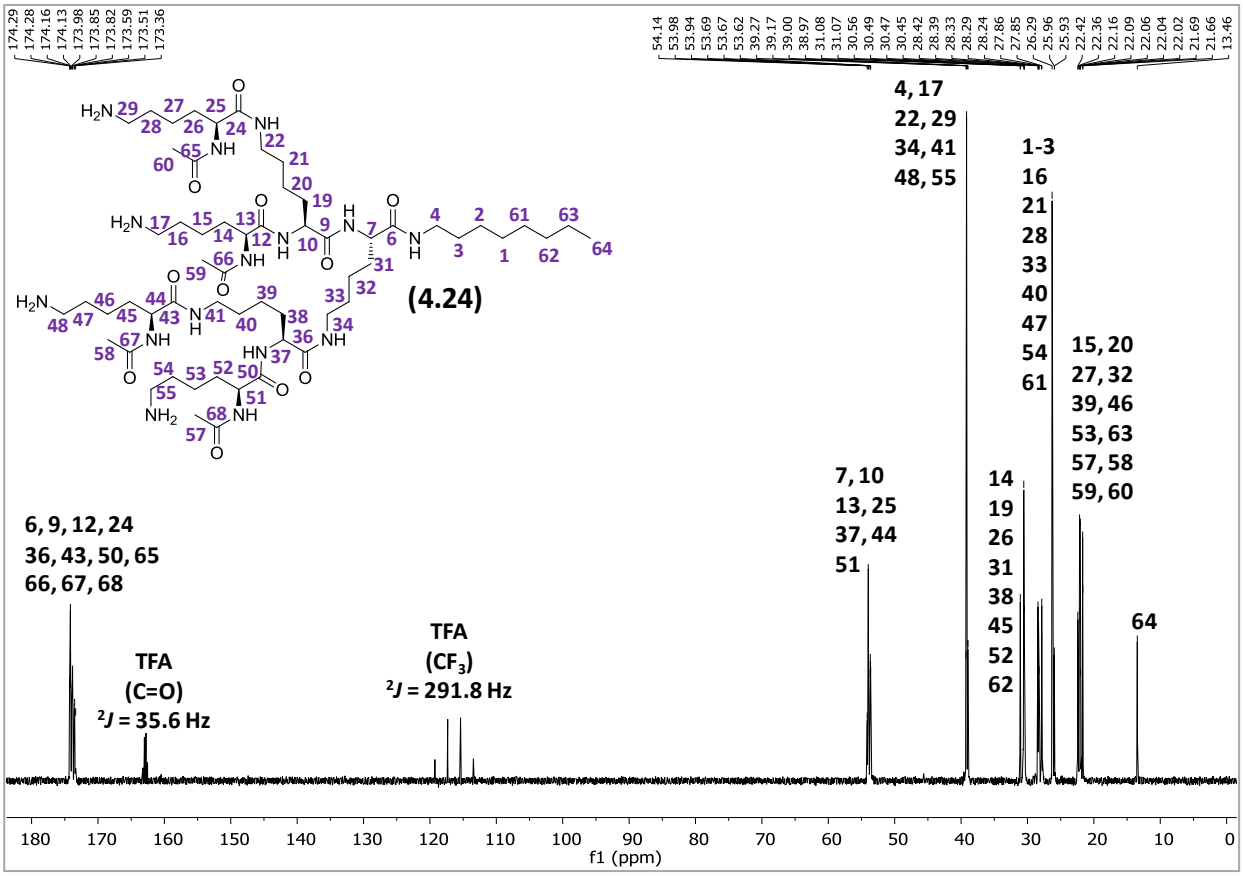
(4.24)
6, 9, 12, 24
36, 43, 50, 65
66, 67, 68
TFA
(C=O)
²J = 35.6 Hz
TFA
(CF3)
²J = 291.8 Hz
7, 10
13, 25
37, 44
51
4, 17
22, 29
34, 41
48, 55
14
19
26
31
38
45
52
62
1-3
16
21
28
33
40
47
54
61
15, 20
27, 32
39, 46
53, 63
57, 58
59, 60
64
f1 (ppm)

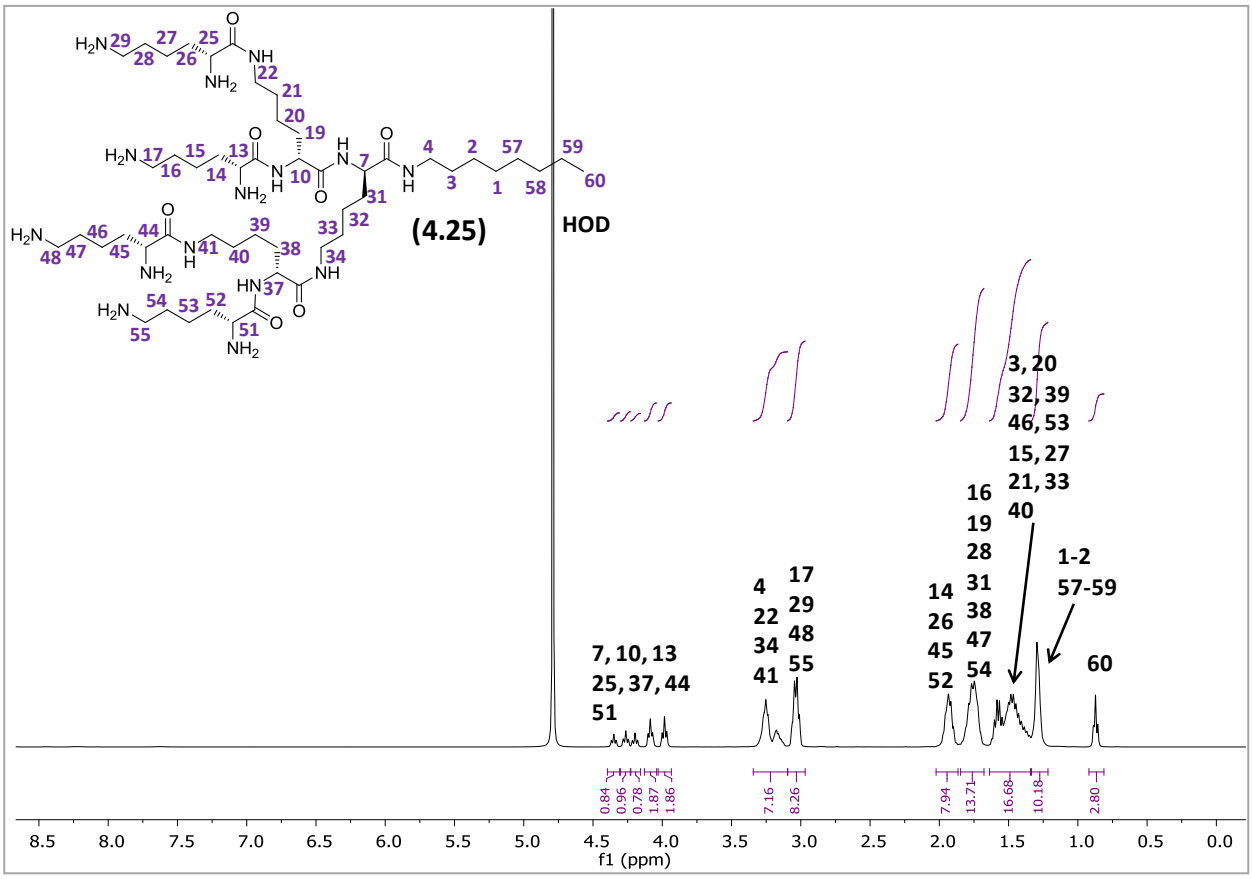
(4.25)
HOD
7, 10, 13
25, 37, 44
51
4
22
34
41
17
29
48
55
14
26
45
52
16
19
28
31
38
47
54
3, 20
32, 39
46, 53
15, 27
21, 33
40
1-2
57-59
60
0.84
0.96
0.78
1.87
1.86
7.16
8.26
7.94
13.71
16.68
10.18
2.80
f1 (ppm)

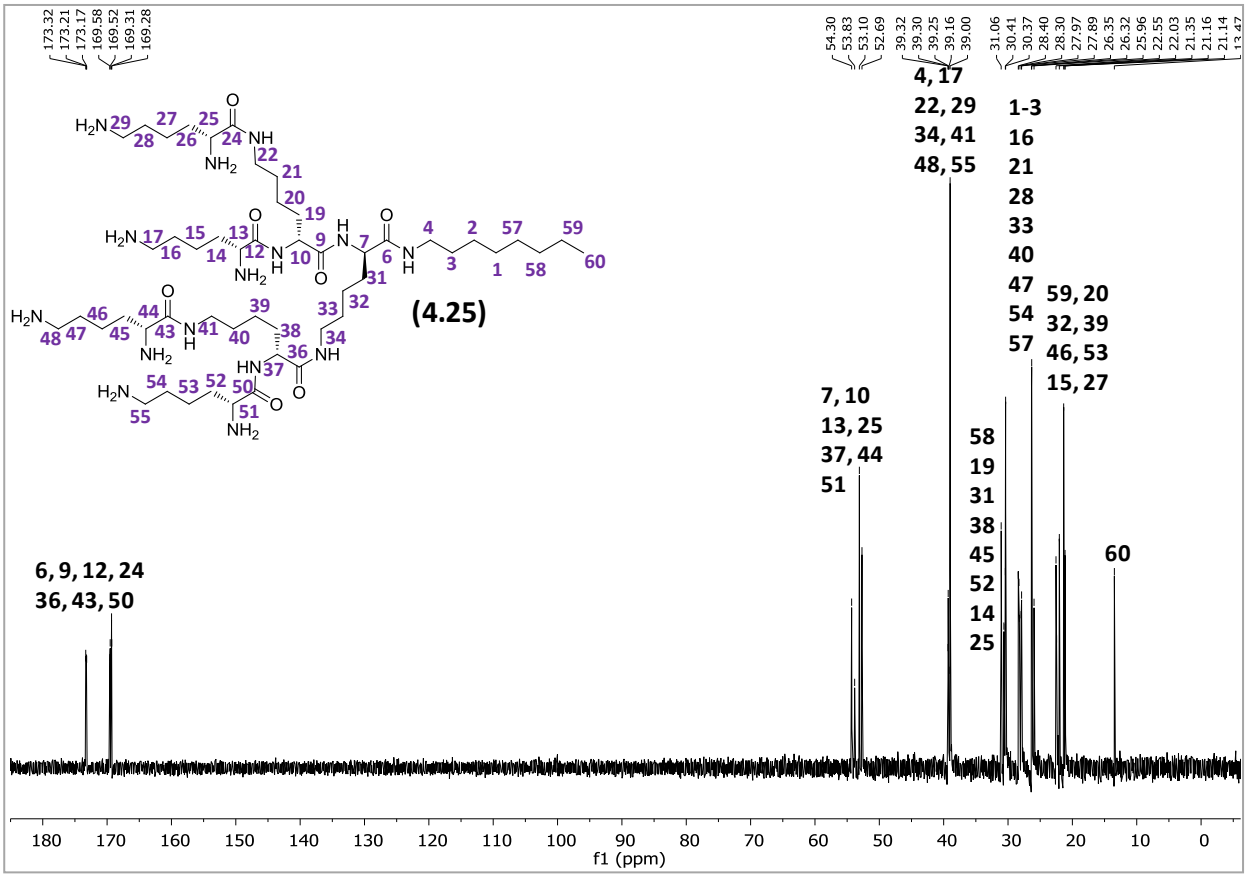
(4.25)
6, 9, 12, 24
36, 43, 50
7, 10
13, 25
37, 44
51
4, 17
22, 29
34, 41
48, 55
58
19
31
38
45
52
14
25
1-3
16
21
28
33
40
47
54
57
59, 20
32, 39
46, 53
15, 27
60
f1 (ppm)

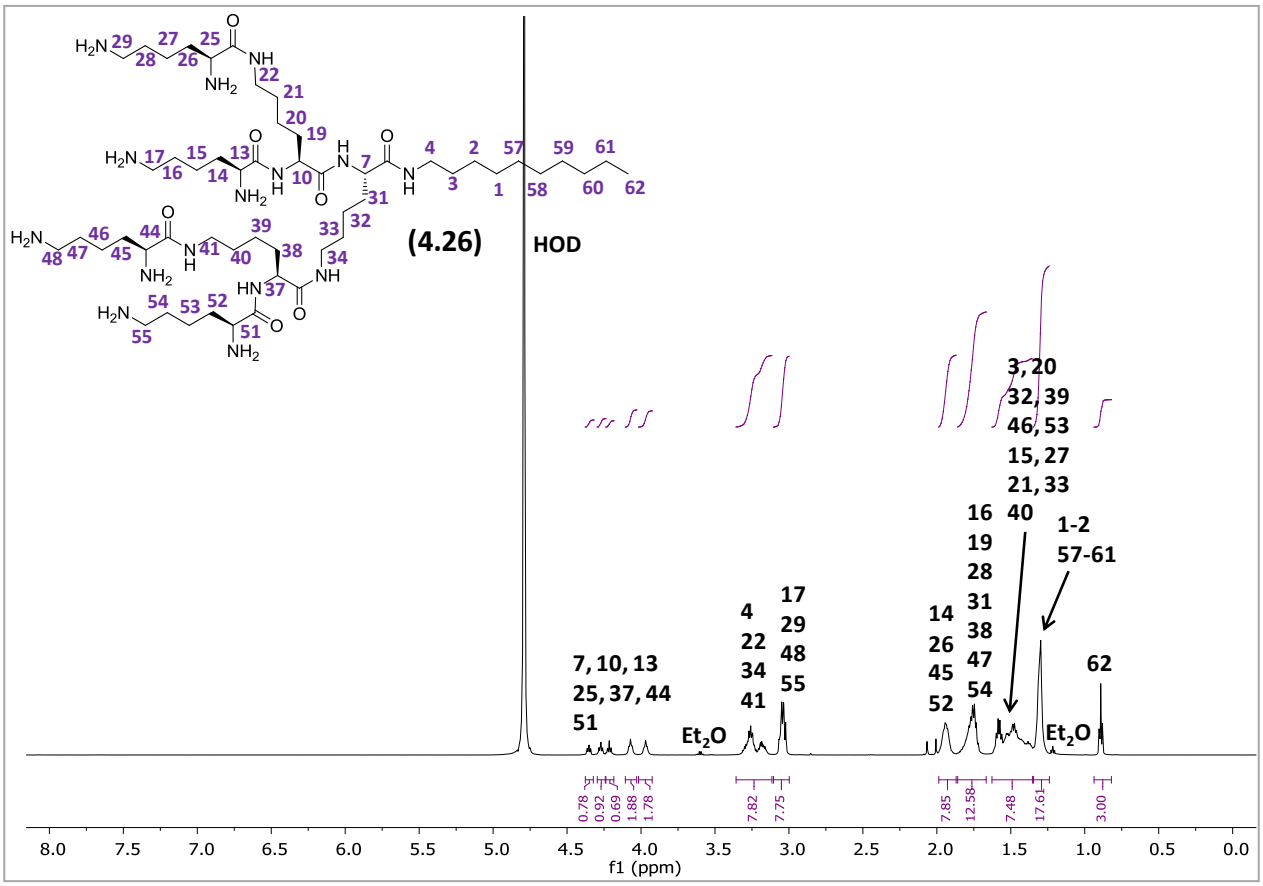
(4.26)
HOD
Et2O
Et2O
7, 10, 13
25, 37, 44
51
4
22
34
41
17
29
48
55
14
26
45
52
16
19
28
31
38
47
54
3, 20
32, 39
46, 53
15, 27
21, 33
40
1-2
57-61
62
f1 (ppm)

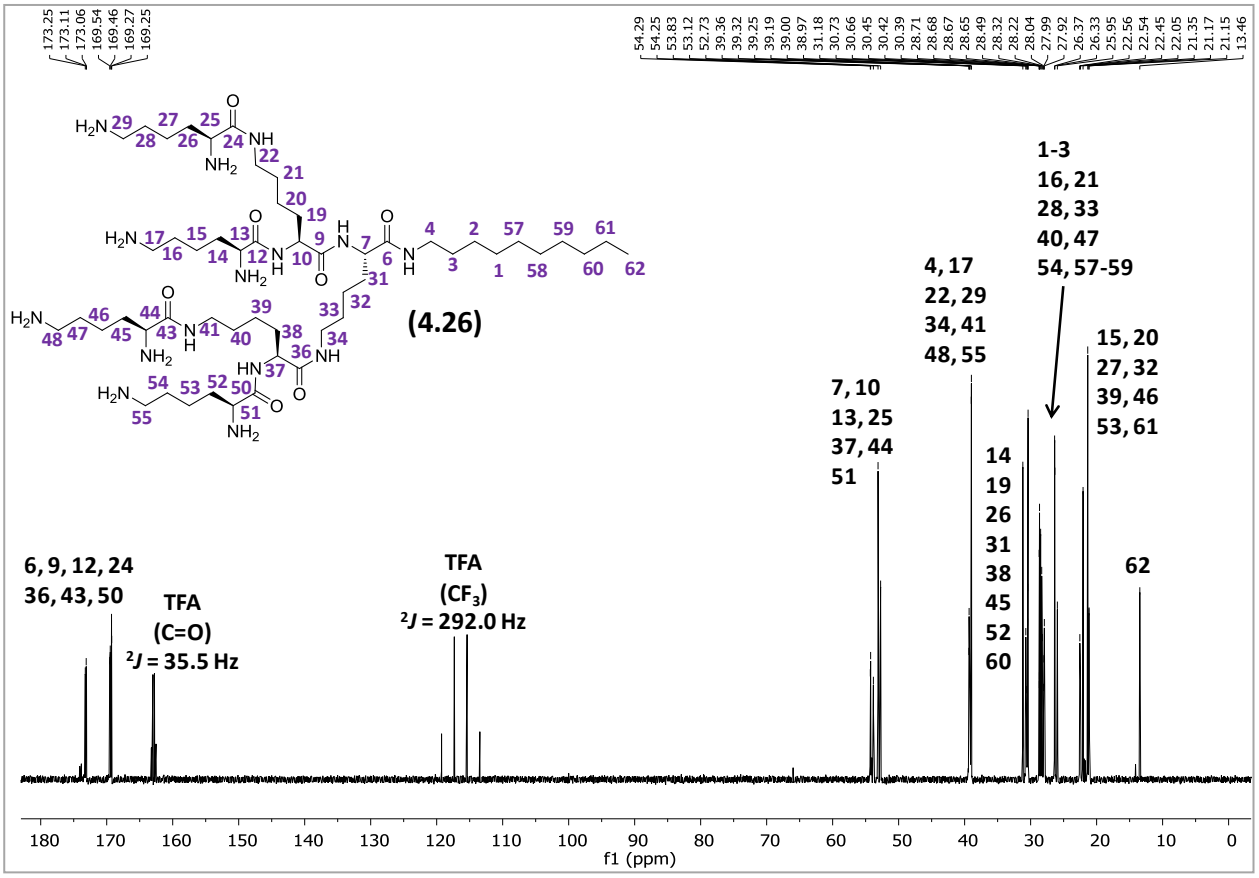
(4.26)
6, 9, 12, 24
36, 43, 50
TFA
(C=O)
2J = 35.5 Hz
TFA
(CF3)
2J = 292.0 Hz
7, 10
13, 25
37, 44
51
4, 17
22, 29
34, 41
48, 55
14
19
26
31
38
45
52
60
1-3
16, 21
28, 33
40, 47
54, 57-59
15, 20
27, 32
39, 46
53, 61
62
f1 (ppm)

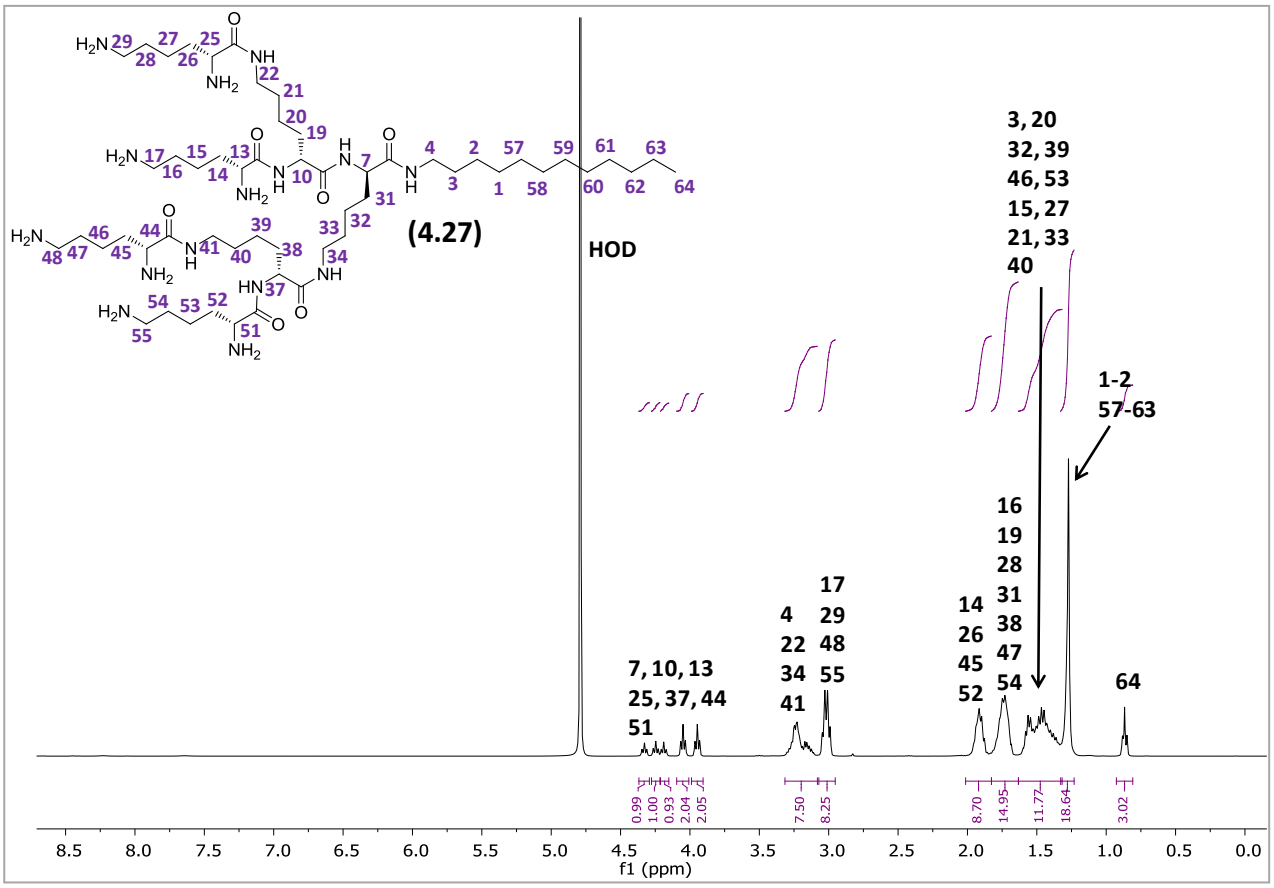
(4.27)
HOD
3, 20
32, 39
46, 53
15, 27
21, 33
40
1-2
57-63
16
19
28
31
38
47
54
14
26
45
52
17
29
48
55
4
22
34
41
7, 10, 13
25, 37, 44
51
64
f1 (ppm)

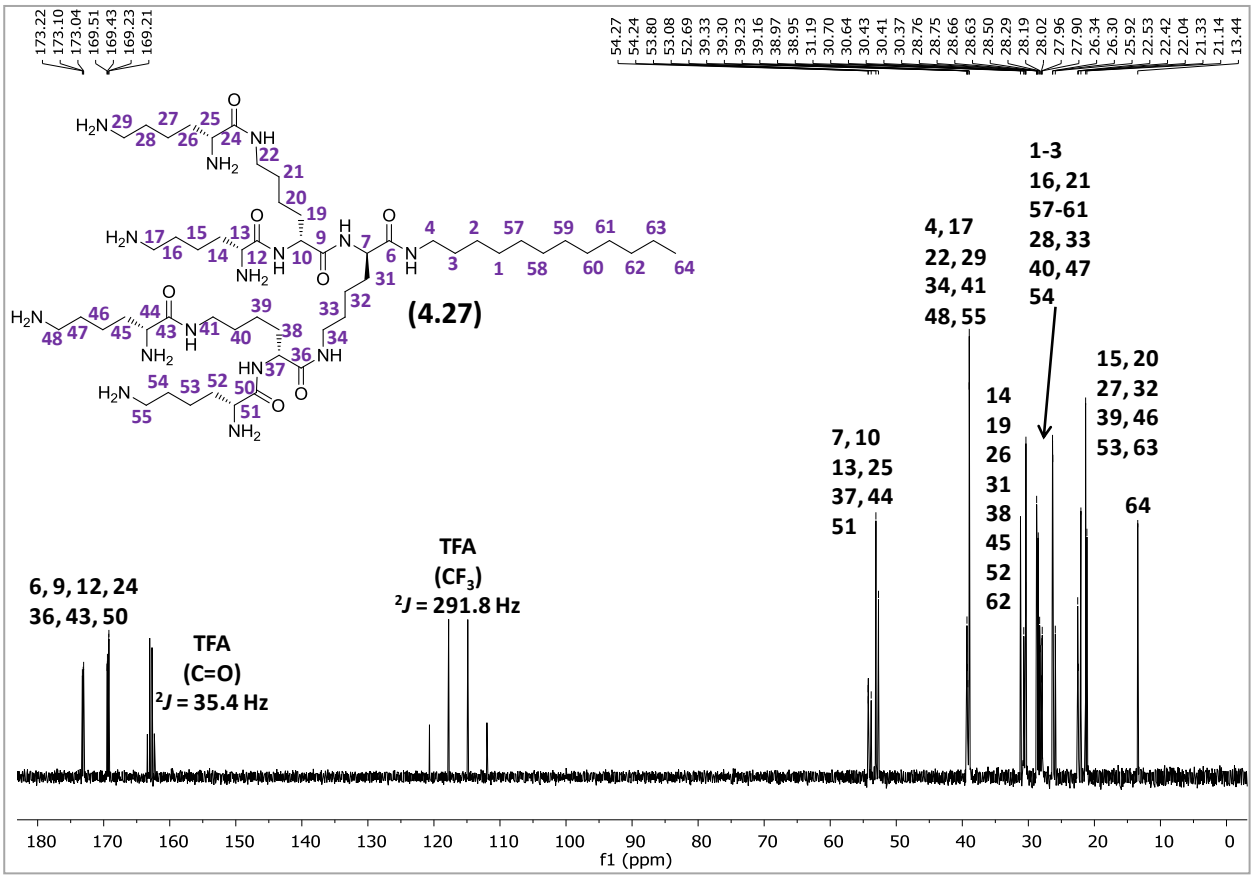
(4.27)
1-3
16, 21
57-61
28, 33
40, 47
54
4, 17
22, 29
34, 41
48, 55
15, 20
27, 32
39, 46
53, 63
14
19
26
31
38
45
52
62
7, 10
13, 25
37, 44
51
64
TFA
(CF3)
2J = 291.8 Hz
6, 9, 12, 24
36, 43, 50
TFA
(C=O)
2J = 35.4 Hz
f1 (ppm)

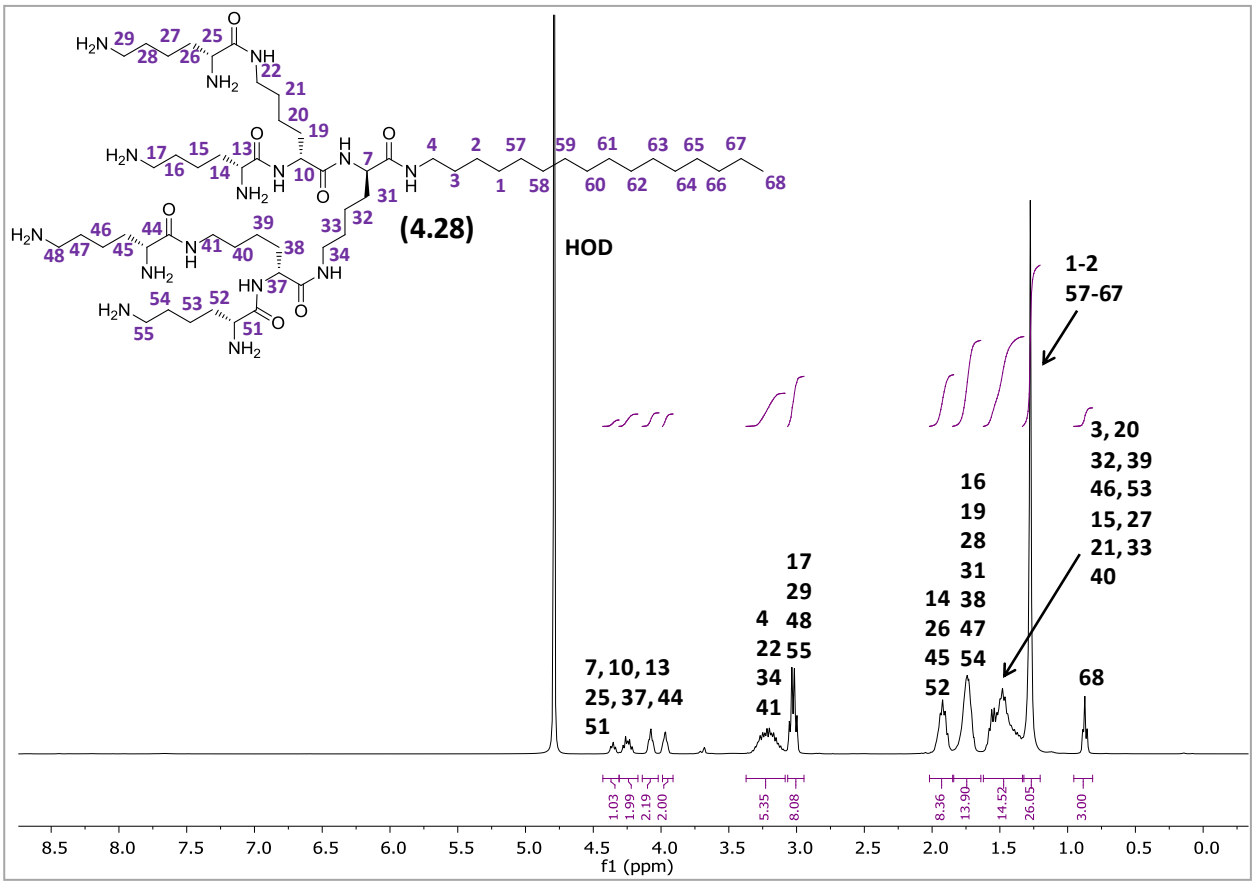
(4.28)
HOD
1-2
57-67
3, 20
32, 39
46, 53
15, 27
21, 33
40
16
19
28
31
14 38
26 47
45 54
52
17
29
4 48
22 55
34
41
7, 10, 13
25, 37, 44
51
68
1.03
1.99
2.19
2.00
5.35
8.08
8.36
13.90
14.52
26.05
3.00
f1 (ppm)

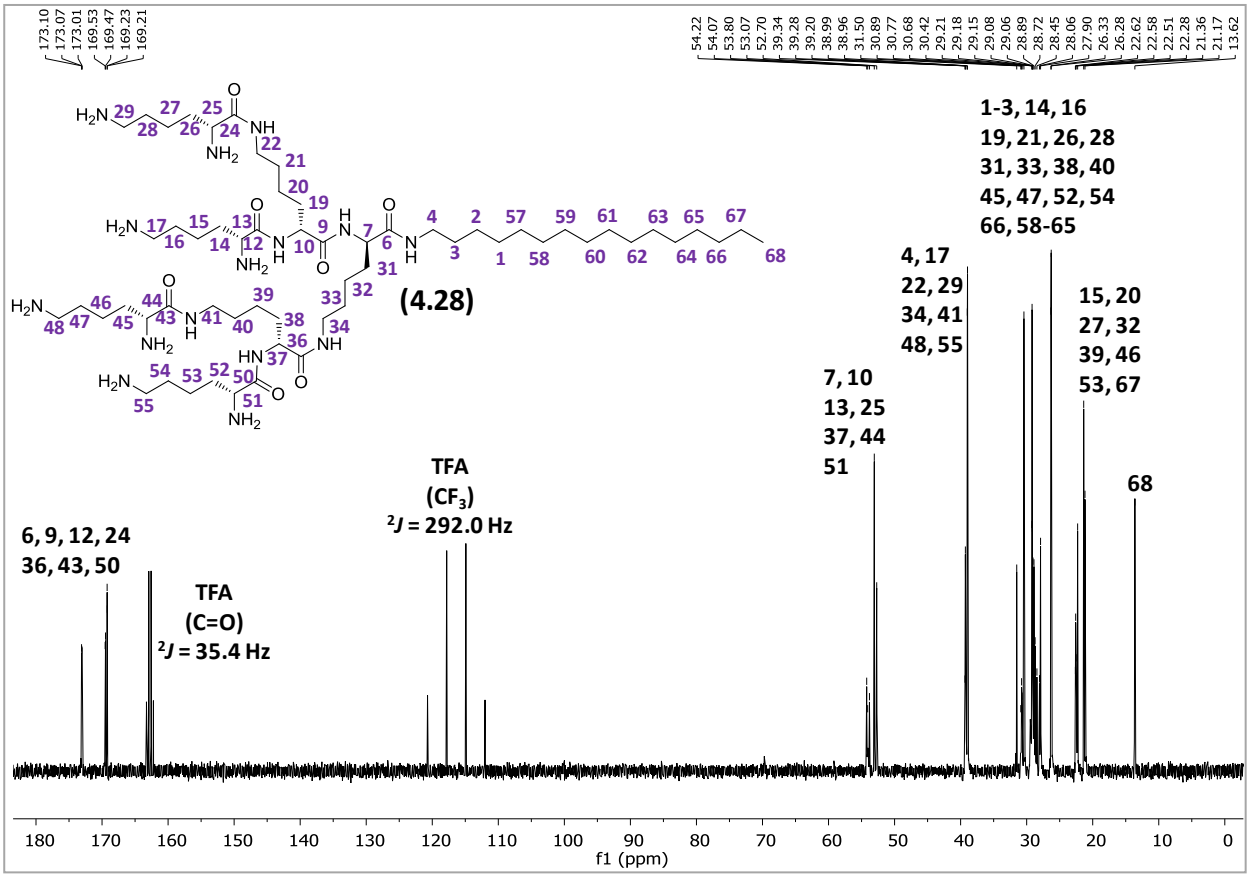
(4.28)
1-3, 14, 16
19, 21, 26, 28
31, 33, 38, 40
45, 47, 52, 54
66, 58-65
4, 17
22, 29
34, 41
48, 55
15, 20
27, 32
39, 46
53, 67
7, 10
13, 25
37, 44
51
68
TFA
(CF3)
2J = 292.0 Hz
6, 9, 12, 24
36, 43, 50
TFA
(C=O)
2J = 35.4 Hz
f1 (ppm)

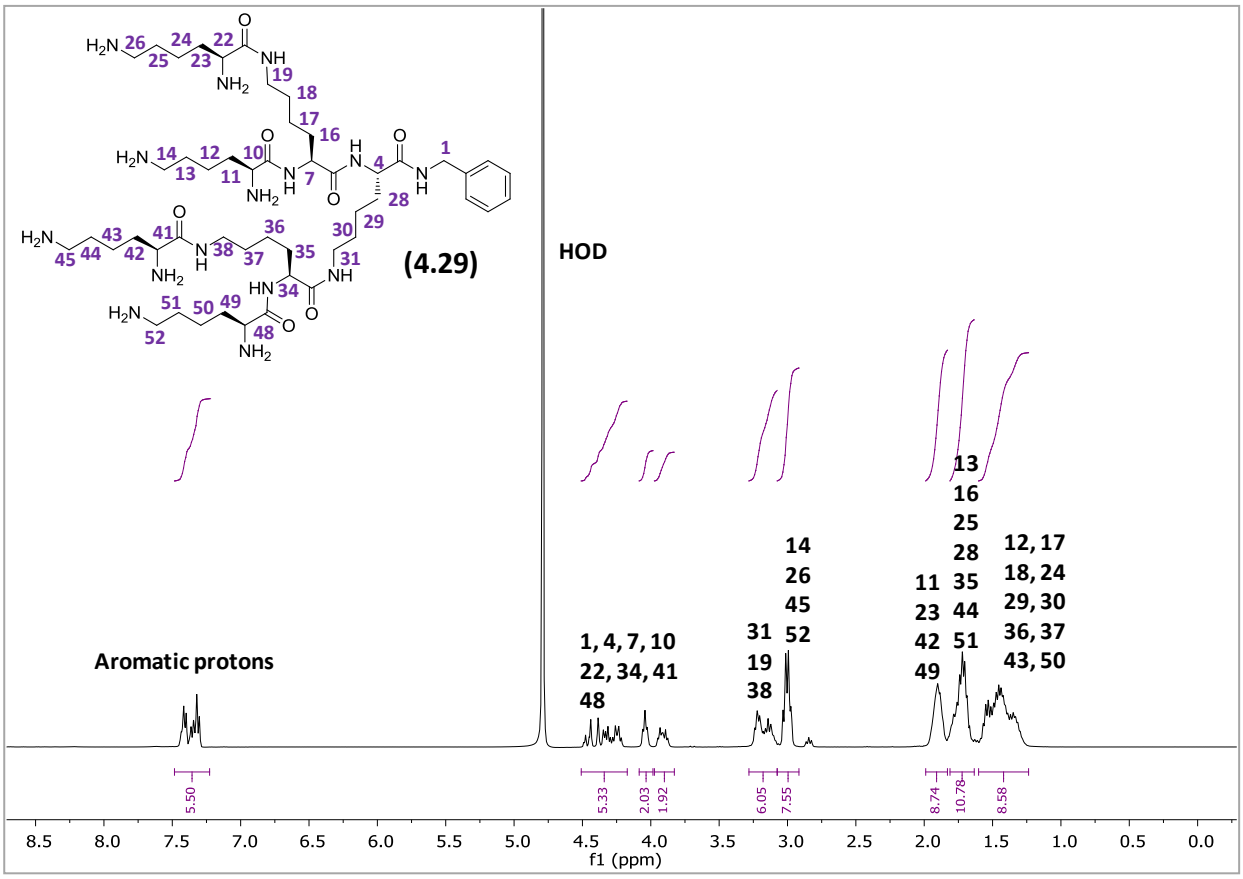
(4.29)
HOD
Aromatic protons
1, 4, 7, 10
22, 34, 41
48
31
19
38
14
26
45
52
11
23
42
49
13
16
25
28
35
44
51
12, 17
18, 24
29, 30
36, 37
43, 50
5.50
5.33
2.03
1.92
6.05
7.55
8.74
10.78
8.58
f1 (ppm)

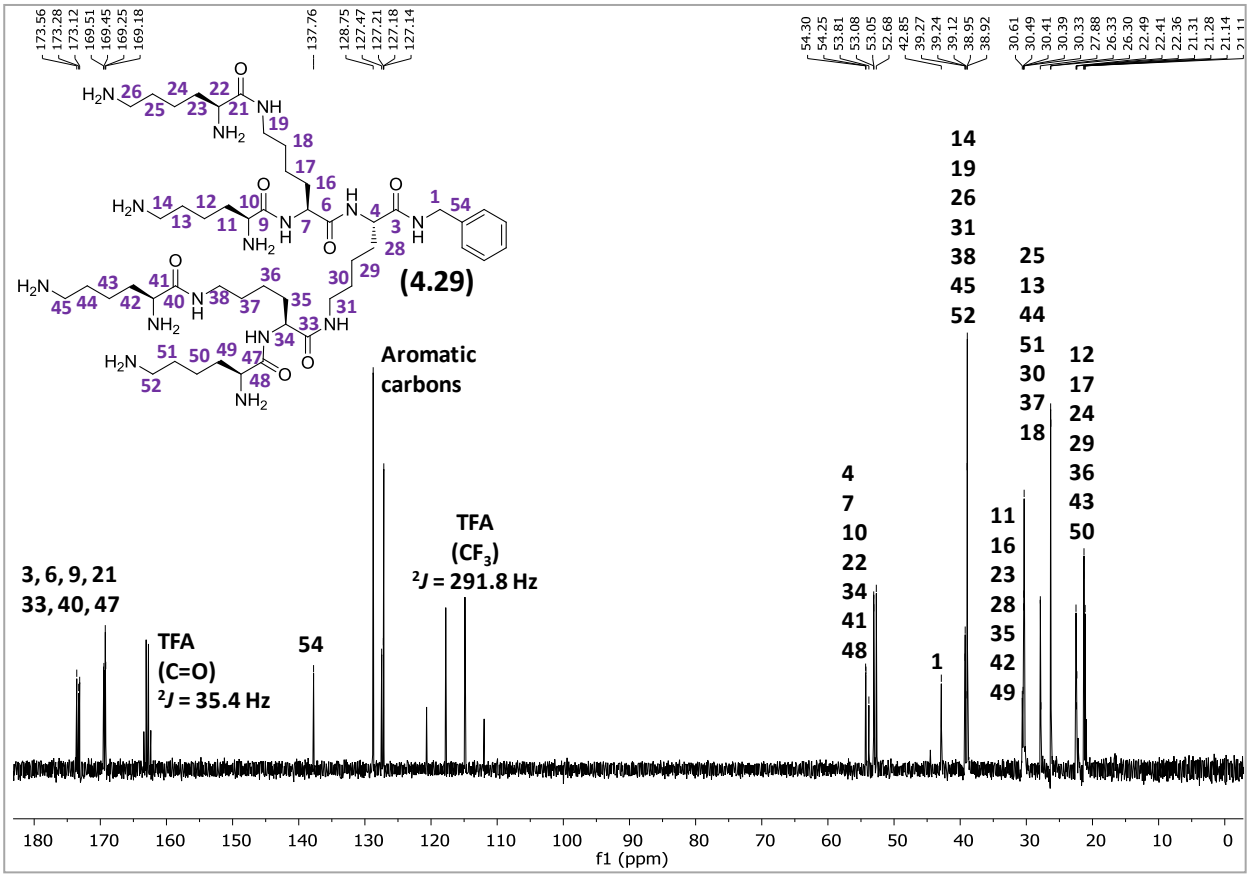
(4.29)
Aromatic carbons
TFA
(C=O)
²J = 35.4 Hz
TFA
(CF3)
²J = 291.8 Hz
3, 6, 9, 21
33, 40, 47
54
4
7
10
22
34
41
48
1
14
19
26
31
38
45
52
11
16
23
28
35
42
49
25
13
44
51
30
37
18
12
17
24
29
36
43
50
f1 (ppm)

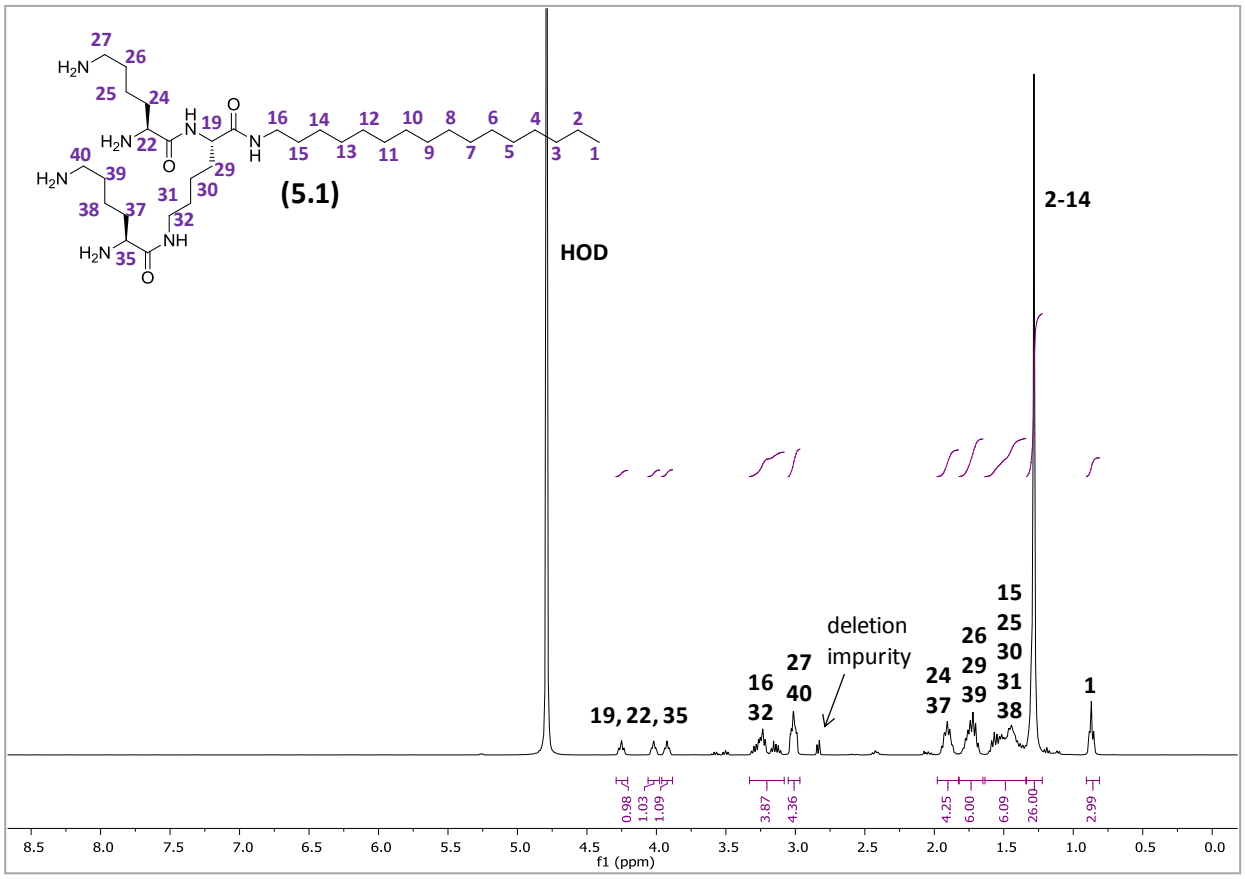
(5.1)
HOD
2-14
19, 22, 35
16
32
27
40
deletion
impurity
24
37
26
29
39
15
25
30
31
38
1
0.98
1.03
1.09
3.87
4.36
4.25
6.00
6.09
26.00
2.99
f1 (ppm)

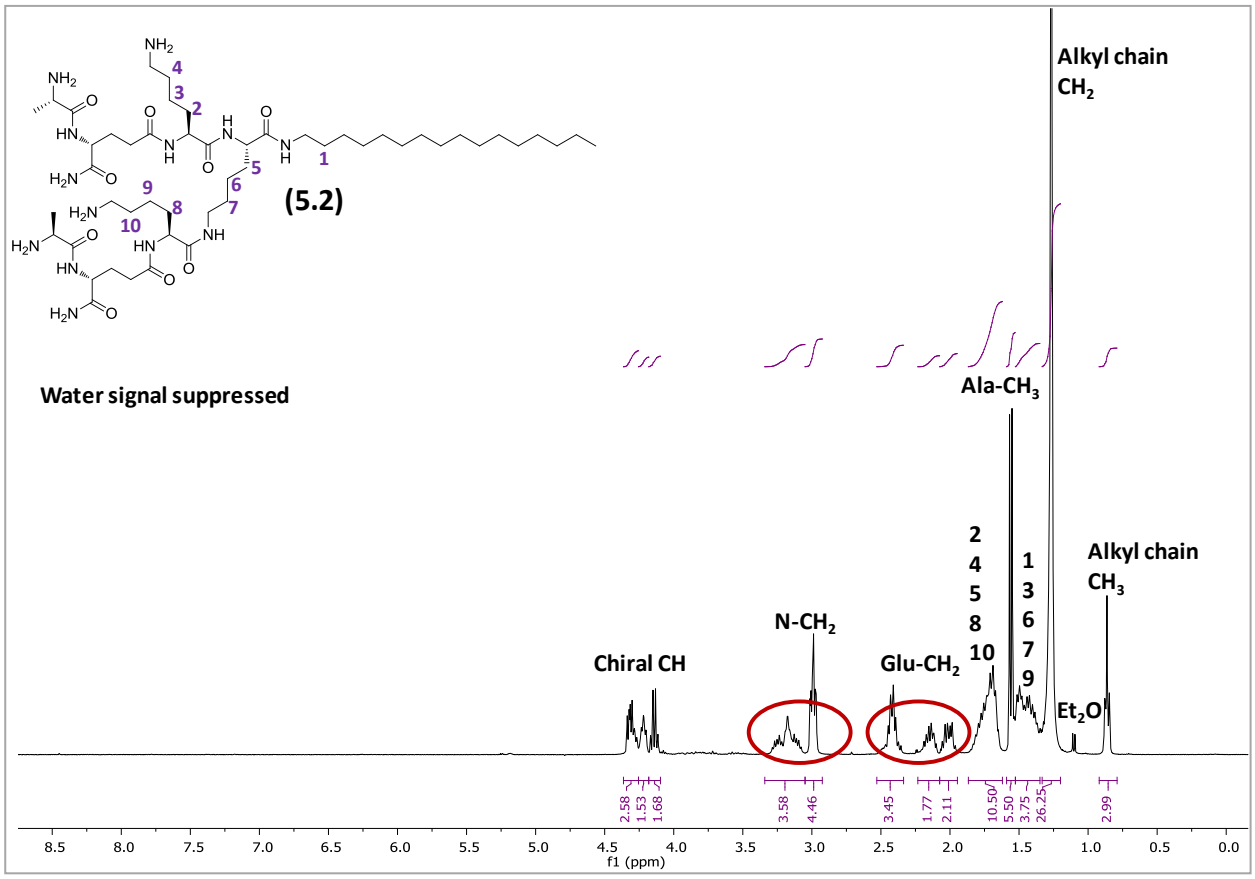
(5.2)
Water signal suppressed
Alkyl chain
CH2
Ala-CH3
Alkyl chain
CH3
N-CH2
Chiral CH
Glu-CH2
Et2O
f1 (ppm)

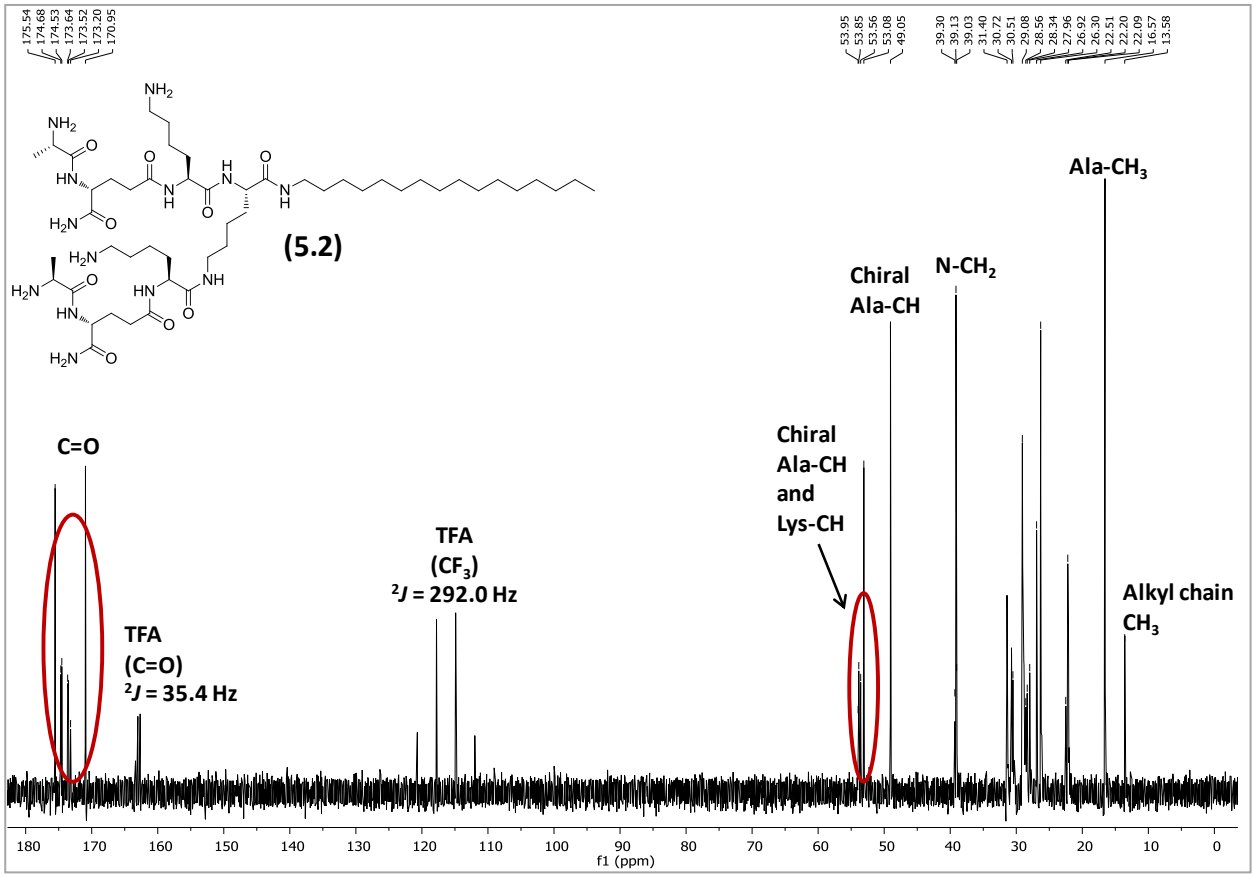
(5.2)
Ala-CH3
Chiral
Ala-CH
N-CH2
Chiral
Ala-CH
and
Lys-CH
C=O
TFA
(CF3)
2J = 292.0 Hz
TFA
(C=O)
2J = 35.4 Hz
Alkyl chain
CH3
f1 (ppm)

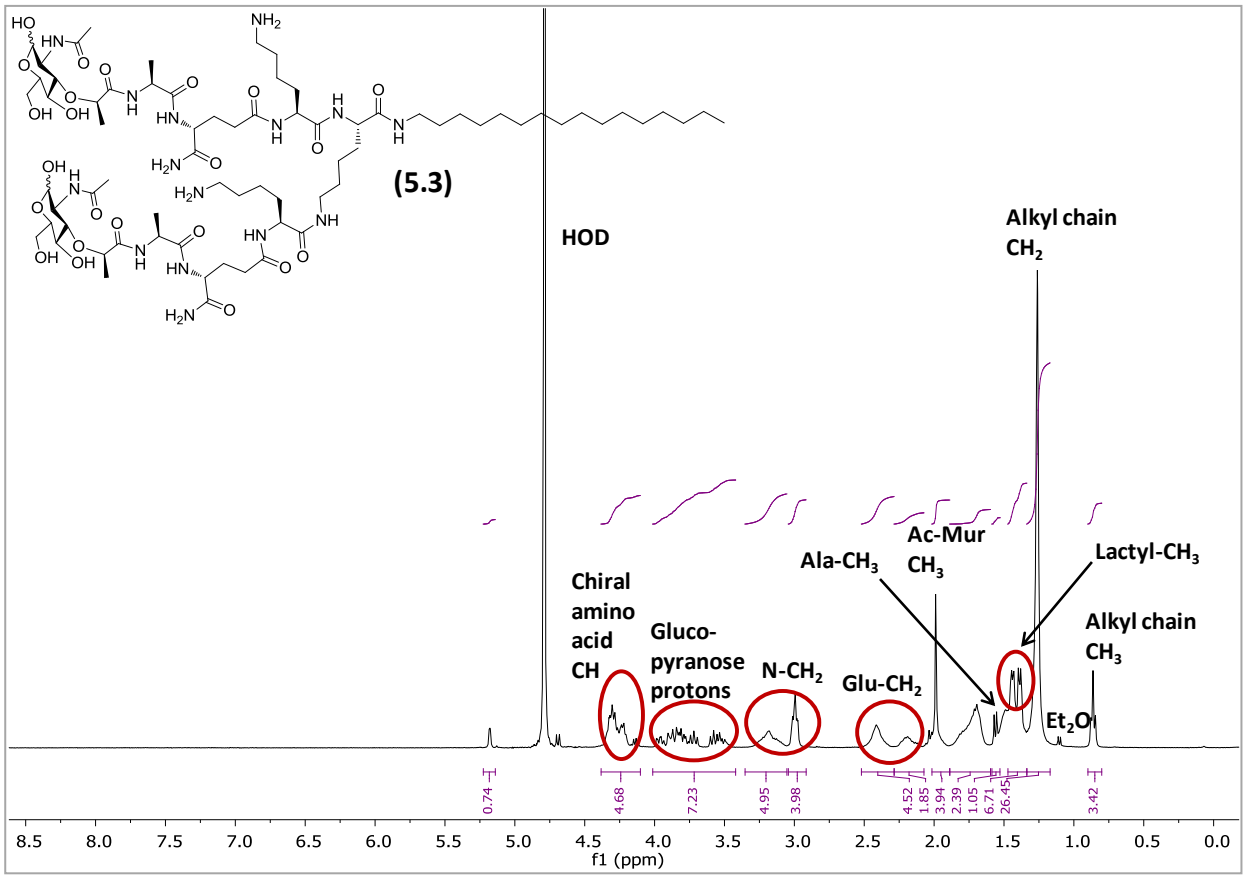
(5.3)
HOD
Alkyl chain
CH2
Ac-Mur
CH3
Ala-CH3
Lactyl-CH3
Chiral
amino
acid
CH
Gluco-
pyranose
protons
N-CH2
Glu-CH2
Alkyl chain
CH3
Et2O
0.74
4.68
7.23
4.95
3.98
4.52
1.85
3.94
2.39
1.05
6.71
26.45
3.42
8.5
8.0
7.5
7.0
6.5
6.0
5.5
5.0
4.5
4.0
3.5
3.0
2.5
2.0
1.5
1.0
0.5
0.0
f1 (ppm)

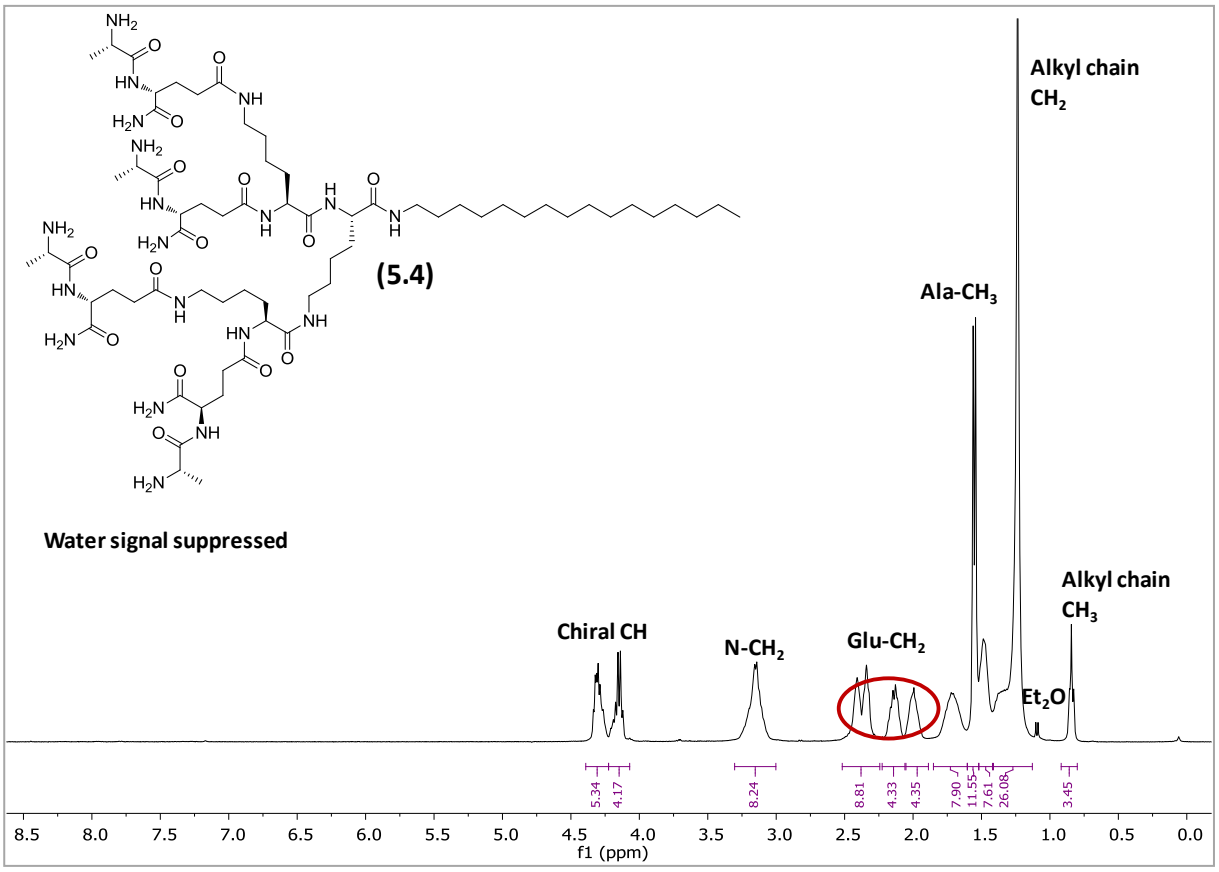
(5.4)
Alkyl chain
CH2
Ala-CH3
Water signal suppressed
Alkyl chain
CH3
Chiral CH
N-CH2
Glu-CH2
Et2O
5.34
4.17
8.24
8.81
4.33
4.35
7.90
11.55
7.61
26.08
3.45
f1 (ppm)

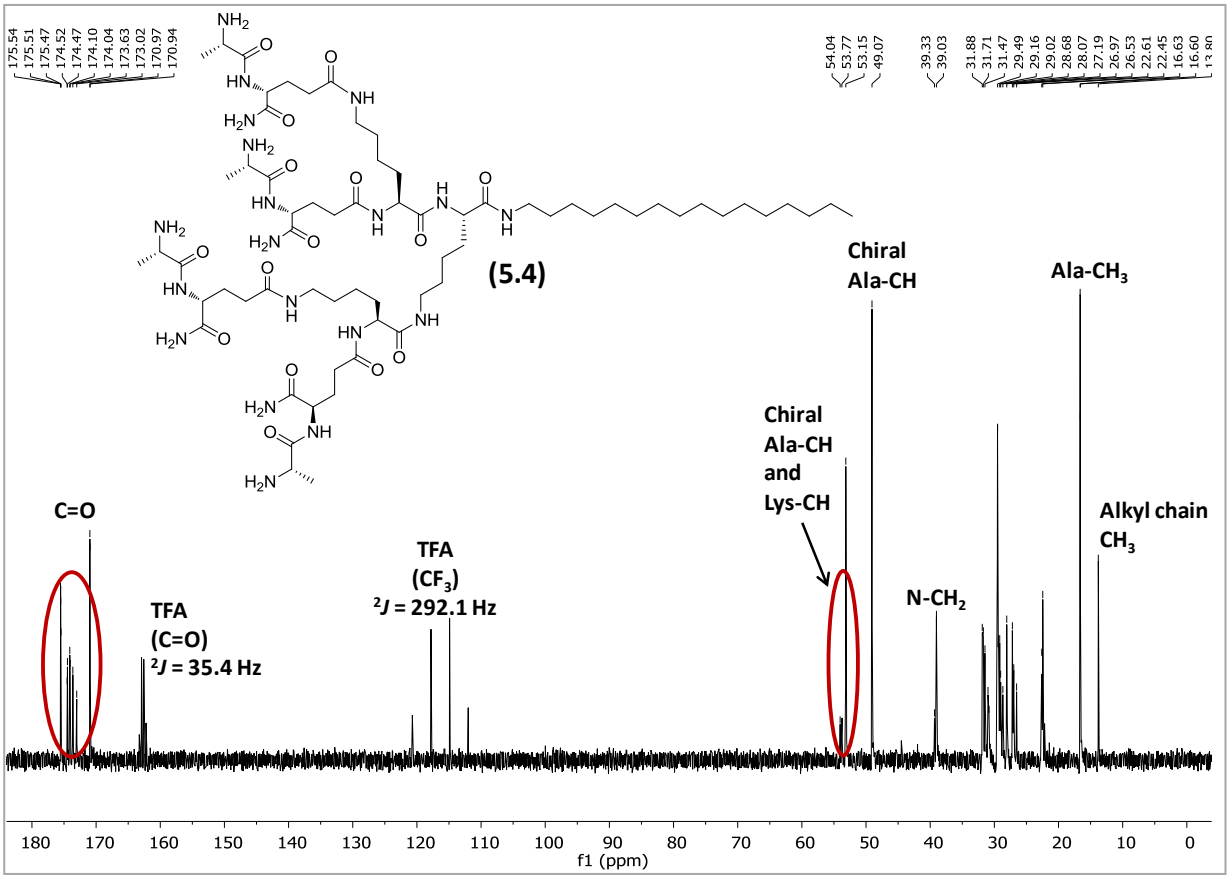
(5.4)
Chiral
Ala-CH
Ala-CH3
Chiral
Ala-CH
and
Lys-CH
C=O
TFA
(CF3)
2J = 292.1 Hz
TFA
(C=O)
2J = 35.4 Hz
N-CH2
Alkyl chain
CH3
f1 (ppm)

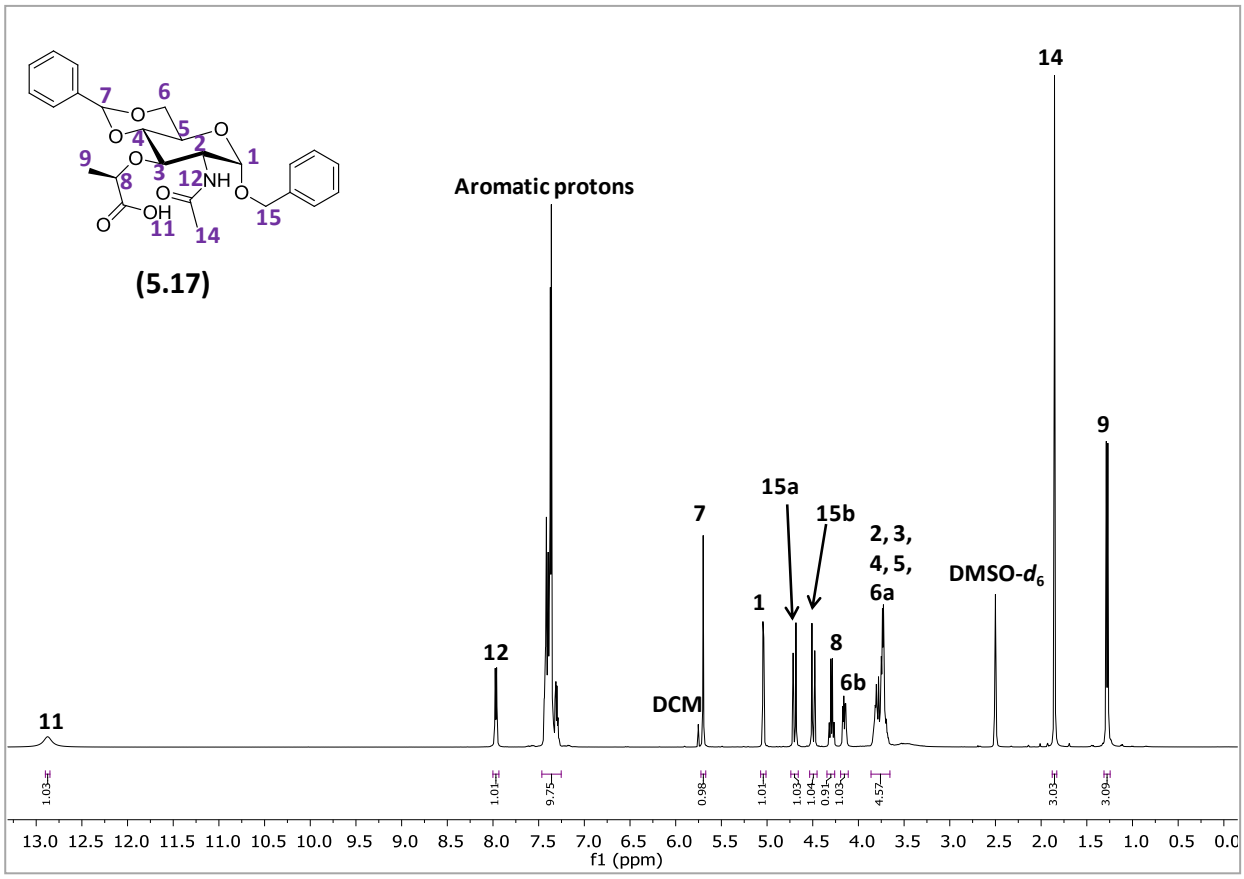
(5.17)
Aromatic protons
14
9
15a
7
15b
2, 3,
4, 5,
6a
DMSO-d_6
1
8
12
6b
DCM
11
f1 (ppm)

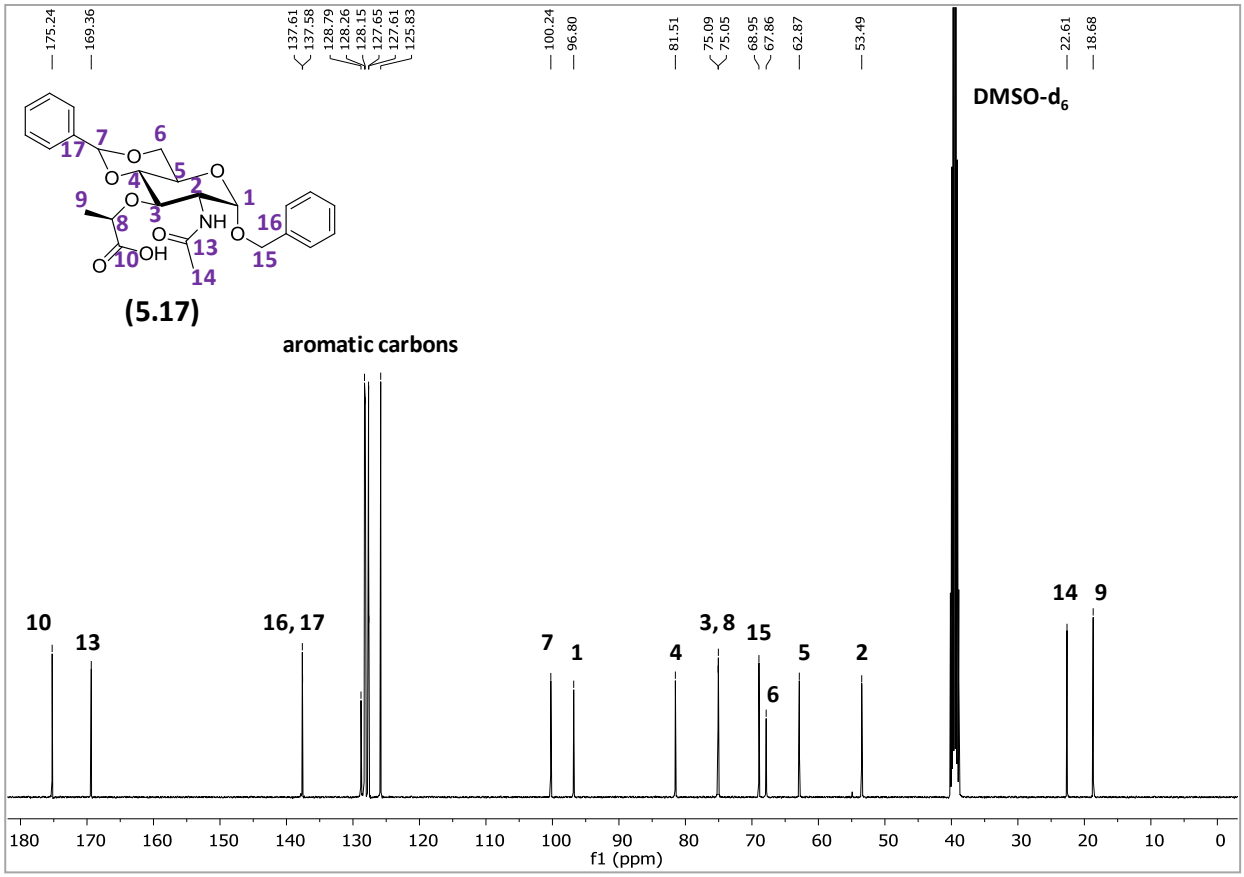
(5.17)
aromatic carbons
DMSO-d_6
10
13
16, 17
7
1
4
3, 8
15
6
5
2
14
9
f1 (ppm)

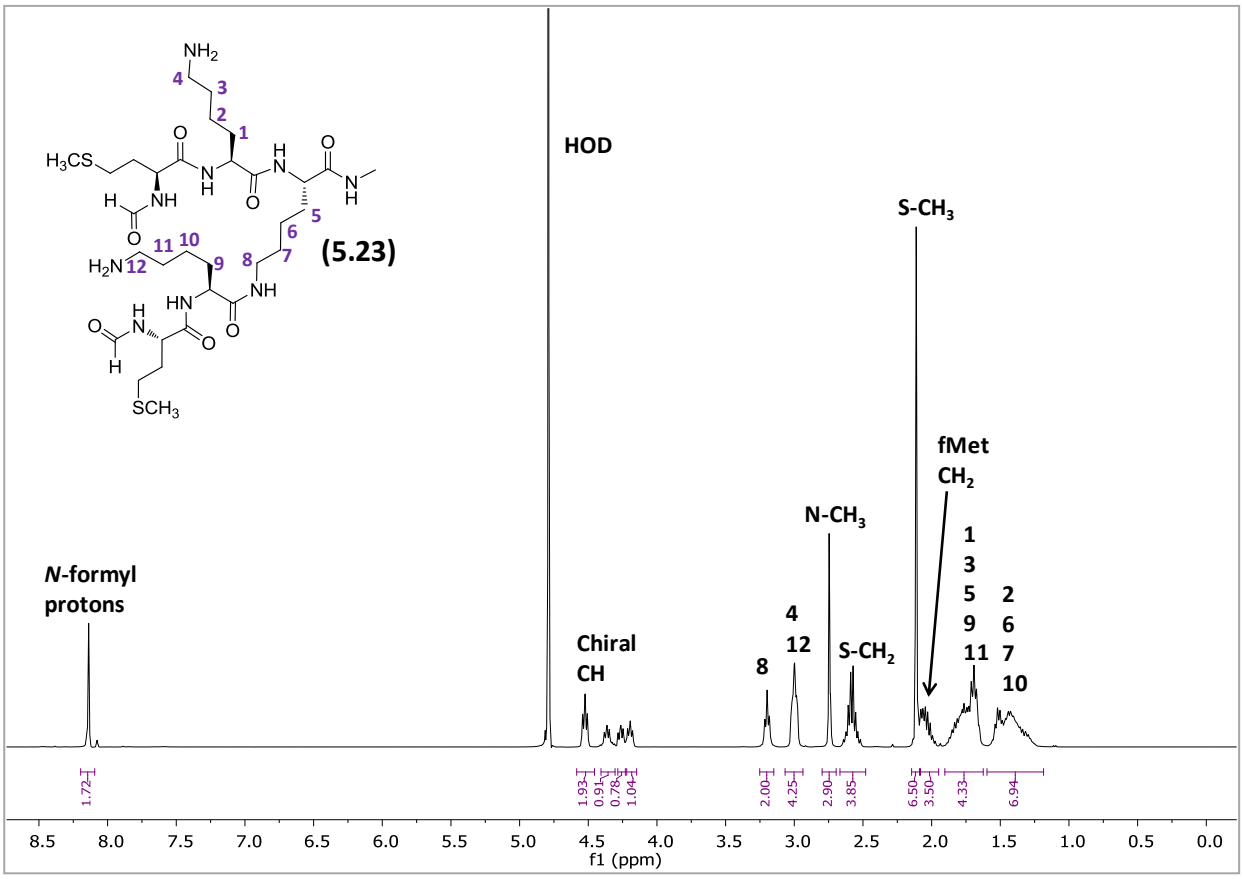
(5.23)
HOD
S-CH3
fMet
CH2
N-CH3
1
3
5
9
11
2
6
7
10
N-formyl
protons
Chiral
CH
8
4
12
S-CH2
1.72
1.93
0.91
0.78
1.04
2.00
4.25
2.90
3.85
6.50
3.50
4.33
6.94
8.5
8.0
7.5
7.0
6.5
6.0
5.5
5.0
4.5
4.0
3.5
3.0
2.5
2.0
1.5
1.0
0.5
0.0
f1 (ppm)

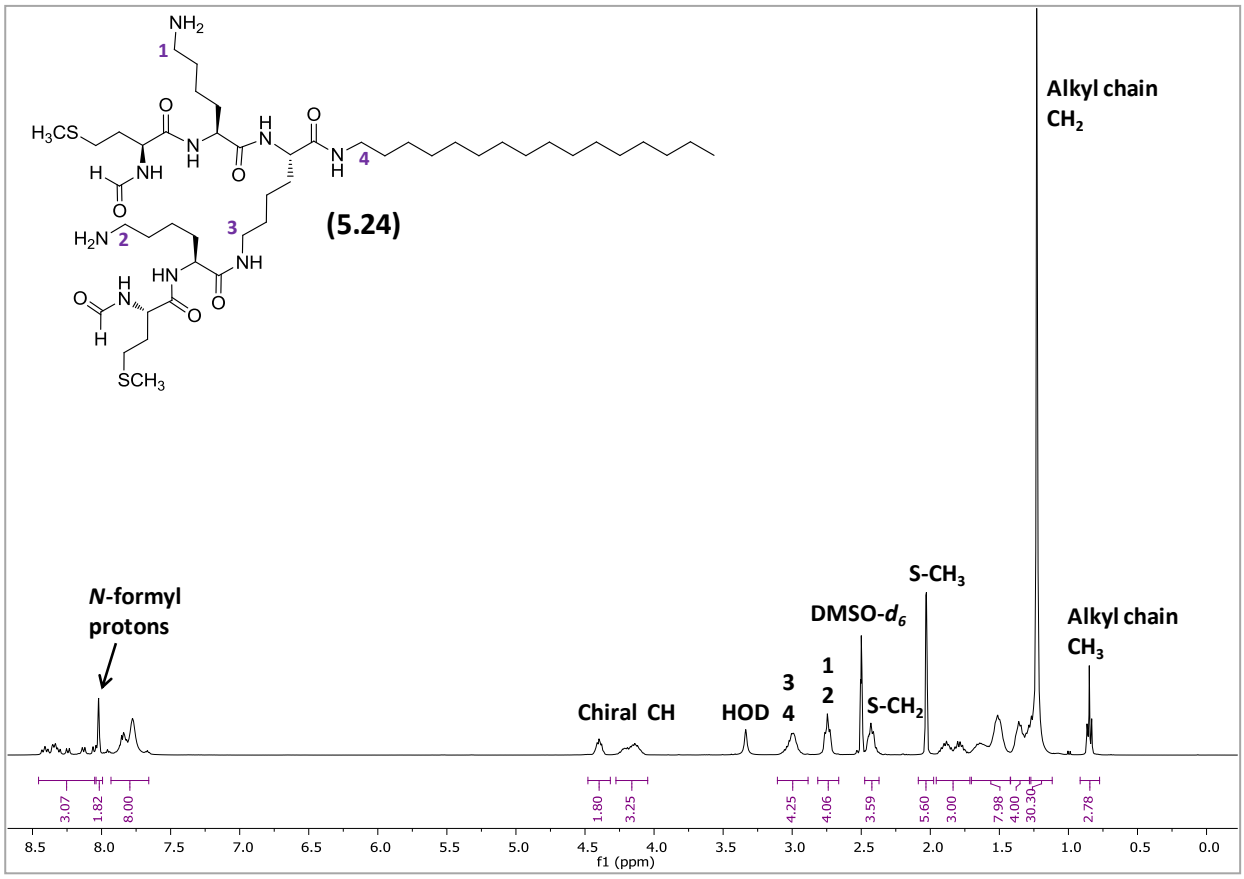
(5.24)
Alkyl chain
CH2
S-CH3
DMSO-d6
Alkyl chain
CH3
N-formyl
protons
Chiral CH
HOD
S-CH2
f1 (ppm)

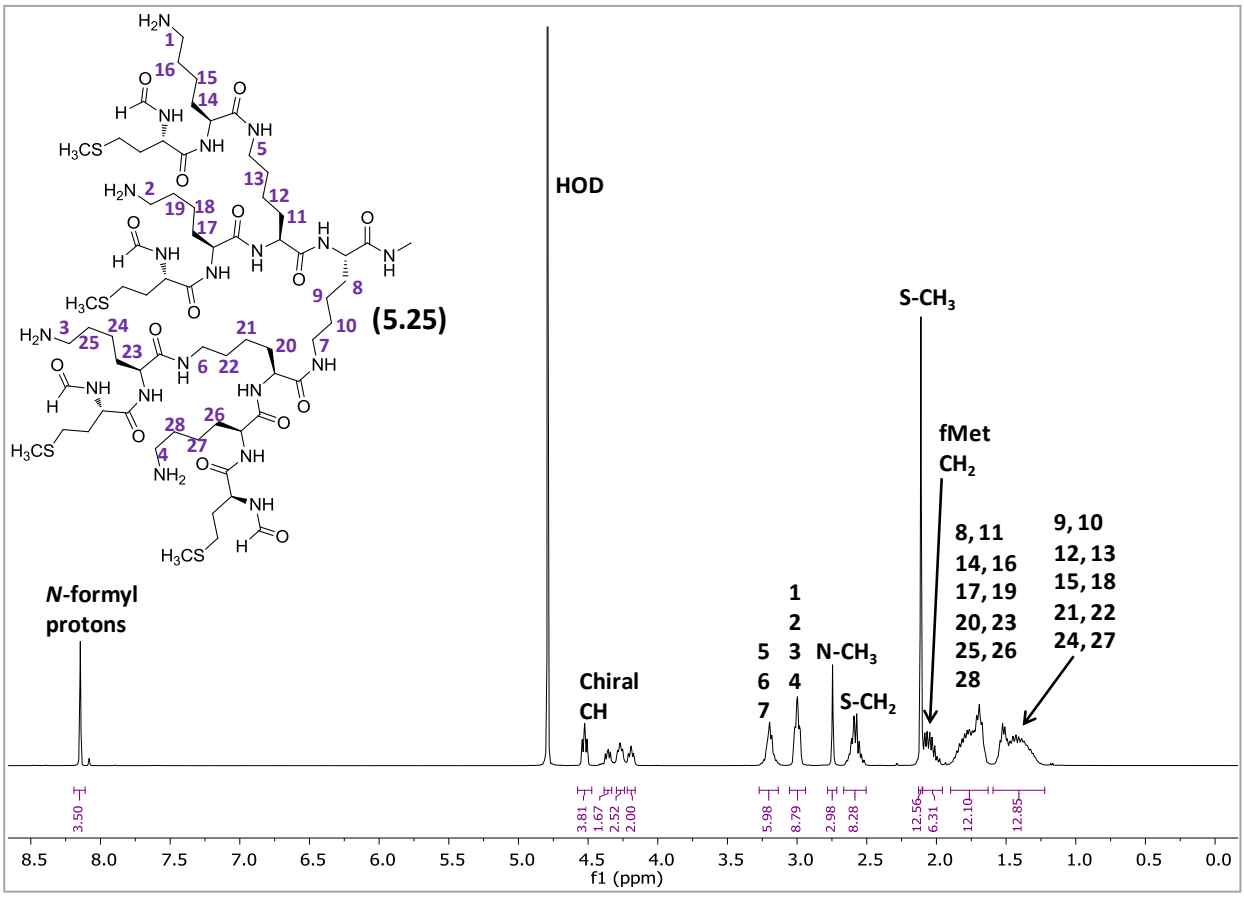
(5.25)
HOD
S-CH3
fMet
CH2
8, 11
14, 16
17, 19
20, 23
25, 26
28
9, 10
12, 13
15, 18
21, 22
24, 27
N-formyl
protons
Chiral
CH
1
2
3
4
5
6
7
N-CH3
S-CH2
3.50
3.81
1.67
2.52
2.00
5.98
8.79
2.98
8.28
12.56
6.31
12.10
12.85
8.5
8.0
7.5
7.0
6.5
6.0
5.5
5.0
4.5
4.0
3.5
3.0
2.5
2.0
1.5
1.0
0.5
0.0
f1 (ppm)

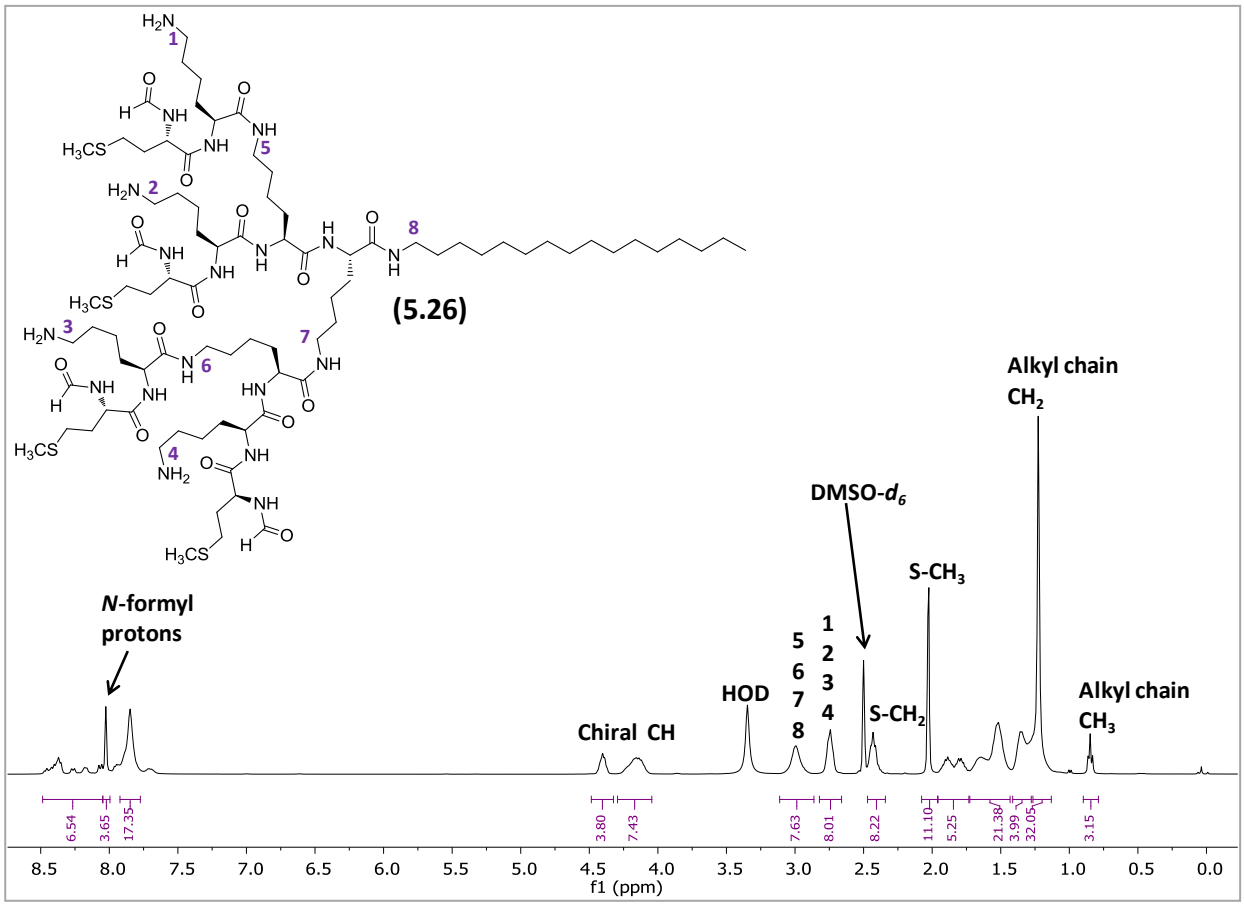
(5.26)
N-formyl protons
Chiral CH
HOD
DMSO-d6
S-CH3
S-CH2
Alkyl chain CH2
Alkyl chain CH3
f1 (ppm)

Mass Spectrum SmartFormula Report

Analysis Info

Analysis Name	D:\Data\PKH\MJE SM 286_RC3_01_39339.d	Acquisition Date	4/1/2016 9:11:16 PM
Method	standard pos low.m	Operator	BDAL@DE
Sample Name	MJE SM 286	Instrument / Ser#	micrOTOF-Q II 10205
Comment			

Acquisition Parameter

Source Type	ESI	Ion Polarity	Positive	Set Nebulizer	0.3 Bar
Focus	Not active	Set Capillary	4200 V	Set Dry Heater	180 °C
Scan Begin	50 m/z	Set End Plate Offset	-500 V	Set Dry Gas	4.0 l/min
Scan End	1500 m/z	Set Collision Cell RF	325.0 Vpp	Set Divert Valve	Source

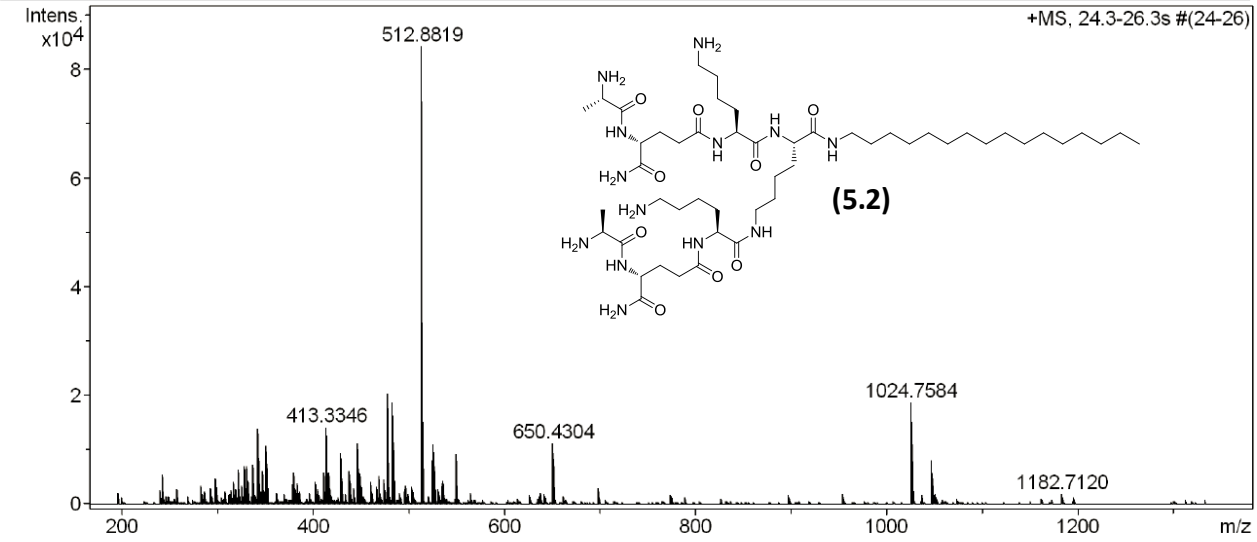

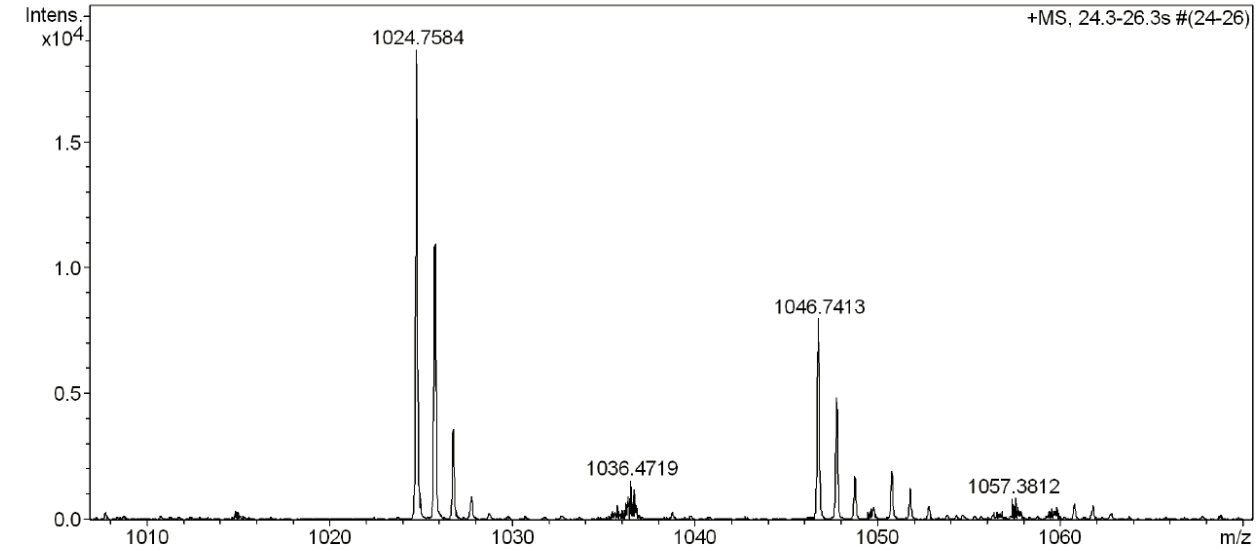

Meas. m/z	#	Formula	Score	m/z	err [ppm]	Mean err [ppm]	mSigma	rdb	e⁻ Conf	N-Rule
1024.7584	1	C 50 H 98 N 13 O 9	100.00	1024.7605	2.0	2.6	6.4	8.5	even	ok

Mass Spectrum SmartFormula Report

Analysis Info

Analysis Name	D:\Data\PKH\MJE SM 284_RA2_01_39179.d	Acquisition Date	3/30/2016 11:44:27 AM
Method	standard pos high.m	Operator	BDAL@DE
Sample Name	MJE SM 284	Instrument / Ser#	micrOTOF-Q II 10205
Comment			

Acquisition Parameter

Source Type	ESI	Ion Polarity	Positive	Set Nebulizer	0.4 Bar
Focus	Not active	Set Capillary	4500 V	Set Dry Heater	180 °C
Scan Begin	300 m/z	Set End Plate Offset	-500 V	Set Dry Gas	4.0 l/min
Scan End	3000 m/z	Set Collision Cell RF	916.7 Vpp	Set Divert Valve	Source

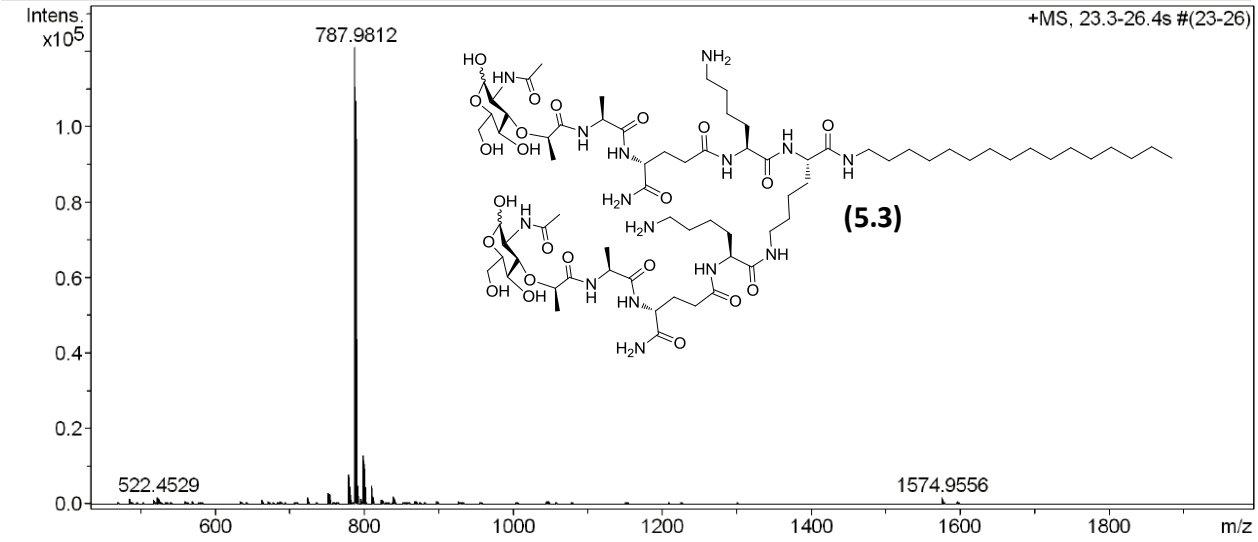

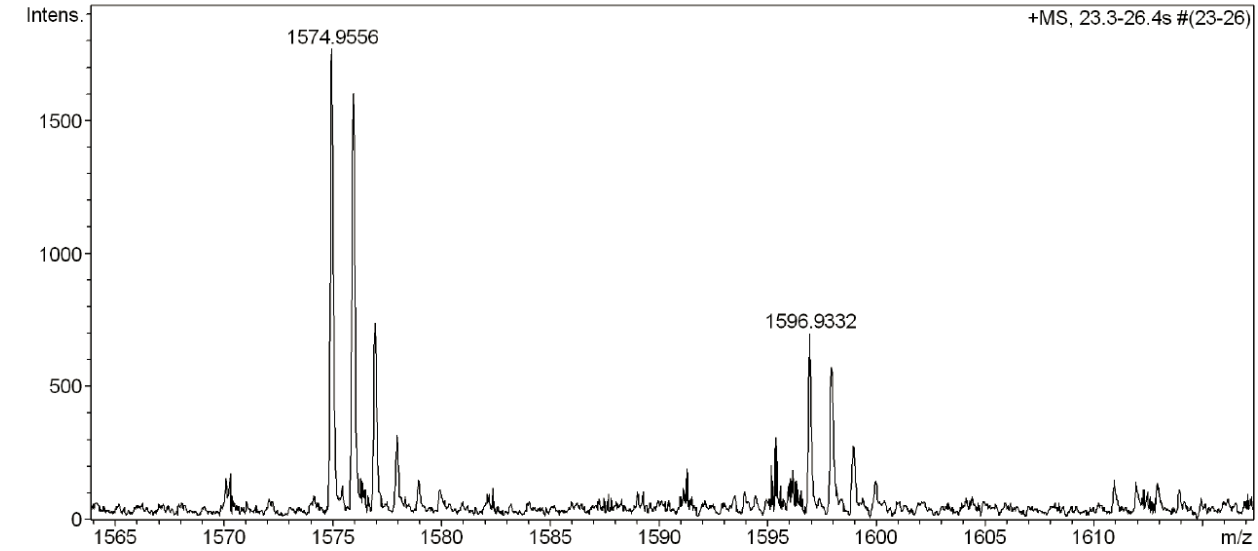

Meas. m/z	#	Formula	Score	m/z	err [ppm]	Mean err [ppm]	mSigma	rdb	e⁻ Conf	N-Rule
1574.9556	1	C 72 H 132 N 15 O 23	100.00	1574.9615	3.8	4.3	29.6	14.5	even	ok

Mass Spectrum SmartFormula Report

Analysis Info

Analysis Name	D:\Data\PKH\MJE SM 285_RC2_01_39335.d	Acquisition Date	4/1/2016 8:39:44 PM
Method	standard pos low.m	Operator	BDAL@DE
Sample Name	MJE SM 285	Instrument / Ser#	micrOTOF-Q II 10205
Comment			

Acquisition Parameter

Source Type	ESI	Ion Polarity	Positive	Set Nebulizer	0.3 Bar
Focus	Not active	Set Capillary	4200 V	Set Dry Heater	180 °C
Scan Begin	50 m/z	Set End Plate Offset	-500 V	Set Dry Gas	4.0 l/min
Scan End	1500 m/z	Set Collision Cell RF	325.0 Vpp	Set Divert Valve	Source

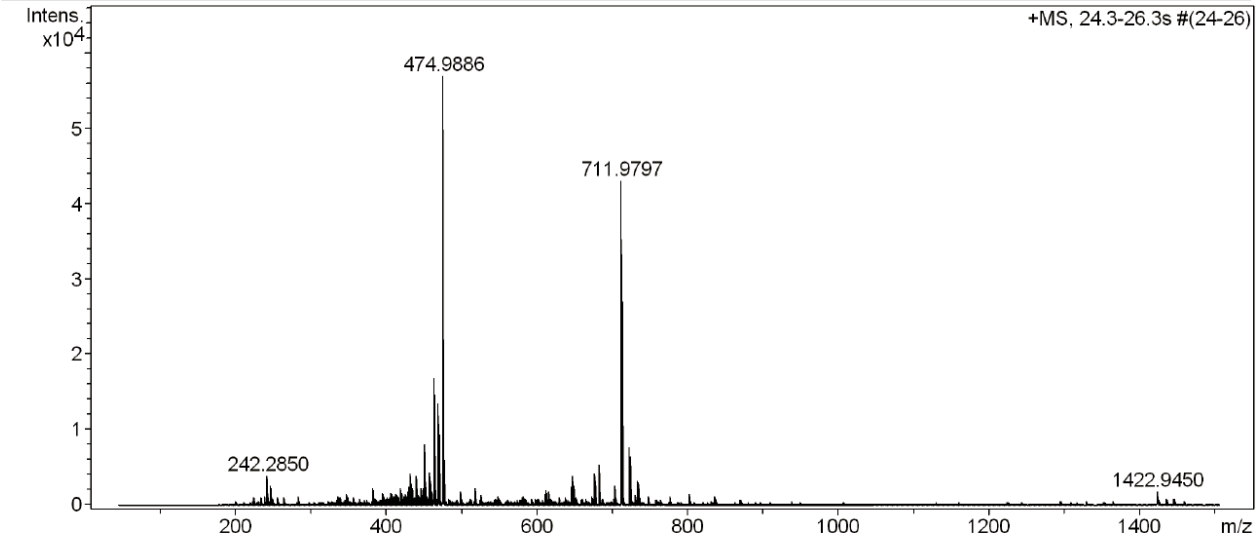

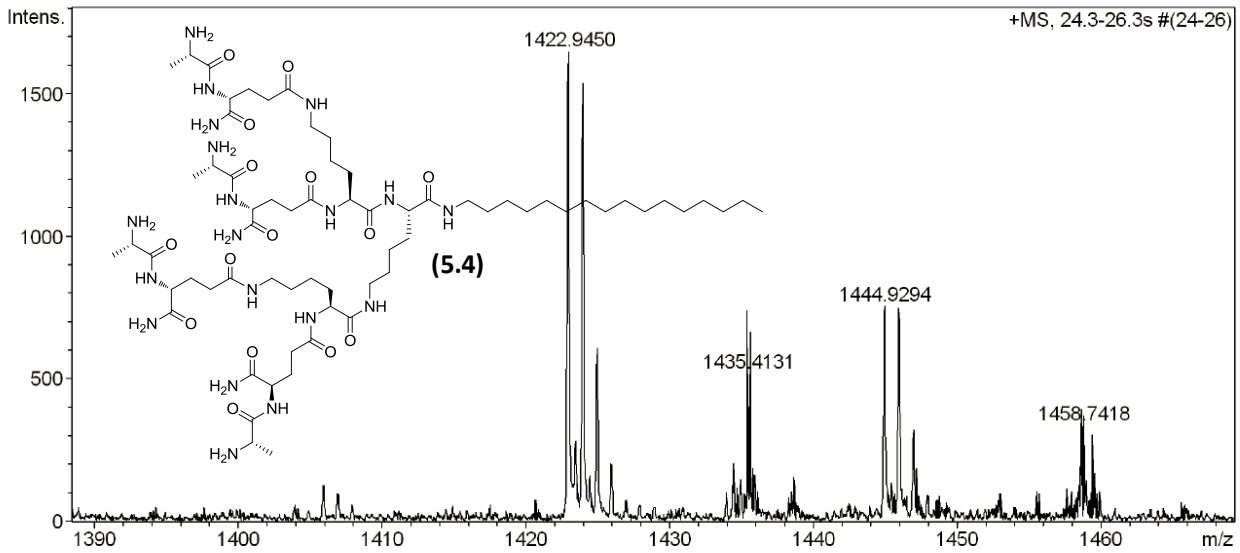

Meas. m/z	#	Formula	Score	m/z	err [ppm]	Mean err [ppm]	mSigma	rdb	e⁻ Conf	N-Rule
1422.9450	1	C 66 H 124 N 19 O 15	100.00	1422.9519	4.8	2.5	76.4	14.5	even	ok

Mass Spectrum SmartFormula Report

Analysis Info

Analysis Name	D:\Data\PKH\MJE SM 317_RC5_01_39347.d	Acquisition Date	4/1/2016 10:14:36 PM
Method	standard pos low.m	Operator	BDAL@DE
Sample Name	MJE SM 317	Instrument / Ser#	micrOTOF-Q II 10205
Comment			

Acquisition Parameter

Source Type	ESI	Ion Polarity	Positive	Set Nebulizer	0.3 Bar
Focus	Not active	Set Capillary	4200 V	Set Dry Heater	180 °C
Scan Begin	50 m/z	Set End Plate Offset	-500 V	Set Dry Gas	4.0 l/min
Scan End	1500 m/z	Set Collision Cell RF	325.0 Vpp	Set Divert Valve	Source

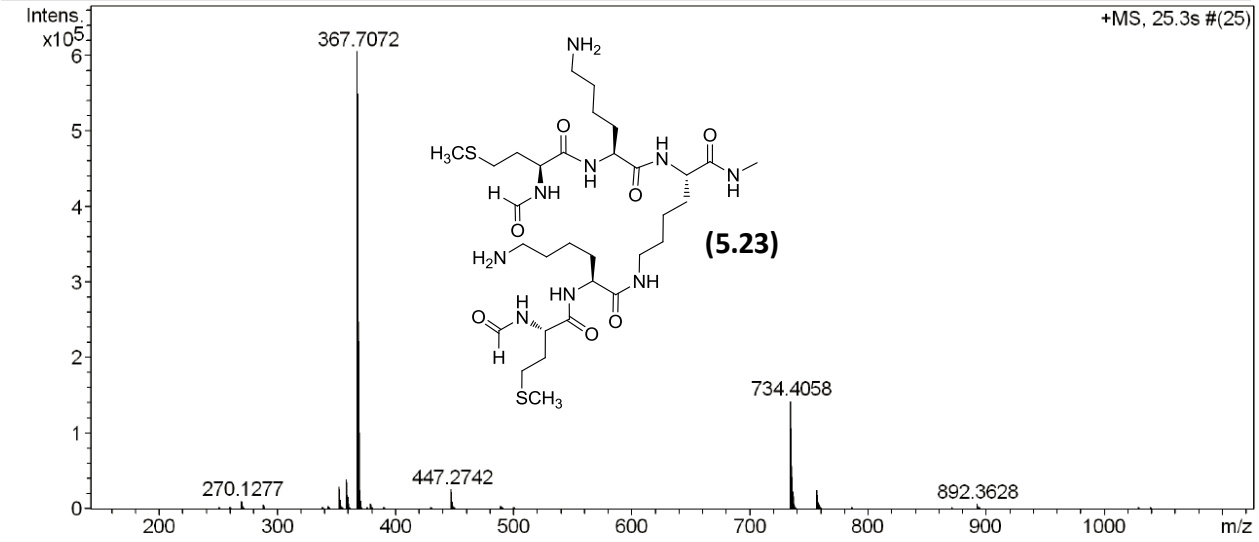

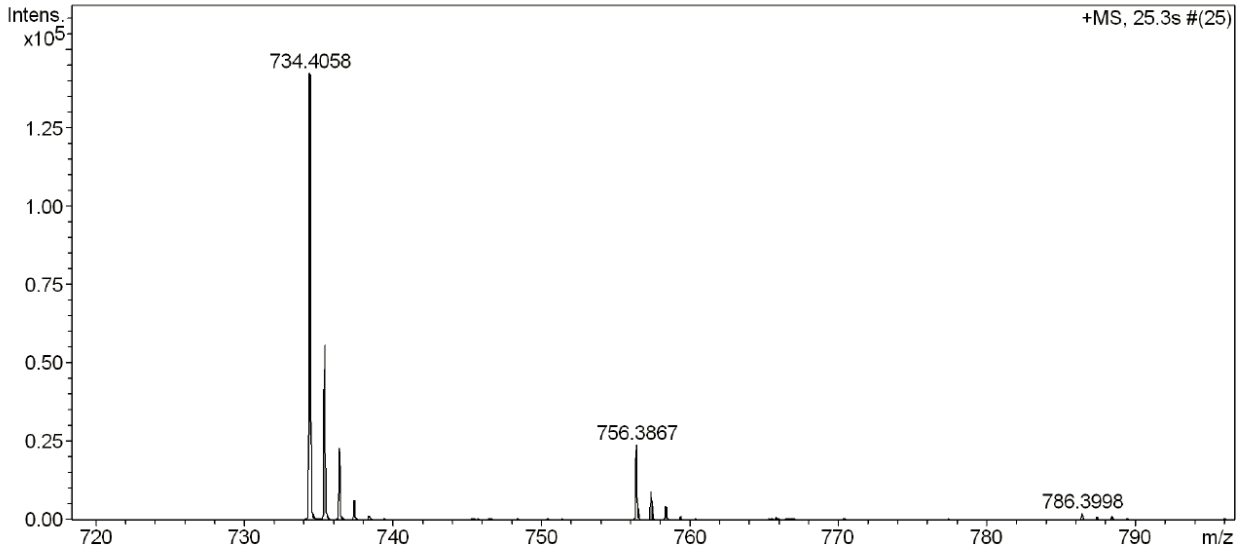

Meas. m/z	#	Formula	Score	m/z	err [ppm]	Mean err [ppm]	mSigma	rdb	e⁻ Conf	N-Rule
734.4058	1	C 31 H 60 N 9 O 7 S 2	100.00	734.4052	-0.9	-1.1	8.3	6.5	even	ok

Mass Spectrum SmartFormula Report

Analysis Info

Analysis Name	D:\Data\PKH\MJE SM 301_RC4_01_39343.d	Acquisition Date	4/1/2016 9:42:49 PM
Method	standard pos low.m	Operator	BDAL@DE
Sample Name	MJE SM 301	Instrument / Ser#	micrOTOF-Q II 10205
Comment			

Acquisition Parameter

Source Type	ESI	Ion Polarity	Positive	Set Nebulizer	0.3 Bar
Focus	Not active	Set Capillary	4200 V	Set Dry Heater	180 °C
Scan Begin	50 m/z	Set End Plate Offset	-500 V	Set Dry Gas	4.0 l/min
Scan End	1500 m/z	Set Collision Cell RF	325.0 Vpp	Set Divert Valve	Source

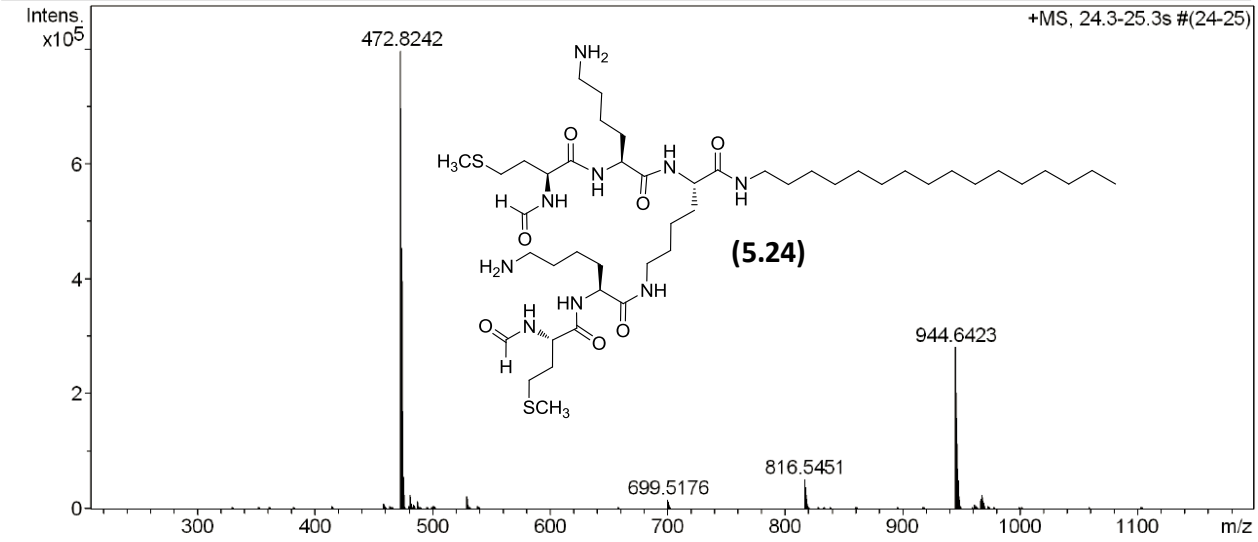

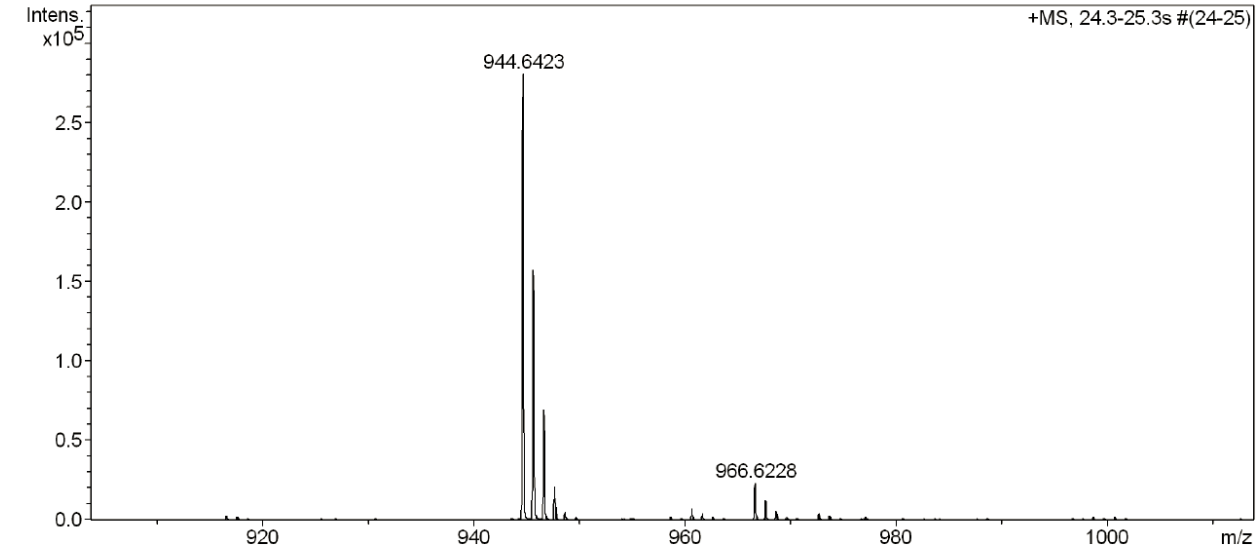

Meas. m/z	#	Formula	Score	m/z	err [ppm]	Mean err [ppm]	mSigma	rdb	e⁻ Conf	N-Rule
944.6423	1	C 46 H 90 N 9 O 7 S 2	100.00	944.6399	-2.5	-1.9	6.5	6.5	even	ok

Mass Spectrum SmartFormula Report

Analysis Info

Analysis Name	D:\Data\PKH\MJE SM 319_RA4_01_39187.d	Acquisition Date	3/30/2016 12:47:48 PM
Method	standard pos high.m	Operator	BDAL@DE
Sample Name	MJE SM 319	Instrument / Ser#	micrOTOF-Q II 10205
Comment			

Acquisition Parameter

Source Type	ESI	Ion Polarity	Positive	Set Nebulizer	0.4 Bar
Focus	Not active	Set Capillary	4500 V	Set Dry Heater	180 °C
Scan Begin	300 m/z	Set End Plate Offset	-500 V	Set Dry Gas	4.0 l/min
Scan End	3000 m/z	Set Collision Cell RF	916.7 Vpp	Set Divert Valve	Source

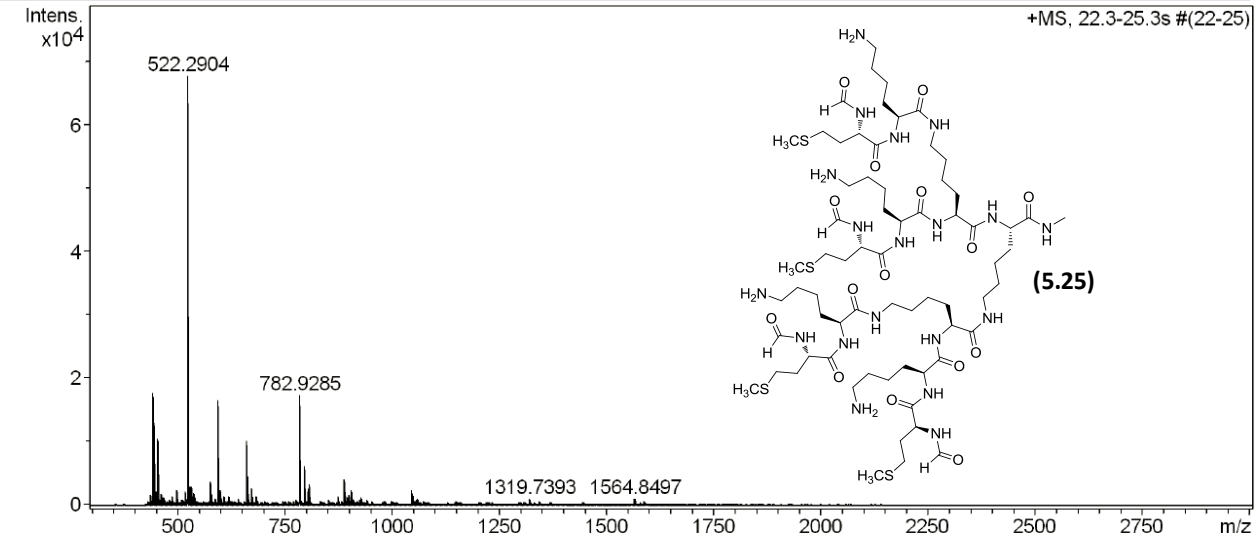

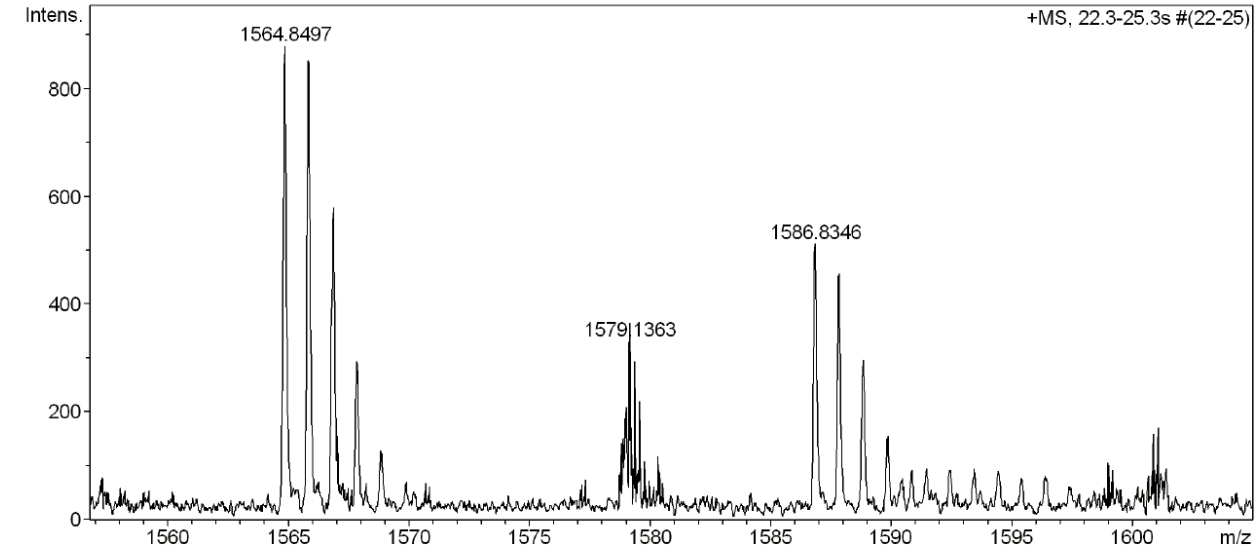

Meas. m/z	#	Formula	Score	m/z	err [ppm]	Mean err [ppm]	mSigma	rdb	e⁻ Conf	N-Rule
1564.8497	1	C 67 H 126 N 19 O 15 S 4	100.00	1564.8558	3.9	4.8	82.8	14.5	even	ok

Tetrahedron Letters 55 (2014) 3942–3945

Contents lists available at ScienceDirect

Tetrahedron Letters

journal homepage: www.elsevier.com/locate/tetlet

Solid-phase synthesis of polyfunctional polylysine dendrons using aldehyde linkers

Daniel K. Svenssen [a], Sahar Mirsharghi [a], Ulrik Boas [a,b,*]

[a] Innate Immunology Group, National Veterinary Institute, The Technical University of Denmark, Bülowsvej 27, DK-1870 Frederiksberg, Denmark
[b] Center for Nanomedicine and Theranostics, The Technical University of Denmark, Building 345E, Ørsteds Plads, DK-2800 Kongens Lyngby, Denmark

ARTICLE INFO

Article history:
Received 4 March 2014
Revised 3 April 2014
Accepted 30 April 2014
Available online 15 May 2014

Keywords:
Polylysine dendron
Solid-phase synthesis
Backbone amide linker
Polyfunctional

ABSTRACT

A straightforward method for the solid-phase synthesis of C-terminally modified polylysine dendrons has been developed by applying bisalkoxybenzaldehyde and trisalkoxybenzaldehyde linkers. The method has been used for the synthesis of polylysine dendrons with a variety of C-terminal 'tail groups' such as alkyl, propargyl, and dansyl to give dendrons in high crude purity. Furthermore, the method was successful for the synthesis of dendrons with multiple N-terminal pentapeptide groups together with C-terminal alkyl and propargyl tail groups. Finally, the method was shown to be well-suited for automated synthesis.

Dendrimers and dendrons belong to a class of molecularly defined/monodisperse hyperbranched molecules that present a high number of functional groups at their surface. The high number of functionalities on the surfaces of dendrons and dendrimers enables these structures to act as high affinity ligands for various biological receptors. Therefore, these structures have a great potential in the development of new biomaterials.[1] Dendrimers and dendrons are categorized both by the monomers they comprise and by the number of branching points following a chain from the core, or in lysine dendrons, from the C-terminal to the periphery (N-terminal). The number of branching points in the chain is denoted by the generation number (Gn) of the dendron.[2] Hence the dendrimer/dendron structure grows larger for each generation in a defined manner.

Dendrimers and dendrons based on the amino acid L-lysine were initially developed by Denkewalter[3] and their application in biological research was pioneered by Tam et al.[4] In this regard, there have been several reports on the synthesis of poly-L-lysine (PLL) dendrons by solid-phase synthesis (SPS), both by Tam's group[5,6] and subsequently by other research groups.[7–10] The reported SPS of PLL dendrons applies a Rink amide or Rink acid linker to give dendrons with a primary amide or carboxylic acid as the C-terminal functional group. However, being C-terminal protective groups, these linkers give only limited possibility to modify the C-terminus of the dendron with an additional functionality during the solid-phase synthesis.

The ability to tailor specific polyvalent structures with several functionalities may be valuable in the preparation of, for example, biologically active compounds. As we are interested in preparing multifunctional dendron ligands for a large variety of receptors, we set out to develop a straightforward strategy for the solid-phase synthesis of a large variety of polyfunctional dendron scaffolds. A peptide linker allowing both C-terminal and N-terminal modification would pave the way for the facile introduction of several functional groups during the synthetic sequence.

Linkers based on bis- and trisalkoxybenzaldehydes such as the backbone amide linker (BAL, with an *ortho* or *para* substituted spacer) and a 4-(4-formyl-3-methoxyphenoxy)butanoic acid (FMPB) linker (Fig. 1) were initially developed for the solid-phase synthesis of C-terminally modified peptides. Subsequently, they have found a wide use in the synthesis of modified and cyclic peptides as well as small non-oligomeric molecules.[11–14]

In the solid-phase synthesis of dendrons the 'backbone amide linkage approach' enables the introduction of a large variety of C-terminal 'tail' functionalities early in the synthetic sequence, without the need to introduce additional orthogonal protecting groups (Scheme 1). The initial step in the synthesis is the formation of a secondary amine by reductive amination between the linker aldehyde group and a C-terminal functionality which contains an amino group. By subsequent acylation of the secondary amine with lysine, a dendron can be synthesized on the resin by divergent synthesis. Due to stabilization of the alkoxybenzyl carbonium ion, the

* Corresponding author. Tel.: +45 35886215.
E-mail address: uboa@vet.dtu.dk (U. Boas).

http://dx.doi.org/10.1016/j.tetlet.2014.04.127
0040-4039/

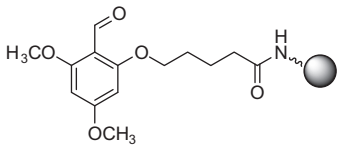

ortho-BAL derivatized resin

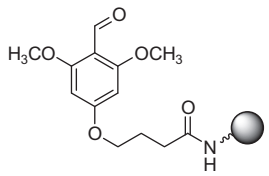

para-BAL derivatized resin

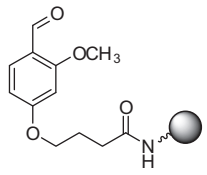

FMPB derivatized resin

Figure 1. Bis- and trisalkoxybenzaldehyde derivatized aminomethylated polystyrene resins.

dendron substrate with the secondary amide anchor point can be released in a 'traceless' manner from the resin under mild acidic conditions (Scheme 1).

The bisalkoxybenzaldehyde (FMPB) and trisalkoxybenzaldehyde (*ortho*-/*para*-BAL) linkers[15] were linked to aminomethylated polystyrene resin [1% divinylbenzene (DVB) cross-linked] or high loading rigid macroporous polystyrene (10% DVB cross-linked) by an amide linkage using (benzotriazol-1-yloxy)tripyrrolidinophosphonium hexafluorophosphate (PyBOP) and diisopropyl amine (DIPEA).[15,16] The introduction of the linker onto the resin was monitored by infrared spectroscopy (attenuated total reflectance). Here an aldehyde band appeared at approximately 1715 cm^{-1} (rigid macroporous resin) or at approximately 1670 cm^{-1} (1% DVB cross-linked resin) together with an amide band (approx. 1650 cm^{-1} for the rigid macroporous resin and 1600 cm^{-1} for the 1% DVB cross-linked resin). Hence, a red-shift was generally observed with the 1% DVB cross-linked resin compared to the rigid macroporous resin.[17,18] The presence of aldehyde groups on the resin was furthermore visualized colorimetrically by either the purpald test[19] (where the presence of resin aldehyde groups gave purple beads), or by reaction with 2,4-dinitrophenylhydrazine (DNPH) in sulfuric acid (orange–red to deeply red beads with resin aldehyde groups).[20] The loading of linker groups on the resin was reduced to avoid 'crowding' on the resin during synthesis of the more bulky dendrons.[21] The dendron C-terminal functionality was introduced onto the aldehyde linker resin via reductive amination using sodium cyanoborohydride in a dipolar aprotic solvent (DMF or NMP) under mild acidic catalysis (5% acetic acid). In this step, amines with a large variety of functional groups could be introduced. The reductive amination reactions were generally complete within 2–3 h according to IR and purpald or DNPH tests.

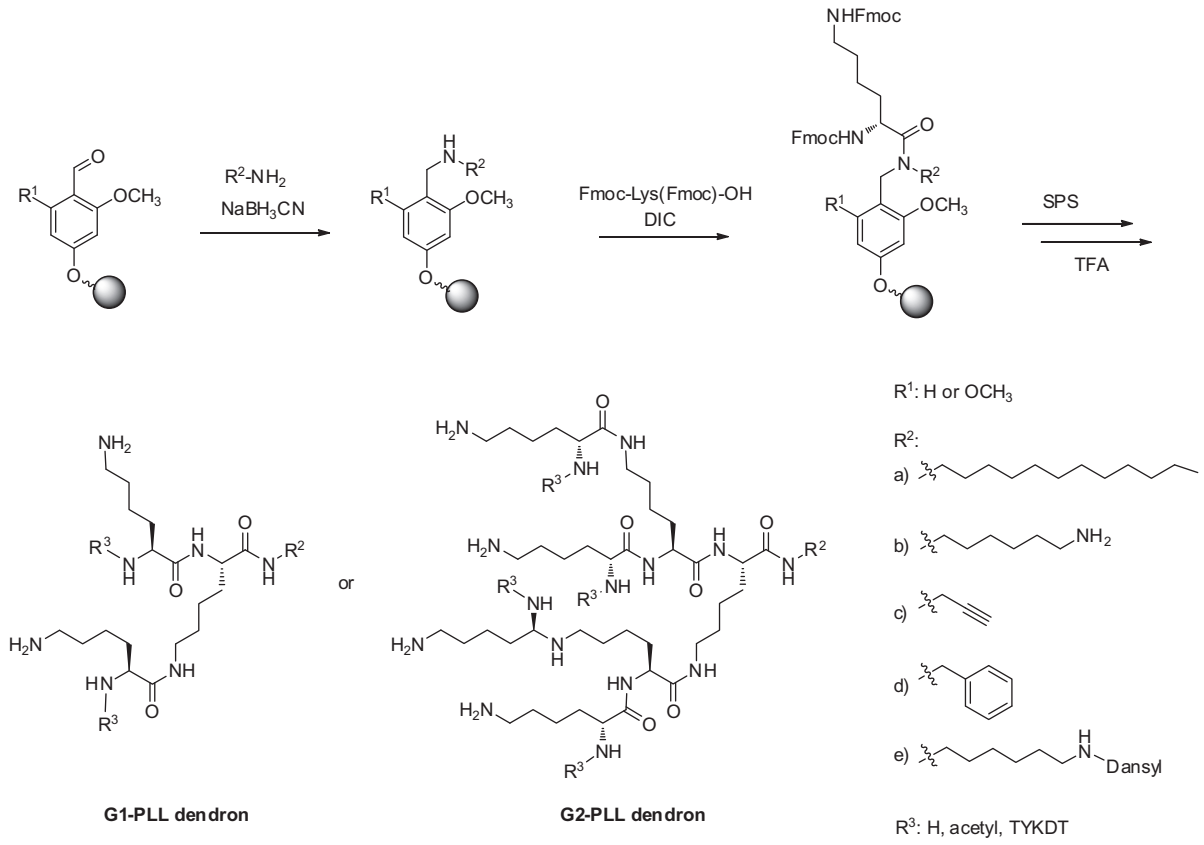

Scheme 1. Synthetic sequence for the formation of poly-L-lysine dendrons with a variety of C-terminal groups.

On-resin IR analysis of the rigid macroporous resin after reductive amination of the aldehyde generally showed a strong reduction of the aldehyde band (approx. 1715 cm^{-1}) in accordance with the negative DNPH test. In contrast, with the 1% DVB cross-linked resin, only a slight reduction of the aldehyde band (approx. 1670 cm^{-1}) was observed relative to the amide band, although purpald and DNPH tests were negative. However, upon reductive amination with long chain alkyl amines, both resins showed a significantly increased C—H stretching band (approx. 2900 cm^{-1}) relative to the aldehyde band, which was indicative of a successful reductive amination.[17,19,20] With long chain alkyl amines, for example, dodecylamine, a precipitate formed in NMP, so in these cases, a less polar solvent mixture [THF/NMP (9:1)] was applied to better dissolve the amine during the reaction.

The subsequent acylation of the secondary amine on resin with Fmoc-Lys(Fmoc)-OH was generally performed using *N*,*N*′-diisopropylcarbodiimide (DIC) twice over two hours (which worked better compared to a 4 h reaction time). In this procedure, the insoluble *N*,*N*′-diisopropylurea byproduct precipitated within 10 min. This urea byproduct could be removed by washing the resin with MeOH and NMP. By employing the coupling agent fluoro-*N*,*N*,*N*′,*N*′-tetramethylformamidinium hexafluorophosphate (TFFH) for the acylation of the secondary amine and reaction times two hours (twice), this precipitation could be avoided and similar coupling yields were obtained. Phosphonium or uronium peptide coupling agents such as PyBOP or *O*-(benzotriazol-1-yl)-*N*,*N*,*N*′,*N*′-tetramethyluronium hexafluorophosphate (HBTU), did not give complete acylation of the secondary amine under these reaction conditions. For this step the content (loading) of the amines was determined by measuring the UV absorption of the released dibenzofulvene-piperidine adduct (λ = 290 nm) from the Fmoc protected amines on the resin.[22] Generally, in the synthesis of dendron substrates, higher loadings (loading ~0.3 mmol/g) were obtained with the *ortho*-BAL linker compared to the *para*-BAL and FMPB linkers (loading $\leqslant$ 0.1 mmol/g).

Subsequent dendron synthesis was carried out by Fmoc-based SPS. In some cases, Fmoc-Lys(Boc)-OH was applied in the coupling step to release free ε-amines in the dendron product upon acidolytic release of the dendron from the resin. In the divergent build-up of the dendron, only two equivalents of the activated amino acids per amine were applied to afford complete acylation of the terminal amines. This is a lower excess than the 4–5 equiv generally needed to complete acylations in the synthesis of peptides on solid phase. The acylations were complete within one hour in the formation of G1-dendrons (indicated by a negative ninhydrin test). However, upon stepwise divergent formation of G1- and G2-dendrons carrying N-terminal peptide groups (TYDKT, which is a partial T cell epitope[23]), the coupling times in the synthesis of the peptide sequence usually increased to 2–3 h before obtaining a negative ninhydrin test. In the synthesis of dendrons with N-terminal TYDKT peptides, delayed coloring during the ninhydrin test was occasionally observed. This led to false negative results after the Fmoc deprotection of the amino acids with bulky side-chain groups (e.g., aspartic acid with a *tert*-butyl ester side-chain group, or threonine). However, inconclusive ninhydrin results could be overcome by prolonged heating during the analysis (5 min at 80 °C), which then gave reliable colorimetric results.

In order to use the method as a tool for C-terminal fluorescence labeling of dendrons we first reductively aminated the aldehyde linker with 1,6-diaminohexane followed by reaction of the primary amine with fluorescein isothiocyanate. However, the introduction of fluorescein at the C-terminus led to complex product mixtures. This may be due to the presence of two phenolic groups and a carboxylic acid on the fluorescein structure, which are prone to reaction during the subsequent synthesis of the dendron. However, two routes to introduce an alternative dansyl fluorophore gave a satisfactory outcome, albeit with somewhat lower crude purities of the products. The dansyl group could be introduced via reductive amination with a mono-dansyl modified hexane diamine,[24] followed by acylation and Fmoc-based SPS of the dendron. Alternatively, a similar result could be obtained by reductive amination with 1,6-diaminohexane followed by selective dansylation of the primary amine. To increase the selectivity toward the reaction with a primary amine in the presence of a secondary amine, we found it necessary to deactivate the dansyl chloride by reaction with hydroxybenzotriazole (HOBt) to form an intermediate HOBt-sulfonic acid ester.[25]

Amino groups at the dendron surface could be released as free amines or acetylated amines. Also, a triglycine peptide was successfully introduced by segment coupling, opening up possible segment coupling by other peptide sequences comprising a C-terminal glycine residue. The G1- and G2 dendronized triglycine derivatives were synthesized in 37–44% isolated yields possessing either dodecyl or 6-aminohexyl tail groups (Table 1). To further investigate the scope of the present method, the automated synthesis of dendron structures with N-terminal peptide groups was carried out on a peptide synthesizer. Here, we synthesized two G1-dendrons with a C-terminal dodecyl and propargyl tail and two N-terminal peptide groups. G1- and G2-dendrons with a propargyl tail group (**8** and **18**) and with two and four N-terminal TYKDT peptide groups, respectively, were successfully synthesized by automated synthesis (Table 1). Here, product **18** was of high crude purity according to HPLC–MS, whereas crude product **8** showed a minor impurity with an M + 96 mass. The M + 96 mass could result from either the TFA ester or trifluoroacetamide adduct of **8** formed during the acidolytic cleavage from the resin. The propargyl tail group was chosen, since it allows the introduction of a large variety of functionalities by click chemistry. The G1-dendron with a dodecyl tail group **7** was synthesized both manually and by automated synthesis, the crude product **7** prepared by automated synthesis showed some minor impurities according to HPLC-MS with an M + 96 (TFA ester or TFA amide) together with a minor HPLC peak with mass M − 128. The M − 128 mass was found to be a deletion sequence missing one lysine residue.[17] As deletion byproducts were not observed in the automated synthesis of dendrons with a propargyl group at the C-terminus, this could indicate that the hydrophobic dodecyl chain influences the acylation steps due to steric effects, occasionally giving deletion sequences. Hence, in these cases, the automated

Table 1
Synthesized dendrons and their isolated yields[24]

	Compound	Yield (%)
1	G1-PLL($(NH_2)_4$)-N-dodecyl	47
2	G1-PLL($(NH_2)_4$)-N-(6-aminohexyl)	72
3	G1-PLL($(NH_2)_2$ $(AcNH)_2$)-N-dodecyl	69
4	G1-PLL($(NH_2)_2$ $(AcNH)_2$)-N-(6-aminohexyl)	52
5	G1-PLL($(NH_2)_2$ $(AcNH)_2$)-N-propargyl	56
6	G1-PLL($(NH_2)_2(AcNH)_2$)-N-(6-dansylaminohexyl)	67
7	G1-PLL($(NH_2)_2(TYKDT)_2$)-N-dodecyl	42
8	G1-PLL($(NH_2)_2(TYKDT)_2$)-N-propargyl	44
9	G1-PLL$(GGG)_4$-N-dodecyl	44
10	G1-PLL$(GGG)_4$-N-(6-aminohexyl)	44
11	G2-PLL($(NH_2)_8$)-N-dodecyl	31
12	G2-PLL($(NH_2)_8$)-N-(6-aminohexyl)	42
13	G2-PLL-($(NH_2)_4(AcNH)_4$)-N-dodecyl	55
14	G2-PLL($(NH_2)_4(AcNH)_4$)-N-(6-aminohexyl)	60
15	G2-PLL($(NH_2)_4(AcNH)_4$)-N-benzyl	35
16	G2-PLL($(NH_2)_4(AcNH)_4$)-N-propargyl	68
17	G2-($(NH_2)_4(GGG)_4$)-N-dodecyl	37
18	G2-PLL($(NH_2)_4(TYKDT)_4$)-N-propargyl	32[a]

[a] A somewhat higher loading (0.11 mmol/g) and a lower isolated yield was obtained due to the lack of capping of the free amine groups on the resin.

synthesis protocol may be further optimized to resolve this problem. However, pure product **7** was obtained by manual solid-phase synthesis. To further determine the structure of the dendronized TYDKT peptides, derivatives **7** and **18** were analyzed by amino acid analysis (AAA) and found to be in accordance with the expected amino acid compositions, $Lys_5Thr_4Asp_2Tyr_2$ and $Lys_{11}Thr_8Asp_4Tyr_4$, respectively.

In summary, a straightforward method for the preparation of polyfunctional lysine dendrons in good yields and crude purities is presented. The method paves the way for the introduction of a large variety of C-terminal functionalities including molecular labels or functionalities which allow further derivatization in solution, for example, by click chemistry. Peptide N-terminal endgroups can be introduced by solid-phase segment coupling or by stepwise synthesis. The method can furthermore be implemented in automated SPS of dendrons.

Supplementary data

Supplementary data associated with this article can be found, in the online version, at http://dx.doi.org/10.1016/j.tetlet.2014.04.127.

References and notes

1. For example, see: (a) Tomalia, D. A.; Christensen, J. B.; Boas, U. *Dendrimers, Dendrons and Dendritic Polymers*; Cambridge University Press, 2012; (b) Boas, U.; Christensen, J. B.; Heegaard, P. M. H. *Dendrimers in Medicine and Biotechnology*; RSC Publishing, 2006.
2. In this Letter we apply a nomenclature which is a combination of peptide nomenclature and dendrimer nomenclature where a generation of poly-L-lysine dendron is named as follows: Gn-PLL (N-terminal end groups)*n* –N-(C-terminal end group) where *n* = number of N-terminal end groups, and G = generation and *n* = the generation number.
3. Denkewalter, R. G.; Kole, J.; Lukasavage, W. J. US patent 4,289,872 (1981).
4. Tam, J. P. *Proc. Natl. Acad. Sci.* **1988**, *85*, 5409–5413.
5. Posnett, D. N.; McGrath, H.; Tam, J. P. *J. Biol. Chem.* **1988**, *263*, 1719–1725.
6. Lu, Y. A.; Tam, J. P. *Proc. Natl. Acad. Sci.* **1989**, *86*, 9084–9088.
7. (a) Kantchev, E. A. B.; Chang, C.-C.; Cheng, S.-F.; Roche, A.-C.; Chang, D.-K. *Org. Biomol. Chem.* **2008**, *6*, 1377–1385; (b) Kantchev, E. A. B.; Chang, C.-C.; Chang, D.-K. *Biopolymers Pept. Sci.* **2006**, *84*, 232–240.
8. Tang, Y. H.; Huang, A. Y. T.; Chen, P. Y.; Chen, H. T.; Kao, C. L. *Pharm. Des.* **2011**, *17*, 2308–2330.
9. Papadopoulos, A.; Shiao, T. C.; Roy, R. *Mol. Pharm.* **2012**, *9*, 394–403.
10. Shiao, T. C.; Roy, R. *New J. Chem.* **2012**, *36*, 324–339.
11. Jensen, K. J.; Alsina, J.; Songster, M. F.; Vágner, J.; Albericio, F.; Barany, G. *J. Am. Chem. Soc.* **1998**, *120*, 5441–5452.
12. Boas, U.; Brask, J.; Jensen, K. J. *Chem. Rev.* **2009**, *109*, 2092–2118.
13. Swayze, E. E. *Tetrahedron Lett.* **1997**, *38*, 8465–8468.
14. Sarantakis, D.; Bicksler, J. J. *Tetrahedron Lett.* **1997**, *38*, 7325–7328.
15. The *ortho*-BAL linker was not commercially available and was therefore synthesized according to: Boas, U.; Brask, J.; Christensen, J. B.; Jensen, K. J. *J. Comb. Chem.* **2002**, *4*, 223–228.
16. *Procedure for anchoring the aldehyde linker to aminomethylated polystyrene resin*: the aldehyde linker, for example, FMPB or *ortho*-/*para*-BAL (1 equiv), PyBOP (1 equiv) and HOBt (1 equiv) were suspended in NMP (approximately 7.3 mL/g resin). However, it was later concluded that HOBt could be omitted from the general procedure. DIPEA (2 equiv) was added and the mixture was swirled for 5 min at rt. The mixture was transferred to a filter syringe/glass container with a glass filter containing the aminomethylated polystyrene resin (0.5 or 1 equiv, loading: 2 mmol/g) and shaken for 1 h at rt, and then washed with NMP (5 × 10 mL) and CH_2Cl_2 (5 × 10 mL). The resin was capped with Ac_2O/DIPEA/CH_2Cl_2 10/5/85 (7–10 mL/g resin) for 2 h, or until the ninhydrin test showed negative. The derivatized resin was washed with NMP (5 × 10 mL), CH_2Cl_2 (5 × 10 mL) and MeOH (2 × 5 mL), and then air-dried followed by drying in vacuo. The IR spectrum was recorded showing bands at 1680 cm^{-1} (C=O stretch, amide), around 1700 cm^{-1} (C=O stretch, aldehyde); positive purpald and DNPH tests were observed.
17. Analytical data including spectra and chromatograms can be found in the Supporting information.
18. A strong IR band from residual acetic anhydride was seen at approximately 1790 cm^{-1} after capping of the rigid macroporous resin and the anhydride proved difficult to remove by washing. Treatment with 20% MeOH/5% DIPEA in CH_2Cl_2 overnight removed the band, but sometimes gave rise to a smaller band at approximately 1770 cm^{-1}, presumably due to a methyl acetate (C=O stretch) formed during the MeOH treatment. However, with the 1% DVB cross-linked resin, no band from residual acetic anhydride was observed. We conclude that the reduced swelling ability of the rigid macroporous resin must somehow have an effect on entrapment of acetic anhydride inside the beads.
19. The purpald aldehyde test was performed as described by Cournoyer, J. J.; Kshirsagar, T.; Fantauzzi, P. P.; Figliozzi, G. M.; Makdessian, T.; Yan, B. *J. Comb. Chem.* **2002**, *4*, 120–124.
20. The DNPH test on the aldehyde functionality was performed according to the procedure described by Shannon, S. K.; Barany, G. *J. Comb. Chem.* **2004**, *6*, 165–170.
21. Tam, J. P.; Lu, Y. A. *J. Am. Chem. Soc.* **1995**, *117*, 12058–12063.
22. Determination of the resin loading was carried out as follows: resin (3 × 5 mg) was transferred to falcon tubes and a solution of piperidine in NMP (1:4, 25 mL) was added and the tube shaken for 30 min along with a reference tube containing only the piperidine solution. Each of the four samples were transferred to a cuvette and the absorbance measured by photospectrometry at 290 nm. The absorbance was used to calculate the loading of the resin according to the formula: loading in mmol/g = 4.76 Abs/mass of resin in mg.
23. Bay, S.; Lo-Man, R.; Isinaga, E.; Nakada, H.; Leclerc, C.; Cantacucene, D. *J. Peptide Res.* **1997**, *49*, 620–625.
24. Detailed experimental procedures on the synthesized compounds can be found in the Supporting information.
25. Data not shown.

Supplementary material for: D.K. Svenssen, S. Mirsharghi and U. Boas. Solid-phase synthesis of polyfunctional polylysine dendrons using aldehyde linkers

General remarks:

All starting materials were purchased from Sigma-Aldrich, IRIS Biotech and Merck Chemicals and used without further purification. Solvents were purchased from Fischer Scientific and VWR International and were of HPLC grade. High-loading (2mmol/g) aminomethylated polystyrene (1% divinylbenzene (DVB) crosslinked or rigid macroporous) was employed and the solid-phase reactions were performed in polypropylene syringes equipped with a polyethylene filter placed on a shaker or a glass container with a glass filter and manual washing of the resins was carried out on Torviq plates. Automated solid-phase syntheses of dendrons were carried out on a Intavis AG ResPep synthesizer. Nuclear magnetic resonance spectroscopy, NMR (^{1}H) was performed in deuterium oxide on a 300MHz Bruker Avance 300 equipped with a BBO probe and autosampler operating at 300 MHz. Spectra were calibrated relative to TMS as an internal standard or residual solvent peak (D_2O: 4.79 ppm). Reverse-phase HPLC-MS analysis was performed on a Shimadzu LCMS 2010, using a Phenomenex Jupiter C5 column (5µm, 300Å) and a 1 mL/min linear gradient from 3 to 95% over 18 min (buffer A: 0.025% TFA in 10% aqueous acetonitrile; buffer B: 0.025% TFA in 90% aqueous acetonitrile). Additionally UPLC-MS analysis was carried out on an equipment comprising of a Shimadzu Nexera X2 and a Bruker MicrOTOF-Q III, using a Ascentis Express Peptide ES-C18 column (2.7µm, 160Å) and a 1 mL/min linear gradient from 0 to 100% over 5.00 min with buffer A and B as above. Initial mass analysis was carried out in conjunction with HPLC on a quadrupole mass spectrometer in electronspray ionization (ESI^+) mode. Infrared spectroscopy (IR) was performed directly on the resin beads by a Shimadzu IRaffinity spectrometer using attenuated technique of reflectance (ATR). Amino acid analysis (AAA) was performed with Waters pico-tag in duplicate after hydrolyzing resin samples for 15 h at 130°C with concentrated HCl/propionic acid (1:1).

1-N-Dansyl-6-diaminohexane (20): N-Boc-1,6-hexanediamine hydrochloride (750 mg, 3.47 mmol, 1 equiv.), dansyl chloride (842 mg, 3.12 mmol, 0.9 equiv.) and DIPEA (1.5 mL, 8.67 mmol, 2.5

equiv.) were dissolved in dry DCM (25 mL) and stirred. After 2 h the reaction was complete. The organic phase was washed with 1 N $KHSO_4$ (2 x 25 mL) and brine (2 x 25 mL) before drying with Na_2SO_4. Upon filtration the solvent was removed in vacuo giving 1-N-dansyl-6-N-Boc-diaminohexane (**19**). Then **19** was treated with a TFA/DCM 1:1 mixture (20 mL) for 1 h. followed by concentration in vacuo. The product was obtained as a yellow syrup which was stirred with Et_2O (10mL), petroleum ether (10mL) and freeze-dried to remove the remaining TFA. Yield: 636,1mg (44 %), HPLC data: t_R 16.2 min., MS(ESI^+) calcd $C_{18}H_{27}N_3O_2S$: 349.18, Found: m/z 350 $[MH]^+$, NMR data: ^1H NMR (D_2O, 300MHz): δ 1.08 (4H, m, 2 x CH_2-$\underline{CH_2}$-CH_2), 1.25 (2H, p, J = 6.5 Hz, CH_2-$\underline{CH_2}$-CH_2), 1.40 (2H, p, *J* = 7.5 Hz, CH_2-$\underline{CH_2}$-CH_2), 2.79 (2H, t, *J* = 7.5 Hz, CH_2-$\underline{CH_2}$-NH_2), 2.85 (2H, t, *J* = 6.8 Hz, CH_2-$\underline{CH_2}$-NH), 3.44 (6H, s, 2 x N-$\underline{CH_3}$), 4.63 (2H, s, CH_2-$\underline{NH_2}$), 4.70 (solvent peak), 7.83 (2H, t, J = 8.7 Hz, ArH), 8.02 (1 H, d, J = 7.8 Hz, ArH), 8.31 (2 H, dd, J_1 = 8.8 Hz, J_2 = 21.5, ArH), 8.70 (1 H, d, J = 8.8 Hz, ArH), Missing: N-H (sulfonamide) due to exchange.

G1-PLL(NH_2)$_4$ dendron with C-terminal Dodecyl and Aminohexyl groups, general procedure (I): The FMPB or BAL derivatized resin (100 mg, 0.10 mmol, 1 equiv.), $NaBH_3CN$ (62 mg, 1.00 mmol, 10 equiv.), and amine (1.00 mmol, 10 equiv.) were suspended in a 5 % AcOH in NMP solution (2 mL) and shaken. After 16 h, the resin was washed with NMP (10 x 5 mL), DCM (5x5 mL) and MeOH (2 x 5 mL) before air-drying and drying on oil-pump overnight. IR spectrum was recorded. Purpald test (-). Fmoc-Lys(Fmoc)-OH (295 mg, 0.50 mmol, 5 equiv.) and DIC (32 mg, 39 µL, 0.25 mmol, 2.5 equiv.) was suspended in DCM/NMP (9:1, 1 mL) in a falcontube and shaken for 15 min and transferred to the filter syringe containing the BAL-derivatized resin and DCM (1 mL), the suspension was shaken. After 16 h the resin was washed (NMP (10 x 5 mL), DCM (5 x 5 mL), and MeOH (3 x 5 mL)) and air-dried for 15 min. The loading was determined to 0.31 mmol/g on 3 x 5 mg resin by Fmoc quantification. Fmoc removal was carried out with piperidine/NMP (1:4) for 3 +

20 min followed by washing of the resin (DCM (5 x 5 mL) and NMP (10 x 5 mL)). Ninhydrin test (+). Fmoc-Lys(Fmoc)-OH (236 mg, 0.40 mmol, 4 equiv.), PyBOP (198 mg, 0.38 mmol, 3.8 equiv.), HOBt (54 mg, 0.40 mmol, 4 equiv.) and DIPEA (136 µL, 0.78 mmol, 7.8 equiv.) were preactivated in NMP (2 mL) for 5 min and transferred to the filter syringe containing the BAL-derivatized resin and shaken for 3 h, washed (NMP (5 x 5 mL), DCM (5 x 5 mL) and MeOH (1 x 5 mL)). Ninhydrin test (-). Fmoc groups were removed with piperidine/NMP (1:4) for 3 + 20 min followed by washing (DCM (5 x 5 mL), NMP (5 x 5 mL)). Ninhydrin test (+). The resin was treated with TFA/DCM (1:1, 4 mL) and shaken for 2 h, followed by filtration and collection of the cleavage mixture in a round bottomed flask. Evaporation in vacuo and precipitation in Et_2O gave the product as a white powder. **G1-PLL($(NH_2)_4$)-N-dodecyl (1)**: Yield 8.1 mg (47 %), HPLC data: t_R, 16.6 min. MS(ESI^+), calcd $C_{30}H_{63}N_7O_3$: 569.87, Found: m/z 571 $[MH]^+$, 286 $[MH]^{2+}$. **G1-PLL($(NH_2)_4$)-N-(6-Aminohexyl) (2):** Yield 11.2 mg (72 %), HPLC data: t_R, 7.4 min. MS(ESI^+), calcd $C_{24}H_{52}N_8O_3$: 500.72, Found: m/z 502 $[MH]^+$, 251 $[MH]^{2+}$.

G1-PLL($(NH_2)_2(AcNH)_2$) dendron with C-terminal Dodecyl, Aminohexyl, Dansyl and Propargyl groups, general procedure (II): The FMPB or BAL derivatized resin (100 mg, 0.10 mmol, 1 equiv), $NaBH_3CN$ (62 mg, 1.00 mmol, 10 equiv.), and amine (1.00 mmol, 10 equiv.) were suspended in a 5 % AcOH in NMP solution (2 mL) and shaken. After 16 h, the resin was washed with NMP (10 x 5 mL), DCM (5x5 mL) and MeOH (2 x 5 mL) before air-drying and drying on oil-pump overnight. IR spectrum was recorded which showed disappearance of the IR band (C=O stretch, benzaldehyde) at 1700 cm^{-1}. In case of reaction with propargyl amine an IR band at 2150 cm^{-1} (C≡C stretch, alkyn) was observed. Purpald test for aldehydes was negative. Fmoc-Lys(Fmoc)-OH (295 mg, 0.50 mmol, 5 equiv.) and DIC (32 mg, 39 µL, 0.25 mmol, 2.5 equiv.) were suspended in DCM/NMP (9:1, 1 mL) in a 15 mL polypropylene tube and shaken for 15 min and transferred to the filter syringe

containing the BAL-derivatized resin and DCM (1 mL), the suspension was shaken. After 2 h the resin was washed (NMP (10 x 5 mL), DCM (5 x 5 mL), and MeOH (3 x 5 mL)) and air-dried for 15 min. Loading was determined on 3 x 5 mg resin by Fmoc quantification (see general remarks above). Fmoc removal was carried out with piperidine/NMP (1:4) for 3 + 20 min followed by washing of the resin (DCM (5 x 5 mL) and NMP (10 x 5 mL)). Ninhydrin test (+). Fmoc-Lys(Boc)-OH (187 mg, 0.40 mmol, 4 equiv.), PyBOP (198 mg, 0.38 mmol, 3.8 equiv.), HOBt (54 mg, 0.40 mmol, 4 equiv.) and DIPEA (136 µL, 0.78 mmol, 7.8 equiv.) were preactivated in NMP (2 mL) for 5 min and transferred to the filter syringe containing the BAL-derivatized resin and shaken for 2 h, washed (NMP (5 x 5 mL), DCM (5 x 5 mL) and MeOH (1 x 5mL)). Ninhydrin test (-).Fmoc removal was carried out with piperidine/NMP (1:4) for 3 + 20 min followed by washing of the resin (DCM (5 x 5 mL) and NMP (10 x 5 mL)). Ninhydrin test (+). The free amine groups were acetylated with a solution of 10 % Ac_2O and 5 % DIPEA in NMP (3 mL), the mixture was shaken overnight and washed (NMP (10 x 5 mL), DCM (5 x 5 mL) and MeOH (2 x 5 mL)). Ninhydrin test (-). The resin was treated with TFA/DCM (1:1, 4 mL) and shaken for 2 h, followed by filtration and collection of the cleavage mixture in a round bottomed flask. Evaporation in vacuo and precipitation in Et_2O gave the product as a white powder. Yields and analytical data: **G1-PLL($(NH_2)_2$($(AcNH)_2$)-N-Dodecyl (3):**14.9 mg (loading: 0.33mmol/g, 69 %), HPLC data: t_R, 19.2 min. MS(ESI^+), calcd $C_{34}H_{67}N_7O_5$: 653.52 Found: m/z 655 $[MH]^+$, 328 $[MH]^{2+}$. **G1-PLL($(NH_2)_2$($(AcNH)_2$)-N-(6-Aminohexyl) (4):** Yield 9.5 mg (loading: 0.31 mmol/g, 52 %), HPLC data: t_R, 7.3 min. MS(ESI^+), calcd $C_{28}H_{56}N_7O_5$: 584.44 Found: m/z 585 $[MH]^+$, 293 $[MH]^{2+}$. **G1-PLL($(NH_2)_2$($(AcNH)_2$)-N-Progargyl (5):** Yield 4.8 mg (loading: 0.18mmol/g, 56 %), HPLC data: t_R, 7.7 min. MS(ESI^+), calcd $C_{25}H_{45}N_7O_5$: 523.35 Found: m/z 524 $[MH]^+$, 263 $[MH]^{2+}$. IR (ATR) ν 2150 cm-1. **G1-PLL($(NH_2)_2$($(AcNH)_2$)-N-(6-Dansylaminohexyl) (6):**

Yield 1.1 mg (loading: 0.02mmol/g, 67 %), HPLC data: t_R, 15.2 min. MS(ESI^+), calcd $C_{40}H_{67}N_9O_7S$: 817.49 Found: m/z 410 $[MH]^{2+}$.

G1-PLL($(NH_2)_2$($TYKDT)_2$)-N-Dodecyl (7): The FMPB-derivatized resin (200 mg, 0.2 mmol, 1 equiv.), $NaBH_3CN$ (117 mg, 1.86 mmol, 9.28 equiv.) and Dodecylamine (371 mg, 2.0 mmol, 10 equiv.) were suspended in a 5 % AcOH in NMP solution (2.5 mL) and shaken. After 2.5 h, the resin was washed with NMP (4 x 10 mL), DCM (5 x 10 mL), MeOH (2 x 10mL) before air-drying. DNPH test (+). Reaction repeated once with $NaBH_3CN$ (117 mg, 1.86 mmol, 9.28 equiv.) and Dodecylamine (372 mg, 2.0 mmol, 10 equiv.) in a 5 % AcOH in NMP solution (2.5 mL) and shaken. After 1 h, the resin was washed with NMP (4 x 10 mL), DCM (5 x 10 mL) and MeOH (2 x 10 mL) and dried overnight on vacuum. DNPH test (-). Fmoc-Lys(Fmoc)-OH (591 mg, 1.0 mmol, 5 equiv.) and DIC (63 mg, 77 µL, 0.5 mmol, 2.5 equiv.) were suspended in DCM/NMP (9:1, 2 mL) in a falcontube and shaken for 15 min and transferred to the filter syringe containing the BAL-derivatized resin and DCM (2 mL), the suspension was shaken. After 2 h the resin was washed (NMP (4 x 10 mL) and DCM (5 x 10 mL). The reaction was repeated once with Fmoc-Lys(Fmoc)-OH (591 mg, 1.0 mmol, 5 equiv.), and DIC (63 mg, 77 µL, 0.5 mmol, 2.5 equiv.) under the same conditions as before, but without preactivation of the aa. After 2 h the resin was washed (NMP (4 x 10 mL), DCM (2 x 10 mL), and MeOH (2 x 10 mL) and dried overnight on vacuum. Loading was determined on 3 x 5 mg resin by Fmoc quantification to 0.04 mmol/g. Fmoc removal was carried out with piperidine/NMP (1:4) for 3 + 20 min followed by washing of the resin (DCM (5 x 10 mL) and NMP (8 x 10 mL)). Ninhydrin test (+). Fmoc-Lys(Boc)-OH (375 mg, 0.8 mmol, 4 equiv.), PyBOP (417 mg, 0.8 mmol, 4 equiv.) and DIPEA (0.28 mL, 1.6 mmol, 8 equiv.) suspended in NMP (4mL) were added to the filter syringe containing the BAL-derivatized resin and shaken for 2 h, washed (NMP (3 x 10 mL), DCM (3 x 10 mL) and MeOH (2 x 10 mL)) and dried overnight on vacuum. Ninhydrin test (-). Fmoc removal was

carried out with piperidine/NMP (1:4) for 3 + 20 + 30 min followed by washing of the resin (DCM (5 x 10 mL) and NMP (8 x 10 mL)). Ninhydrin test (+). The 5 aa long partial T-cell epitope was anchored to the growing dendron in 5 acylation steps employing 4 equiv. of each aa (starting from Thr-Asp-Lys-Tyr-Thr) with PyBOP (4 equiv.) and DIPEA (8 equiv.) dissolved in NMP (4mL). Each acylation step was shaken at r.t. for 2.5 h and followed by ninhydrin test. In between the acylation steps Fmoc removal was carried out with piperidine/NMP for 3 + 20 + 30 min and followed by ninhydrin test. The resin was treated with TFA/DCM (1:1, 4 mL) and shaken for 2 h at r.t., followed by filtration and collection of the cleavage mixture in a round bottomed flask. Evaporation by N_2 flow and precipitation in cold Et_2O gave the product as a white powder. Yield 6.1 mg (42 %), HPLC data: t_R, 3.4 min., MS(ESI$^+$): calcd $C_{84}H_{143}N_{19}O_{23}$: 1787.07, found: m/z 894.00 $[MH]^{2+}$, 596.68 $[MH]^{3+}$. AAA: calcd: $Lys_5Thr_4Asp_2Tyr_2$, found: $Lys_{4.99}Thr_{4.02}Asp_{2.02}Tyr_{2.00}$

G1-PLL($(NH_2)_2$($TYKDT)_2$)-N-propargyl (8): The BAL-derivatized resin (200 mg, 0.2 mmol, 1 equiv.), $NaBH_3CN$ (126 mg, 2.0 mmol, 10 equiv.), and Propargylamine hydrochloride (183 mg, 2.0 mmol, 10 equiv.) were suspended in a 5 % AcOH in NMP solution (4 mL) and shaken. After 2 h, the resin was washed, NMP (8 x 10 mL) and DCM (5 x 10 mL) before air-drying. DNPH test (-). Fmoc-Lys(Fmoc)-OH (591 mg, 1.0 mmol, 5 equiv.) and DIC (63 mg, 77 µL, 0.5 mmol, 2.5 equiv.) was added directly to the filter syringe containing the BAL-derivatized resin and DCM/NMP (9:1, 4 mL) and shaken. After 2 h the resin was washed, NMP (5 x 10 mL), DCM (5 x 10 mL), and MeOH (2 x 10 mL) and dried overnight on vacuum. The reaction was repeated twice with Fmoc-Lys(Fmoc)-OH (591 mg, 1.0 mmol, 5 equiv.) and DIC (63 mg, 77 µL, 0.5 mmol, 2.5 equiv.) under the same conditions as before. After 2 h the resin was washed, NMP (5 x 10 mL), DCM (5 x 10 mL), and MeOH (2 x 10 mL) and dried on vacuum overnight. Loading was determined on 3 x 5 mg resin by Fmoc quantification to 0.11 mmol/g. The derivatized resin (50 mg, 0.006mmol) was used in a peptide synthesizer

employing 16 equiv. of aa's for the acylation steps with TBTU (0.4M in NMP) and NMM (4M in NMP). Fmoc removal was performed by feeding the peptide synthesizer a solution of piperidine/NMP (1:4). Following the peptide synthesizer the resin was washed with NMP (5 x 2 mL) and DCM (5 x 2 mL) and left to air-dry 1 h on vacuum suction. The resin was treated with TFA/DCM (1:1, 2 mL) and shaken for 2 h, followed by filtration and collection of the cleavage mixture in a round bottomed flask. Evaporation by N_2 flow and precipitation in cold Et_2O gave the product as a white powder. Yield 3.8 mg (44 %), HPLC data: t_R, 0.4-0.6 min. MS(ESI^+), calcd $C_{75}H_{121}N_{19}O_{23}$: 1656.90, found: m/z 828.92 $[MH]^{2+}$, 552.95 $[MH]^{3+}$, 415.22 $[MH]^{4+}$. In the LC-MS another peak is seen for the TFA ester of the dendron at t_R: 1.3-1.4, which can be cleaved by treatment with 0.1M ammonium bicarbonate.

G1-PLL$(GGG)_4$ dendron with C-terminal Dodecyl and Aminohexyl groups, general procedure (III): Resins with G1-PLL $(FmocNH_2)_4$ having C-terminal dodecyl and aminohexyl groups were synthesized according to the above procedure (***I***) leaving out the last deprotection and cleavage steps, and 50 mg of each of these resins were used. Fmoc groups were removed with piperidine/NMP (1:4) for 3 + 20 min followed by washing (DCM (5 x 2 mL), NMP (5 x 2 mL)). Ninhydrin test (+). Fmoc-Gly-Gly-Gly-OH (54 mg, 0.12 mmol, 8 equiv.), PyBOP (61 mg 0.12 mmol, 7.6 equiv.), HOBt (17 mg, 0.12 mmol, 8 equiv.) and DIPEA (41 µL, 0.24 mmol, 15.6 equiv.) were preactivated in NMP (2 mL) for 15 min. and transferred to the filter syringe containing the BAL-derivatized resin and shaken for 16 h, washed (NMP (5 x 2 mL), DCM (5 x 2 mL) and MeOH (1 x 2 mL)). Ninhydrin test (-). Fmoc groups were removed with piperidine/NMP (1:4) for 3 + 20 min followed by washing (DCM (5 x 2 mL), NMP (5 x 2 mL)). Ninhydrin test (+). The resin was treated with TFA/DCM (1:1, 2 mL) and shaken for 2 h, followed by filtration and collection of the cleavage mixture in a round bottomed flask. Evaporation in vacuo and precipitation in Et_2O gave the

product as a white powder. **G1-PLL(GGG)$_4$-N-Dodecyl (9):** Yield 10.0 mg (loading: 0.31 mmol/g, 44%), HPLC data: t_R, 16.3 min. MS(ESI$^+$), calcd $C_{54}H_{99}N_{19}O_{15}$: 1253.76, Found: m/z 628 $[MH]^{2+}$, 419 $[MH]^{3+}$. **G1-PLL(GGG)$_4$-N-(6-aminohexyl) (10):** Yield 8.8 mg (loading 0.31 mmol/g, 44%), HPLC data: t_R, 7.5 min. MS(ESI$^+$), calcd $C_{48}H_{88}N_{20}O_{15}$: 1184.67, Found: m/z 594 $[MH]^{2+}$, 396 $[MH]^{3+}$.

G2-PLL(NH_2)$_8$ dendrons with C-terminal Dodecyl and Aminohexyl groups, general procedure (IV): Resins with G1-PLL (FmocNH_2)$_4$ having C-terminal dodecyl and aminohexyl groups were synthesized according to the above procedure (**I**) without the last deprotection and cleavage steps, and 50 mg of each of these resins were used. Fmoc groups were removed with piperidine/NMP (1:4) for 3 + 20 min followed by washing (DCM (5 x 2 mL), NMP (5 x 2 mL)). Ninhydrin test (+). Fmoc-Lys(Boc)-OH (57 mg, 0.12 mmol, 8 equiv.), PyBOP (60 mg, 0.12 mmol, 7.6 equiv.), HOBt (17 mg, 0.12 mmol, 8 equiv.) and DIPEA (41 µL, 0.24 mmol, 15.6 equiv.) were preactivated in NMP (2 mL) for 5 min and transferred to the filter syringe containing the BAL-derivatized resin and shaken for 16 h, washed (NMP (5 x 2 mL), DCM (5 x 2 mL) and MeOH (1 x 2 mL)). Ninhydrin test (-). Fmoc groups were removed with piperidine/NMP (1:4) for 3 + 20 min followed by washing (DCM (5 x 2 mL), NMP (5 x 2 mL)). Ninhydrin test (+). The resin was treated with TFA/DCM (1:1, 2 mL) and shaken for 2 h, followed by filtration and collection of the cleavage mixture in a round bottomed flask. Evaporation in vacuo and precipitation in Et_2O gave the product as a white powder. **G2-PLL((NH_2)$_8$)-N-Dodecyl (11):** Yield 10.2 mg (loading: 0.31 mmol/g, 31 %), HPLC data: t_R, 14.4 min. MS(ESI$^+$), calcd $C_{54}H_{111}N_{15}O_7$: 1082.56, Found: m/z 542 $[MH]^{2+}$, 362 $[MH]^{3+}$. **G2-PLL((NH_2)$_8$)-N-(6-Aminohexyl) (12):** Yield 13.3 mg (loading: 0.31 mmol/g, 42 %), HPLC data: t_R, 7.5 min. MS(ESI$^+$), calcd $C_{48}H_{100}N_{16}O_7$: 1013.41, Found: m/z 508 $[MH]^{2+}$, 339 $[MH]^{3+}$.

G2-PLL-($(NH_2)_4(AcNH)_4$)- with C-terminal Dodecyl, 6-aminohexyl, Benzyl and Propargyl groups, general procedure (V): Resins with G1-PLL $(FmocNH)_4$ having C-terminal dodecyl, aminohexyl, benzyl and propargyl groups were synthesized according to procedure (**I**) and 50 mg of each of these resins were used for the synthesis of G2 dendrons. Fmoc groups were removed with piperidine/NMP (1:4) for 3 + 20 min followed by washing (DCM (5x), NMP (5x)). Ninhydrin test (+). Fmoc-Lys(Boc)-OH (57 mg, 0.12 mmol, 8 equiv.), PyBOP (60 mg, 0.12 mmol, 7.6 equiv.), HOBt (17 mg, 0.12 mmol, 8 equiv.) and DIPEA (41 µL, 0.24 mmol, 15.6 equiv.) were preactivated in NMP (2 mL) for 5 min and transferred to the filter syringe containing the BAL-derivatized resin and shaken for 16 h, washed (NMP (5 x 2 mL), DCM (5 x 2 mL) and MeOH (1 x 2 mL)). Ninhydrin test (-). Fmoc protection groups were removed with piperidine/NMP (1:4) for 3 + 20 min followed by washing (NMP (5 x 2 mL) and DCM (5 x 2 mL)). The free amino groups were acetylated with a solution (4 mL) of 10 % Ac_2O and 5 % DIPEA in NMP followed by ninhydrin test. The resin was treated with TFA/DCM (1:1, 2 mL) and shaken for 2 h, followed by filtration and collection of the cleavage mixture in a round bottomed flask. Evaporation in vacuo and precipitation in Et_2O gave the product as a white powder. Yields and analytical data: **G2-PLL-($(NH_2)_4(AcNH)_4$)-N-Dodecyl (13):** Yield 11.0 mg (55 %, loading 0.31 mmol/g), HPLC data: t_R, 16.61 min. MS (ESI^+), calcd $C_{62}H_{119}N_{15}O_{11}$: 1250.70, Found: m/z 1252 $[MH]^+$, 626 $[MH]^{2+}$, 418 $[MH]^{3+}$. **G2-PLL($(NH_2)_4(AcNH)_4$)-N-(6-aminohexyl) (14):** Yield 13.5 mg (60 %, loading 0.31 mmol/g), HPLC data: t_R, 7.61 min. MS(ESI^+), calcd $C_{56}H_{108}N_{16}O_{11}$: 1181.56, Found: m/z 592 $[MH]^{2+}$, 395 $[MH]^{3+}$. **G2-PLL($(NH_2)_4(AcNH)_4$)-N-Benzyl (15):** Yield 8.3 mg (35 %, loading 0.39 mmol/g), HPLC data: t_R, 11.35 min. MS(ESI^+), calcd $C_{57}H_{101}N_{15}O_{11}$: 1172.51, Found: m/z 587 $[MH]^{2+}$, 392 $[MH]^{3+}$. **G2-PLL($(NH_2)_4(AcNH)_4$)-N-Progargyl (16):** Yield: 9.2mg (68 %, loading 0.24 mmol/g). HPLC data: t_R, 7.5 min. MS(ESI^+), calcd $C_{53}H_{97}N_{15}O_{11}$:1119.75. Found: m/z 561 $[MH]^{2+}$, 375 $[MH]^{3+}$.

G2-PLL($(NH_2)_4$($(GGG)_4$)-N-Dodecyl (17): 50 mg of the resin with G1-PLL ($FmocNH_2)_4$ having a C-terminal dodecyl group synthesized according to the above procedure (**I**) without the last deprotection and cleavage steps was used. The loading was determined to 0.31 mmol/g. Fmoc groups were removed with piperidine/NMP (1:4) for 3 + 20 min followed by washing (DCM (5 x 2 mL), NMP (5 x 2 mL)). Ninhydrin test (+). Fmoc-Lys(Boc)-OH (57 mg, 0.12 mmol, 8 equiv.), PyBOP (60 mg, 0.12 mmol, 7.6 equiv.), HOBt (17 mg, 0.12 mmol, 8 equiv.) and DIPEA (41 µL, 0.24 mmol, 15.6 equiv.) were preactivated in NMP (2 mL) for 5 min and transferred to the filter syringe containing the BAL-derivatized resin and shaken for 16 h, washed (NMP (5 x 2 mL), DCM (5 x 2 mL) and MeOH (1 x 2 mL)). Ninhydrin test (-). Fmoc protection groups were removed with piperidine/NMP (1:4) for 3 + 20 min followed by washing (NMP (5 x 2 mL) and DCM (5 x 2 mL)). Fmoc-Gly-Gly-Gly-OH (54 mg, 0.12 mmol, 8 equiv.), PyBOP (60 mg, 0.13 mmol, 7.6 equiv.), HOBt (17 mg, 0.12 mmol, 8 equiv.) and DIPEA (43 µL, 0.24 mmol, 15.6 equiv.) were preactivated in NMP (2 mL) for 5 min and transferred to the filter syringe containing the BAL-derivatized resin and shaken for 16 h, washed (NMP (5 x 2 mL), DCM (5 x 2 mL) and MeOH (1 x 2 mL)). Ninhydrin test (-). The resin was treated with TFA/DCM (1:1, 2 mL) and shaken for 2 h, followed by filtration and collection of the cleavage mixture in a round bottomed flask. Evaporation in vacuo and precipitation in Et_2O gave the product as a yellow-reddish powder. Yield 9.9mg (37 %), HPLC data; t_R: 14.5 min. MS(ESI^+), calcd $C_{78}H_{147}N_{27}O_{19}$: 1766.14, Found: m/z 590 $[MH]^{3+}$, 443 $[MH]^{4+}$.

G2-PLL($(NH_2)_4$($(TYKDT)_4$)-N-propargyl (18): The BAL-derivatized resin (200 mg, 0.2 mmol, 1 equiv.), $NaBH_3CN$ (126 mg, 2.0 mmol, 10 equiv.), and Propargylamine hydrochloride (183 mg, 2.0 mmol, 10 equiv.) were suspended in a 5 % AcOH in NMP solution (4 mL) and shaken. After 2 h, the resin was washed, NMP (8 x 10 mL) and DCM (5 x 10 mL) before air-drying. DNPH test (-). Fmoc-Lys(Fmoc)-OH (591 mg, 1.0 mmol, 5 equiv.) and DIC (63 mg, 77 µL, 0.5 mmol, 2.5 equiv.) was added directly

to the filter syringe containing the BAL-derivatized resin and DCM/NMP (9:1, 4 mL) and shaken. After 2 h the resin was washed, NMP (5 x 10 mL), DCM (5 x 10 mL), and MeOH (2 x 10 mL) and dried overnight on vacuum. The reaction was repeated twice with Fmoc-Lys(Fmoc)-OH (591 mg, 1.0 mmol, 5 equiv.) and DIC (63 mg, 77 µL, 0.5 mmol, 2.5 equiv.) under the same conditions as before. After 2 h the resin was washed, NMP (5 x 10 mL), DCM (5 x 10 mL), and MeOH (2 x 10 mL) and dried on vacuum over the weekend. Loading was determined on 3 x 5 mg resin by Fmoc quantification to 0.11 mmol/g. The derivatized resin (50 mg, 0.006mmol) was used in a peptide synthesizer employing 16 equiv. of aa's for the acylation steps with TBTU (0.4M in NMP) and NMM (4M in NMP). Fmoc removal was performed by feeding the peptide synthesizer a solution of piperidine/NMP (1:4). Following the peptide synthesizer the resin was washed with NMP (6 x 10 mL) and DCM (5 x 10 mL) and left to air-dry 1 h on vacuum suction. The resin was treated with TFA/DCM (1:1, 2 mL) and shaken for 2 h, followed by filtration and collection of the cleavage mixture in a round bottomed flask. Evaporation by N_2 flow and precipitation in cold Et_2O gave the product as a white powder. Yield 6 mg (32 %), HPLC data: t_R, 0.3 min. MS(ESI^+), calcd $C_{153}H_{249}N_{39}O_{47}$: 3386.84, found: m/z 1129.55 $[MH]^{3+}$, 847.68 $[MH]^{4+}$. AAA: calcd: $Lys_{11}Thr_8Asp_4Tyr_4$, found: $Lys_{11.39}Thr_{8.09}Asp_{4.24}Tyr_{4.00}$

Selected IR data:

ortho-BAL derivatized resin (polystyrene 1% DVB crosslinked):

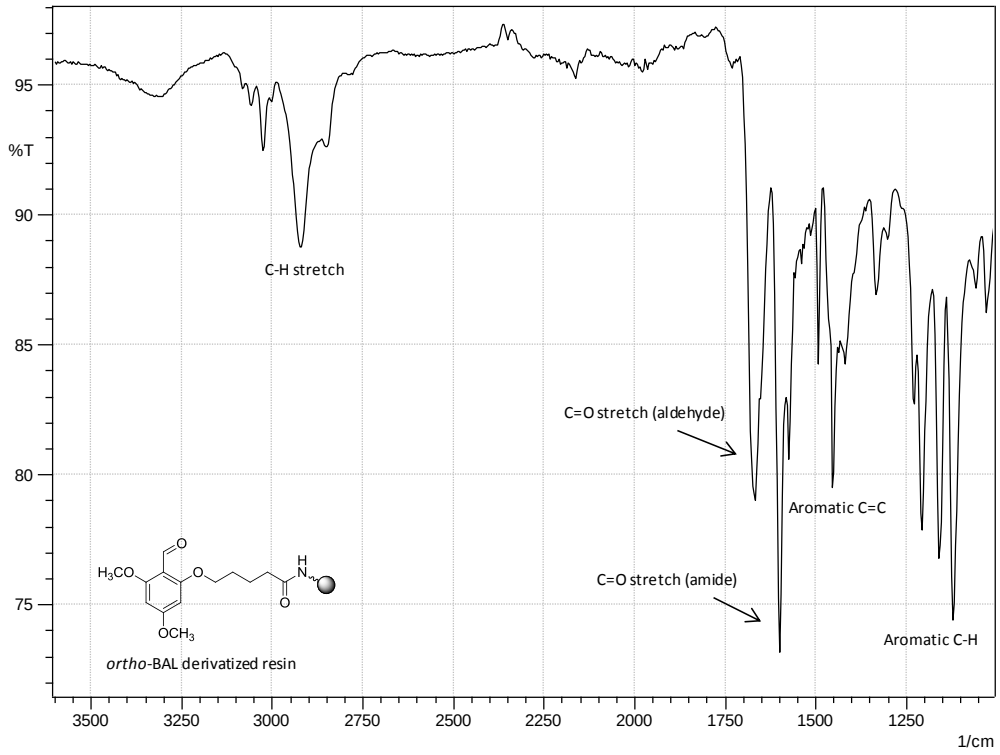

N-Dodecyl *ortho*-BAL derivatized resin (polystyrene 1% DVB crosslinked):

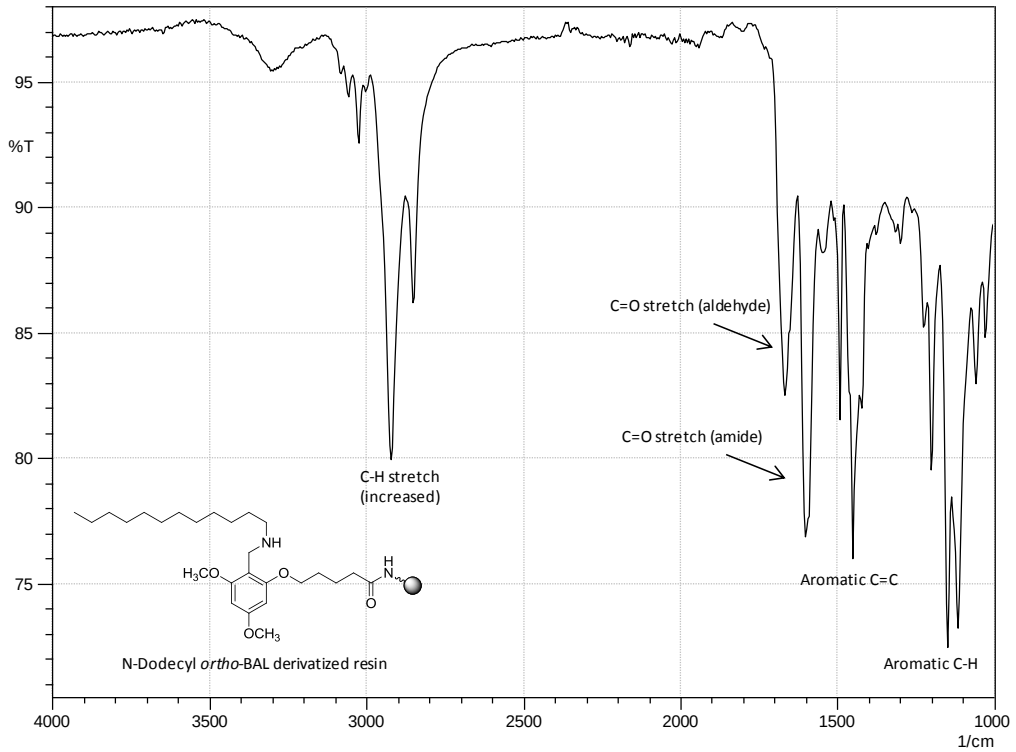

N-(6-Bocaminohexyl) *ortho*-BAL derivatized resin (polystyrene 1% DVB crosslinked):

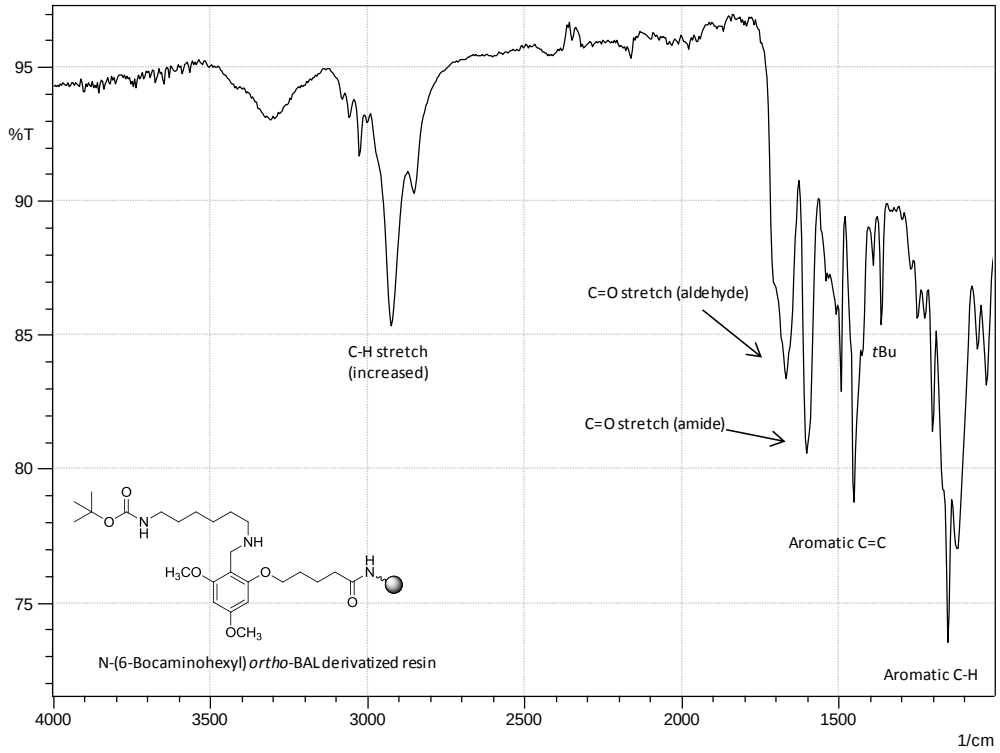

N-Propargyl *ortho*-BAL derivatized resin (polystyrene 1% DVB crosslinked):

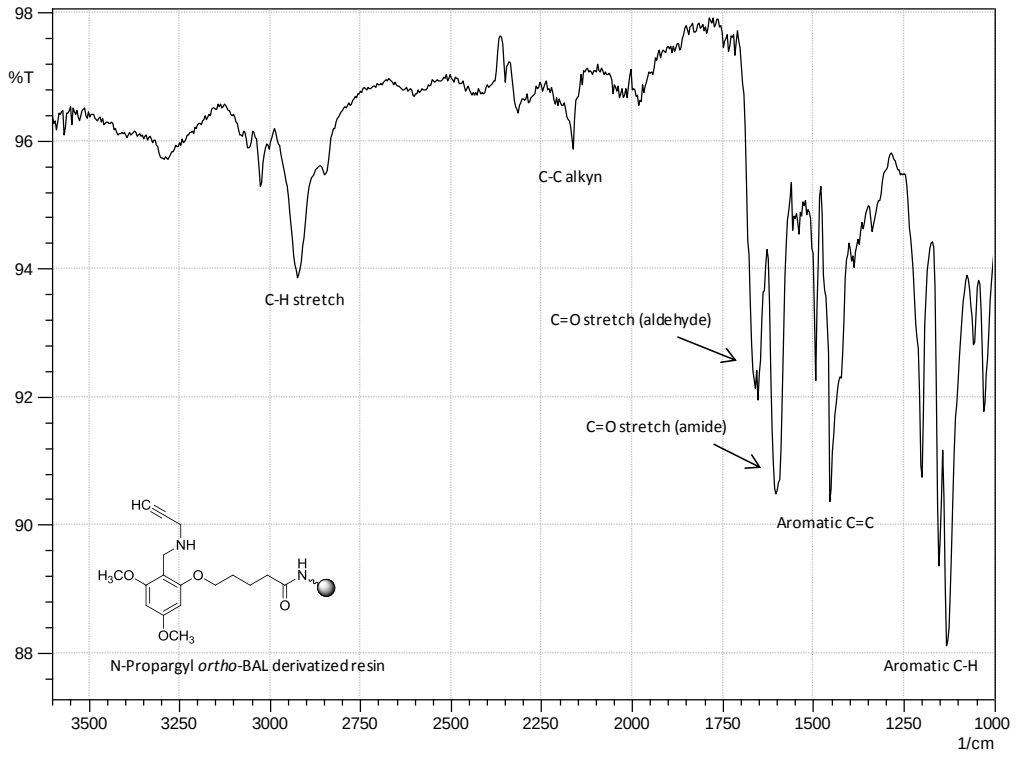

FMPB derivatized resin (rigid macroporous polystyrene, 10% DVB crosslinked):

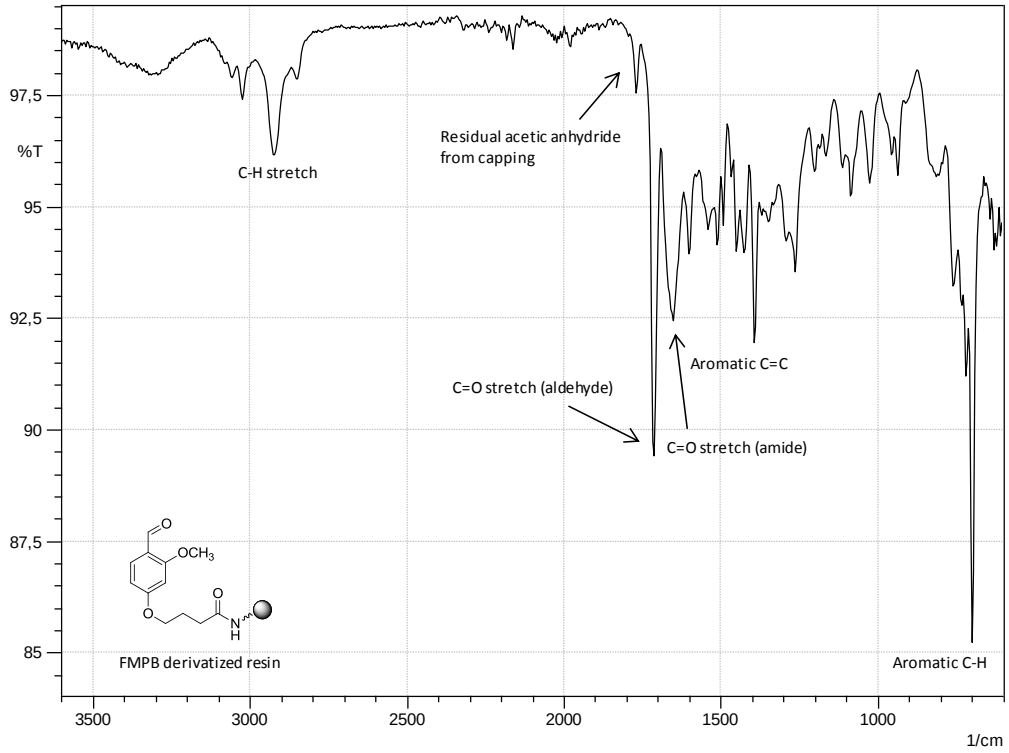

N-Dodecyl FMPB derivatized resin (rigid macroporous polystyrene, 10% DVB crosslinked):

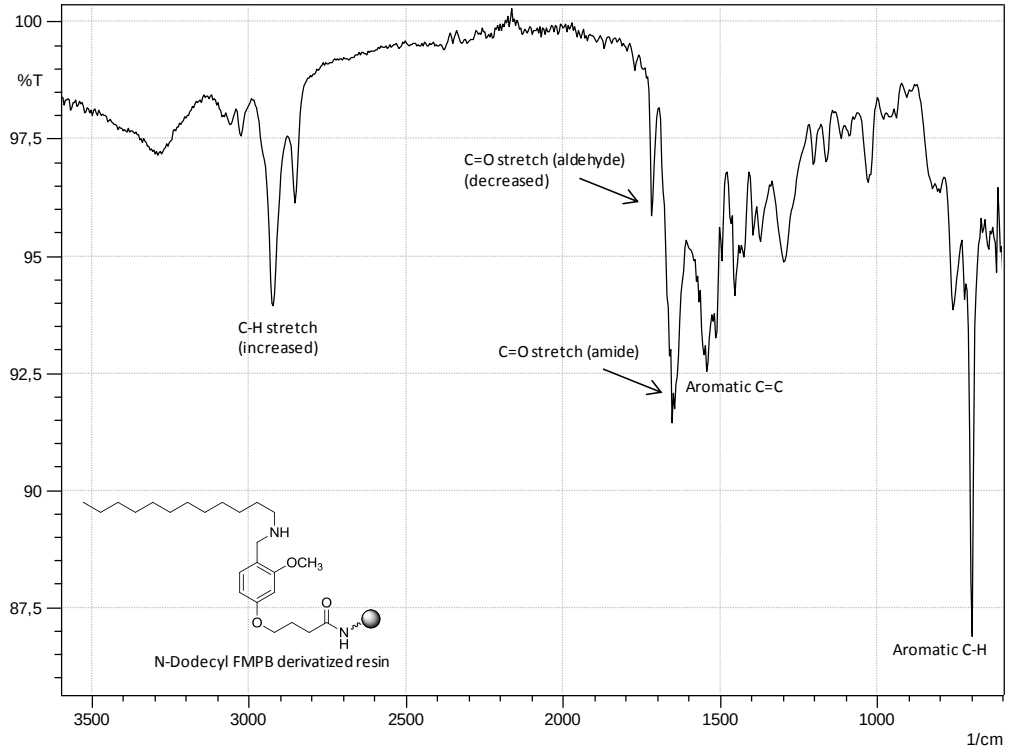

para-BAL derivatized resin (rigid macroporous polystyrene, 10% DVB crosslinked):

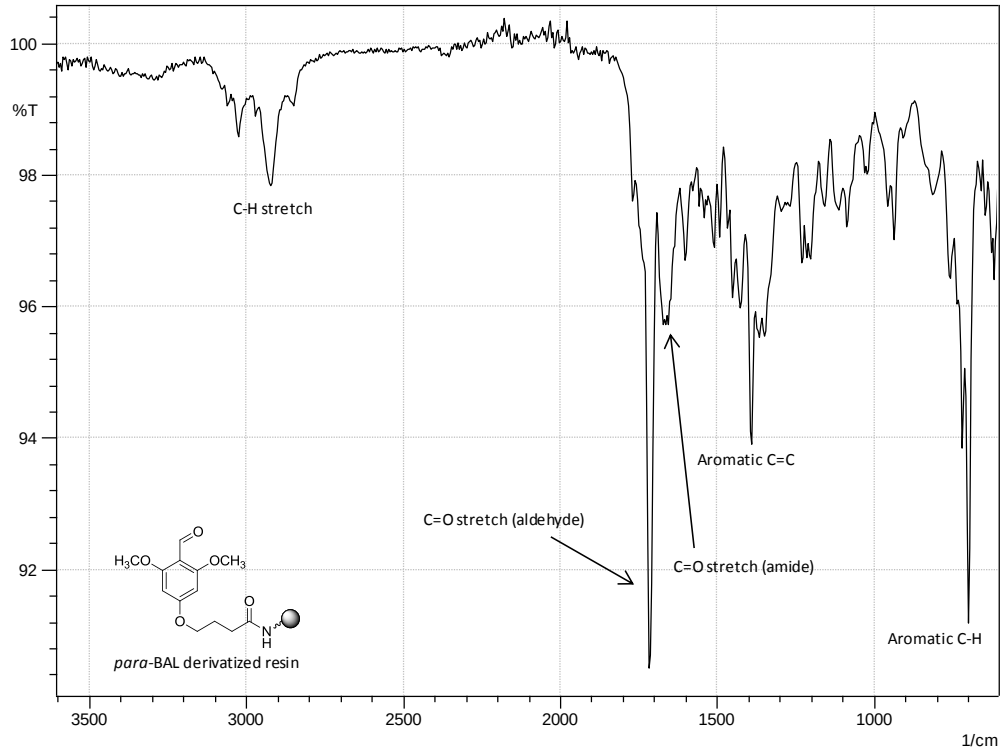

N-Dodecyl *para*-BAL derivatized resin (rigid macroporous polystyrene, 10% DVB crosslinked):

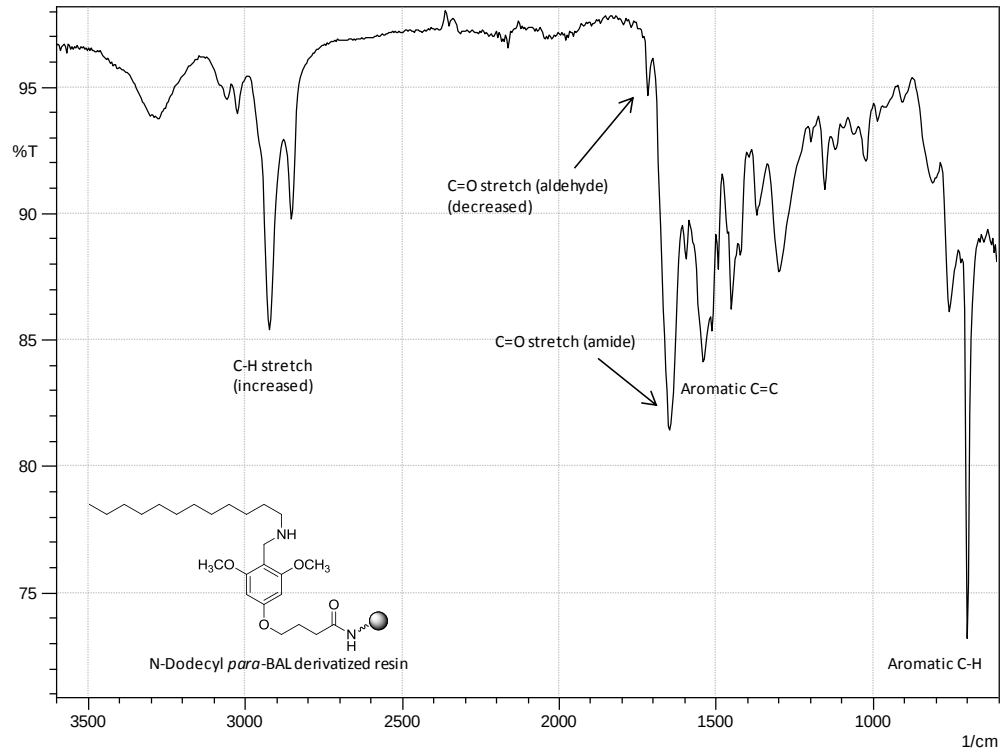

HPLC-MS data on crude products:

G1-PLL($(NH_2)_4$)-N-Dodecyl (1):

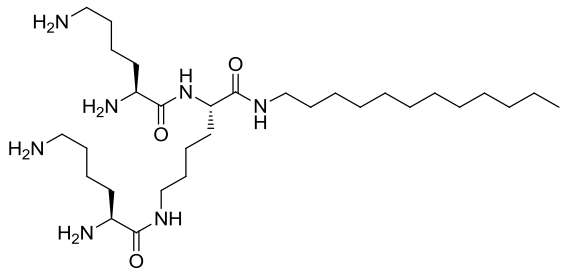

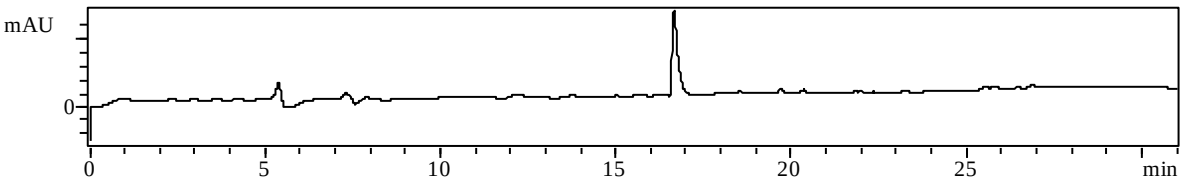

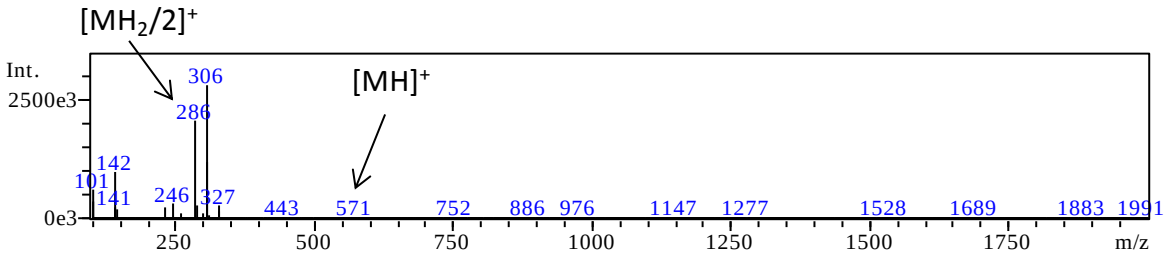

G1-PLL($(NH_2)_4$)-N-(6-Aminohexyl) (2):

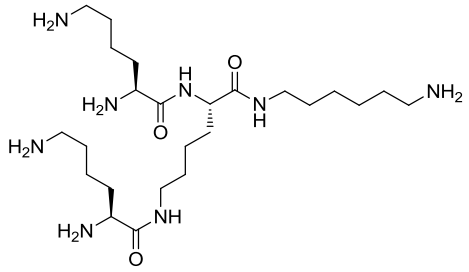

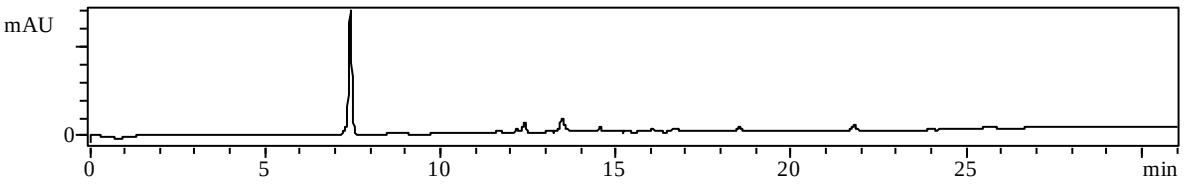

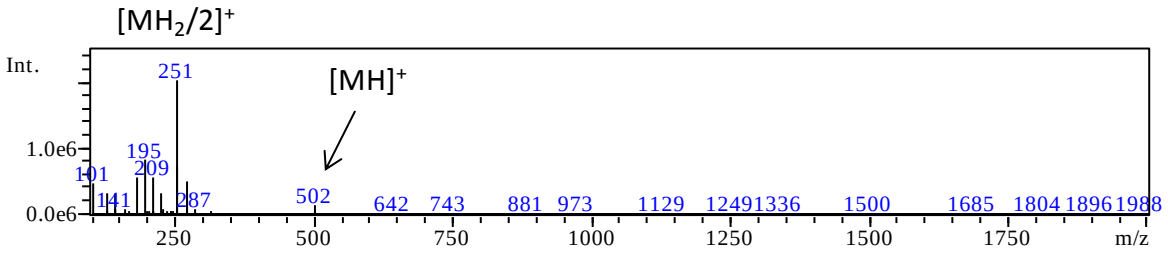

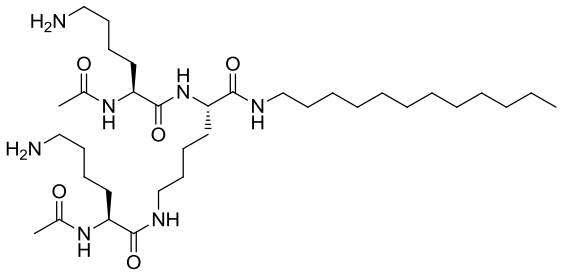

G1-PLL($(NH_2)_2$ $(AcNH)_2$)-N-Dodecyl (3):

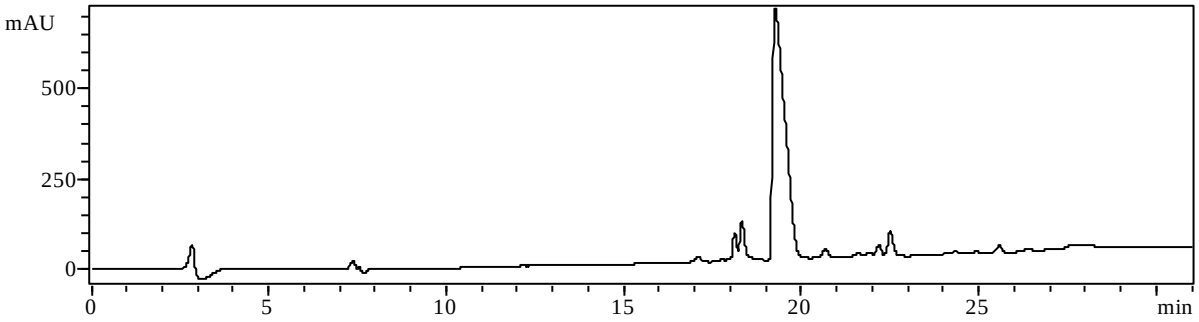

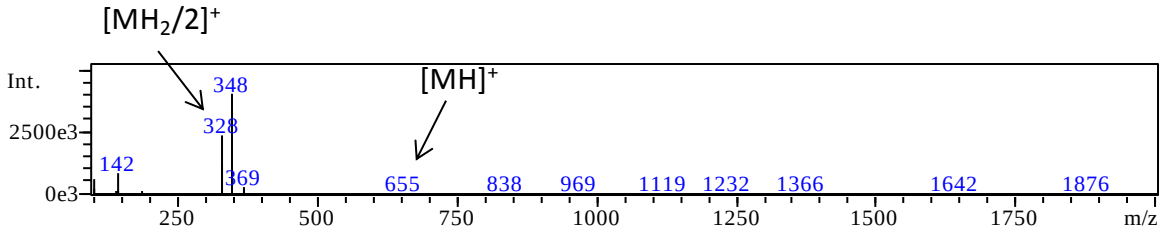

G1-PLL($(NH_2)_2$ $(AcNH)_2$)-N-(6-Aminohexyl) (4):

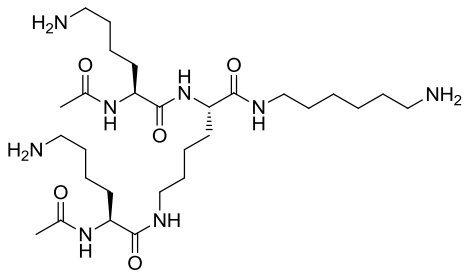

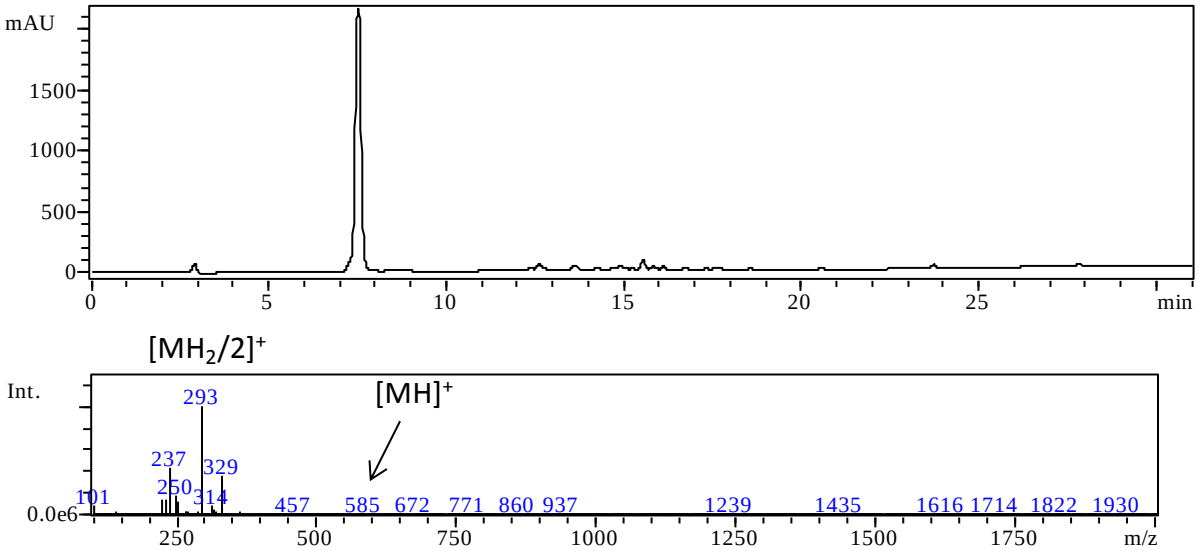

G1-PLL(NH_2)$_2$ (AcNH)$_2$)-N-Propargyl (5):

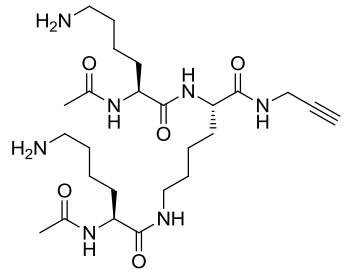

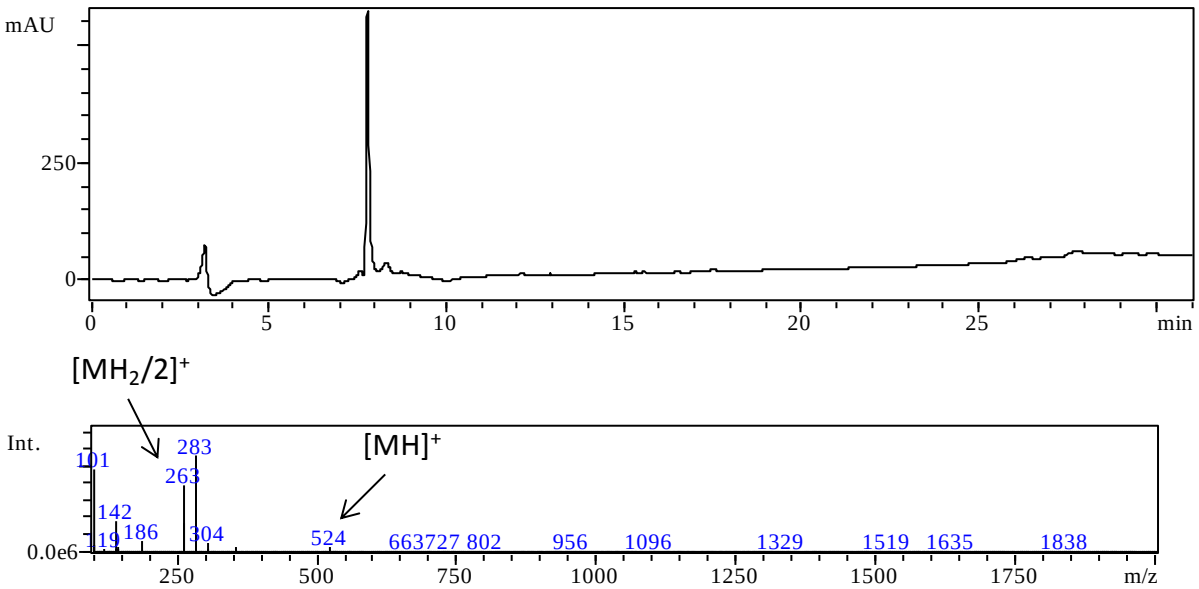

G1-PLL($(NH_2)_2$ $(AcNH)_2$)-N-(6-Dansylaminohexyl) (6):

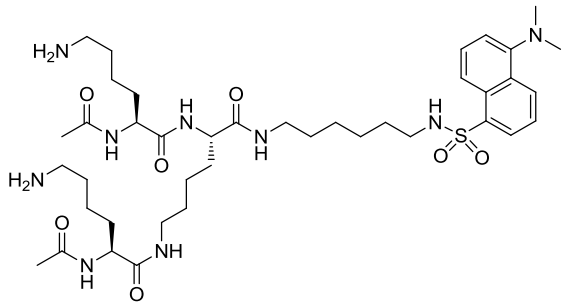

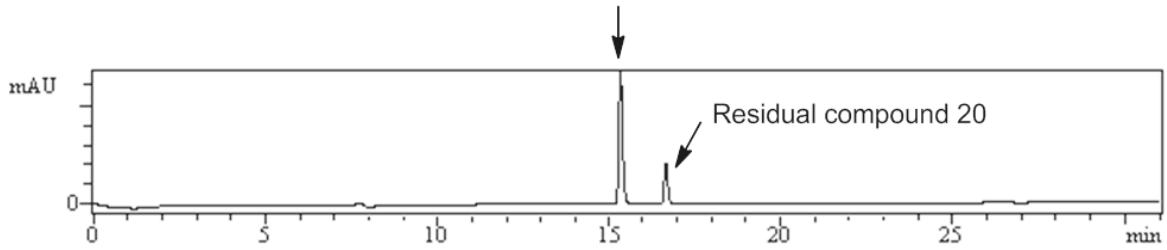

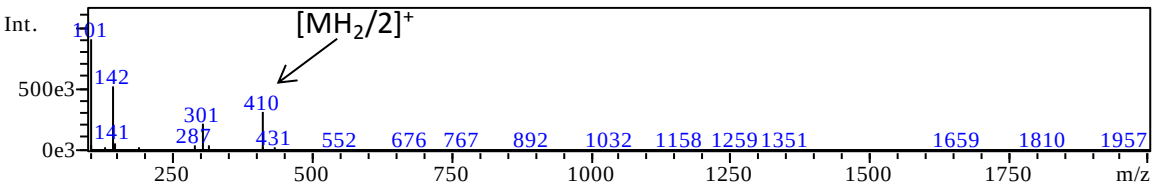

G1-PLL($(NH_2)_2$($TYKDT)_2$)-N-Dodecyl (7), manual synthesis:

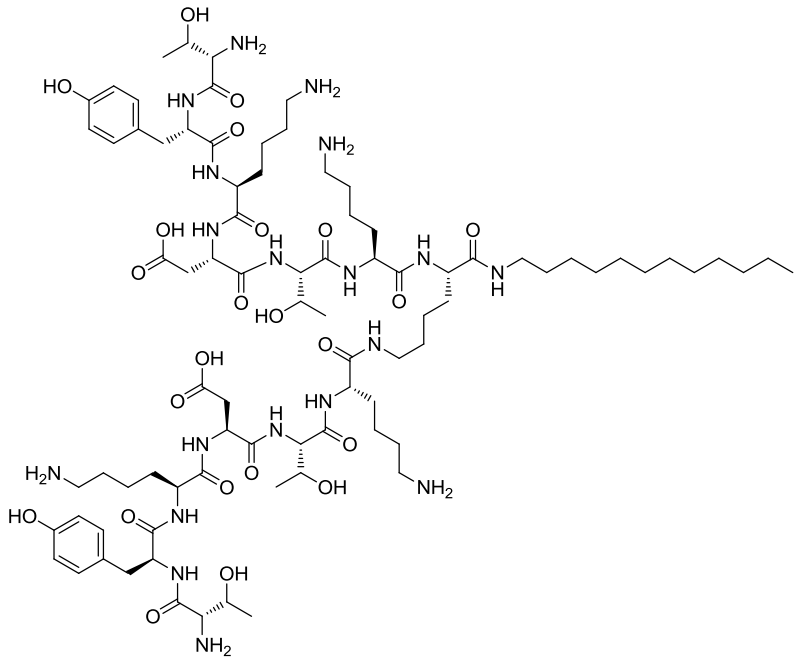

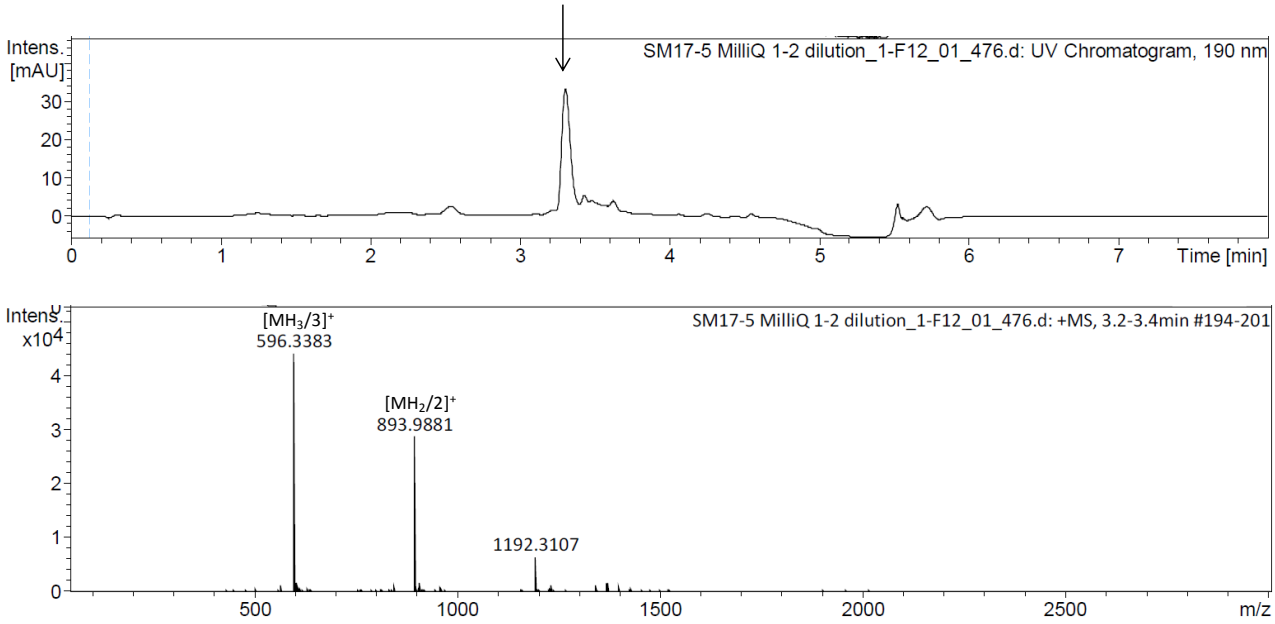

HPLC performed on MilliQ water for measurement of the background:

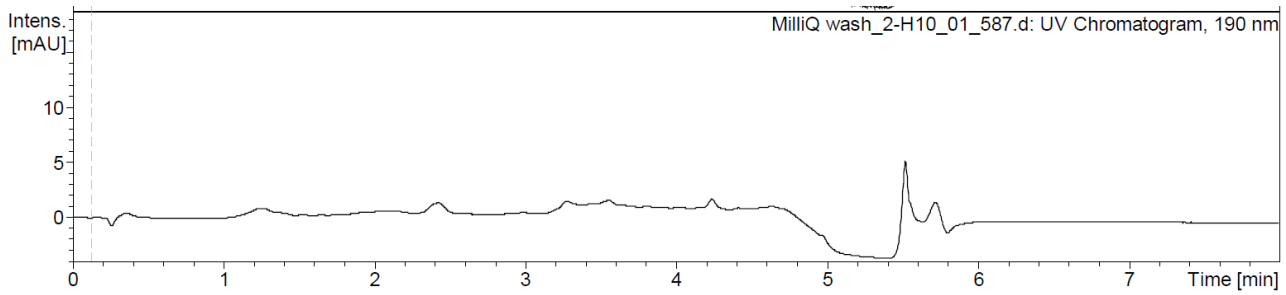

Amino acid analysis of (7) (calcd.: $Lys_5Thr_4Asp_2Tyr_2$, found: $Lys_{4.99}Thr_{4.02}Asp_{2.02}Tyr_{2.00}$):

Peak Results

	Name	RT	nmol/injvol.	mol%	ug prot./injvol.	Height	Area
1	Asp	10.86	3.573	15.50	0.411	772774	28957671
2	Thr	12.82	7.115	30.87	0.719	1783854	61295303
3	Ser	14.26					
4	Glu	17.02					
5	Pro	18.88					
6	Gly	22.46					
7	Ala	23.89					
8	TPCys	25.53					
9	Val	27.85					
10	Met	29.86					
11	Ile	31.43					
12	Leu	32.47					
13	Tyr	34.39	3.539	15.35	0.578	715313	25655352
14	Phe	35.46					
15	His	45.01					
16	Lys	50.59	8.825	38.28	1.131	1644446	53547547
17	Arg	57.21					
Sum			23.051		2.839		

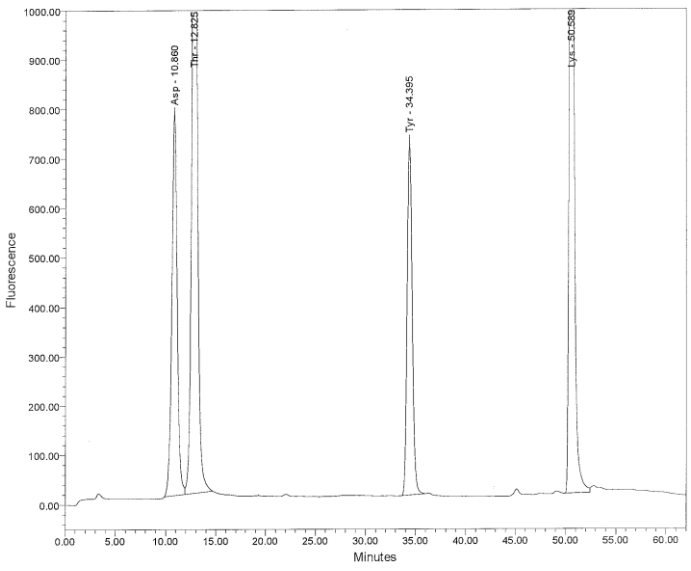

G1-PLL($(NH_2)_2$($TYKDT)_2$)-N-Dodecyl (7), automated synthesis:

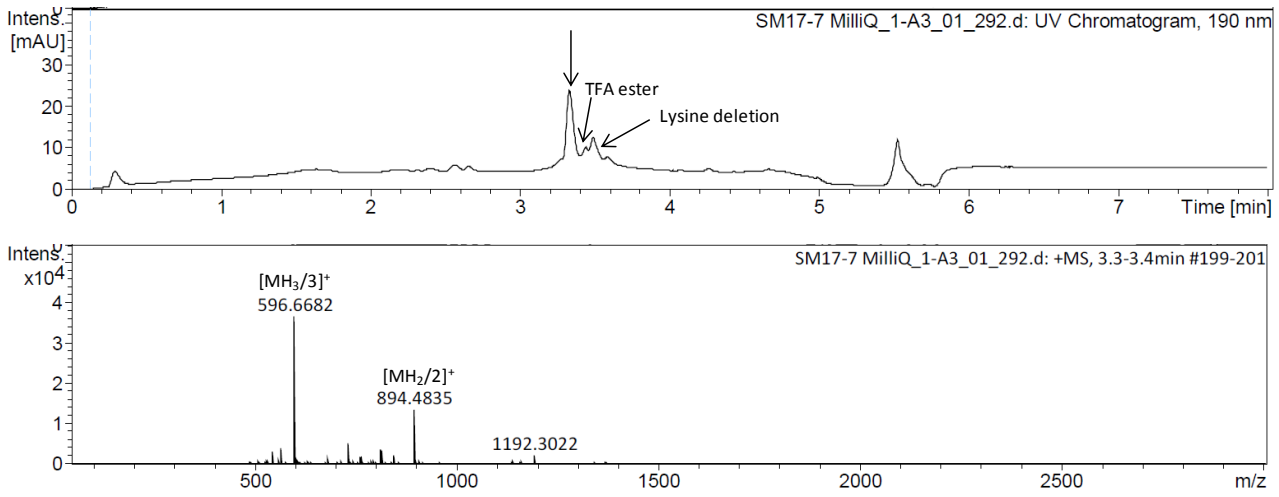

G1-PLL($(NH_2)_2$($TYKDT)_2$)-N-Propargyl (8), automated synthesis:

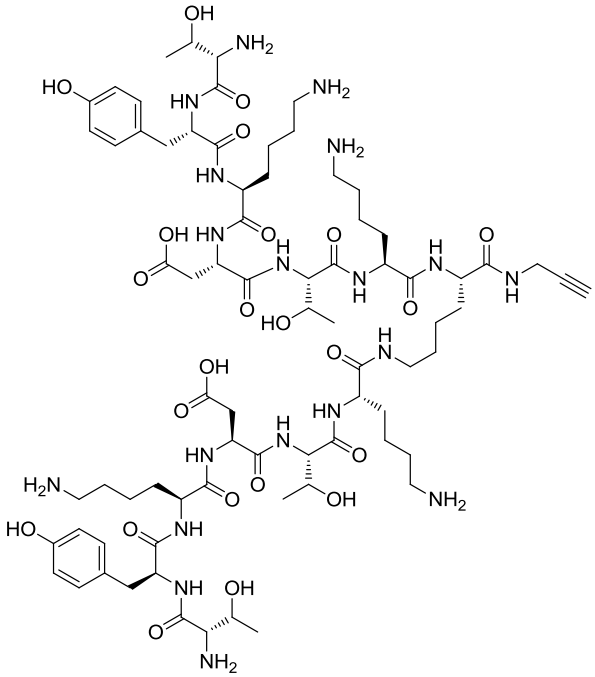

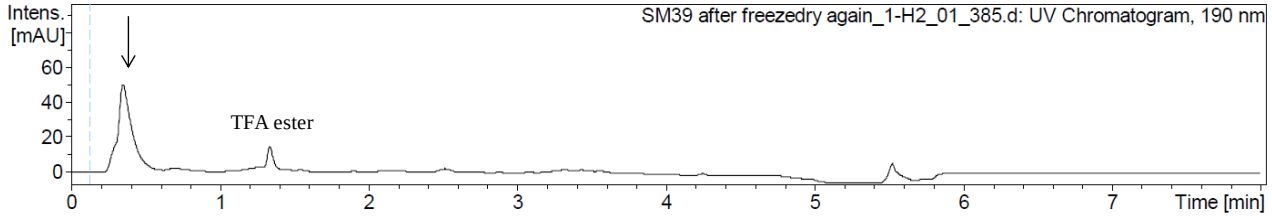

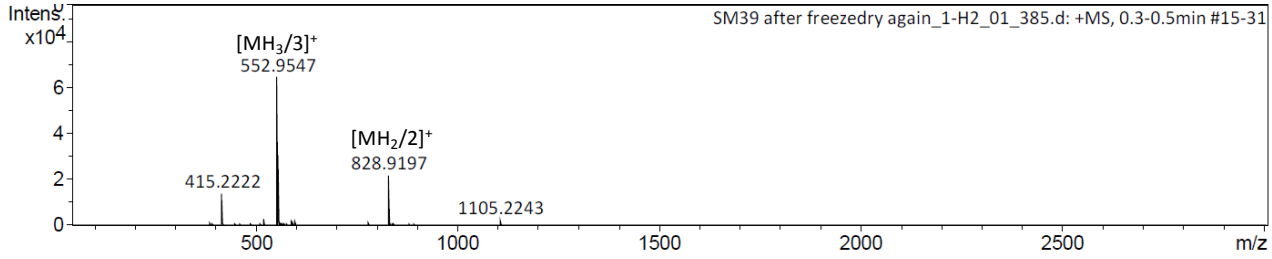

G1-PLL(GGG)$_4$-N-Dodecyl (9):

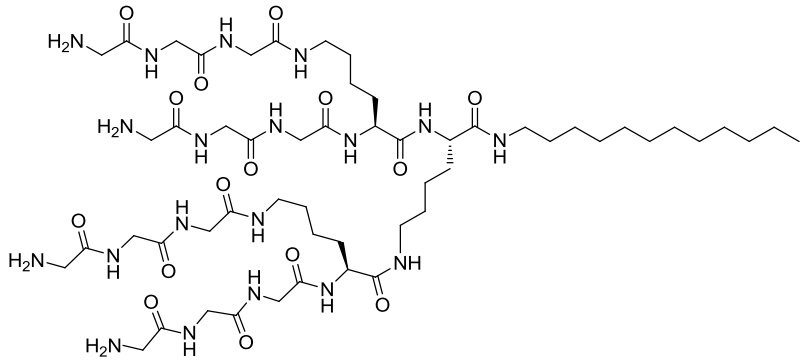

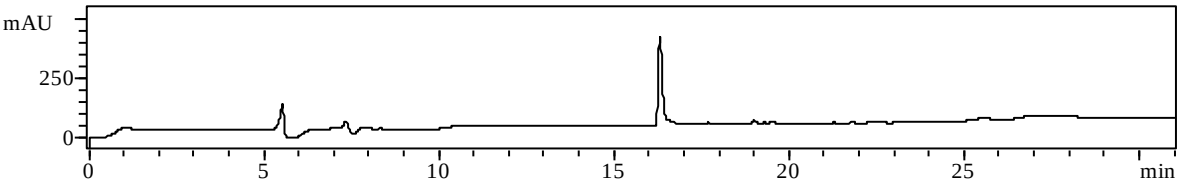

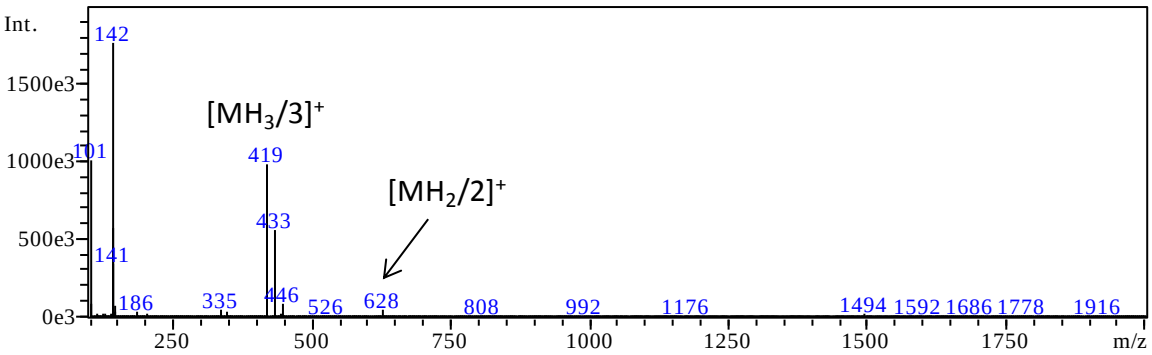

G1-PLL(GGG)$_4$-N-(6-Aminohexyl) (10):

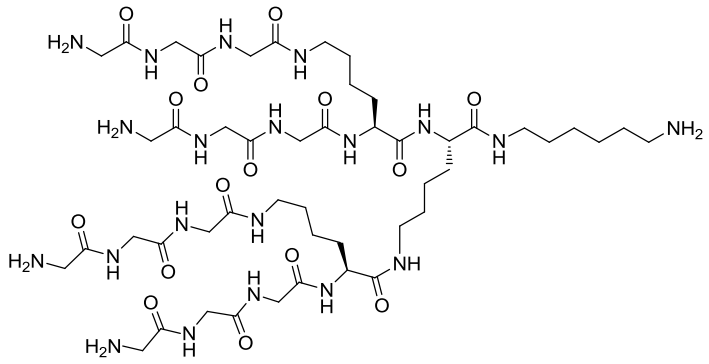

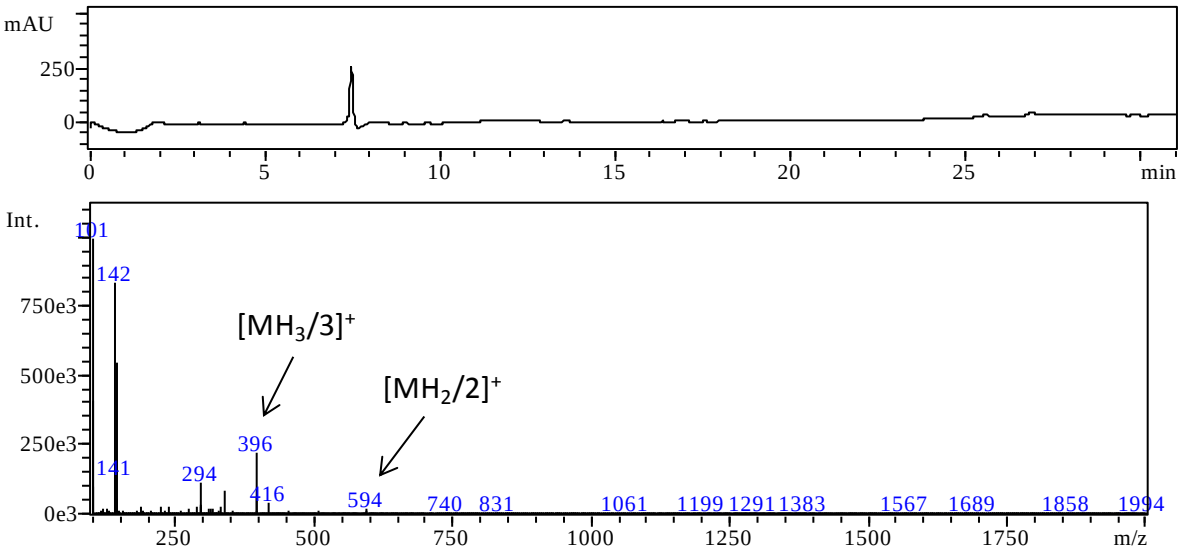

G2-PLL((NH$_2$)$_8$)-N-Dodecyl (11):

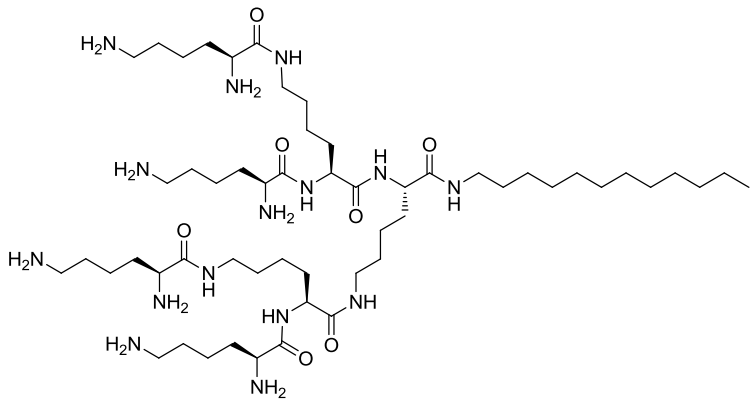

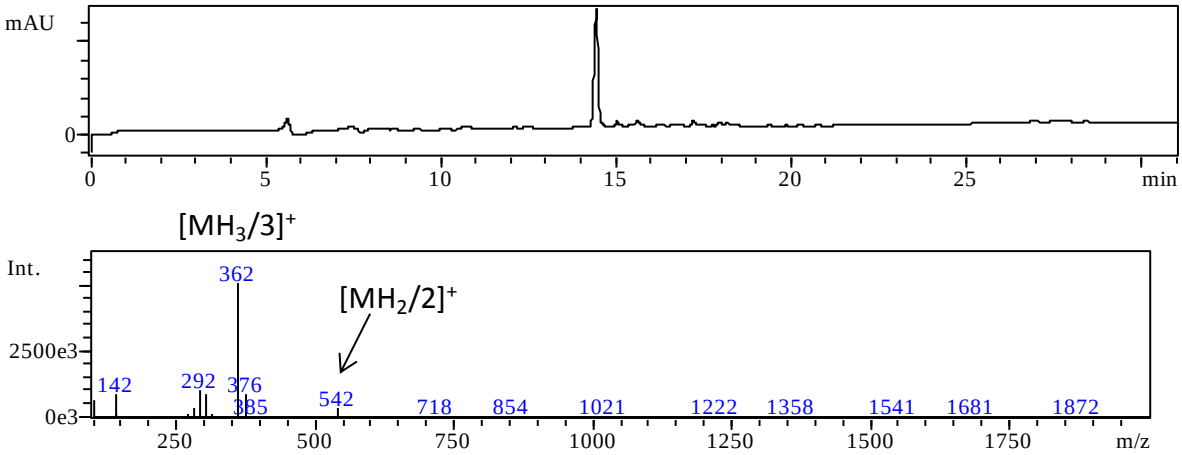

G2-PLL($(NH_2)_8$)-N-(6-Aminohexyl) (12):

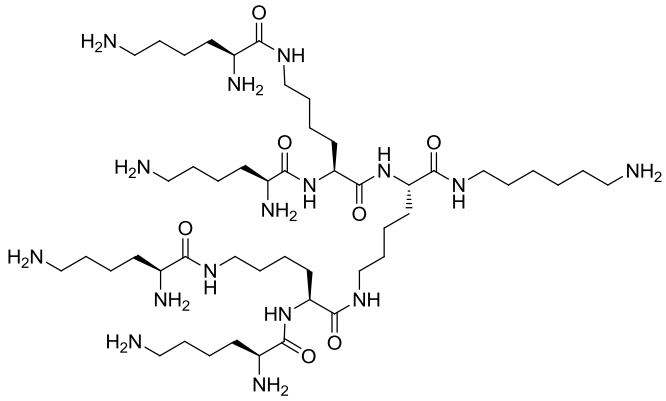

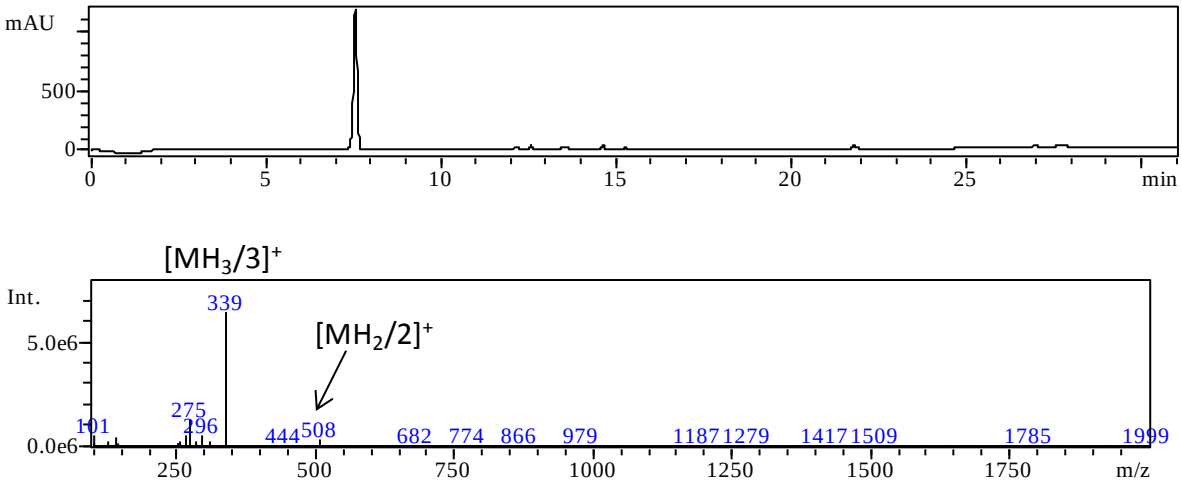

G2-PLL($(NH_2)_4(AcNH)_4$)-N-Dodecyl (13):

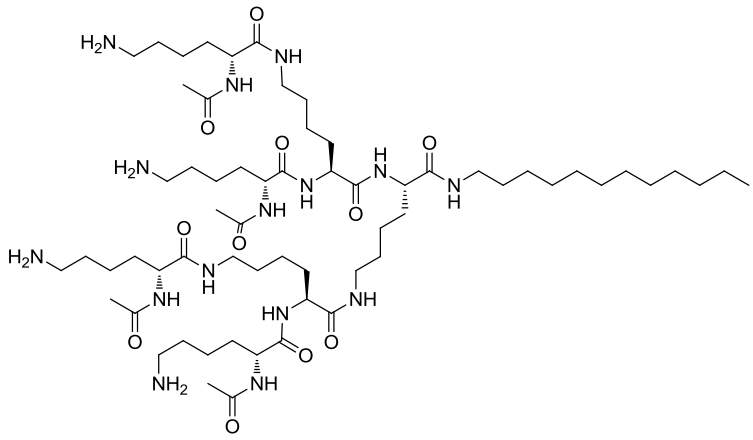

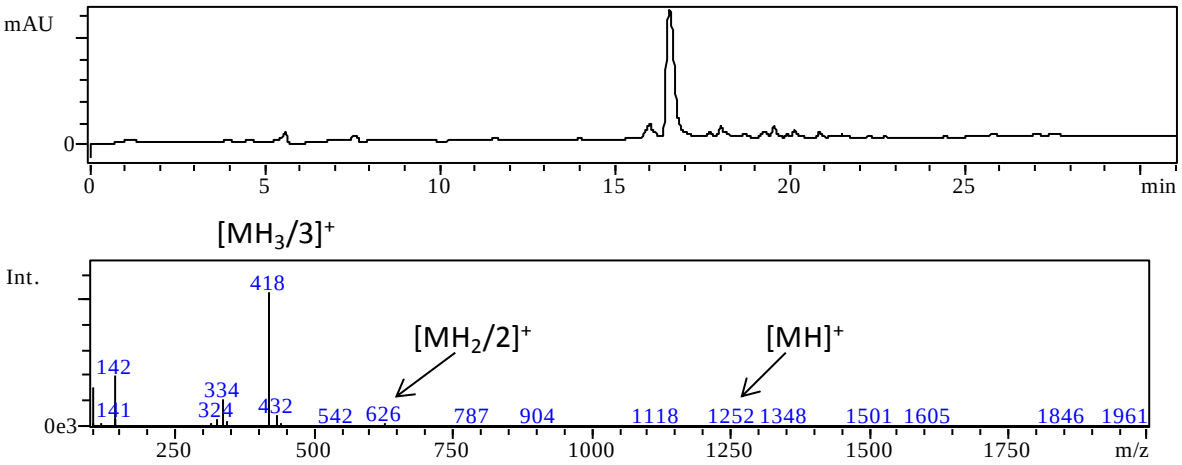

G2-PLL($(NH_2)_4(AcNH)_4$)-N-(6-Aminohexyl) (14):

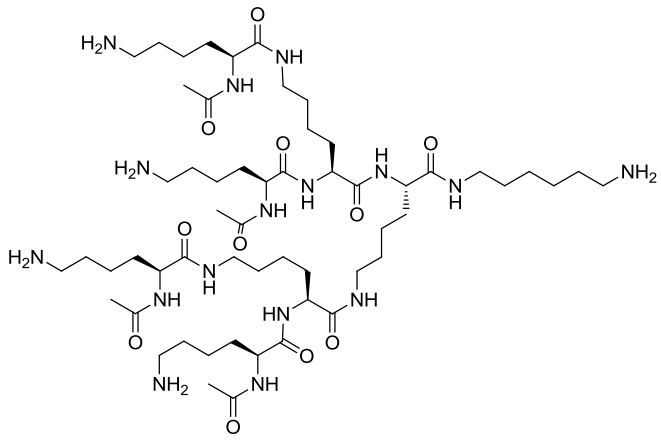

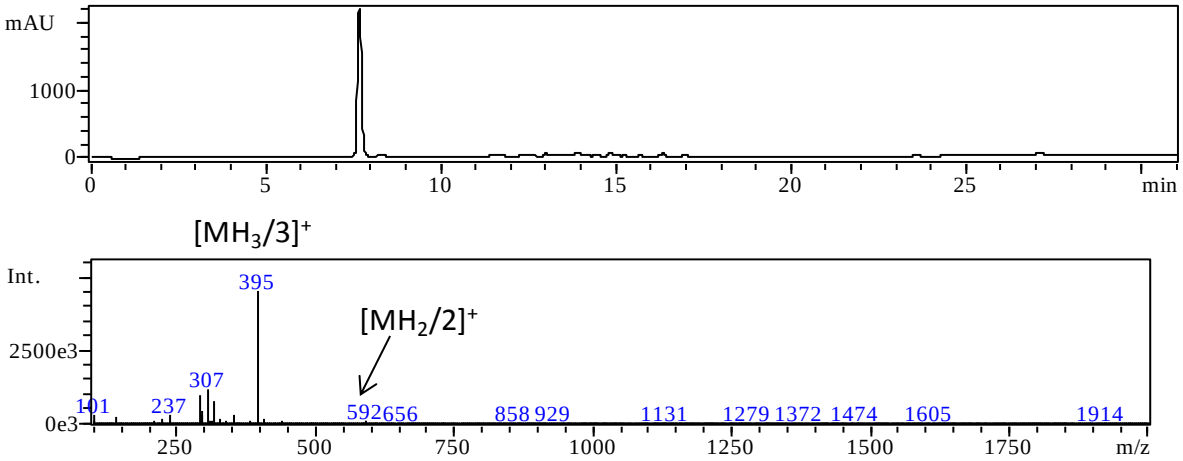

G2-PLL($(NH_2)_4(AcNH)_4$)-N-Benzyl (15):

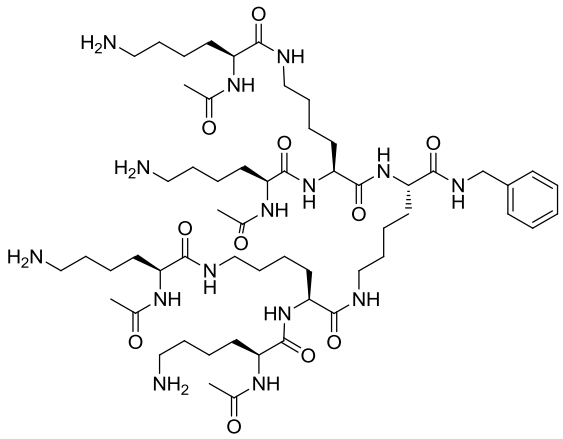

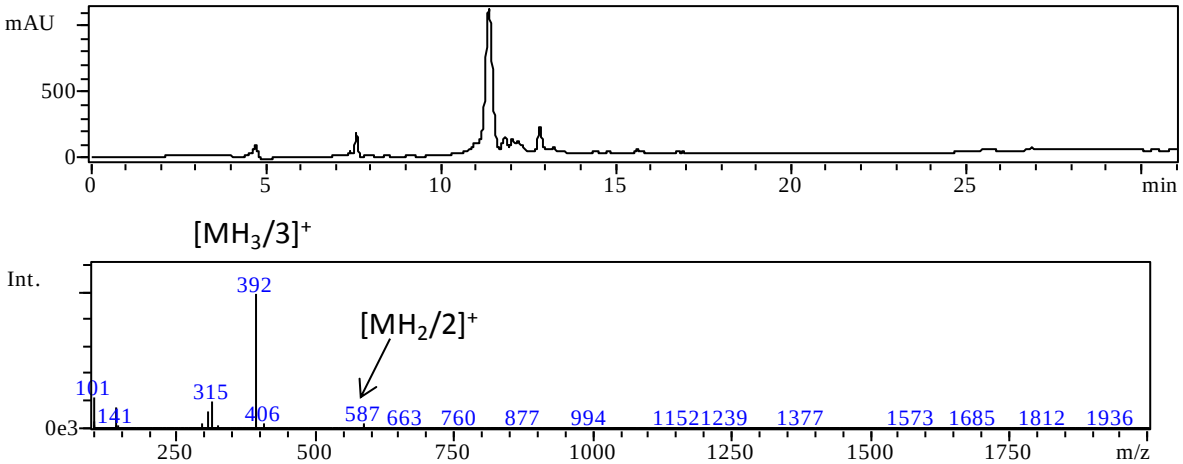

G2-PLL((NH$_2$)$_4$(AcNH)$_4$)-N-Propargyl (16):

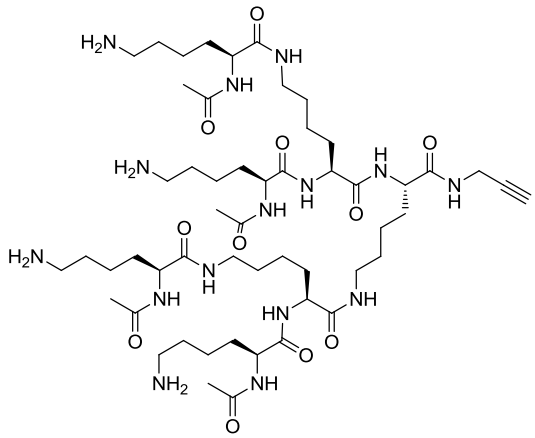

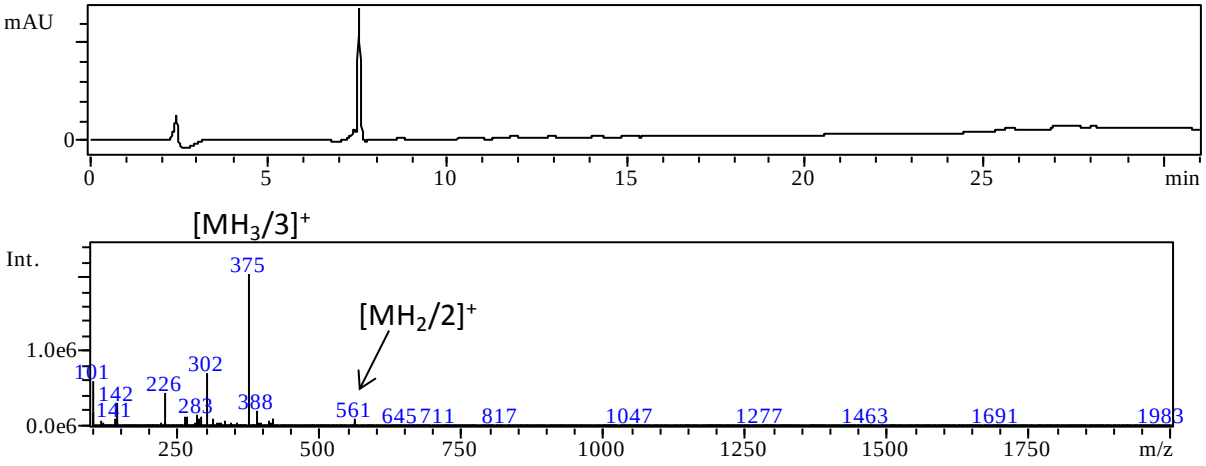

G2-PLL((NH$_2$)$_4$(GGG)$_4$)-N-Dodecyl (17):

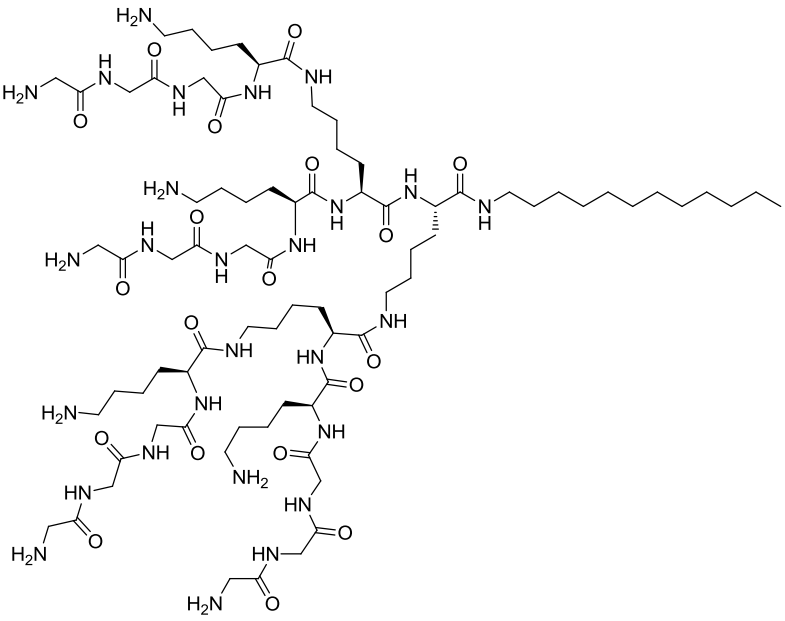

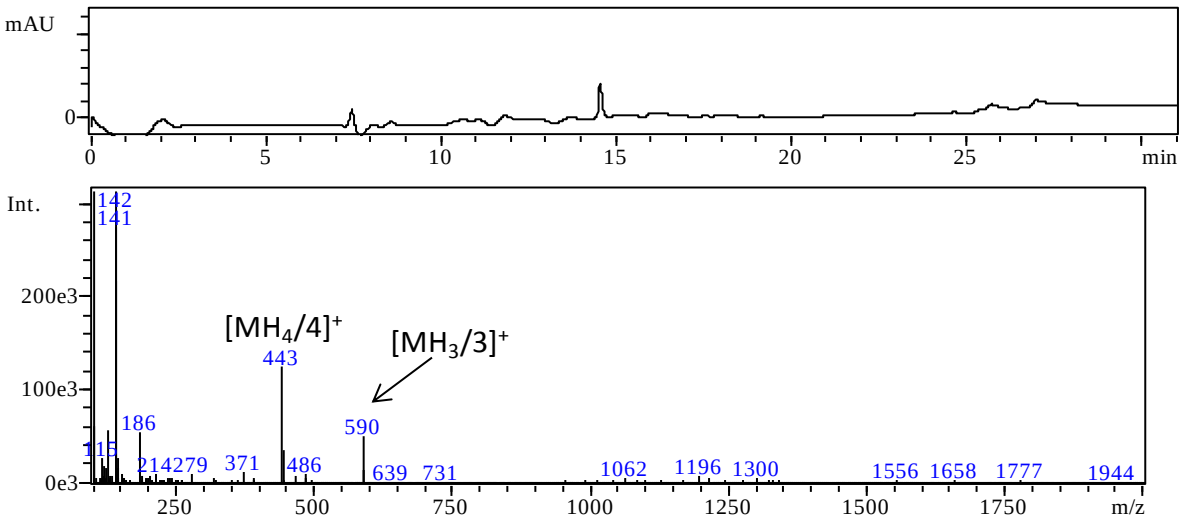

G2-PLL($(NH_2)_4$(TYKDT)$_4$)-N-Propargyl (18), automated synthesis:

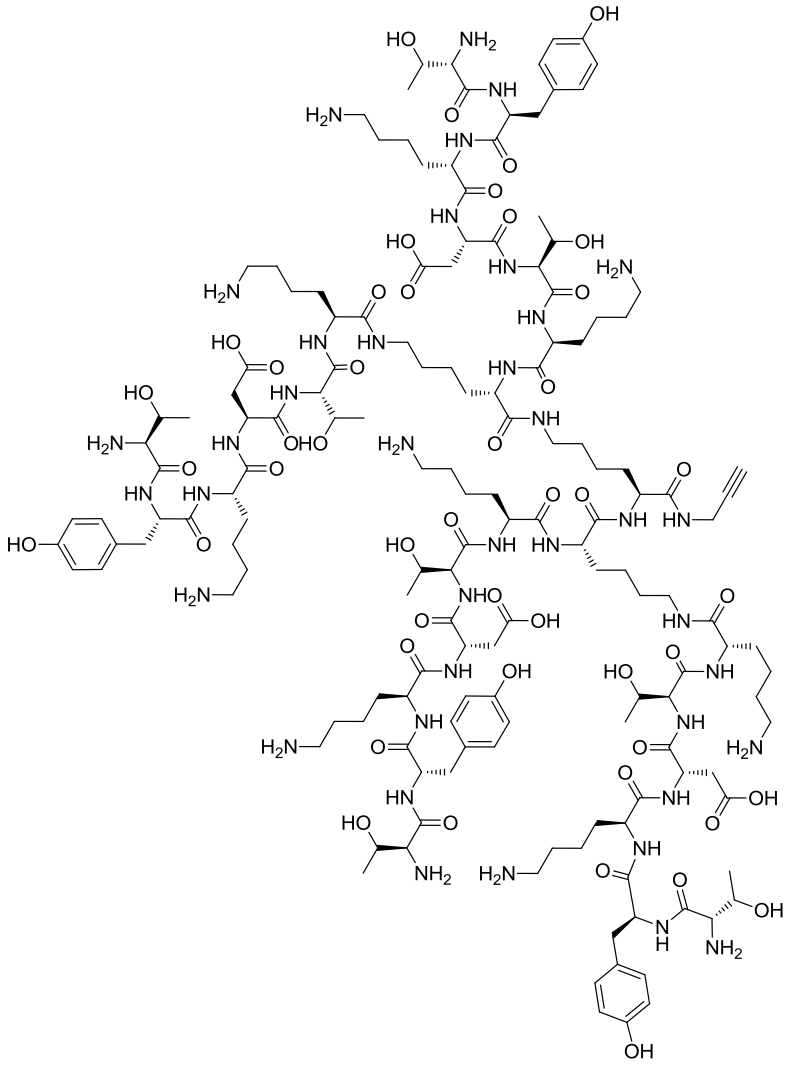

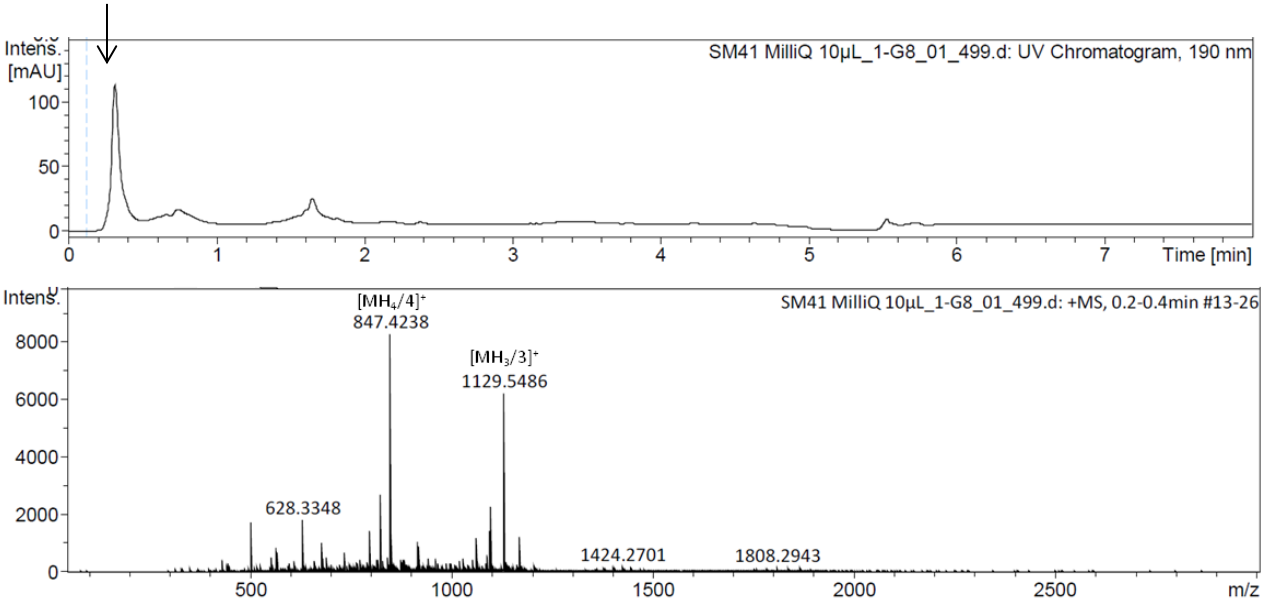

Amino acid analysis of (18) (calcd.: $Lys_{11}Thr_8Asp_4Tyr_4$, found: $Lys_{11.39}Thr_{8.09}Asp_{4.24}Tyr_{4.00}$):

Peak Results

	Name	RT	nmol/injvol.	mol%	ug prot./injvol.	Height	Area
1	Asp	10.84	2.315	15.29	0.266	492573	18761472
2	Thr	12.86	4.419	29.18	0.447	1071354	38066899
3	Ser	14.26					
4	Glu	17.02					
5	Pro	18.88					
6	Gly	22.46					
7	Ala	23.89					
8	TPCys	25.53					
9	Val	27.85					
10	Met	29.86					
11	Ile	31.43					
12	Leu	32.47					
13	Tyr	34.45	2.186	14.43	0.357	442544	15846172
14	Phe	35.46					
15	His	45.01					
16	Lys	50.56	6.225	41.10	0.798	1173360	37771447
17	Arg	57.21					
Sum			15.144		1.868		

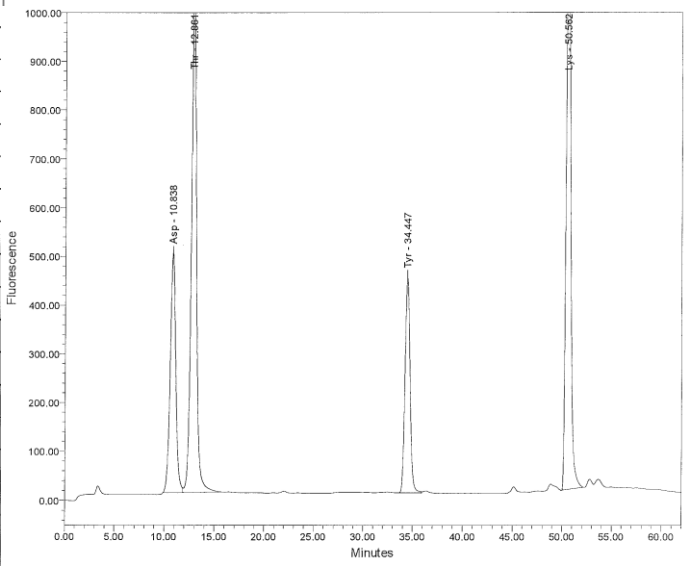

1-N-Dansyl-6-N-Boc-diaminohexane (19)

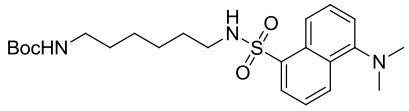

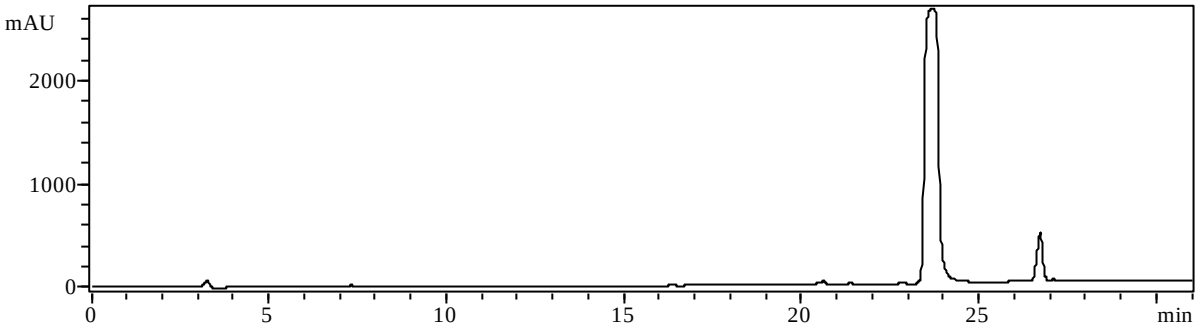

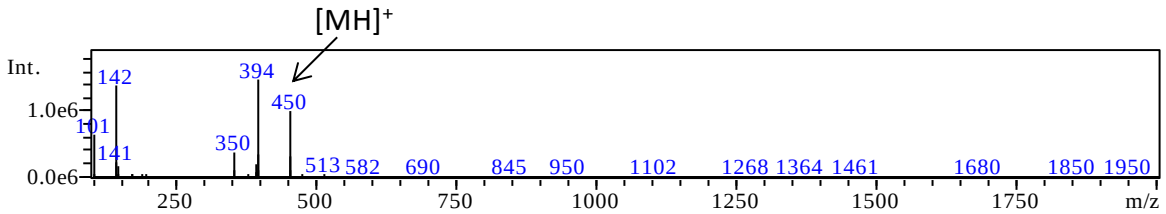

1-N-Dansyl-6-diaminohexane (20):

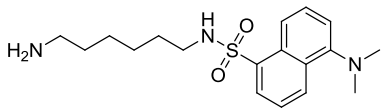

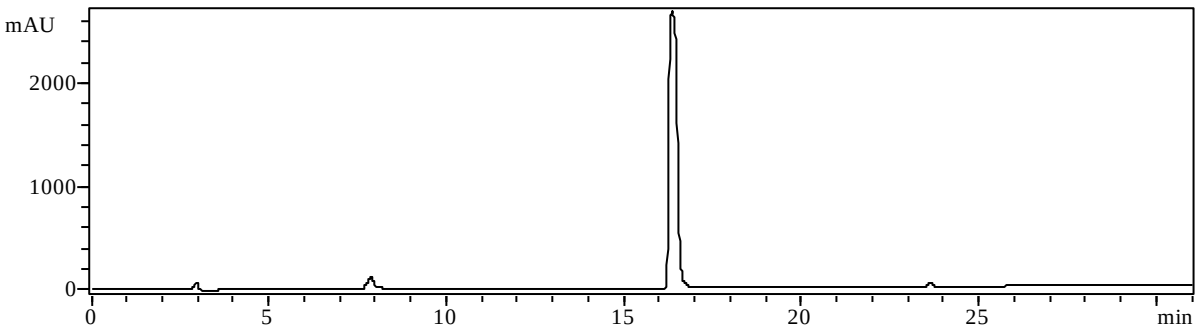

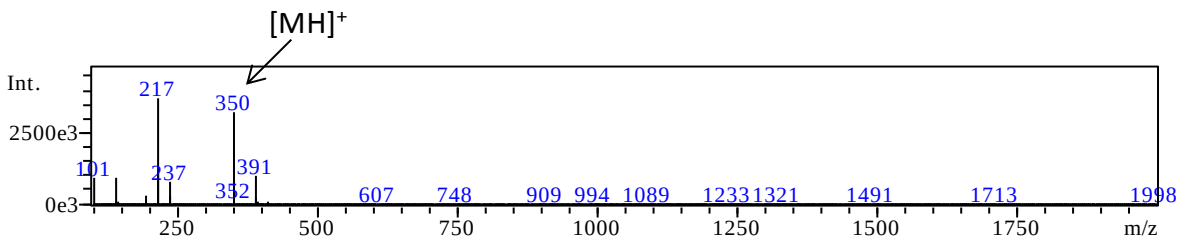

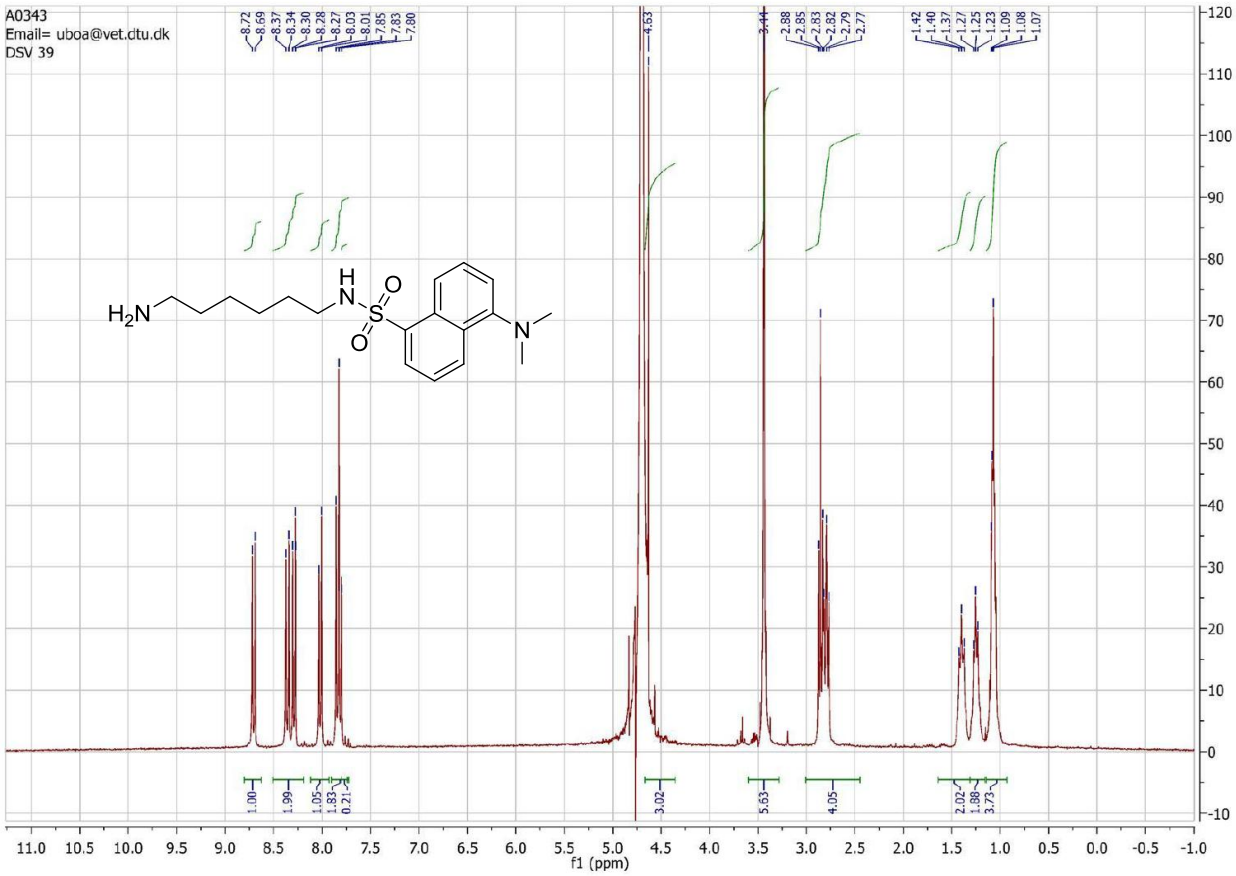
A0343
Email= uboa@vet.dtu.dk
DSV 39
8.72
8.69
8.37
8.34
8.30
8.28
8.27
8.03
8.01
7.85
7.83
7.80
4.63
3.44
2.88
2.85
2.83
2.82
2.79
2.77
1.42
1.40
1.37
1.27
1.25
1.23
1.09
1.08
1.07
1.00
1.99
1.05
1.83
0.21
3.02
5.63
4.05
2.02
1.88
3.73
H
N
O
S
O
H_2N
N
f1 (ppm)

Organic LETTERS

Letter

pubs.acs.org/OrgLett

Color Test for Selective Detection of Secondary Amines on Resin and in Solution

Ulrik Boas* and Sahar Mirsharghi

The National Veterinary Institute, Technical University of Denmark. Department of Immunology and Vaccinology, Bülowsvej 27, DK-1870, Frederiksberg, Denmark

DTU Center for Nanomedicine and Theranostics, Technical University of Denmark, Building 345Ø, DK-2800, Kgs. Lyngby, Denmark

Supporting Information

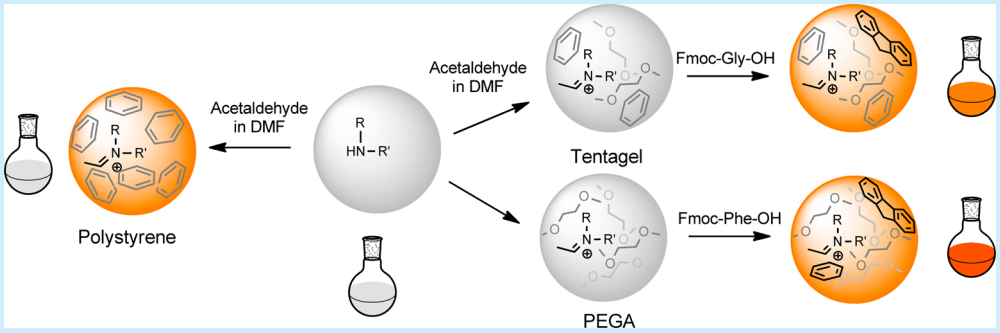

ABSTRACT: Resins for solid-phase synthesis give orange to red-brown resin beads selectively when secondary amines are present on the resin when treated with a solution of acetaldehyde and an Fmoc-amino acid in NMP. The method shows good specificity and gives colorless beads when exposed to a variety of other functional groups. Furthermore, the acetaldehyde/Fmoc amino acid method can be used as a selective colorimetric test for secondary amines in solution.

Amines are important functional groups in synthesis, both in solution and on solid phase. In solid-phase synthesis, direct spectroscopic "on-resin" analysis of amines is limited and a variety of colorimetric methods have been developed to monitor the presence and transformation of amines during the course of the solid-phase synthesis.[1] For the visualization of primary amines, the ninhydrin test developed by Kaiser has found extensive use both in solid-phase peptide synthesis (SPPS) and in solid-phase organic chemistry (SPOC).[2] Later, reported methods for the colorimetric visualization of amines on solid phase involve the use of dyes such as 1-methyl-2-(4′-nitrophenyl)-imidazol[1,2-*a*]pyrimidinium perchlorate (DESC) which form orange to red colored beads in the presence of primary and secondary amines as well as thiols.[3] Other methods involve the use of trinitrobenzenesulfonic acid (TNBSA),[4] substituted naphthoquinones, and 4-*N*,*N*′-dimethylaminoazobenzene-4-isothiocyanate (DABITC) which detect both primary and secondary amines.[5,6] Also nondestructive "reversible" colorimetric monitoring methods for primary, secondary amines and thiols have been reported.[7] The isatin test is the hitherto only reported method for the selective detection of secondary amino acid residues (proline) on solid phase.[8] A single paper by Feigl and Anger[9] reported that acetaldehyde combined with sodium nitroprusside could selectively detect secondary amines in solution, and the method was used for quantitative analysis of secondary amines as well. Here, the authors reported that the color of the solution faded out after a few minutes.[10] A method which has been extensively applied for the visualization of both primary and secondary amines on solid phase is the chloranil method which is performed by adding two drops of a 2% acetaldehyde in DMF followed by the addition of two drops of 2% chloranil in DMF. Applying DMF as solvent instead of toluene increases the sensitivity of the chloranil test.[11,12] As our research involves the formation of various secondary amine intermediates on solid phase in the synthesis of peptides by the backbone amide linker strategy[13,14] we wanted to implement the chloranil test as a versatile test to visualize the presence and reaction of secondary amines on the resin. Whereas the chloranil test has no selectivity between primary and secondary amines, we surprisingly found that, upon adding only one of the test solutions, 2% acetaldehyde in DMF, onto a secondary amine substrate on polystyrene resin (Table 1, entry 3), the resin changed color within 3−5 min at room temperature resulting in orange to dark red resin beads. Upon exposing a primary amine resin to the acetaldehyde solution, no color change of the beads was observed (Table 1, entry 7). To investigate whether this was a general phenomenon or only specific for *N*-methylamine substrates we applied the test to other secondary amine substrates and found a similar color change. In some cases, e.g. with long chain

Received: October 4, 2014
Published: October 31, 2014

dx.doi.org/10.1021/ol502936d | *Org. Lett.* 2014, 16, 5918−5921

Table 1. Micrographs of the Acetaldehyde Test Selectivity toward Different Functional Groups on Polystyrene Beads[15]

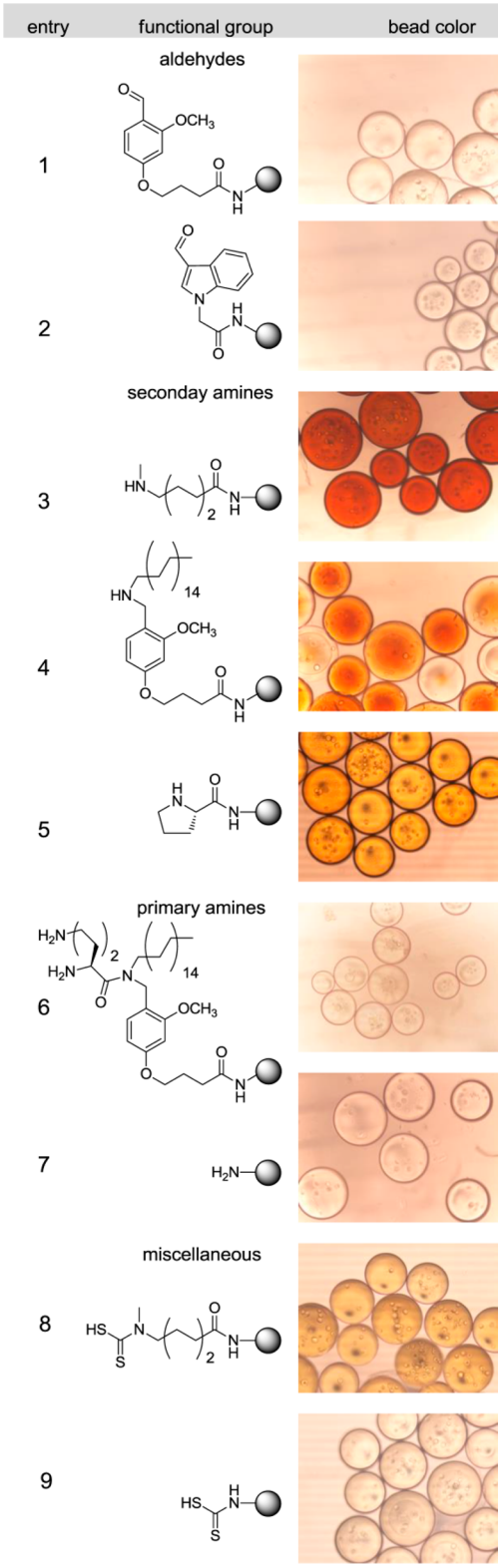

alkyl amine substrates, the color change was somewhat slower and needed 5 min for proper visualization (Table 1, entry 4).

To evaluate the applicability of the method to differentiate between primary and secondary amino acids we conjugated Fmoc-protected lysine,[15,16] proline (Table 1, entry 5), and alanine[15,16] to aminomethylated polystyrene. Performing the acetaldehyde test on the Fmoc-protected amino acids resulted in colorless beads,[16] whereas the unprotected amino acids, the proline secondary amine, gave a positive reaction displaying orange colored beads. Here, the acetaldehyde test proved useful as a complementary test to the Kaiser test for primary amines (Figure 1).

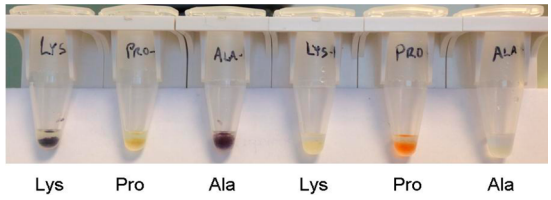

Figure 1. Analysis of primary and secondary amino acids on polystyrene resin. (Left) Ninhydrin test detecting primary amines on lysine and alanine (blue colored beads), but giving weakly yellow beads with proline. (Right) "Acetaldehyde test" detecting the secondary amine on proline (orange colored beads) but giving colorless beads with primary amino acids.

As a reference, we investigated several solvents for the solution of acetaldehyde with NMP and THF, which gave similar results.[17] Also different batches of acetaldehyde and polystyrene resins gave the same effect.

The specificity of the test was investigated on a variety of substrates synthesized on solid phase (Figure 1). The type of polystyrene resin resulted in minor differences in the color, where the 1% DVB polystyrene resin gave orange to deep red colors and the rigid macroporous polystyrene gave a more brown-red coloration of the beads. We found that it was necessary to quench the reaction by washing the resin beads with NMP; otherwise colorless beads gradually turned orange upon standing overnight. When the color reaction was quenched both positive and negative test samples could be stored at room temperature without alteration of their color. In comparison, colored resin beads from a positive Kaiser test gradually lost their color upon standing. Upon derivatization of the primary amine with carbon disulfide to form the corresponding dithiocarbamate, the acetaldehyde test showed a negative result (Table 1, entry 9).

However, upon formation of the dithiocarbamate of the secondary amine (Table 1, entry 8) the acetaldehyde test gave a weak positive readout. This is an indication that it is not the nucleophilic dithiocarbamate that gives a positive reaction but merely its decomposition to the (secondary) amine and carbon disulfide.

Acylation of secondary amines to form substituted amides gave colorless beads in the test (Table 1, entry 6). After having observed that the formation of Schiff base adducts between acetaldehyde and secondary amines does not give rise to colored products in solution we investigated the utility of the test on other types of resins by derivatizing PEGA and Tentagel (TG) resins with proline. On these resins we did not observe any color change specific to the presence of secondary amines.[18] The resins changed color upon heating for a few minutes; however, this coloration was unspecific and presumably due to decomposition of the resin. This indicates that this color reaction is dependent on specific properties of the polystyrene resin and with resins such as TG and PEGA the color reaction does not occur. Upon carrying out the acetaldehyde test on primary amino acid polystyrene resins we observed an orange-red colored supernatant. We assumed

dx.doi.org/10.1021/ol502936d | Org. Lett. 2014, 16, 5918−5921

the coloration arose from the combination of acetaldehyde and traces of piperidine and dibenzofulvene (DBF) from the preceding Fluorenyloxycarbonyl (Fmoc) deprotection step in the synthesis. As the Fmoc amino acid will rapidly liberate DBF selectively with secondary amines, a small amount of Fmoc-amino acid (Fmoc-Gly-OH) was added to the acetaldehyde solution prior to the retesting of the secondary amino acid proline on Tentagel.[19] Indeed then the proline-Tentagel resin became rapidly colored. In comparison, Tentagel with a primary amine gave no color reaction, indicating the preserved selectivity of the test (Figure 2).

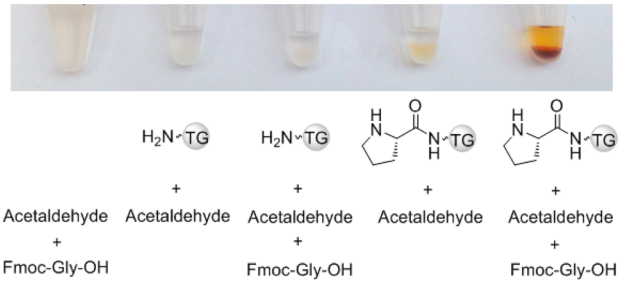

Figure 2. Analysis of primary and secondary amino acids on Tentagel, effect of adding Fmoc-Glycine to the acetaldehyde solution.

The yellow colored supernatant formed during the color test could be removed by washing with NMP, while the beads remained orange-red colored. Proline on PEGA resin which has a very low content of aromatic residues also gave a color reaction with the acetaldehyde/Fmoc-Gly-OH solution. Here, it was investigated whether the addition of aromatic amino acids such as Fmoc-phenylalanine or Fmoc-tryptophane would give a stronger "readout". The acetaldehyde/Fmoc-phenyl alanine mixture gave a more rapid coloration (approximately 1 min) of the PEGA resin compared to the acetaldehyde/Fmoc-glycine mixture (3 min) and a somewhat more deep red-brown coloration of the resin beads. The sensitivity of the acetaldehyde/Fmoc-phenyl alanine method was tested on polystyrene and tentagel resins similar to the methods described by Claerhout et al.[3] and Yang et al.[7] Here a visible color change could be observed in loadings down to ca. 3−6 μmol/g where Tentagel gave visible coloration within 5 min compared to the reference resin; polystyrene resin required 10 min for a clear visual readout.[16]

The utility of the acetaldehyde/Fmoc-amino acid method for colorimetric analysis of secondary amines in solution was also investigated. We used *N*-benzylmethylamine (**A**) as a model system. Mixing of acetaldehyde and **A** in NMP or DMF gave no coloration; however, upon the use of acetaldehyde/Fmoc amino acid mixtures the solution became colored within 1−3 min. As a reference, benzyl amine (**B**) was exposed to the same treatment and here no color development was observed (Figure 3).

We tested the sensitivity of the method for the test of secondary amines in solution and found that the coloration could be visually observed in concentrations down to 0.3−0.6 mM.[16] At low concentrations (0.25 mM) no increased sensitivity was observed upon using 10% acetaldehyde solution or upon increasing the concentration of the Fmoc-amino acid (data not shown). Although we are not certain of the mechanism behind the color reaction, it is evident from our solid-phase experiments that polystyrene exposed to the

Figure 3. Color test carried out in solution (amine concentration 500 mM). (1) **A** and acetaldehyde; (2) **A**, acetaldehyde, and Fmoc-Gly-OH; (3) **A**, acetaldehyde, and Fmoc-Phe-OH; (4) **B** and acetaldehyde; (5) **B**, acetaldehyde, and Fmoc-Gly-OH; (6) **B**, acetaldehyde, and Fmoc-Phe-OH.

iminium/enamine adduct from acetaldehyde and the secondary amine gives the coloration, whereas in more "polystyrene deficient" resins such as Tentagel and PEGA, or in solution, this color reaction is not observed. Furthermore, small amounts of DBF from the Fmoc-amino acid seem to play a key role in the formation of colored adducts with the iminium/enamine, both on resin and in solution. It is known that DBF undergoes spontaneous anionic polymerization when exposed to nucleophiles such as e.g. alkoxides,[20−23] and enamines can perform Michael type addition to electrophilic alkenes.[24] Therefore, it may be proposed that the enamine formed between the secondary amine and acetaldehyde reacts with small amounts of DBF released *in situ* from the Fmoc-amino acid by the secondary amine and the resulting adduct reacts further with DBF to undergo polymerization (Figure 4).

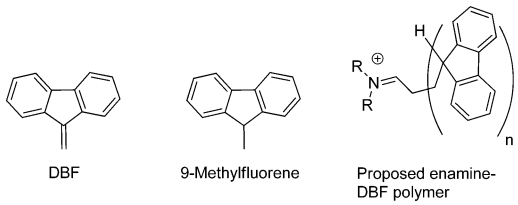

Figure 4. Structures of DBF, 9-methylfluorene, and the proposed structure for iminium-Poly-DBF.

To investigate the assumption of enamine induced polymerization of DBF, we set up an experiment where 9-methylfluorene was added to the acetaldehyde test solution instead of the Fmoc-amino acid. Being saturated at the 9 position, 9-methylfluorene would not be prone to Michael addition from the enamine (Figure 4). Whereas the reaction between amine **A** and acetaldehyde in the presence of Fmoc-Phe-OH resulted in coloring of the solution, no color reaction was observed in the presence of acetaldehyde and 9-methylfluorene under similar conditions.[16] This could imply that the role of dibenzofulvene as a Michael acceptor is important for the formation of colored dyes. The MS and IR spectra obtained from the isolated colored dye precipitates from amine **A** and acetaldehyde with Fmoc-Gly-OH or Fmoc-Phe-OH showed similar peaks. This indicates that the same dye is formed regardless of the Fmoc-amino acid used. MS analysis showed molecular ions which could be assigned to several oligomers of the poly-DBF-iminium structure shown in Figure 4.[16] Also the IR of the solid dyes showed a band at 1660 cm^{-1} relating to the iminium group.[16,25] In divinylbenzene (DVB) cross-linked polystyrene resins residual alkenes from DVB may be present from incomplete polymerization.[26] These reactive alkenes may react with the enamine formed from the secondary amine so

dx.doi.org/10.1021/ol502936d | *Org. Lett.* 2014, 16, 5918−5921

that no additional Fmoc-amino acid is needed to induce coloring in this case. Furthermore, an increased amount of aromatic residues in the system also seems to play a role in the intensity of the color.

In summary, the acetaldehyde test is a simple and fast test to detect secondary amines on polystyrene resins with high specificity. The sensitivity of the method can be enhanced by the addition of Fmoc-amino acids, which makes the method generic for colorimetric analysis of secondary amines on a variety of resin types as well as for visualizing secondary amines in solution. Finally, the 2% acetaldehyde and the 2% acetaldehyde/Fmoc amino acid solutions gave reproducible results after several weeks of storage in the fridge.[27,28]

■ ASSOCIATED CONTENT

Supporting Information

Experimental details on synthesis and analysis on selected resin bound substrates; experimental details and results on the following: Measurements of the test sensitivity on solid-phase and in solution; the use of 9-methylfluorene versus Fmoc amino acid; experimental procedures on the preparation and isolation of colored dye precipitates together with MS and IR spectra on isolated colored dye precipitates from exposure of *N*-benzylmethyl amine to the acetaldehyde/Fmoc-amino acid test solution. This material is available free of charge via the Internet at http://pubs.acs.org.

■ AUTHOR INFORMATION

Corresponding Author

*E-mail: uboa@vet.dtu.dk.

Notes

The authors declare no competing financial interest.

■ REFERENCES

(1) For a review, see: Kay, C.; Lorthioir, O. E.; Parr, N. J.; Congreve, M.; McKeown, S. C.; Scicinski, J. J.; Ley, S. V. *Biotechnol. Bioeng.* **2000/2001**, *71*, 110−118.
(2) Kaiser, E.; Colescott, R. L.; Bossinger, C. D.; Cook, P. I. *Anal. Biochem.* **1970**, *34*, 595.
(3) Claerhout, S.; Ermolat'ev, D. S.; Van der Eycken, E. V. *J. Comb. Chem.* **2008**, *10*, 580−585.
(4) Hancock, W. S.; Battersby, J. E. *Anal. Biochem.* **1976**, *71*, 260−264.
(5) Blackburn, C. *Tetrahedron Lett.* **2005**, *46*, 1405−1409.
(6) Shah, A.; Rahman, S. S.; de Biasi, V.; Camilleri, P. *Anal. Commun.* **1997**, *34*, 325−328.
(7) Yang, S.-J-; Tian, X. Z.; Shin, I. *Org. Lett.* **2009**, *11*, 3438−3441.
(8) Kaiser, E.; Bossinger, C. D.; Colescott, R. L.; Olsen, D. B. *Anal. Chim. Acta* **1980**, *118*, 149−151.
(9) Feigl, F.; Anger, V. *Mikrochim. Acta* **1937**, *1*, 138.
(10) Cullis, C. F.; Waddington, D. J. *Anal. Chim. Acta* **1956**, *15*, 158−163.
(11) Vojkovsky, T. *Peptide Res.* **1995**, *8*, 236−237.
(12) Christensen, T. *Acta Chem. Scand.* **1979**, *B 33*, 763−766.
(13) Boas, U.; Brask, J.; Jensen, K. J. *Chem. Rev.* **2009**, *109*, 2092−2118.
(14) For a recent report on peptide synthesis by the backbone amide linker, see: Svenssen, D.; Mirsharghi, S.; Boas, U. *Tetrahedron Lett.* **2014**, *55*, 3942−3945.
(15) The resin functional groups were verified by infrared spectroscopy; selected spectra can be found in the Supporting Information.
(16) See Supporting Information.
(17) We found that NMP was preferred to DMF as solvent. DMF decomposes upon standing under formation of small amounts of dimethylamine which consumes the acetaldehyde and quenches the color reaction.
(18) Proline on Tentagel gave a weak positive reaction (yellow beads) upon standing for 10 min.
(19) For the seminal paper on the fluorenyloxycarbonyl (Fmoc) group, see: Carpino, L. A.; Han, G. Y. *J. Org. Chem.* **1972**, *37*, 3404−3409.
(20) Nakano, T.; Takewaki, K.; Yade, T.; Okamoto, Y. *J. Am. Chem. Soc.* **2001**, *123*, 9182−9183.
(21) Nakano, T.; Yade, T. *J. Am. Chem. Soc.* **2003**, *125*, 15474−15484.
(22) Nakano, T.; Yade, T.; Fukuda, Y.; Yamaguchi, T.; Okumura, S. *Macromolecules* **2005**, *38*, 8140−8148.
(23) Nakano, T.; Tanikawa, M.; Nakagawa, O.; Yade, T.; Sakamoto, T. *J. Polym. Sci., Part A: Polym. Chem.* **2009**, *47*, 239−246.
(24) For example, see: *Enamines: Synthesis, Structure, and Reactions*, 2nd ed.; Cook, G., Ed.; M. Dekker: 1987.
(25) Furusawa, K.; Ogawa, T.; Itabashi, T.; Miyahara, T.; Kitahara, S.; Kawanaka, T. *Colloid Polym. Sci.* **1994**, *272*, 1514−1520.
(26) Sherrington, D. C. *Chem. Commun.* **1998**, 2275−2286.
(27) Color test for secondary amines on resin by acetaldehyde/Fmoc amino acid: The test solution was prepared by dissolving Fmoc-Gly-OH (2 mg, 6.7 mmol) or Fmoc-Phe-OH (3 mg, 6.7 mmol) in 2% acetaldehyde in NMP (1 mL). Then a few resin beads were placed in an Eppendorf tube, two drops of the acetaldehyde/Fmoc-amino acid solution were added, and the resin suspension was allowed to stand for 3−5 min at room temperature. Upon the presence of secondary amines the resin beads turned red. The resin beads were washed five times with NMP to quench the color reaction.
(28) Color test for secondary amines in solution: To an amine containing a sample in NMP (200 μL), a test solution (40 μL) comprising Fmoc-Phe-OH (2.6 mg, 6.7 μmol) dissolved in 2% acetaldehyde in NMP (1 mL) was added. The solution incubated for 5 min; orange to red-brown coloring of the solution indicates the presence of a secondary amine in the mixture.

Supporting information

Color test for selective detection of secondary amines on resin and in solution

Ulrik Boas* and Sahar Mirsharghi.

Department of Immunology and Vaccinology, The National Veterinary Institute, The Technical University of Denmark, Bülowsvej 27, DK-1870 Frederiksberg

DTU Center for Nanomedicine and Theranostics, The Technical University of Denmark, Building 345Ø, DK-2800, Kgs. Lyngby

**uboa@vet.dtu.dk*

Contents

1. General remarks. Polystyrene (aminomethylated, Indole aldehyde) and Tentagel resins were purchased from Sigma-Aldrich and Iris Biotech, amino-PEGA resin was purchased from Merck (Novabiochem). All chemicals were purchased from Sigma-Aldrich and solvents from Fischer Scientific and of HPLC grade. 2-methoxy-4-alkoxy-benzaldehyde (FMPB) resin was prepared as previously described. [1] The amine loading was determined by UV of the Dibenzofulvene-piperidine adduct at λ (290nm) as earlier described. [2] On-resin functional group determination was carried out by IR (attenuated technique of reflectance). Micrographs were taken on a Leica DMLS microscope with a 10x/0.22 PH1 lense. The microscope was equipped with a Leica DFC290 camera. The beads were suspended in NMP and dropped onto the microscope glass (no cover glass used). HPLC-MS analysis was performed on an equipment comprising of a Shimadzu Nexera X2 with diode array UV detection in conjunction with a Bruker MicrOTOF-Q III mass spectrometer (positive ionization mode), using a Ascentis Express Peptide ES-C18 column (2.7μm, 160Å) and a 1 mL/min linear gradient from 0 to 100% over 5.00 min (buffer A: 0.025% TFA in 10% aqueous acetonitrile; buffer B: 0.025% TFA in 90% aqueous acetonitrile) with buffer A and B.

2. Acetaldehyde/Fmoc-amino acid test: Sensitivity on solid-phase (method by Claerhout et al.[3])

Fmoc-Proline and Boc-Glycine were mixed in five ratios and coupled to Rink Amide aminomethylated polystyrene (loading 0.36mmol/g) or Tentagel S NH2 (loading 0.29mmol/g) using HBTU as the coupling agent. The resulting loadings of proline (secondary amine) on resin 1-5 were determined by Fmoc-quantization in triplicate (Table S1, measurement A, B and C)

Stock solutions:

Fmoc-Pro-OH stock (0.144mmol/mL): Fmoc-Pro-OH (972mg, 2.88mmol) in NMP (20mL)

Boc-Gly-OH stock(0.144mmol/mL): Boc-Gly-OH (505mg, 2.88mmol) in NMP (20mL)

HBTU stock solution: HBTU (1g, 2.6 mmol) was dissolved in NMP (10mL)

1) To Rink amide resin (deprotected) or Tentagel S NH2 (0.2g, approx. 0.072 mmol) was added Boc-Gly-OH (1mL, 0.144mmol) and Fmoc-Pro-OH (1mL, 0.144 mmol) followed by addition of DIPEA (97μL, 0.56 mmol) and HBTU stock solution (1 mL, 0.26 mmol) followed by shaking for 1 hr at r.t. Washing of the resin with NMP (5times) and DCM (5 times), shrinking with methanol. Secondary amine loading was determined by Fmoc-quantization to be: 172 μmol/g (Rink amide resin) and 87 μmol/g (Tentagel).

2) To Rink amide resin (deprotected) or Tentagel S NH2 (0.2g, approx. 0.072 mmol) was added Boc-Gly-OH (1.75 mL, 0.252mmol) and Fmoc-Pro-OH (250μL, 0.036 mmol) followed by addition of DIPEA (97μL, 0.56 mmol) and HBTU stock solution (1 mL, 0.26 mmol) followed by shaking for 1 hr at r.t. Washing of the resin with NMP (5times) and DCM (5 times), shrinking with methanol. Secondary

amine loading was determined by Fmoc-quantization to be: 63.1 μmol/g (Rink amide resin) and 33 μmol/g (Tentagel).

3) To Rink amide resin (deprotected) or Tentagel S NH2 (0.2g, approx. 0.072 mmol) was added Boc-Gly-OH (1.875 mL, 0.270mmol) and Fmoc-Pro-OH (125 μL, 0.018 mmol, mg) followed by addition of DIPEA (97μL, 0.56 mmol) and HBTU stock solution (1 mL, 0.26 mmol) followed by shaking for 1 hr at r.t. Washing of the resin with NMP (5times) and DCM (5 times), shrinking with methanol. Secondary amine loading was determined by Fmoc-quantization to be: 35.7 μmol/g (Rink amide resin) and 14.1 μmol/g (Tentagel).

4) To Rink amide resin (deprotected) or Tentagel S NH2 (0.2g, approx. 0.072 mmol) was added Boc-Gly-OH (1.94mL, 0.279mmol) and Fmoc-Pro-OH (63 μL, 0.009 mmol) followed by addition of DIPEA (97μL, 0.56 mmol) and HBTU stock solution (1 mL, 0.26 mmol) followed by shaking for 1 hr at r.t. Washing of the resin with NMP (5times) and DCM (5 times), shrinking with methanol. Secondary amine loading was determined by Fmoc-quantization to be: 16.1 μmol/g (Rink amide resin) and 6.2 μmol/g (Tentagel).

5) To Rink amide resin (deprotected) or Tentagel S NH2 (0.2g, approx. 0.072 mmol) was added Boc-Gly-OH (1.97 mL, 0.284mmol) and Fmoc-Pro-OH (31 μL, 0.0045 mmol, mg) followed by addition of DIPEA (97μL, 0.56 mmol) and HBTU stock solution (4 mL, 0.26 mmol) followed by shaking for 1 hr at r.t. Washing of the resin with NMP (5times) and DCM (5 times), shrinking with methanol. Secondary amine loading was determined by Fmoc-quantization to be: 7.3 μmol/g (Rink amide resin).

Table S1

Sample - Abs (Mass/mg)	Sample - Abs (Mass/mg)	Sample - Abs (Mass/mg)	Mean loading
	Rink amide-PS resin		
1A: 0.208(6.1)	1B: 0.207(5.5)	1C: 0.179(4.9)	172 μmol/g
2A: 0.078(6.1)	2B: 0.083(6.5)	2C: 0.081(5.7)	63.1 μmol/g
3A: 0.054(7.7)	3B: 0.061(8.0)	3C: 0.058(7.4)	35.7 μmol/g
4A: 0.037(10.3)	4B: 0.038(10.9)	4C: 0.034(11.0)	16.1 μmol/g
5A: 0.023(14.8)	5B: 0.018(12.3)	5C: 0.021(13.6)	7.3 μmol/g
	Tentagel resin		
1A: 0.120(6.5)	1B: 0.092(4.9)	1C: 0.109(6.2)	87 μmol/g
2A: 0.041(5.5)	2B: 0.055(8.5)	2C: 0.053(7.7)	33 μmol/g
3A: 0035(10.8)	3B: 0.035(11.5)	3C: 0.034(13.0)	14.1μmol/g
4A: 0.019(13.2)	4B: 0.020(13.3)	4C: 0.011(11.9)	6.2 μmol/g

After determination of loading the resins were Fmoc-deprotected to expose the various amounts of secondary amines present on the resins.

2. Acetaldehyde/Fmoc-amino acid test: Sensitivity on solid-phase (method by Yang et al.[4])

The sensitivity test was performed on Rink amide-PS resins 2A and 3A and Tentagel resins 1A and 2A from Table S1. Resins suspended in two drops of NMP were applied as references.

Fmoc removal was performed on all four derivatized resins with piperidine/NMP (1:4, 2mL) for 3 + 30 min.

1) Rink amide-PS resin 3A (50mg, 1.8µmol, loading: 35.7µmol/g, 1 equiv.), Fmoc-Leu-OH (0.6mg, 1.6µmol, 0.9 equiv.), PyBOP (0.8mg, 1.6µmol, 0.9 equiv.), DIPEA (1.0µL, 6.4µmol, 3.6 equiv.) were suspended in NMP (1.0mL) and shaken at rt. After 1h the resin was washed with NMP (6x), DCM (5x) and MeOH (2x). Acetaldehyde/Fmoc-amino acid test was carried out as described and visualized after 5 min and 10 min. (see figure S1)

2) Rink amide-PS resin 2A (50mg, 3.2µmol, loading: 63.1µmol/g, 1 equiv.), Fmoc-Leu-OH (1.0mg, 2.8µmol, 0.9 equiv.), PyBOP (1.5mg, 2.8µmol, 0.9 equiv.), DIPEA (1.9µL, 11.4µmol, 3.6 equiv.) were suspended in NMP (0.5mL) and shaken at rt. After 1h the resin was washed with NMP (6x), DCM (5x) and MeOH (2x). Acetaldehyde/Fmoc-amino acid test was carried out as described and visualized after 5 min and 10 min. (see figure S1)

3) Tentagel resin 2A (50mg, 1.7µmol, loading: 33µmol/g, 1 equiv.), Fmoc-Leu-OH (0.5mg, 1.5µmol, 0.9 equiv.), PyBOP (0.8mg, 1.5µmol, 0.9 equiv.), DIPEA (1.0µL, 5.9µmol, 3.6 equiv.) were suspended in NMP (0.5mL) and shaken at rt. After 1h the resin was washed with NMP (6x), DCM (5x) and MeOH (2x). Acetaldehyde/Fmoc-amino acid test was carried out as described and visualized after 5 min and 10 min. (see figure S1)

4) Tentagel resin 1A (50mg, 4.4µmol, loading: 87µmol/g, 1 equiv.), Fmoc-Leu-OH (1.4mg, 3.9µmol, 0.9 equiv.), PyBOP (2.0mg, 3.9µmol, 0.9 equiv.), DIPEA (2.7µL, 15.7µmol, 3.6 equiv.) were suspended in NMP (0.5mL) and shaken at rt. After 1h the resin was washed with NMP (6x), DCM (5x) and MeOH (2x). Acetaldehyde/Fmoc-amino acid test was carried out as described and visualized after 5 min and 10 min. (see figure S1)

Acetaldehyde/Fmoc-Phenylalanine test after 5min.: References: Resins in NMP

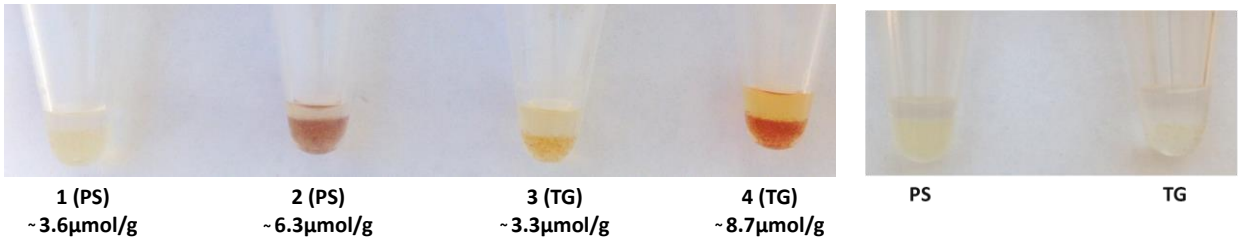

Acetaldehyde/Fmoc-Phenylalanine test after 10min.:

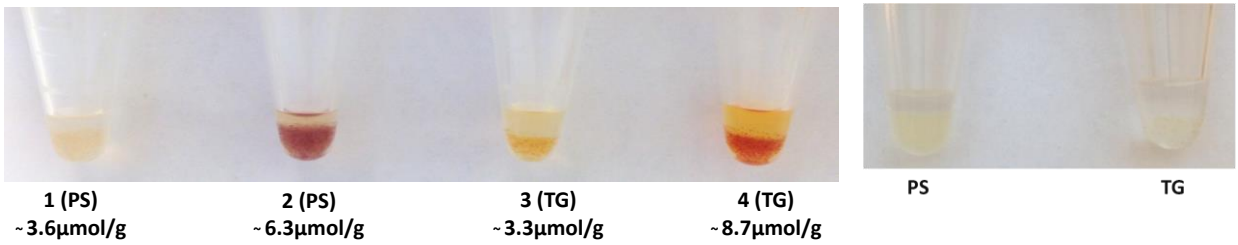

Figure S1. Sensitivity tests on polystyrene and tentagel

Preparation of Stock A, B and C used for the experiments below

Stock A: Acetaldehyde (1.1mL, 20mmol, d 0.79, MW 44) was dissolved in DMF (8mL)

Stock B: N-Benzylmethyl amine (0.52 mL, 4 mmol, d 0.94, MW 121.2) was dissolved in DMF (8mL)

Stock C: Benzyl amine (0.44mL, 4mmol, d 0.98, MW 107.2) in DMF (8mL)

3. Acetaldehyde/Fmoc-amino acid test in solution: N-Benzylmethyl amine compared to benzyl amine (Figure 3 in article)

1: Stock A (10µL) + Stock B (10µL) in DMF (5mL), shaking for 3 min
2: Stock A (10µL) + Fmoc-Gly-OH (1mg, 3.4 µmol) in DMF (5mL), to this solution is added Stock B (10µL), shaking for 3 min
3: Stock A (10µL) + Fmoc-Phe-OH (1.3mg, 3.4 µmol) in DMF (5mL), to this solution is added Stock B (10µL), shaking for 3 min
4: Stock A (10µL) in DMF (5mL), addition of Stock C (10µL), shaking for 3 min
5: Stock A (10µL) + Fmoc-Gly-OH (1mg, 3.4µmol) in DMF (5mL), to this solution is added Stock C (10µL) shaking for 3 min
6: Stock A (10µL) + Fmoc-Phe-OH (1.3mg, 3.4µmol) in DMF (5mL), to this solution is added Stock C (10µL), shaking for 3 min

4. Acetaldehyde/Fmoc-amino acid test: Sensitivity in solution

Stock B (5.2µL) was diluted in DMF (8mL) to give an amine concentration of 5mM. In the first well of the two rows diluted stock B (200 µL) was added and subjected to a two-fold dilution from 5mM-0.2mM concentration. In the first row, 40 µL of a test solution containing Fmoc-Glycine (2.0 mg, 7 µmol) in 2% Acetaldehyde in DMF (1mL) was added to each well. In the second row, 40 µL of a test solution containing Fmoc-Phenylalanine (2.6 mg, 7 µmol) in 2% Acetaldehyde in DMF (1mL) was added to each well. The total volume in each well was then 240 µL. Incubation for 5 minutes at room temperature (Figure S2).

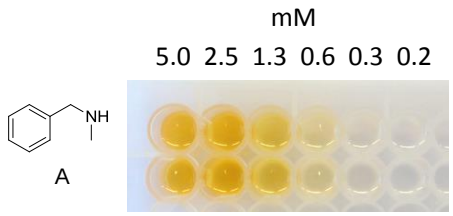

Figure S2. Two-fold dilution of amine **A** in DMF (total volume per well = 240 µL) visualized with acetaldehyde/Fmoc-Gly-OH (top row) and acetaldehyde/Fmoc-Phe-OH (bottom row)

5. 9-Methylfluorene compared to Fmoc-Phenylalanine in the acetaldehyde test solution.

1: Stock A (20uL) in DMF (10mL), addition of stock B (20uL)

2: Stock A (20uL) and 9-methylfluorene (1.2 mg, 6 µmol) in DMF (10mL), addition of stock B (20µL)

3: Stock A (20uL) and Fmoc-Phenylalanine (2.4mg, 6 µmol) in DMF (10mL), addition of Stock B (20µL)

4: Stock A (20uL) and 9-methylfluorene (1.2 mg, 6 µmol) in DMF (10mL), addition of Stock C (20µL)

5: Stock A (20uL) and Fmoc-Phenylalanine (2.4mg, 6 µmol) in DMF (10mL), addition of Stock C (20µL)

All the mixtures were shaken for 5 min before transfer to a 96 well plate. The results of the experiment and the structures of 9-methyl-fluorene and dibenzofulvene are shown in figure S3.

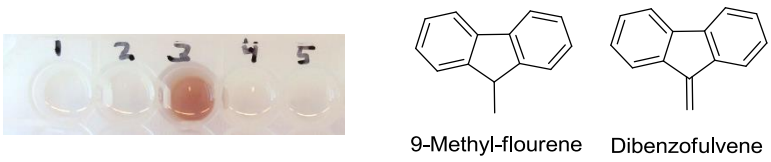

Figure S3. Effect of dibenzofulvene versus 9-methyl-fluorene in the formation colored solutions.

6. MS, UV and FT-IR analysis of colored dye precipitates

N-Benzylmethylamine (amine **A**, 130uL, 1mmol) was dissolved in DMF (2mL) and a mixture of acetaldehyde (280uL, 5mmol, MW 44, d 0.79) and Fmoc-amino acid (0.3mmol) dissolved in DMF (2mL) was added while stirring and the mixture turned rapidly dark brown. The mixture was stirred for 10 min. Acetonitrile (10mL) was added and the mixture was centrifuged and the dark brown/black

precipitate was isolated. The brown precipitate was wased 5 times with acetonitrile. A small amount of the precipitate was dissolved in DMF, filtered through a micro-filter and analyzed by MS (Figure S4, S5), which gave similar mass spectra regardless of using Fmoc-Gly-OH or Fmoc-Phe-OH in the color test indicative of the structure proposed in Figure S4. UV-VIS on the dye precipitated from Acetaldehyde/Fmoc-Phe-OH test showed UV absorption maxima at λ=198, 216 and 425nm (Figure S6). The solid precipitates were analyzed by FT-IR (attenuated technique of reflection) which showed a band at 1660 cm-1 characteristic for the presence of a dialkyliminium group (Figure S7).

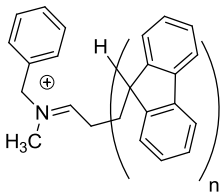

Figure S4. Proposed structure of DBF polymer formed by reaction between amine **A**, acetaldehyde and Fmoc-amino acid.

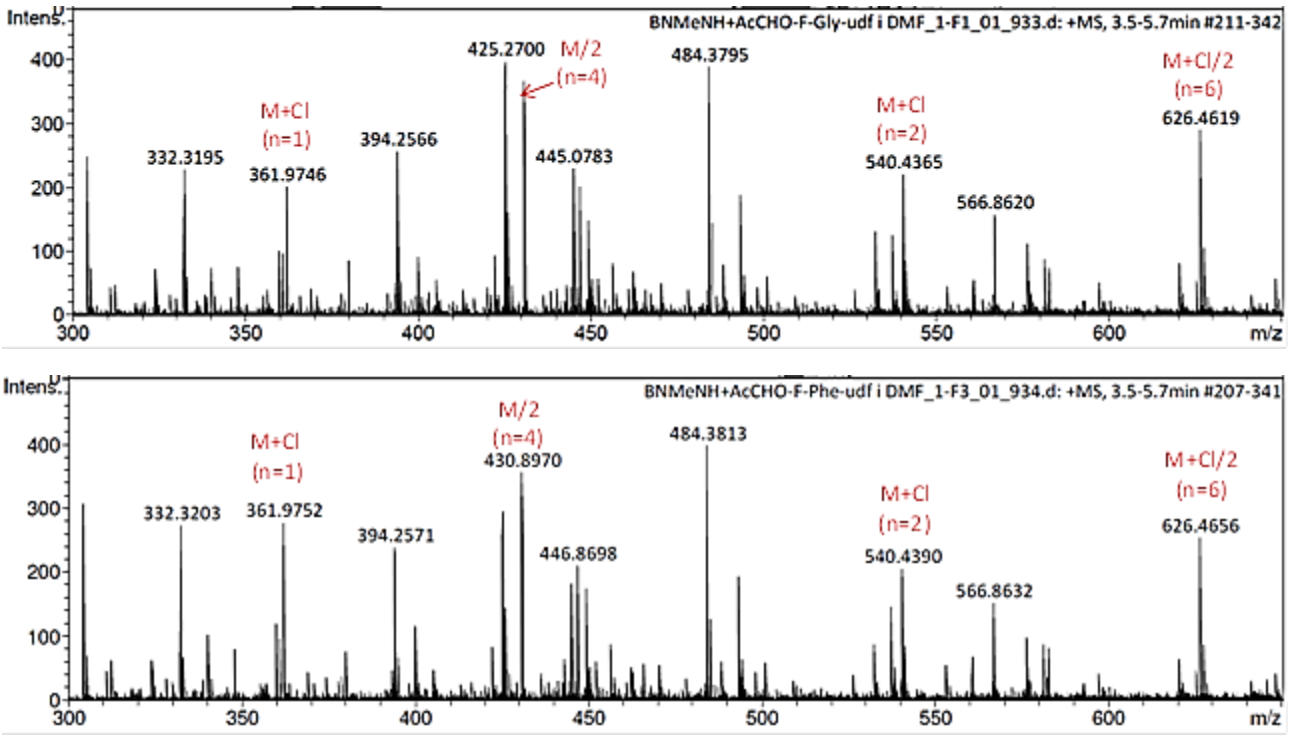

Figure S5. Interpreted MS spectra of dyes isolated as described above from: Amine **A** mixed with acetaldehyde/Fmoc-Gly-OH test mixture (top) and Amine **A** mixed with acetaldehyde/Fmoc-Phe-OH test mixture (bottom)

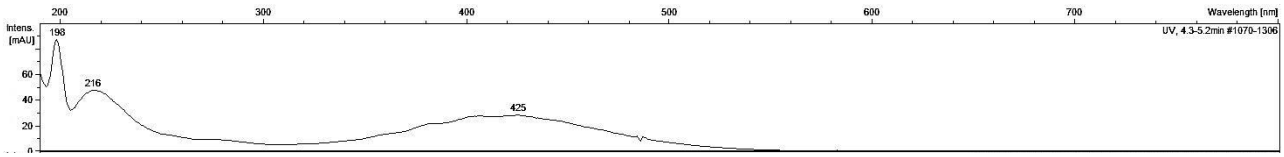

Figure S6. UV-VIS (diode array) spectrum of dye isolated as above from: Amine **A** mixed with acetaldehyde/Fmoc-Phe-OH test mixture

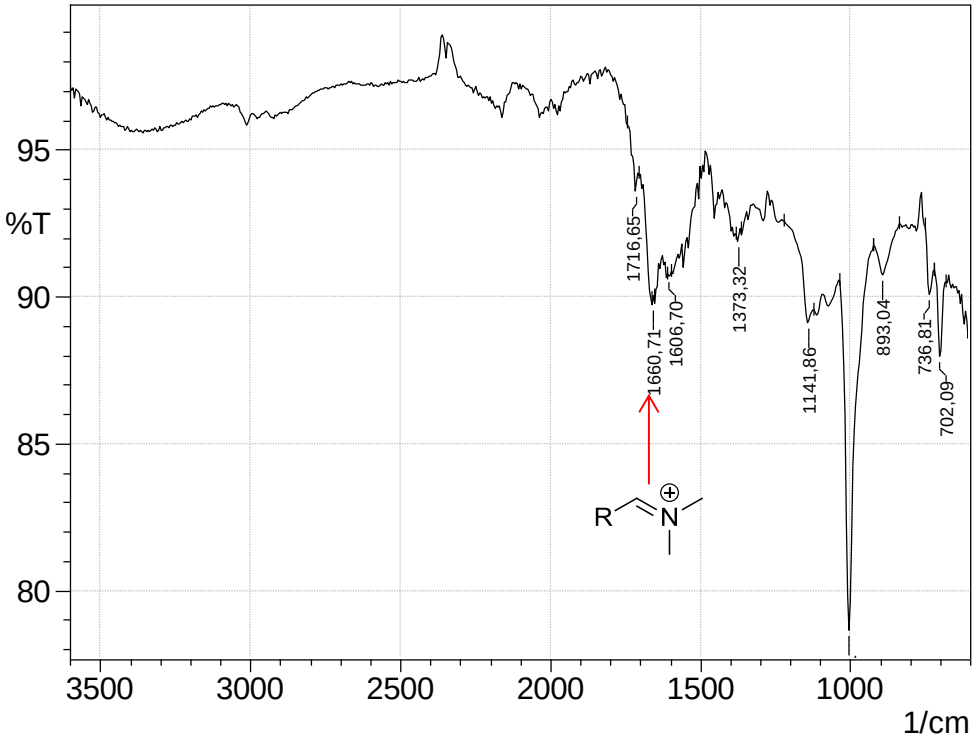

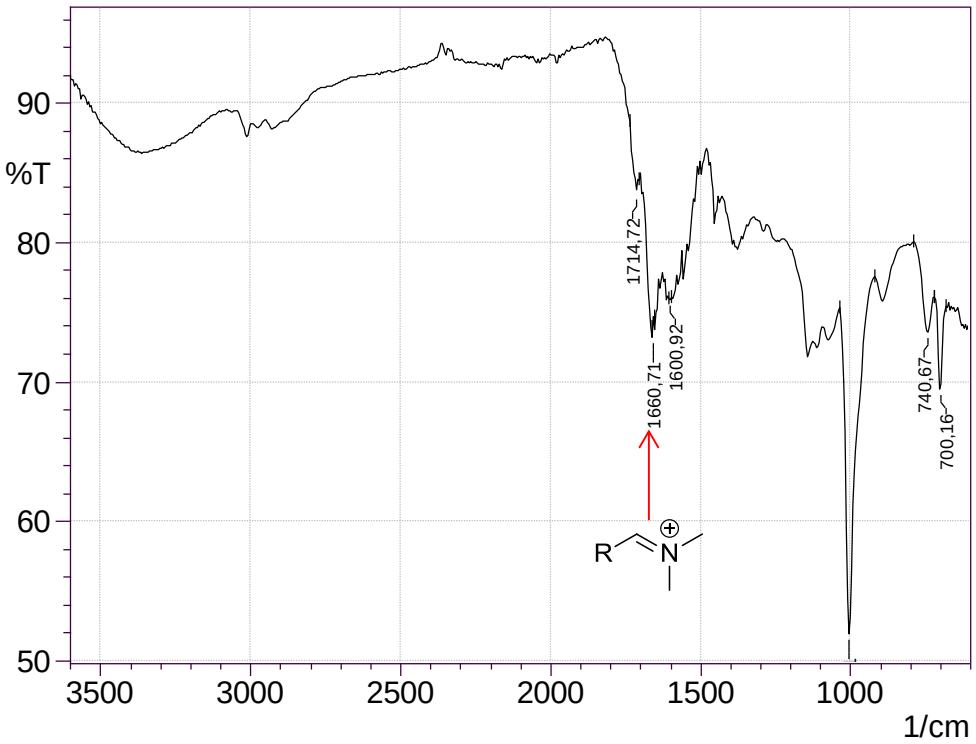

Figure S7. Analysis of dye precipitates by FT-IR of dyes isolated as described above from: Amine **A** mixed with acetaldehyde/Fmoc-Gly-OH mixture (top) and Amine **A** mixed with acetaldehyde/Fmoc-Phe-OH mixture (bottom)

7. Procedures for the synthesis of resin substrates

Proline/lysine/alanine on aminomethylated polystyrene resin (compounds 5, 10 and 11, respectively)

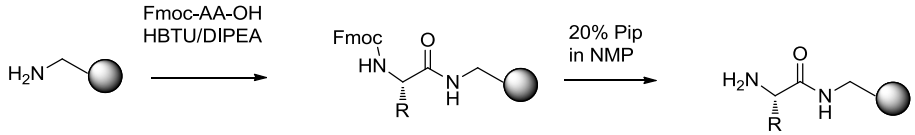

Procedure: Aminomethylated polystyrene resin (0.3g, 0.6mmol, load 2mmol/g) was swelled in dry NMP (5mL). PyBOP (1.24g, 4equiv., 2.4mmol, MW 520.4) and dry DIPEA (0.82mL, 4equiv., 4.8mmol, MW129.3) were added followed by Fmoc protected aa (4equiv., 2.4mmol). The resin suspension was shaken for 1h at r.t. and washed with 6x NMP, 5x DCM and 3x MeOH. Ninhydrin test, negative. Cleavage of Fmoc group by 20% Piperidine in NMP (5mL, 3+20min), wash (6x NMP, 5x DCM, 2x MeOH). Ninhydrin test was positive. IR-(ATR) ν (Cm^{-1}). Alanine: 2922 (C-H stretch), 1668 (C=O stretch, amide), 758 (N-H bend). Lysine: 2922 (C-H stretch), 1660 (C=O stretch, amide), 758 (N-H bend). Proline: 2922 (C-H stretch), 1668 (C=O stretch, amide), 759 (N-H bend)

Proline on Tentagel S NH2 and Amino PEGA resins (compound 5a and 5b)

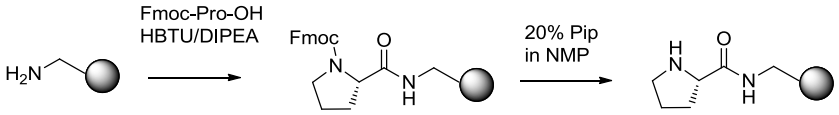

Procedure (Tentagel S NH2): Fmoc-Pro-OH (0.4 mmol, 135mg, MW 337.4) was suspended in dry NMP (4 mL) and HBTU (0.4mmol, 152 mg, MW 379) was added followed by DIPEA (0.8mmol, 138 uL, MW 129.3, d 0.75) the mixture was stirred for 5 minutes and added to tentagel resin (0.3g, 0.09 mmol, load 0.29mmol/g) was swelled in NMP (3mL). The resin suspension was shaken for 2 hr at r.t. and washed (DCM x5, NMP x5), Ninhydrin test, negative Cleavage of Fmoc group by 20% Piperidine in NMP(3mL, 3+20min), wash (5xDCM, 5x NMP, 2xmethanol), Ninhydrin test (should be negative). IR (ATR) ν (Cm^{-1}) 3468 (N-H stretch, amide), 2870 (C-H, stretch), 1667 (C=O, amide),

Procedure (Amino PEGA): Fmoc-Pro-OH (0.4 mmol, 135mg, MW 337.4) was suspended in dry NMP (4 mL) and HBTU (0.4mmol, 152 mg, MW 379) was added followed by DIPEA (0.8mmol, 138 uL, MW 129.3, d 0.75) the mixture was stirred for 5 minutes and added to Amino PEGA resin (0.2g, 0.08 mmol, load 0.4mmol/g, Novabiochem) was swelled in NMP (3mL). The resin suspension was shaken for 2 hr at r.t. and washed (DCM x5, NMP x5), Ninhydrin test? Cleavage of Fmoc group by 20% Piperidine in NMP(3mL, 3+20min), wash (5xDCM, 5x NMP, 2xmethanol), Ninhydrin test (should be negative). IR (ATR) ν (Cm^{-1}) 3446 (N-H stretch, amide)2927, 2875 (C-H stretch), 1659 (C=O stretch, amide)

N,N-methyl-(6-amidohexyl)amine on aminomethylated polystyrene resin (Compound 3)

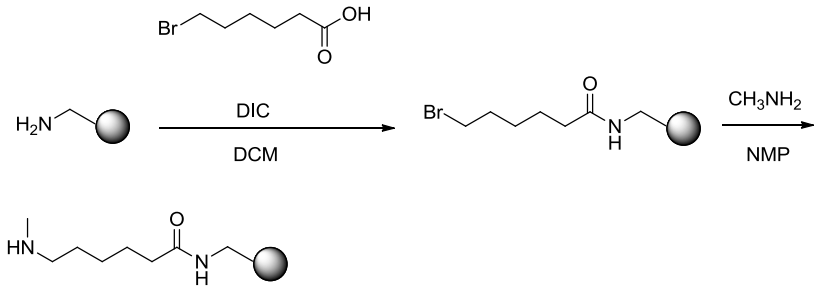

Procedure: 6-Bromohexanoic acid (3.9 g, 20 mmol, MW 195.05) was suspended in dry DCM (15mL) and the mixture was cooled on an icebath. After 5 minutes DIC (1.6 mL, 10 mmol, d=0.81, MW 126.2) was added and the mixture was stirred for 30 minutes on ice. The stirring bar was removed and Aminomethylated polystyrene resin (1g, 2 mmol, loading 2 mmol/g) was added and the resin mixture was shaken 3 h in the round bottomed flask. The resin suspension was transferred to a filter syringe and washed with NMP (x5) and DCM (x5) and methanol (x2). Ninhydrin test was performed and was negative (otherwise capping with acetic anhydride (5%Ac2O/10% DIPEA in DCM for 30 min). The bromo resin was suspended in dry NMP (10 mL) and 2M methyl amine in THF (10 mmol, 5 mL) and the suspension was shaken 16 h. The resin was washed with NMP (5x), DCM (5x) and shrunk with methanol (2x) and kept under vacuum (oilpump). IR (ATR) ν (Cm^{-1}) 2922 (C-H stretch), 1668 (C=O stretch, amide), 1367 (methyl, bend), 758 (N-H, bend)

Secondary amine substrate on aminomethylated polystyrene resin (Compound 4)

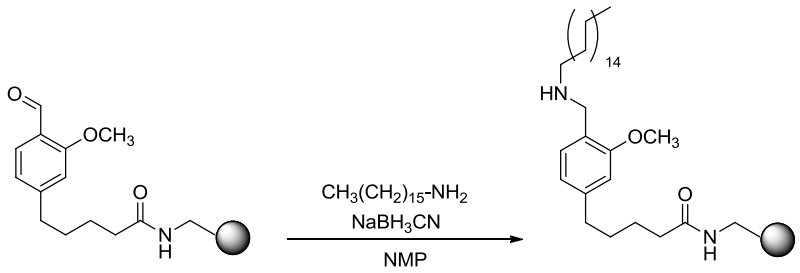

Procedure: Aldehyde (FMPB) derivatized resin (0.5g, 1mmol, 1 equiv.) was swelled in 5% acetic acid in dry NMP/THF (1:9) (14mL). $NaBH_3CN$ (0.63g, 10 equiv., 10mmol, MW 62.84) and hexadecylamine (2.41g, 10equiv., 10mmol, MW 241.46) were added. The resin suspension was shaken for 24h at r.t. and washed with 3x MeOH, 6x NMP, 5x DCM. DNPH test, positive. Reaction repeated 2h at r.t. and washed as above. DNPH test, negative. IR (ATR) ν (Cm^{-1}) 2922 (C-H stretch), 1651 (C=O stretch, amide), 1375 (methyl, bend), 759 (N-H, bend), 698 (C-H bend, aromatic)

Primary amine substrate on aminomethylated polystyrene resin (Compound 6)

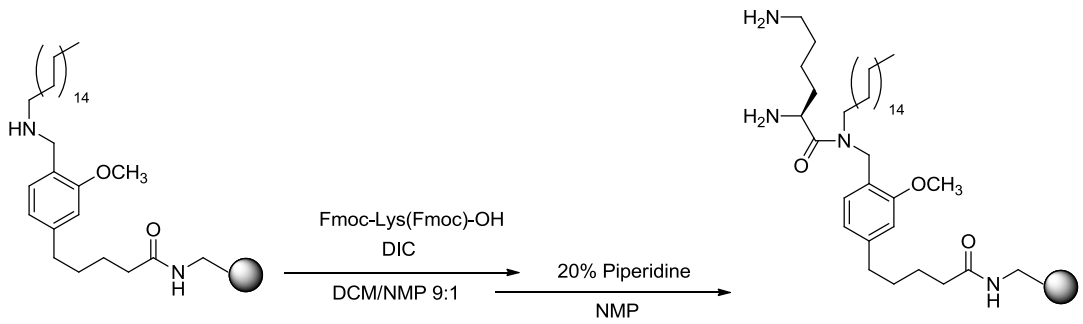

Procedure: Secondary amine-FMPB derivatized resin, (0.5g, 1mmol, 1 equiv.) was swelled in dry NMP (5mL). Et_3N (1.40mL, 10mmol, 10 equiv., MW 101.2, d=0.73), DMAP (0.12g, 1mmol, 1 equiv., MW 122.2) and TFFH (1.32g, 5mmol, 5 equiv., MW 264.1) were added followed by Fmoc-Lys(Fmoc)-OH (2.95g, 5mmol, 5 equiv., MW 590.7). The resin suspension was shaken 22.5h at r.t. and washed with 6x NMP, 5x DCM, 2x MeOH. Cleavage of Fmoc groups by 20% Piperidine in NMP (10mL, 3+30min), wash (6x NMP, 5x DCM, 2x MeOH). Ninhydrin test was positive. IR (ATR) ν (Cm^{-1}) 2922 (C-H stretch), 1651 (C=O stretch, amide), 1375 (methyl, bend), 759 (N-H, bend), 698 (C-H bend, aromatic)

Resin bound dithiocarbamate (Compound 8)

Procedure: N-methyl-(6-amidohexyl)amine on polystyrene (20 mg, 0.04mmol, loading 2 mmol/g) was put in an Eppendorf test tube and swelled in NMP (0.1 mL). Carbon disulfide (0.2mL) was added and the mixture was shaken for 1 h at r.t. The yellow resin suspension was transferred to a syringe equipped with a filter and washed with NMP (5 times), DCM (5 times) and methanol and air dried. IR (ATR) ν (cm^{-1}) 2922 (C-H stretch), 1651 (C=O stretch, amide), 1512 (C=S stretch), 1371 (methyl, bend), 758 (N-H bend)

Resin bound dithiocarbamate (Compound 9)

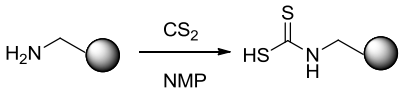

Procedure: Aminomethylated polystyrene (20 mg, 0.04mmol, loading 2 mmol/g) was put in an Eppendorf test tube and swelled in NMP (0.1 mL). Carbon disulfide (0.2mL) was added and the mixture was shaken for 1 h at r.t. The yellow resin suspension was transferred to a syringe equipped with a filter and washed with NMP (5 times), DCM (5 times) and methanol and air dried. IR (ATR) ν (cm^{-1}) 2920 (C-H stretch), 1506 (C=S stretch), 758 (N-H bend)

8. Selected FT-IR spectra for resin substrates

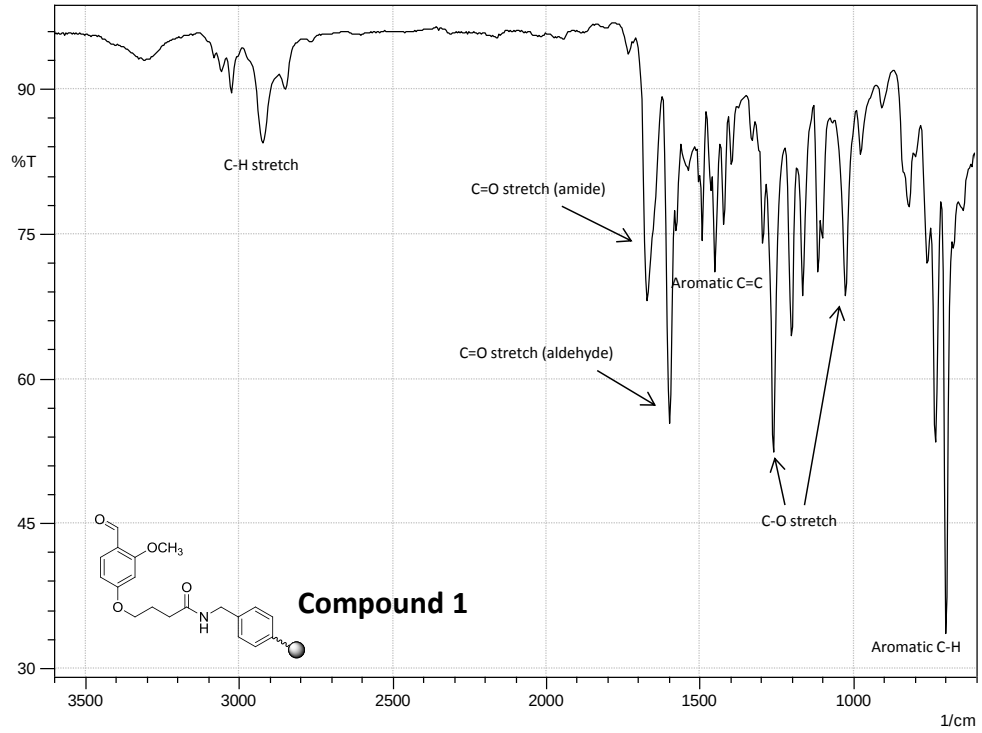

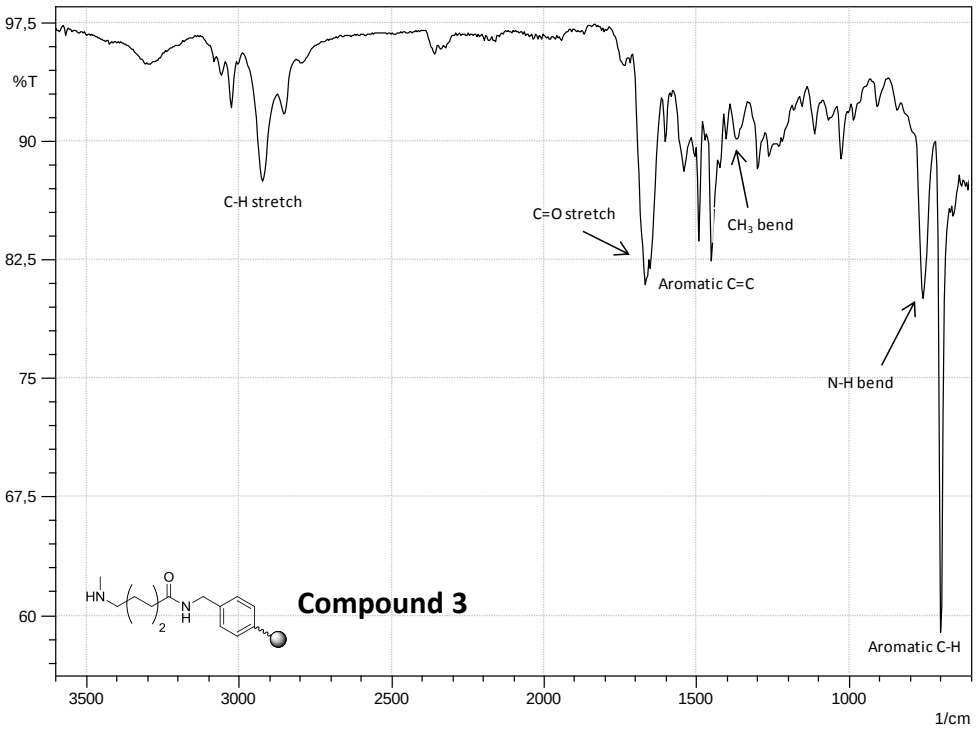

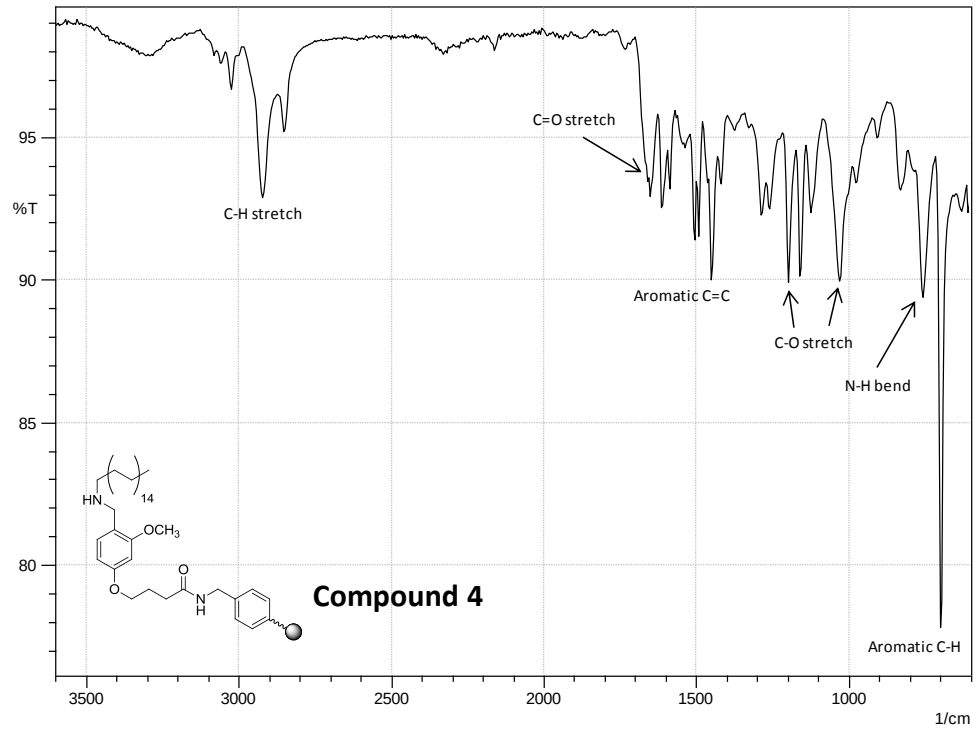
95
%T
90
85
80
C=O stretch
C-H stretch
Aromatic C=C
C-O stretch
N-H bend
Aromatic C-H
HN
14
OCH3
O
O
N
H
Compound 4
3500
3000
2500
2000
1500
1000
1/cm

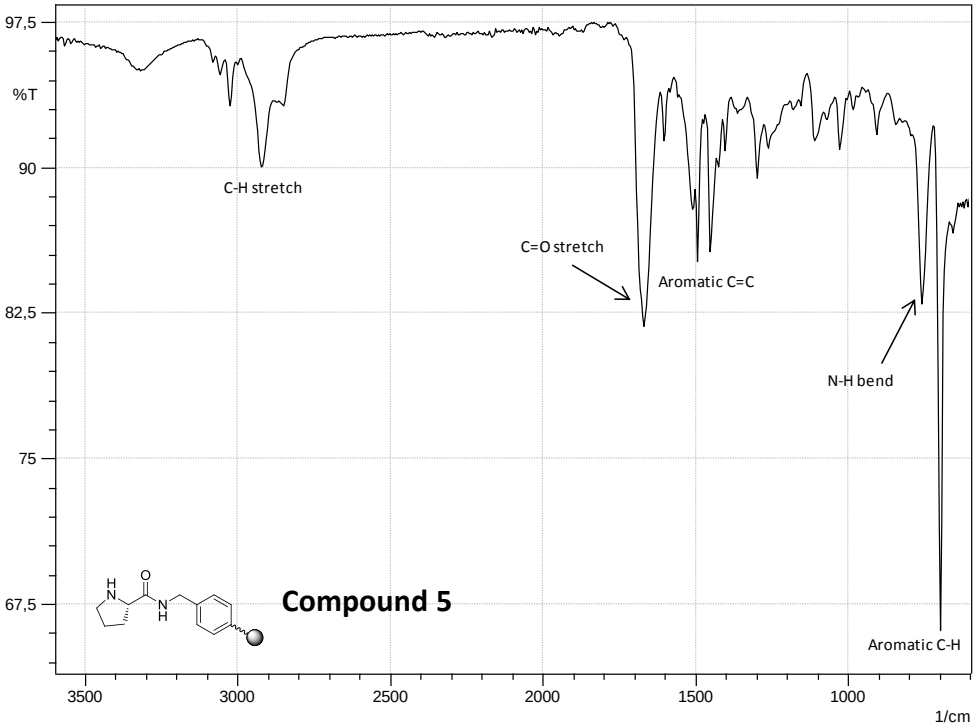
97,5
%T
90
82,5
75
67,5
C-H stretch
C=O stretch
Aromatic C=C
N-H bend
Aromatic C-H
H
N
O
N
H
Compound 5
3500
3000
2500
2000
1500
1000
1/cm

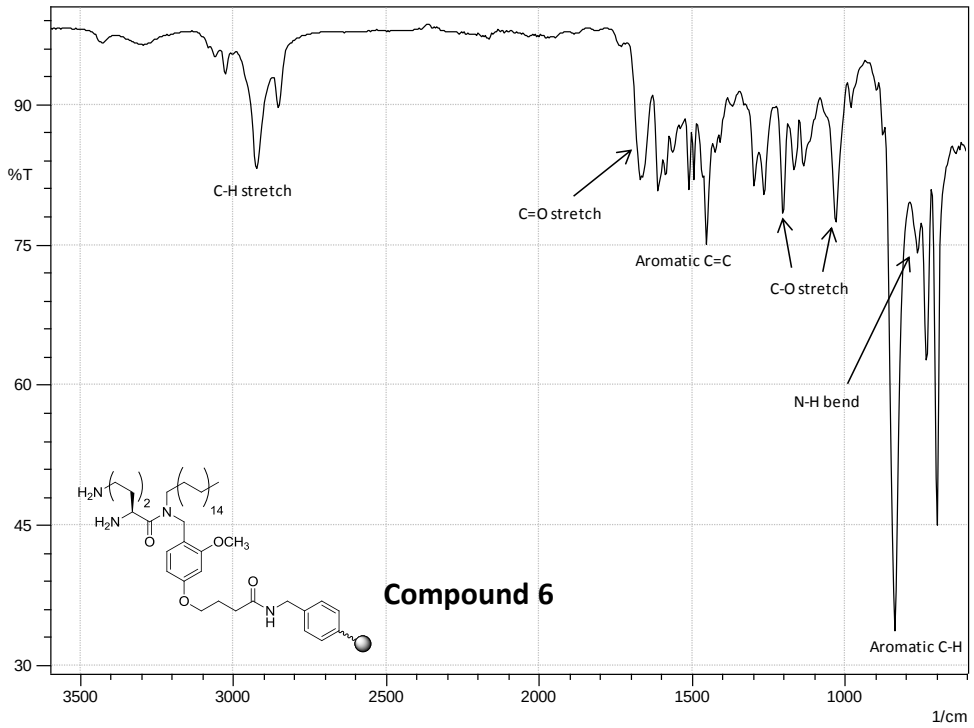
%T
90
75
60
45
30
C-H stretch
C=O stretch
Aromatic C=C
C-O stretch
N-H bend
Aromatic C-H
Compound 6
3500
3000
2500
2000
1500
1000
1/cm

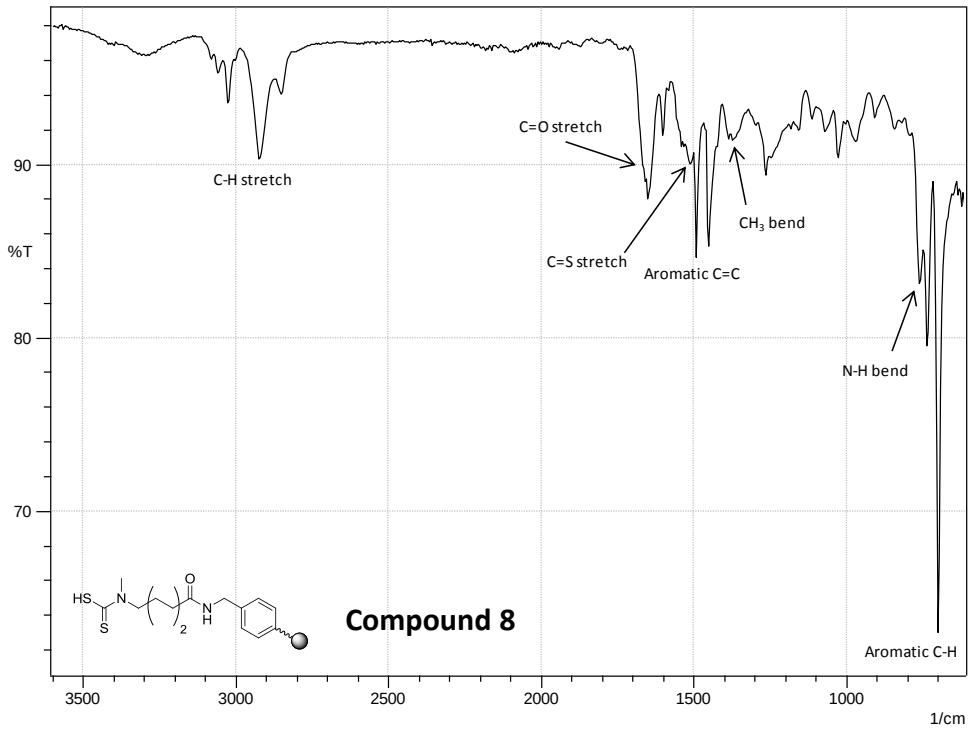
%T
90
80
70
C-H stretch
C=O stretch
C=S stretch
Aromatic C=C
CH3 bend
N-H bend
Aromatic C-H
Compound 8
3500
3000
2500
2000
1500
1000
1/cm

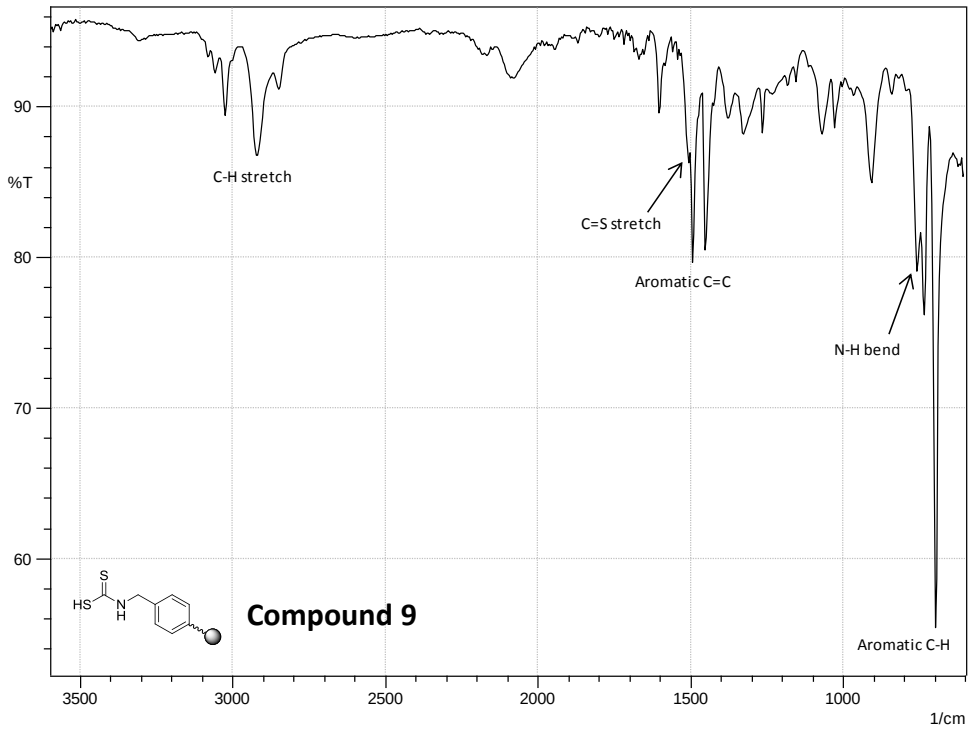
90
%T
80
70
60
C-H stretch
C=S stretch
Aromatic C=C
N-H bend
Aromatic C-H
Compound 9
3500
3000
2500
2000
1500
1000
1/cm

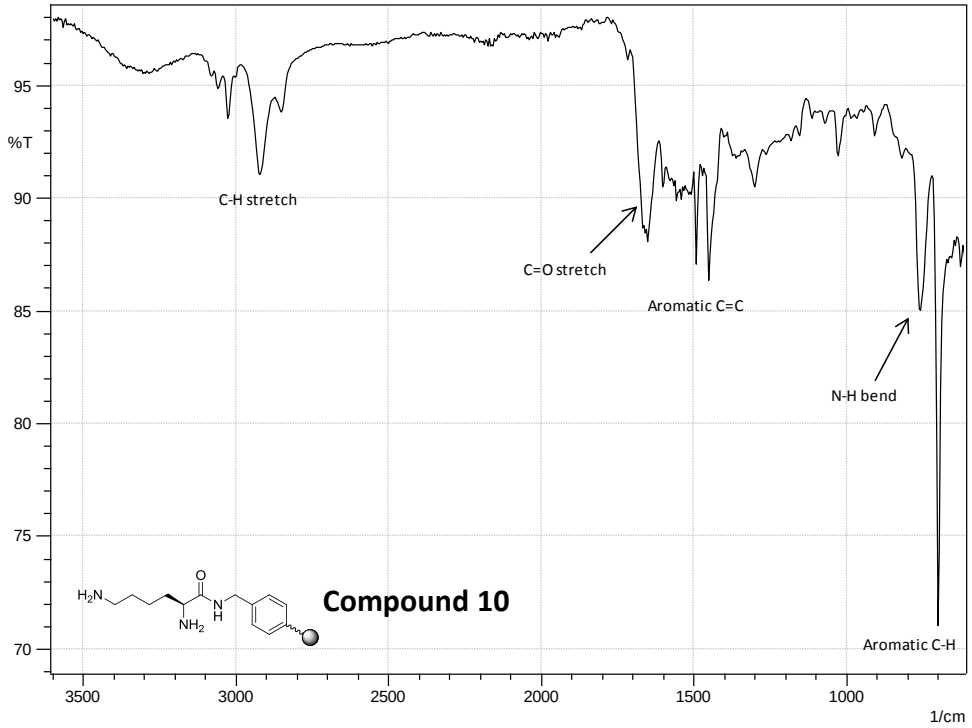
95
%T
90
85
80
75
70
C-H stretch
C=O stretch
Aromatic C=C
N-H bend
Aromatic C-H
Compound 10
3500
3000
2500
2000
1500
1000
1/cm

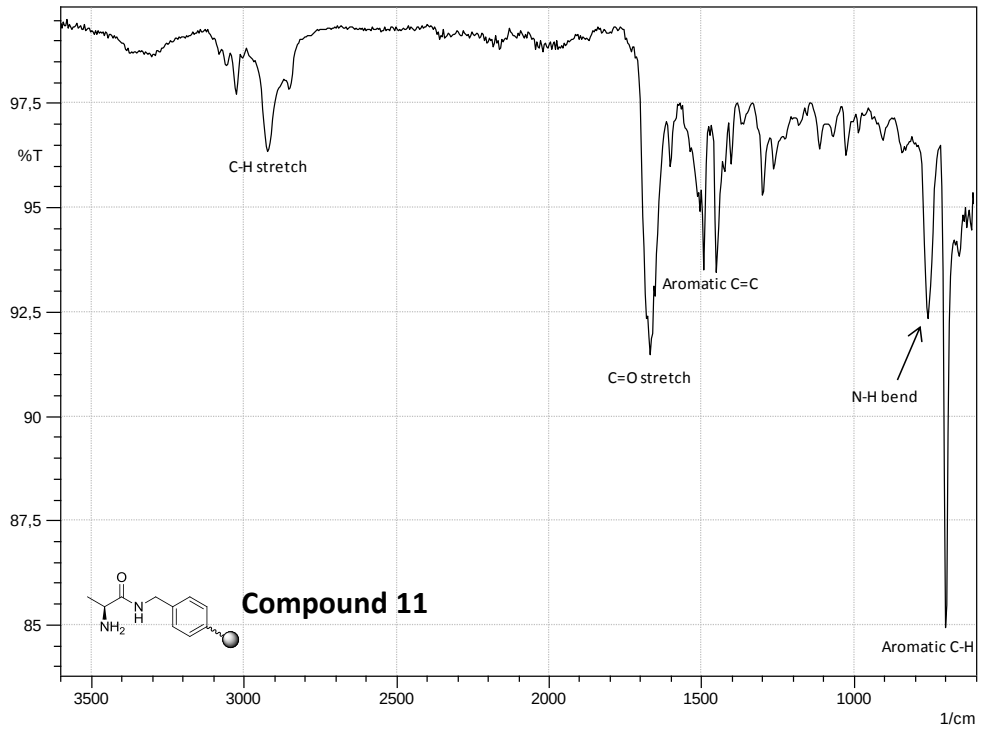

9. Test carried out on Fmoc-protected amines (primary and secondary) and alkyl chlorides

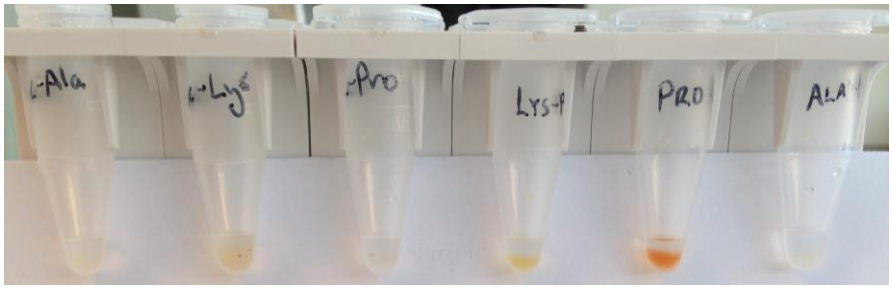

Picture S1: The acetaldehyde test performed on Fmoc-protected amino acids, alanine, lysine and proline (three tubes to the left) and unprotected amino acids (three tubes to the right)

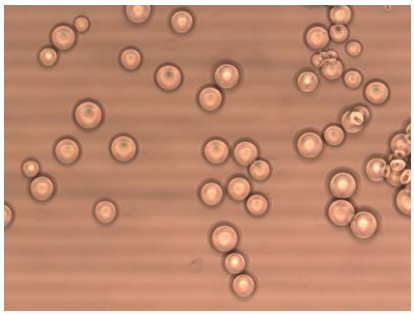

Picture S2: Micrograph of the colorless beads of chloromethylated polystyrene after performing the acetaldehyde test.

10. References

1) Svenssen, D. K.; Mirsharghi, S.; Boas. U. *Tetrahedron Lett.* **2014**, *55*, 3942-3945

2) Boas, U.; Gertz, H.; Christensen, J. B.; Heegaard, P. M. H. *Tetrahedron Lett.* **2004**, *45*, 269-272

3) Claerhout, S.; Ermolat'ev, D. S.; Van der Eycken, E. V. *J. Comb. Chem.* **2008**, *10*, 580-585

4) Yang, S.-J-; Tian, X. Z.; Shin, I. *Org. Lett.* **2009**, *11*, 3438-3441

NJC

PAPER

Cite this: *New J. Chem.*, 2016, 40, 3597

Preparation and self-assembly of amphiphilic polylysine dendrons†

Sahar Mirsharghi,[a] Kenneth D. Knudsen,[b] Shahla Bagherifam,[cd] Bo Nyström[c] and Ulrik Boas*[a]

Herein, we present the synthesis of new amphiphilic polylysine dendrons with variable alkyl chain lengths (C1–C18) at the C-terminal. The dendrons were synthesized in moderate to quantitative yields by divergent solid-phase synthesis (SPS) employing an aldehyde linker. The self-assembling properties of the dendrons in aqueous solutions were studied by small angle neutron scattering (SANS) and dynamic light scattering (DLS). The self-assembling properties were influenced by the length of the alkyl chain and the generation number (G*n*). Increasing the temperature and concentration did not have significant impact on the hydrodynamic diameter, but the self-assembling properties were influenced by the pH value. This demonstrated the need for positively charged amines in the head groups for the successful formation of controlled self-assemblies. Dendrons having alkyl chains below C8 did not self-assemble. Well-defined micellar structures observed with SANS were formed with alkyl chain lengths above C12. Large structures detected with DLS for dendrons with alkyl chain lengths above C12 are ascribed to intermicellar aggregates stabilized by hydrophobic and electrostatic forces in accordance with the observed pH effect. Finally, the cytotoxicity of the dendrons was evaluated in mouse fibroblast (NIH/3T3) and human embryonic kidney (HEK 293T) cells at 5, 10 and 20 μM concentrations. The dendrons showed low cytotoxicity, displaying cell viability well above 80%.

Received (in Montpellier, France) 1st October 2015,
Accepted 15th February 2016

DOI: 10.1039/c5nj02690c

www.rsc.org/njc

Introduction

Dendrimers and dendrons belong to a class of well-defined/monodisperse hyperbranched molecules. The first molecular dendritic structures reported in the literature were poly(propylene imine) (PPI or POPAM) initially named "cascade" molecules by Buhleier *et al.*[1] in 1978. However, it was Tomalia *et al.*[2] who defined and named dendrimers in 1985 and described the synthesis of bigger structures, *i.e.*, poly(amidoamine) (PAMAM) dendrimers. Independently around the same time Newkome *et al.*[3] reported the synthesis of similar macromolecules, poly(etheramide) (Arborol) dendrimers. The first peptide-based dendrimers and dendrons were developed by Denkewalter and co-workers in the early 1980s, and were composed of L-lysine as the repeating monomer.[4,5] Here, lysine has two amine functionalities available to serve as branching units. These structures were later revisited by Tam and co-workers, who constructed the well-defined multiple antigenic peptide (MAP) system that was originally intended for vaccines. MAPs are mainly based on polylysine. They have found additional use in other applications, *e.g.*, diagnostics, drug delivery, and gene delivery.[6–8] Dendrimers and dendrons are classified by their generation numbers (G*n*) according to the number (*n*) of branching points of repeating units from the core, or for polylysine dendrons, from the C-terminal to the periphery (N-terminal). With each generation number, the number of surface functionalities will increase. The surface groups can be modified with the molecular motifs of interest giving dendrimers and dendrons the ability of multivalent display. This multivalency makes dendrimers and dendrons promising for a variety of biomedical applications.[9–11] Recent studies on dendrons carrying a lipid tail have shown that they hold great promise as non-viral transfectants for genetic materials such as siRNA.[12–14] Hence, the ability to form self-assembled structures may be an important feature when applying dendrimers as carriers for drugs and genes.

In the present study, we synthesized novel polylysine dendrons with different alkyl chain lengths at the C-terminal to investigate the self-assembly behavior as a function of the alkyl chain length and dendron generation. We hypothesized that the lipid functionality on the dendrons would induce self-assembly into micelle-like structures

[a] *National Veterinary Institute, Technical University of Denmark (DTU), Bülowsvej 27, DK-1870 Frederiksberg C, Denmark. E-mail: uboa@vet.dtu.dk*
[b] *Department of Physics, Institute for Energy Technology, PO Box 40, N-2027 Kjeller, Norway*
[c] *Department of Chemistry, University of Oslo, PO Box 1033, Blindern N-0315, Oslo, Norway*
[d] *Department of Biology, University of Oslo, Blindernveien 31, N-0316 Oslo, Norway*

† Electronic supplementary information (ESI) available: Measured zeta potentials for G1 and G2 dendrons. IR data for four selected derivatized resins. Assigned NMR spectra (^{1}H-NMR, ^{13}C-NMR, DEPT-135 ^{13}C-NMR, HSQC and COSY) and UPLC-MS chromatograms are provided for all compounds. See DOI: 10.1039/c5nj02690c

by mainly hydrophobic interactions. Further modification of the surface functional groups of these dendritic structures with relevant ligands for a multivalent presentation can increase receptor recognition and binding due to the ''dendritic effect''.[9] The aim of this work is to elucidate the self-assembling features of these new systems and to gain insight into their potential to form supermolecular structures. For this purpose, it is highly relevant that the self-assembling properties of unmodified dendrons are well understood.

Results and discussion

Synthesis of polylysine dendrons

Dendrons were synthesized by step-wise divergent solid-phase synthesis, using a backbone amide linker strategy (Scheme 1),[15,16] which opens up the way for the preparation of dendrons with a large variety of C-terminal modifications. Here, a bisalkoxybenzaldehyde (4-(4′-formyl-3′-methoxyphenoxy) butanoic acid, FMPB) linker was attached to amino methylated polystyrene (AM PS) resin by an amide bond employing *N*,*N*,*N*′,*N*′-tetramethyl-*O*-(1*H*-benzotriazol-1-yl)uronium hexafluorophosphate (HBTU) or (benzotriazol-1-yloxy)tripyrrolidinophosphonium hexafluorophosphate (PyBOP) as the coupling reagent together with *N*,*N*-diisopropylethylamine (DIPEA).

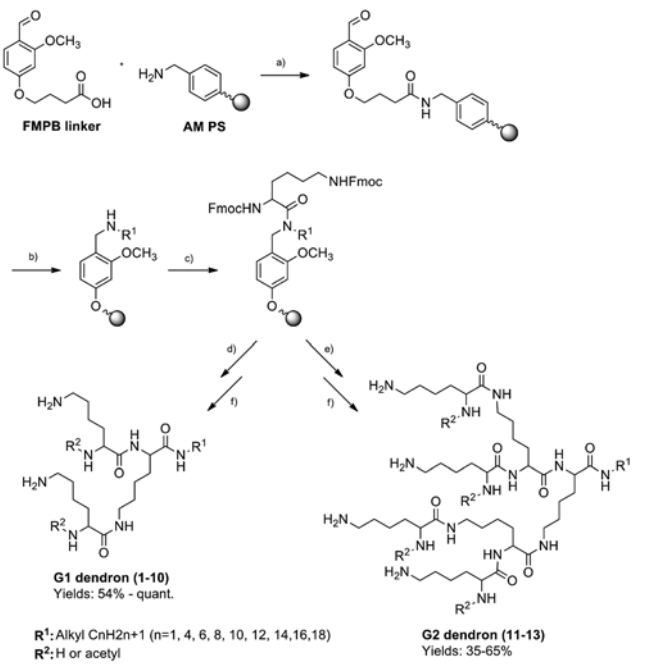

Scheme 1 Synthesis of G1 and G2 polylysine dendrons. (a) PyBOP or HBTU, DIPEA, NMP, rt, 22 h; (b) alkyl amine, $NaBH_3CN$, 5% AcOH, NMP, rt, 20 h; (c) Fmoc-Lys(Fmoc)-OH, DIC, DCM/NMP (95 : 5), rt, 20 h; (d) Fmoc deprotection: piperidine/NMP (1 : 4), rt, 3 + 30 + 20 min; linkage of the second lysine group: Fmoc-Lys(Boc)-OH, PyBOP, DIPEA, NMP, rt, 3 h or until ninhydrin test negative; (e) Fmoc deprotection: piperidine/NMP (1 : 4), rt, 3 + 30 + 20 min; linkage of the second lysine group: Fmoc-Lys(Fmoc)-OH, PyBOP, DIPEA, rt, 3 h or until ninhydrin test negative; Fmoc deprotection: piperidine/NMP (1 : 4), rt, 3 + 30 + 20 min; linkage of the third lysine group: Fmoc-Lys(Boc)-OH, PyBOP, DIPEA, rt, 3 h or until ninhydrin test negative; Fmoc deprotection: piperidine/NMP (1 : 4), rt, 3 + 30 + 20 min; (f) R^2 = H: TFA/DCM (1 : 1), rt, 2 h; R^2 = acetyl: Ac_2O/DIPEA/DCM (10/5/85), rt, 3 h; TFA/DCM (1 : 1), rt, 2 h.

The completion of the reaction on the resin bead was monitored by infrared (IR) spectroscopy (attenuated total reflectance) showing new bands at approximately 1670 cm^{-1} (C═O stretch, amide) and 1600 cm^{-1} (C═O stretch, aldehyde). Additionally, the reaction was monitored colorimetrically with 2,4-dinitrophenylhydrazine (DNPH) in sulfuric acid giving dark orange-red beads for resin-bound aldehyde groups according to the procedure by Shannon *et al.*[17] Subsequently, reductive amination between the FMPB aldehyde group and an alkyl amine allowed a C-terminal modification by an alkyl chain of choice (Scheme 1). The reductive amination was carried out by employing sodium cyanoborohydride ($NaBH_3CN$) in *N*-methyl-2-pyrrolidone (NMP) under mild acidic conditions (5% acetic acid). The reaction completion was monitored by IR, which showed an increase in the C–H stretch band around 2922 cm^{-1} and a decrease in the aldehyde band around 1610 cm^{-1}.[18] This increase was more pronounced for dendrons modified with long chain alkyl amines at the C-terminal. Furthermore, the reaction was monitored by two complementary on-resin colorimetric methods: DNPH test (pale orange to yellow beads in accordance with a negative readout) and a newly developed secondary amine test,[19,20] which gives orange-brown resin beads in the presence of resin-bound secondary amines. After this, acylation of the secondary amine on the resin by the first lysine residue was performed by Fmoc-Lys(Fmoc)-OH and *N*,*N*′-diisopropylcarbodiimide (DIC) as the coupling reagent in a dichloromethane (DCM)/NMP mixture. An insoluble waxy *N*,*N*′-diisopropylurea byproduct formed after 5 minutes and was removed after reaction completion by washing the resin thoroughly with NMP and MeOH. Also here, the reaction completion was monitored colorimetrically giving a negative secondary amine test (colorless beads). In order to determine the final yield of the solid-phase synthesis, resin loadings were determined after the first lysine group had been added by measuring the UV-vis absorbance at 290 nm (dibenzofulvene–piperidine adduct released upon Fmoc cleavage) upon treatment of the resin-bound Fmoc-derivative with 20% piperidine in NMP. The loadings typically ranged from 0.14 to 0.35 mmol g^{-1}.

Deprotection of the Fmoc-amines was conducted by the addition of a solution of 20% piperidine in NMP resulting in free primary amine groups for further reaction with the next lysine residue. The successful deprotection and subsequent coupling process were monitored colorimetrically by ninhydrin test (positive: purple-blue supernatant, negative: pale grey/yellow supernatant).[21,22] The second lysine was attached by employing PyBOP as the coupling reagent in NMP, and the reaction completion was again monitored by ninhydrin test. Either Fmoc-Lys(Boc)-OH or Fmoc-Lys(Fmoc)-OH was used as the second lysine depending on the product being a G1 or G2 dendron, respectively. For the G2 dendron the coupling was repeated with the attachment of Fmoc-Lys(Boc)-OH after the deprotection step. Cleavage of the dendron from the resin was carried out with a 1 : 1 mixture of trifluoroacetic acid (TFA) and DCM giving the dendrons in moderate to good yields and high

Table 1 Synthesized G1 and G2 dendrons

#	Compound	Yield[a] (%)
1	G1-C1	70
2	G1-C8	64
3	G1-C12	54
4	G1-C14	Quantitative
5	G1-C16	79
6	G1-C18	Quantitative
7	G1(acetyl)-C4	81
8	G1(acetyl)-C6	73
9	G1(acetyl)-C10	Quantitative
10	G1(acetyl)-C16	72
11	G2-C1	35
12	G2-C12	43
13	G2-C16	65

[a] TFA salt.

crude purity (see Table 1 for compound numbers and yields). To obtain dendrons having partially acetylated N-terminal amines, the Fmoc groups were removed and the dendrons having Bocylated side chain amines were treated with Ac_2O/DIPEA/DCM (10/5/85) prior to the release of the dendron from the resin by treatment with acid (Scheme 1).

The chemical structure of the synthesized dendrons was confirmed by ^{1}H-NMR, ^{13}C-NMR, DEPT-135 ^{13}C-NMR, COSY and HSQC and the molecular weight was determined by UPLC-MS. An example of typical 1D and 2D NMR spectra can be seen for the G1-C8 dendron in Fig. 1.[23]

Self-assembly probed by small angle neutron scattering

In order to obtain information on a mesoscopic length scale and to reveal the structure of the self-assembled species, small angle neutron scattering (SANS) was performed on synthesized G1-C1/C8/C12/C14/C16/C18, G1(acetyl)-C10/C16 and G2-C1/C12/C16 dendrons. Dendron concentrations of 9, 18 and 27 mM were chosen to observe the effect of concentration on the size and shape of the self-assembled entities. It should be noted that the considered concentrations are well above the critical aggregation concentration (cac) for the studied systems. To illustrate the scattering behavior, we show here initially SANS scattering data for two selected dendron types, G1-C16 and G1-C18, in aqueous solution (Fig. 2).

Strong interparticle interactions are observed in the form of a correlation peak at intermediate q-values (around q = 0.045 Å^{-1}), corresponding to an interparticle distance $d_i = 2\pi/q$ around 140 Å (14 nm). This allows for some separation between the micelles, since the overall diameter of these micelles was found to be *ca.* 5 nm (Table 2). The dynamic light scattering (DLS) results discussed below reveal that for these dendrons also some larger clusters (in the range around 100 nm) are formed in solution (*cf.* Fig. 9). These entities have, however, a size outside the range for the SANS detection, and will not contribute to the characteristic micellar SANS pattern that we have seen, apart from a possible weak contribution at the lowest q-range where the SANS data are noisy. The SANS measurements therefore probe the micellar range only, but this does not exclude the presence of larger structures that we in some cases observe by DLS.

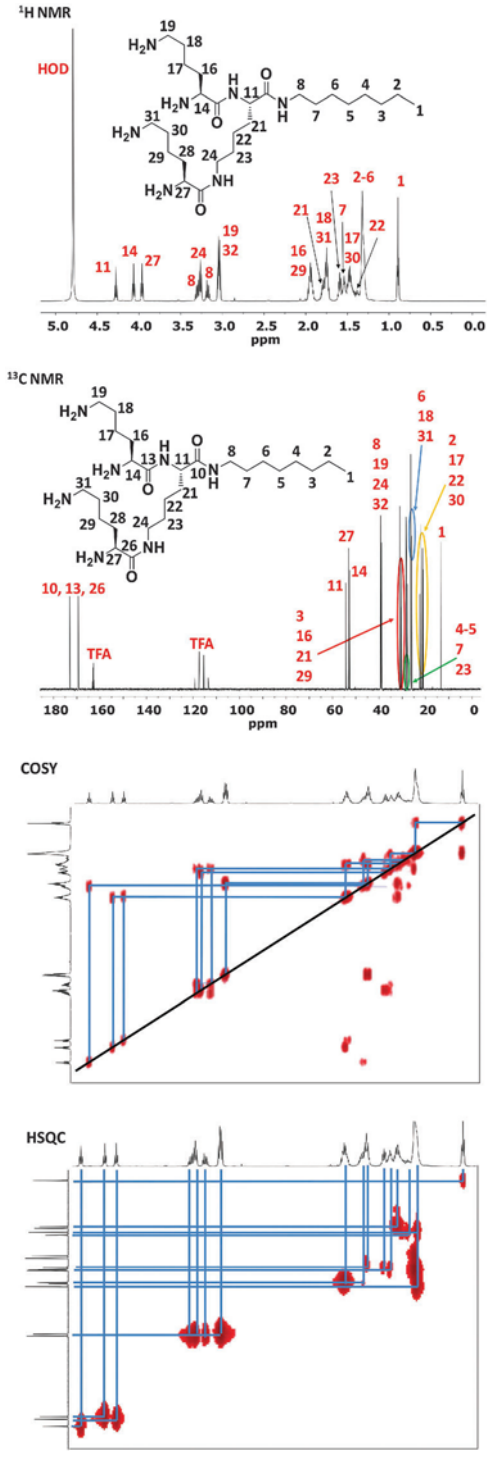

Fig. 1 Top: Assigned 1D NMR spectra of the G1-C8 dendron in D_2O (^{1}H-NMR 600 MHz and ^{13}C-NMR 151 MHz). Bottom: 2D NMR spectra of the G1-C8 dendron showing the coupling between ^{1}H–^{1}H nuclei (COSY) and ^{13}C–^{1}H nuclei (HSQC).

The data can be well portrayed by a core–shell particle model when a repulsive interaction term between the particles is included. For interacting spherical entities the scattered intensity can be expressed through the product of a form factor $P(q)$ and an interaction term $S(q)$ (structure factor). The following form factor

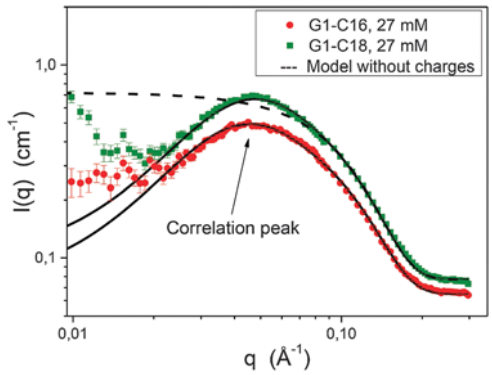

Fig. 2 SANS profiles of the G1-C16 and G1-C18 dendrons in aqueous solutions at a concentration of 27 mM. Continuous lines are fits with a spherical core–shell model (see text). The dashed line for G1-C18 represents the same core–shell model, but without charges.

Table 2 Fitted parameters for the G1-C16 and G1-C18 micelles. Error in the sizes is ±0.4 Å, in the charge ±0.5 *e*, and in the aggregation number ±5

	Concentration [mM]	*R* (core) [Å]	Thickness (shell) [Å]	*R* (total) [Å]	Charge (+)	*N*(agg)
G1-C16	27	12.0	12.3	24.3	7.9	33
G1-C18	27	12.8	11.9	24.7	8.0	35

$P(q)$, representing a spherical core–shell structure, was employed in the analysis:[24]

$$P(q) = \frac{\text{scale}}{V_s}\left[\begin{array}{l} 3V_c(\rho_c - \rho_s)\dfrac{[\sin(qr_c) - qr_c \times \cos(qr_c)]}{(qr_c)^3} \\ +3V_s(\rho_s - \rho_{solv})\dfrac{[\sin(qr_s) - qr_s \times \cos(qr_s)]}{(qr_s)^3} \end{array}\right]^2 + \text{bkg} \quad (1)$$

Here V_c is the volume of the core while V_s is the volume of the shell. The parameter r_s is the outer radius of the shell (with respect to the particle center) and r_c that of the core, while ρ_c, ρ_s and ρ_{solv} are the scattering length densities of the core, shell, and solvent, respectively. In the modelling, ρ_{solv} and ρ_c were set to the theoretical values for the scattering length density of D_2O (ρ_{solv} = 6.3 × 10^{-6} Å^{-2}) and the alkyl chain (ρ_c = −0.34 × 10^{-6} Å^{-2}), respectively. The parameter ρ_s corresponds to the average scattering length density of the atoms in the dendron head groups, together with the water molecules located inside the shell, and was adjusted for a best fit to the data. The value of ρ_s was approximately 4 × 10^{-6} Å^{-2}, indicating that the shell was significantly hydrated. The term scale is a factor proportional to the concentration, and bkg is the background due to incoherent scattering. To illustrate the significance of electrostatic interactions, the dashed line for G1-C18 in Fig. 2 represents the same core–shell model without charges. It is obvious that this model does not portray the data well and this emphasizes the importance of including charges in the model for a good description of the data.

Since these micelles are likely to be charged, due to the presence of amine groups, the structure factor employed was that corresponding to particles with Coulomb interaction, as developed by Hayter and Penfold. Below the structure factor is written in dimensionless form, where $K = q\sigma$, with σ being the diameter of the spherical particle:[25]

$$S(K) = \frac{1}{1 - 24\eta a(K)} \quad (2)$$

where $\eta = \pi n\sigma^3/6$ is the volume fraction (n being the particle number density). The parameter $a(K)$ is a sum of polynomial terms (not shown here), which includes the effect of particle charge and counterions, as well as that of possible screening from additional ions in the solution.

Table 2 shows the extracted values for the core size and shell thickness using this model. The core radius is found to be 12 Å for the G1-C16 micelle, and in the same range (12.8 Å) for the G1-C18 micelle. Even though the difference is small, and within the error level, one may in fact expect a slightly larger core radius for G1-C18 due to the longer alkyl chain (two more C atoms) that has to be accommodated into the micellar core.

The overall size of the micelles is found to be the same (within errors), *i.e.*, about 25 Å or 2.5 nm radius, corresponding to a diameter of *ca.* 5 nm. When compared with the average distance between the micelles found earlier, *ca.* 14 nm, we see that the surfaces of two neighboring micelles are separated by a distance of roughly two micellar diameters.

The aggregation number *N*(agg), *i.e.*, the number of dendron molecules taking part in each micelle, has also been estimated for these systems, as shown in Table 2. *N*(agg) can be calculated based on the volume of one micelle, given by $(4/3)\pi R^3$, where R is the total radius listed in Table 2, divided by the volume of one dendron molecule. The latter is given by $M_w/(N_A{\cdot}\rho)$, where M_W is the weight average molecular weight, N_A is Avogadro's constant (6.02 × 10^{23} mol^{-1}), and ρ is the density (g cm^{-3}). When calculating M_w one must take into account that for the G1 dendrons with four free amine groups, a minimum of four TFA molecules (each with M_w of 114.02 g mol^{-1}) will be directly associated with the dendron. For other dendrons employed, such as the G1(acetyl)-C16 and Lys-C16 having two free amine groups (see later), one should take into account a minimum of two TFA and HCl molecules, respectively. For the estimate of *N*(agg) we have assumed the number of associated TFA or HCl molecules being equal to the minimum number mentioned above, and furthermore employed the same density (1 g cm^{-3}) for the different dendrons. We note that the aggregation numbers observed for G1-C16 and G1-C18 are 33 ± 5 and 35 ± 5 and they are significantly smaller than that of micelles of SDS having a radius of about 2 nm and an aggregation number of *ca.* 60.[26] This difference is expected because of the bulky head groups of the dendrons reported in this paper.

We also find that there is a charge on the micelles, corresponding to *ca.* 7 charge units. This charge is due to protonated amines in the head groups of the dendrons. Since the head group is the same (G1) for the two dendrons above, it is also reasonable that the effective charge is found to be nearly the same in the two cases. This charge is responsible for quite a strong repulsion between the micelles, reflected in the structure factor $S(q)$, and leading to the depression of the curve to the left

side of the correlation peak. As an illustration of the effect of charges on the scattering profile, the pattern of the same core–shell model without any charges present (all other parameters unchanged) is also shown (Fig. 2). We observe in Fig. 2 that the scattering signal tends to rise again at the lowest q-values and the upturn is strongest for the dendron (G1-C18) with the longest alkyl chain. This is most likely due to some large aggregates also present in the sample (*cf.* discussion of the DLS data below), and this part of the pattern (below q = 0.15 Å^{-1}) was not included in the fitting.

The charges present in the head groups of these dendrons are expected to have an influence on the stability of the created micelles, hindering the tendency to intermicellar aggregation. However, one may expect that these charges also can have an effect on the ability of the dendrons to assemble into micelles, due to Columbic repulsion that will occur between the head groups in the micellar shell. We therefore synthesized a variant of G1-C16 having less charges, G1(acetyl)-C16, with two acetylated amines and two free amines in the head group to compare the results with the SANS data on G1-C16 shown above, having four free amino groups in the head group. This turned out to considerably affect the SANS pattern, indicating an even stronger tendency to micelle formation. From a visual inspection of the results obtained (Fig. 3) we find that the characteristic micellar scattering pattern is significantly more developed for the less positively charged compound G1(acetyl)-C16 than for G1-C16. The intensity is higher (for the same concentration) and the correlation peak is narrower, demonstrating a well-defined average distance between similar entities (micelles).

We argue that the difference in behavior between the two dendrons is due to the stronger electrostatic repulsion within the corona of the micelles from compound G1-C16 that has four positively charged amine groups. This additional repulsion acts as a force working against the self-assembly of sufficient dendron molecules to create the most stable micelles. The SANS data on G1(acetyl)-C16 were also fitted using the spherical core–shell model described earlier, with the results shown in Fig. 3C. Table 3 shows the result of the fitting for this system. The radius of the core and the thickness of the shell of the micelle, as well as the extracted value for the micellar charge, are listed.

It is found that both the core radius (13–17 Å) and the total radius (25–28 Å) of the micelles increase slightly with increasing concentration. When comparing the core radius obtained earlier for the G1-C16 micelle (Table 2) with the value for G1(acetyl)-C16 at the same concentration (27 mM), we find a larger size for the latter (*ca.* 16 *vs.* 12 Å), whereas the thickness of the shell is nearly the same, and practically constant (roughly 12 Å) for the G1(acetyl)-C16 micelles over the concentration range considered in this study.

The size of the core radius is compatible with the expected size of an extended C16 chain, and the shell size matches with the approximate size of the head groups (roughly 10 Å). The slight expansion of the micelle size with increasing concentration is an indication that more unimers (dendrons) are incorporated into each micelle. This is reflected in the estimated aggregation number, and is also consistent with the finding that the effective charge density of the shell increases as the dendron concentration increases.

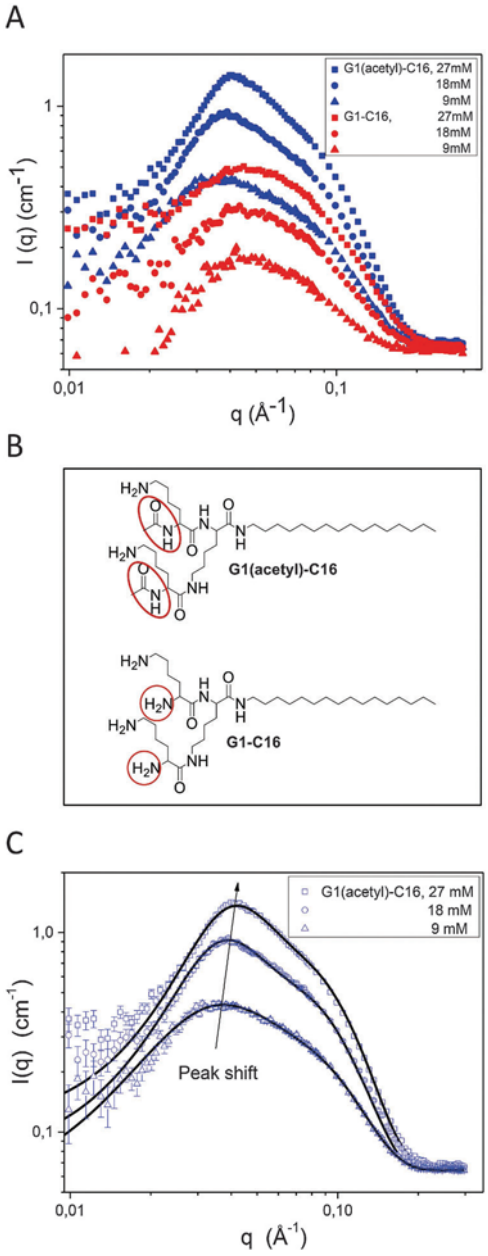

Fig. 3 (A) Comparison of SANS profiles from the two different G1-C16 dendrons, with 4 amine groups (G1-C16) and 2 amine groups (G1(acetyl)-C16). (B) The molecular structures of the two different G1-C16 dendrons with head group differences marked by red circles. (C) SANS profiles of the G1(acetyl)-C16 dendron fitted with a spherical core–shell model.

Table 3 Fitted parameters for the G1(acetyl)-C16 micelles. The error in the sizes is ±0.2 Å and in the charge ±0.5 e

	Concentration [mM]	R (core) [Å]	Thickness (shell) [Å]	R (total) [Å]	Charge (+)	N(agg)
G1(acetyl)-C16	9	13.4	12.5	25.9	10	47
	18	15.7	11.7	27.4	15	55
	27	16.7	11.3	28.0	16	59

The position of the correlation peak in Fig. 3C is seen to move to slightly higher q-values with increasing concentration,

demonstrating that the average distance between the micelles becomes smaller due to the formation of more micelles. Thus the main effect of concentration increase for this system is the formation of additional micelles, with just a slight simultaneous increase in the micellar size.

We have now demonstrated the behavior and fitting procedure for some stable micellar structures, and to achieve that dendrons with a relatively long alkyl chain were selected. However, we also looked at the effect of different lengths of the alkyl chain, and found that there is a certain critical length necessary for micelles of these dendrons to be formed. SANS results for G1 dendrons with three different lengths of the alkyl chain and at various concentrations are depicted in Fig. 4A, and a visual inspection of the data gives important information about these systems.

For the sample with the shortest alkyl chain shown here (G1-C14), the correlation peak is virtually absent at the lowest concentration, but appears and is strengthened as the concentration increases. This behavior is consistent with the hypothesis that more molecules facilitate self-assembly and thereby favor the formation of core–shell like structures. Correlation peaks are seen to exist at all concentrations for G1-C16 (as commented earlier), reflecting the formation of organized spherical core–shell micelles, although this effect was found to be even stronger for G1(acetyl)-C16. This behavior is also found to be the case for G1-C18 at the three concentrations employed (Fig. 4A). These findings show that when the alkyl tails are sufficiently long, regular structures can emerge even at low concentration, and a longer alkyl chain (with the head group unchanged) enhances the formation of stable micelles. On the other hand, for the C14 alkyl chain, a higher concentration is needed to develop micelle-like structures. As mentioned before (*cf.* Fig. 2), although there is significant noise in the SANS data at low q-values, one can identify a significant upturn in the scattered intensity at low q for most of the samples, indicating the existence of also some large structures in the system (see the discussion below on DLS results).

Furthermore, a comparison between two generations of dendrons, G1 and G2, was made. This is shown in Fig. 4C at a concentration of *ca.* 20 mg mL^{-1}. In addition, the SANS scattering profiles for dendrons with the shortest alkyl chain, G1-C1 and G2-C1, are also shown in the figure. These patterns are observed to be very similar and indicate that no regular micelle structures are formed, but the strong upturn at low q may signalize the presence of large irregular aggregates. It should be mentioned that patterns for other alkyl chain lengths, G1-C8/C12 and G1(acetyl)-C10, were also collected (not shown here), but were practically overlapping with those of G1-C1, thus presenting no indication of micelle formation. When the data for G1-C16 and G2-C16 are compared, it is noticed that the SANS scattering profile for G2-C16 displays quite a different behavior than that of the former sample. For G2-C16 a plateau region is observed at intermediate q-values,

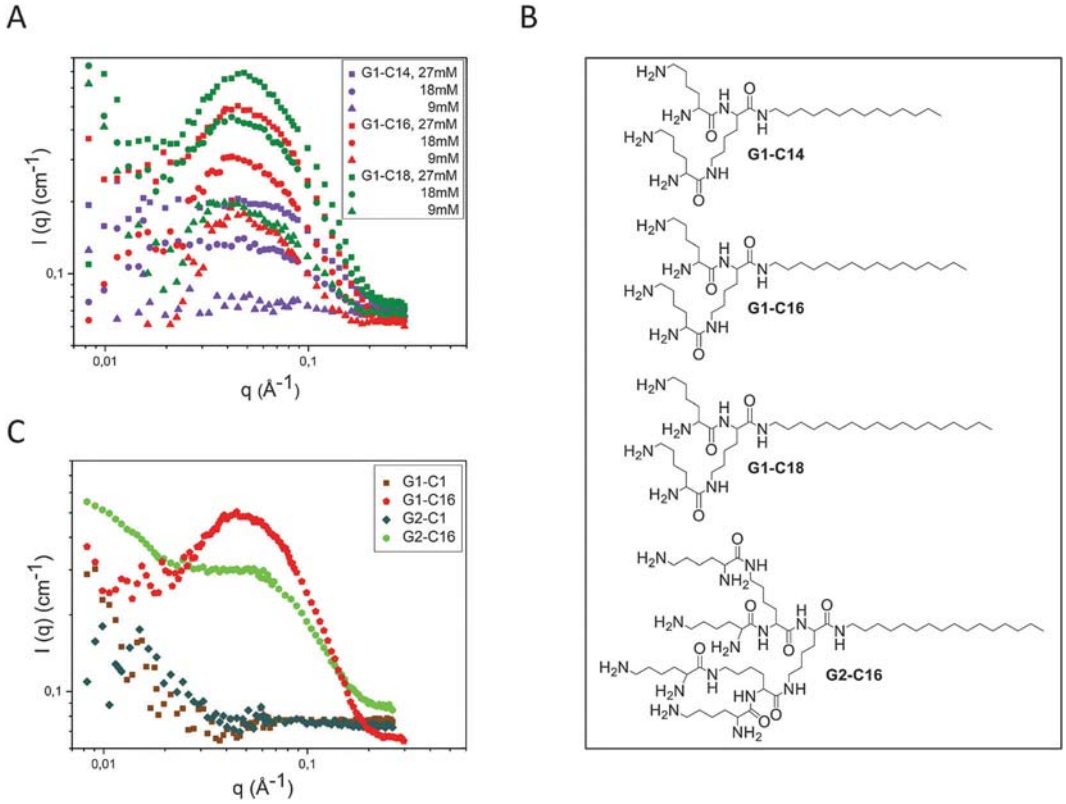

Fig. 4 (A) SANS profiles for G1-C14, G1-C16 and G1-C18 at different concentrations. (B) The molecular structures of G1 dendrons shown with different alkyl chain lengths (C14, C16 and C18) and the G2-C16 dendron. (C) SANS profiles of G1 and G2 dendrons with variable C-terminal alkyl tails at a concentration of about 20 mg mL^{-1}.

followed by a strong upturn of the scattered intensity at low q. This clearly suggests the presence of large clusters in the solution, and indicates that the larger head groups in the G2 dendrons (compared to G1) may obstruct the formation of regular micelles. It is reasonable to assume that the efficiency of forming micelles should depend on the size and population of both polar and non-polar groups, lysine head group and alkyl chain, respectively. Thus for a moderate alkyl length (*e.g.*, C16 as here), the size of the head group can easily become too large for efficient packing in the micellar corona.

Based on the previous observation of the effect of the head group, we also decided to investigate another variant of the C16-type dendron, namely Lys-C16 where the G1 head group (three lysine groups) has been replaced by an even smaller unit (one lysine group). This was in order to see if reducing the head group even further had any effect on the micelle formation. In Fig. 5, the SANS profiles for solutions of Lys-C16 are shown. The characteristic features are similar to those of the G1(acetyl)-C16 system (Fig. 3), with strong micellar scattering of nearly the same magnitude, being more accentuated than for the G1-C16 dendron. The same core–shell model as employed earlier was used in fitting these data, and the results are shown in Table 4.

Lys-C16 and G1(acetyl)-C16 are quite different in terms of size of the head group, but comparable with respect to charge, with both having two amines available for protonation, instead of the four amines in G1-C16. This is a strong indication that charge density is highly important with respect to micelle formation. This comes in addition to the earlier observation that for a given charge the size of the head group can work against the formation of stable micelles. Also for Lys-C16 more unimers are located in the micelle as the concentration increases.

A comparison of the results of the fitting for the Lys-C16 and the G1(acetyl)-C16 systems discloses (apart from the lowest concentration, where the data quality is moderate) that the thickness of the shell for Lys-C16 is slightly smaller than that for G1(acetyl)-C16. This is reasonable taking into account that Lys-C16 has a marginally smaller head group. We also see that the aggregation number has now increased considerably with respect to the G1-type dendrons, most likely since the smaller Lys head group reduces the steric hindrance in the micellar corona, thus allowing for the hydrophobic interaction between the alkyl chains to assemble more dendrons in each micelle. Overall, the results for solutions of these dendrons demonstrate that both systems form spherical core–shell micelles with a total diameter between 5 and 6 nm, where C16 alkyl chains constitute the core and the head group designs the shell.

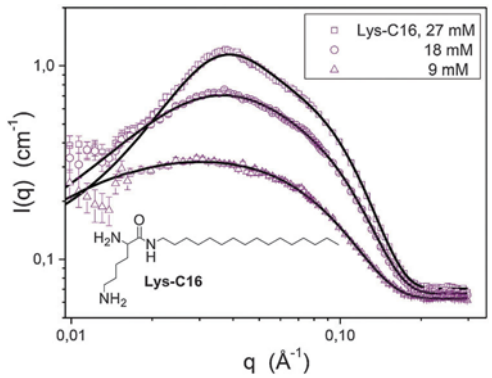

Fig. 5 SANS profiles of Lys-C16 (see the molecular structure inseted below the curves) in aqueous solutions at different concentrations. The curves are well fitted with a spherical core–shell model of charged micelles.

Table 4 Fitted parameters for the Lys-C16 micelles. The error in the radii is ±0.2 Å and in the charge ±0.5 *e*

	Concentration [mM]	*R* (core) [Å]	Thickness (shell) [Å]	*R* (total) [Å]	Charge (+)	*N*(agg)
Lys-C16	9	13.5	14.4	27.9	4	124
	18	17.9	10.7	28.6	7	133
	27	18.6	10.5	29.1	12	140

Self-assembly probed by dynamic light scattering

The effects of the C-terminal alkyl group on the self-assembling properties of the G1 and G2 dendrons were investigated by DLS to gain insight into the sizes and structures formed in the self-assembly process on a more global dimensional scale than SANS. The influence of temperature, pH and concentration on the behavior of these systems was examined to obtain detailed information on the effects of these parameters on dynamics and structure.

Since our ultimate aim is to employ the synthesized polylysine dendrons for drug delivery purposes, four relevant temperatures were chosen: 8 °C (refrigerated storage conditions), 25 °C (shelf storage at rt), 37 °C (physiological) and 42 °C (hyperthermic case). We chose to investigate three different pH values: pH 5 (present in lysosomes and tumors), pH 7.4 (physiological conditions) and pH 9 to understand the behavior of the polylysine dendrons under basic conditions. To obtain these pH values, a phosphate buffered saline (PBS) solution was employed and the pH adjusted with 0.1 M HCl or 0.1 M NaOH. Dendron concentrations of 4, 9 and 18 mM were chosen to see whether an alteration in concentration may lead to changes in the size of the self-assembled entities.

In solutions of dendrons and other solutes, the experimentally recorded intensity autocorrelation function $g^2(q,t)$ is directly linked to the theoretically amenable first-order electric field autocorrelation $g^1(q,t)$ through the Siegert[27] relationship $g^2(q,t) = 1 + B|g^1(q,t)|^2$, where B (≤ 1) is an instrumental parameter. The wave vector is determined by $q = (4\pi n/\lambda)\sin(\theta/2)$, where λ is the wavelength of the incident light in vacuum, θ is the scattering angle, and n is the refractive index of the medium.

For most dendrons, the decay of the correlation functions generally showed a unimodal behavior and was fitted by a stretched exponential with only one relaxation mode:

$$g^1(t) = A\exp\left[-\left(\frac{t}{\tau_e}\right)^{\beta}\right] \quad (3)$$

Here A is the amplitude of the relaxation mode, τ_e is the effective relaxation time, and β ($0 \leq \beta \leq 1$) is a measure of the distribution of relaxation times. The average relaxation time

is given by $\tau = (\tau_e/\beta)\Gamma(1/\beta)$, where $\Gamma(1/\beta)$ is the gamma function of β^{-1}.

For the G1-C14/C16/C18 dendrons, the relaxation process was found to be more complex because large clusters are formed. In this case, bimodal decay is observed and the correlation functions are well portrayed by the sum of two stretched exponentials:

$$g^1(t) = A_f \exp\left[-\left(\frac{t}{\tau_{fe}}\right)^{\beta_f}\right] + A_s \exp\left[-\left(\frac{t}{\tau_{se}}\right)^{\beta_s}\right] \quad (4)$$

where $A_f + A_s = 1$. The subscripts f and s of the amplitudes denote parameters for the fast and slow relaxation mode, respectively.

The correlation functions were analyzed by a non-linear fitting algorithm obtaining best-fit values for the relaxation times and stretched exponentials in eqn (3) or eqn (4). The relaxation time τ is always diffusive and therefore q^2 dependent. The relaxation time is related to the mutual diffusion coefficient D by $\tau^{-1} = D{\cdot}q^2$ and the apparent hydrodynamic diameter d_h assuming spherical structures can be calculated *via* the Stokes–Einstein relationship:

$$d_h = \frac{k_B T}{3\pi\eta D} \quad (5)$$

where k_B is the Boltzmann constant, T is the absolute temperature, and η is the viscosity of the medium.

DLS was employed to investigate the concentration effects on the self-assembling properties of the G2-C12 and G2-C16 dendrons, and the results indicate that the concentration did not have any notable effect on the sizes of the aggregates. The hydrodynamic diameters d_h were found to be 95 nm and 65 nm, respectively (Fig. 6). In these cases the correlation functions could be well-described by a single stretched exponential (eqn (3)). However, the sizes of the species are outside the q-window probed in our SANS experiments.

These large hydrodynamic diameters observed by DLS are attributed to aggregates, since they are much larger than the sizes detected by SANS. We suggest that the large aggregates are due to intermicellar entities formed for these dendrons that show micellar structures by SANS. However, for dendrons not exhibiting micellar structures by SANS, *i.e.* alkyl lengths of C12 and below, the association process is probably due to the formation of more random assemblies. Our conjecture is that the intermicellar structures are partly held together by electrostatic forces between the positively charged amine groups on the lysine heads and negatively charged trifluoroacetate present in the solution (the dendrons were synthesized as trifluoroacetate salts, Scheme 1). A more detailed discussion about the formation of micelles and intermicellar associations is given below.

In addition, the temperature effect was examined for some G1 dendrons (*e.g.* G1-C8, G1-C16 and G1(acetyl)-C16) and G2 dendrons (*e.g.* G2-C12 and G2-C16) showing no influence on the self-assembly, as illustrated for G1-C16 and G2-C16 in Fig. 7 at a solute concentration of 18 mM. To compensate for simple temperature-induced changes in solvent viscosity, the first-order electric field autocorrelation function, $g^1(t)$, was plotted against $t{\cdot}T/\eta$ (where t is the time, T is the absolute solution temperature, and η is the solvent viscosity). Since fairly high temperatures are considered and no influence of temperature is detected on the decay of the correlation function, the results indicate that hydrogen bonds should not play an important role in the self-assembling behavior of these dendrons since hydrogen bonds are expected to be disrupted at elevated temperatures. This effect would lead to faster decay of the correlation function and therefore smaller size of the entities. Since neither solute concentration nor temperature seems to affect the self-assembling process and the species are stable over time, the formation of these very large supramolecular structures appears to be controlled by a mechanism that is not directly related to the conventional hydrogen and hydrophobic interactions. Another interesting feature observed in Fig. 7 is that for the G2-C16 sample the correlation functions at different temperatures can be portrayed by a single stretched exponential with d_h = 65 nm and a value of β = 0.8, which indicates fairly monodisperse entities. In contrast, for the G1-C16 sample the correlation functions reveal a bimodal relaxation mode that can be well described by eqn (4). In this case, micelles (d_{hf} = 6 nm) coexist with intermicellar structures (d_{hs} = 88 nm). The reason for this difference in the self-assembling behavior of the dendrons is not clear, but it seems that the bulky G2-C16 dendrons are more inclined

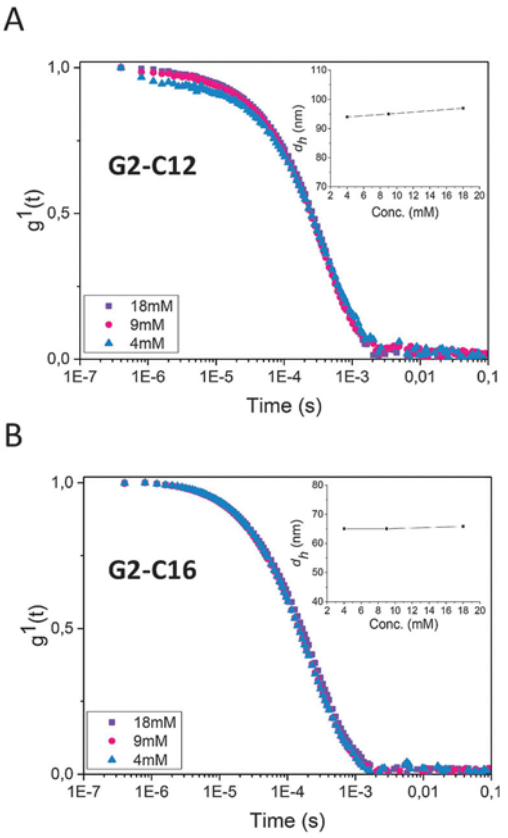

Fig. 6 First-order electric field autocorrelation function *versus* time obtained for (A) G2-C12 and (B) G2-C16 for different concentrations at 25 °C and pH ranging from 3 to 5. The insets show the effect of concentration on the hydrodynamic radius.

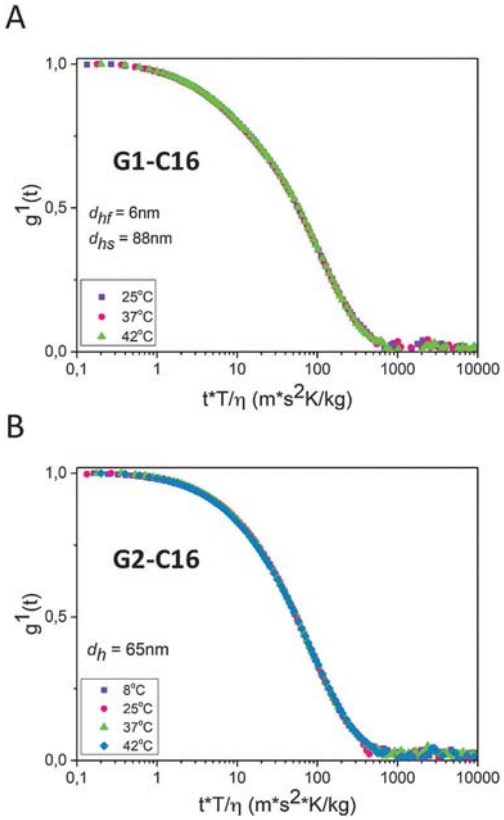

Fig. 7 First-order electric field autocorrelation function at a scattering angle of 124° *vs.* $t{\cdot}T/\eta$ obtained for (A) G1-C16 and (B) G2-C16 at different temperatures and at a solute concentration of 18 mM.

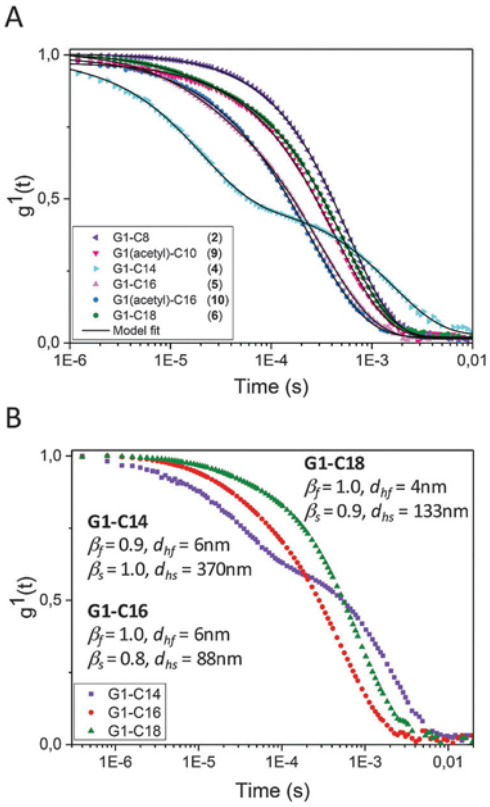

Fig. 8 (A) First-order electric field autocorrelation functions at a scattering angle of 124° obtained for G1 dendrons with a tail length equal to or above C8. Only G1-C14, G1-C16 and G1-C18 exhibit a bimodal behavior and the other systems exhibit unimodal decay. (B) First-order electric field autocorrelation functions *versus* time for G1-C14, G1-C16, and G1-C18 systems at a scattering angle of 90° and a temperature of 25 °C.

to form intermicellar structures. It is interesting to note that the lower value of d_{hf} around 6 nm corresponds well with the sizes found by SANS, *i.e.* a radius of 2.5–2.9 nm (depending on the dendron type, *cf.* Tables 2–4), giving a diameter of 4.9 to 5.8 nm.

Since we did not observe any concentration effects, a concentration of 18 mM was chosen for the analysis of the rest of the dendrons, besides G1-C16 and G1(acetyl)-C16, which were analyzed at a concentration of 27 mM. The DLS measurements indicate that a minimum C-terminal alkyl tail length of C8 was needed for the dendrons to form clusters, since no correlation functions were obtained with dendrons having tail lengths below C8 (Fig. 8A).

Surprisingly, no self-assembly was observed for G1-C12 by DLS, even though the corresponding dendrons with shorter alkyl tail groups were showing association behavior. Zeta potentials were determined for the different dendrons and ranged from 11 to 55 mV. However, there was no clear correlation between zeta potential values and the ability of the dendrons to self-assemble.[28,29] The hydrodynamic diameters d_h of the aggregates obtained by DLS for G1-C8/C14/C16/C18, G1(acetyl)-C10/C16 and G2-C12/C16 ranged from approximately 65 to 370 nm showing the formation of large interchain architectures.[30] It is obvious from Fig. 8A that the correlation function for the G1-C14 dendron exhibits the most pronounced bimodal appearance and this behavior supports the coexistence of micelles and intermicellar structures.

The stretched exponential β characterizes the width of the distribution of relaxation times and β is 1.0 for a single exponential. In this study β is in the range 0.8–1.0 showing a fairly narrow size distribution. In Fig. 8B, $g^1(q,t)$ is plotted *versus* time for the G1-C14, G1-C16, and G1-C18 samples and both the fast and slow relaxation modes are diffusive. The appearance of two relaxation modes for these samples can probably be attributed to increased hydrophobicity due to the long alkyl chains in these dendrons. This feature should make them more inclined to form intermicellar structures. The bimodal profile of the correlation functions is most pronounced for the G1-C14 system, but the bimodal appearance can also be established for the other displayed systems. The results disclose the coexistence of micelles ($d_{hf} \approx$ 4–6 nm) and large intermicellar species. The sizes of the micelles from DLS are close to the values observed for the same systems by SANS. The largest hydrodynamic diameter (d_{hs} = 370 nm) is observed for the G1-C14 sample, whereas the smallest (d_{hs} = 88 nm) is found for the G1-C16 system. It seems that the sample with the shortest carbon chain is more inclined to form large interchain structures. When the alkyl chain is longer, the effect of steric hindrance may come into play and this may prevent the formation of large intermicellar associations.

The hydrodynamic diameters obtained from DLS are summarized in Fig. 9 for the systems indicated in the figure. Fig. 9A

reveals that only the G1-C14/C16/C18 dendrons show a bimodal behavior with a fast and a slow relaxation mode. The value of d_{hs} in Fig. 9A shows a maximum for the G1-C14 dendron and this suggests that this system is inclined to form large associated structures. The dendrons with longer alkyl chains (C16 and C18) seem to form smaller aggregates. The values of d_{hf} from the fast relaxation mode do not give a specific trend. In spite of the fact that SANS data for the G1(acetyl)-C16 dendron system suggest the formation of well-developed micelles, we are not able to detect a fast relaxation mode in the correlation function, representing the micelles, for this system. The reason for this is attributed to the small amplitude of the fast mode, compared to the slow mode representing the intermicellar clusters. As a result, the fitting procedure is not able to catch the fast relaxation mode.

The results for the G2-C12 and G2-C16 dendrons show that the correlation functions can be described by a single relaxation mode (eqn (3)) and the value of d_h decreases as the alkyl chain becomes longer (*cf.* Fig. 9B). The hypothesis for the absence of the fast mode (micelles) is that the larger head groups in the G2 dendrons can obstruct the formation of regular micelles and this conjecture is supported by the previous SANS results. The decrease of d_h may indicate that the packing efficiency inside the species may be augmented for longer alkyl chains.

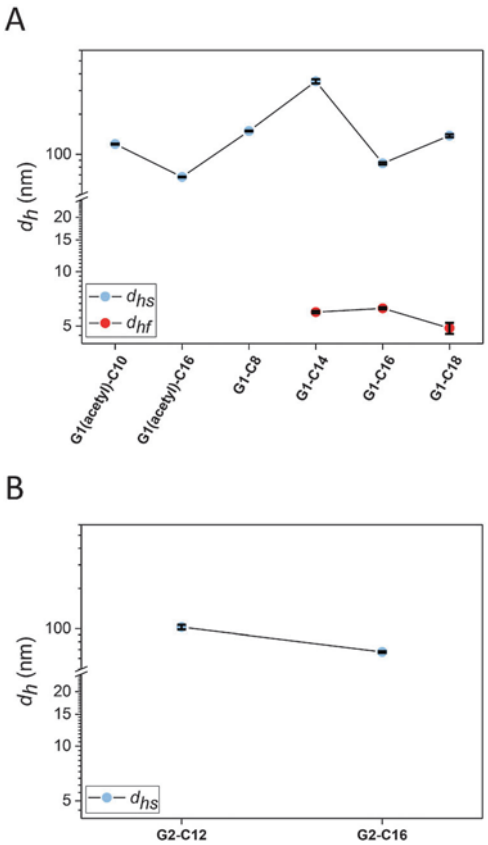

Fig. 9 The hydrodynamic diameter (d_h) obtained by DLS presented with error bars (approximately of the same size as the symbols) as a logarithmic function. (A) G1 dendrons with G1-C14/C16/C18 showing a bimodal behavior with the fast mode giving d_{hf} and the slow d_{hs}. (B) G2 dendrons only showing unimodal behavior.

Next, we studied the pH effect on the sizes of the moieties formed by the dendrons. By examining the self-assembling ability of the G2-C16 dendron at pH 5, 7.4 and 9 in a phosphate buffer, we could conclude that an acidic pH was best suited to evoke self-assembly. The G2-C16 dendron precipitated at pH 7.4 and 9. However, at pH 5, the G2-C16 dendron was solvated showing increased size for the intermicellar aggregates giving a d_h value of 212 nm, in comparison to the d_h value of 117 nm measured at pH 4 (Fig. 10). The observed pH effect confirmed our hypothesis that the formation of intermicellar aggregates could be due to electrostatic forces between micelles. At higher pH values these forces would not be effective due to the removal of the positive charge from the amines in the lysine head groups.

In Fig. 11, we have summarized our main findings in a schematic way, based on information obtained from both DLS and SANS data. As indicated in the figure, the length of the alkyl chain is an important parameter with respect to micelle formation. Micelles (with a diameter of approx. 5 nm) were created only for chain lengths of C14 and above, and their core–shell structure could be described in detail by SANS. Below this length the alkyl chain is too short for micelle formation, since the total interaction energy is not sufficient to compensate for the bulky head group of the dendrons. However, due to their hydrophobic character, the alkyl chains will interact in other ways to form ill-defined aggregates. In addition to single dendrons (unimers), it is therefore likely that they also form dynamic irregular clusters with a size detected by DLS. A simplified image of such structures is illustrated in the upper right of Fig. 11 (for $C \leq 12$). The alkyl chain is generally not expected to be straight when the dendron is in solution allowing different kinds of internal arrangements within such clusters. When the condition for micelle formation is satisfied (in terms of chain length, *i.e.* $C \geq 14$), large intermicellar structures can exist, as schematically illustrated in the lower right of Fig. 11. These were found by DLS to be in the range of 65 to 370 nm. In the intermicellization process sticky micelles collide and they form intermicellar aggregates. Due to the size limitation of SANS (*ca.* 70 nm, as indicated at the bottom of Fig. 11), these

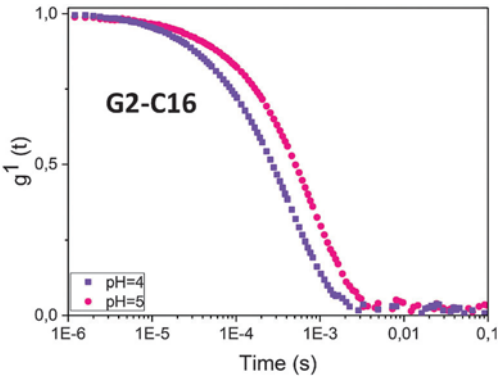

Fig. 10 First-order electric field autocorrelation functions *versus* time for G2-C16 at 25 °C and at the pH values indicated. A PBS buffer was used and it was adjusted to the considered pH values.

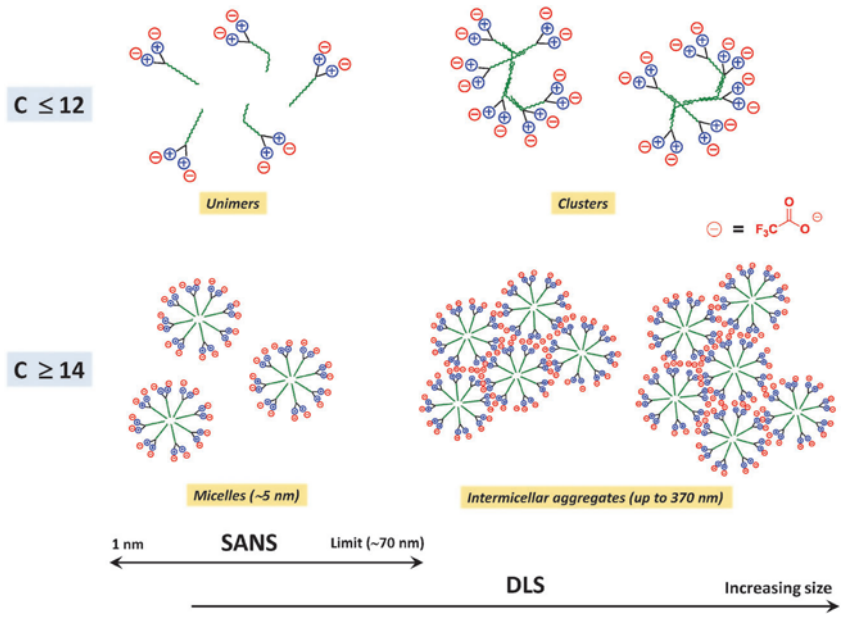

Fig. 11 Schematic view of micellar and intermicellar structures formed by dendrons in this study. For alkyl chain lengths of 12 carbons or less (C ≤ 12), micelles are not formed, and the dendrons exist in solution as unimers and large irregular clusters, where the latter are detected by DLS. For alkyl chain lengths of 14 carbons or more (C ≥ 14), micelles are formed with a core–shell structure as detailed by SANS, and with an overall diameter of approx. 5 nm. For these alkyl lengths, large intermicellar structures also exist. These are not detectable by SANS due to the upper SANS-limit of approx. 70 nm, but were followed by DLS.

structures are generally not seen by SANS, apart from occasional signs of a tail in the SANS scattering pattern at the lowest *q*-values.

Cell viability

To explore the biocompatibility of dendrons, they were subjected to *in vitro* cytotoxicity testing on mouse fibroblast (NIH/3T3) and human embryonic kidney (HEK 293T) cells. The cytotoxicity in NIH/3T3 cells was examined in this study, because they are the most common cells used in cell experiments as models for connective tissues in the body. NIH/3T3 cells have a number of properties that make them attractive as cell culture models. They are hypertriploid and relative to other primary explant cultures, they are easy to establish and maintain. They proliferate rapidly and as a result large numbers of cells can be produced within several days. In addition, we have chosen HEK 293T as a chemical sensitive cell line model. This model was chosen because the kidney is a major site of organ damage caused by drug toxicity. MTS [3-(4,5-dimethylthiazol-2-yl)-5-(3-carboxymethoxyphenyl)-2-(4-sulfophenyl)-2*H*-tetrazolium] assay was used as a colorimetric assay to evaluate cell viability measured as the quantity of formazan product[31] after treating the cells with dendrons at three different concentrations (5, 10 and 20 μM). Chosen concentrations were inspired from the results published by Dong Ma *et al.*[32] Since Dong Ma and co-workers did not observe any cytotoxicity for a G2 polylysine dendron cyclodextrin conjugate at concentrations up to 6.3 μM (50 μg mL^{-1}) we chose 5 μM as the lowest concentration for our much smaller dendrons and increased 4-fold to obtain 20 μM as the highest concentration (corresponding to 8–23 μg mL^{-1}).

We expected the G1 dendrons with four free amine groups to show an increased cytotoxicity relative to G1 dendrons that were partially acetylated (two free amine groups), since it is known that positively charged amine groups are toxic to cells.[9,33] Additionally, the cytotoxicity was expected to rise with higher concentrations. However, as seen in Fig. 12A and B, this is not the case. The two types of G1 dendrons exhibit similar non-cytotoxic behavior with increasing concentration.

Furthermore, we wanted to study the effect on cytotoxicity for a G2 dendron. For this we examined the G2-C16 dendron. The G2 dendron was expected to show an increased cytotoxicity profile relative to the G1 dendrons due to a greater number of positively charged amine groups on the surface (G2 dendrons having eight amine groups relative to four present on G1 dendrons). However, also here we observed high cell viability (Fig. 12). Overall it can be concluded that the dendrons do not display cytotoxicity (cell viability >80%) at concentrations up to 20 μM.

Conclusion

A series of novel amphiphilic polylysine dendrons containing variable alkyl chain lengths were successfully prepared by solid-phase synthesis using the backbone amide linker approach. From the obtained small angle neutron scattering (SANS) results it could be concluded that ordered micellar structures only formed for dendrons with alkyl chain lengths above C12. For dendrons with longer alkyl chains than C12, the SANS data could be adequately fitted by a spherical core–shell model,

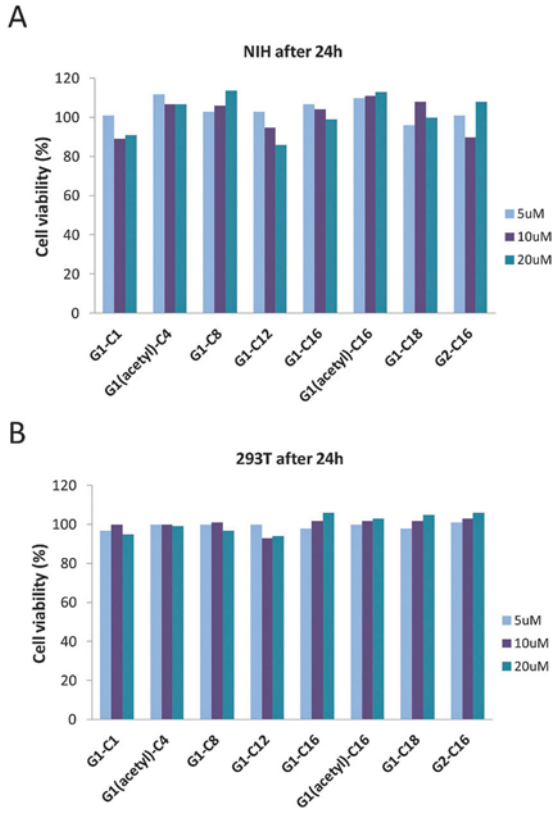

Fig. 12 Cell viability of NIH/3T3 (A) and HEK 293T (B) cells relative to untreated control cells of G1 and G2 dendrons at three different concentrations. The standard deviation was calculated to be less than 0.05 and 0.01 for NIH/3T3 and HEK 293T, respectively.

taking into account Coulombic interaction between the micelles. The overall size of the micellar structures formed by G1 dendrons was found to be around 5 nm corresponding well with the micellar diameter being spanned by two dendrons. Also, the number of dendrons per micellar structure in G1 dendrons, *i.e.* the aggregation number *N*(agg), was estimated and ranged from 33 to 59 depending on the acetylation degree. Furthermore, it was observed that the bigger head groups in G2 dendrons may have a destabilizing effect on the micelle formation resulting in less regular micelles compared to the corresponding G1 dendrons. Based on this study, G1 dendrons with a minimum alkyl chain length of C14 would be best suited for the formation of stable micelles. Moreover, a modification of the head groups rendering them less positive would increase the micelle forming ability of the dendrons, but this must be balanced against the increased tendency for intermicellar aggregate formation when the surface charge is reduced. In addition to the micelle formation disclosed by the SANS and dynamic light scattering (DLS) results, the DLS experiments also revealed the presence of large intermicellar structures having sizes of 65–370 nm.

The *in vitro* cytotoxicity of selected G1 and G2 dendrons was evaluated in mouse fibroblast (NIH/3T3) and human embryonic kidney (HEK 293T) cells by employing MTS [3-(4,5-dimethylthiazol-2-yl)-5-(3-carboxymethoxyphenyl)-2-(4-sulfophenyl)-2*H*-tetrazolium] assay. Some level of cytotoxicity was expected due to the presence of positively charged amines on the lysine head groups. However, all dendrons display similar cytotoxicity profiles regardless of surface modification and generation number with no increased cytotoxicity at higher concentrations. Furthermore, there are no significant differences in cytotoxicity profiles when considering short *versus* long alkyl chain lengths. Given that the cell viabilities are well above 80–90%, this indicates the possibility for further development of these dendritic systems for biomedical applications.

Experimental section

Materials and methods

All commercially available starting materials were purchased from Sigma-Aldrich, IRIS Biotech GmbH and Merck Chemicals and used without further purification. Solvents were purchased from Fischer Scientific and were of HPLC grade. Aminomethylated polystyrene resin (50–100 mesh size; 2 mmol g^{-1} loading; 1% cross-linked with divinylbenzene) was employed and the solid-phase reactions were performed in polypropylene syringes equipped with a polyethylene filter, or a glass container with a glass filter which was placed on a shaker. Washing of the resin was carried out manually on Torviq plates using 10 mL for each wash if not stated otherwise. After the reductive amination step, the resin was typically washed with MeOH (3×), NMP and DCM (15×), MeOH (3×), NMP (5×), DCM (5×), and MeOH (2×). Washing for the subsequent steps was typically performed with NMP and DCM (10×) and MeOH (3×). Fmoc deprotection was typically carried out with piperidine/NMP (1 : 4, 10 mL) for 3 + 30 + 20 min, or until ninhydrin test gave a positive read out. Dendrons were characterized by ^{1}H-NMR (600 MHz), ^{13}C-NMR (151 MHz), COSY (^{1}H–^{1}H coupling), HSQC (^{13}C–^{1}H coupling) and DEPT-135 ^{13}C-NMR using a Bruker Ultrashield AVANCE or AVANCE II 600 with a cryo platform. Spectra were calibrated relative to the residual solvent peak (D_2O: 4.79 ppm). UPLC-MS analysis was conducted on an instrument comprising a Shimadzu Nexera X2 and a Bruker MicrOTOF-Q III, using a Phenomenex Kinetex C8 column (2.6 μm, 100 Å, 50 × 2.1 mm) or an Ascentis Express Peptide ES-C18 column (2.7 μm, 160 Å, 50 × 2.1 mm) and a 1 mL min^{-1} linear gradient 0–2.7 min (0–20% buffer B), 2.7–6.0 min (20–100% buffer B), 6.0–7.0 min (100–0% buffer B), stop time 8.2 min. Buffer A: 0.025% TFA in 10% aqueous MeCN. Buffer B: 0.025% TFA in 90% aqueous MeCN. Infrared spectroscopy (IR) was performed directly on the resin beads using a Shimadzu IR-affinity spectrometer based on the technique of attenuated total reflectance (ATR). The compound Lys-C16 was prepared according to the procedure published by Gallot *et al.*[34]

Preparations

FMPB derivatized resin[15]. Aminomethylated polystyrene resin (1 equivalent, 5 g) was added to a filter syringe/glass container with a glass filter and swelled in NMP (7.8 mL g^{-1} resin). FMPB linker (1 equiv.), HBTU or PyBOP (0.95 equiv.) and DIPEA (1.9 equiv.) were added and the mixture was swirled for 24 h at rt and then washed with NMP (15 × 100 mL) and DCM

(15 × 100 mL). The resin was capped with Ac_2O/DIPEA/DCM (10/5/85; 30 mL g^{-1} resin) for 2–4 h at rt. The derivatized resin was washed as above and additionally with MeOH (3 × 100 mL) followed by air-drying and drying *in vacuo*. Ninhydrin test (negative, yellow/pale grey supernatant) and DNPH test (positive, dark orange-red resin) were carried out.

Cleavage of the final dendron from the resin, procedure A. The derivatized resin was treated with TFA/DCM (1 : 1, 10 mL) and shaken for 2 h, followed by filtration and collection of the cleavage mixture in a round bottomed flask. Evaporation *in vacuo* and precipitation in cold Et_2O gave the product as a white powder.

G1 dendron with C-terminal C1, C8, C12, C14, C16 and C18 chains, procedure B. The FMPB-derivatized resin (500 mg, 0.5 mmol, 1 equiv.), $NaBH_3CN$ (315 mg, 5 mmol, 10 equiv.), and amine (5 mmol, 10 equiv.) were suspended in a 5% AcOH in NMP solution (6 mL) in a 20 mL filter syringe and shaken. After 20 h, the resin was washed followed by air-drying and drying *in vacuo*. DNPH test (negative, pale orange to yellow resin) and secondary amine test (positive, orange-brown resin) were carried out. Fmoc-Lys(Fmoc)-OH (1.48 g, 2.5 mmol, 5 equiv.) and DIC (0.20 mL, 1.25 mmol, 2.5 equivalents) were added to the filter syringe containing the derivatized resin and DCM/NMP (95 : 5, 10 mL). The suspension was mixed using a spatula until a waxy mass was obtained. After 20 h the resin was washed followed by air-drying and drying *in vacuo*. Secondary amine test (negative, colorless resin) was conducted. Fmoc removal was carried out followed by washing. Fmoc-Lys(Boc)-OH (937 mg, 2 mmol, 4 equiv), PyBOP (989 mg, 2 mmol, 3.8 equiv.) and DIPEA (0.68 mL, 3.9 mmol, 7.8 equiv.) were transferred to the filter syringe containing the derivatized resin and NMP (6 mL) and shaken for 3 h, or repeated until the ninhydrin test was negative.[35] The resin was washed followed by Fmoc removal. Cleavage of the dendron was performed by procedure A.

Partially acetylated G1 dendron with C-terminal C4, C6, C10 and C16 chains. Procedure B was followed; however, before the cleavage step the derivatized resin was treated with Ac_2O/DIPEA/DCM (10 mL, 10/5/85) and shaken for 3 h. The resin was washed followed by air-drying. Ninhydrin test (negative, yellow/pale grey supernatant) was carried out. Cleavage of the dendron was performed by procedure A.

G2 dendron with C-terminal C1, C12 and C16 chains, procedure C. The FMPB-derivatized resin (500 mg, 0.5 mmol, 1 equiv.), $NaBH_3CN$ (315 mg, 5 mmol, 10 equiv.) and amine (5 mmol, 10 equiv.) were suspended in a 5% AcOH in NMP solution (6 mL) in a 20 mL filter syringe and shaken. After 20 h, the resin was washed followed by air-drying and drying *in vacuo*. DNPH test (negative, pale orange to yellow resin) and secondary amine test (positive, orange-brown resin) were carried out. Fmoc-Lys(Fmoc)-OH (1.48 g, 2.5 mmol, 5 equiv.) and DIC (0.20 mL, 1.25 mmol, 2.5 equiv.) were added to the filter syringe containing the derivatized resin and DCM/NMP (95 : 5, 10 mL). The suspension was mixed using a spatula creating a waxy mass. After 20 h the resin was washed followed by air-drying and drying *in vacuo*. Secondary amine test (negative, colorless resin) was conducted. Fmoc removal was carried out followed by washing. Fmoc-Lys(Fmoc)-OH (1.18 g, 2 mmol, 4 equiv.), PyBOP (989 mg, 2 mmol, 3.8 equiv.) and DIPEA (0.68 mL, 3.9 mmol, 7.8 equiv.) were added to the filter syringe containing the derivatized resin and NMP (6 mL) and shaken for 3 h, or repeated until the ninhydrin test was negative. The resin was washed followed by Fmoc deprotection. Fmoc-Lys(Boc)-OH (937 mg, 2 mmol, 4 equiv.), PyBOP (989 mg, 2 mmol, 3.8 equiv.) and DIPEA (0.68 mL, 3.9 mmol, 7.8 equiv.) were transferred to the filter syringe containing the derivatized resin and NMP (6 mL) and shaken for 3 h, or repeated until the ninhydrin test was negative. The resin was washed followed by Fmoc removal. Cleavage of the dendron was performed by procedure A.

Physicochemical measurements

Small angle neutron scattering. The SANS instrument at the 2MW JEEP II reactor at the Institute for Energy and Technology (IFE) at Kjeller (Norway) was employed for the measurements. A velocity selector (Dornier) was used, with a wavelength spread of $\Delta\lambda/\lambda$ = 10%. Two different sample detector distances (1.0 m and 3.4 m) and two different neutron wavelengths (5.1 Å and 10.2 Å) were used in order to obtain a total scattering range (q-range) from 0.008 $Å^{-1}$ to 0.25 $Å^{-1}$ corresponding to an observable particle size range of 2.5–78.5 nm. The neutron detector was a circular 128 × 128 pixel ^{3}He-filled RISØ type inside a shielded detector chamber with vacuum to reduce air scattering. All samples were dissolved in D_2O to reduce incoherent scattering and maximize the scattering contrast. The samples were inspected before being introduced to 2 mm quartz cuvettes and placed in the sample chamber. The transmission was measured separately and the scattering was normalized to absolute units (cm^{-1}) by taking into account data from the empty cell, the beam without cell and blocked-beam background scattering for data reduction. Chosen dendron samples were measured and all measurements were performed at room temperature.

Dynamic light scattering. DLS experiments were carried out using an ALV/CGS-8F goniometer system with 8 fiber-optical detection units, from ALV-GmbH, Langen, Germany. The intensity correlation functions were measured at 8 scattering angles simultaneously in the range 22–141°. The beam from a Uniphase cylindrical 22 mW HeNe-laser, operating at a wavelength of 632.8 nm with vertically polarized light, was focused on the sample cell (10 mm NMR tubes, Wilmad Glass Co., of highest quality) through a temperature-controlled cylindrical quartz container (with 2 plane-parallel windows), which was filled with a refractive index matching liquid (*cis*-decalin). The temperature in the container was controlled to within ±0.01 °C with a heating/cooling circulator. The samples were dissolved in MilliQ water and filtered in an atmosphere of filtered air through 0.45 μm filters directly into pre-cleaned and dust free 10 mm NMR tubes.

Zeta potential and pH measurements. All zeta potential measurements were performed at 25 °C on a Zetasizer Nano ZS (ZEN3600, Malvern Instruments Ltd) using a "dip" cell with palladium electrodes. Laser Doppler micro-electrophoresis was employed to determine the electrophoretic mobility and automatically calculate the zeta potential from this value.

Samples were prepared by dissolving the dendron samples in MilliQ water to give a final concentration of 18 mM and 800 μL was transferred to a PCS1115 cuvette to be placed in the sample chamber. Five to ten measurements were made for each sample and an average was taken for the zeta potential.

An InLab Micro pH electrode from Mettler Toledo made of glass (3 M KCl as reference electrolyte) was employed for pH measurements. The pH values were measured at room temperature on 18 mM solutions of dendrons in MilliQ water.

Cell viability. In this study cytotoxicity assay was carried out by using NIH/3T3 as a standard mouse fibroblast cell line and the human embryonic kidney cell line, HEK 293T, as a chemical sensitive model. The kidney model was used because the kidney is a major site of organ damage caused by drug toxicity.[36–38]

NIH/3T3 and HEK 293T were purchased from ATCC (American Type Culture Collection) and cultured in T75 cell culture flasks in Dulbecco's modified Eagle's cell culture medium (DMEM) containing 10% fetal bovine serum (FBS) and 1% penicillin–streptomycin (Sigma Aldrich). The monolayer was then trypsinized and the cells were seeded in 96-well plates at a density of 6×10^3 cells per well (100 μL per well) in the culture medium. Following 24 h incubation and attachment, the cells were treated with dendrons with concentrations of 5, 10 and 20 μM and incubated for an additional 24 h. Cell viability of cells treated with dendrons was evaluated using MTS assay as a colorimetric assay in solution with an electron coupling reagent, phenazine ethosulfate (CellTiter 96 AQ_{ueous} One Solution Cell Proliferation Assay, Promega Corporation). 20 μL MTS was added to each well and incubated for 2 h following the 24 h incubation with dendrons. The absorbance of the soluble formazan product was quantified by measuring the absorbance at 490 nm using a plate reader (Synergy Mx-Monochromator-based Multi-mode Microplate Reader, BioTek Instruments, Vermont, USA). The experiment was repeated four times for each group and relative cell viability was calculated as below:

$$\text{Relative cell viability } (\%) = \frac{(A_{\text{sample}} - A_{\text{ref}})}{A_{\text{control}} - A_{\text{ref}}} \times 100 \qquad (6)$$

where A_{sample} is the absorbance obtained from the wells containing dendron-treated cells, A_{ref} the absorbance of blank medium (100 μL medium + 100 μL MilliQ + 20 μL MTS) and A_{control} the absorbance of control cells (untreated cells).

Acknowledgements

B. N. gratefully acknowledges a grant from the Norwegian Research Council, SYNKNØYT for the project with the number 8411/F50. S. M. acknowledges Sandra Medel for assisting in the collection of DEPT-135 ^{13}C-NMR data.

References

1 E. Buhleier, W. Wehner and F. Vögtle, *Synthesis*, 1978, 155–158.
2 D. A. Tomalia, H. Baker, J. R. Dewald, M. Hall, G. Kallos, S. Martin, J. Roeck, J. Ryder and P. Smith, *Polym. J.*, 1985, **17**, 117–132.
3 G. R. Newkome, Z. Q. Yao, G. R. Baker and V. K. Gupta, *J. Org. Chem.*, 1985, **50**, 2003–2006.
4 R. G. Denkewalter, J. Kolc and W. J. Lukasavage, *US pat.*, 4 289 872, 1981.
5 R. G. Denkewalter, J. Kolc and W. J. Lukasavage, *US pat.*, 4 410 688, 1983.
6 K. Sadler and J. P. Tam, *Rev. Mol. Biotechnol.*, 2002, **90**, 195–229.
7 J. P. Tam, *Proc. Natl. Acad. Sci. U. S. A.*, 1988, **85**, 5409–5413.
8 D. N. Prosnett, H. McGrath and J. P. Tam, *J. Biol. Chem.*, 1988, **263**, 1719–1725.
9 D. A. Tomalia, J. B. Christensen and U. Boas, *Dendrimers, Dendrons and Dendritic Polymers*, Cambridge University Press, 2012.
10 U. Boas, J. B. Christensen and P. M. H. Heegaard, *Dendrimers in Medicine and Biotechnology*, RSC Publishing, 2006.
11 M. Malkoch, E. Malmström and A. M. Nyström, *Polymer Science: A Comprehensive Reference*, 2012, **6**, 113–175.
12 T. Yu, X. Liu, A.-L. Bolcato-Bellemin, Y. Wang, C. Liu, P. Erbacher, F. Qu, P. Rocchi, J.-P. Behr and L. Peng, *Angew. Chem., Int. Ed.*, 2012, **51**, 8478–8484.
13 X. Liu, J. Zhou, T. Yu, C. Chen, Q. Cheng, K. Sengupta, Y. Huang, H. Li, C. Liu, Y. Wang, P. Posocco, M. Wang, Q. Cui, S. Giorgio, M. Fermeglia, F. Qu, S. Pricl, Y. Shi, Z. Liang, P. Rocchi, J. J. Rossi and L. Peng, *Angew. Chem.*, 2014, **126**, 12016–12021.
14 X. Liu, C. Liu, J. Zhou, C. Chen, F. Qu, J. J. Rossi, P. Rocchi and L. Peng, *Nanoscale*, 2015, **7**, 3867–3875.
15 D. K. Svenssen, S. Mirsharghi and U. Boas, *Tetrahedron Lett.*, 2014, **55**, 3942–3945.
16 U. Boas, J. Brask and K. J. Jensen, *Chem. Rev.*, 2009, **109**, 2092–2118.
17 S. K. Shannon and G. Barany, *J. Comb. Chem.*, 2004, **6**, 165–170.
18 See selected IR data in ESI†.
19 The test solution was prepared by dissolving Fmoc-phenylalanine (3 mg) in 2% (v/v) acetaldehyde in NMP (1 mL). A few resin beads were put in a test tube and two drops of the test solution was added. After 3–5 minutes at room temperature, the formation of orange-brown resin beads indicates the presence of a secondary amine.
20 U. Boas and S. Mirsharghi, *Org. Lett.*, 2014, **16**, 5918–5921.
21 E. Kaiser, R. L. Colescott, C. D. Bossinger and P. I. Cook, *Anal. Biochem.*, 1970, **34**, 595–598.
22 S. Yokoyama and J.-I. Hiramatsu, *J. Biosci. Bioeng.*, 2003, **95**, 204–205.
23 See fully assigned NMR data on all compounds in ESI†.
24 A. Guinier and G. Fournet, *Small-Angle Scattering of X-Rays*, 1955.
25 J. B. Hayter and J. Penfold, *Mol. Phys.*, 1981, **42**, 109–118.
26 N. J. Turro and A. Yekta, *J. Am. Chem. Soc.*, 1978, **100**, 5951–5952.
27 A. J. F. Siegert, *Rad. Lab. Rep.*, No 465, Massachusetts Institute of Technology, 1943.
28 See Table S1 in ESI† for zeta potentials.
29 The zeta potential is a measure of the charge density of the particles in solution. Generally, solutions or suspensions of

particles with a zeta potential at or above ±30 mV are considered electrostatically stable, whereas at lower values flocculation may occur.

30 The length of a C–C bond is 0.154 nm. Taking into account that the bonds are in a zig-zag pattern with respect to the main axis of the alkyl chain, the projection of the chain can be calculated to be 0.8 and 1.8 nm for a C8 and C18 chain, respectively. Assuming that the chain is fully stretched and that the lysine head groups in a G1 and G2 dendron are roughly 1–2 nm, the dendron length will be roughly 1.8–3.8 nm. If the micellar diameter is spanned by two dendrons this would give a diameter in the range of 3.6–7.6 nm, *i.e.* well below 10 nm. Hence, obtained sizes ranging from 65 to 370 nm must be due to intermicellar aggregates.

31 The MTS assay is an enzyme-based colorimetric method for cell viability assessment. In the mitochondria of metabolic active (living) cells MTS is reduced to a colored formazan product. Therefore, the quantity of formazan measured by the absorbance at 490 nm is directly proportional to the number of living cells in the culture.

32 D. Ma, H.-B. Zhang, Y.-Y. Chen, J.-T. Lin and L.-M. Zhang, *J. Colloid Interface Sci.*, 2013, **405**, 305–311.

33 K. Jain, P. Kesharwani, U. Gupta and N. K. Jain, *Int. J. Pharm.*, 2010, **394**, 122–142.

34 B. Gallot and H. H. Haj, *Mol. Cryst. Liq. Cryst.*, 1989, **170**, 195–214.

35 The liability of the ninhydrin test was low when synthesizing dendron derivatives on resin with alkyl chain lengths above C12 leading to false negative ninhydrin read-outs.

36 G.-E. Séralini, J. S. de Vendômois J, D. Cellier, C. Sultan, M. Buiatti, L. Gallagher, M. Antoniou and K. R. Dronamraju, *Int. J. Biol. Sci.*, 2009, **5**, 438–443.

37 R. Mesnage, E. Clair, S. Gress, C. Then, A. Székács and G.-E. Séralini, *J. Appl. Toxicol.*, 2013, **33**, 695–699.

38 G.-E. Séralini, R. Mesnage R, E. Clair, S. Gress, D. Cellier and J. S. de Vendômois, *Environ. Sci. Eur.*, 2011, **23**, 10.

Supporting information

Preparation and self-assembly of amphiphilic polylysine dendrons

Sahar Mirsharghi,[a] Kenneth D. Knudsen,[b] Shahla Bagherifam,[c,d] Bo Nyström[c] and Ulrik Boas*[a]

[a] *Section of Immunology and Vaccinology, National Veterinary Institute, Technical University of Denmark (DTU), Bülowsvej 27, DK-1870 Frederiksberg C, Denmark. E-mail: uboa@vet.dtu.dk*

[b] *Department of Physics, Institute for Energy Technology, PO Box 40, N-2027 Kjeller, Norway*

[c] *Department of Chemistry, University of Oslo, PO Box 1033, Blindern N-0315 Oslo, Norway*

[d] *Department of Biology, University of Oslo, Blindernveien 31, N-0316 Oslo, Norway*

List of contents

Table of compounds with page numbers of spectra and chromatograms

Zeta potential data

Table S1 G1 and G2 dendrons together with zeta potentials and DLS measurements.

Compound	Zeta potential (mV)[a]	DLS
G1-C1	12	÷
G1-C8	12	+
G1-C12	20	÷
G1-C14	ND	+
G1-C16	55	+
G1-C18	52	+
G1(acetyl)-C4	11	÷
G1(acetyl)-C6	18	÷
G1(acetyl)-C10	42	+
G1(acetyl)-C16	54	+
G2-C1	25	÷
G2-C12	34	+
G2-C16	45	+

Selected IR data

FMPB derivatized resin:

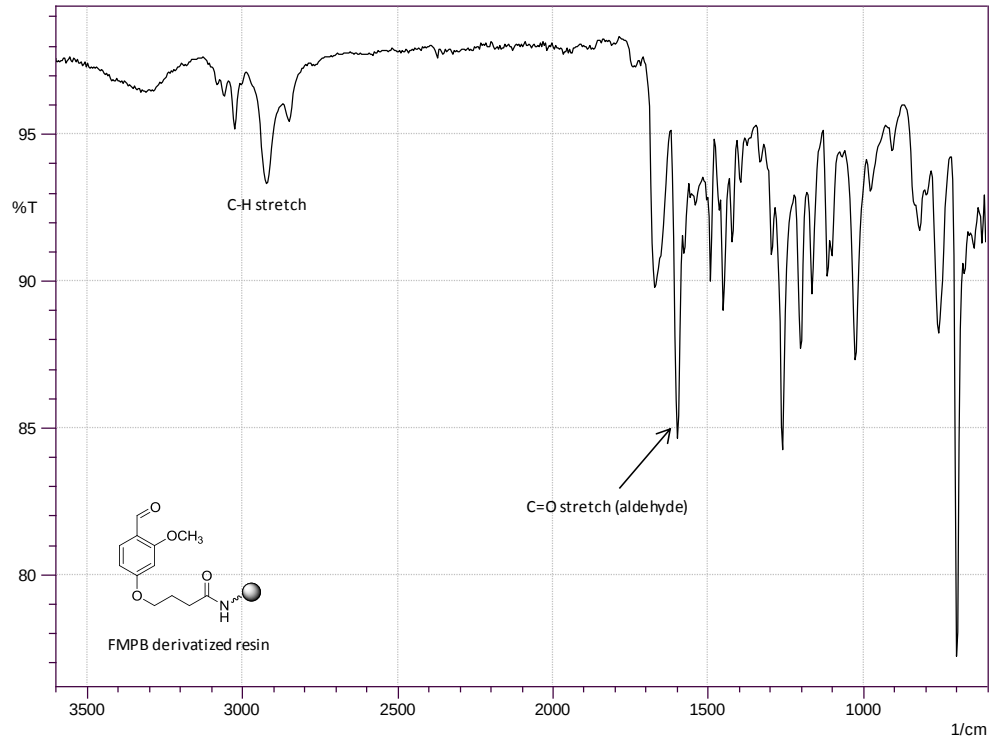

N-hexyl FMPB derivatized resin:

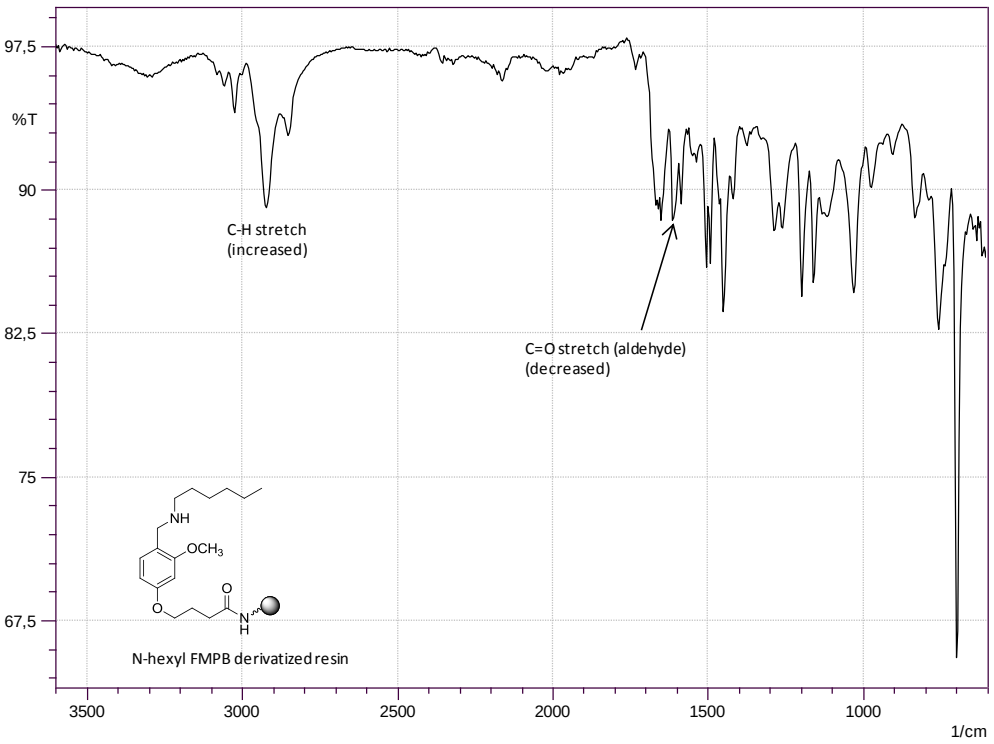

N-tetradecyl FMPB derivatized resin:

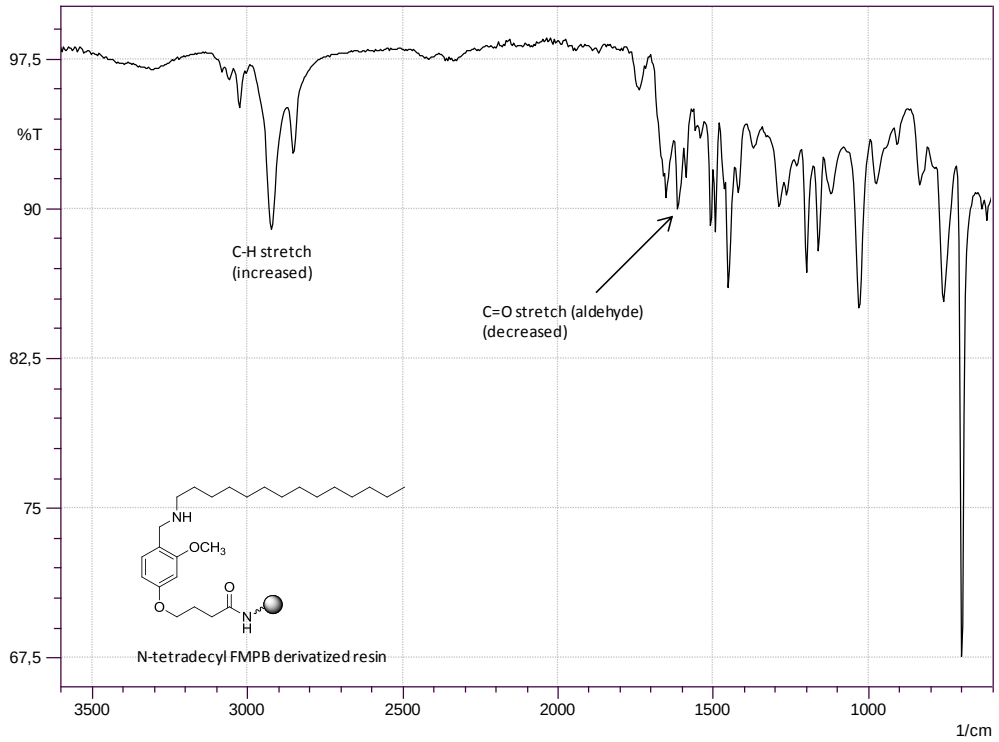

N-octadecyl FMPB derivatized resin:

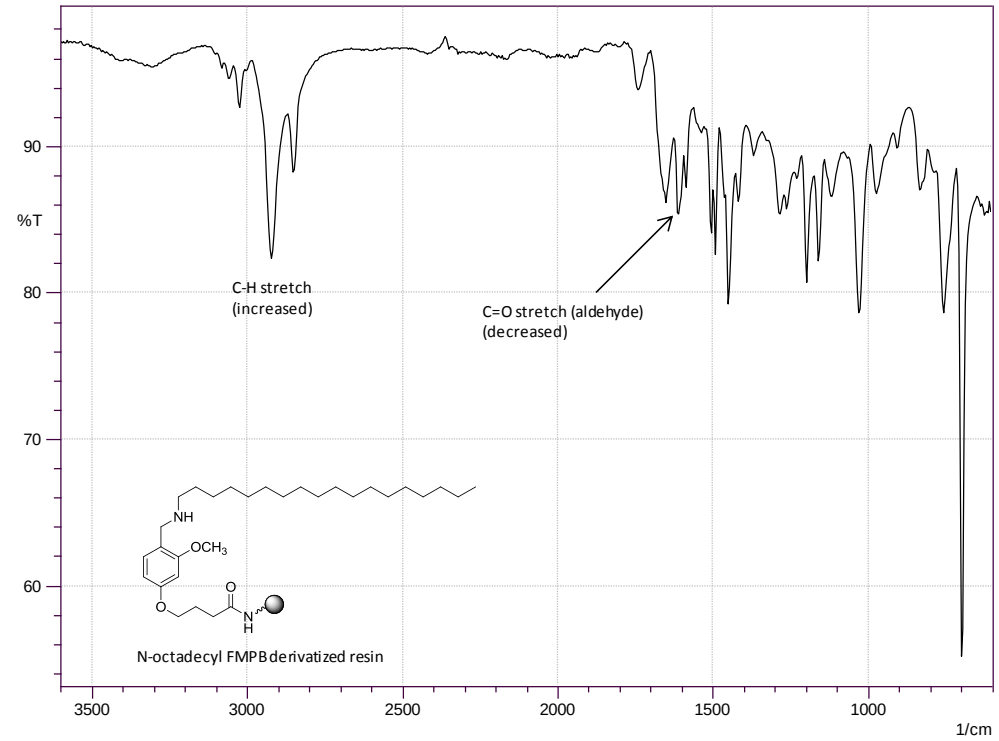

NMR spectra and UPLC-MS data on synthesized compounds

Background signals observed in UPLC-MS

Peaks 295; 369; 430; 760; 1072; 1859 and 2333 on some spectras are due to some residual impurity in the system (capillary (nebulizer), column, hexapole).

UPLC-MS (Acetonitril)

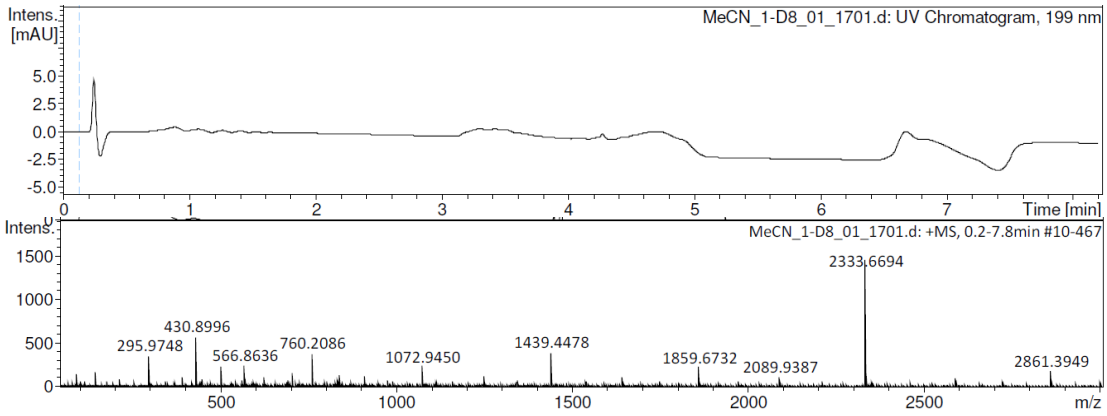

UPLC-MS (Acetonitril)

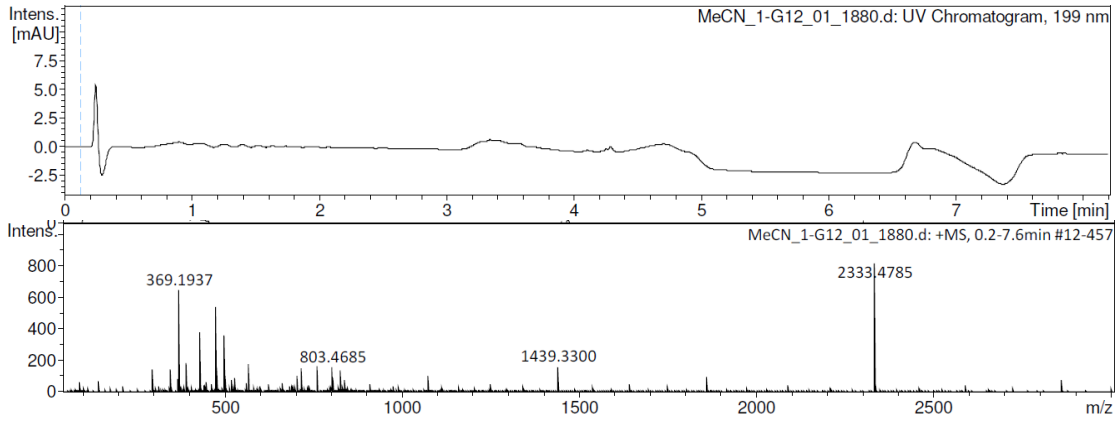

UPLC-MS (MilliQ water)

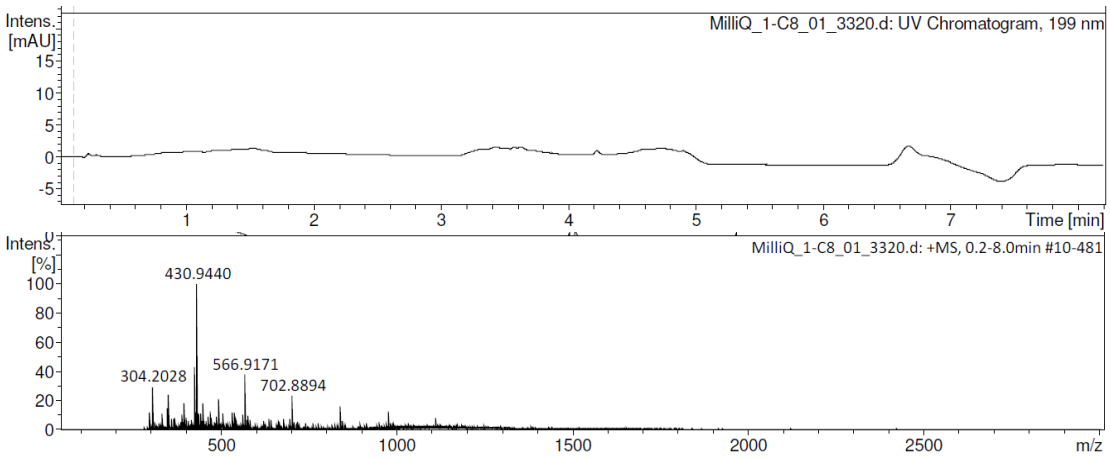

G1-C1 (1)

Yield (TFA salt; loading: 0.25 mmol/g): 56.6 mg (70 %). LC-MS data R_t: 0.2-0.4 min. MS(ESI^+), calcd $C_{19}H_{41}N_7O_3$: 415.33 g/mol, found: m/z 416.32 $[MH]^+$. ^1H NMR (600 MHz, D_2O): δ 4.27 (t, *J* = 7.38 Hz, 1H), 4.07 (t, *J* = 6.56 Hz, 1H), 3.96 (t, *J* = 6.71 Hz, 1H), 3.26 (td, *J* = 7.13, 1.92 Hz, 2H), 3.04 (q, *J* = 7.80 Hz, 4H), 2.78 (s, 3H), 2.02 – 1.87 (m, 4H), 1.84 – 1.69 (m, 6H), 1.58 (p, *J* = 7.48 Hz, 2H), 1.53 – 1.31 (m, 6H). ^{13}C NMR (151 MHz, D_2O): δ 173.84, 169.50, 169.30, 54.27, 53.12, 52.70, 39.25, 39.00, 38.97, 30.47, 30.37, 30.36, 27.87, 26.36, 26.34, 25.75, 22.41, 21.33, 21.03.

UPLC-MS (1)

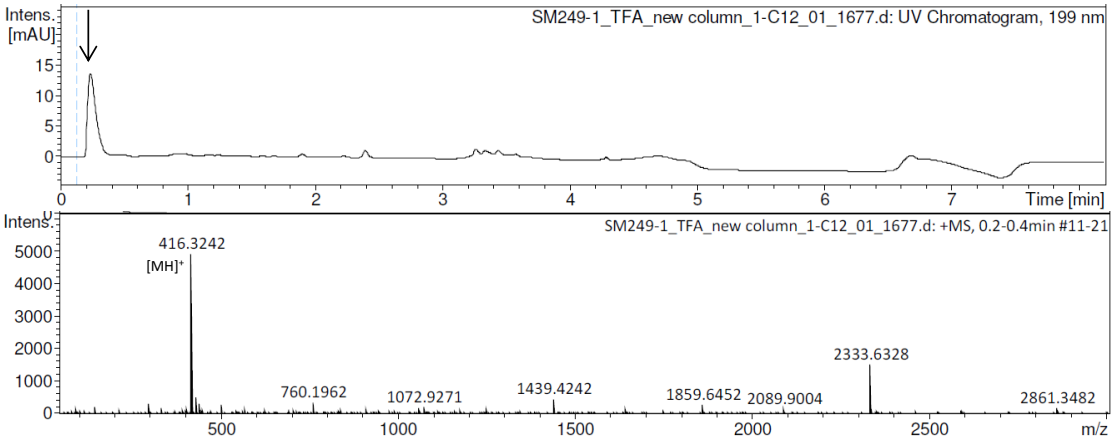

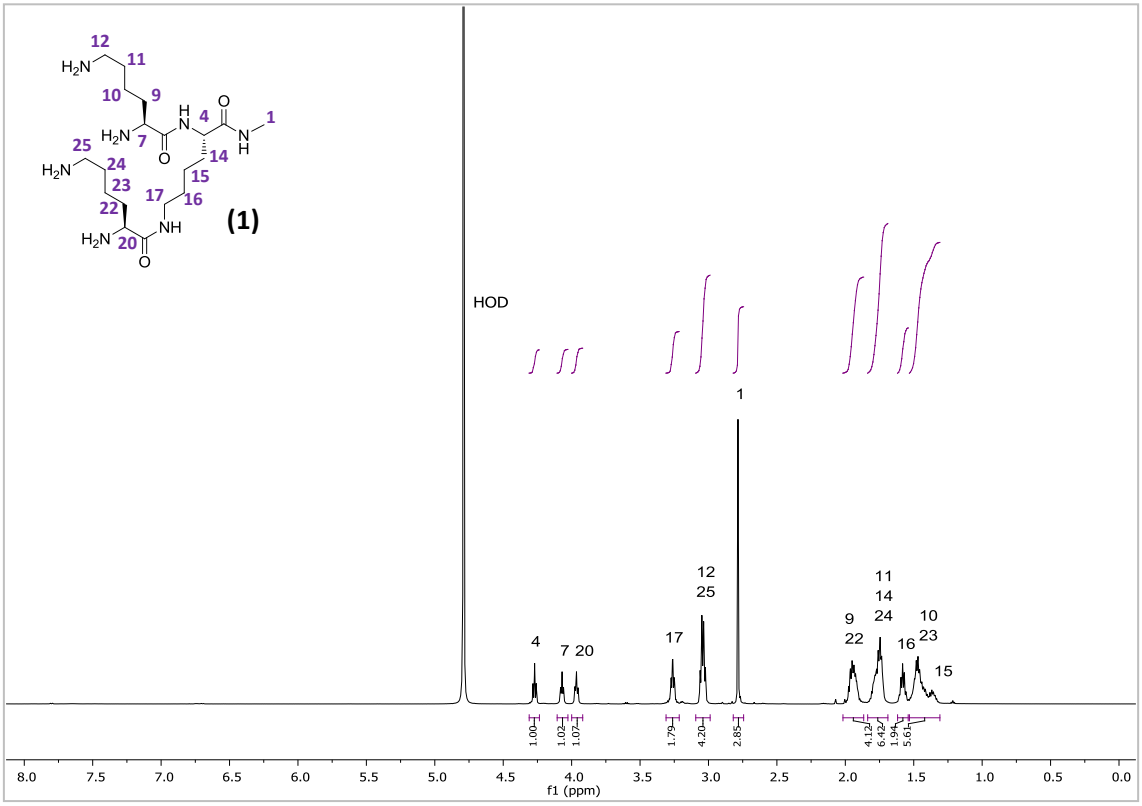

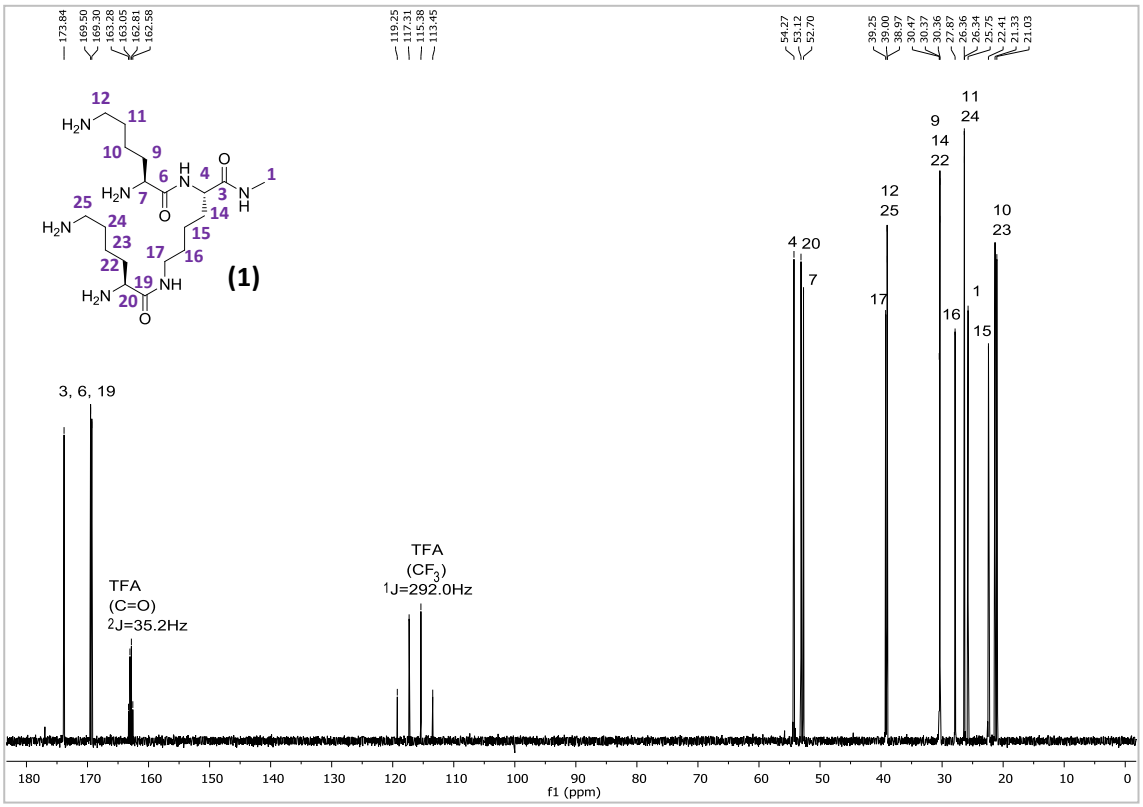
(1)
3, 6, 19
TFA
(C=O)
2J=35.2Hz
TFA
(CF3)
1J=292.0Hz
f1 (ppm)

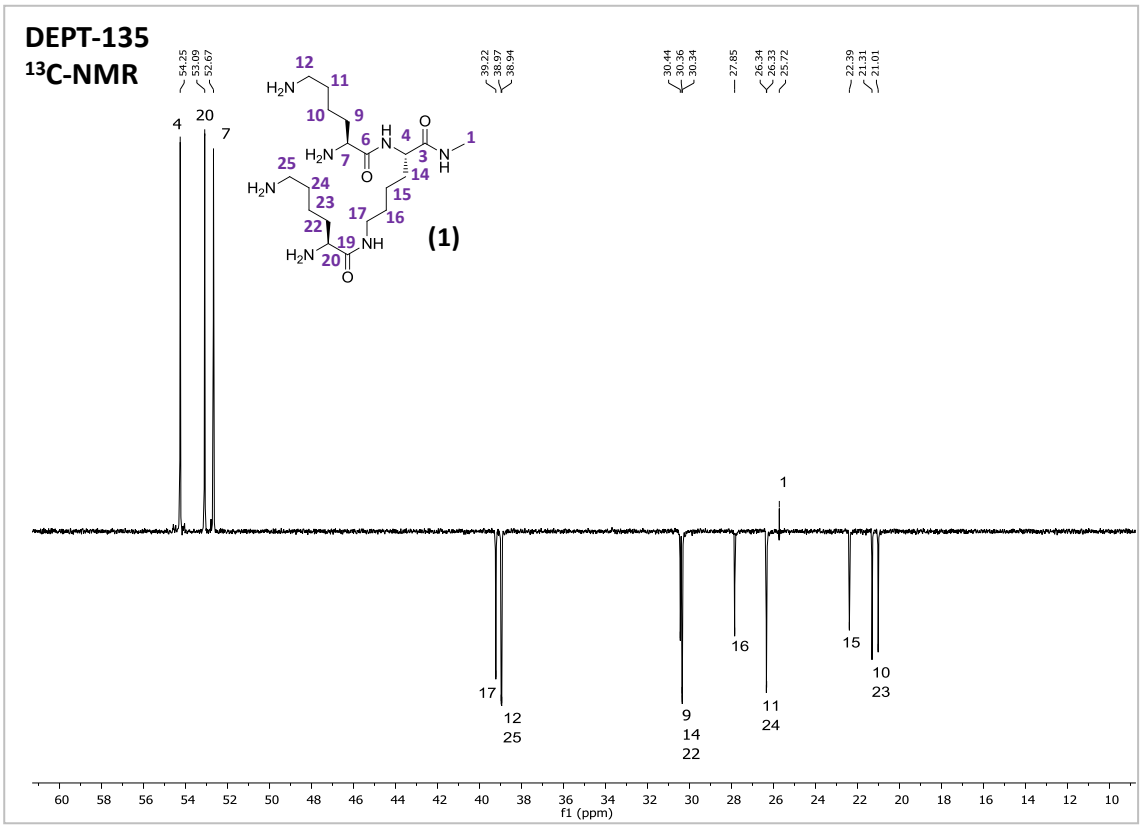
DEPT-135
13C-NMR
(1)
f1 (ppm)

HSQC (1)

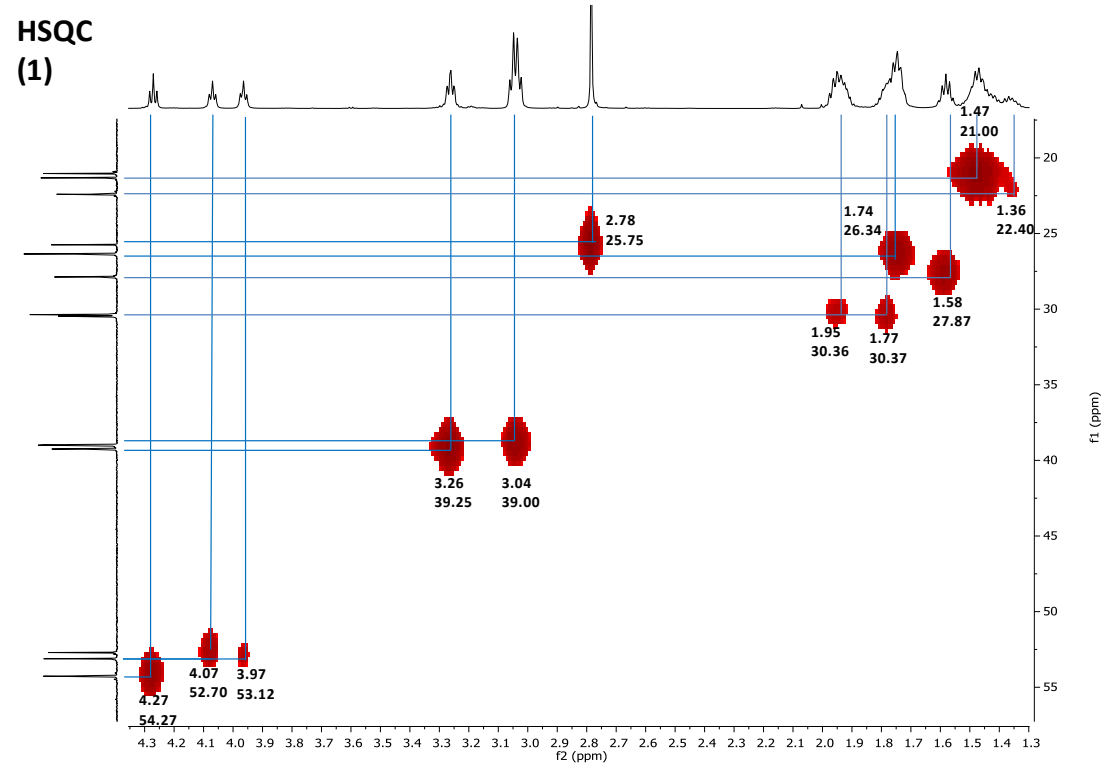
1.47
21.00
1.36
22.40
1.74
26.34
2.78
25.75
1.58
27.87
1.95
30.36
1.77
30.37
3.26
39.25
3.04
39.00
4.27
54.27
4.07
52.70
3.97
53.12
f2 (ppm)
f1 (ppm)

COSY (1)

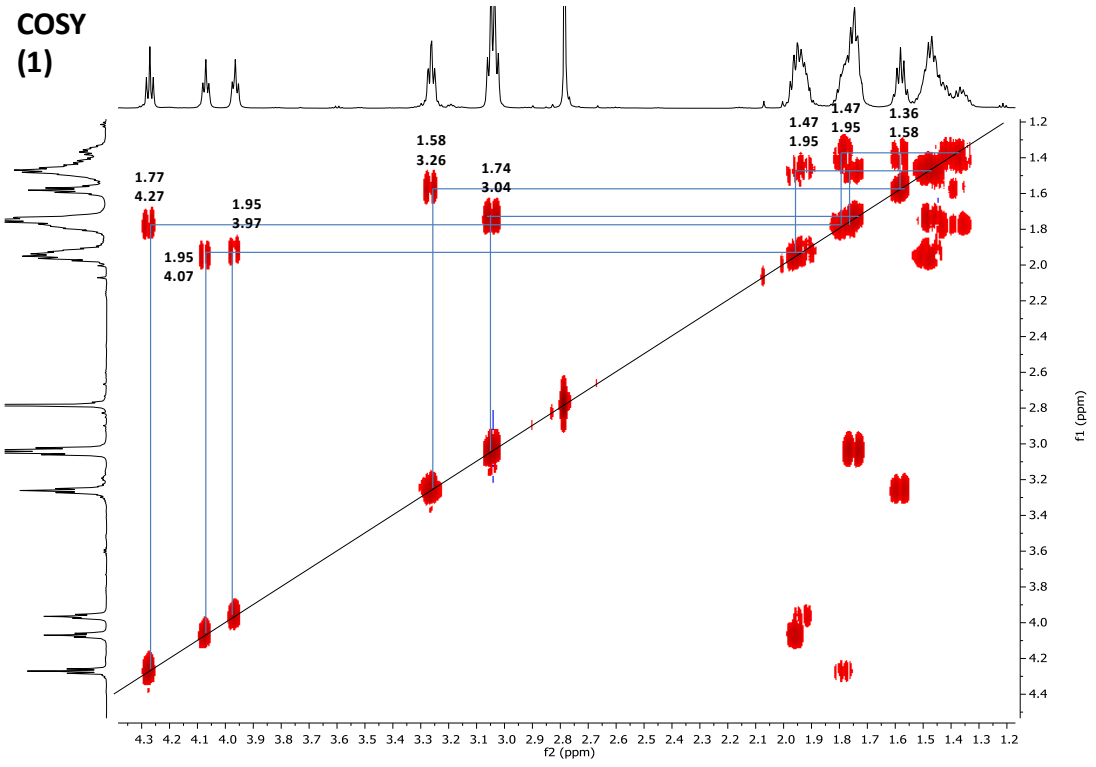
1.77
4.27
1.95
3.97
1.95
4.07
1.58
3.26
1.74
3.04
1.47
1.95
1.47
1.95
1.36
1.58
f2 (ppm)
f1 (ppm)

G1-C8 (2)

Yield (TFA salt; loading: 0.33 mmol/g): 102.8 mg (64 %). LC-MS data R_t: 1.0-1.4 min. MS(ESI^+), calcd $C_{26}H_{55}N_7O_3$: 513.44 g/mol, found: m/z 514.42 $[MH]^+$. ^1H NMR (600 MHz, D_2O): δ 4.28 (t, *J* = 7.39 Hz, 1H), 4.06 (t, *J* = 6.55 Hz, 1H), 3.96 (t, *J* = 6.73 Hz, 1H), 3.33 – 3.24 (m, 3H), 3.17 (dt, *J* = 13.42, 6.68 Hz, 1H), 3.07 – 3.01 (m, 4H), 2.01 – 1.87 (m, 4H), 1.84 – 1.69 (m, 5H)[1], 1.65 – 1.36 (m, 7H), 1.35 – 1.23 (m, 11H), 0.92 – 0.86 (m, 3H). ^{13}C NMR (151 MHz, D_2O): δ 173.01, 169.35, 169.27, 54.31, 53.11, 52.70, 39.31, 39.00, 38.97, 31.06, 30.59, 30.42, 30.38, 28.38, 28.28, 28.20, 27.90, 26.36, 25.98, 22.48, 22.00, 21.34, 21.07, 13.41.

UPLC-MS (2)

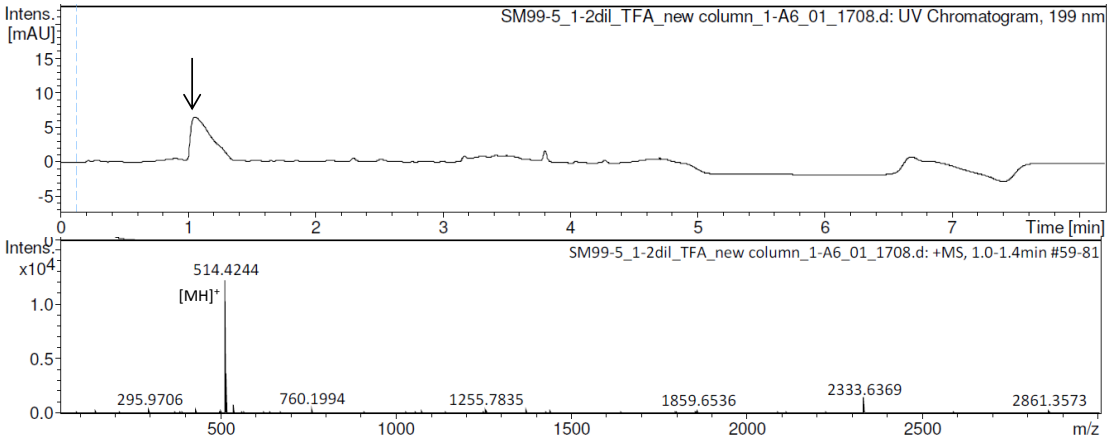

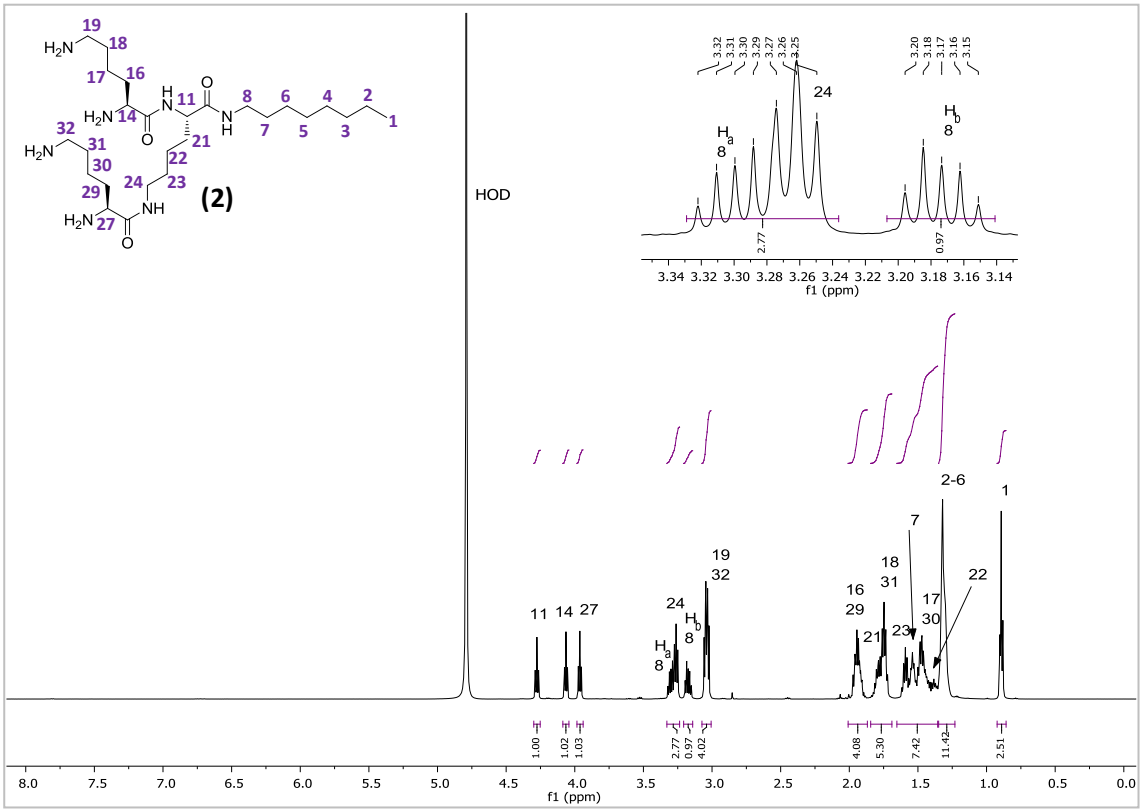

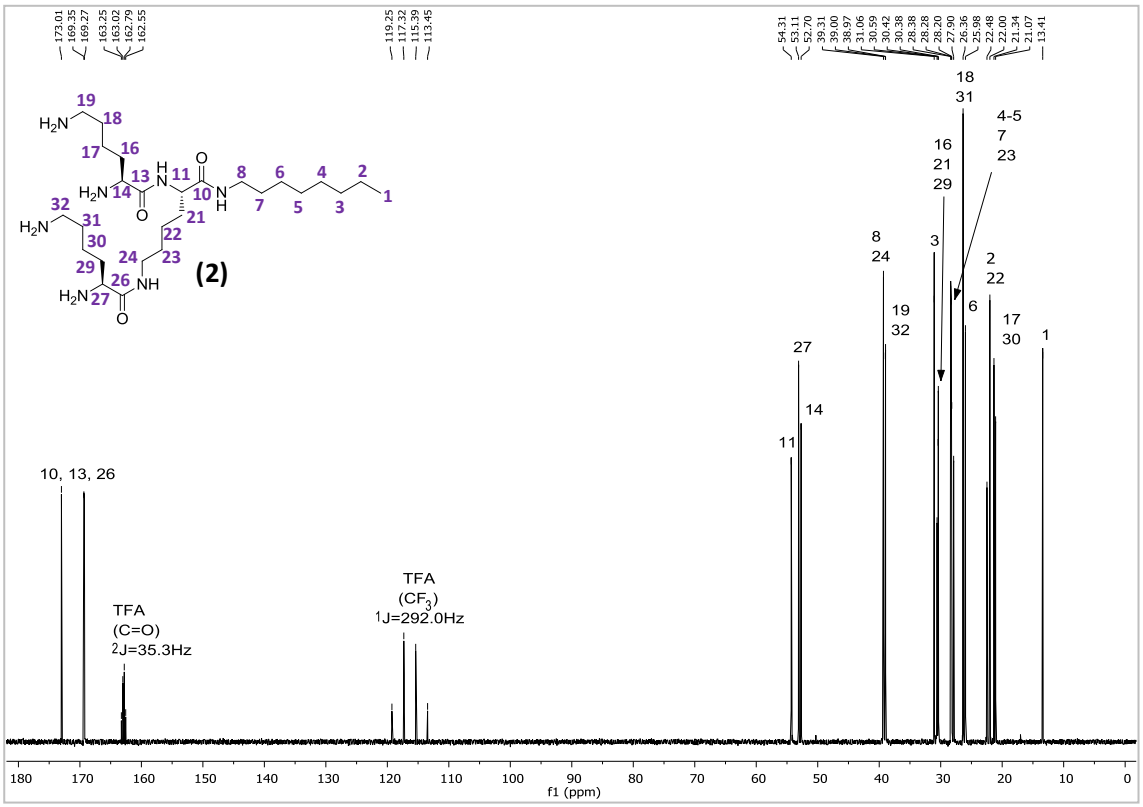
(2)
TFA
(C=O)
2J=35.3Hz
TFA
(CF3)
1J=292.0Hz
10, 13, 26
f1 (ppm)

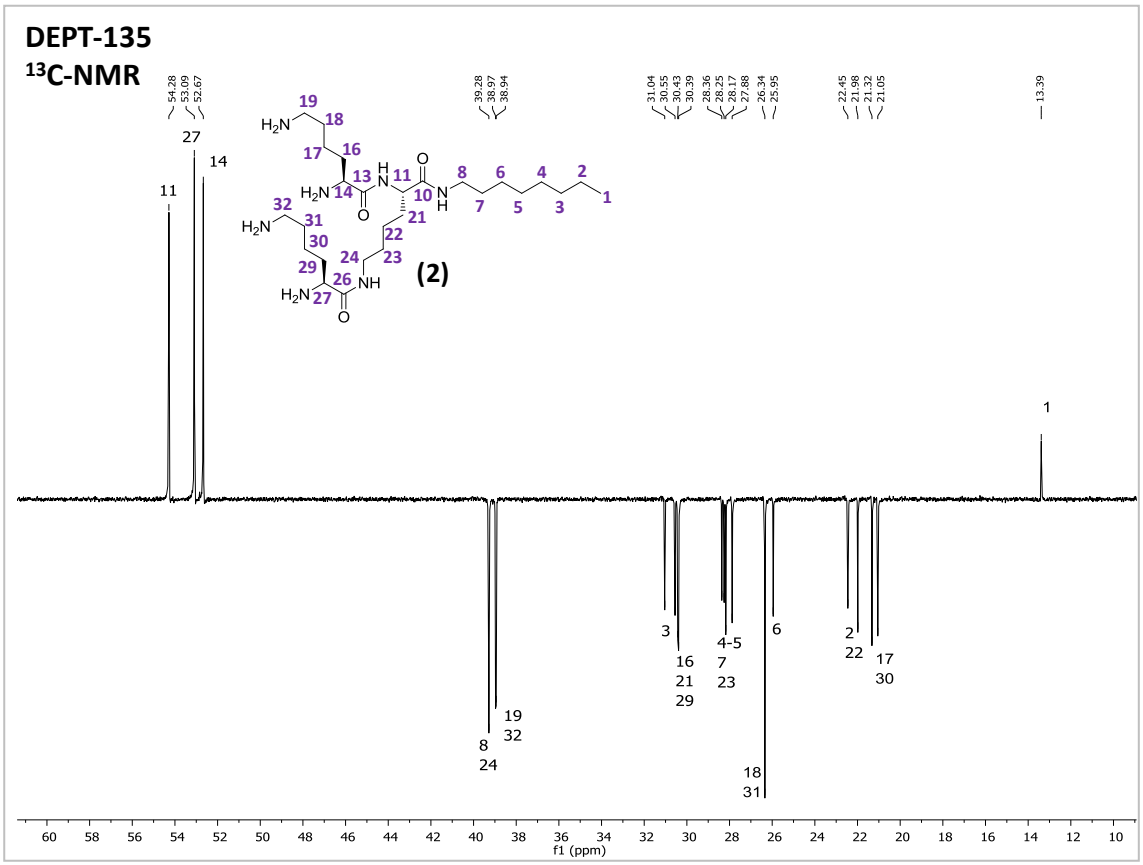
DEPT-135
13C-NMR
(2)
f1 (ppm)

HSQC (2)

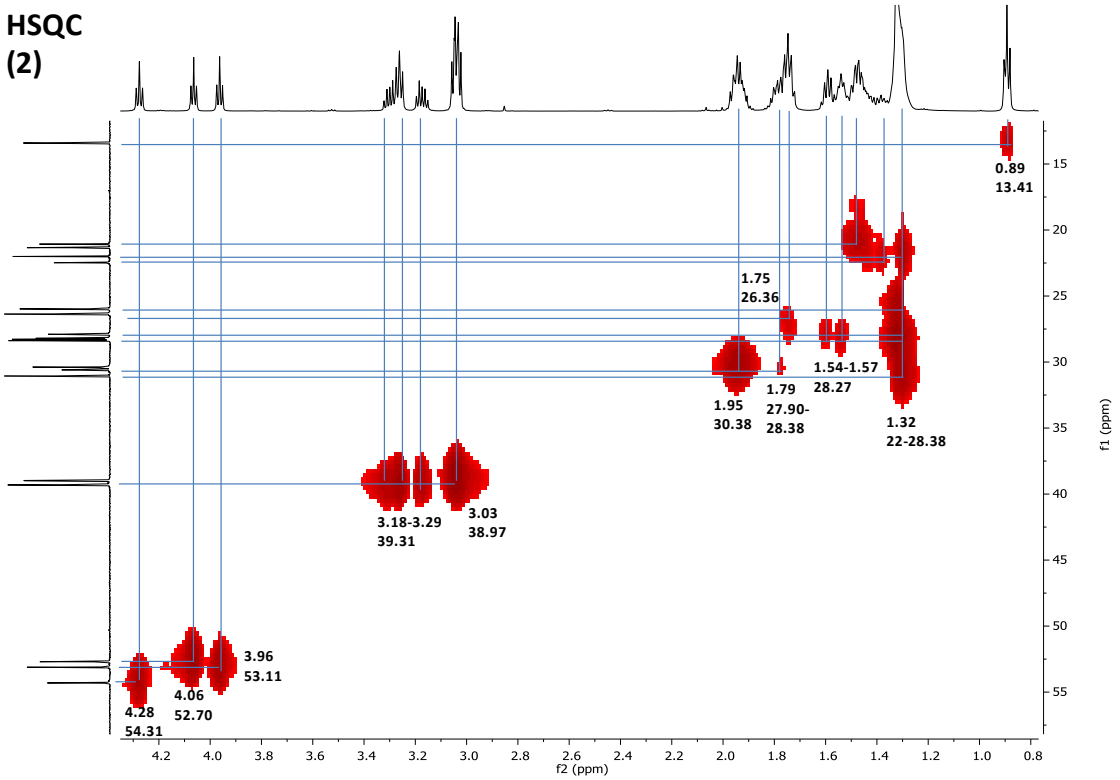
0.89
13.41
1.75
26.36
1.95
30.38
1.79
27.90-
28.38
1.54-1.57
28.27
1.32
22-28.38
3.18-3.29
39.31
3.03
38.97
3.96
53.11
4.06
52.70
4.28
54.31
f2 (ppm)
f1 (ppm)

COSY (2)

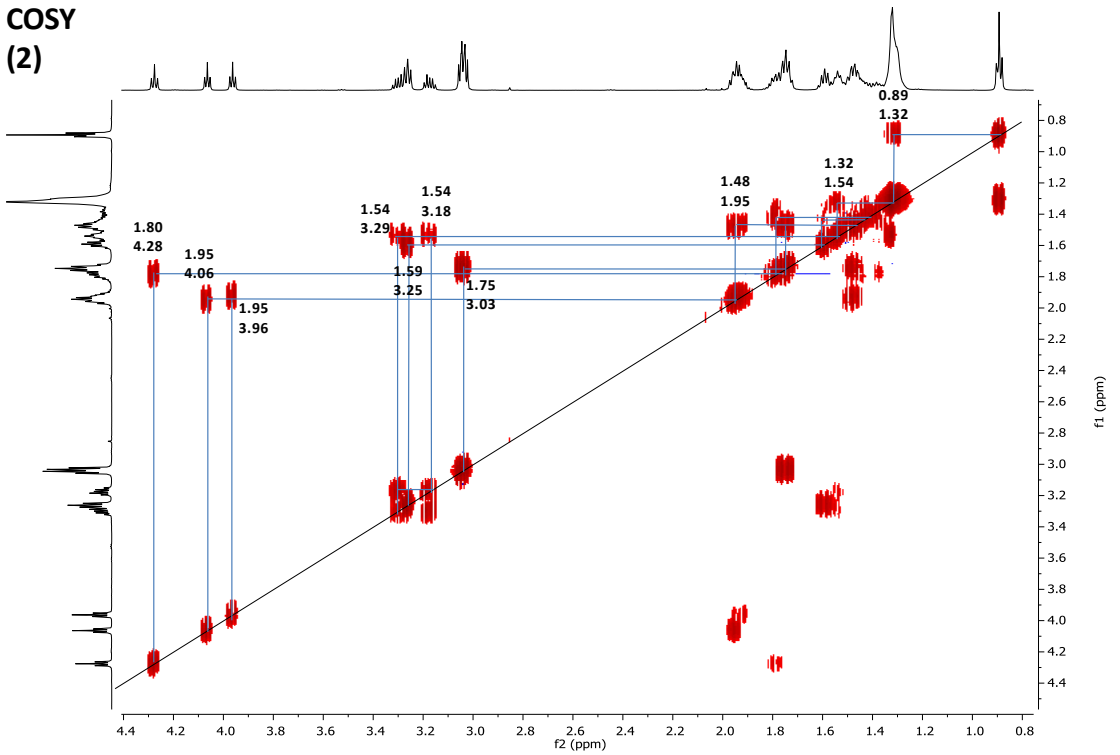
0.89
1.32
1.32
1.54
1.48
1.95
1.54
3.29
1.54
3.18
1.80
4.28
1.95
4.06
1.59
3.25
1.75
3.03
1.95
3.96
f2 (ppm)
f1 (ppm)

G1-C12 (3)

Yield (TFA salt; loading: 0.34 mmol/g): 93.3 mg (54 %). LC-MS data R_t: 2.7-3.1 min. MS(ESI^+), calcd $C_{30}H_{63}N_7O_3$: 569.50 g/mol, found: m/z 570.49 $[MH]^+$. ^1H NMR (600 MHz, D_2O): δ 4.26 (t, *J* = 7.36 Hz, 1H), 4.03 (t, *J* = 6.59 Hz, 1H), 3.93 (t, *J* = 6.74 Hz, 1H), 3.32 – 3.18 (m, 3H), 3.14 (dt, *J* = 13.45, 6.71 Hz, 1H), 3.06 – 2.96 (m, 4H), 1.98 – 1.83 (m, 4H), 1.82 – 1.66 (m, 6H), 1.62 – 1.33 (m, 8H)[2], 1.33 – 1.21 (m, 21H), 0.87 (t, *J* = 6.94 Hz, 3H). ^{13}C NMR (151 MHz, D_2O): δ 172.94, 169.48, 169.34, 54.24, 53.09, 52.69, 39.30, 39.27, 38.97, 38.93, 31.26, 30.64, 30.46, 30.43, (28.85, 28.84, 28.75, 28.73, 28.59, 28.37, 28.23, 27.90, 26.34, 26.32, 26.03, 22.48, 22.09, 21.34, 21.08, 13.45.

UPLC-MS (3)

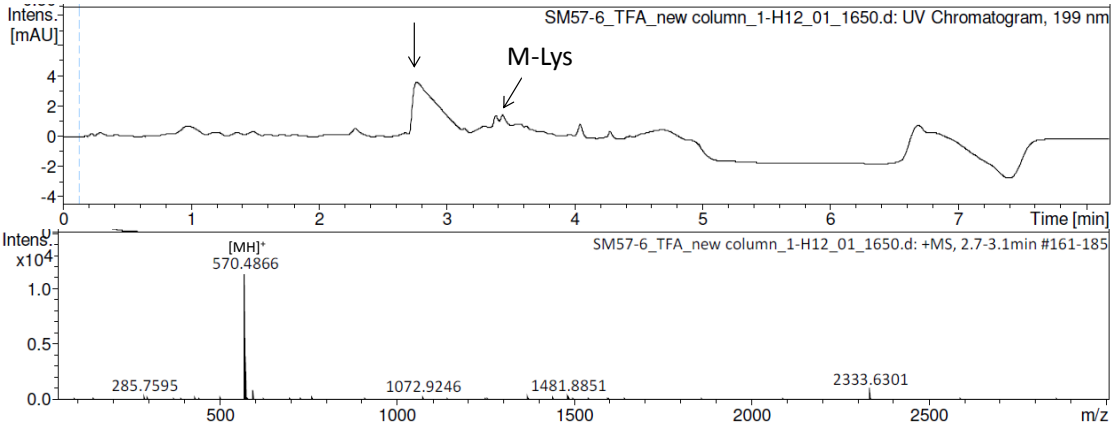

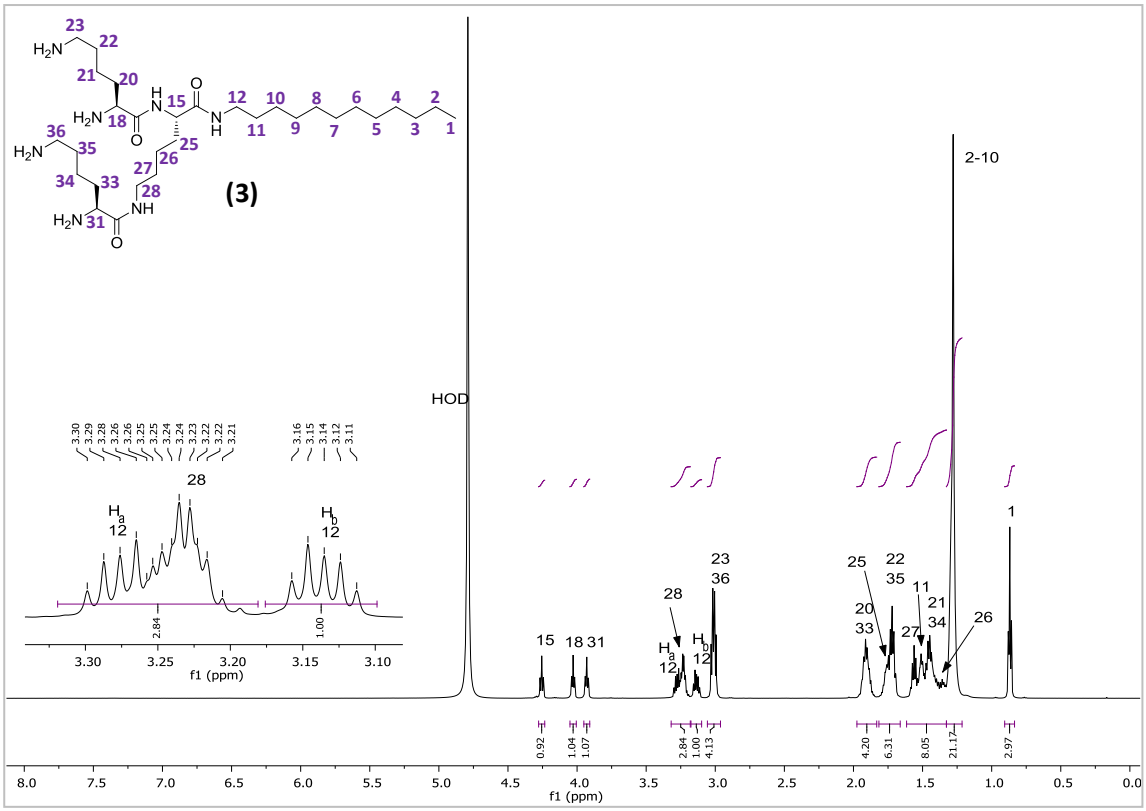

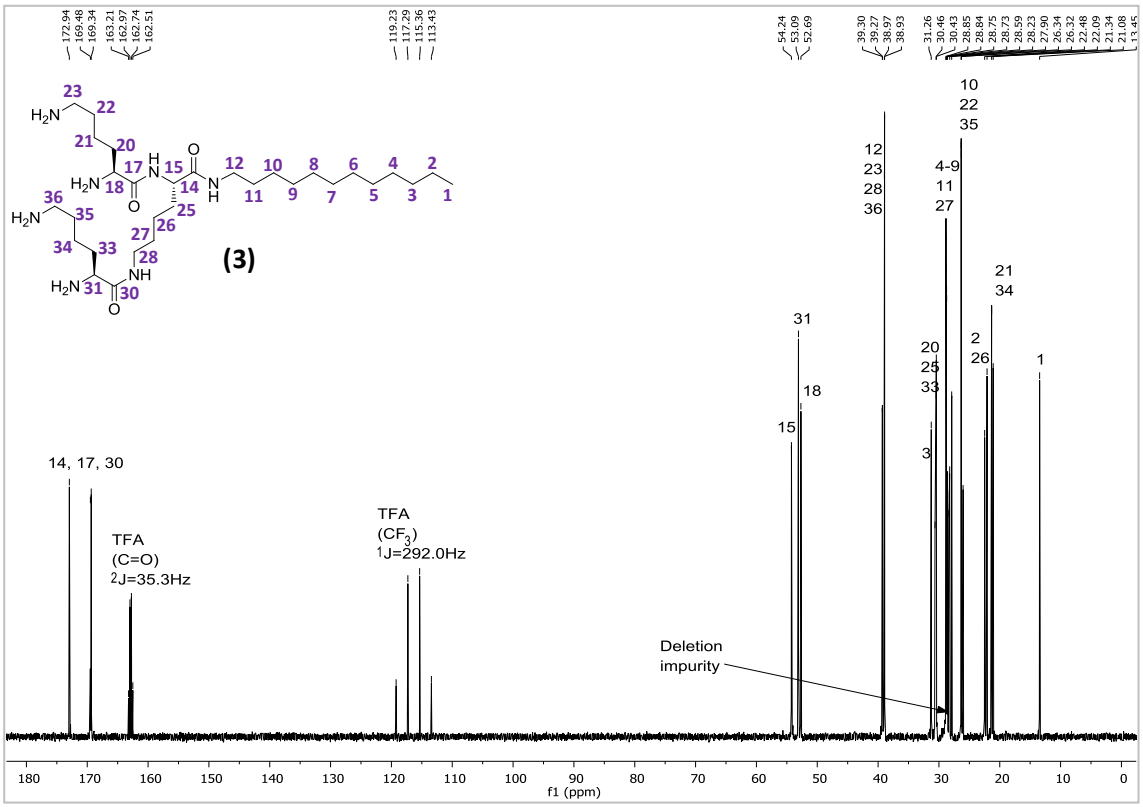
(3)
14, 17, 30
TFA
(C=O)
2J=35.3Hz
TFA
(CF3)
1J=292.0Hz
Deletion
impurity
f1 (ppm)

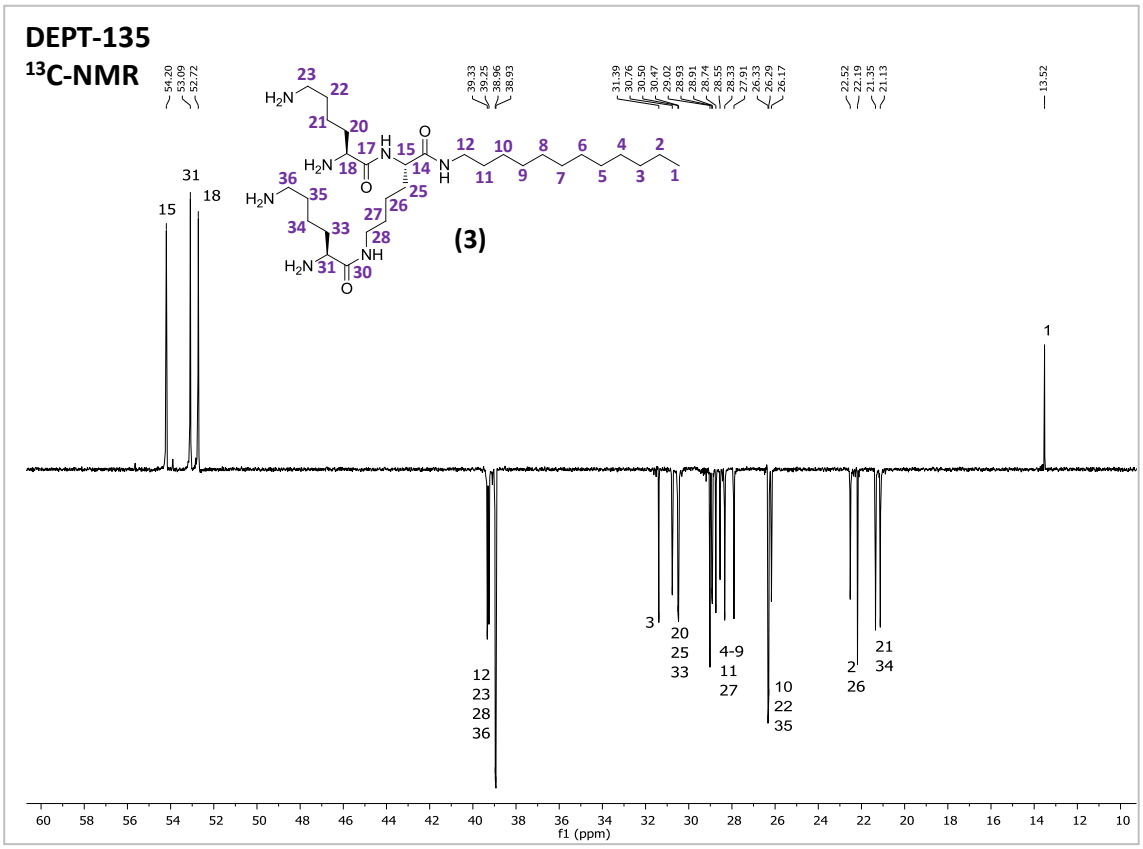
DEPT-135
13C-NMR
(3)
f1 (ppm)

HSQC (3)

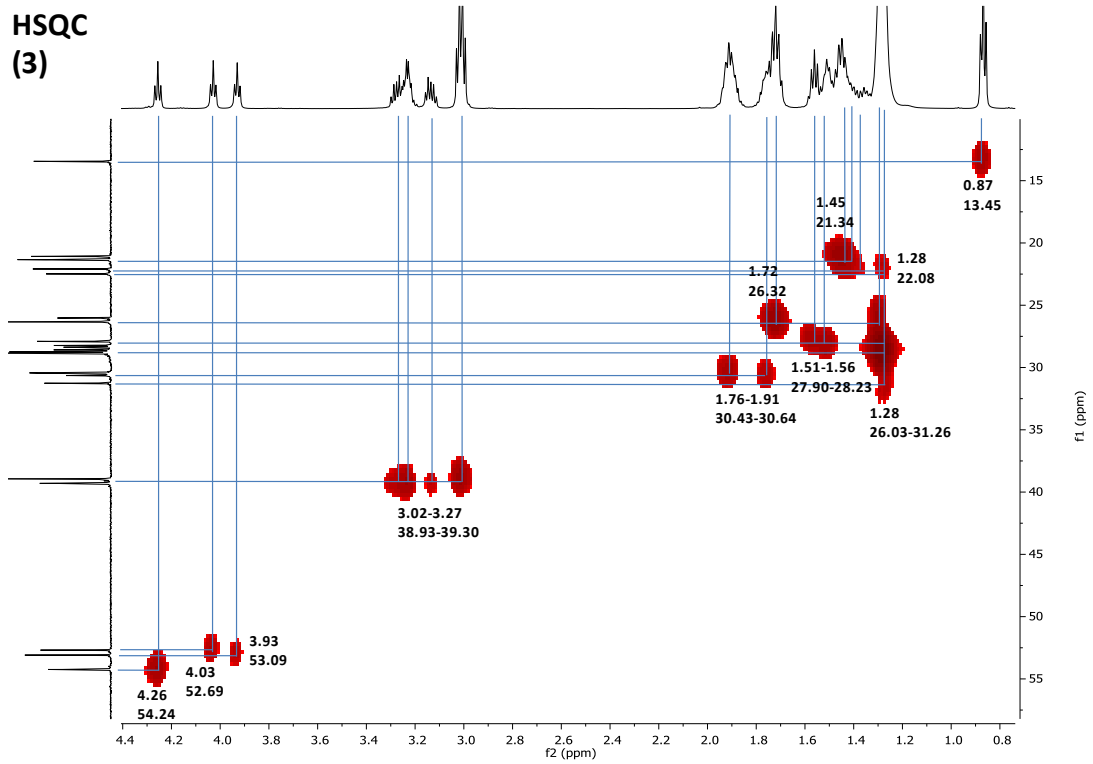
0.87
13.45
1.45
21.34
1.28
22.08
1.72
26.32
1.51-1.56
27.90-28.23
1.76-1.91
30.43-30.64
1.28
26.03-31.26
3.02-3.27
38.93-39.30
3.93
53.09
4.03
52.69
4.26
54.24
f2 (ppm)
f1 (ppm)

COSY (3)

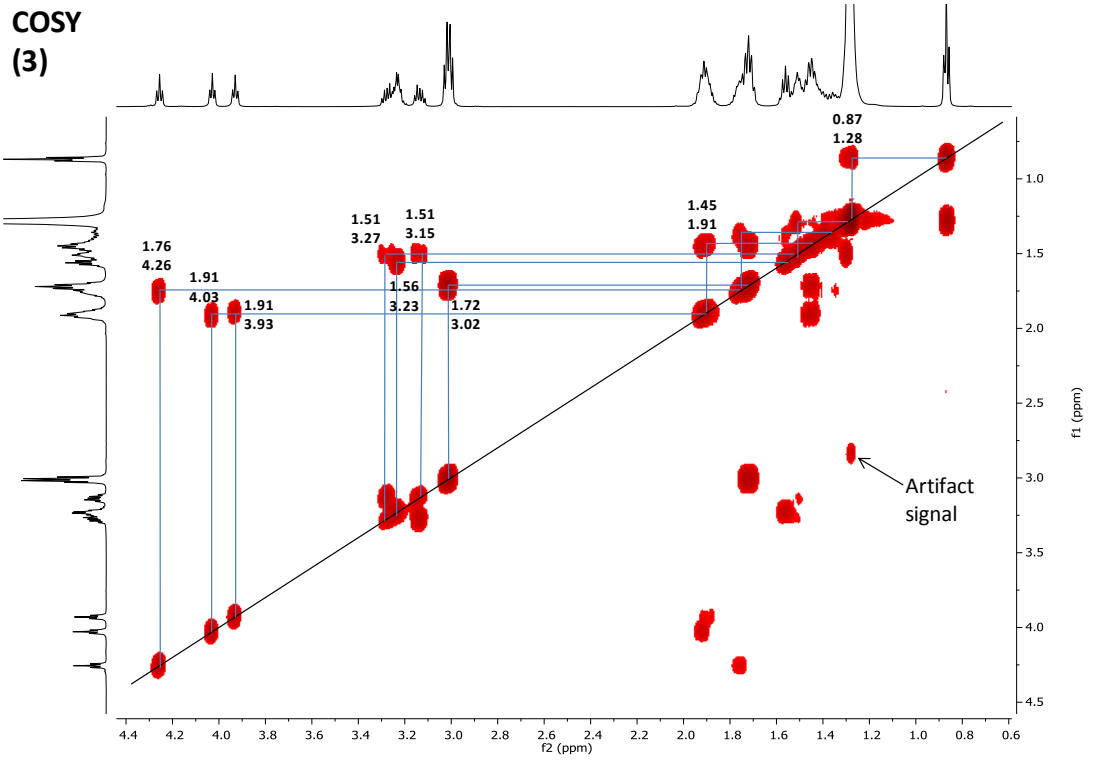
0.87
1.28
1.45
1.91
1.51
3.27
1.51
3.15
1.76
4.26
1.91
4.03
1.91
3.93
1.56
3.23
1.72
3.02
Artifact signal
f2 (ppm)
f1 (ppm)

G1-C14 (4)

Yield (TFA salt; loading: 0.22 mmol/g): 147.1 mg (quant.). LC-MS data R_t: 3.4-3.6 min. MS(ESI^+), calcd $C_{32}H_{67}N_7O_3$: 597.53 g/mol, found: m/z 598.52 $[MH]^+$; 299.77 $[MH_2/2]^+$. ^1H NMR (600 MHz, D_2O): δ 4.33 (t, *J* = 7.29 Hz, 1H), 4.14 – 4.04 (m, 1H), 3.99 (t, *J* = 6.71 Hz, 1H), 3.33 – 3.09 (m, 2H)[2], 3.04 (q, *J* = 7.23 Hz, 4H), 2.03 – 1.88 (m, 3H), 1.75 (m, 6H), 1.62 – 1.43 (m, 7H), 1.31 (s, 22H), 0.93 – 0.88 (m, 3H). ^{13}C NMR (151 MHz, D_2O): δ 172.75, 169.37, 169.21, 54.15, 53.07, 52.75, 39.42, 39.27, 38.99, 38.96, 31.69, 31.04, 30.47, 30.43, 29.67, 29.55, 29.45, 29.42, 29.36, 29.29, 29.12, 28.95, 28.60, 26.51, 26.32, 26.25, 22.42, 21.37, 21.22, 21.16, 13.70.

UPLC-MS (4)

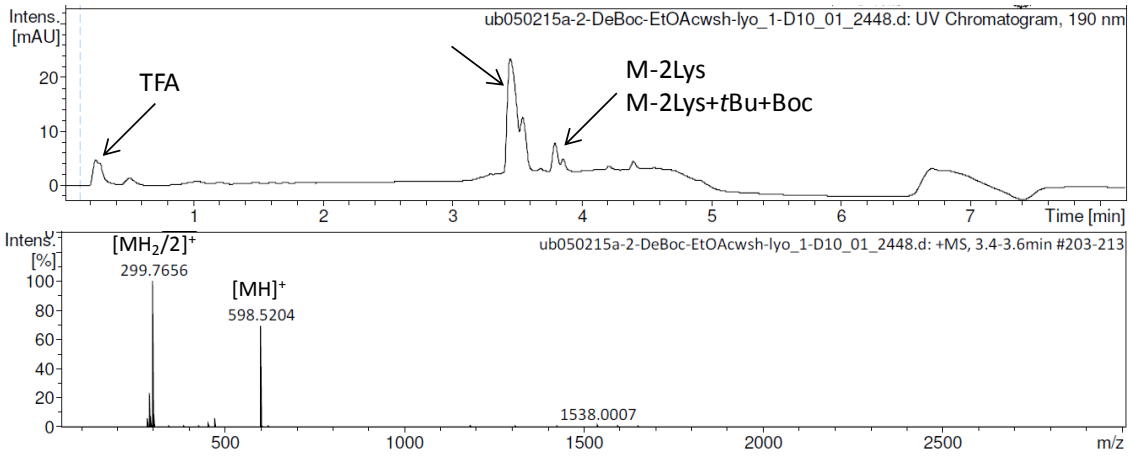

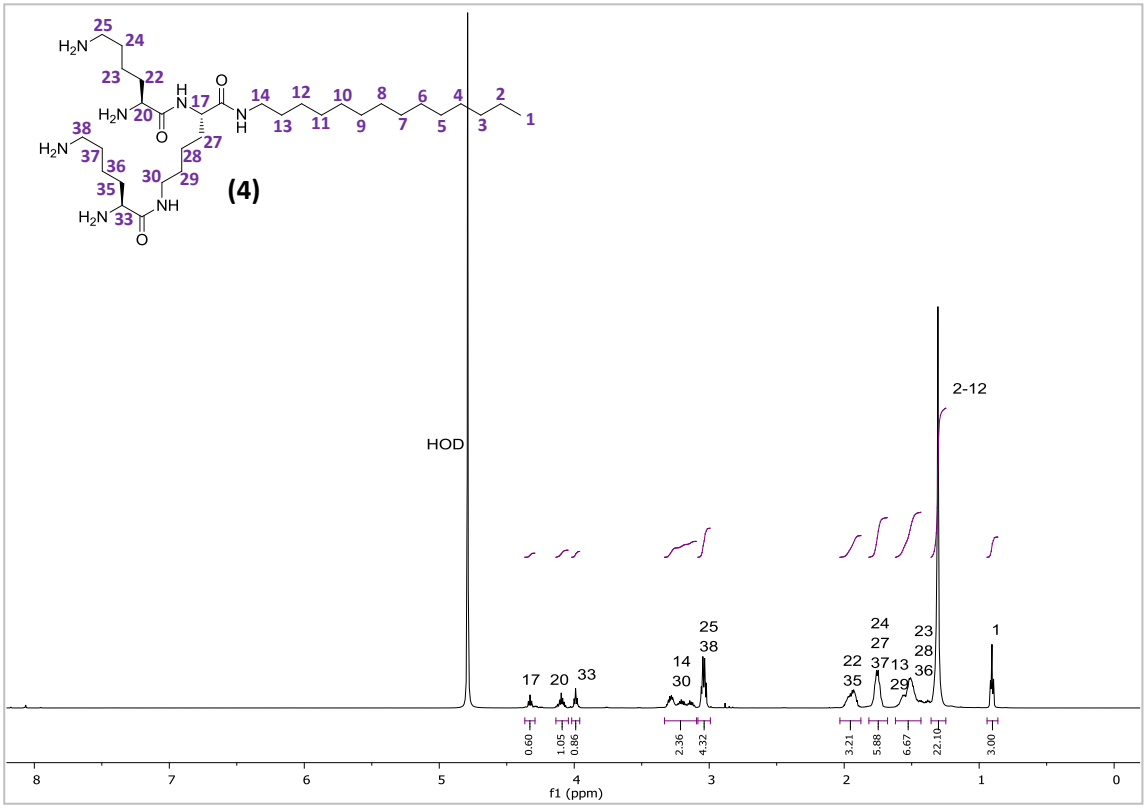

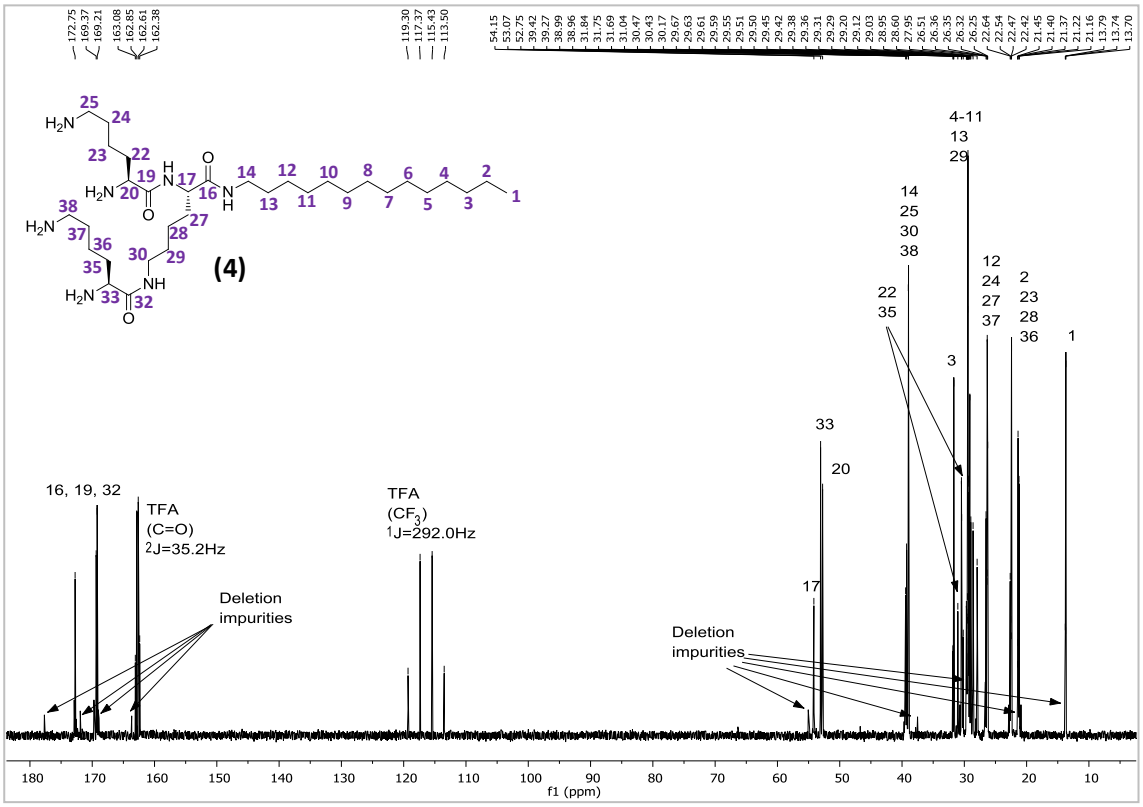
(4)
16, 19, 32
TFA
(C=O)
2J=35.2Hz
TFA
(CF3)
1J=292.0Hz
Deletion
impurities
Deletion
impurities
4-11
13
29
14
25
30
38
12
24
27
37
2
23
28
36
22
35
3
33
20
17
1
f1 (ppm)

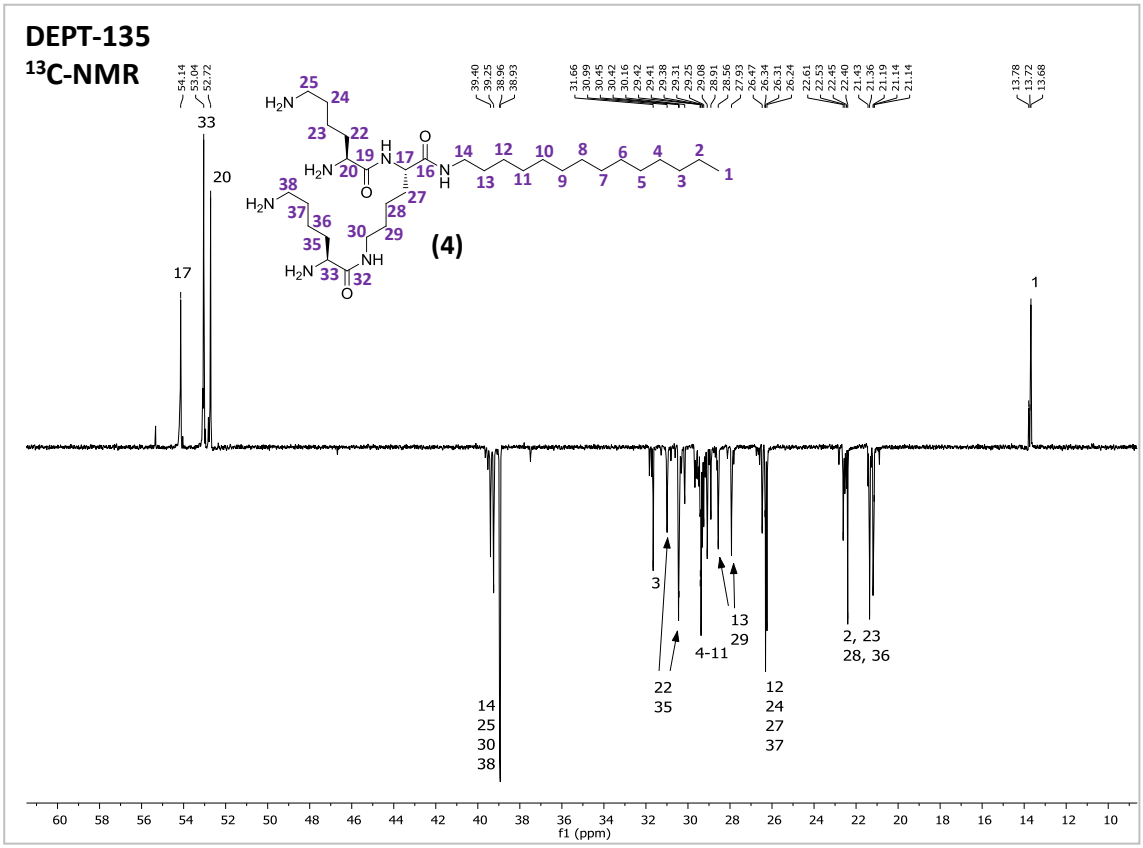
DEPT-135
13C-NMR
(4)
33
20
17
1
3
22
35
4-11
13
29
12
24
27
37
14
25
30
38
2, 23
28, 36
f1 (ppm)

HSQC (4)

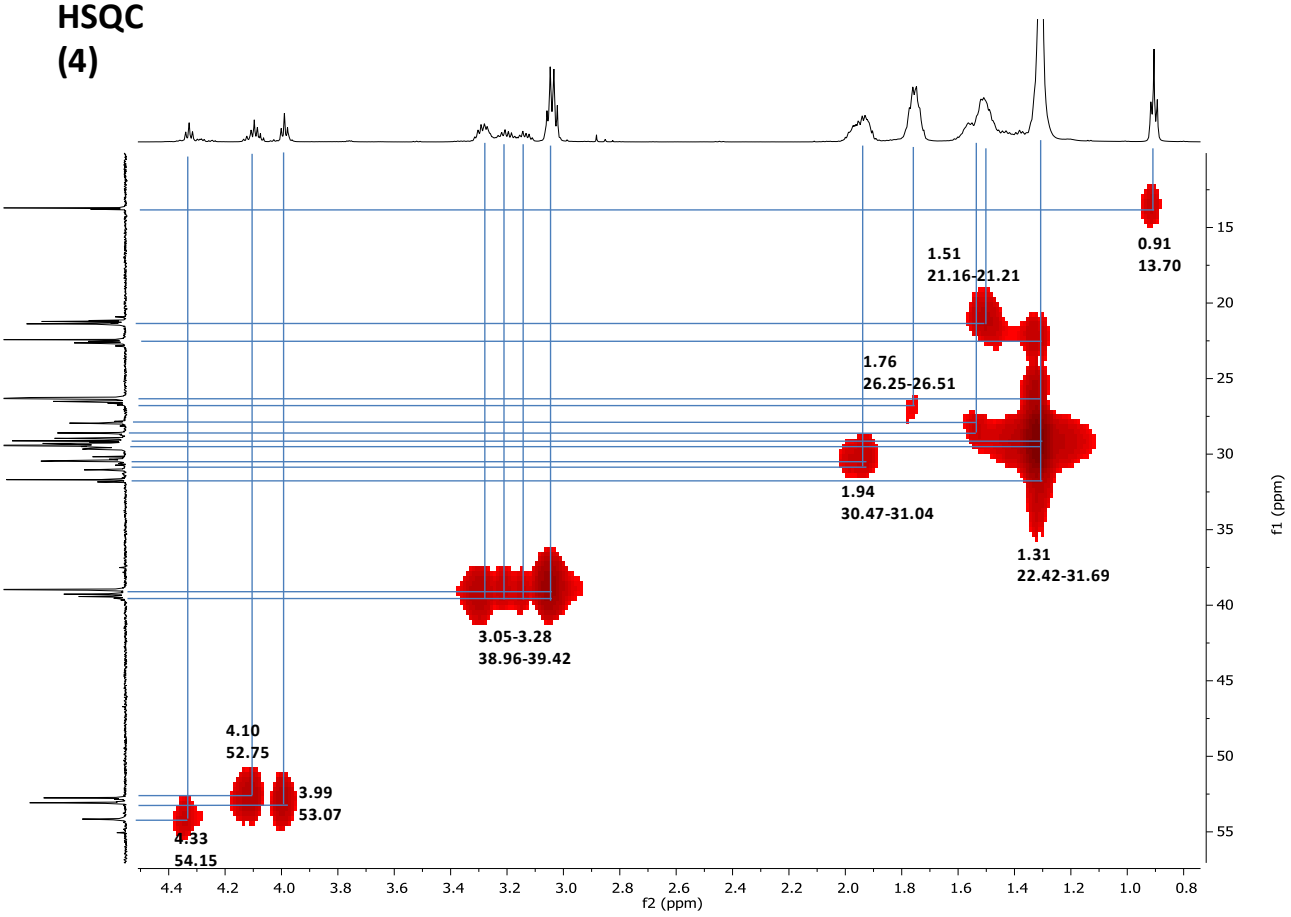
0.91
13.70
1.51
21.16-21.21
1.76
26.25-26.51
1.94
30.47-31.04
1.31
22.42-31.69
3.05-3.28
38.96-39.42
4.10
52.75
3.99
53.07
4.33
54.15
f2 (ppm)
f1 (ppm)

COSY (4)

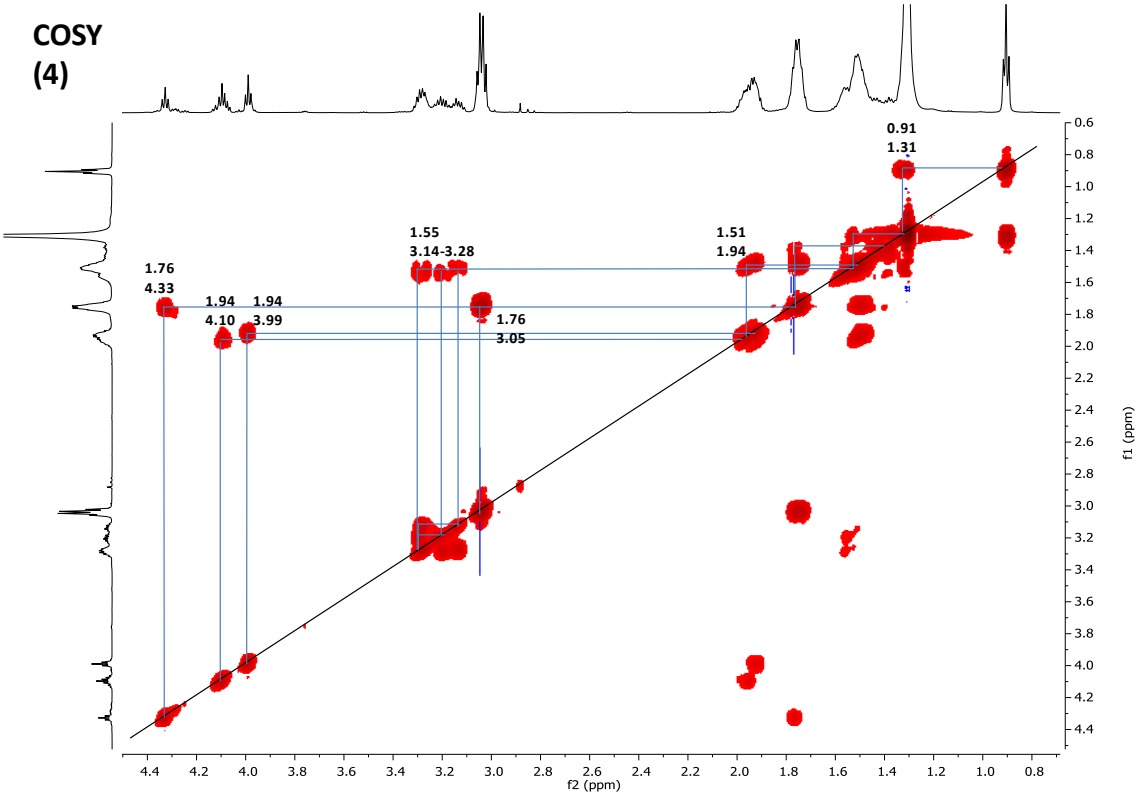
0.91
1.31
1.55
3.14-3.28
1.51
1.94
1.76
4.33
1.94
4.10
1.94
3.99
1.76
3.05
f2 (ppm)
f1 (ppm)

G1-C16 (5)

Yield (TFA salt; loading: 0.21 mmol/g): 71.4 mg (79 %). LC-MS data R_t: 3.5-3.6 min. MS(ESI^+), calcd $C_{34}H_{71}N_7O_3$: 625.56 g/mol, found: m/z 626.54 $[MH]^+$; 313.78 $[MH_2/2]^+$. ^1H NMR (600 MHz, D_2O): δ 4.32 (t, *J* = 7.39 Hz, 1H), 4.13 – 4.03 (m, 1H), 3.97 (t, *J* = 6.80 Hz, 1H), 3.32 – 3.21 (m, 2H), 3.20 – 3.06 (m, 1H), 3.02 (q, *J* = 7.44 Hz, 4H), 2.01 – 1.83 (m, 4H), 1.79 – 1.66 (m, 6H), 1.61 – 1.36 (m, 8H)[2], 1.28 (s, 29H), 0.89 (t, *J* = 6.68 Hz, 3H). ^{13}C NMR (151 MHz, D_2O): δ 172.69, 169.38, 169.20, 54.09, 53.05, 52.75, 39.44, 39.24, 38.97, 38.94, 31.83, 31.14, 30.48, 30.45, 29.82, 29.75, 29.66, 29.62, 29.60, 29.57, 29.48, 29.38, 29.29, 29.14, 28.71, 27.94, 26.66, 26.31, 26.22, 22.53, 21.38, 21.26, 13.78.

UPLC-MS (5)

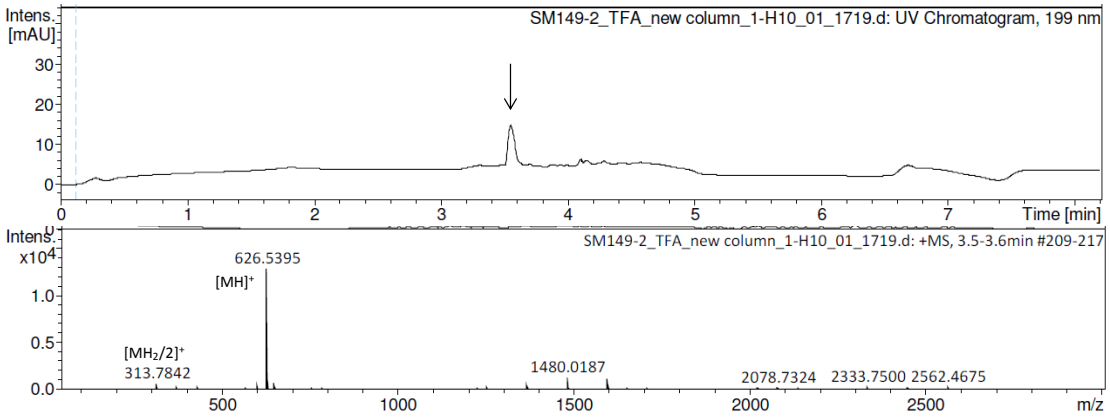

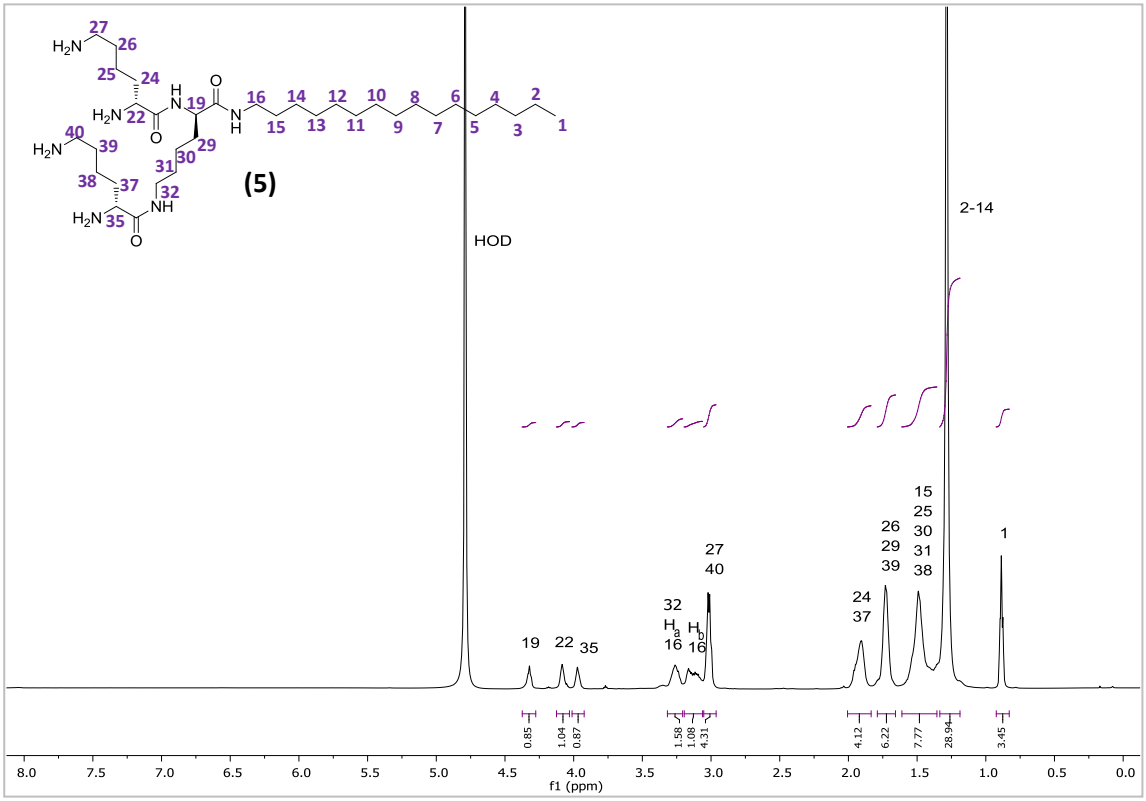

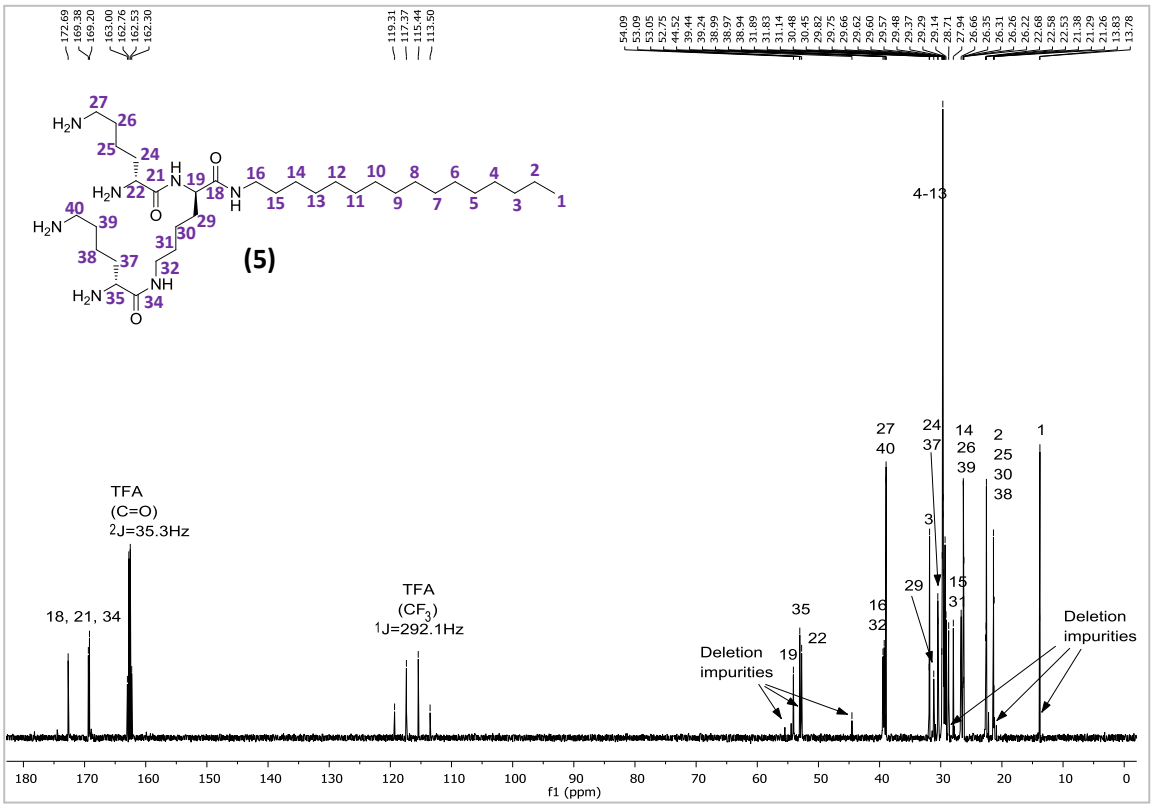
(5)
TFA
(C=O)
2J=35.3Hz
TFA
(CF3)
1J=292.1Hz
18, 21, 34
Deletion impurities
Deletion impurities
4-13
f1 (ppm)

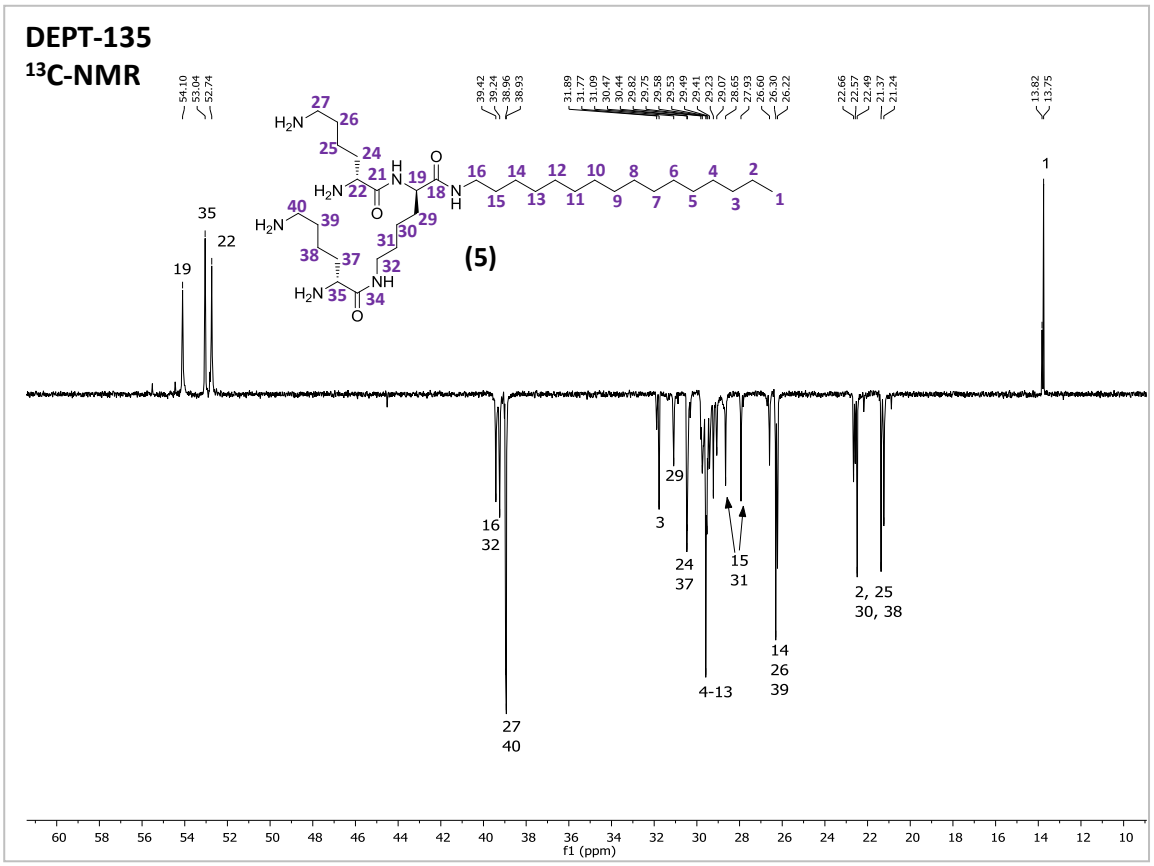
DEPT-135
13C-NMR
(5)
16 32
27 40
3
29
24 37
15 31
4-13
14 26 39
2, 25 30, 38
f1 (ppm)

HSQC (5)

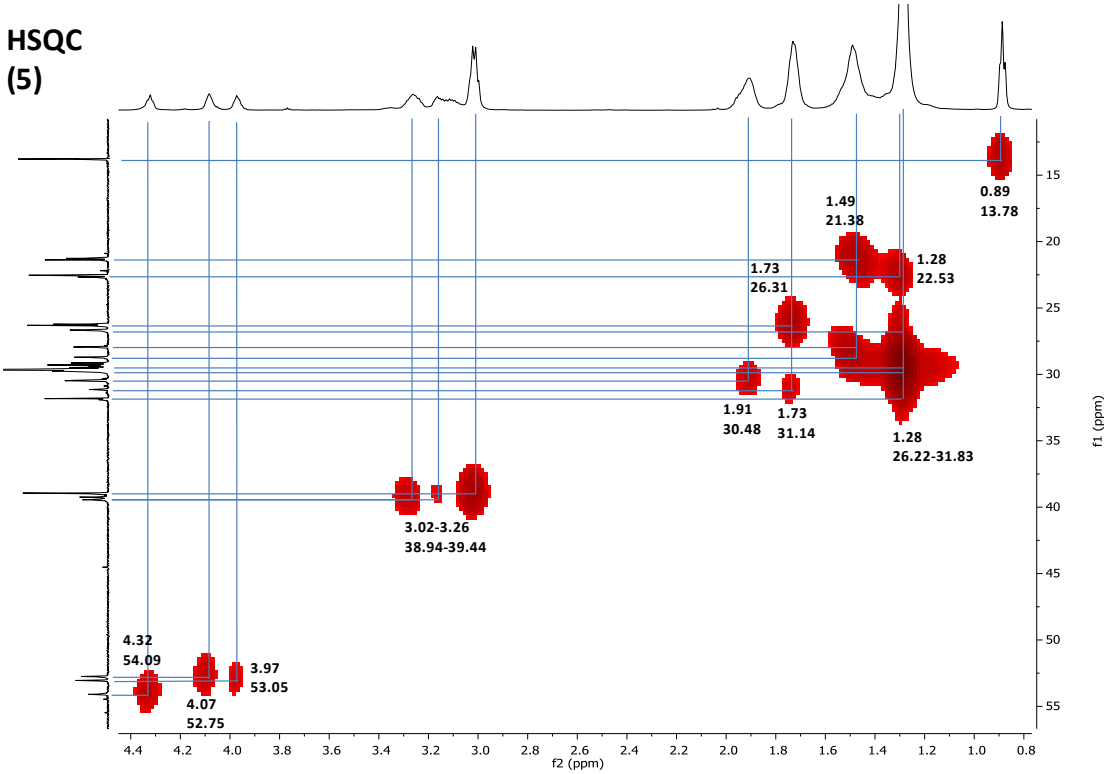
0.89
13.78
1.49
21.38
1.28
22.53
1.73
26.31
1.91
30.48
1.73
31.14
1.28
26.22-31.83
3.02-3.26
38.94-39.44
4.32
54.09
3.97
53.05
4.07
52.75
f2 (ppm)
f1 (ppm)

COSY (5)

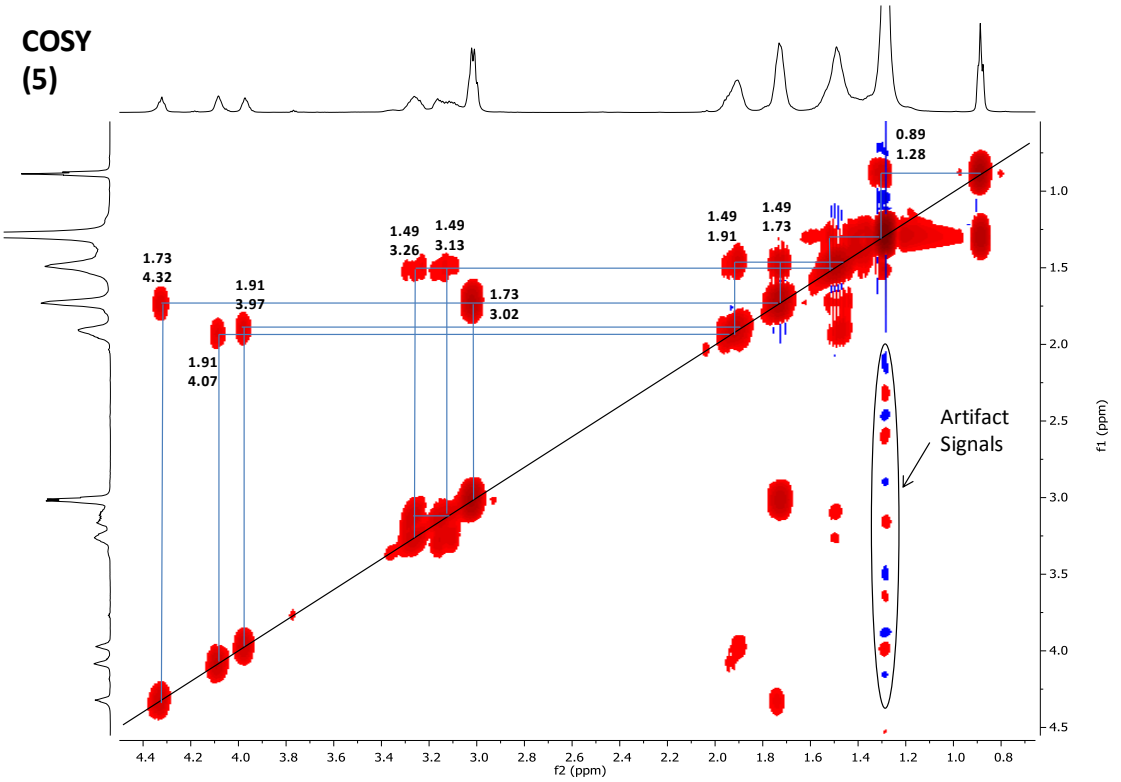
0.89
1.28
1.49
1.91
1.49
1.73
1.49
3.26
1.49
3.13
1.73
4.32
1.91
3.97
1.73
3.02
1.91
4.07
Artifact
Signals
f2 (ppm)
f1 (ppm)

G1-C18 (6)

Yield (TFA salt; loading: 0.14 mmol/g): 101.2 mg (quant.). LC-MS data R_t: 3.7-3.9 min. MS(ESI^+), calcd $C_{36}H_{75}N_7O_3$: 653.59 g/mol, found: m/z 654.58 $[MH]^+$; 327.80 $[MH_2/2]^+$. ^1H NMR (600 MHz, D_2O): δ 4.33 (t, *J* = 7.20 Hz, 1H), 4.09 (t, *J* = 7.07 Hz, 1H), 3.97 (t, *J* = 7.29 Hz, 1H), 3.33 – 3.06 (m, 3H)[2], 3.02 (q, *J* = 7.34 Hz, 4H), 2.01 – 1.85 (m, 4H), 1.79 – 1.67 (m, 6H), 1.59 – 1.38 (m, 7H), 1.29 (s, 30H), 0.89 (t, *J* = 6.76Hz, 3H). ^{13}C NMR (151 MHz, D_2O): δ 172.66, 169.40, 169.21, 54.09, 53.04, 52.75, 39.45, 39.23, 38.97, 38.93, 31.90, 31.19, 30.50, 30.45, 29.77, 29.72, 29.69, 29.66, 29.59, 29.56, 29.39, 29.22, 28.75, 27.94, 26.72, 26.29, 26.19, 22.59, 21.38, 21.27, 21.15, 13.83.

UPLC-MS (6)

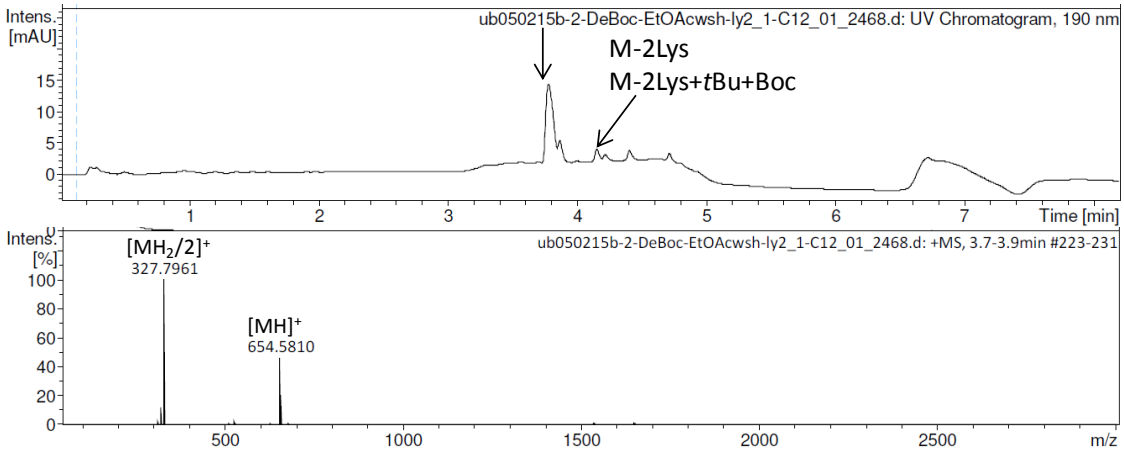

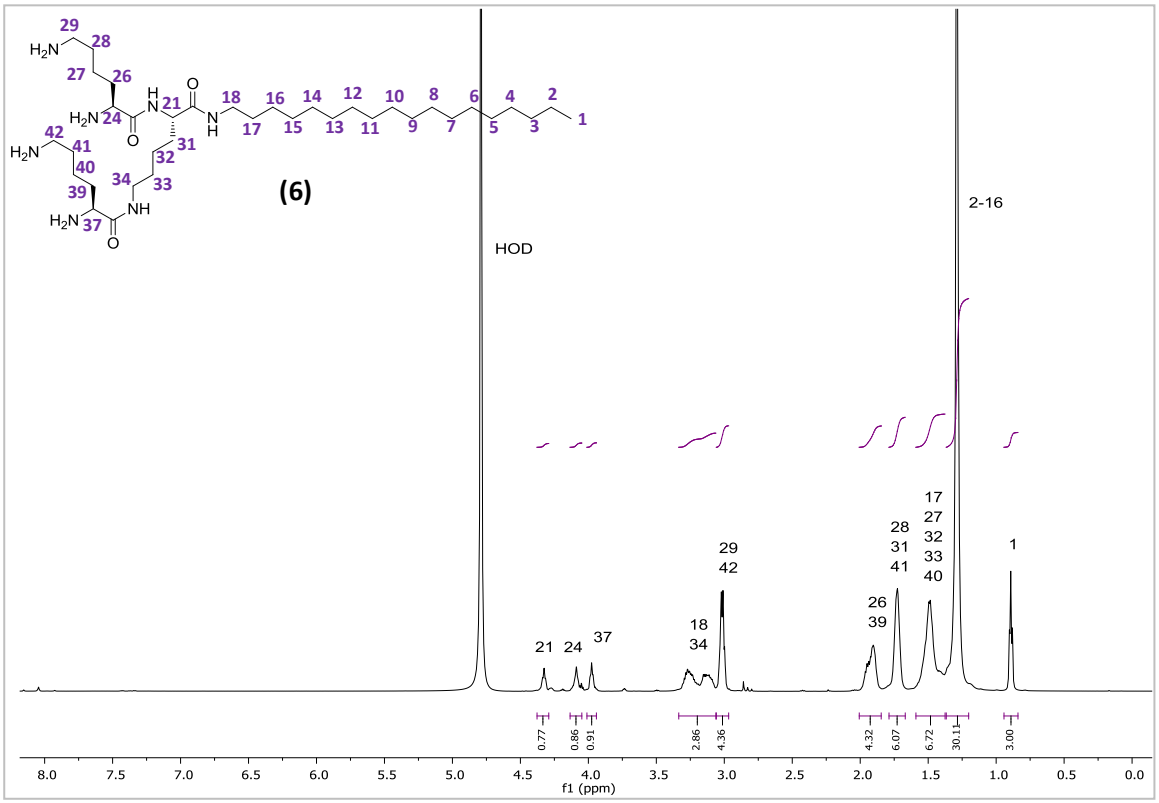

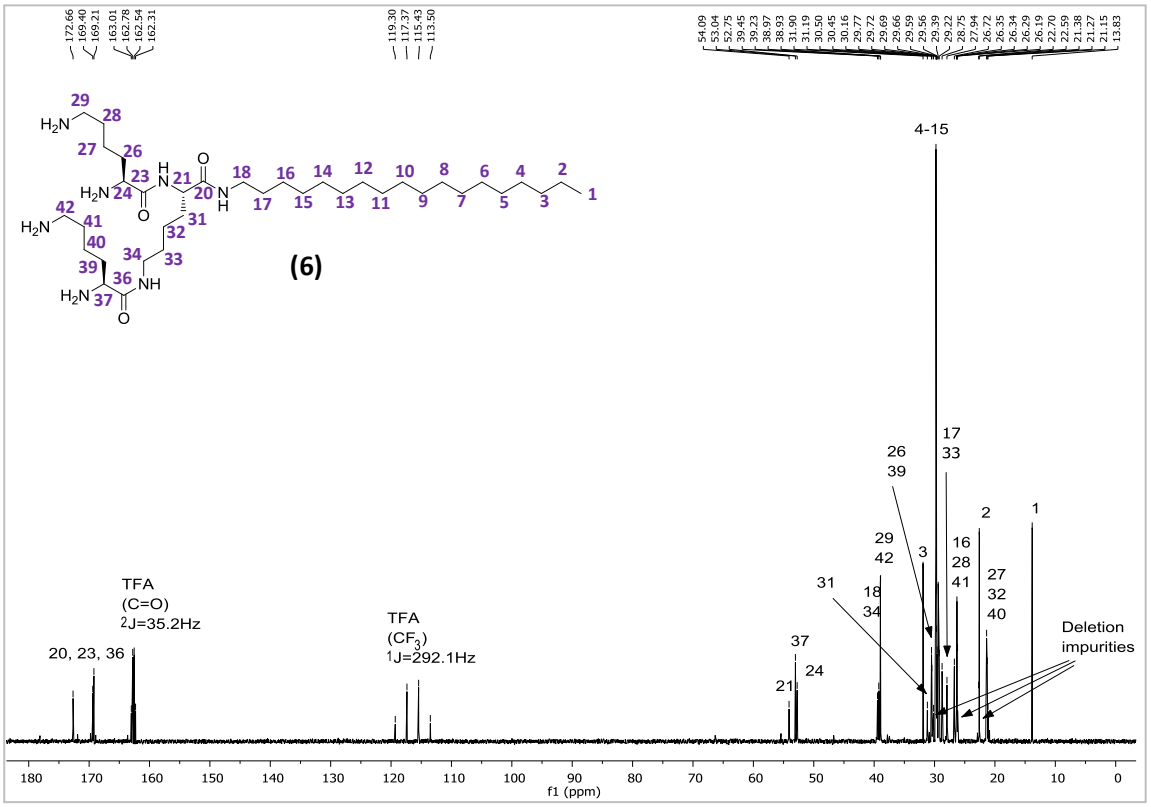
(6)
TFA
(C=O)
2J=35.2Hz
TFA
(CF3)
1J=292.1Hz
20, 23, 36
Deletion
impurities
f1 (ppm)

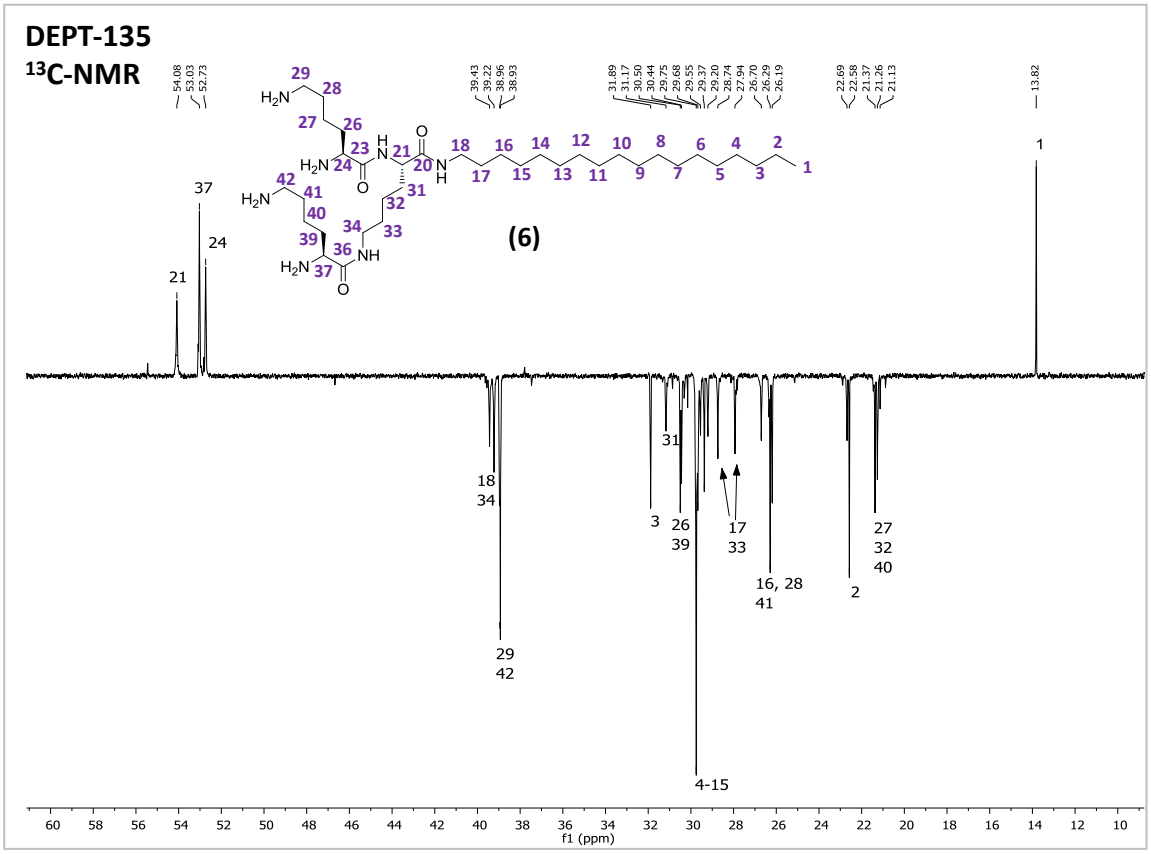
DEPT-135
13C-NMR
(6)
f1 (ppm)

HSQC (6)

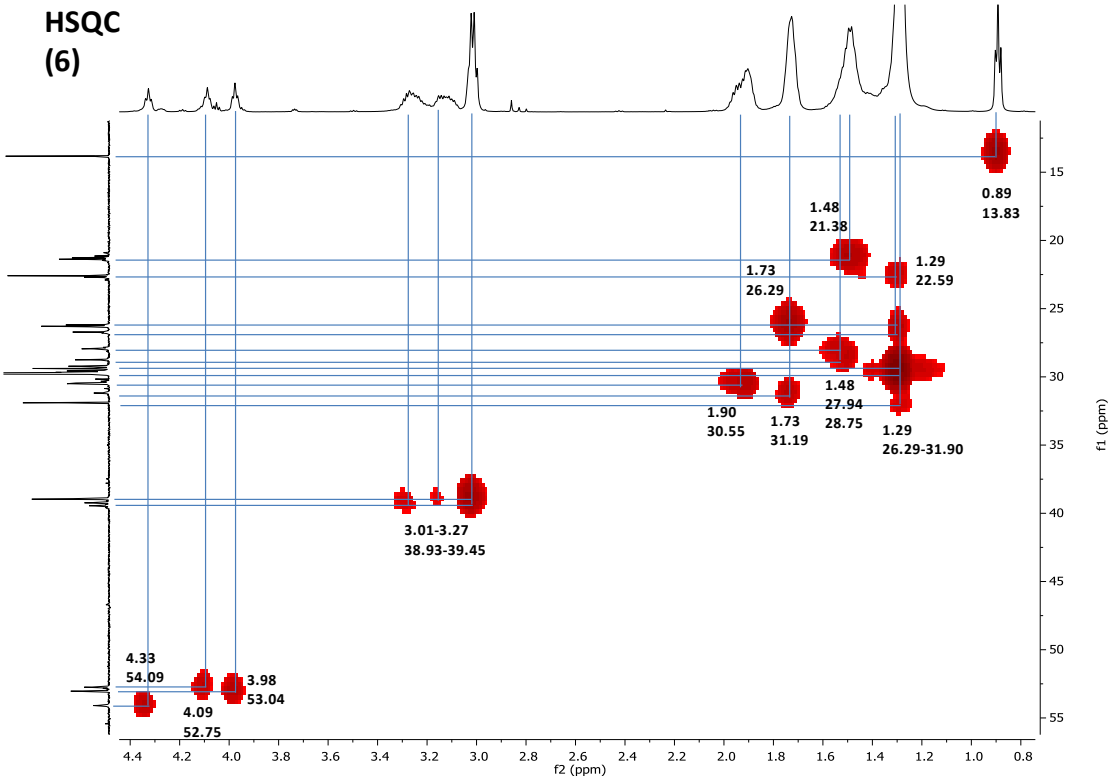
0.89
13.83
1.48
21.38
1.29
22.59
1.73
26.29
1.48
27.94
28.75
1.90
30.55
1.73
31.19
1.29
26.29-31.90
3.01-3.27
38.93-39.45
4.33
54.09
3.98
53.04
4.09
52.75
f2 (ppm)
f1 (ppm)

COSY (6)

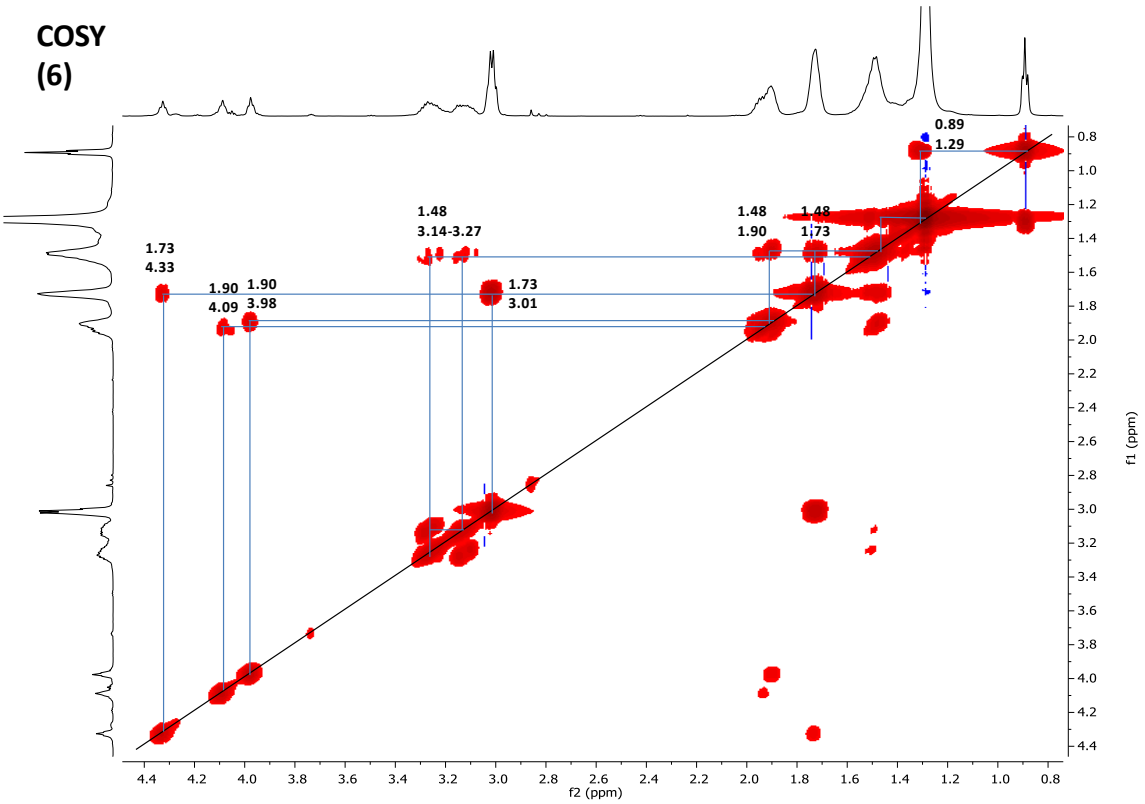
0.89
1.29
1.48
3.14-3.27
1.48
1.90
1.48
1.73
1.73
4.33
1.90
4.09
1.90
3.98
1.73
3.01
f2 (ppm)
f1 (ppm)

G1(acetyl)-C4 (7)

Yield (TFA salt; loading: 0.32 mmol/g): 99.8 mg (81 %). LC-MS data R_t: 0.4-0.6 min. MS(ESI^+), calcd $C_{26}H_{51}N_7O_5$: 541.40 g/mol, found: m/z 542.38 $[MH]^+$. ^1H NMR (600 MHz, D_2O): δ 4.27 (dd, *J* = 8.39, 5.96 Hz, 1H), 4.24 – 4.16 (m, 2H), 3.28 – 3.13 (m, 4H), 3.00 (td, *J* = 7.76, 3.80 Hz, 4H), 2.04 (s, 6H), 1.85 – 1.64 (m, 7H)[1], 1.57 – 1.35 (m, 6H), 1.31 (h, *J* = 7.36 Hz, 3H), 0.89 (t, *J* = 7.38 Hz, 3H). ^{13}C NMR (151 MHz, D_2O): δ 174.24, 174.18, 173.94, 173.86, 173.45, 53.99, 53.98, 53.60, 39.14, 38.98, 38.92, 30.50, 30.45, 30.37, 27.78, 26.28, 26.25, 22.34, 22.11, 21.99, 21.64, 21.58, 19.28, 12.91.

UPLC-MS (7)

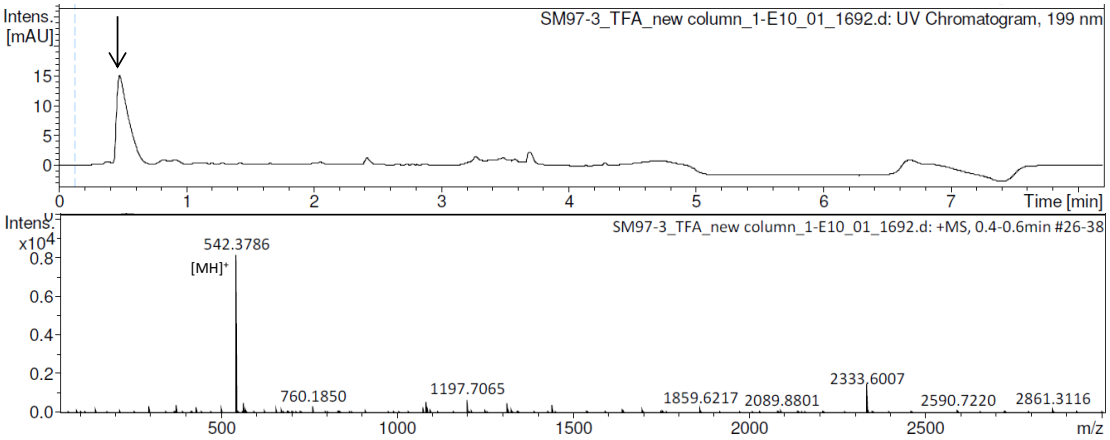

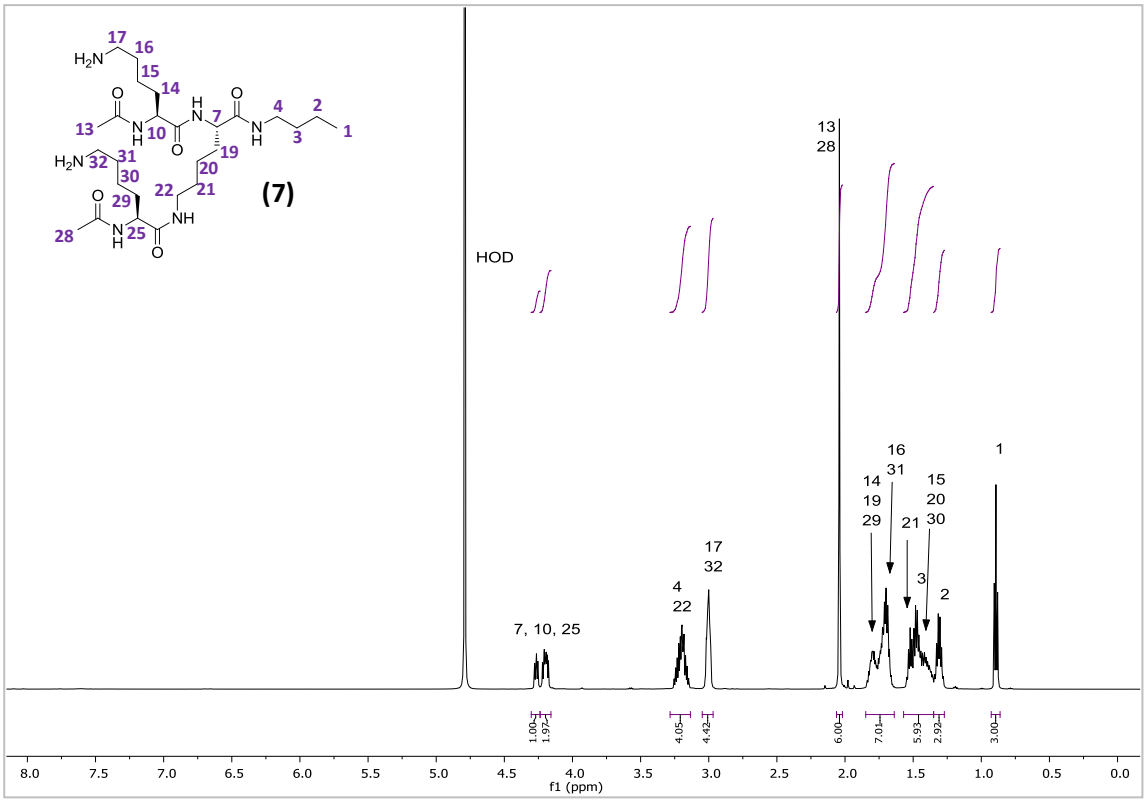

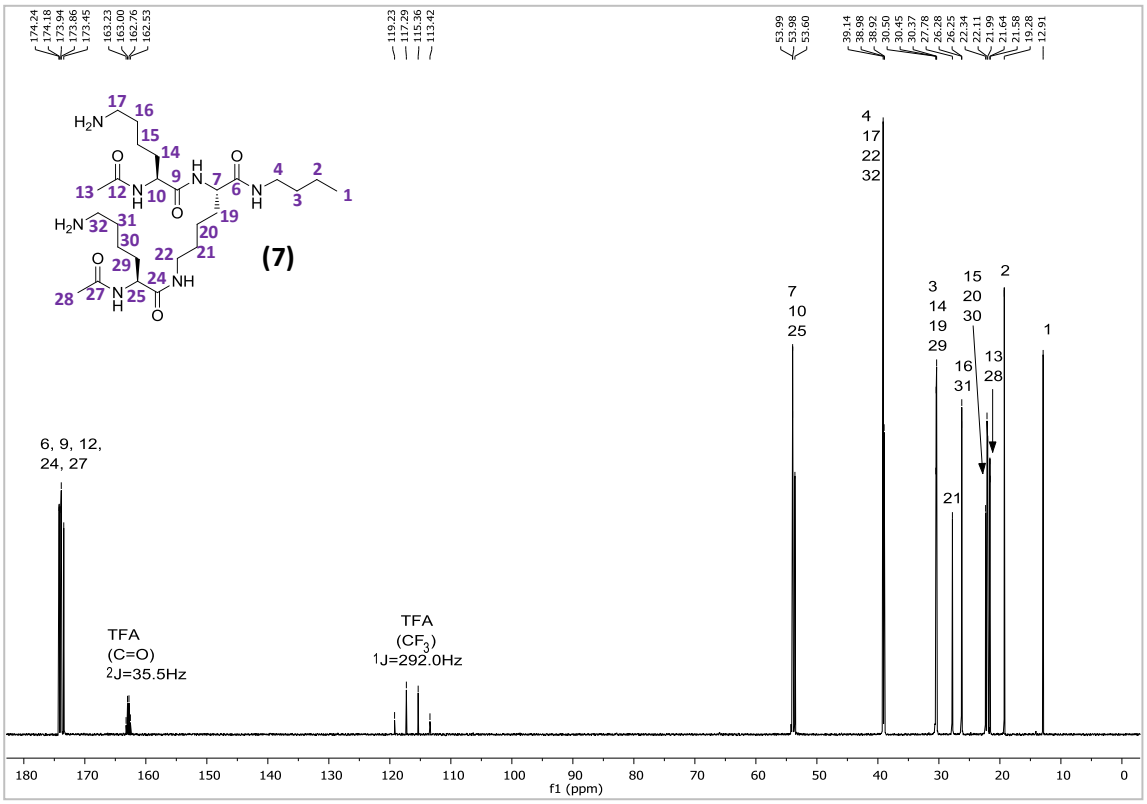
(7)
6, 9, 12,
24, 27
TFA
(C=O)
2J=35.5Hz
TFA
(CF3)
1J=292.0Hz
f1 (ppm)

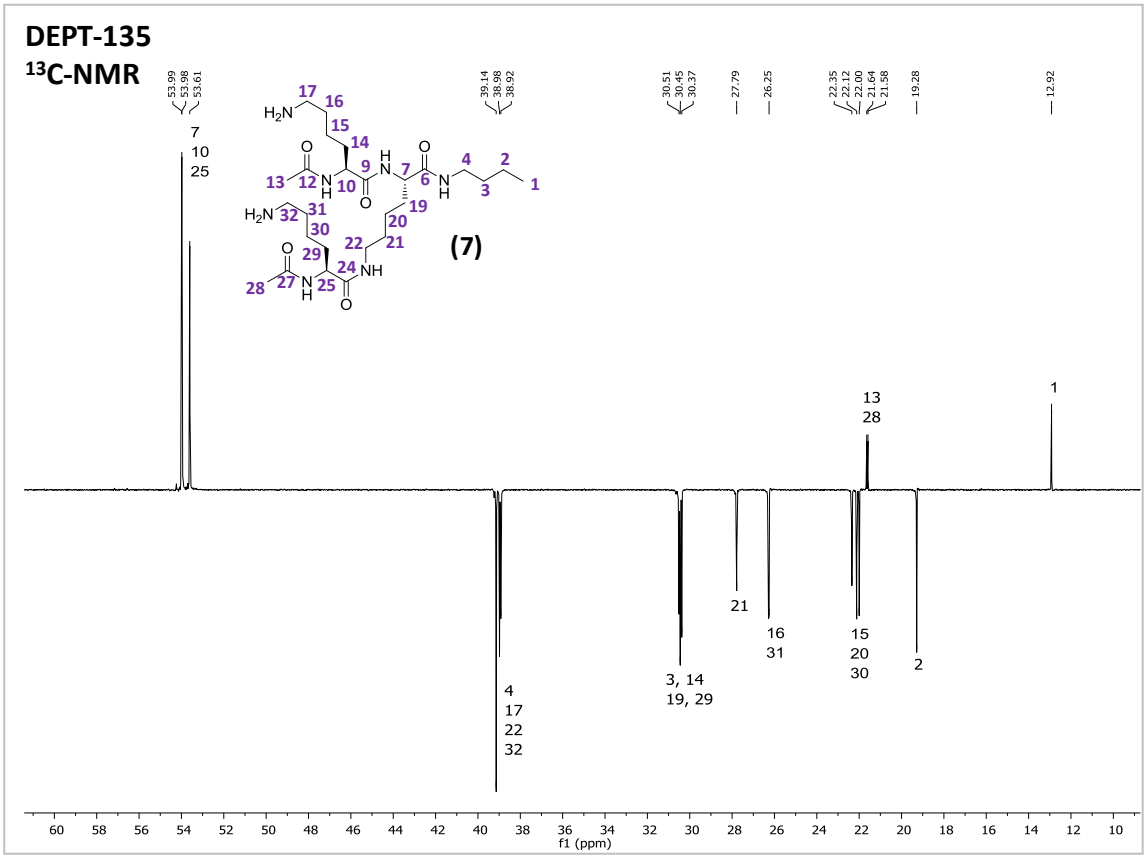
DEPT-135
13C-NMR
(7)
4
17
22
32
3, 14
19, 29
21
16
31
15
20
30
2
13
28
1
f1 (ppm)

HSQC (7)

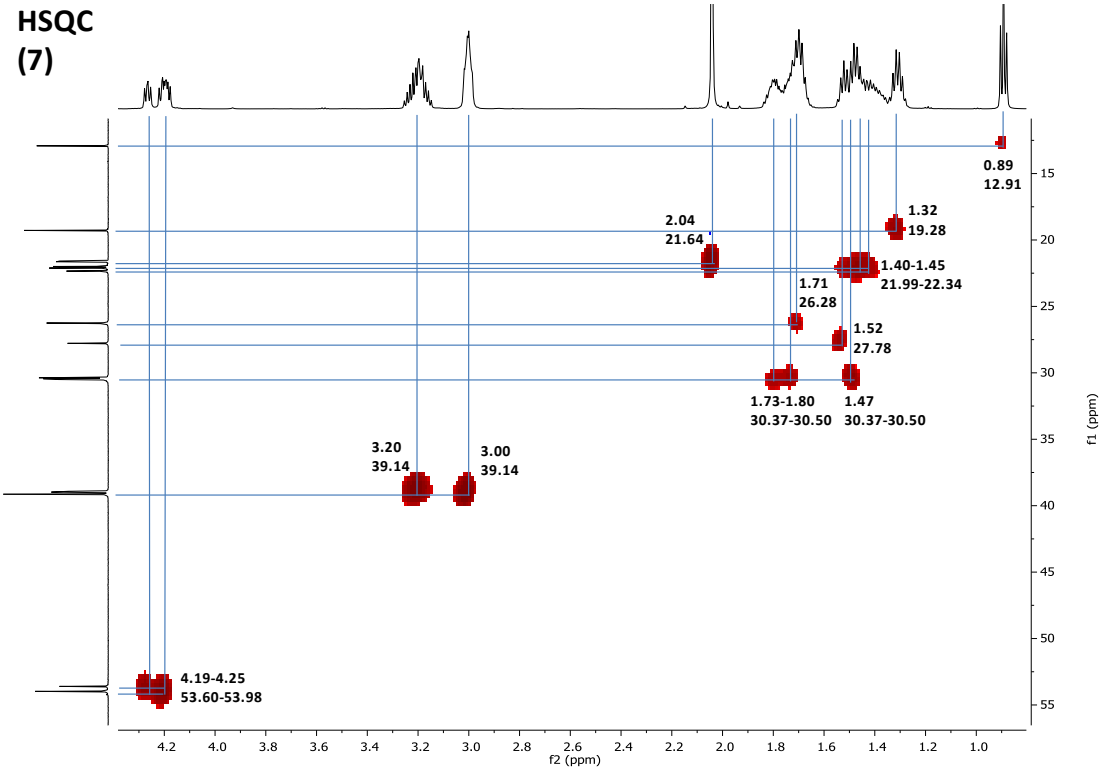
0.89
12.91
1.32
19.28
2.04
21.64
1.40-1.45
21.99-22.34
1.71
26.28
1.52
27.78
1.73-1.80
30.37-30.50
1.47
30.37-30.50
3.20
39.14
3.00
39.14
4.19-4.25
53.60-53.98
f2 (ppm)
f1 (ppm)

COSY (7)

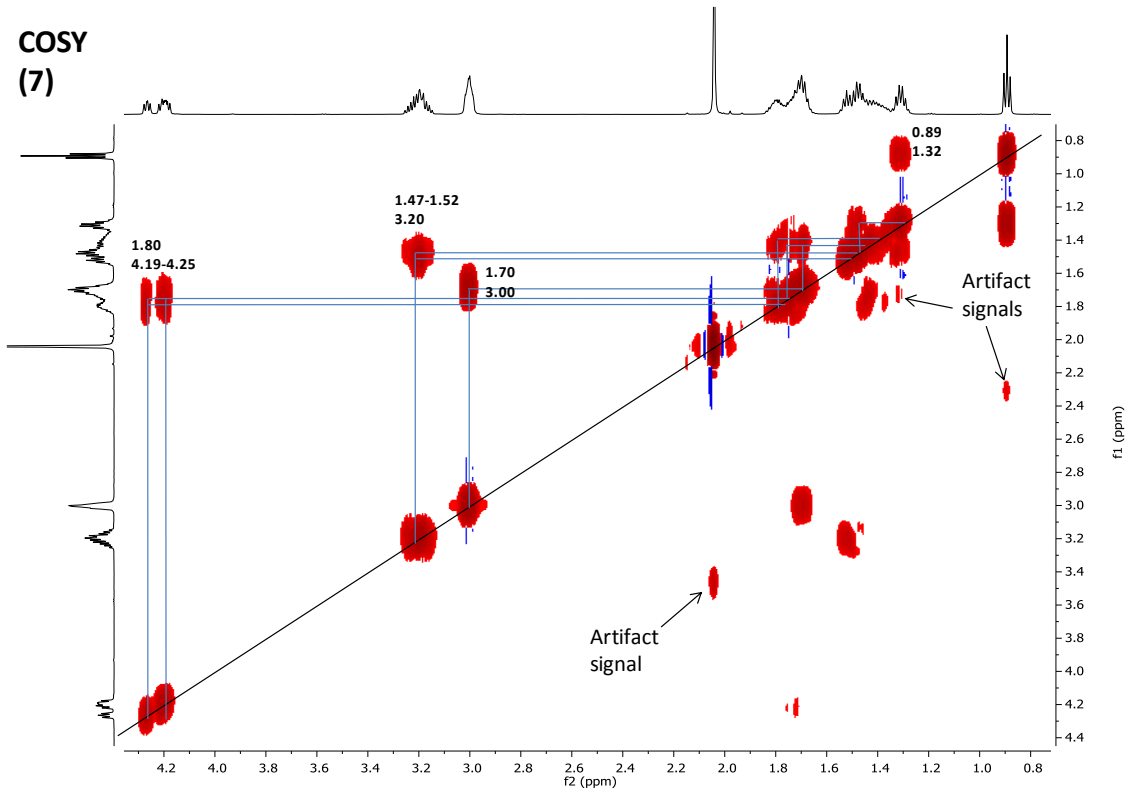
0.89
1.32
1.47-1.52
3.20
1.80
4.19-4.25
1.70
3.00
Artifact signals
Artifact signal
f2 (ppm)
f1 (ppm)

G1(acetyl)-C6 (8)

Yield (TFA salt; loading: 0.34 mmol/g): 98.8 mg (73 %). LC-MS data R_t: 1.2-1.5 min. MS(ESI^+), calcd $C_{28}H_{55}N_7O_5$: 569.43 g/mol, found: m/z 570.41 $[MH]^+$. ^1H NMR (600 MHz, D_2O): δ 4.29 (dd, *J* = 8.44, 5.91 Hz, 1H), 4.27 – 4.18 (m, 2H), 3.33 – 3.13 (m, 4H), 3.03 (td, *J* = 7.49, 3.43 Hz, 4H), 2.10 – 2.03 (m, 6H), 1.88 – 1.66 (m, 6H)[1], 1.60 – 1.33 (m, 10H), 1.33 – 1.28 (m, 6H), 0.92 – 0.87 (m, 3H). ^{13}C NMR (151 MHz, D_2O): δ 174.27, 174.19, 173.90, 173.86, 173.44, 53.99, 53.98, 53.62, 39.27, 39.17, 38.96, 30.63, 30.54, 30.51, 30.48, 28.18, 27.80, 26.30, 26.28, 25.61, 22.36, 22.13, 22.03, 21.93, 21.68, 21.62, 13.32.

UPLC-MS (8)

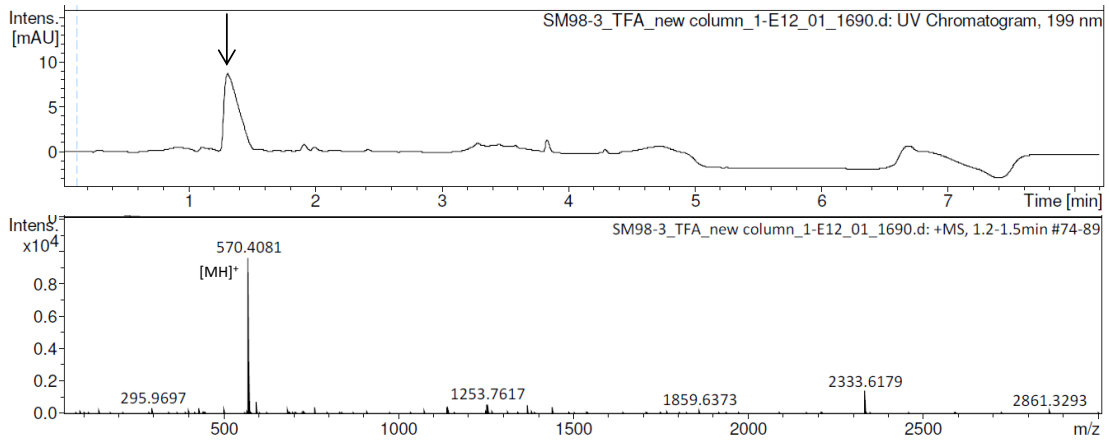

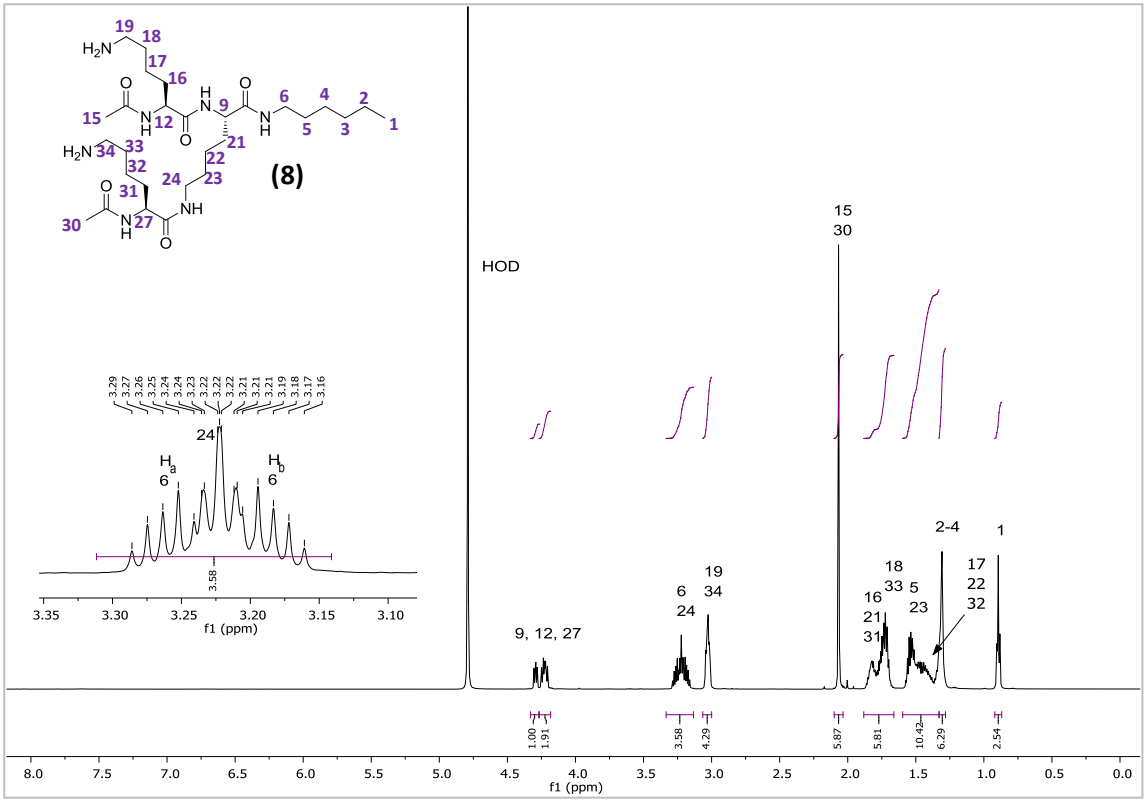

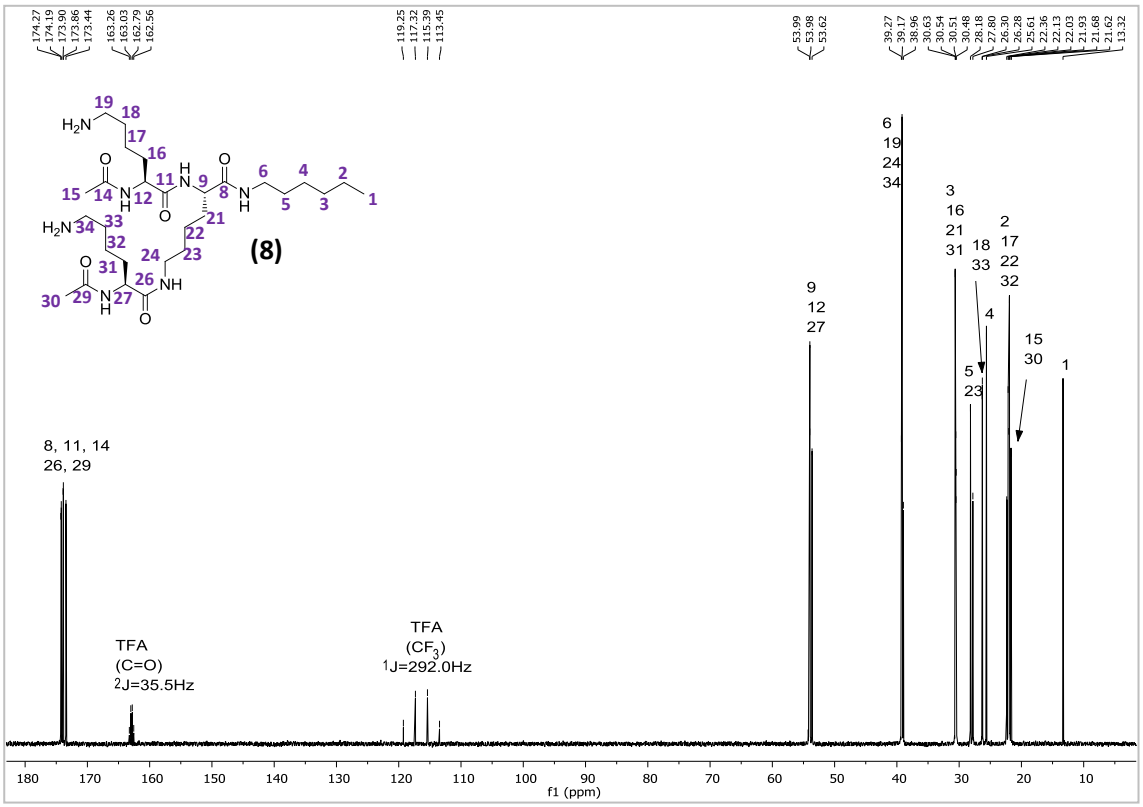
(8)
8, 11, 14
26, 29
TFA
(C=O)
2J=35.5Hz
TFA
(CF3)
1J=292.0Hz
f1 (ppm)

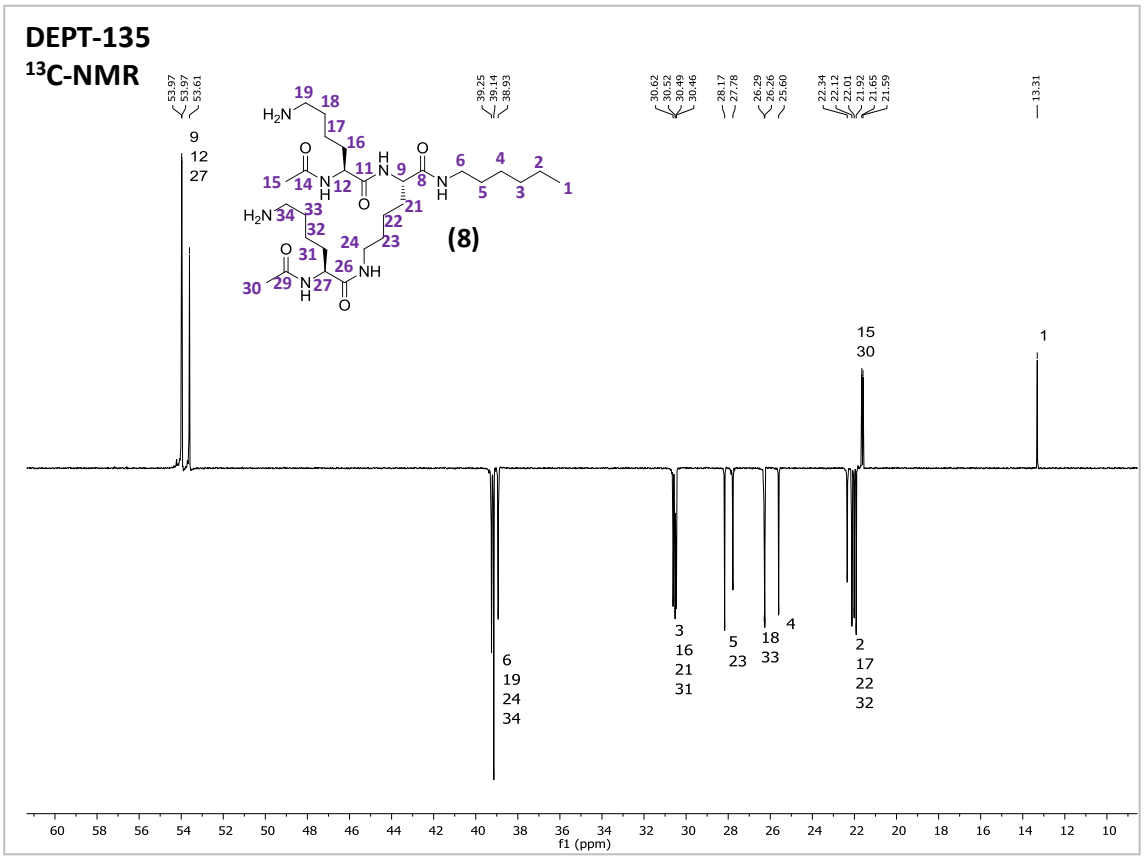
DEPT-135
13C-NMR
(8)
f1 (ppm)

HSQC (8)

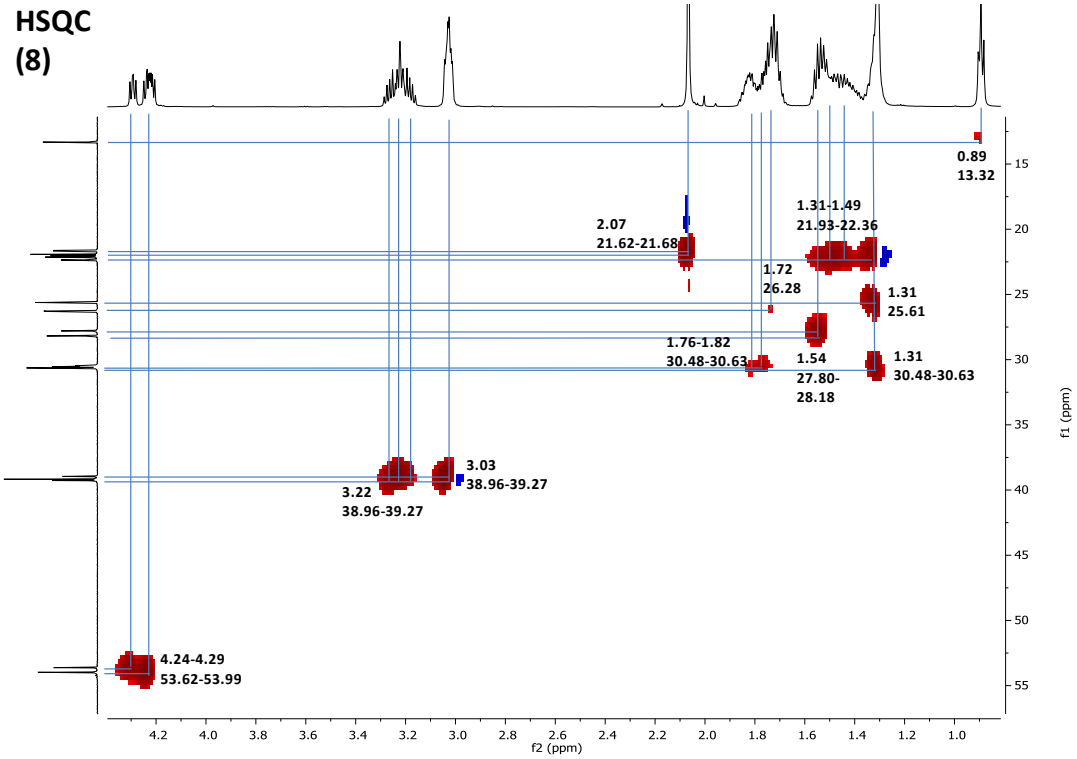
0.89
13.32
2.07
21.62-21.68
1.31-1.49
21.93-22.36
1.72
26.28
1.31
25.61
1.76-1.82
30.48-30.63
1.54
27.80-28.18
1.31
30.48-30.63
3.03
38.96-39.27
3.22
38.96-39.27
4.24-4.29
53.62-53.99
f2 (ppm)
f1 (ppm)

COSY (8)

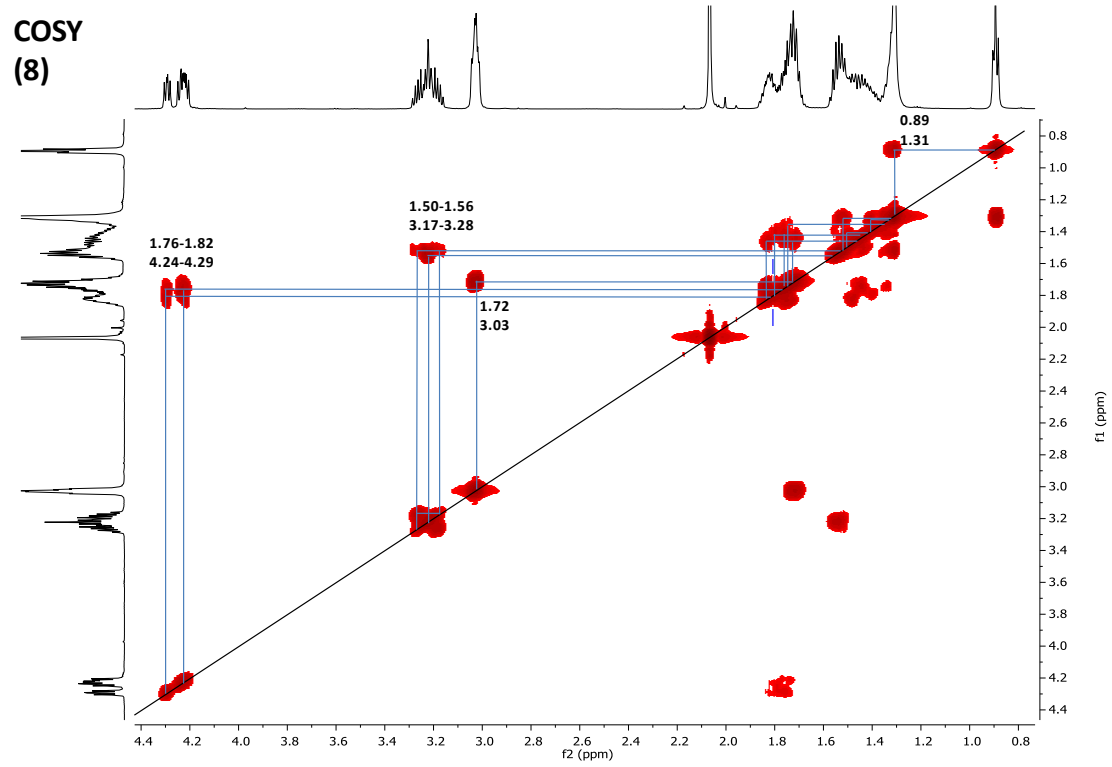
0.89
1.31
1.50-1.56
3.17-3.28
1.76-1.82
4.24-4.29
1.72
3.03
f2 (ppm)
f1 (ppm)

G1(acetyl)-C10 (9)

Yield (TFA salt; loading: 0.32 mmol/g): 139.8 mg (quant.). LC-MS data R_t: 3.2-3.4 min. MS(ESI^+), calcd $C_{32}H_{63}N_7O_5$: 625.49 g/mol, found: m/z 626.47 $[MH]^+$. ^1H NMR (600 MHz, D_2O): δ 4.35 – 4.18 (m, 3H), 3.27 (dt, *J* = 13.64, 6.90 Hz, 1H), 3.21 (t, *J* = 6.98 Hz, 2H), 3.16 (dt, *J* = 13.45, 6.75 Hz, 1H), 3.03 (td, *J* = 7.74, 4.08 Hz, 4H), 2.07 (s, 6H), 1.88 – 1.65 (m, 8H), 1.59 – 1.35 (m, 5H)[2], 1.34 – 1.23 (m, 16H), 0.89 (t, *J* = 6.91 Hz, 3H). ^{13}C NMR (151 MHz, D_2O): δ 174.14, 173.98, 173.83, 173.72, 173.24, 53.91, 53.87, 53.70, 39.32, 39.18, 38.98, 31.41, 30.80, 30.68, 30.52, 28.98, 28.95, 28.76, 28.62, 28.39, 27.92, 26.31, 26.20, 22.47, 22.23, 22.19, 22.11, 21.74, 21.70, 13.58.

UPLC-MS (9)

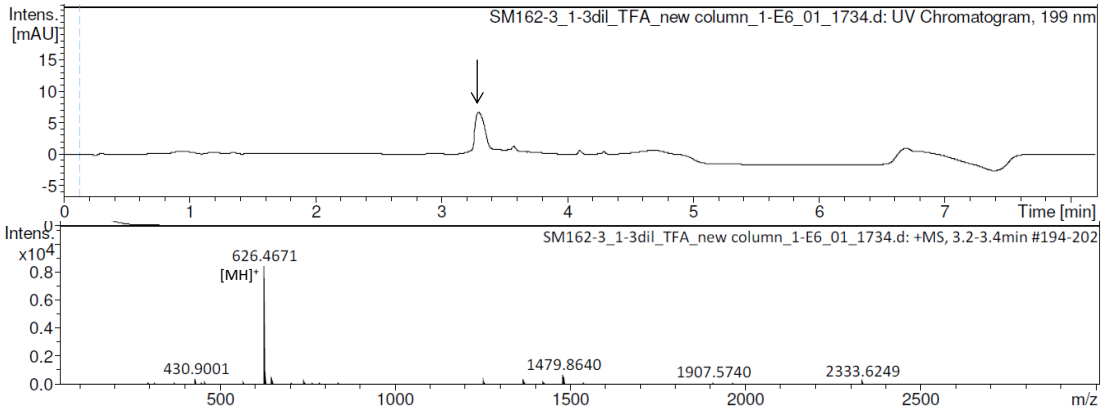

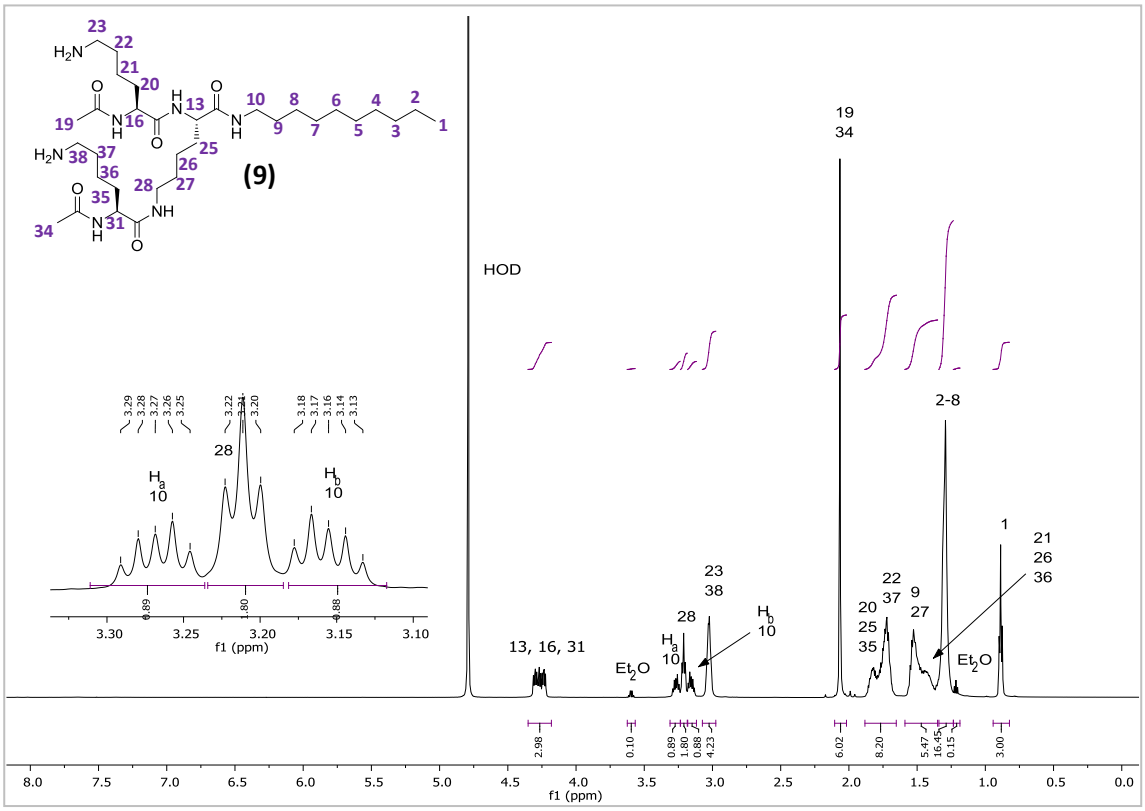

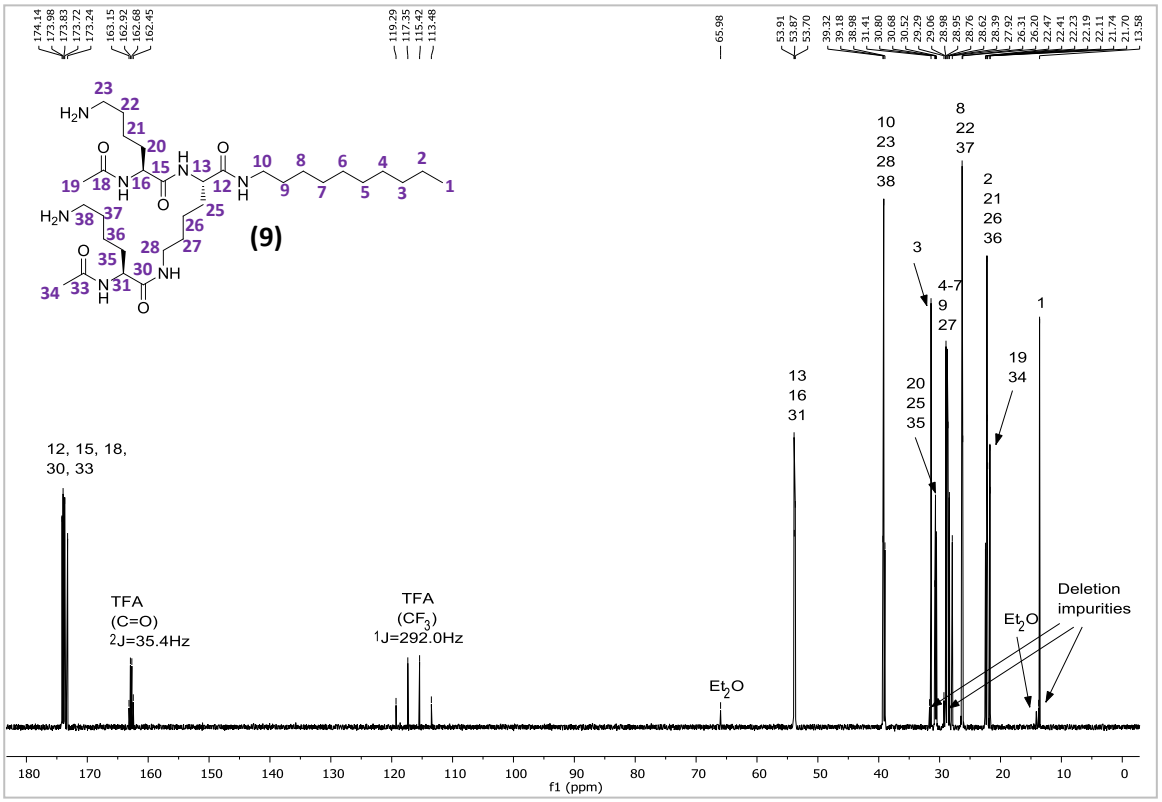
(9)
12, 15, 18, 30, 33
TFA (C=O) 2J=35.4Hz
TFA (CF3) 1J=292.0Hz
Et2O
13 16 31
10 23 28 38
8 22 37
2 21 26 36
3
4-7 9 27
1
19 34
20 25 35
Et2O
Deletion impurities
f1 (ppm)

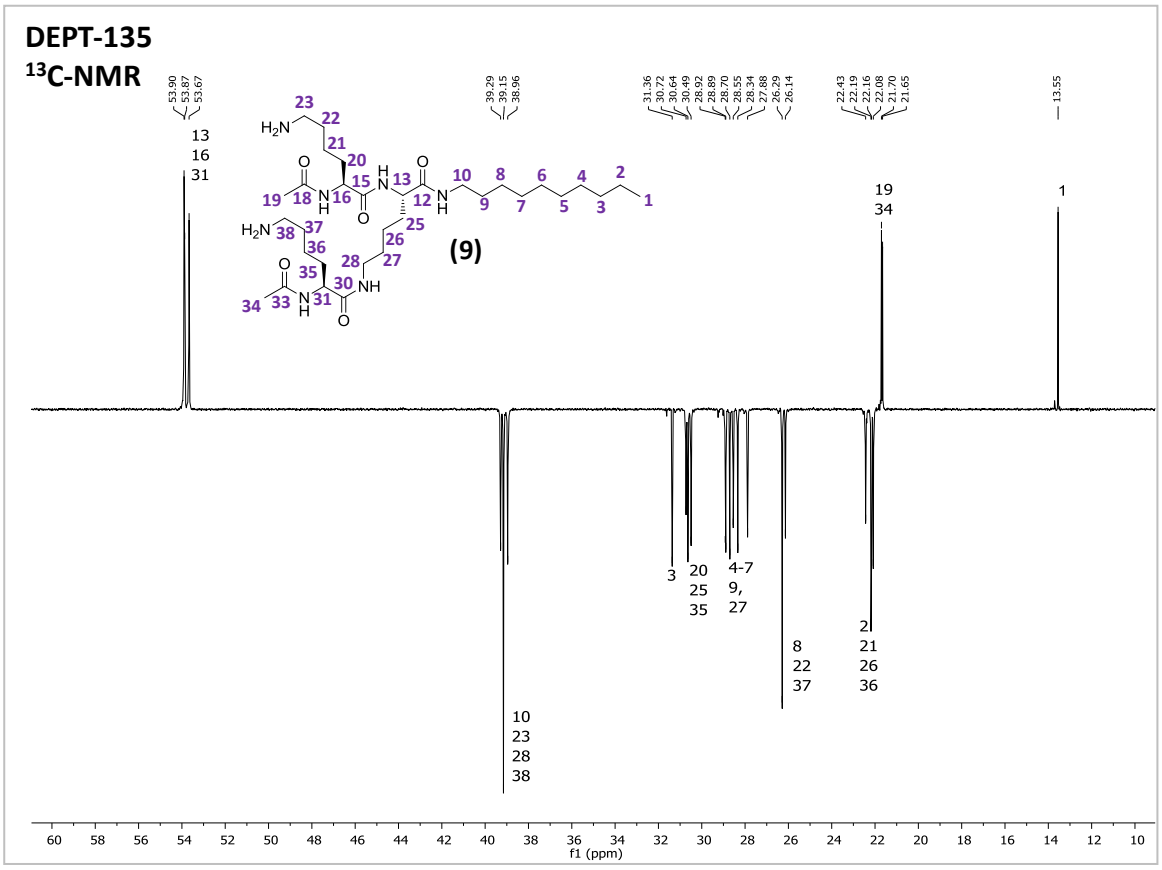
DEPT-135
13C-NMR
(9)
13 16 31
10 23 28 38
3
20 25 35
4-7 9, 27
8 22 37
2 21 26 36
19 34
1
f1 (ppm)

HSQC (9)

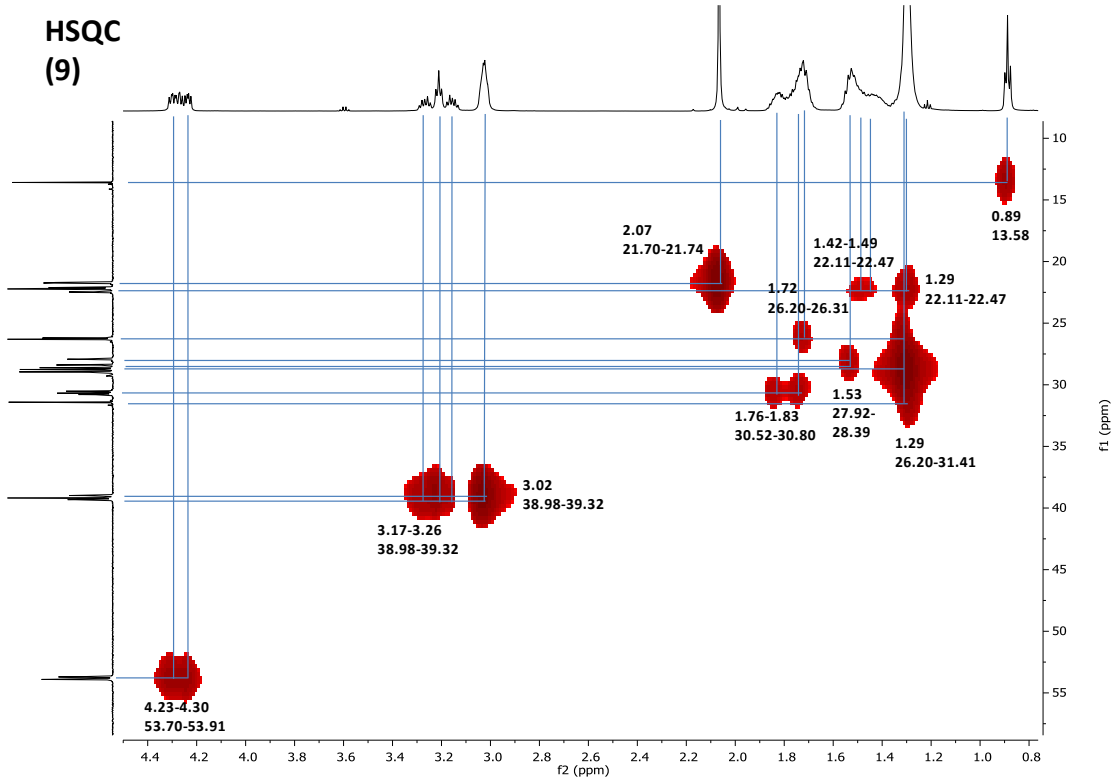
2.07
21.70-21.74
1.42-1.49
22.11-22.47
1.29
22.11-22.47
1.72
26.20-26.31
0.89
13.58
1.53
27.92-28.39
1.76-1.83
30.52-30.80
1.29
26.20-31.41
3.02
38.98-39.32
3.17-3.26
38.98-39.32
4.23-4.30
53.70-53.91
f2 (ppm)
f1 (ppm)

COSY (9)

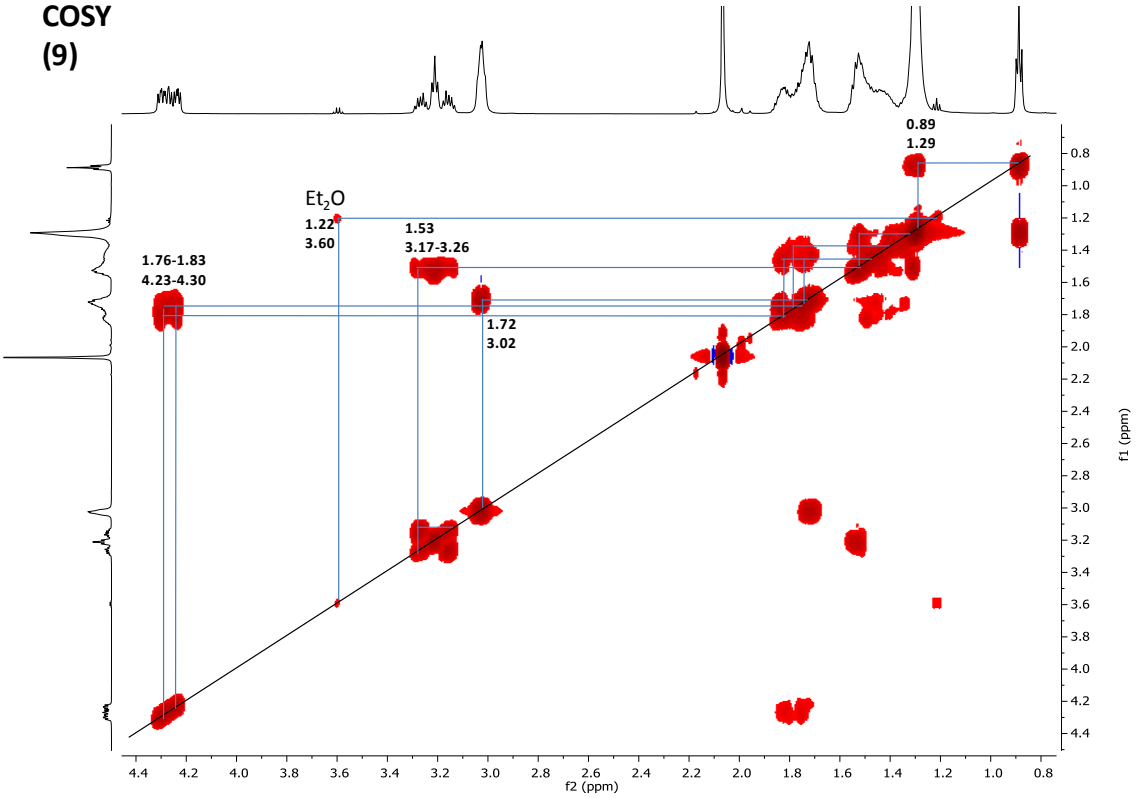
0.89
1.29
Et2O
1.22
3.60
1.53
3.17-3.26
1.76-1.83
4.23-4.30
1.72
3.02
f2 (ppm)
f1 (ppm)

G1(acetyl)-C16 (10)

Yield (TFA salt; loading: 0.25 mmol/g): 84.9 mg (72 %). LC-MS data R_t: 3.8 min. MS(ESI$^+$), calcd $C_{38}H_{75}N_7O_5$: 709.58 g/mol, found: m/z 710.55 $[MH]^+$. ^{1}H NMR (600 MHz, D_2O): δ 4.33 – 4.26 (m, 2H), 4.24 (dd, *J* = 9.12, 5.26 Hz, 1H), 3.25 – 3.08 (m, 2H) [1], 3.00 (td, *J* = 7.67, 2.68 Hz, 4H), 2.04 (m, 6H), 1.87 – 1.63 (m, 6H), 1.55 – 1.34 (m, 6H), 1.27 (s, 26H), 0.88 (t, *J* = 6.74 Hz, 3H). ^{13}C NMR (151 MHz, D_2O): δ 173.77, 173.74, 173.56, 173.55, 172.90, 53.92, 53.82, 53.62, 39.43, 39.16, 38.97, 31.90, 31.16, 30.85, 30.61, 29.81, 29.79, 29.78, 29.74, 29.70, 29.65, 29.39, 29.33, 28.84, 28.03, 26.82, 26.31, 22.68, 22.59, 22.30, 22.26, 21.83, 13.85.

UPLC-MS (10)

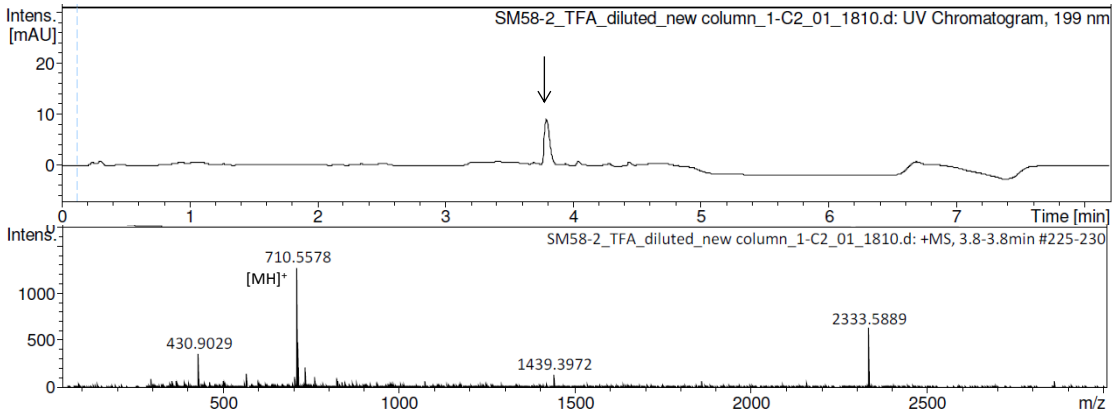

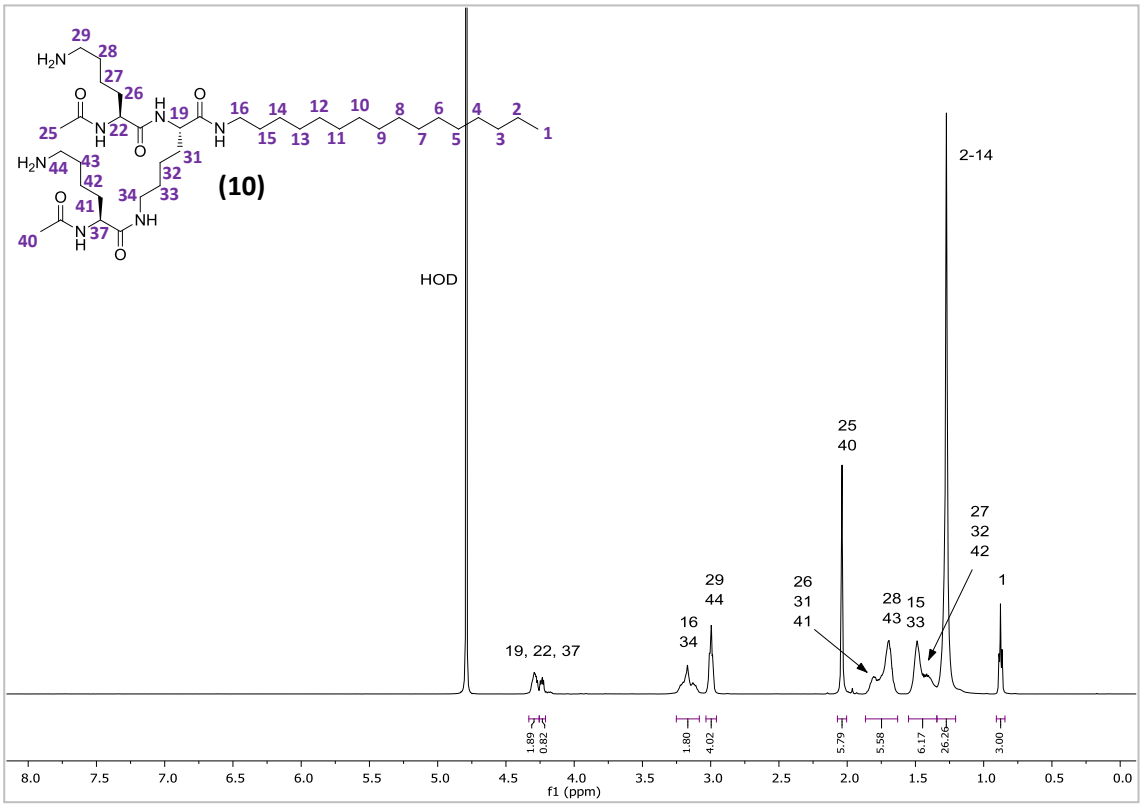

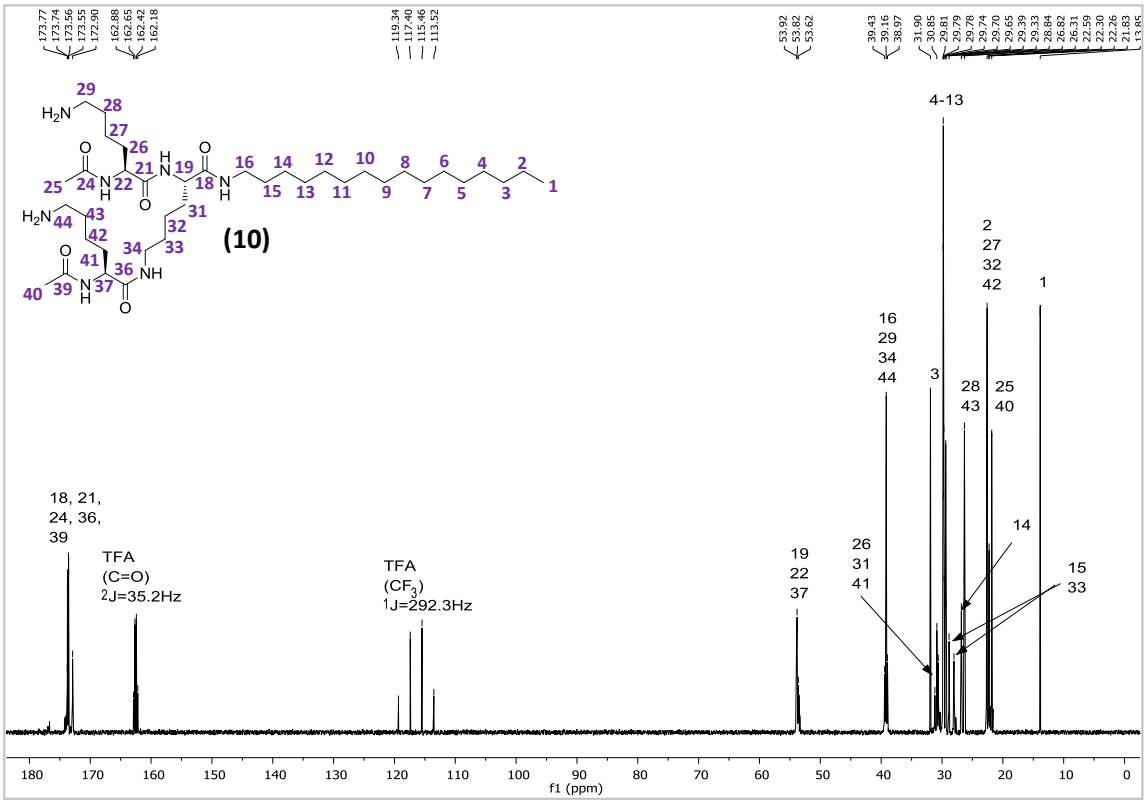
(10)
18, 21,
24, 36,
39
TFA
(C=O)
2J=35.2Hz
TFA
(CF3)
1J=292.3Hz
19
22
37
26
31
41
16
29
34
44
4-13
3
28
43
2
27
32
42
25
40
1
14
15
33
f1 (ppm)

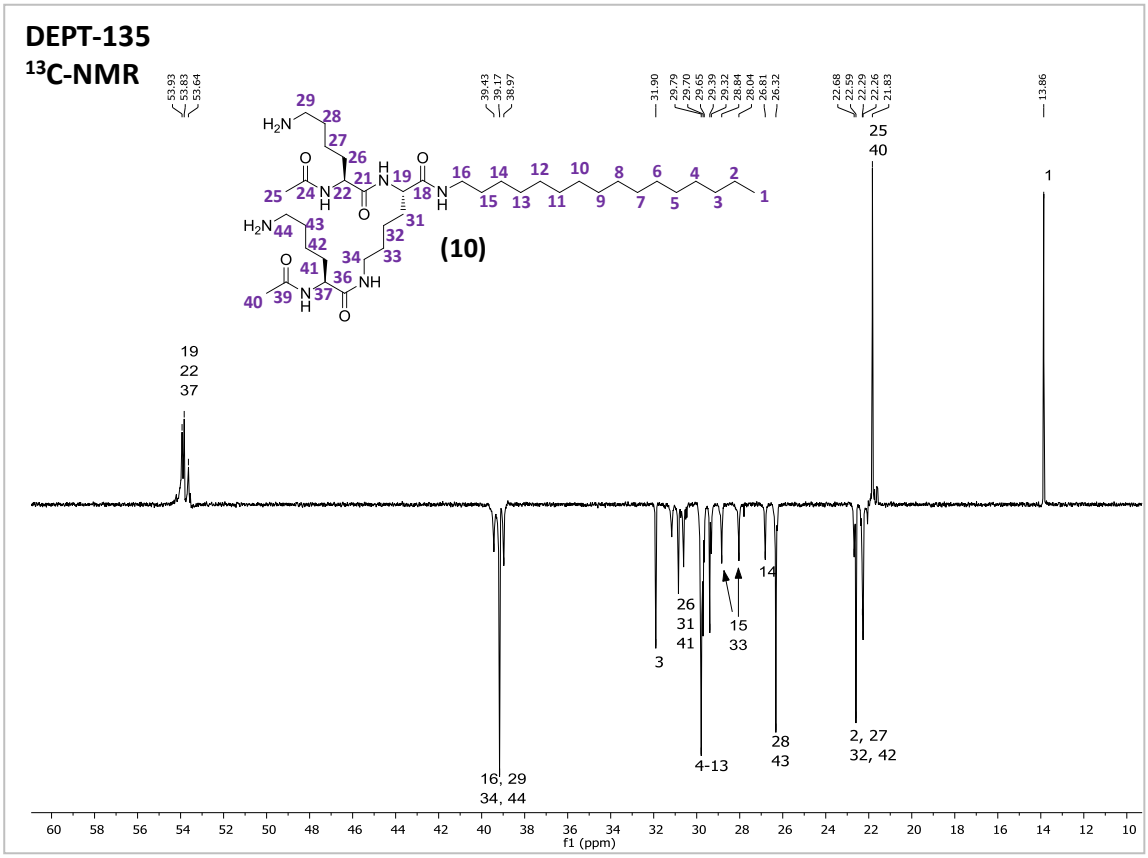
DEPT-135
13C-NMR
(10)
19
22
37
16, 29
34, 44
3
26
31
41
4-13
15
33
14
28
43
2, 27
32, 42
25
40
1
f1 (ppm)

HSQC (10)

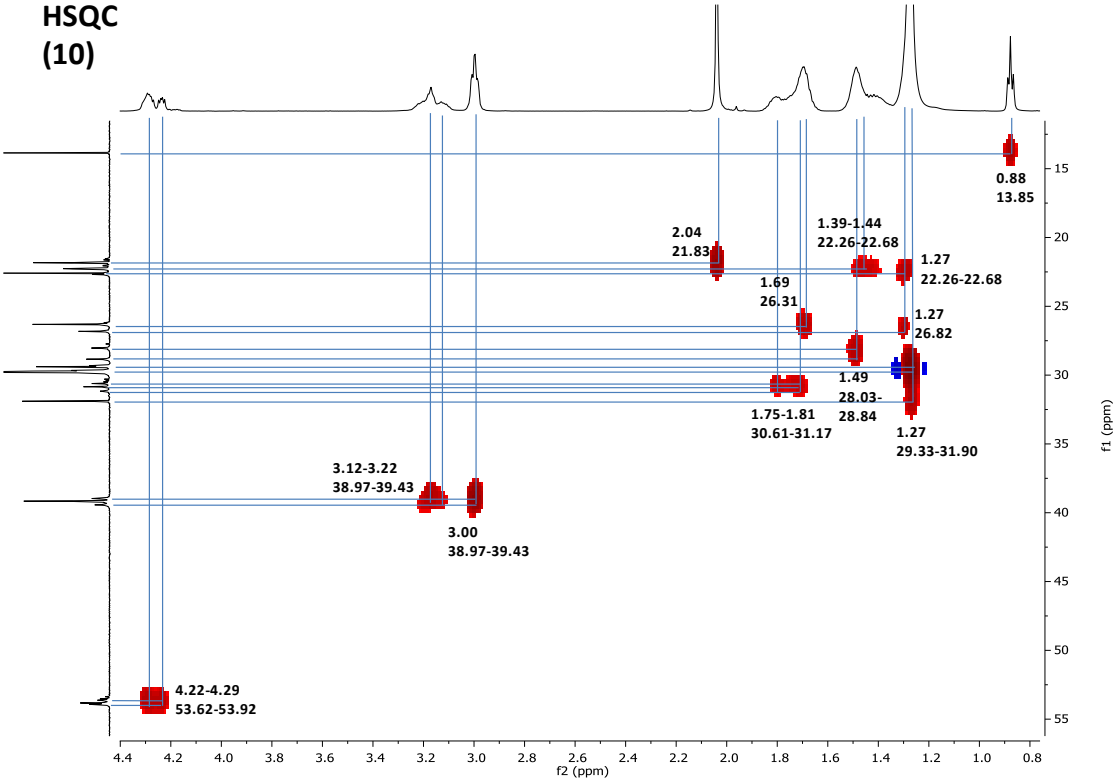

COSY (10)

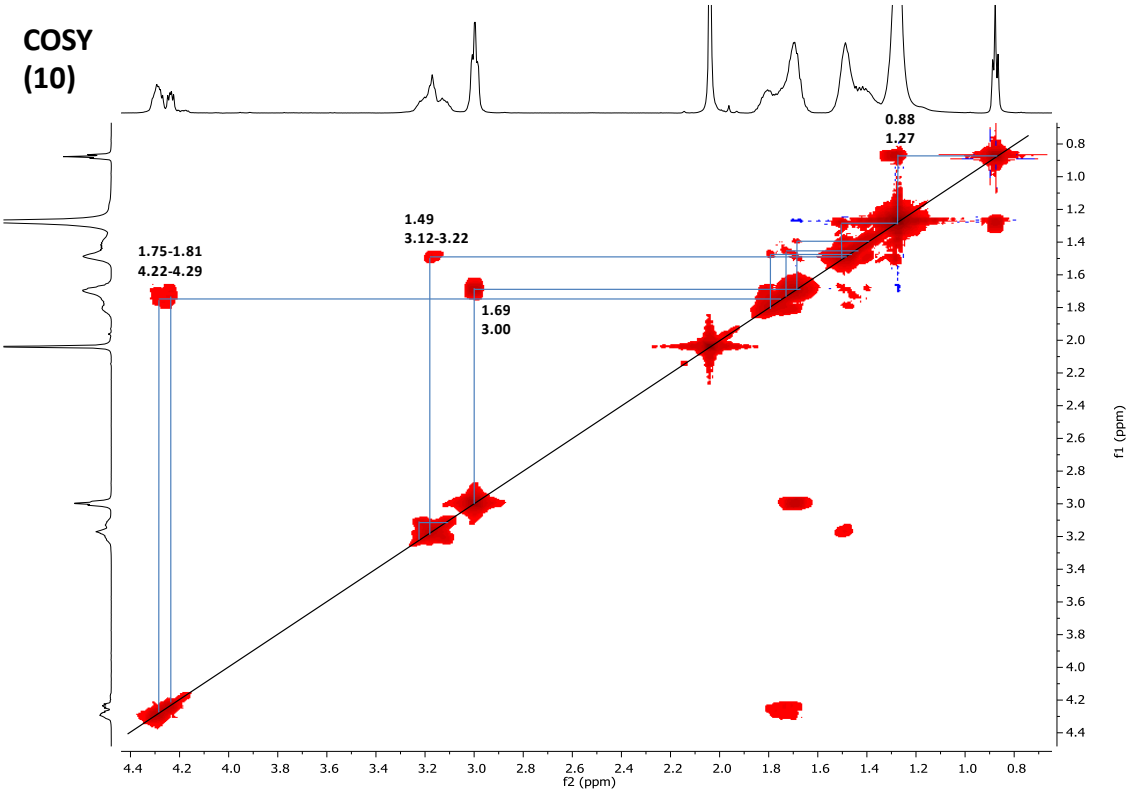

G2-C1 (11)

Yield (TFA salt; loading: 0.24 mmol/g): 77.3 mg (35 %). LC-MS data R_t: 0.2-0.3 min. MS(ESI^+), calcd $C_{43}H_{89}N_{15}O_7$: 927.71 g/mol, found: m/z 464.89 $[MH_2/2]^+$. ^1H NMR (600 MHz, D_2O): δ 4.39 – 4.33 (m, 1H), 4.26 (t, *J* = 7.34 Hz, 1H), 4.20 (t, *J* = 7.32 Hz, 1H), 4.07 (s, 2H), 3.97 (s, 2H), 3.33 – 3.13 (m, 5H)[2], 3.04 (q, *J* = 7.93 Hz, 6H), 2.81 – 2.73 (m, 3H), 1.99 – 1.87 (m, 7H), 1.86 – 1.66 (m, 13H), 1.64 – 1.29 (m, 18H). ^{13}C NMR (151 MHz, D_2O): δ 174.10, 173.35, 173.17, 169.56, 169.50, 169.45, 169.29, 54.28, 54.24, 54.08, 53.80, 53.14, 53.12, 52.72, 39.34, 39.30, 39.12, 39.06, 38.99, 38.97, 30.62, 30.55, 30.53, 30.45, 30.41, 30.37, 30.35, 28.00, 27.95, 27.90, 26.36, 26.33, 25.77, 22.52, 22.49, 22.41, 21.85, 21.71, 21.47, 21.33, 21.32, 21.16, 21.14.

UPLC-MS (11)

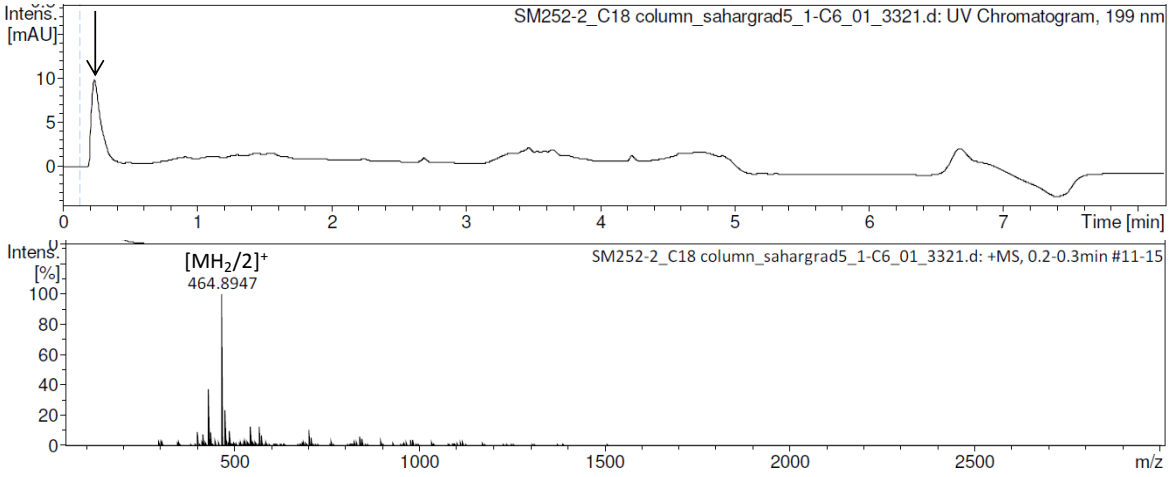

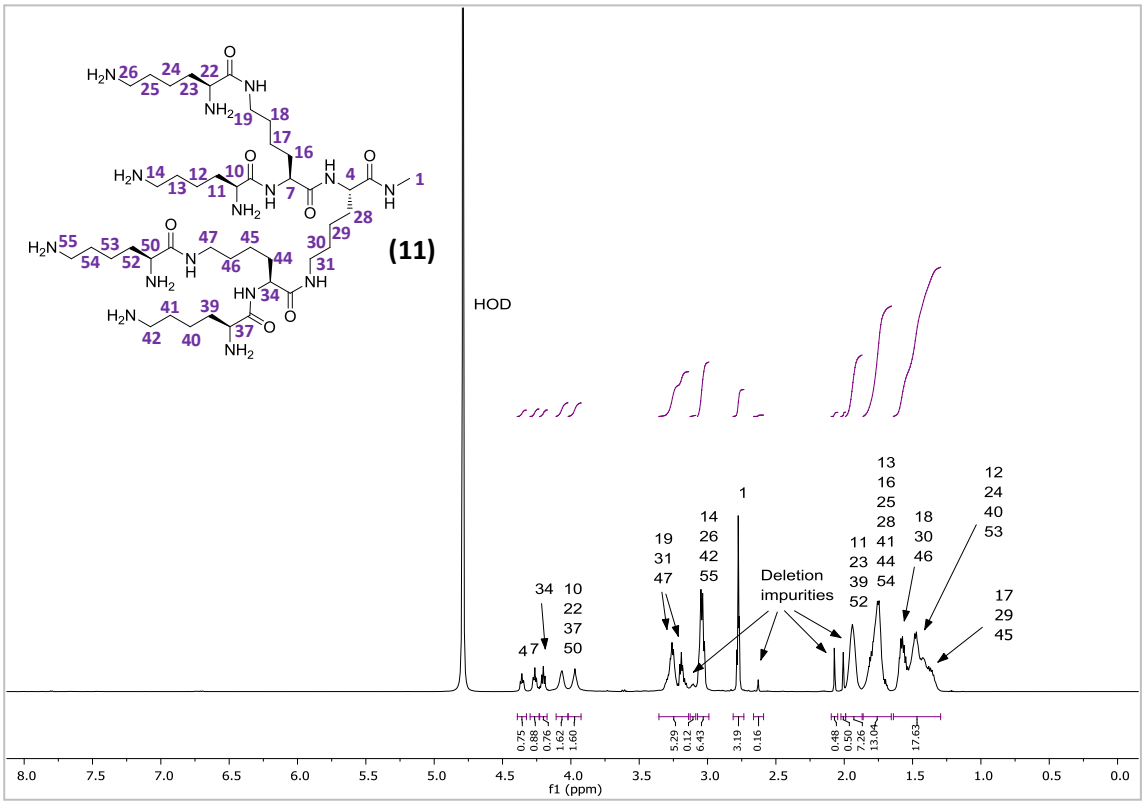
(11)
HOD
Deletion impurities
f1 (ppm)

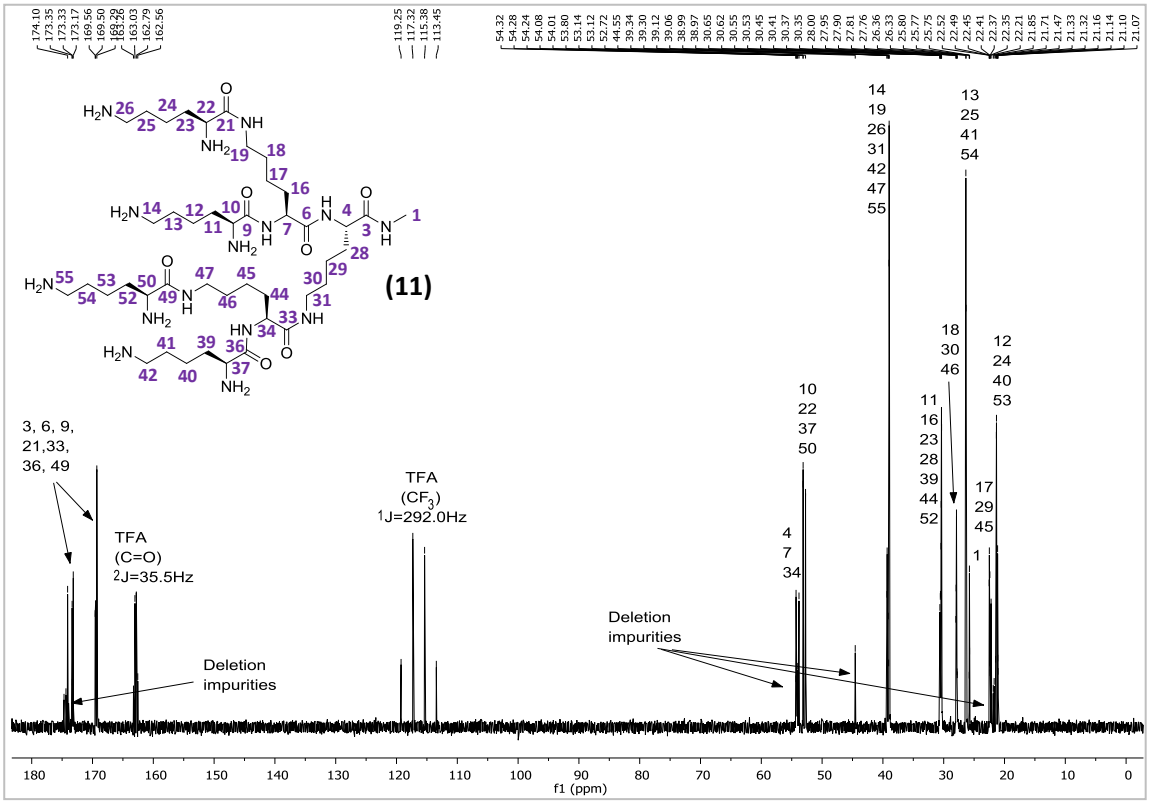
(11)
3, 6, 9, 21,33, 36, 49
TFA (C=O) 2J=35.5Hz
TFA (CF3) 1J=292.0Hz
Deletion impurities
Deletion impurities
f1 (ppm)

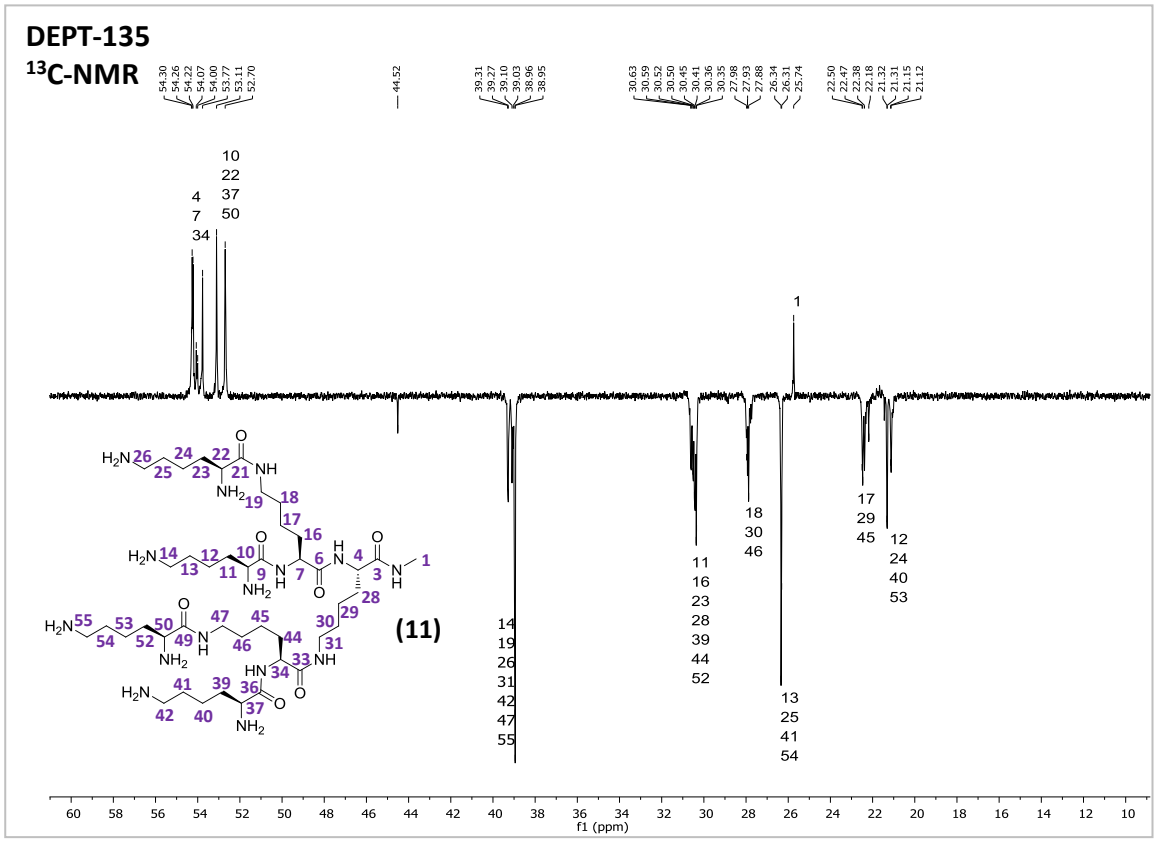
DEPT-135
13C-NMR
(11)
f1 (ppm)

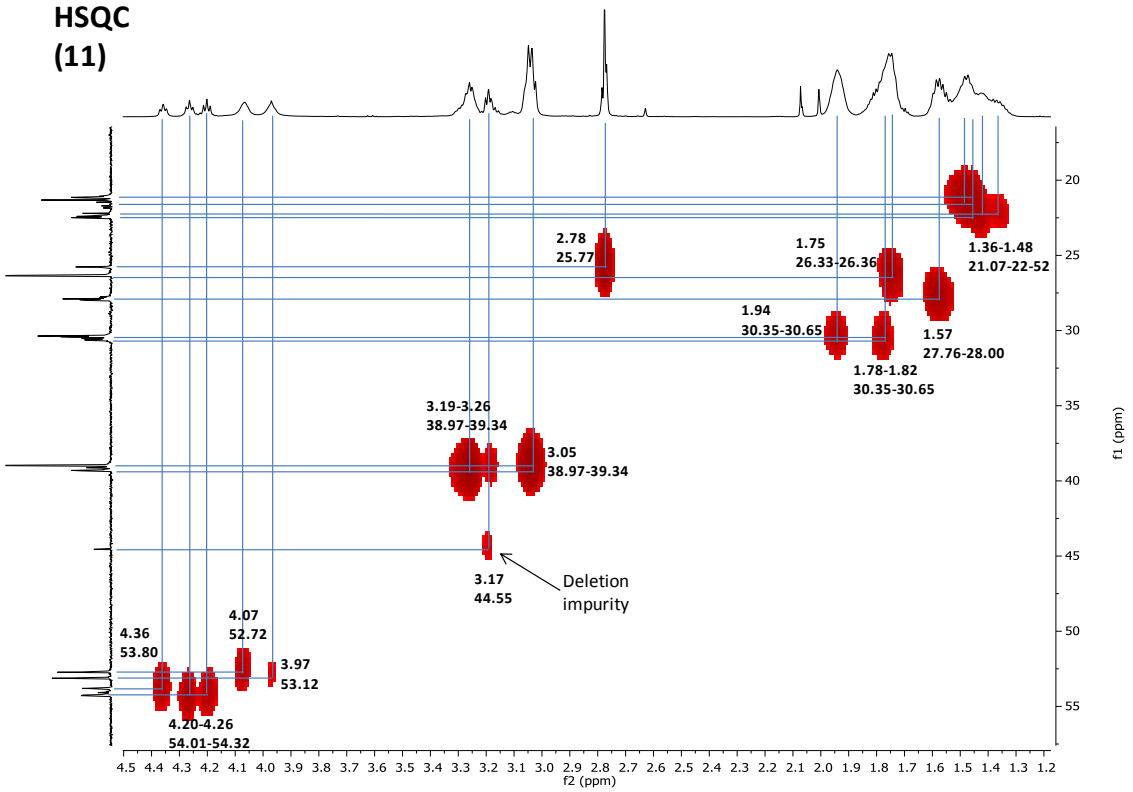
HSQC
(11)
2.78
25.77
1.75
26.33-26.36
1.36-1.48
21.07-22-52
1.94
30.35-30.65
1.57
27.76-28.00
1.78-1.82
30.35-30.65
3.19-3.26
38.97-39.34
3.05
38.97-39.34
3.17
44.55
Deletion
impurity
4.36
53.80
4.07
52.72
3.97
53.12
4.20-4.26
54.01-54.32
f2 (ppm)
f1 (ppm)

COSY (11)

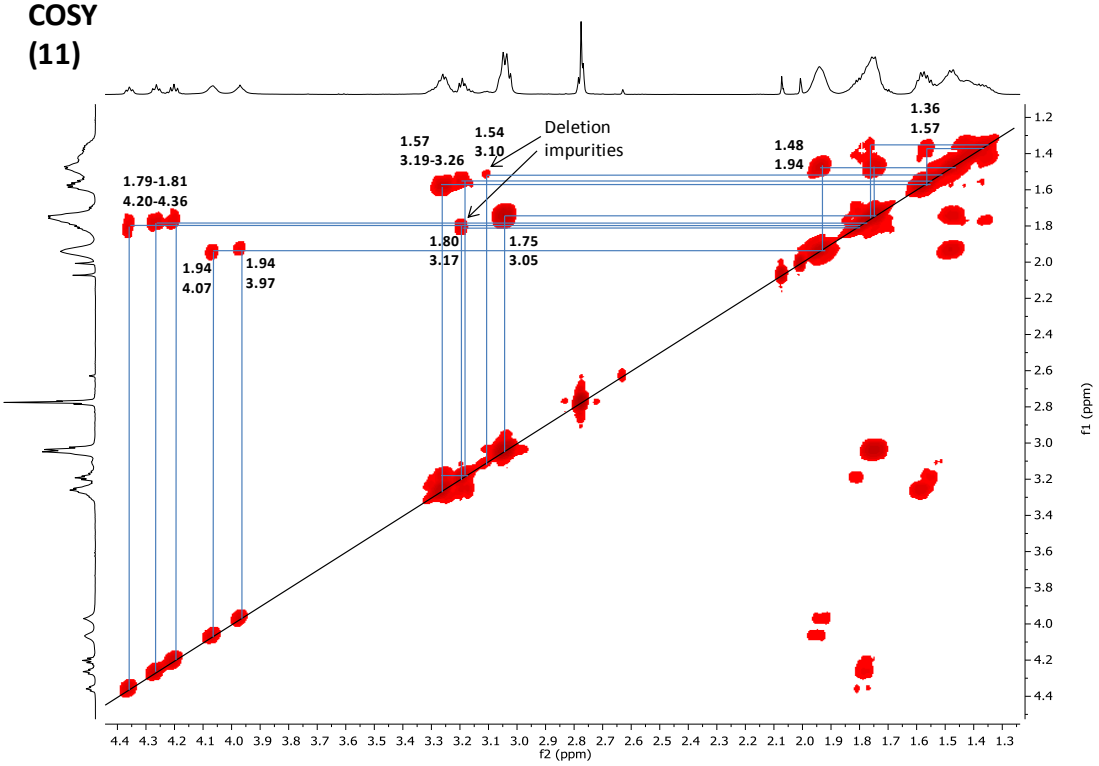
1.79-1.81
4.20-4.36
1.94
4.07
1.94
3.97
1.57
3.19-3.26
1.54
3.10
Deletion impurities
1.80
3.17
1.75
3.05
1.48
1.94
1.36
1.57
f2 (ppm)
f1 (ppm)

G2-C12 (12)

Yield (TFA salt; loading: 0.35 mmol/g): 151.4 mg (43 %). LC-MS data R_t: 2.0-2.2 min. MS(ESI^+), calcd $C_{54}H_{111}N_{15}O_7$: 1081.88 g/mol, found: m/z 1082.82 $[MH]^+$; 541.93 $[MH_2/2]^+$. ^1H NMR (600 MHz, D_2O): δ 4.32 (t, *J* = 7.15 Hz, 1H), 4.25 (td, *J* = 7.16 Hz, 4.53 Hz, 1H), 4.19 (t, *J* = 7.40 Hz, 1H), 4.03 (t, *J* = 6.67 Hz, 2H), 3.93 (td, *J* = 6.77 Hz, 2.0 Hz, 2H), 3.32 – 3.09 (m, 6H)[2], 3.06 – 2.97 (m, 6H), 1.96 – 1.84 (m, 6H), 1.83 – 1.67 (m, 11H), 1.62 – 1.33 (m, 9H), 1.32 – 1.21 (m, 18H), 0.87 (t, *J* = 6.81 Hz, 3H). ^{13}C NMR (151 MHz, D_2O): δ 173.21, 173.10, 173.03, 169.64, 169.56, 169.33, 169.30, 54.27, 54.21, 53.78, 53.10, 52.71, 52.67, 39.32, 39.29, 39.22, 39.17, 39.14, 39.10, 38.96, 38.94, 31.21, 31.18, 30.70, 30.63, 30.48, 30.46, 30.43, 30.40, 28.78, 28.75, 28.73, 28.67, 28.65, 28.61, 28.52, 28.49, 28.30, 28.28, 28.18, 28.02, 27.97, 27.90, 26.34, 26.31, 25.90, 22.52, 22.41, 22.03, 21.33, 21.14, 13.42.

UPLC-MS (12)

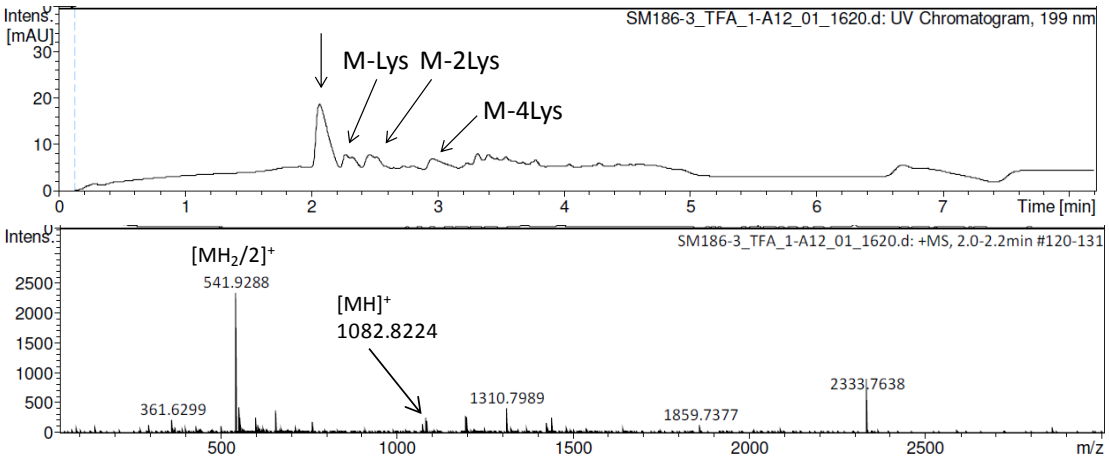

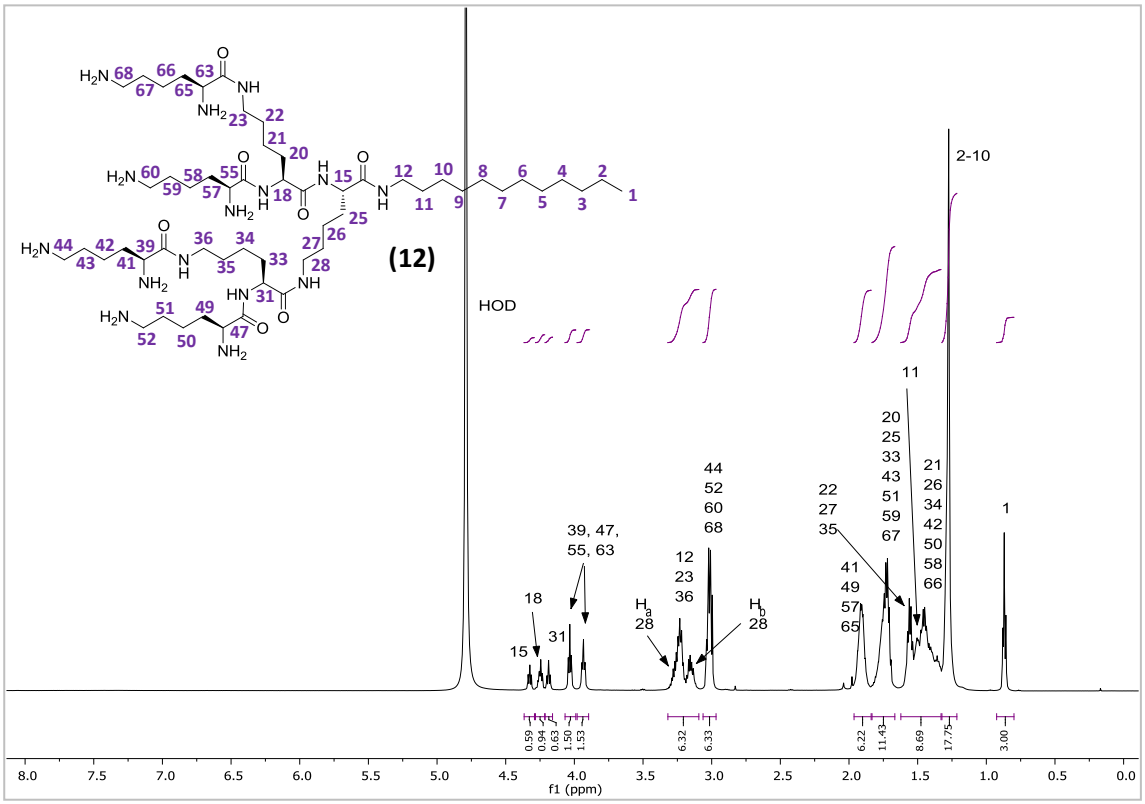
(12)
HOD
2-10
11
20 25 33 43 51 59 67
21 26 34 42 50 58 66
44 52 60 68
22 27 35
39, 47, 55, 63
12 23 36
41 49 57 65
18
31
15
1
f1 (ppm)

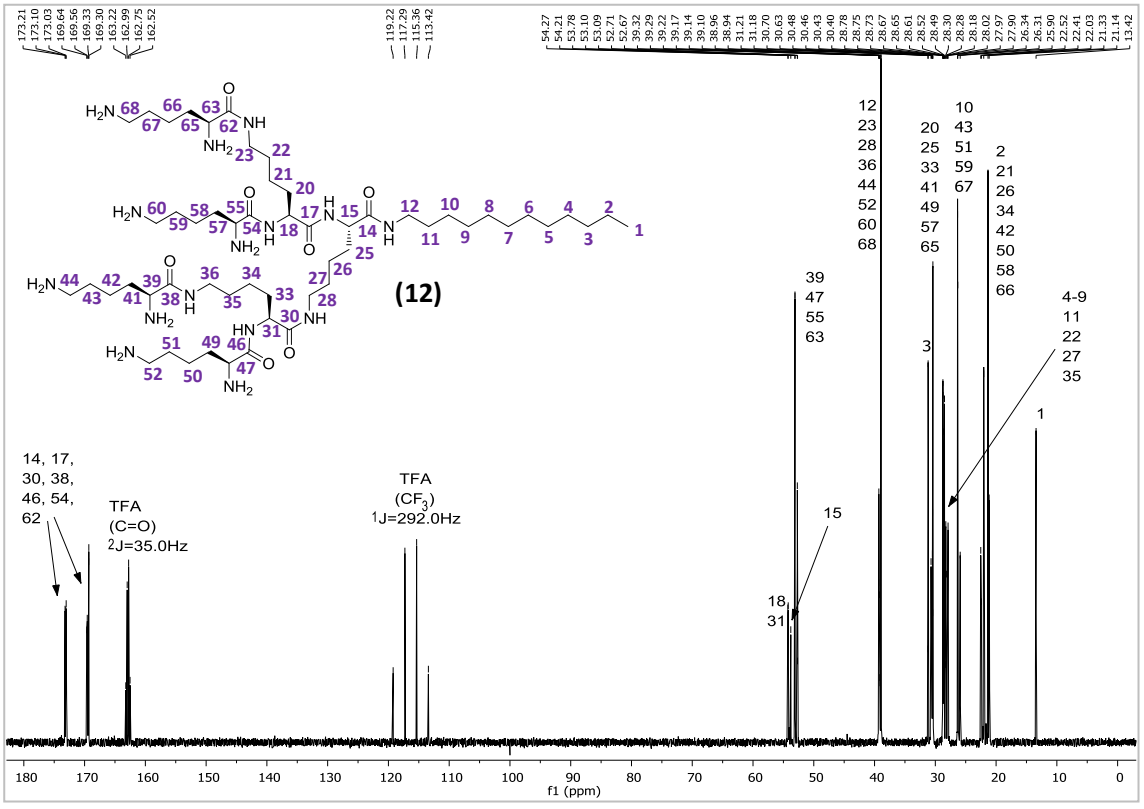
(12)
14, 17, 30, 38, 46, 54, 62
TFA (C=O) 2J=35.0Hz
TFA (CF3) 1J=292.0Hz
12 23 28 36 44 52 60 68
20 25 33 41 49 57 65
10 43 51 59 67
2 21 26 34 42 50 58 66
39 47 55 63
4-9 11 22 27 35
3
1
15
18 31
f1 (ppm)

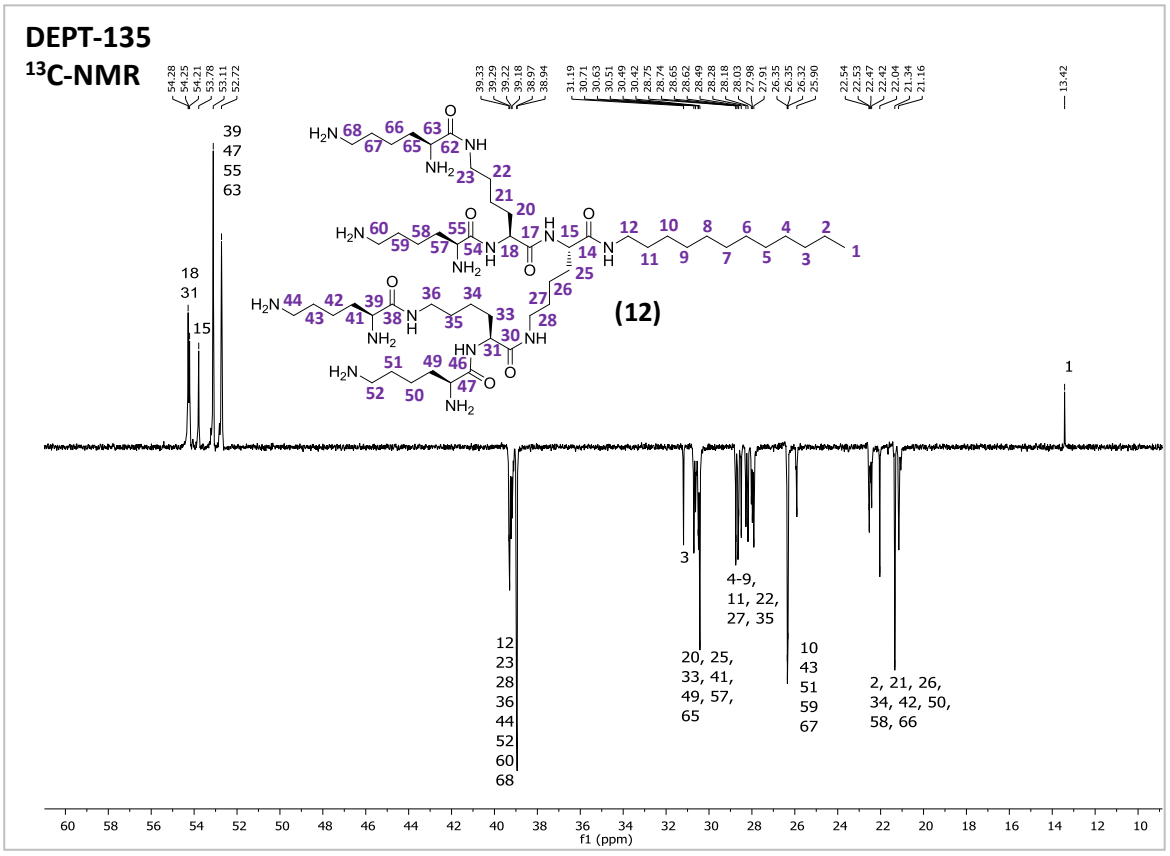
DEPT-135
13C-NMR
(12)
f1 (ppm)

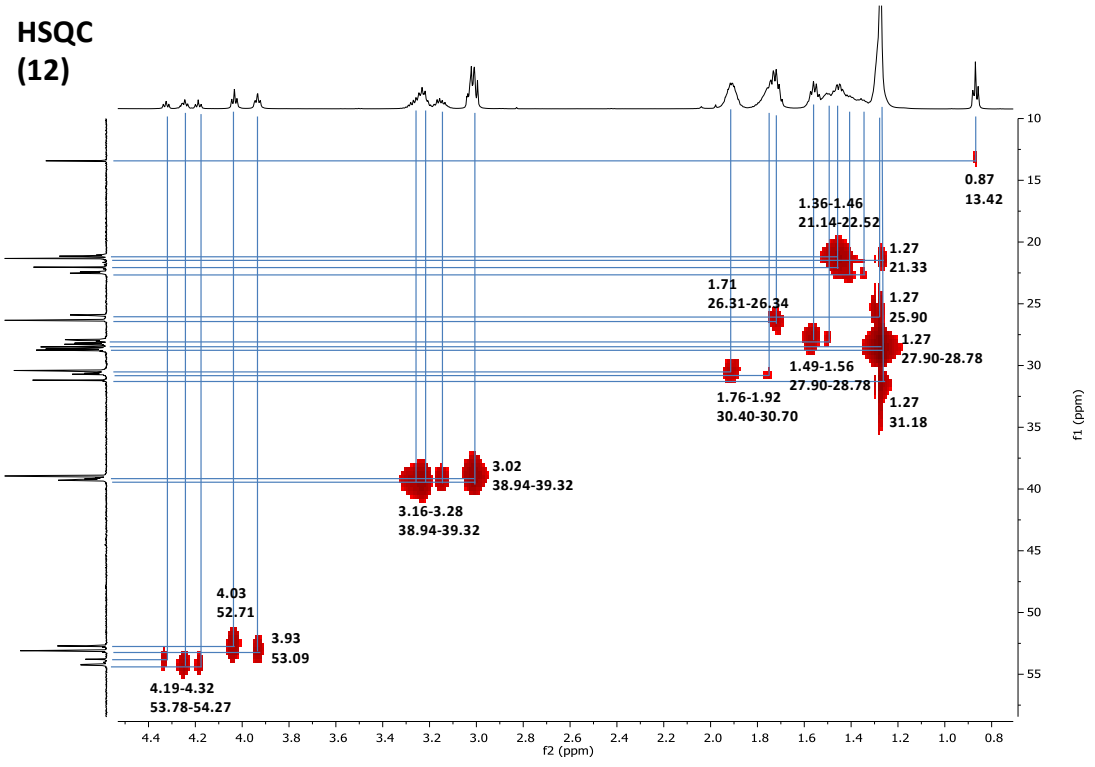
HSQC
(12)
f2 (ppm)
f1 (ppm)

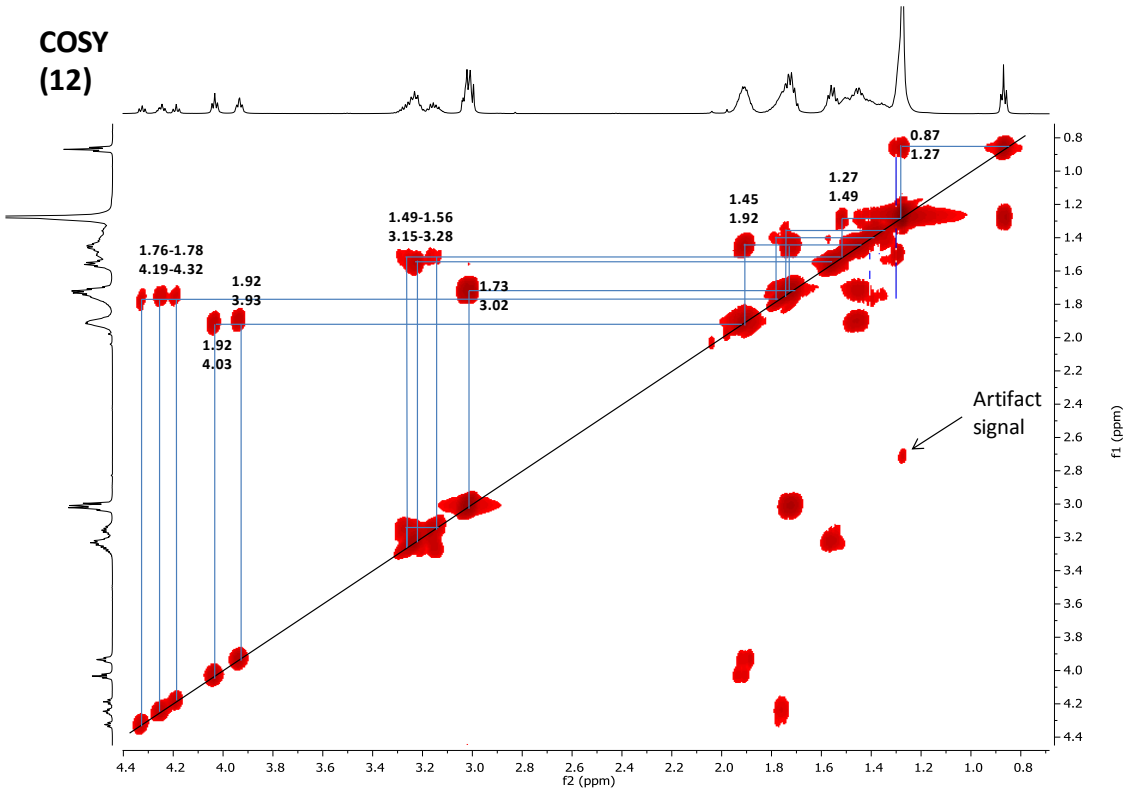
COSY
(12)
0.87
1.27
1.27
1.49
1.45
1.92
1.49-1.56
3.15-3.28
1.76-1.78
4.19-4.32
1.92
3.93
1.73
3.02
1.92
4.03
Artifact
signal
f2 (ppm)
f1 (ppm)

G2-C16 (13)

Yield (TFA salt; loading: 0.23 mmol/g): 152.6 mg (65 %). LC-MS data R_t: 3.2-3.3 min. MS(ESI^+), calcd $C_{58}H_{119}N_{15}O_7$: 1137.84 g/mol, found: m/z 1138.88 $[MH]^+$; 569.96 $[MH_2/2]^+$. ^{1}H NMR (600 MHz, D_2O): δ 4.44 – 4.18 (m, 3H)[1], 4.15 – 4.04 (m, 2H), 4.02 – 3.94 (m, 2H), 3.36 – 3.09 (m, 4H), 3.09 – 3.00 (m, 9H), 2.02 – 1.86 (m, 10H), 1.85 – 1.67 (m, 16H), 1.65 – 1.35 (m, 21H), 1.34 – 1.18 (m, 50H), 0.90 (t, *J* = 5.94 Hz, 5H). ^{13}C NMR (151 MHz, D_2O): δ 173.19, 173.08, 173.01, 169.53, 169.46, 169.25, 169.23, 54.28, 54.23, 53.82, 53.12, 53.10, 52.74, 39.37, 39.34, 39.26, 39.23, 38.99, 38.97, 31.90, 31.24, 30.74, 30.45, 30.43, 30.40, 29.74, 29.38, 28.81, 28.78, 28.76, 28.72, 28.67, 28.61, 28.55, 28.32, 28.23, 28.08, 28.01, 27.95, 27.90, 26.37, 26.34, 26.27, 25.96, 22.60, 22.57, 22.46, 22.21, 22.09, 21.47, 21.40, 21.36, 21.18, 13.85.

UPLC-MS (13)

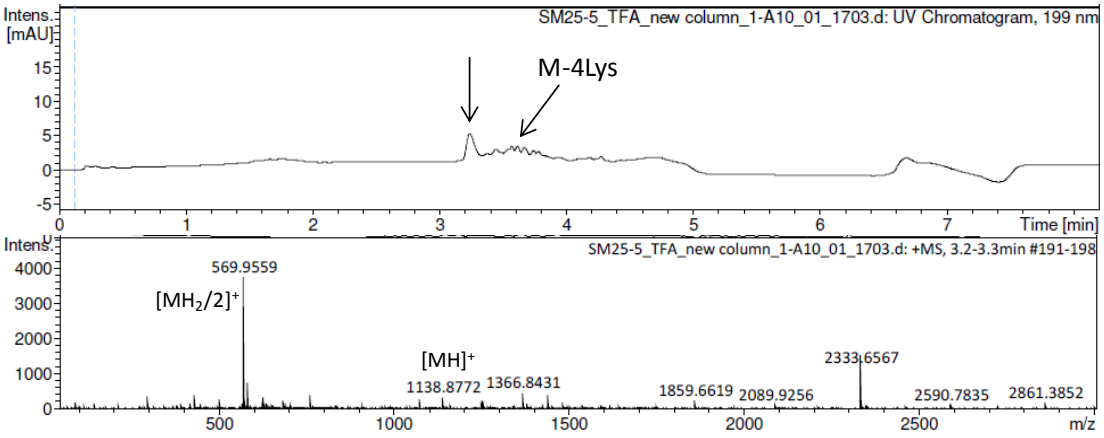

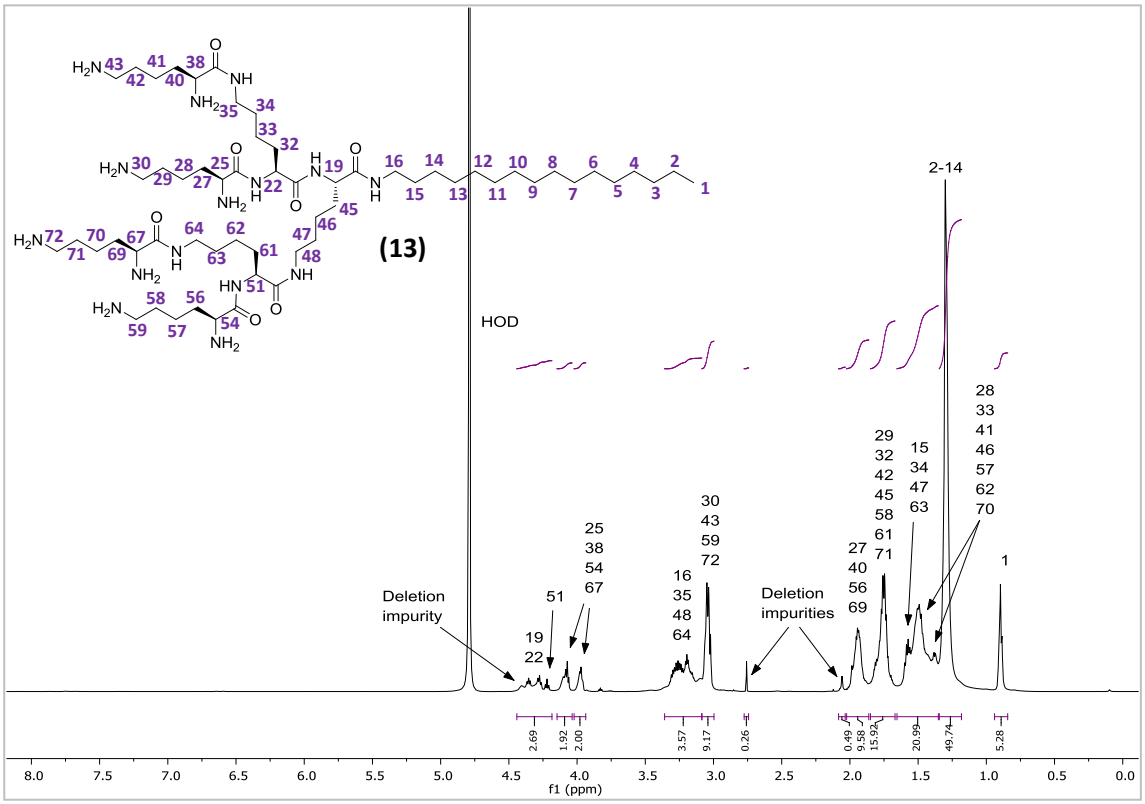
(13)
HOD
2-14
Deletion impurity
Deletion impurities
f1 (ppm)

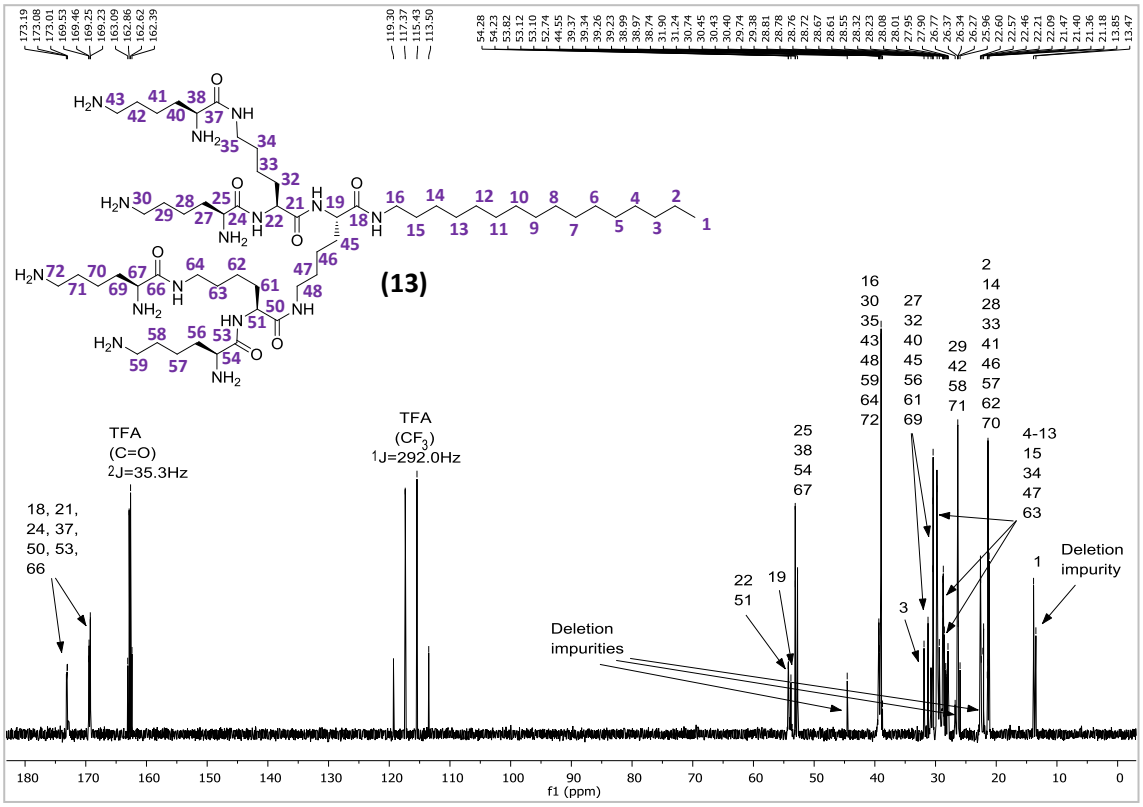
(13)
TFA (C=O) 2J=35.3Hz
TFA (CF3) 1J=292.0Hz
18, 21, 24, 37, 50, 53, 66
Deletion impurities
Deletion impurity
4-13
f1 (ppm)

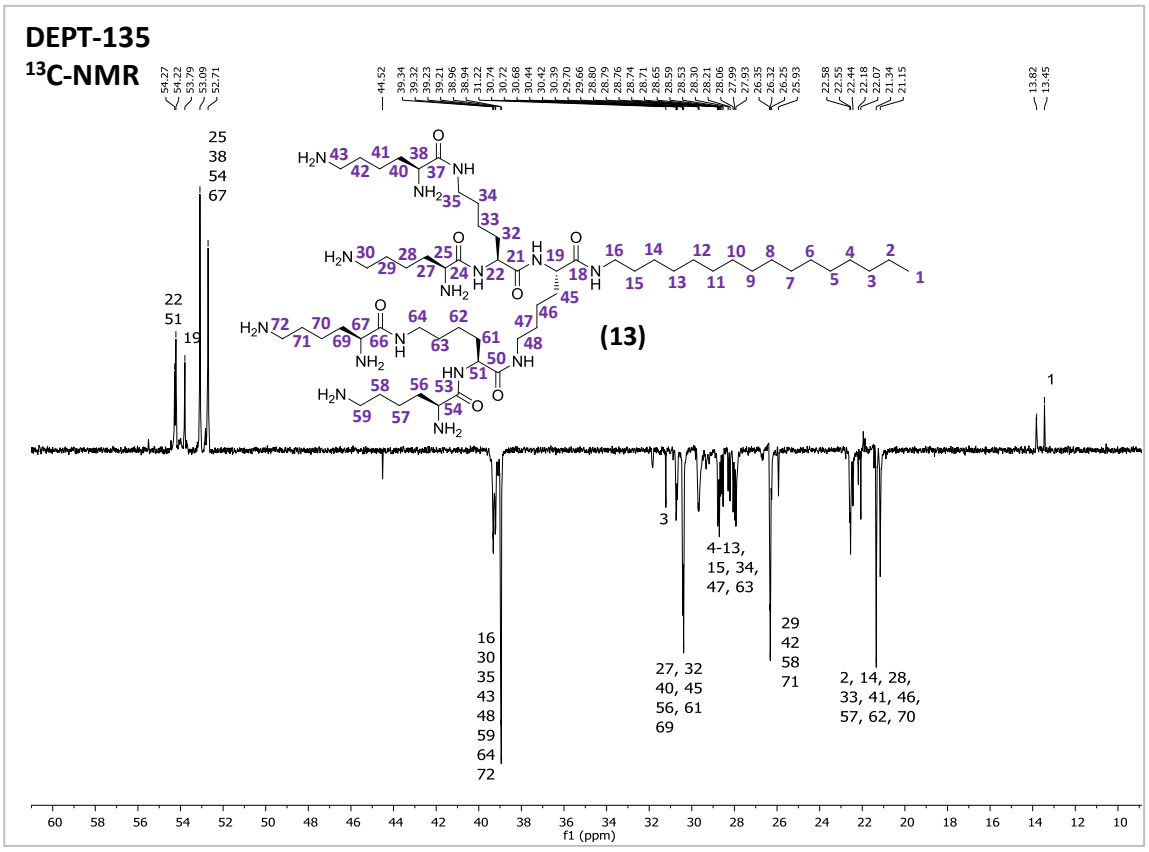
DEPT-135
13C-NMR
(13)
f1 (ppm)

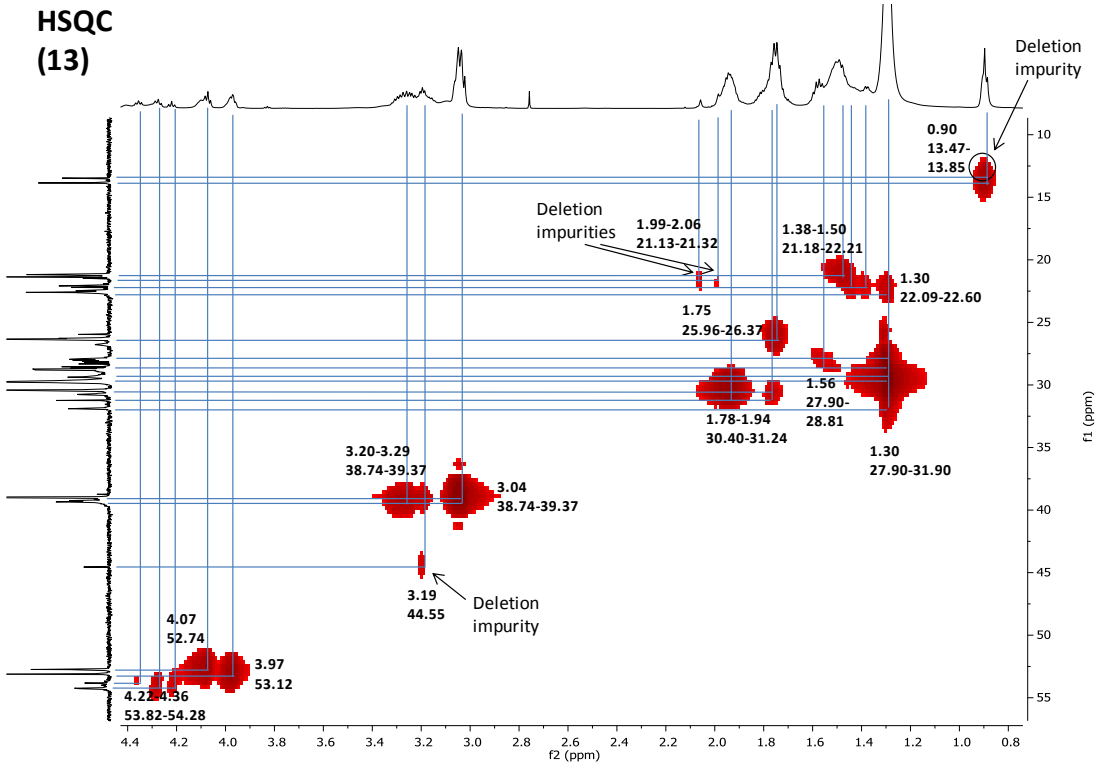
HSQC
(13)
Deletion impurity
Deletion impurities
1.99-2.06
21.13-21.32
1.38-1.50
21.18-22.21
1.30
22.09-22.60
1.75
25.96-26.37
1.56
27.90-28.81
1.78-1.94
30.40-31.24
1.30
27.90-31.90
3.20-3.29
38.74-39.37
3.04
38.74-39.37
3.19
44.55
Deletion impurity
4.07
52.74
3.97
53.12
4.22-4.36
53.82-54.28
f2 (ppm)
f1 (ppm)

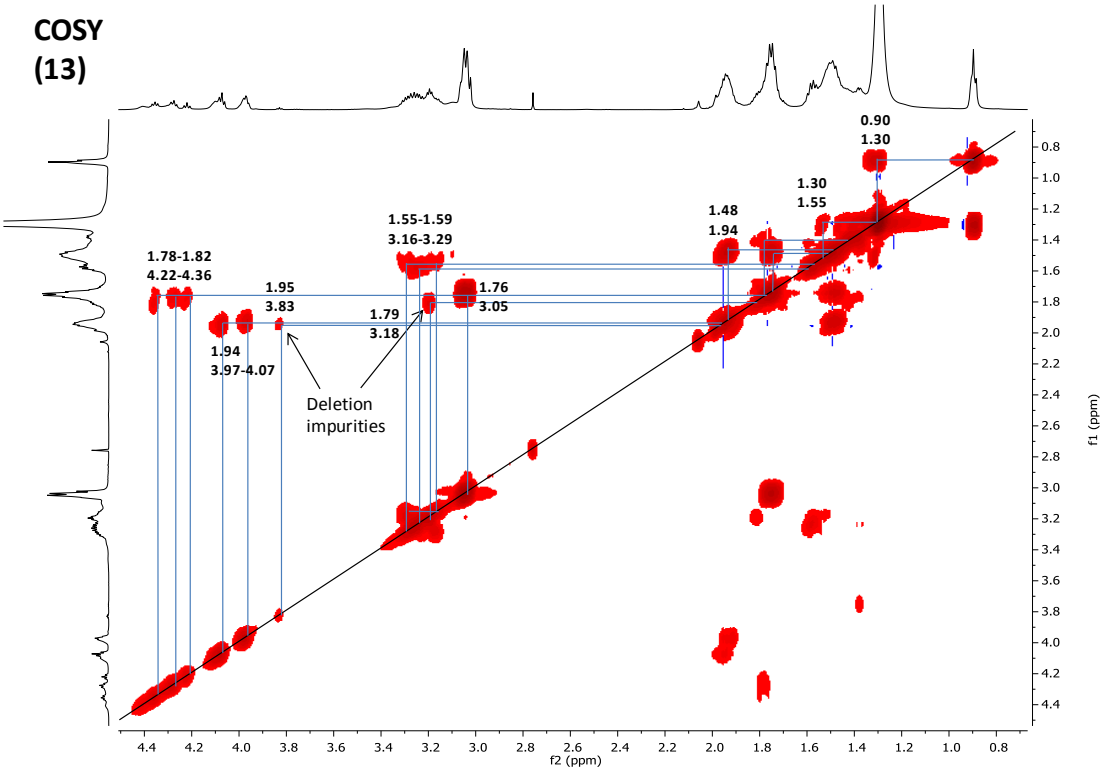
COSY
(13)
0.90
1.30
1.30
1.55
1.48
1.94
1.55-1.59
3.16-3.29
1.78-1.82
4.22-4.36
1.95
3.83
1.76
3.05
1.79
3.18
1.94
3.97-4.07
Deletion
impurities
f2 (ppm)
f1 (ppm)

Notes

1 In some of the compounds of high generation with long alkyl chains the ^{1}H integrals on some protons sometimes deviates from the proposed structure, presumably due to slow relaxation. However, UPLC-MS chromatograms and ^{13}C spectra correlate nicely with the proposed structure.

2 In some of the compounds deviations in the ^{1}H integrals are seen due to the presence of lysine deletion adducts with/without Boc/*t*Bu impurities.